Investigating the degree of Induced Disorder in Mechanicaly Combined Pharmaceutical Materials

Woodhead, Brendon

Awarding institution:
King's College London

Investigating the degree of induced disorder in mechanically comminuted pharmaceutical materials

Brendon Woodhead B.Sc., M.Sc.

Institute of Pharmaceutical Science

King's College London

A Thesis submitted in partial fulfillment of the requirements for the degree of Doctor of Philosophy

April 2014

Abstract

Particle size reduction or comminution by milling is often required to enhance the bioavailability of pharmaceutical solid dosage formulations through increased dissolution rate or solubility inherent in small particulate powders[1-4]. However, these unit operations have the highest risk of inadvertently generating process induced disorder (PID) due to their intense mechanical nature and associated high processing input energies[5-10]. It is therefore important to develop strategies to control, characterise and optimise the particle properties to ensure the safety and quality of the final product.

The work presented in this thesis describes a novel analytical approach using a combination of techniques and analytical responses to give a single normalised value that can be used to represent the relative level of disorder present in material due to a given process without the need for standard mixtures or calibration curves.

A model set of 10 materials: salbutamol sulphate, loperamide HCl, γ-indomethacin, caffeine, sulfamerazine, sulfadiazine, acetylsalicylic acid, phenacetin, acetaminophen and methyl paraben were selected that encompassed the whole of the amorphous-crystalline continuum when subjected to mechanical comminution. These materials were then characterised by a core set of techniques: X-ray powder diffraction (XRPD), gravimetric vapor sorption (GVS), differential scanning calorimetry (DSC), thermal gravimetric analysis, scanning electron microscopy, polarised light microscopy, particle size analysis, high performance liquid chromatography, and Fourier transform infrared spectroscopy both before and after comminution by ball- and jet-milling under different conditions.

The presence of PID was identified and semi-quantified for each comminuted material based upon the relative changes in a combination of XRPD, DSC and GVS responses give a score (D_{Pro}) out of 10. The larger the D_{Pro} value the more likely disorder is present. This successfully allowed the materials to be ranked based on their relative PID contents and the effect of the different comminution processes to be assessed, confirming the validity of the new analytical approach. The high frequency ball-milled materials of salbutamol sulphate, loperamide HCl, and γ-indomethacin exhibited the highest levels of disorder (D_{Pro} 6 to 10), while phenacetin, acetaminophen and methyl paraben exhibited the least (D_{Pro} 0 to 3). The remaining materials exhibited some degree of disorder depending on the comminution process employed. High frequency ball-milling induced the most disorder followed by low frequency ball-milling and jet-milling (micronisation).

Acknowledgement

I would like to express my sincere thanks to the following people:

First and foremost a big thank you goes to my wife Nicola, for her love, understanding, patience, and encouragement not only during the preparation of this thesis but for the many years we have been together.

To my supervisors at King's College London (KCL), Dr Paul Royall, and Professor Gary Martin for their guidance, support, patience and perseverance over the years both in person and over the phone.

To Brian Stockton (ex-manager and industrial supervisor at GlaxoSmithKline Tonbridge) for his support and understanding and allowing me the opportunity to gain experience in a number of solid state characterisation techniques over the 10 years I worked with him.

To GlaxoSmithKline for their previous financial support, supply of materials and free reign of the equipment during my employment.

To Hartley Atkinson and AFT pharmaceuticals, for their kind support and encouragement in the final stages of this thesis.

To my parents and friends, for their encouragement and advice and, finally I would like to thank my two children (Benjamin and Olivia) who appeared in this world during the course of this research, providing the occasional welcome "distraction" and taught me the true meaning of chaos and disorder.

Table of Contents

Table of Figures

Table of tables

Abbreviations

API	Active pharmaceutical ingredient
APF	Atomic packing factor
APR	Analytical property response
ATR	Attenuated total reflectance
BCR	Ball/charge ratio
CCV	Calculated cell volume
Cpg	Cost per gram (£/g)
CRA	Comparative response analysis
CSD	Cambridge Structural Database
Cts	Counts (XRPD peak height)
DSC	Differential scanning calorimetry
DMA	Dynamic mechanical analysis
DVS	Dynamic vapour sorption
FTIR	Fourier transform infrared spectroscopy
FR	Feed rate
GSK	GlaxoSmithKline
GVS	Gravimetric vapour sorption
HBDA	Hydrogen bond donors and acceptors
HA	Hydrogen bond acceptors
HD	Hydrogen bond donors
HDSC	Hyper differential scanning calorimetry
HSM	Hot stage microscopy
KCL	King's College London
HPLC	High performance Liquid Chromatography
JM	Jet mill or micronisation
LoD	Level of detection
LoQ	Level of quantification
LRD	Long range disorder
LRO	Long range order
MDSC	Modulated differential scanning calorimetry
MIP	Most intense peak
MSC	Material selection criteria
MSDS	Material safety data sheet
NMR	Nuclear magnetic resonance spectroscopy
OHC	Occupational health category
PCA	Principle component analysis
PDA	Process disorder analysis
PID	Process induced disorder
PLM	Polarised light microscopy
PLS	Partial least squared
PSA	Particle size analysis
PSC	Particle size class (Sieve fraction)
PSD	Particle size distribution
RA	Response analysis
RAM	Raman spectroscopy
RCS	Refrigerated cooling system
RDA	Response disorder analysis
RDS	Response disorder score
RH	Relative humidity
RMD	Research Material database
RPI	Relative peak intensity
RSD	Relative standard deviation
RT	Room temperature
SC	Selection criteria
SCC	Size classification code
SEM	Scanning electron microscopy
SPG	Space group number
SRO	Short range order
SSA	Specific surface area
SXRPD	Single crystal X-ray diffraction
TGA	Thermal gravimetric analysis
VBM	Vibrational ball-milling
XRPD	X-ray powder diffraction

1 Introduction

Drug products are typically solid dosage forms (inhaled powders or oral solid dose tablets or capsules) manufactured using powdered crystalline active pharmaceutical ingredients (APIs) due to their good physiochemical stability and ease of handling[11]. However, during the manufacturing of these pharmaceutical products, the crystalline API and associated excipients can be subjected to a number of thermal and mechanical unit operations (processes) that can cause process-induced phase transformations resulting in the formation of new solid-state forms or phases[11,12]. As a consequence, the physicochemical properties of the original starting material can be altered and this may ultimately change the pharmaceutical product's physiochemical stability and therapeutic performance[13-17]. When the manufacturing process results in the inadvertent generation of disorder or the formation of amorphous domains, process induced disorder (PID) or mechanical activation is said to have occurred[17-28]. The amount of induced disorder will not only depend on the type and conditions of the pharmaceutical process employed but also on the intrinsic properties of the material itself. However, quantifying the amount of disorder is typically only achieved by the use of calibration curves constructed using "pure" amorphous and crystalline standards that are both problematic and complex to generate[29,30].

In recent years our knowledge of the crystalline (ordered) and amorphous (disordered) solid-state has vastly improved[11,12,14,15,17,31]. However, little is known of the propensity of crystalline materials to undergo process induced disorder. The work presented in this thesis will concentrate on developing an analytical approach using a combination of techniques to investigate the propensity for PID without the need of amorphous/crystalline standards and calibration curves of the material being investigated. The selectivity and sensitivity of this approach will be investigated using a model set of pharmaceutical relevant materials that will be mechanically processed under different conditions and changes in the material's molecular, particulate and bulk properties assessed with respect to the presence of PID. However, in this introductory chapter it is important that the different solid-states or phases of organic matter are firstly defined (Section 1.1), secondly their associated properties examined (Section 1.2), and finally the relevant pharmaceutical mechanical processes reviewed in the context of their potential to generate PID (Section 1.4).

1.1 Solid-states of organic matter

In terms of solid-state structure, organic solids can be ordered (crystalline), disordered (amorphous) or be comprised of varying degrees of both (mesophases) (Figure 1-1). This diversity can be influenced by the relative molecular structure, composition[15,32-35] and by the strength of the intermolecular linkages of the constituent molecules with respect to each other[36].

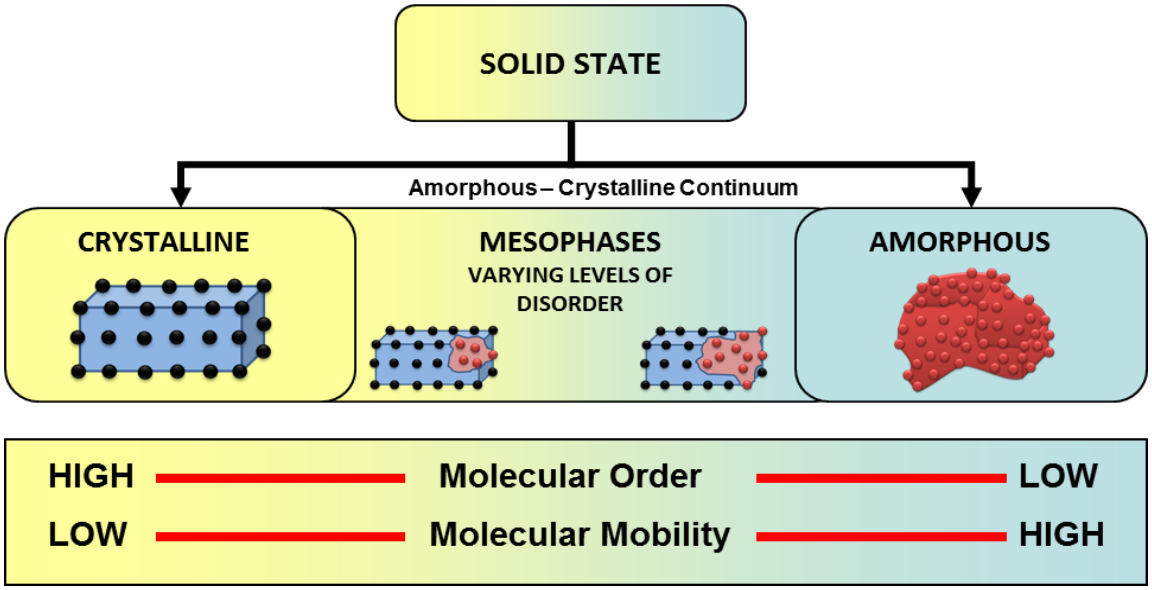

Figure 1-1 Top level classification for the solid-states of matter based on molecular equilibrium

1.1.1 Crystalline solids

Molecules within crystalline solids are packed into a repeated three-dimensional highly ordered rigid structure exhibiting long-range order (LRO)[30]. Crystalline solids exhibit limited amounts of molecular mobility and can be considered rigid with respect to the other states of matter. However, structural differences in molecular conformation and/or packing for a given crystalline solid with the same chemical composition can give rise to what is termed "polymorphism"[17,37-39].

1.1.2 Amorphous solids

Amorphous or disordered solids can be differentiated from the crystalline state by the absence of LRO whereby molecules appear in a random orientation but may still exhibit some form of short-range order (SRO), *i.e.* molecular interactions between the first- or second-nearest neighbours of an atom[40] which may be similar or identical to that in the crystalline state allowing interactions such as hydrogen bonding patterns to also be similar[34,41,42]. Slight changes in the interaction between molecules or the molecular network motifs, *i.e.* changes in their SRO can alter pharmaceutical functions and thermodynamic stability and potentially lead to amorphous instability and

recrystallisation to a new polymorphic form[41,43]. For example, at different temperatures changes in the hydrogen-bond (H-bond) patterns for amorphous indomethacin resulted in molecular recognition events that can lead to the self-assembly (crystallisation) of either the γ- or α-indomethacin polymorphic forms[44,45].

Amorphous solids are more molecularly mobile allowing them to behave more like a liquid[40]. This enhanced molecular mobility can imply conformational diversity for amorphous solids. The number of conformations will depend on the flexibility of the molecule and the preparation route along with any processing history, *i.e.* how the material has been processed and/or stored. This conformational diversity has often been regarded as a type of polymorphism of the disordered state and as such has been referred to as "polyamorphism"[32,33,35,46-48].

Two different classes of polyamorphism are said to occur: "true" and "apparent" polyamorphs[32]. "True" polyamorphism occurs when a material has two distinct meta-stable amorphous states which are separated by a clear phase transition between them[32]. However, evidence for this type of polyamorphism has only been reported for inorganic and polymer substances and not for small organic pharmaceuticals[34,49-55].

"Apparent" polyamorphs which are also referred to as relaxation polyamorphs or pseudo-polyamorphs arise when there is an energy release or structural relaxation process that occurs when the mobility of the amorphous material is sufficient to allow movement of the system towards the meta-stable pseudo-equilibrium state of the liquid or glassy phase under certain processing or experimental conditions[18,32,34,35,56,57].

A number of examples of this type of polyamorphism for pharmaceutical materials have been observed and reported over the last few decades as a result of differences in their kinetic and mobility properties imparted by their previous processing history *e.g.* modes of preparation, storage conditions and thermal and mechanical treatments[34,46,49-55,58-62]. For example, Yamaguchi *et al.* reported different isolated amorphous forms of an antibiotic compound (MAT) prepared by spray drying that exhibited different thermal properties and dissolution behaviours depending on the preparation conditions employed[62]. While, Yonemochi *et al.*, concluded that different molecular states of amorphous ursodeoxycholic acid can exist that exhibit different crystallisation behaviours as a result of the preparation method (quench cooled or grinding)[56,63].

For the two classes of polyamorphism, new terms and definitions are proposed here in this thesis according to the processes used to generate them (Table 1-1). True

polyamorphs, are defined as being metamorphs as they represent meta-stable amorphous states separated by a phase transition. In contrast, relaxation or "apparent" polyamorphs which are generated as a result of differences in their kinetic properties but are related by structural relaxations are defined as kinetamorphs.

Table 1-1 Proposed classification and definitions for different types of polyamorphs

Historical Classification	New Classification	New Definition
True polyamorph	Metamorph	The existence of distinct amorphous states of the same material separated by a phase transition.
Relaxation, pseudo or apparent polyamorph	Kinetamorph	The existence of distinct amorphous states of the same material as a result of differences in their kinetic and mobility properties imparted by their previous processing history.

Amorphous solids are by definition not at thermodynamic equilibrium with their surroundings as they contain an excess of Gibbs free energy (ΔG) relative to the crystalline phase at a stated storage temperature and humidity (Equation [1-1]).

$$\Delta G = \Delta H - T\Delta S \qquad [1\text{-}1]$$

where the enthalpy difference between the phases (ΔH) reflects the lattice or structural energy (enthalpy) differences, while, the entropy difference (ΔS) is related to the disorder and lattice vibrations at absolute temperature (T).

As amorphous solids are unstable they may lie in a number of positions in the energy landscape relative to the crystalline phase as illustrated in (Figure 1-2). Therefore, the Gibbs free energy value for amorphous solids should be considered to represent an average position or value.

Figure 1-2 can also be used to illustrate the existence of metamorphs. An amorphous material (metamorph 1) may exist as a collection of states separated by an activation energy barrier E_{a1} from another polyamorph (metamorph 2) which is at a lower energy state. E_{a1} represents the energy required to transform metamorph 1 to metamorph 2 and is smaller than the energy required to overcome the activation energy barrier (E_{a2}) for a phase transformation from the amorphous to crystalline phase. The stored or excess energy of amorphous solids can be released completely via recrystallisation if ΔG is negative, or partially by means of an irreversible structural relaxation process[64]. The rate at which the recrystallisation process takes place is determined by the molecular mobility of the material[40].

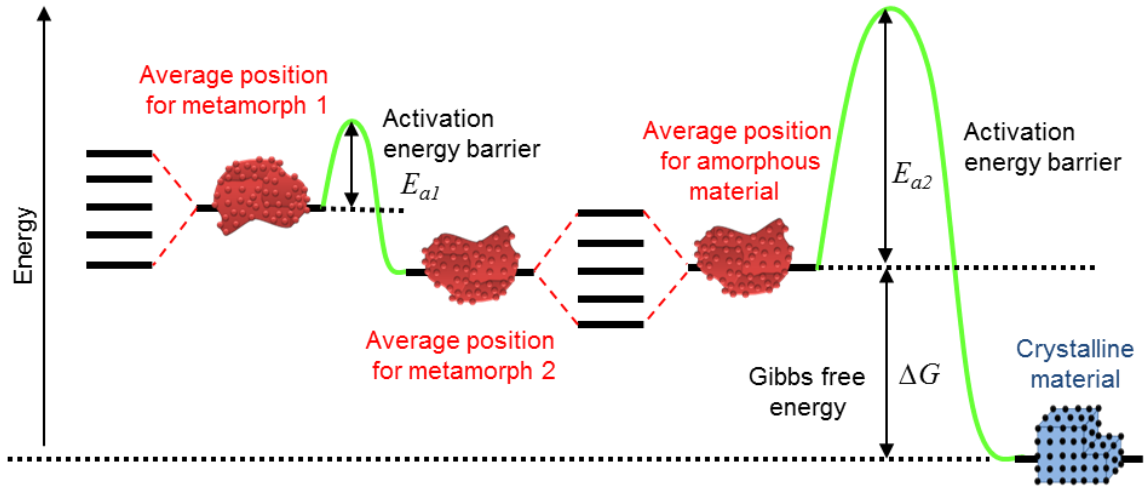

Figure 1-2 ***Schematic showing the energy landscape and relationship between metastable amorphous (metamorphs) and the crystalline material***
E_{a1} is the activation energy barrier to overcome for the transition of metamorph 1 to metamorph 2. E_{a2} is the activation energy barrier to overcome going from amorphous material to a crystalline material.

Figure 1-3 represents a plot of the enthalpy (H) or specific volume (V) of a solid substance as a function of its temperature[65]. For a crystalline material it can be seen, that as the temperature increases there is a small increase in enthalpy and volume at low temperatures, where the slope is equivalent to the heat capacity (C_p) of the material. Once the temperature reaches the melting point (T_m) of the crystalline phase, a first order transition occurs to the liquid state[65].

When the liquid is rapidly cooled below T_m, a super-cooled liquid is obtained where the thermal molecular motions are significantly reduced down to a time scale larger than that of any structural relaxation. This is often referred to as the "rubbery state"[40,65]. In theory, if the super-cooled liquid was cooled and remained in equilibrium as shown by the blue dashed line in Figure 1-3 then at some point the volume and enthalpy of the system would be equal to that of the crystalline material. This hypothetical point is referred to as the Kauzmann temperature (T_K) or the Kauzmann paradox[66-68]. Kauzmann in 1948 postulated that upon cooling, the entropy of the super cooled liquid would became less than that of the crystalline solid[68]. However, this point can never be reached without violating the Third Law of Thermodynamics[66,67]. Instead, as the temperature decreases the molecular volume of the super-cooled liquid correspondingly decreases and the material becomes increasingly viscous or less mobile, and in such a milieu the molecules can adopt a number of different conformations. The point at which the material deviates from that of a super-cooled liquid resulting in a "frozen" non-equilibrium state (amorphous or glassy material) is called the glass transition temperature (T_g)[65,67]. The T_g is associated with a reduction in the heat capacity and molecular mobility of the material. Below the T_g viscosity reaches a high value (>10^{12}

Pa.s) and over time the glass may age and relax to a lower energy state. This slow relaxation in glasses towards the equilibrium state is known as structural relaxation, physical aging or annealing[65,69].

In theory, an infinite number of different glasses or kinetamorphs may be generated with different glass transition temperatures and potentially distinct physical and chemical properties[32,70] by adjusting the cooling rate of a material below its melting temperature (Figure 1-3). In general, the faster the cooling rate the higher the T_g and therefore the greater the molecular volume and molecular mobility.

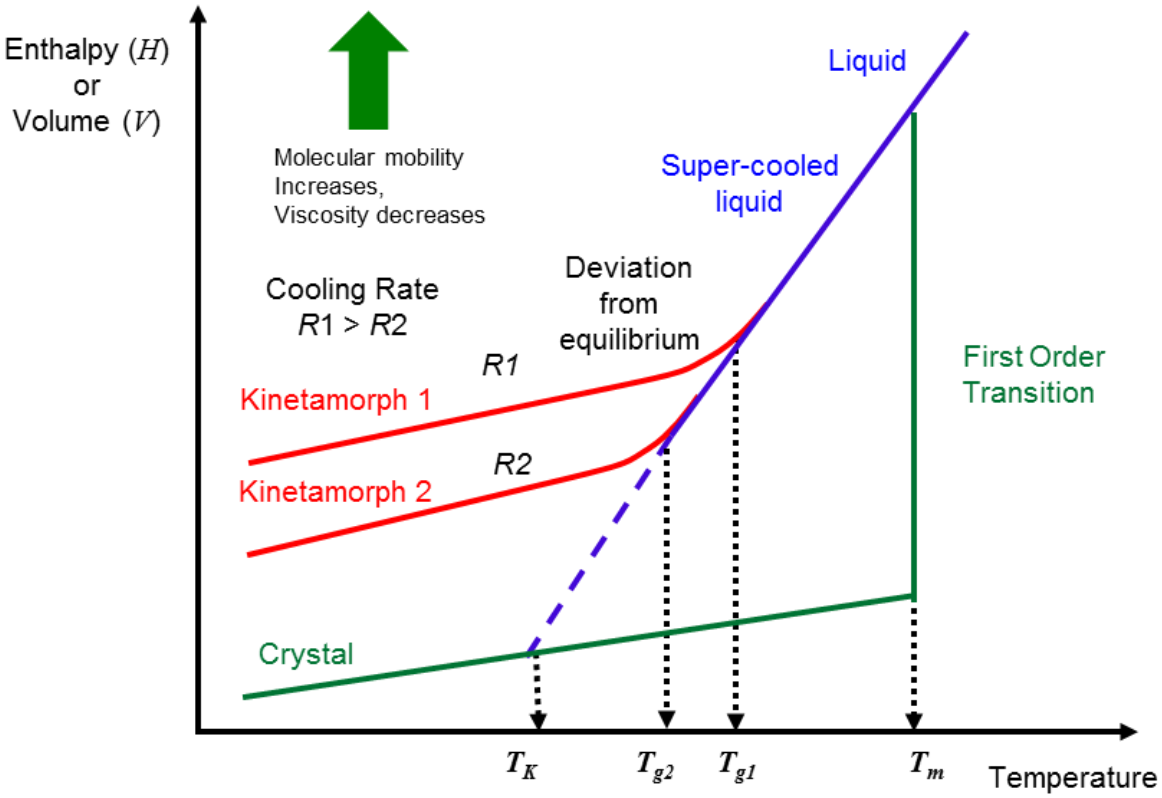

Figure 1-3 ***Schematic for the variation of enthalpy (or volume) as a function of temperature [Adapted[18,64,65]]***

The red line denotes the pathway of an amorphous material while the green line denotes the behaviour of a crystalline material. Varying the cooling rate (R1 and R2) can result in the formation of different amorphous solids i.e. kinetamorphs (1 and 2). These kinetamorphs can exhibit different glass transition temperatures, T_{g1} and T_{g2} respectively. The melting point temperature (T_m) is a thermodynamic first order transition from the crystalline to the liquid state. T_K:Kauzmann temperature.

The physical property changes that occur during glass transition can be detected and quantified by several techniques[65,71] but most commonly the T_g and heat capacity (C_p) changes are measured using techniques such as differential scanning calorimetry (DSC). The determination of T_g for amorphous and PID materials can provide information around the material's chemical reactivity and physical stability. As the storage temperature approaches the T_g, physical stability is reduced while chemical reactivity

increases. For pharmaceutical processes operating near or above the T_g uncontrolled phase transformations may occur which could result in new solid state forms that may lead to detrimental effects on downstream processing and affect the pharmaceutical performance of the final product[9,72-78].

It has been observed that the T_g region occurs over a temperature range that is approximately two-thirds of the melting point (T_m) (in kelvin)[40]. This observation can be used to estimate the location of T_g based on T_m. If both values are known then the temperature dependency of molecular mobility in the regions just above T_g can be estimated by determining the amount of deviation from the "two-thirds rule". If T_g/T_m is significantly greater than 2/3 then molecular mobility for material is likely to be strongly temperature dependent around the T_g region and can be classed as "fragile". However, there is no simple method to estimate the temperature dependence of molecular mobility in the temperature region below T_g where a large proportion of pharmaceutical materials are processed and stored[79-81].

1.1.3 The amorphous-crystalline continuum: mesophases

The amorphous-crystalline continuum[12,64,82] can be considered to be composed of material (mesophases) of differing proportions of both pure disordered (amorphous) and pure ordered (crystalline) phases[83]. These heterogeneous systems are composed of various distinct domains, each of which is in itself homogeneous in composition, but separated from the other by distinct boundary surfaces[38]. The amorphous-crystalline continuum can be visualised by a number of models based on their phase composition and location.

The first model often referred to as the "one-state" model[18,47,65,84,85] arises where there exists a completely crystalline solid with a high degree of order. As the amount of crystal defects and/or distortions increases, so does the level of disorder until a highly disordered (amorphous) material is generated (Figure 1-4). Lattice defects of this type predominately occur on the surfaces of crystals as a consequence of mechanical processes by processes such as ball-milling and micronisation and are quite often difficult to detect[82,86]. Crystal defects are discussed further in Section 1.3.

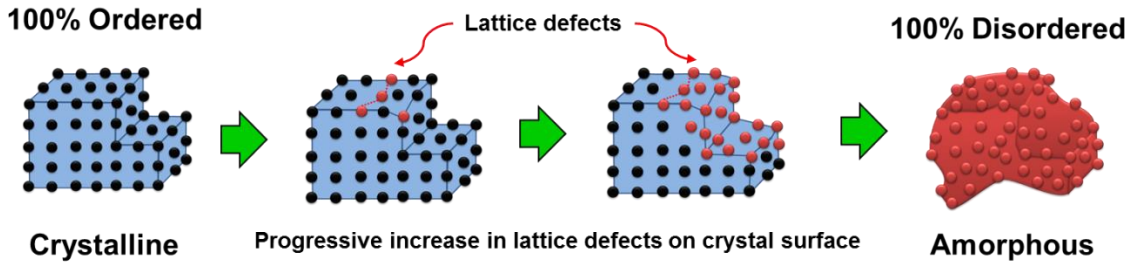

Figure 1-4 ***Depiction of the "One-State" Model for the conversion of 100% crystalline material to 100% amorphous via progressive incorporation of lattice defect***

A progressive increase in lattice defects within a crystalline solid causes a subsequent decrease in crystallinity until a highly disordered solid is generated

A second model often referred to as the "two-state"[34,42,47,65,84,85] model arises due to the presence of pure amorphous or pure crystalline phases co-existing either within a single crystal as domains (Figure 1-5A) or within a molecular mixture (Figure 1-5B).

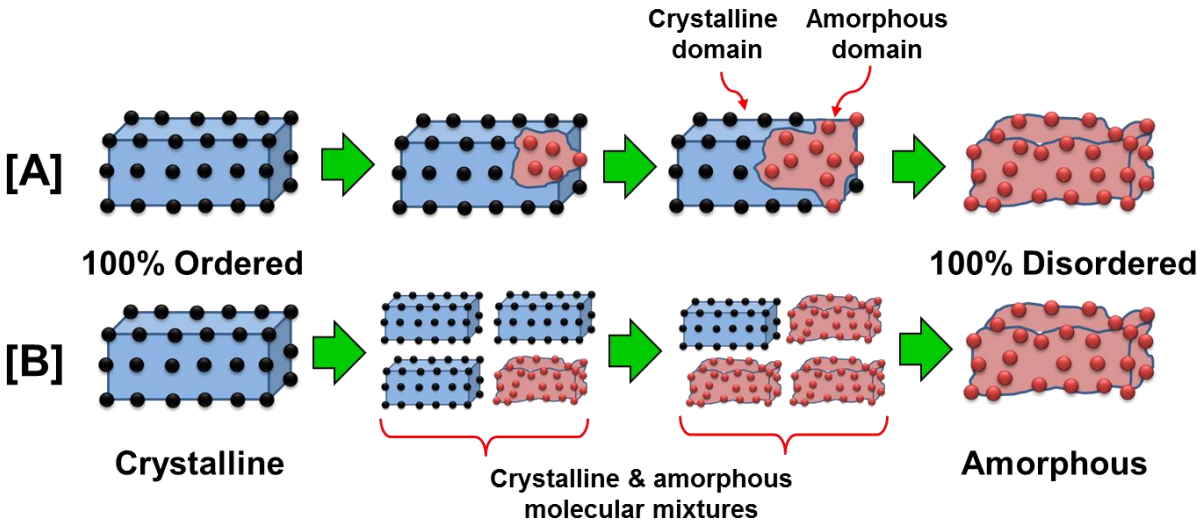

Figure 1-5 ***Depiction of the "Two-State" model for describing pure amorphous/crystalline domains within a solid (A) or a mixture (B)***

Often in literature, mixtures of pure amorphous and crystalline material are used to construct calibration curves to quantify the levels of disorder that maybe present[23,87]. However, these "pure" amorphous standards are typically prepared by processes such as spray drying or melt-quenching resulting in complete disorder of the bulk of the material which may not necessarily best represent the material or the analytical responses for materials where disorder is generally surface located as a consequence of mechanical pharmaceutical unit processes such as ball-milling or micronisation[47,84,88]. If standard curves are to be employed it is important that the standards used reflect not only the type and location of the disorder, *i.e.* surface or bulk as described by the one- and two-state models, but also the associated analytical response for the desired physical property being investigated.

1.2 Properties of the crystalline solid-state

Properties of solids can be broadly classified into two levels; primary (intrinsic) and secondary (derived) properties. The former defines the fundamental properties such as structure and solid-state form, while the latter defines the solid's behavioural and manufacturability properties[17,39,89,90,91] (Table 1-2). Only the primary properties or molecular characteristics will be discussed in this chapter. Further information regarding the other properties listed can be found in the numerous well documented reviews in the literature[91-93].

Table 1-2 Some typical primary and secondary properties of solids [Adapted[91]]

Primary (Inherent) properties [Molecular characteristics]	Secondary (derived) properties [Particulate & bulk characteristics]	
Molecular packing	Chemical and physical stability	Brittleness/elasticity
Morphology	Thermal behaviour (melting etc)	Moisture uptake
Hydrogen bonding	Bulk and tapped density	Powder flow
Absolute or true density	Electrostatic properties	Compactability
Lattice energies and entropies	Dissolution rate and solubility	Surface area
Molecular mobility	Fracturability and cleavage planes	Particle size

1.2.1 Molecular structure and packing

Knowledge of the molecular packing and conformation of solids as well as their thermodynamic properties provides important information on how a solid may act under certain conditions such as pressure, temperature and relative humidity. This information can be used to highlight the propensity for potential phase transformations and hence the solids' respective relative stabilities[94].

The geometry of crystal packing can be described by a number of molecular descriptors (see Section 1.2.1.1). However, it is important to understand the nature of the molecular interactions or bonds that hold the crystal together, or in the case of disordered or amorphous materials the reduction of molecular interaction.

Chemical bonds can be classified in decreasing strength as ionic, covalent, metallic, van der Waals and hydrogen bonds[95-97]. Materials possessing strong bonds such as ionic, covalent and metallic bonds typically have much stronger or larger mechanical properties such as hardness as well as higher melting points than small organic crystalline materials such as pharmaceuticals which are held together by the weaker van der Waals and hydrogen bonds[95-97]. For materials such as pharmaceuticals, these weak interactions must be maximised to ensure optimal molecular packing[95-97]. This optimisation of the non-covalent interactions is based on three fundamental principles. These are, (i) to maximise density and minimise free volume[98], (ii) maximise hydrogen

bond (H-bond) interactions[97,99,100] and (iii), minimise electrostatic energy[98]. Using these principles the atoms or molecules of the crystal are arranged into a three dimensional motif called a crystal lattice which represents an array of points with a definite volume (*V*) and defined by the lattice parameters, axial lengths (*a*, *b* and *c*) and angles (α, β and γ) that forms the unit cell[85,91,101] (Figure 1-6[A]). Arranging the unit cells into an ordered molecular array, results in a high density packed lattice exhibiting LRO (Figure 1-6[B]).

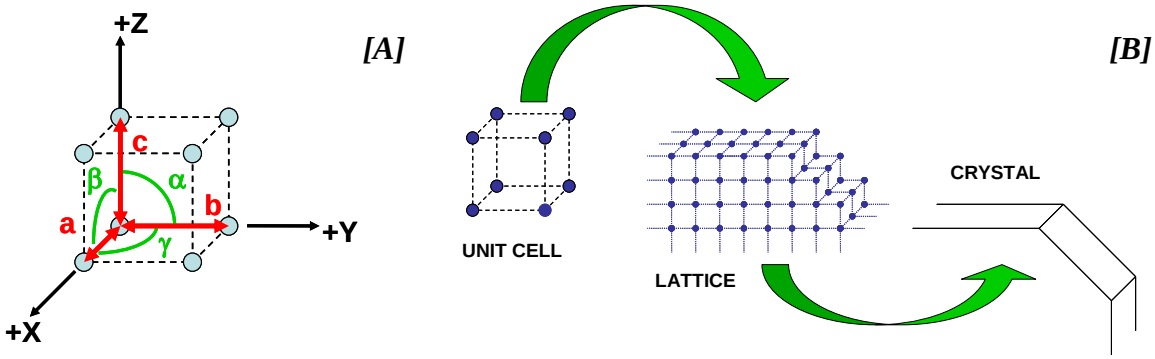

Figure 1-6 ***Schematic of a unit cell [A] and the arrangement of molecules within crystalline solids [B] [Adapted[102]].***

1.2.1.1 *Molecular descriptors for the geometry of crystal packing*

There are only fourteen possible crystal lattice types referred to as Bravais lattices[85,102,103] which can be categorized into seven crystal systems (Table 1-3). Each Bravais lattice is given a space lattice code in brackets next to its respective name as shown in Table 1-3. *P* represents the primitive or simple unit cell with lattice points at the cube corners. *I* refers to a body centered unit cell with lattice points at the corners and in the middle of the cell. *F* refers to a face centered unit cell with lattice points at the corners and in the center of each face. While *C*, represents an end-centered unit cell with lattice points at the corners and in the center of one set of parallel face. Any crystal structure can be described with a unit cell from one of the seven crystal systems.

The unit cell typically contains more than one molecule, and these molecules can also be described on the basis of symmetry. There are five symmetry elements (Table 1-4) that can be used to give a total of 230 possible molecular combinations or space groups[104-106].

Table 1-3 Crystal systems and Bravais lattices for the molecular packing of crystalline unit cells [Adapted[102]]

Crystal system	Bravais lattice	Axial length and angles
Monoclinic	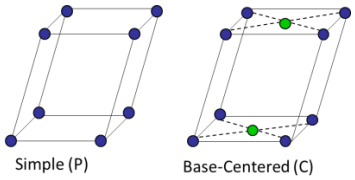	$\alpha = \gamma = 90^o \neq \beta$ $a \neq b \neq c$
Orthorhombic	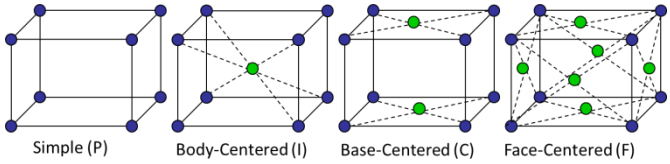	$\alpha = \beta = \gamma = 90^o$ $a \neq b \neq c$
Triclinic	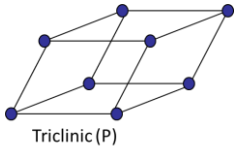	$\alpha \neq \beta \neq \gamma \neq 90^o$ $a \neq b \neq c$
Tetragonal	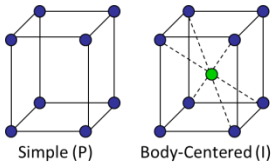	$\alpha = \beta = \gamma = 90^o$ $a = b \neq c$
Trigonal or Rhombohedral	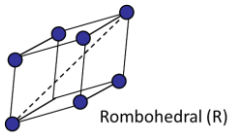	$\alpha = \beta = \gamma \neq 90^o$ $a = b = c$
Hexagonal	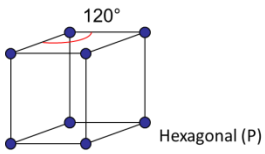	$\alpha = \beta = 90^o$, $\gamma = 120°$ $a = b \neq c$
Cubic	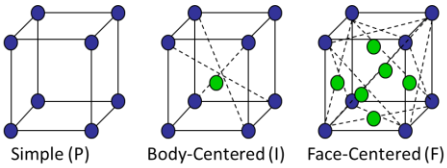	$\alpha = \beta = \gamma = 90^o$ $a = b = c$

A space group starts with a capital letter to indicate the Bravais lattice type, followed by a symbol for the principal axis. If there is a plane of symmetry or a glide plane perpendicular to the principal axis the symbols are combined. This is followed by symbols for the symmetries of the secondary and tertiary axes and the planes of symmetry or glide planes parallel to these axes. For example, in the space group *Pmm2*, *P* refers to a primitive lattice and *mm2* means that the cell contains mirror (*m*) planes perpendicular to both the *a* and *b* axes and a two-fold rotation axis along the *c* axis[103]. In the case of small organic molecules which are typically classed as irregular shaped

molecules there is little or no symmetry and molecules adopt a strategy to optimise intermolecular interactions by packing into arrangements with inversion centers, glide planes and/or two-fold screw axes as is the case for the most abundant group monoclinic space group $P2_1/c$ which contains all three symmetry elements. Approximately 75% of all known organic compounds crystallise in only five space groups[107]: $P2_1/c$, $P2_12_12_1$, $P1$, $P2_1$ and $C2/c$ which correspond to space group numbers 14, 19, 1, 4 and 15 respectively[108,109].

Table 1-4 The symmetry elements of crystal packing [Adapted[15,103]]

Symmetry Element	Description
Rotation axis (n = 2,3,4,6)	Rotation of 360°/n results in the same structure, then the crystal contains a n-fold rotation axis.
Screw axis (n_1)	Rotation of 360°/n followed by a translation parallel to the axis of rotation brings the structure into coincidence.
Rotatory-inversion axis (n = $\underline{2}$, $\underline{3}$, $\underline{4}$, $\underline{6}$)	Rotation of 360°/n followed by inversion results in the same structure.
Mirror plane (m)	Reflection through the plane results in the same structure.
Glide plane (c)	Reflection through a mirror plane followed by translation brings the structure into coincidence.

Molecules with symmetries that allow close packing generally form more ordered crystals and crystallise more easily than irregular molecules[103]. The efficiency of packing defined by the packing coefficient, (C) can be calculated as the amount of filled space in the unit cell divided by the total unit cell volume as shown in Equation [1-2][110,111].

$$C = \frac{Z \,.\, V_m}{V_{cell}} \qquad [1\text{-}2]$$

where Z is the number of molecules in the unit cell, V_m is the molecular volume and V_{cell} is the unit cell volume. Typically most stable crystals have a packing coefficient between 0.65 and 0.80[98,110,111]. However, H-bonded systems tend to have packing coefficients in the lower range (< 0.7) due to their open configuration (positioning) to maximise the H-bond network[99].

1.2.2 Hydrogen bonding and molecular aggregates

H-bonds play a key role in the molecular packing and stability of small organic crystals[100]. The formation of a network of H-bonds within a solid is a means of molecular stabilisation by the creation of a molecular aggregate[97,112]. For example, H-bonding is a primary feature in the crystal structure of acetaminophen Form I a monoclinic crystal[113]. There are two H-bond donors (HD): NH, OH and two H-Bond

acceptors (HA): CO, OH with a total of eight atoms involved in the H-bond pattern. Within the crystal, molecules are linked by hydrogen bonds to form pleated sheets[114]. Each molecule in the sheet is surrounded by six others which are connected to the central molecule by four hydrogen bonds. The sheets are stacked along the *b* plane by relatively strong van der Waals interactions between the benzene rings. These interactions contribute to nearly 60% of the entire lattice energy and define the anisotropy of the crystal properties, such as differences in dissolution for the different faces[113-115]. For disorder to be generated as a consequence of a mechanical processing, destabilisation of the crystal lattice requires that the H-bonding pattern and molecular interactions must be first overcome.

H-bonding patterns have also been shown to influence cleavage along slip planes[116-122]. For example, cleavage was shown to occur between networks of hydrogen bonds for adipic acid and salicylamide while for sucrose and α-lactose monohydrate it involves breaking the weakest hydrogen bonds[119,120]. A structure-property relationship can potentially be derived from H-bonding patterns which may lead to a correlation with the propensity of a material to become disordered upon mechanical processing, *i.e.* solids with weaker or limited hydrogen bonding patterns may fracture more as the strength of the bonds stabilising the molecular aggregate are less. Therefore, the amount of energy required to disrupt the crystal lattice is lower, if too much energy is applied to the solid there is the potential for lattice destabilisation and the formation of process induced disorder.

1.2.3 Crystal morphology (habits)

Crystal morphology is a term often used to describe the external geometry or shape of a crystal[2,123-125]. However, when a material of the same chemical composition and the same solid state form, *i.e.* the same unit cell exhibits different shapes, this is often referred to as exhibiting different crystal habits[125]. Crystal morphology defines the particle shape, size, and other mechanical properties which can affect manufacturing processes and product efficacy[125,126].

The final crystal morphology of a crystal is decided by the ease and speed of attachment of new molecules at each crystal face. The energy released on the attachment of a growth slice to a growing crystal surface or face is called the attachment energy (E_{ATT})[126]. The growth rate of the face is proportional to its E_{ATT}. Faces with the lowest E_{ATT} are the slowest growing and, therefore, have the most morphological importance, *i.e.* faces with the lowest E_{ATT} will be the major habit face and will coincide with the

major cleavage face as this face provides the weakest plane and can give rise to slip planes[119,120,127]. Slip planes can also be characterised by stacked layers of molecules strengthened by a 2D H-bonding network[118].

The relationship between structure and properties can be considered anisotropic. A crystal will contain a lattice of unit cells with potentially different symmetry elements along their axes[126]. As a consequence of this, the properties or functional groups of a crystal may differ in different directions or faces exhibiting different physicochemical and processing properties[126,128]. For example, different habits/faces may have different dissolution rates or they may also exhibit different fracturing behaviour during pharmaceutical processes such as milling, which can result in different levels of disorder[2,123,126,129-131].

1.3 Crystal defects

In theory crystals are generally considered to be a highly ordered molecular array of atoms. However, in reality they are never "100% perfect". A large number of crystal imperfections exist in the form of point, lattice and plane defects[119,120,126,132-134] (Figure 1-7, Figure 1-8 and Figure 1-10 respectively). These defects can develop during crystallisation and act as nuclei for crystal growth or as fracture points during pharmaceutical unit processes such as milling and compaction[12,132,135-137].

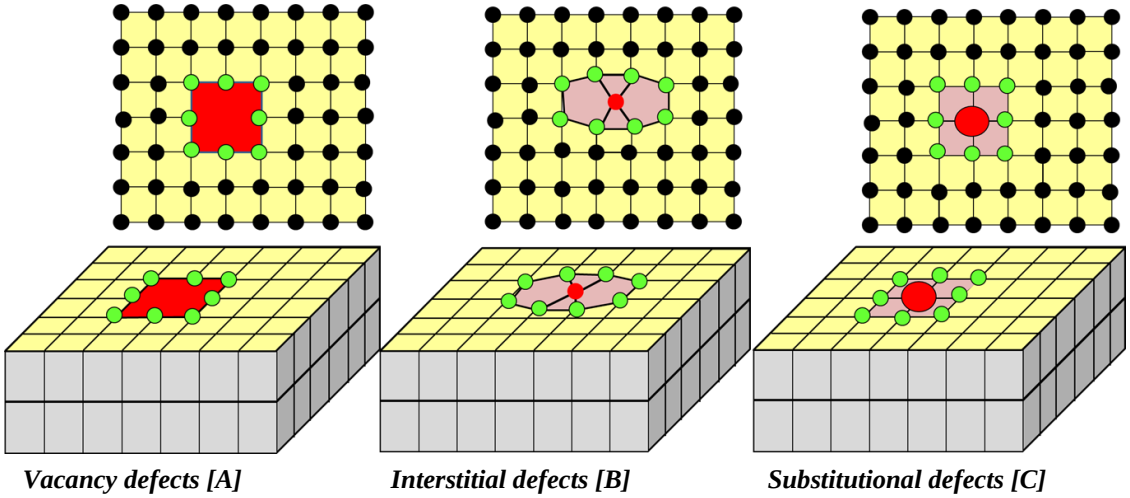

Figure 1-7 Schematics of the three types of point defects: vacancy (A), interstitial (B) & substitutional (C) depicted in 2- and 3-dimensions
Atoms coloured red depict the position of the lattice defect, while the neighbouring atoms are coloured green. For vacancy defects the red depicts the missing atom.

Point defects are imperfections that occur only at or around a single lattice point on a crystal face and are defined as vacancy, interstitial or substitutional defects[133,134,138] (Figure 1-7). A vacancy defect is caused by the absence of an atom at a specific point[134,138] (Figure 1-7[A]). Interstitial defects are atoms that occupy a site in the crystal

structure at which there is usually not an atom[134,138] (Figure 1-7 [B]). Substitutional defects arise due to impurities being incorporated at a regular atomic site in the crystal structure[134,138] (Figure 1-7 [C]). Both interstitial and substitutional defects will cause a displacement of neighbouring atoms and a strain in the crystal[134].

Impurities or additives can lead to lattice defects such as line (edge) and screw dislocations (Figure 1-8)[133,134,138]. A line dislocation is an extra half-plane of atoms that is inserted midway into the crystal lattice, distorting nearby planes of atoms (Figure 1-8[A]). When enough force is applied from one side of the crystal structure as occurs in a shear stress, this extra plane passes through the planes of other atoms breaking and remaking bonds until it reaches the grain boundary (Figure 1-9). Grain boundaries are interfaces where crystals of different orientations meet, and contain atoms that have been perturbed and migrated from their original lattice sites by dislocations and impurities. Dislocation migration can provide a mechanism for strain release or structural relaxation as a consequence of mechanical processing. The stresses and strains associated with mechanical processing will be discussed in Section 1.4.1 and 1.4.2.

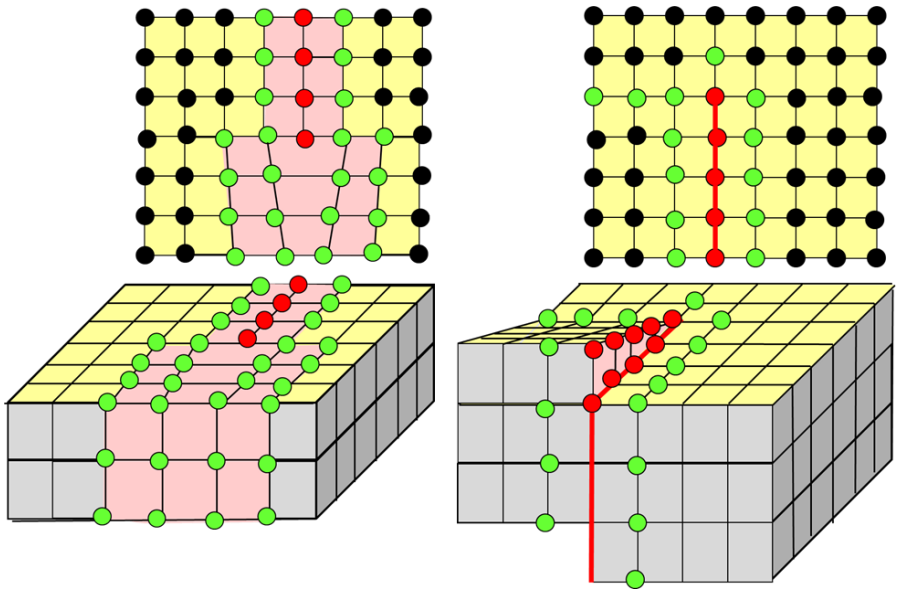

Line or edge dislocation [A] ***Screw dislocation [B]***

Figure 1-8 ***Schematics of the two types of lattice defects: line or edge dislocations (A) and screw dislocations (B) depicted in 2- and 3-dimensions [Adapted[119,132,134]]***
Atoms coloured red depict the position of the lattice defect, while the neighbouring atoms are coloured green.

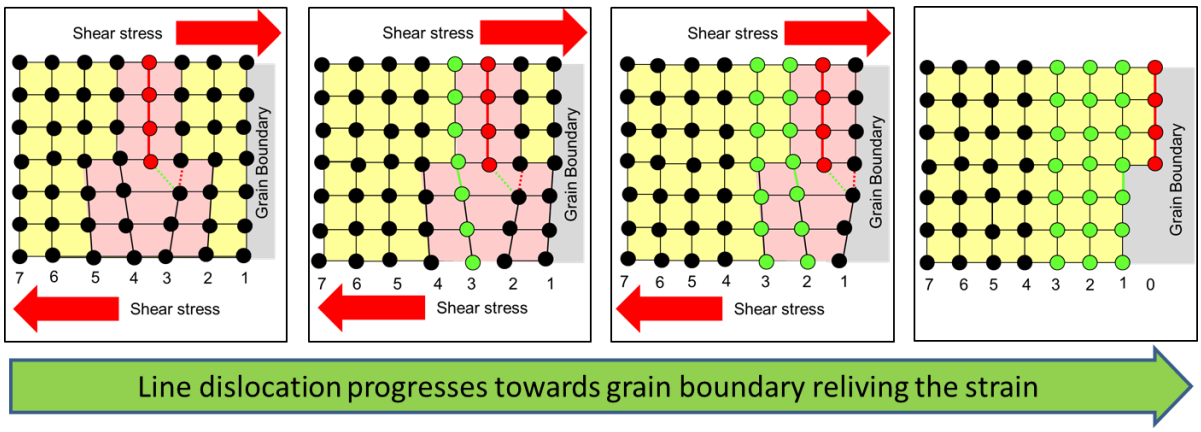

Figure 1-9 ***Movement of an edge dislocation during the application of a shear stress [Adapted[119]].***

The solid red line and atoms represent the position of the line dislocation. The dashed red line identifies the bond which is broken as the line dislocation traverses the planes of atoms (numbered) in the crystal lattice. Dashed and solid green lines show the next and newly formed bonds respectively. Green atoms show the progress of the line dislocation along the planes of atoms towards the grain boundary. The amount of internal strain is released as the dislocation travels towards the grain boundary

Screw dislocations provide a number of additional exposed crystal faces that normally are not exposed thereby potentially changing the behaviour of the material (Figure 1-8[B]). For example, screw dislocations can expose a number of hydrophobic groups which could alter the solubility and dissolution characteristics of the material. Or the presence of exposed surfaces can act as nuclei for further crystal growth thereby changing the crystal habit.

A crystal solid (particle) can be thought to consist of a number of small crystals called crystallites which are held together by grain boundaries[133,134,138] (Figure 1-10). These grain boundaries can be considered to be an array of dislocations and defects resulting in plane defects and areas in which the crystalline lattice can fracture when exposed to an external force[12,132,137]. The mechanical process of crystal fracture will be discussed in Section 1.4.2.

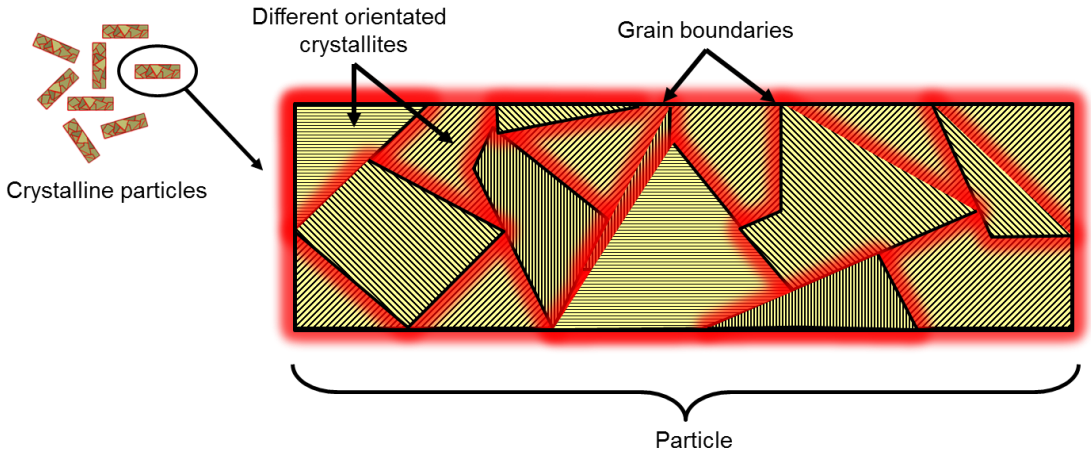

Figure 1-10 ***Schematic of a crystalline particle containing different orientated crystallites separated by grain boundaries.***

1.4 Pharmaceutical processes and process induced disorder

In the manufacture of inhaled and non-inhaled pharmaceutical solid dosage formulations the primary focus is on converting a molecule to a crystal, a crystal to particles and then particles to a dosage form. During these processes, the API and excipients can be subjected to a number of thermal and mechanical processes as shown in Figure 1-11. Pharmaceutical unit operations that are associated with the API only such as crystallisation and particle size reduction (comminution) processes are referred to as primary processes. While, pharmaceutical unit operations which are employed to formulate the API and excipients into a product such as mixing, blending and compaction are referred to as secondary processes. During each step of the primary and secondary manufacturing process there is a need to develop strategies to control, characterise and optimise the particle properties.

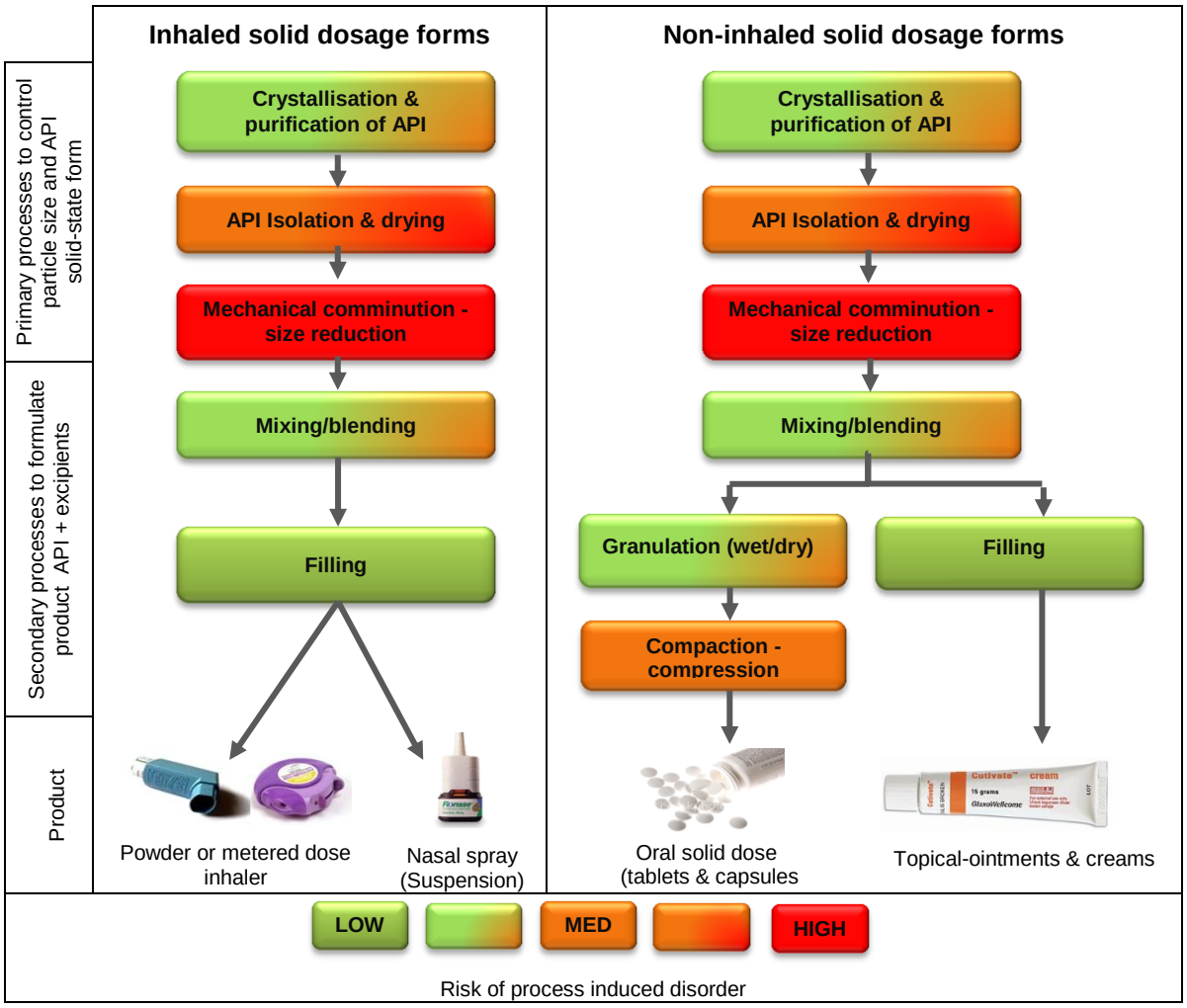

Figure 1-11 General pharmaceutical manufacturing process map showing the associated mechanical and thermal processes for the manufacturing of inhaled and non-inhaled solid dosage formulations

Each manufacturing process is colour coded to reflect the risk of inducing disorder from low risk (green) to red (high risk). [Product images courtesy of GSK]

Mechanical processes are pharmaceutical unit operations such as agitated drying, high energy milling, compaction and high shear granulation, which employ or involve physical processes or media without a chemical reaction to modify or obtain a desired behaviour or physical property. While thermal processes are pharmaceutical unit operations that are associated with changes in temperature such as cooling (crystallisation) or heating (drying). For a number of mechanical unit operations, changes in temperature can also occur. For example, during the compaction of a powder into a tablet an increase in temperature from 5 – 30 °C above ambient is typically observed which can influence not only compaction behaviour but also tensile strength of the material[139-141]. Both thermal and mechanical processes can inadvertently cause process-induced phase transformations such as the generation of lattice disorder or PID which is a significant concern to the pharmaceutical industry[17-28,65]. Typically PID can result in a number of significant changes to the material which can affect the performance and quality of the intended product. These changes are exemplified by; (i) the formation of agglomerates during or post processing[19-21], (ii) physical and chemical instabilities[4,83,142-144], (iii) solid state form or phase transformations[6,17-28,145-150], (iv) electrostatic and surface energy changes[151-159] and (v) increased hygroscopicity[19,20].

In Figure 1-11 each pharmaceutical unit operation has been colour coded to reflect its potential to induce disorder, *i.e*. the PID risk. Units coloured red signify a high PID risk, those coloured orange a medium risk, while unit operations with the lowest PID risk are green. The unit operations with the highest PID risk are the particle size reduction or comminution processes due to their intense mechanical nature and associated high processing input energies[5-10]. It is for this reason that two commonly used mechanical comminution processes, vibrating ball-milling and air jet-milling (fluid energy mill) were selected as the units of operation to potentially generate PID to investigate the presence or absence of disorder in a selection of model pharmaceutical materials.

1.4.1 Mechanical process stresses and material responses (strains)

Pharmaceutical mechanical processes can subject the API and associated excipients to a number of external forces or stresses as illustrated in Figure 1-12. When exposed to a stress, the solid will attempt to resist the force and prevent permanent deformations, distortions and fractures. How much the material resists the applied force depends on the intrinsic properties of the material and the energy associated with the process[160].

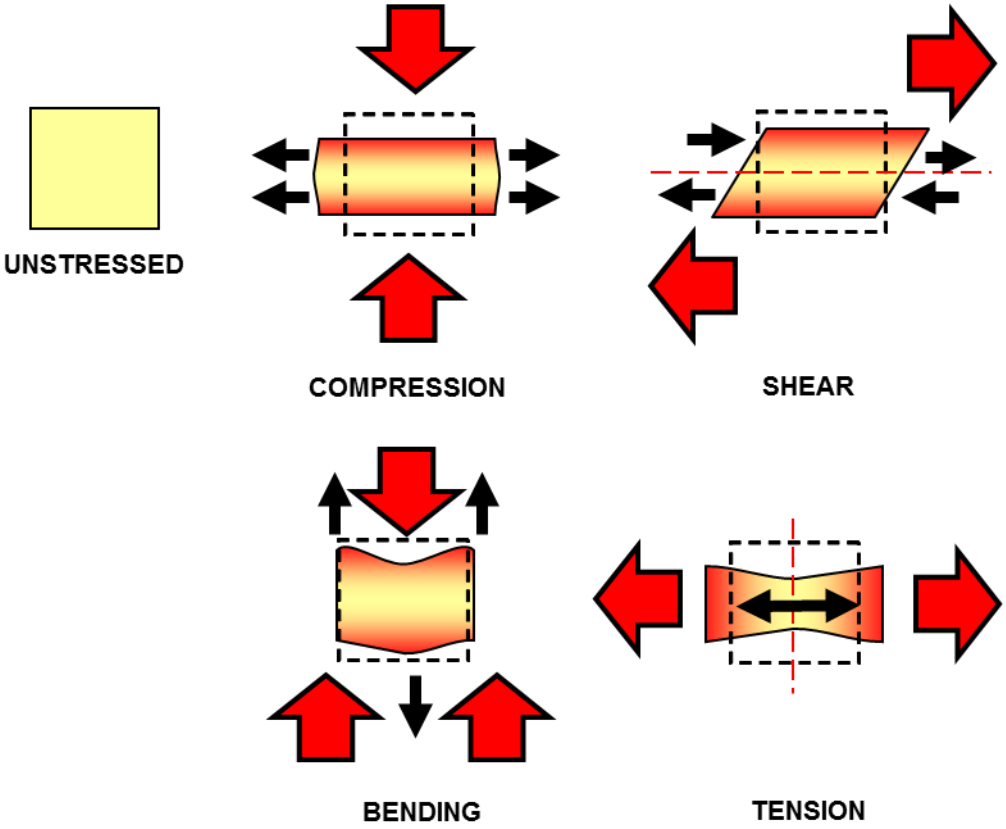

Figure 1-12 Four types of mechanical stresses that can be applied to materials during pharmaceutical unit operations

Direction of applied stress is shown by the red arrows. Black arrows show the direction of the resulting deformation, i.e. the direction of the materials response. The square box shows the shape of the unstressed material

When a change occurs in the materials dimensions as a result of an applied stress then the material is said to be strained. When the external stress is removed the material attempts to recover to its original state. If there is no permanent deformation the material is said to have behaved elastically. However, if the elastic limit has been reached and the material does not return to its original state after removal of the external stress, the material is said to have behaved plastically and this results in a permanent deformation. Materials which can undergo significant permanent or irreversible deformation prior to fracture are termed ductile (Figure 1-13[A]), while materials that fracture immediately are defined as brittle[161-165] (Figure 1-13[B]). As shown in Figure 1-13, when a stress is applied to a solid the material behaves elastically whereby the amount of strain is proportional to the applied stress until an elastic limit is reached. Plastic deformation will occur beyond the elastic limit until the yield point is reached and fracture or lattice collapse occurs releasing the strain in the lattice. For brittle materials the amount of deformation and subsequent fracturing is a function of not only the stress but also the rate at which it is applied.

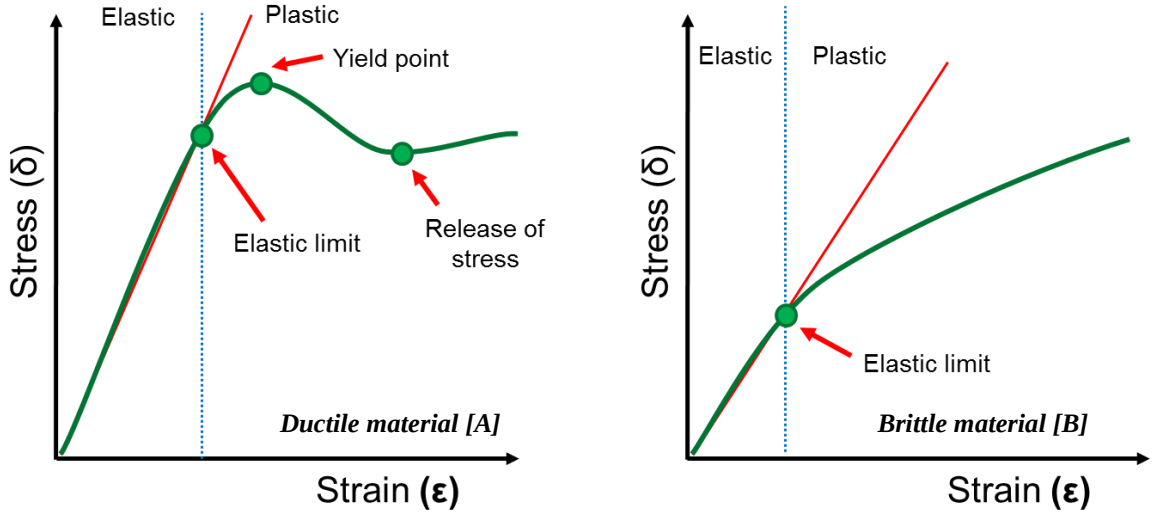

Figure 1-13 Depiction of material deformation profiles for ductile [A] and brittle [B] materials as a consequence of and applied mechanical stress

The amount of plastic deformation in crystals is influenced by: (i) lattice structure, (ii) the types of bonding present and (iii) the type and number of crystal defects present[166]. For example, crystallographic features, such as the existence of slip planes, can greatly facilitate the ability of crystals to deform plastically[121]. Slip planes are molecular planes in the crystal structure that have relatively stronger intra-planar interactions and weaker inter-planar interactions[122]. This can be demonstrated by acetaminophen, which forms H-bonded molecular pleated sheets which are stacked together by van der Waals forces allowing slip planes to exist in which fracture can occur allowing a strain release and plastic deformation[166,167]. Conversely, the absence of slip planes in methyl paraben crystal structure results in significantly poorer tableting performance due to poor plasticity[121]. It was also demonstrated by Shekunov and York (2000)[168] that relatively large molecules and those with a certain degree of rotational flexibility tend to form a disordered state as a result of plastic deformation by mechanical processes.

1.4.2 The mechanical comminution process

Particle size reduction or comminution is often required to enhance the bioavailability of inhaled and non-inhaled pharmaceutical solid dosage formulations through increased dissolution rate or solubility[1-4].

During comminution processes, material is mechanically broken down (ground) into smaller fragments with a consequential increase in surface area to produce particles within a specified particle size range. This process typically involves high energies and stresses such as shearing (attrition and abrasion) and compression depending on the type of comminution process employed. Two types of mechanically comminuted processes

will be utilized in this thesis, vibrational ball-milling (VBM) and jet micronisation or milling (JM) (Table 1-5). VBM involves attrition, abrasion and compression mechanisms using solid grinding balls, while JM involves impact, attrition and some abrasion processes using gas as the comminution media[169]. Both VBM and JM processes are routinely used to reduce particle sizes of materials but the selection of which technique to use is dependent on the final particle size that is required[170]. For example, JM is frequently used in the pharmaceutical industry to obtain particles of respirable size (<10 μm)[21].

Table 1-5 The comminution processes employed in this thesis

Mill type	Size range (μm)	Scale of use	Breakage mechanism(s)	Comminution media
Vibrational ball-milling (VBM)	<100	Laboratory	Attrition Abrasion Compression	Mechanical grinding
Jet micronisation (JM)	<10	Pilot-manufacturing	Impact Attrition Some abrasion	Gas (air)

The two types of shear stresses typically encountered in VBM and JM comminution processes are attrition and abrasion. Attrition refers to a force applied to only part of the particle surface resulting in a small amount of breakage at the edges of the particle and the generation of fine particles and larger rounded particles[171]. This can be analogous to using a chisel on the edge of a stone block. While abrasion is analogous to using sandpaper, as a shear force is applied tangentially to the particle resulting in very fine particles. The original particle is smoother with little change in size or shape[171]. Compressive stresses commonly used in comminution processes do not cause fracturing directly but rather generate distortions by tensile or shear stresses to form a crack tip away from initial point of primary stress application.

During a mechanical comminution process, a mechanical load or force is applied to a particle creating a state of stress, *i.e.* a stress field. Once subjected to the stress the particle will initiate a response relative to the intrinsic properties of the material, the type of comminution process and the strength of the stress field employed. This initially involves absorbing the applied mechanical energy and storing this as a strain energy within the lattice enabling mechanical activation (higher free energy state), defects and dislocations typically on the surface of the crystal lattice[150,9-13,158,162] (Figure 1-14[i]). The lattice will then fracture by plastic deformation thereby relieving the stress (Figure 1-14[ii]). The presence of slip planes, defects and dislocations enable the stress to be concentrated in this vicinity so failure (fracture) can occur at much lower applied

strength. Hence the more defects present, the less stress needed to cause fracturing. This can explain why material becomes progressively difficult to grind as particle size decreases as the probability of the particle containing an effective defect also decreases. Larger particles fracture better as there is more chance that defects exist.

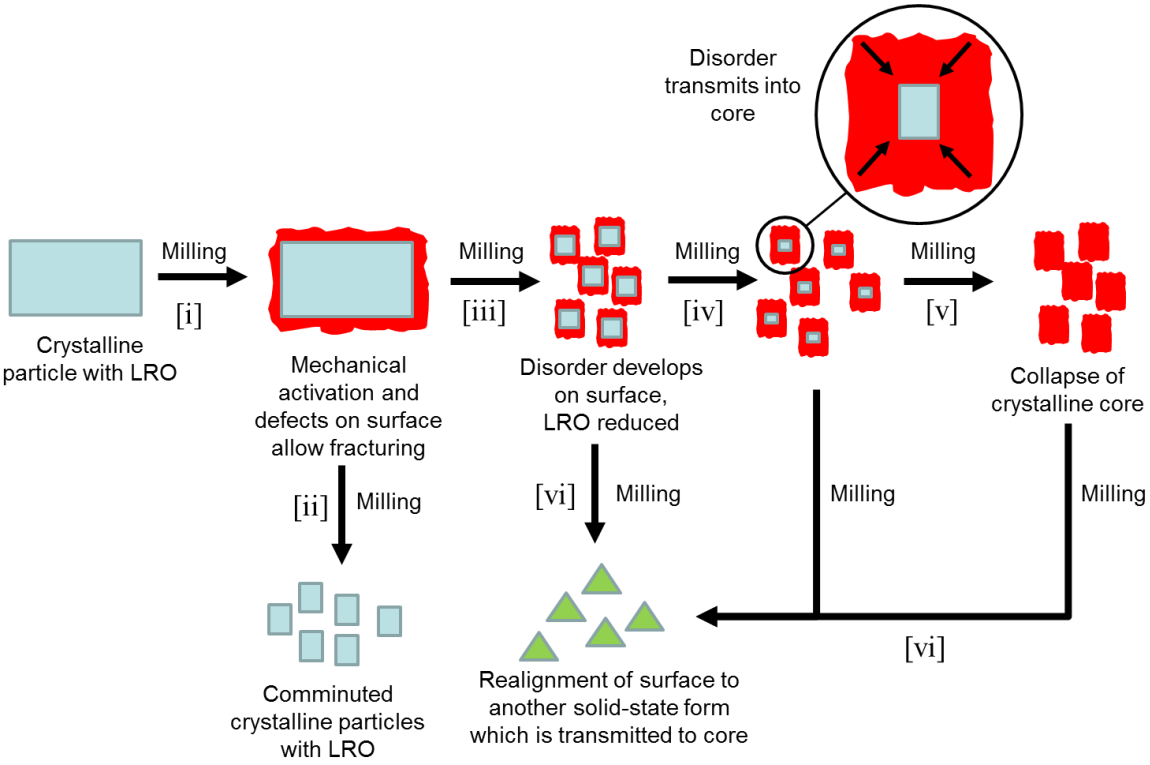

Figure 1-14 Comminution process for the milling of a crystalline particle

Initial milling results in a particle which can fracture into smaller fragments due to the presence of concentrated defects [i &ii]. Extensive milling can result in the formation of surface disorder [iii] which can be transmitted into the crystalline core [iv] and cause complete lattice collapse to an amorphous form [v]. Energy from milling process can also allow for increased molecular mobility and realignment resulting in the transformation into a new solid-state form [vi].

Comminution will continue as long as the stress field is applied. Extensive and prolonged comminution results in the reduction in crystal particle size through fragmentation mechanisms until a minimum particle size limit is reached. However, the majority of applied energy is lost to other processes other than particle breakage such as the production of sound, heat and plastic deformation. Disorder induced by mechanical stress during milling is expected to occur preferentially on the surface regions of particles and decreases moving towards the lattice core[17,23,25-28,150](Figure 1-14[iii]). If the number of defects increases beyond a limit the lattice can collapse completely and an amorphous material can be formed[17,25-28,150,172] (Figure 1-14[iv & v]).

For some materials during the comminution process a transformation to another solid-state form may occur[6,17-28,145-150] (Figure 1-14[vi]). This transformation may be a result of the applied and absorbed milling energy causing increased molecular mobility of the

molecules or surface PID realigning into a more favourable energetic orientation resulting in a new solid-state form.

Comminution is in general a simple operation but the outcomes or product can be complex. This complexity can be material specific and driven by the fundamental molecular or particulate properties of the molecule being milled.

Initial particle size can have an influence on the material properties of the comminuted material. Particle strength increases as particle size decreases therefore the energy to break smaller particles must be larger. Smaller particles will also contain less defects hence will require more energy to cause comminution.

Crystal morphology or habit can also influence the breakage behavior. Non-spherical particles become more spherical as a result of attrition. Corners are knocked off during collisions and particles are exposed to unequal distribution of stress compared to more spherical particles. For example, Chikhalia (2006)[2] investigated the influence of crystal shape on ball-milling and jet milling using different crystal habits of β-succinic acid. It was observed that crystallinity was reduced more when plate morphologies were used as the input material compared to milling needle-like (acicular) crystals. It was also observed that ball-milling caused the greatest decrease in crystallinity.

1.4.3 Vibrational ball-milling

Ball-milling is a high-energy mechanical grinding process that breaks down particles by physical interactions between the particles and the grinding ball and container (Figure 1-15 [A]). The grinding jars perform oscillations at a frequency (*f*) in a horizontal position up to 1800 impacts per minute. The inertia of the grinding balls causes them to impact with high energy on the sample material at the rounded ends of the grinding jars resulting in attrition, abrasion and compression stresses (Figure 1-15 [B]).

Ball-milling can be described as a closed comminution system as the coarse input material and the resulting fines are retained within the grinding jar until the milling process is completed and this can result in over grinding, caking to the side of the grinding jar and ball as well as the potential generation of PID. The caking of comminuted material to the grinding ball is illustrated in (Figure 1-15) and provides a new type of stress particle-particle impact or abrasion and could in fact reduce the efficiency of milling by dampening the effect of the grinding ball.

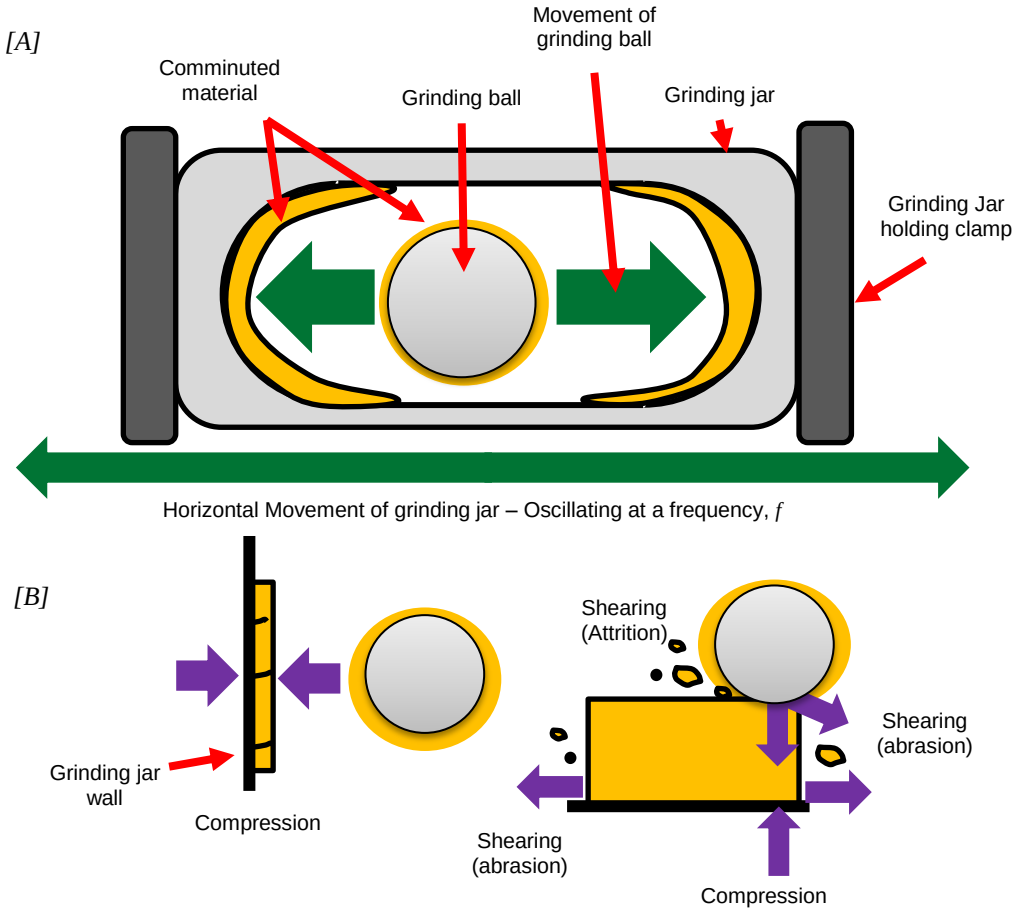

Figure 1-15 Cross-section of a vibrational ball-milling grinding jar [A] and the associated comminution stresses that can occur within it [B]

Purple arrows show the direction of the applied stress

Milling energy is determined by the mass and material density of the grinding balls, whilst milling efficiency depends on the intensity of the applied stress and the number of contacts between the grinding ball, material and jar. In theory, the greater the density and mass of the balls the higher the milling energy (shear stress), while increasing the number of balls increases the number of contact points and therefore increases the shear rate.

It has been noted that ball-milling is more likely to generate surface PID than jet milling but it depends on the processing parameters as well as the properties of the material itself[2]. In the literature there are a number of theories relating to the mechanisms that might be involved in the process of amorphous generation by ball-milling[5,173,174]. One such theory is that localised melting of the material and its subsequent quenching can result in amorphous material[7,175]. However it has been shown that amorphous material can be generated when ball-milling under controlled temperatures using liquid nitrogen (cryomilling), at a temperature far below the glass transition temperature (T_g)[22,26,175-177] and the analytical responses of material obtained by melt-quenching differs to that

generated by ball-milling[5,7,27,177,178]. Therefore it is more likely that the primary mechanism for amorphous generation by ball-milling is by the accumulation of defects and associated loss in lattice structure and LRO[7,179]. It is also likely that the use of cryomilling can increase fracturing as the extreme cold temperature can make the particles more brittle and therefore more susceptible to breaking thus increasing the probability of defect formation and reducing both the energy and time required for effective milling.

1.4.4 Jet-milling (micronisation)

Jet-milling (JM) or micronisation is a high energy mechanical process used to produce a fine powder with a narrow particle size distribution, typically less than 10 μm[4]. A major characteristic of JM is the absence of mechanical parts for particle breakage and the use of a gas as the grinding media which can help to cool or dissipate any generated heat thereby avoiding excessive heat and contamination during its operation[180].

During the operation of a JM, the coarse input particles are fed into the feed funnel at a defined rate (Figure 1-16). These coarse particles are then sucked into the grinding zone due to a pressure gradient or differential between the venturi/feed (P1) and grinding pressure (P2) using pressurised air or nitrogen. P1 must be much higher than P2 to ensure material is not blown back out of the JM. Within the grinding chamber, the grinding gas enters the grinding zone through nozzles in the grinding ring wall and entrains and accelerates the feed particles to sub-sonic velocities in a spiral pattern[180]. Particle breakage occurs when the slower incoming particles and the faster particles in the spiral path collide (inter-particle collisions) and by particle impacts on the grinding ring walls[181]. Particle-particle impaction induces particle fracture via the weakest binding face and also by particle attrition. The fracture mode is the predominating mode when micronisation energy is low. But when micronisation energy is high the attrition mode predominates. It is possible based on the crystal packing that these two modes produce surfaces exhibiting different physical properties such as hydrophobicity and surface energies which could affect the stability and performance of the formulated product.

JM can be defined as an open comminution system as material is removed once it is comminuted to a suitable size. Centrifugal force retains the larger, heavier particles for further grinding while the smaller and lighter comminuted particles exit with the exhaust gas through the central outlet to the collection chamber. Very fine material is collected in a mill bag at the top of the grinding chamber.

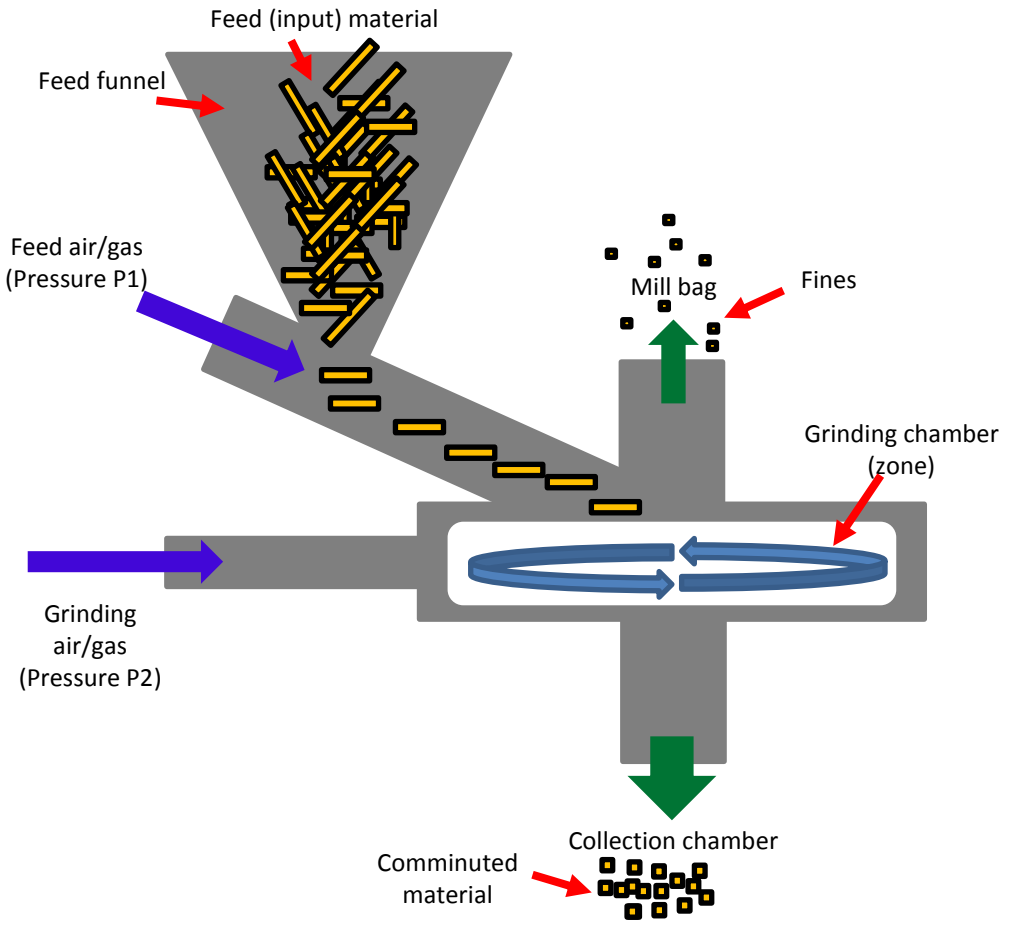

Figure 1-16 Schematic of a jet- mill (microniser)

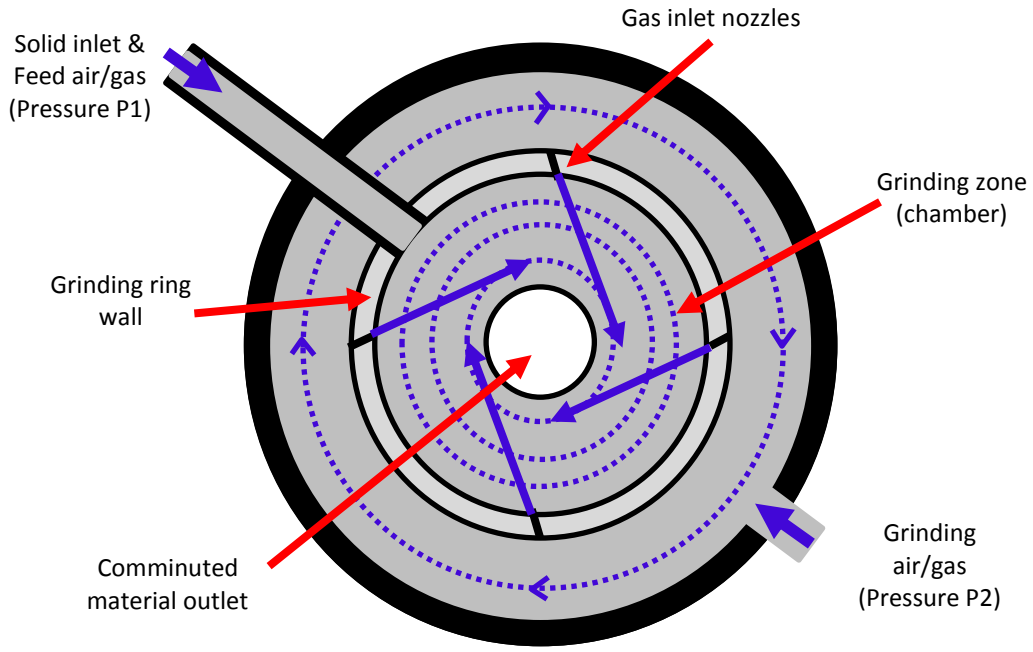

Figure 1-17 Schematic of the inside of a jet-mill grinding chamber (top view)

Blue arrows and dotted lines depict the direction of air/gas flow

The most important operating parameters that control the extent of micronisation are the amount of material to be micronised (feed material) and feed rate, the grinding media (gas) pressure and the differential between the feed and grinding gas pressure[182-184].

Feed pressure controls the acceleration of particles into the grinding chamber but does not promote collisions[182], while feed rate influences the concentration of the material supplied to the grinding zone. The greater the feed rate, the less efficient the micronisation and the larger the comminuted materials as there is less energy per particle meaning particle velocities are slower which leads to less collisions[181-184]. Grinding pressure can influence the amount of amorphisation generated. For example it has been observed that the optimal grind pressure for the micronisation of salbutamol sulphate was 6 bar, below this pressure JM was unable to produce the desired particle size, but above 6 bar amorphous content increased but with no further reduction in particle size[21]. However, the differential between the feed and grinding gas pressure is the main parameter that controls the extent of micronisation. The greater the differential the greater the velocity imparted upon the particles[180].

It is important to note that even though JM is less likely to lead to potential unintentional and unwanted changes to the surfaces of particles such as PID and surface energies compared to other high energy comminution processes such as VBM theses can still occur, so care must be taken to reduce these affects as well as identifying any PID that may be generated as a consequence of the unit operation[2,160,184-189].

1.5 Research objectives

Comminution of pharmaceutical materials can be a challenging process with many potential critical parameters. Knowledge of the molecular structure and mechanical properties of the input material and the potential pre-existing structural flaws could enable the development of more robust pharmaceutical comminution processes and lead to a better understanding of the propensity of materials to undergo process induced disorder. However, once PID has been generated it is of equal importance to be able to identify and potentially quantify the amount of PID that is generated.

Typically the qualitative detection of PID or amorphous domains is performed using individual techniques such as XRPD, DSC and GVS[21,28,88,175,190-193]. However, quantitating the amount of disorder is typically only achieved with the use of calibration curves using mixtures of “pure” amorphous and crystalline standards which can be both problematic and complex to generate[23,24,65,87,194-198].

The primary aim of this thesis was to develop a combined analytical approach to define the level of PID present in pharmaceutically relevant materials as well as their propensities to generate PID as a consequence of mechanical comminution processes such as ball- and jet-milling without the need of "pure" amorphous and crystalline calibration standards and curves.

To achieve this aim, several research objectives needed to be accomplished, these where to;

- Define a small set of pharmaceutical relevant materials using literature and online databases that encompasses the amorphous-crystalline continuum when subjected to mechanical comminution processes, this test set should also possess crystallographic and molecular property diversity (Chapter 2).
- Define a core set of analytical techniques and associated analytical response that can be used to characterise the physical and chemical properties of the model test set before and after comminution (Chapter 3).
- Characterise the comminution input materials using the core analytical techniques and associated responses (Chapter 4).
- Perform mechanical comminution (micronisation and ball-milling) under different operating conditions on the selected materials to potentially generate different levels of PID (Chapter 5).
- Characterise the comminuted materials using the core analytical techniques and associated responses and compare these responses with those of the input materials by a novel Comparative Response Analysis (CRA) approach (Chapter 6).
- Investigate the potential generation and presence of PID in the study materials under different comminution conditions by defining a novel scoring system called Response Disorder Analysis (RDA) that links changes in analytical technique responses with the presence of disorder (Chapter 7).

2 Material selection

2.1 Introduction

Historically, studies that were carried out to investigate the properties of amorphous materials were typically performed using only one or two materials[1,22,44,149,155,175,176,179,199-220]. However, there are some investigations which encompass a much larger model set but often these do not include an explanation as to the rationale for the selection of a particular material and can appear to over process the materials in an attempt to generate "pure" amorphous phases using different processes and/or conditions[160,221]. For example Lin *et al.* (2009)[221] investigated the physical state of 23 compounds after cryogenic milling for up to 5 h and attempted to correlate the presence of disorder with known material properties in order to predict the disordering potential or propensity. Milling times varied between 1-5 h and it was reported that disorder occurred in 15 or 65% of the compounds (Table 2-1).

Table 2-1 Observed disorder in 23 compounds after milling for up to 5 h [Adapted[221]]

Material	Observed disorder after milling for X h					Overall observed disorder Lin *et al.* [221]	Observed disorder (scaled - mill time)
	1 hr	2 hr	3 hr	4 hr	5 hr		
Sucrose	No	No	Yes			Yes	3
Salicylamide	No	No	No	No	No	No	0
Aspirin	No	No	No	No	No	No	0
Acetaminophen	No	No	No	No	No	No	0
γ-Indomethacin	No	No	Yes			Yes	3
Sulfadiazine	No	No	No	No	Yes	Yes	1
β-D-mannitol	No	No	No*			No	3
α-D-lactose-monohydrate	No	No	Yes			Yes	3
D(+)-trehalose dihydrate	No	No	No	Yes		Yes	2
β-D-lactose	No	Yes				Yes	4
D-trehalose	Yes					Yes	5
Theophylline	No	No	No	No	Yes	Yes	1
Tolbutamide I	No	No	No	No	No	No	0
Ibuprofen	No	No	No	No	No	No	0
Cimetidine A	No	No	Yes			Yes	3
Ketoprofen	No	No	Yes			Yes	3
Naproxen	No	No	No	No	No	No	0
β-Piroxicam	Yes					Yes	5
Carbamazepine III	No	No	No	No	Yes	Yes	1
β-Sulfanilamide	No	No	No	No	No	No	0
Sulfathiazole III	No	No	Yes			Yes	3
PFZ1	No	No	Yes			Yes	3
PFZ2	No	No	Yes			Yes	3

** Polymorphic phase transformation observed, this may have indicated the material was disordered. Green cell – Milling continued. Red cell – Milling stopped when disorder observed*

It is important to note that the investigators only used the overall observation of disorder in their correlation models and did not take into account the different milling times. This may skew the data in favour of amorphous materials and lead to misinterpretations with respect to the property-phase relationships. It would have been more appropriate to mill all the materials for the same period of time or maybe include a weighting/scale factor as suggested in the last column of Table 2-1 that takes into account the time required to generate disorder.

Based on the example given and to ensure the accuracy and sensitivity of the generated data, it was decided that the material selection process for this thesis would be based on a defined acceptance criterion that would take into account the materials molecular and crystallographic properties as well as their behaviour upon mechanical comminution. The selected materials would also be subjected to the same mechanical processes and operating conditions (See Chapter 5). This would allow comparisons to be made between the behaviour of materials and correlations to be established between the observed phase(s) and material properties.

To this end a number of objectives were set to: (i) search the literature for pharmaceutical relevant materials *i.e*. small organic molecules typically used as APIs or excipients in pharmaceutical products (See Section 2.2.1), (ii) list the relevant materials in a database and collate the associated crystallographic and molecular properties (See Section 2.2.2), (iii) extract from the literature qualitative assessments for the presence or absence of PID in the materials as a consequence of mechanical comminution (See Section 2.2.2.4), (iv) define the material selection criteria (MSC) (See Section 2.2.3), (v) apply the MSC and use these to define a model set of pharmaceutical relevant materials that might be expected to encompass different levels of PID across the whole of the amorphous-crystalline continuum as well as diversity in their crystallographic and molecular properties.

2.2 Methods and processes

2.2.1 Literature search for pharmaceutically relevant materials

An extensive literature search was performed using the online search engine, EMBASE[222] and the search terms defined in Table 2-2. The results from this search were then exported to the electronic reference manager EndNoteX7 (Thomson Reuters) where the citations were manually reviewed to identify appropriate pharmaceutically relevant materials. These materials were then entered into an Excel© based database called the Research Material Database (RMD) specifically developed for the work reported in this thesis. It is important to note that a material may have multiple entries in the RMD as different solid-state forms can exist and these will possess different crystallographic and other physical properties.

Table 2-2 Search terms employed to identify suitable materials using online search engines.

Search No.	Reason for search	Search terms used in EMBASE
1	To identify only pharmaceutically relevant papers (pharmaceuticals, excipients, solid dosage forms etc)	pharmaceut*.ab. or pharmaceut*.kw. or API.af. or active pharmaceutical ingredient*.af. or excipient.af. or inactive.af. or dosage*.af. or inhalation.af. or inhaled.af. or tablet.af. or solid*.af.
2	Search based on phase and solid- state classes (Amorphous to crystalline, polymorphs and polyamorphs)	((Amorphous or disorder* or crystal* or mesophase or polymorph* or polyamorph*) not inorganic not metal not zinc not copper not Cu not iron not virus not barium not Nickel not silicon not titanium not calcium not selenium not magnesium not carbon not silver not Ag).af.
3	Search based on pharmaceutical unit operations (Crystallisation, comminution , granulation and compression etc)	(micronisation or micronization).af. or mill*.ab. or mill*.kw. or comminut*.af. or mechanical*.af. or granulat*.af. or compression.af. or crystal*.af. or spray.af. or freeze.af.
4	Search based on physical property techniques (X-ray crystallography, differential scanning calorimetry and gravimetric vapour sorption etc)	(crystallography or pxrd or xrpd or diffraction or thermogravimetric or TGA or differential scanning or DSC or microscopy or gravimetric or GVS or sorption or DVS or calorimetry).af.
5	Combining the searches to identify pharmaceutically relevant papers based on phase, pharmaceutical unit operations and analytical techniques	Combine searches 1 to 4 with "and"

Ab – *abstract,* af – *all fields,* kw – *key words*

2.2.2 Material properties from on-line sources

For each material listed in the RMD, molecular and crystallographic properties were obtained and collated along with safety, sourcing and PID information (Table 2-4). This information was acquired from a variety of online databases such as the Cambridge Structural Database (CSD)[223], PubChem[224], NIST Chemistry WebBook[224], Drugbank[225] ChemSpider[226], MSDSxchange[226], SIGMA[227], Fisher[228] MP Biomedical[229] and from the relevant literature citations.

Table 2-3 Collated material properties obtained from the CSD and other online databases/software programs

Property	Description	Property Category	Source
Compound name	Systematic and trivial name	GEN	CSD[223] or PubChem[224]
CAS No	Chemical Abstracts Service registry numbers	GEN	CSD[223] or PubChem[224]
Molecular formula	A moiety formula with stoichiometry (and charges) is given e.g. C8 H9 N1 O2	GEN	PubChem[224]
Solid State form	Hydrate or anhydrate and polymorphic form	GEN	PubChem[224]
CSD ID	Unique Cambridge Structural Database reference code of six letters and potentially 2 numbers that identifies the material crystallographic entry in the CSD. Refer to Section 2.2.2.1	CRYS	CSD[223]
Crystal system	Any crystal must belong to one of seven crystal systems, the symmetry of which introduces constraints on the possible values of the Unit Cell Parameters Refer to Section 1.2.1.1	CRYS	CSD[223] or citation
Space group & Space group number	230 possible arrangements of symmetry elements in the solid state. Refer to Section 1.2.1.1	CRYS	CSD[223] or citation
Unit cell length (*a*, *b* & *c)*	Unit cell vectors that form the edges of a parallelepiped. Refer to Section 1.2.1	CRYS	CSD[223] or citation
Unit cell angle (α, β & γ)	The angles between the vectors (α, the angle between *b* and *c*; β, the angle between *a* and *c*; γ the angle between *a* and *b*) Refer to Section 1.2.1	CRYS	
molecules per unit cell (*Z*)	Number of structural (molecular) units per cell	CRYS	CSD[223] or citation
R factor	A measure of data quality and provides a measure of how well the refined structure agrees with the experimental model. R-factors over 10% may indicate errors with determination of crystal structure. Refer to Section 2.2.2.1	CRYS	CSD[223]
Molar or molecular weight (M_w)	Weight of unit volume of substance, expressed as g/mol	MOLEC	PubChem[224]
Calculated (unit) cell volume (CCV)	Unit cell volume calculated using cell vectors *a*, *b* and *c*, expressed as cm^3. Refer to Section 1.2.1	MOLEC	CSD[223] or citation
Cell Density (ρ_{cell})	Density of the unit cell. See Equation [2-1]	MOLEC	CSD[223] & calculated
Molecular volume (M_v)	Volume occupied by the molecule. See Equation [2-2]	MOLEC	CSD[223] & calculated
Molar Volume (Mr_v)	A volume physically occupied by one mole of substance under normal conditions, expressed as cm^3 See Equation [2-3]	MOLEC	Calculated
Packing coefficient (C)	Efficiency of molecular packing See Equation [1-2] and Section 1.2.1.1	MOLEC	Calculated
Molar refractivity*	Predictor of molar refractivity measuring the total polarizability of a mole of compound, expressed as cm^3	MOLEC	ACD[230,231]
Parachor*	A constant representing the molecular volume of the substance at such temp when its surface tension is equal to unity, expressed as cm^3	MOLEC	ACD[230,231]
Index of refraction*	Ratio of speed of light in vacuum to speed of light in substance. This is an average value for the whole of the molecule and relates to the density of the material	MOLEC	ACD[230,231]
Surface tension*	A value that quantifies the ability of the substance to resist	MOLEC	ACD[230,231]

Property	Description	Property Category	Source
	external forces, expressed as dyne/cm		
Polarizability*	Indicates electron cloud redistribution under the influence of external electric field expressed as cm3	MOLEC	ACD[230,231]
Topological Polar Surface Area*	The surface sum over all polar atoms, primarily oxygen and nitrogen, also including their attached hydrogen atoms	MOLEC	ACD[230,231]
No. rotatable bonds*	Number of rotatable bonds (non-cyclic single bonds between any two atoms having at least two neighbours each This provides an estimate for the flexibility of the molecule	MOLEC	ACD[230,231]
H-bond acceptors*	Number of hydrogen bond acceptors in structure, e.g. the number of O and N atoms Refer to Section 1.2.2	MOLEC	SpresiWeb[232], PubChem[224], ACD[230,231] & MarvinView[233]
H-bond donors*	Number of hydrogen bond donors in structure, e.g. H atoms directly connected to O and N atoms Refer to Section 1.2.2	MOLEC	SpresiWeb[232], PubChem[224], ACD[230,231] & MarvinView[233]
LogP*	Octanol-water partition co-efficient Refer to Section 2.2.2.2	PART	ACD[230,231]
Solubility*	Prediction of solubility in pure water, expressed as mg/ml Refer to Section 2.2.2.2	PART	ACD[230,231]
Melting temperature	The temperature at which the material melts. Note: this is NOT necessarily taken from DSC analysis	PART	CSD[223], NIST[224] or citation
Risk statement codes[234]	Safety risk statement code describing the risks involved in using and handling the material. Refer to Section 2.2.2.3	LGST	MSDSxchange[226], Suppliers or SIRI MSDS Index[235]
Sourcing and cost per gram (cpg) (£/g)	Information with respect to how easy the material is to procure and the cost per gram. Refer to Section 2.2.2.3	LGST	SIGMA[227], Fisher[228], MP Biomedical[229]
Literature PID	Qualitative observation of presence or absence of PID as a result of a mechanical comminution process Refer to Section 2.2.2.4	PID	Citations

* *Predicted values calculated using appropriate online software*
GEN – *general property or information,* CRYS – *crystallographic/unit cell properties,* MOLEC – *molecular properties,* PART – *particle properties,* LGST – *logistic or safety information,* PID –*designation of presence of PID from literature citations*

2.2.2.1 *Material crystallographic properties from the CSD*

Crystallographic properties for each material was in general sourced through the CSD database[223]. However, for some materials this information is either not available or not publicly accessible for commercial reasons. In these cases the crystallographic properties were left blank in the RMD.

For those materials that are listed in the CSD, each entry corresponds to an individual determination of a specific crystal structure identified by a unique CSD reference code (refcode), comprising of six alphabetic characters[236] (e.g. HXACAN). Where multiple entries for the same material exists an additional two-digit number is attached to identify a specific experimental determination of the crystal structure or different authors etc (*e.g.* HXACAN06, HXACAN09, etc.)[237]. These entries represent

polymorphs, redeterminations or republications[236]. A redetermination is an entry for a known crystal structure from a different set of experimental data and usually submitted by different authors. A republication is an entry for a compound with the same determination (parameters) without any additional crystallographic experimental data. These typically have lower R-factor values[236]. The R-factor value is a measure of the crystallographic data quality and provides a measure of how well the refined structure agrees with the experimental mode, *i.e.* the R-factor is an indicator of accuracy, the lower the R-factor, the more accurate the determined structure[237,238]. R-factors below 5% indicate a high quality structure determination, while those over 10% may indicate errors in the determination of the crystal structure or the presence of a number of lattice defects[238].

One of the major obstacles in using the CSD database was the difficulty in choosing the most appropriate CSD entry for a particular material. If the material exists in more than one crystal system then a representative from each crystal system was included in the RMD. If there was more than one entry for a given system, then the entry with the lowest reported R-factor value which also had an available X-ray diffraction pattern was included[236,239]. For example, there are over ten entries for acetaminophen in the CSD but there are only two polymorphic forms. On reviewing the entries only two entries were selected one for each crystal system (or polymorph) based on the smallest R-factor value and the availability of the X-ray diffraction patterns[236,239]. Accordingly, HXACAN11 was selected to represent monoclinic Form I, and HXACAN08 was selected to represent orthorhombic Form II acetaminophen.

Cell density (ρ_{cell}) is given by:

$$\rho_{cell} = \frac{1.66 \text{ x } M_w \text{ x } Z}{CCV} \qquad [2\text{-}1]$$

Where M_w is Molar or molecular weight, Z is the number of structural (molecular) units per cell and CCV is Calculated (unit) cell volume.

Molecular volume (M_v) is given by:

$$M_v = \frac{CCV}{Z} \qquad [2\text{-}2]$$

Where Z is the number of structural (molecular) units per cell and CCV is Calculated (unit) cell volume.

Molar volume (Mr_v) is given by:

$$Mr_V = \frac{M_w}{\rho_{cell}} \quad [2\text{-}3]$$

2.2.2.2 *Determination of predicted properties*

A number of predicted properties were obtained from online databases and software programs as indicated with an asterix (*) in Table 2-3. These predicted properties represent molecular descriptors that can be used as qualitative indicators of the material's physicochemical properties such as solubility, molecular flexibility and H-bonding capacity[240].

However, a number of different databases and software programs list or predict the same properties and these values may vary depending on the way they are calculated or predicted. For example, the potential number of H-bond acceptors and donors (HBDA) can be predicted using four different software programs: (i) from SpresiWeb[232] which uses the Chemical Computing Group Inc.'s Molecular Operating Environment (MOE) (version 2004.3) program, (ii) from PubChem[224] which uses Xemistry GmbH's Cactvs program[241], (iii) from ChemSpider[226] which uses the built-in ACD/Labs property predictor software[230,231] and (iv) ChemAxon's Marvin (version 5.4.0.1) program[233]. The HBDA values can vary between the programs for the same material; hence it is important that when listing these types of properties that the source is clearly identified and the prediction algorithm is known.

In this thesis the HBDA values used during the selection process were calculated using the Marvin software whereby sulphur atoms where excluded from acceptors but halogens were included. A more detailed discussion regarding the differences in HBDA values from different software programs can be found in the results and discussion (section 2.3.2).

Other predicted properties such as LogP and solubility were calculated using the ACD/Labs property predictor software[230,231]. The LogP value is a measure of the lipophilicity of a material. The higher the LogP value, then the more hydrophobic a material is and the greater the likelihood that these materials will have low water solubilities (especially when values are 4 or greater). Solubility is defined as the concentration of dissolved solid (solute) in a solvent medium which becomes a saturated solution and is in equilibrium with the solid at a defined temperature and pressure.

2.2.2.3 *Determination of material safety, processing hazards and sources*

For each material, safety (risk statement code[234], See Appendix 1) and handling information were obtained from online sources such as MSDSxchange[226], SIRI MSDS Index[235] and directly from potential suppliers (Sigma-Aldrich[227], MP Biomedical[229] and Fisher-scientific). The cost per gram (cpg) in British Sterling was also reported for each material to assist with the logistics of the investigation.

2.2.2.4 *Determination of the presence of mechanical PID from literature*

A qualitative assessment of the presence or absence of PID in the materials as a consequence of mechanical size reduction processes such as milling and micronisation was determined using information from the literature. The presence of disorder in the literature was predominately based on an observed "amorphous halo" and/or a glass transition event by X-ray powder diffraction (XRPD) and differential scanning calorimetry (DSC) analyses respectively[6,7,23,160,221,242-247]. More information regarding these techniques and associated responses can be found in Chapter 3 (See 3.2 and 3.4 respectively).

When reviewing the literature information, it is important to note that the materials can be mechanically processed differently, therefore they are exposed to differing levels of mechanical loading or stresses (See Section 1.4.2) and this in turn may or may not result in the generation of PID. For some materials, milling may only have been carried out for 2 min, whereas for others this might have occurred over 30 h depending on the objective of the study[5-7,160,195,221,242,248]. This makes it challenging when attempting to qualitatively define the presence or absence of disorder for different materials from different studies as each investigator may interpret the degree of disorder that maybe present differently. However, for the purposes of this screening exercise the observed literature PID data serve as a reasonable assessment that disorder might exist in the compound and therefore can aid material selection so that a more in-depth investigation can be performed under different processing conditions (Chapter 5). To this end, materials were qualitatively classified as being either disordered (DIS), remaining unchanged (CRYS), or exhibiting some degree of disorder after processing (SOME). Materials which exhibited some degree of disorder were those where it was not a 100% certain that disorder was present or the literature was ambiguous, *i.e.* in some cases disorder was reported being present and in other studies it was not. For materials where no comminution information was available, these were classified as unknown (UKWN).

2.2.3 Material selection process

Initial material selection was made using the material selection criteria (MSC) as defined in Table 2-4. Justifications for the criteria values are given below :

Table 2-4 Material selection criteria (MSC)

ID	Property	Acceptance Criteria
A1	Anhydrous	Only anhydrous material and where possible the parent molecule
A2	Crystallographic properties	Only materials with known and measured crystallographic properties
A3	Safety & handling	Only materials with a low safety risk
A4	Source & cost	Only materials that can be easily sourced commercially and cpg <£15
A5	Melting onset temperature (T_m)	> 80 °C
A6	Storage conditions	Room Temperature (ambient) in light or away from light
A7	Solubility*	Less than 50 mg/mL
A8	LogP*	Greater than 0
A9	No. of rotatable bonds*	Less than 10
A10	Literature PID	Only observed PID (complete or some) or no PID observed will be selected if PID by mechanical processes unknown for the material then they are excluded

* *Predicted property*

Only anhydrous materials were selected to reduce the complexity that hydrates may introduce when milled or micronised, *i.e*. the presence of hydrated water may act as a plasticizer lowering the T_g allowing recrystallisation to occur more easily, thereby effectively removing any induced disorder before it could analytically be observed[65,85,249-252] (A1 Table 2-4). Where appropriate only the parent molecule of the material was chosen to minimise any complications due to the presence of the counter ion. A counter ion is often used to overcome the crystallisation problems which maybe encountered during crystallisation and to improve overall solubility[253]. However, in this research the presence of counter ions could increase the stability of the crystal lattice and restrict the susceptibility for PID during mechanical processing, so where possible only the parent molecule was selected. For example, the salt forms of γ-indomethacin show an increase in T_g compared to the parent molecule, hence they are potentially thermally more stable[253].

It was also important that crystallographic properties of the materials were included to investigate any relationship with PID. Hence materials which had no crystallographic properties reported were excluded (A2 Table 2-4).

Due to the quantity (grams) of the material required to be mechanically comminuted in this research, it was deemed appropriate to mitigate the operational risk by excluding those materials with very high toxicity, high inhalation danger, and those with risk statement codes[234] as shown in red in Appendix 1 (A3 Table 2-4). Due to logistical and

time constraints materials which could not be sourced commercially or with a cpg greater than £15 were excluded (A4 Table 2-4). For example only the acetaminophen form 1 is commercially available and form 2 would need to be prepared in-house which would require additional resource (time) to develop and validate an appropriate method, as well as characterise the generated solid.

Materials with a melting temperature (T_m) less than 80 °C were excluded from selection due to the fact that a lower T_m will likely mean a lower T_g and the presence of any absorbed water will potentially lower the T_g further allowing recrystallisation to occur[65,85,249-252](A5 Table 2-7). It has been suggested that for every 1% w/w water present the T_g can be lowered by approximately 10 °C as was shown for amorphous indomethacin[254]. It has also been noted that mechanically processes such as ball-milling can result in localised heating which can cause material melting[137,160,192,221]. Since it was planned to employ ball-milling at low and high frequencies in this research to potentially produce PID, only materials with a melting temperature greater than 80 °C were retained (A5 Table 2-4). The 80 °C limit was selected as experimental temperatures within ball-milling grinding jars have been shown to be in excess of +45 °C when used under non-cryogenic conditions[255]. Though these temperatures represent bulk average values it is expected that at "localised hot spots" the temperatures could be much higher[255].

To reduce the influence of external environmental parameters and ensure all the materials were handled identically only materials which were stable under ambient conditions were included for selection (A6 Table 2-4).

Typically a large number of compounds selected for product development have poor solubilities, poor permeabilities, or both and therefore require particle size reduction to enhance their bioavailability through increased dissolution rates or solubilities[234;235]. Hence, materials which are unlikely to need size reducing because of good oral bioavailability were excluded from selection. Solubility (A7 Table 2-4), LogP (A8 Table 2-4), and the number of rotatable bonds (A9 Table 2-4) have been shown to be very good descriptors of oral bioavailability[256]. LogP values are a measure of the lipophilicity of a compound and the higher the value) the more hydrophobic-like the material and the greater the likelihood that the material exhibits poor water solubility. While the number of rotatable bonds is a measure of molecular flexibility and have also been shown to be good descriptor s of oral bioavailability[256,257].

To ensure that the final materials selected covered the full range of the amorphous-crystalline continuum as a consequence of mechanical processing materials were classified based on literature observations for PID post mechanical processing (See Section 2.2.2.4). Materials where no milling PID information was reported were excluded (A10 Table 2-4).

Using the MSC, a pool of potentially acceptable materials was obtained. The final selection of materials was made from this pool with the aid of a principle component analysis model (PCA) to ensure that the final materials selected exhibited molecular and crystallographic diversity (See Section 2.2.3.1). The number of materials in this final test set was limited to ten, based on observed PID behaviour and for logistical reasons. These comprised of four materials which will represent materials that maybe resistant to PID, three materials that may exhibit some PID and three materials where PID may likely to be observed as a consequence of mechanical comminution.

2.2.3.1 *Principle Component Analysis (PCA) for final material selection*

Multivariate techniques such as PCA can handle a large number of variables simultaneously and can provide a powerful means to elucidate complex multivariate relationships between properties and process parameters[258].

In a PCA model, the original dimensions of the data set consisting of a matrix of X variables are transformed into another coordinate system through projection. The new coordinate axes are called principal components. The first principal component covers as much of the variation in the data set as possible. The second principal component is orthogonal to the first and covers as much of the remaining variation as possible and so on[259]. Further information about the principles of PCA and its applications can be found in a number of good reviews and books such as that by Esbensen *et al.* (2009) [260], Wold *et al*. (1987)[261] and others[259].

For the materials that passed the MSC, the molecular and crystallographic properties as defined in Table 2-5 were used as the *x* variables to generate a PCA model using the SIMCA-P+ software, version 11.0.0.0 (Umetrics AB, Umea, Sweden). The SIMCA-P+ software automatically scales the data using centering and unit variance (UV) to ensure correct and equal weighting of the *x* variables. The PCA model is displayed graphically as a Bi-plot which displays loadings scaled as correlation and the scores scaled inside the correlation circle.

Table 2-5 X variables used to generate a PCA model to aid in material selection

Property	Xvar ID	Source
Compound name/ID	CMPD	PubChem[224]
Molar weight (M_w)	Mw	PubChem[224]
Calculated (unit) cell volume (CCV)	CCV	CSD[223]
Z	Z	CSD[223]
Cell Density	CD	CSD[223]
Molecular volume	Mv	CSD[223]
Molar Volume	Mrv	calculated
Molar refractivity*	MrR	ACD[230,231]
Parachor*	Par	ACD[230,231]
Index of refraction*	RI	ACD[230,231]
Surface tension*	ST	ACD[230,231]
Polarizability*	Pz	ACD[230,231]
Topological Polar Surface Area*	TPSA	ACD[230,231]
No. rotatable bonds*	RB	ACD[230,231]
LogP*	LogP	ACD[230,231]
Solubility*	Sol	ACD[230,231]
H-bond acceptors*	HA	MarvinView[233]
H-bond donors*	HD	MarvinView[233]
Melting temperature	Tm	CSD[223], NIST[224] or citation

** Predicted property*

2.3 Results and discussions

2.3.1 Literature search for pharmaceutically relevant materials

During the literature search a large number of papers (4000+) were identified using the search terms as defined in Table 2-2. The citations from this search were then exported to create a reference library and 356 pharmaceutically relevant materials (including polymorphs) were identified and entered into the novel Research Material Database (RMD). These materials were used to create a pool from which the investigational materials could be drawn from. This database was not intended to be exhaustive but rather provide a more analytical and logical approach to the selection process. In general the materials listed in the RMD have been well investigated over the last two decades and therefore, any property data and information should be fairly accessible.

2.3.2 Material properties

The molecular and crystallographic properties as defined in Table 2-3 were collated for the RMD materials using information from a variety of online databases. During the search for these properties it was noted that no single database contained all the property data for a particular material and it appeared that for some properties different values can be observed depending on the database and prediction algorithm/program used. As a result there is the potential for ambiguity to occur and highlights an issue over using

calculated properties from different databases. This can be illustrated using HBDA values predicted using different software programs (Table 2-6).

Table 2-6 Software used to predict HBDA values

Database/supplier	Prediction software
PubChem[224]	Xemistry GmbH's Cactvs program
SpresiWeb [232]	MOE v2004.3
ChemSpider[226]	ACD/Labs property predictor [230,231]
ChemAxon[233]	Marvin v5.4.0.1

HBDA values provide an estimate of the degree of H-bonding that may occur within a molecule based upon the availability of H-bond acceptors and donors within the chemical structure. For each material in the RMD, the potential number of H-bond acceptors and donors were reported from three databases (SpresiWeb[232], PubChem[224] and ChemSpider[226]) and calculated using ChemAxon's Marvin view software[233]. Each source appeared to apply different rules to assign the number of H-bond donors and acceptors.

In PubChem[224] the number of H-bond donors and acceptors were calculated using the Xemistry GmbH's Cactvs implementation and classification by Wang *et al.* (1997)[262], *i.e.* the hydrogen donor can be a heteroatom attached to one or two hydrogens. While the hydrogen acceptor, can be any sp^2-hybridized oxygen, fluorine, or hydrogen donor atom.

The H-bond donors reported for materials using the SpresiWeb interface[232] (MOE software) appeared to be incorrect on a number of occasions. For example adipic acid was reported to have four H-bond donors, but the chemical structure only shows two potential donors (Figure 2-1).

The ACD/Labs property predictor software on the ChemSpider[226] website counts the number of N, F and O atoms in the structure and uses these values for the H-bond acceptor count. For example loperamide HCl, indomethacin, caffeine and adipic acid appear to have 4, 5, 6 and 4 H-bond acceptors respectively (Figure 2-1). In contrast both the Marvin and CACTVS programs apply a more detailed set of rules in assigning the H-bond acceptor count, based on the structural motifs of the N and O atoms and their connectivity to other atoms. Only the –N= and =O atoms are counted as H-bond acceptors for caffeine (Figure 2-1).

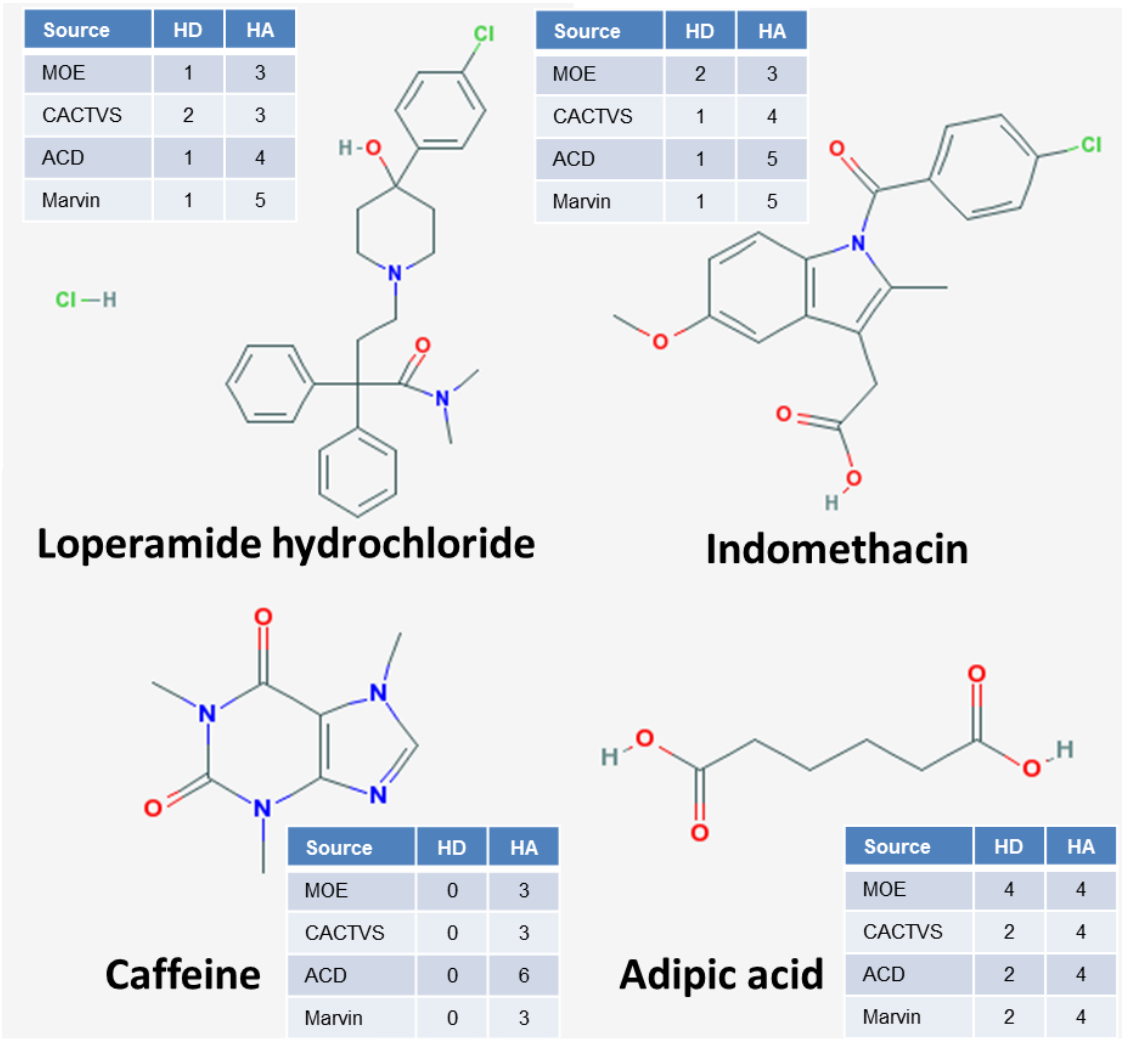

Figure 2-1 HBDA analysis for loperamide HCl, indomethacin, caffeine and adipic acid

HD: Hydrogen bond donors, HA: Hydrogen bond acceptors
MOE: Molecular Operating Environment (version 2004.3) used in SpresiWeb[232]
CACTVS: from Xemistry GmbH[241] *used in PubChem*[224]*, ACD/Labs: property predictor software used in ChemSpider* [226]*, Marvin: From ChemAxon (version 5.4.0.1)*

Of all the programs investigated only the Marvin software included the halogen atoms, and took into account the counter ions such as the chloride ion for loperamide HCl (Figure 2-1). It is important to include any counter ions in the HBDA values as the presence of ions strongly influences the molecular stabilities and physicochemical properties of the crystals such as the solubilities, dissolution rates and hygroscopicity of the materials.

The Marvin software appeared to be the most consistent when assigning both H-bond donors and acceptors, hence it was selected as the program of choice for predicting HBDA values for the individual materials listed in the RMD.

2.3.3 Material selection

Using the material selection criterion (MSC) as defined in Table 2-4 as an initial screen, the number of materials from the RMD pool of 356 was significantly reduced to only 14 (Table 2-7). The MSC includes not only information regarding safety, handling and potential processing considerations but also limits for some of the predicted properties which are good descriptors of the material's potential conformational flexibility and solubility[263].

Table 2-7 The number of materials included/excluded from the RMD with respect to acceptance criteria properties

MSC ID	Property	Number RMD materials included	Number of RMD excluded	% retained from RMD
A1	Anhydrate	303	53	85
A2	Crystallographic properties	170	133	48
A3	Safety & handling	126	44	35
A4	Source & cost	47	79	13
A5	Melting onset temperature	38	9	11
A6	Storage conditions	33	5	9
A7	Solubility*	24	9	7
A8	LogP*	22	2	6
A9	No. Rotatable bonds*	21	1	6
A10	Observed PID from literature	14	7	4

** Predicted properties. MSC ID – material selection criterion property ID from Table 2-4*

The molecular and crystallographic property data for these 14 materials were then used to construct a principle component analysis (PCA) model to discriminate the materials further and aid in the final material selection. The PCA model data can be found in APPENDIX 2.

The PCA model generated could explain 81.5% of the variation in the *x* variables (loadings) in the first three principal components. Using PCA, the values for each of the *x* variables (loadings) for a material are reduced to a single value (score) and relationships (correlations) between loadings and scores can be visualised using a loadings bi-plot where loadings are expressed as correlation coefficients and the scores (observations) (Figure 2-2). Observations (materials) situated near variables are high in these variables and are low in variables situated opposite. For example, in Figure 2-2 caffeine (C88) is in close proximity to the loading Z, the number of structural (molecular) units per cell, hence caffeine is said to be highly correlated to Z and will have a higher Z value (20) than say indomethacin (C11) which is located further away with a Z value of 2.

The bi-plot also allows the easier identifications of groupings between materials. The literature observations for PID were not included in the PCA model but it can be seen that the materials can be easily identified and grouped based on these observations: (i) no PID, (ii) some PID and (iii) observed PID (Figure 2-2).

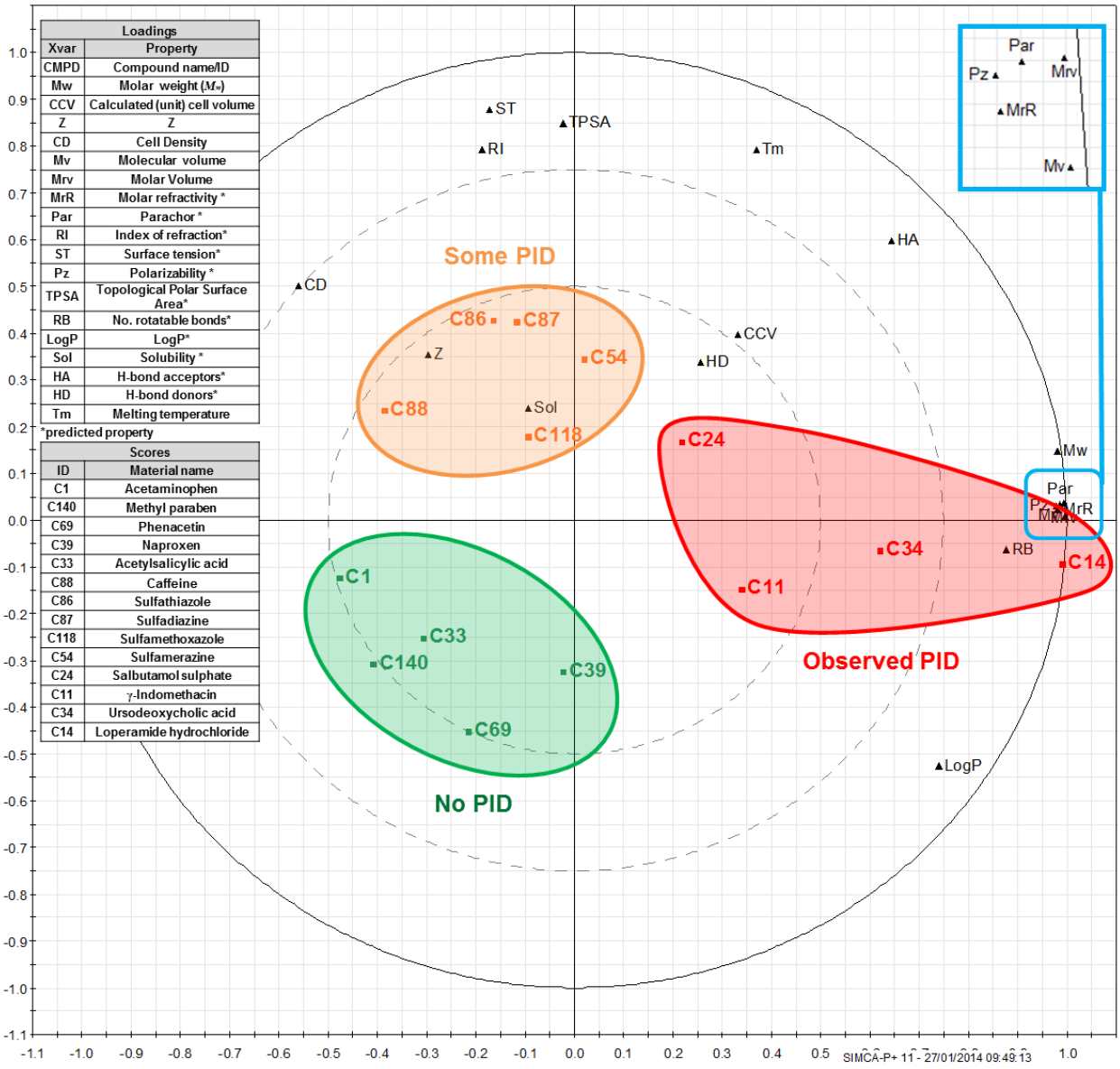

Figure 2-2 Loadings bi-plot for the PCA model for the molecular and crystallographic properties of the screened RMD materials

Colours correlate with the literature PID observations; green (no PID), orange (some PID) and red (observed PID).

From Figure 2-2, it can be seen that in general materials which have higher LogP, Mw, molar and molecular volume, molar refractivity, parachor, polarizability and number of rotatable bonds are more likely to be completely disordered as a consequence of a milling process. This is in line with other observations by other investigators[160,221,264]. Conversely, materials with lower M_w, LogP and number of rotatable bonds etc. will be less likely to have PID as a consequence of milling. It must be noted that these

inferences were made based on the data from only 14 materials and should not be used as a general conclusions for all materials. However, the PCA model reported here was suitable for its intended purpose to discriminate the materials based on observed literature PID so that a final selection of materials for further investigation could be made.

The final selection of 10 materials within the groups was arbitrarily chosen but materials were selected to ensure a good representation of PID behaviour across the amorphous-crystalline continuum. Four out of five materials that did not exhibit any PID were selected: acetaminophen, methyl paraben, acetylsalicylic acid and phenacetin. Three out of five materials possessing some degree of PID were selected: caffeine, sulfadiazine and sulfamerazine, and finally three out of four materials that were mainly disordered were chosen: salbutamol sulphate, γ-Indomethacin and loperamide hydrochloride (Table 2-8).

Table 2-8 Final material selection based on observed PID and PCA model

ID	Material	PCA group	Literature observed PID	Final selection
C1	Acetaminophen	1 (No PID)	No[160,221]	Included
C140	Methyl paraben	1 (No PID)	No[255]	Included
C69	Phenacetin	1 (No PID)	No[265]	Included
C33	Acetylsalicylic acid	1 (No PID)	No[160,221,266,267]	Included
C39	Naproxen	1 (No PID)	No[268]	Excluded
C88	Caffeine	2 (Some PID)	Some[217,269]	Included
C87	Sulfadiazine	2 (Some PID)	Some[221,270]	Included
C54	Sulfamerazine	2 (Some PID)	Some[270,271]	Included
C86	Sulfathiazole	2 (Some PID)	Some[221]	Excluded
C118	Sulfamethoxazole	2 (Some PID)	Some [272-274]	Excluded
C24	Salbutamol sulphate	3 (Yes PID)	Yes[1,20,21,246,247,275-277]	Included
C11	γ-Indomethacin	3 (Yes PID)	Yes [148,160,178,212,221,268,271]	Included
C14	Loperamide hydrochloride	3 (Yes PID)	Yes[278]	Included
C34	Ursodeoxycholic acid	3 (Yes PID)	Yes[279]	Excluded

Following material selection, the materials were purchased and stored under controlled conditions according to the supplier's recommendations, *i.e.* at room temperature and protected from light in a desiccator containing phosphorus pentoxide (P_2O_5). All materials were of pharmaceutical quality and high purity (> 98%) (See APPENDIX 3 for more material information).

2.4 Conclusions

The reasons for a particular material exhibiting or not exhibiting PID are poorly understood and moreover quite often even the nature of the disorder can been misinterpreted[137]. When searching for information regarding a material's PID classification, it was observed that often these materials are over processed and milled under different conditions. This makes it difficult to compare the propensities for PID between materials and further correlate PID with material properties. A PCA approach proved to be very valuable in extracting some correlations between PID and material properties, but it did not take into account the impact of different processing methods such as ball- or jet-milling, control of temperature and length of milling. Hence a more detailed laboratory investigation is warranted where these operating variables can be controlled and applied to all the materials allowing a better comparative investigation, which has not been explored adequately in the literature before.

The systematic selection process as described in this chapter was employed to select ten materials that exhibited sufficient diversity in their structural and molecular properties as well as in their literature PID observations (Table 2-9) to serve as an appropriate cohort of compounds for further in-depth study involving mechanical comminution by ball- and jet-milling under different conditions.

Table 2-9 Structural, molecular and PID diversity within the final 10 selected materials

Property	Range
Literature PID	3 levels
Space groups (SPG)	7 groups
Number of structural (molecular) units per cell (Z)	2 - 20
Calculated (unit) cell volume (CCV) cm^3	604 - 4352
Cell Density (CD)	1.2 - 1.6
Molecular volume (*Mv*) cm^3	163 - 657
Molar Volume (Mr_v) cm^3	98 - 396
Molar or molecular weight (M_w) g/mol	151 - 513
LogP	0 - 5.6
Solubility * (Sol) mg/mL	0 - 33

Property	Range
Number of rotatable bonds* (RB)	0 - 7
H-bond acceptors* (HA)	2 - 6
H-bond donors* (HD)	0 - 5
Melting temperature (T_m) °C	127 - 251
Molar refractivity * (MrR) cm^3	40 - 138
Parachor * (Par) cm^3	326 - 1067
Index of refraction* (RI)	1.5 - 1.7
Surface tension* (ST) dyne/cm	39 - 83
Polarizability * (Pz) cm^3	1.6 - 5.5 ($x10^{-23}$)
Topological Polar Surface Area* (TPSA) $Å^2$	38 - 122

* *predicted property*

3 General physical characterisation methods: Core test set

3.1 Introduction

There is no single test which is capable of assessing all the physical properties of a material. It is for this reason that a number of different techniques are required to measure, monitor and characterise the different properties of the material being examined. The techniques described in this chapter represent a core test set (Table 3-1) which will be utilised in this research for the characterisation of a number of important molecular, particulate and bulk properties of the selected study materials before and after mechanical comminution.

For each technique a brief description is provided of the relevance of the technique in characterising a specific property or properties of the material, along with the associated acquisition method (AM). A description of the relevant analytical responses and how these responses are analysed (response analysis method or RA) is then provided.

Table 3-1 Techniques used for the general characterisation of the study materials (core test set)

Material Property	Technique	Refer to section
Phase detection & identification	X-ray powder diffraction (XRPD)	3.2
	Polarised light microscopy (PLM)	3.5
	Gravimetric vapour sorption (GVS)	3.7
	Differential scanning calorimetry (DSC)	3.4
Chemical structure & H-Bonding	Fourier transform infra-red spectroscopy (FTIR)	3.9
Moisture sorption	Thermogravimetric analysis (TGA)	3.3
	Gravimetric vapour sorption (GVS)	3.7
	Fourier transform infra-red spectroscopy (FTIR)	3.9
Thermal	Differential scanning calorimetry (DSC)	3.4
	Thermogravimetric analysis (TGA)	3.3
Particle shape	Polarised light microscopy (PLM)	3.5
	Scanning electron microscopy (SEM)	3.5
Particle size	Laser light particle size (PSA)	3.6
	Polarised light microscopy (PLM)	3.5
	Scanning electron microscopy (SEM)	3.5
Purity (solid state form & chemical)	Differential scanning calorimetry (DSC)	3.4
	X-ray powder diffraction (XRPD)	3.2
	High pressure liquid chromatography (HPLC)	3.8
	Fourier transform infra-red spectroscopy (FTIR)	3.9

3.2 X-ray powder diffraction (XRPD)

XRPD is a key analytical technique used primarily in the solid state characterisation of crystalline materials[29,93,280,281]. For a given X-ray wavelength, the positions of the diffraction peaks (reflection) are characteristic of the crystal lattice (d-spacing) and intensities are dependent on the crystallographic unit cell content (nature and position of atoms). In this way the XRPD pattern provides a "fingerprint" of the solid state crystalline form present in the solid state bulk of the material and is a representative of the average structure[29,93,280,282,283]. Disordered and amorphous materials however, scatter the incident x-rays in all directions giving rise to a featureless "halo". However, the detection and quantification of partially amorphous materials can be limited by the presence of the much stronger crystalline diffracting peaks which may obscure this characteristic "halo"[29,93,280].

It is important to be aware of the manner in which the physical characteristics of organic pharmaceuticals can influence XRPD responses such as the peak intensity (height), broadening and the overall interpretation of the diffractogram. Typically organic samples have a low X-ray absorption allowing deeper X-ray penetration resulting in greater peak broadening compared to inorganic compounds and metals. The common crystal habits of columnar, acicular particles and plates can also create a texture, which is a non-random or preferred orientation of the particles that alters the XRPD patterns and associated responses making it difficult to identify and quantify solid state phases[29,280].

The particle size of materials can also contribute to misinterpretation of the resultant diffractogram. Materials with particle sizes below 1 μm may exhibit peak broadening and a reduction in peak intensity which could be misinterpreted as disorder[150,284]. Larger particle sizes can influence the crystallographic responses by introducing a preferred orientation effect and could give rise to some sharper and higher intensity diffraction peaks, while other peaks appear much smaller and could be difficult to identify unless they are magnified[29,280]. In general a crystallite size of 1 to 50 μm is sufficient to provide good resolution of diffraction peaks[29,284]. To minimise preferred orientation affects, samples are often ground in a mortar and pestle[29,280]. However, it is the author's opinion that this approach does not fully represent the actual sample as it changes not only the particle size of the material but could also add an element of disorder via the mechanical grinding process. For the purposes of this research, materials were not ground during sample preparation and the presence or absence of preferred orientation

noted so that any observed changes could then be dually assigned to an external process and not to the sample preparation.

3.2.1 XRPD acquisition method

Sample X-ray powder diffraction patterns were obtained using a PANalytical CubiX PRO Fast diffractometer (details in APPENDIX 4). A representative sample of the experimental material was spread thinly on to a lightly silicone greased zero background holder (silicon wafer, PANalytical part number: PW1817/32) and placed on a spinner stage with a spinner revolution time of 1 s. Bragg-Brentano geometry was applied using monochromatic Cu Kα radiation (λ = 1.5406 Å) and soller slits (0.02 rad) for both the incident and diffracted beam paths. The instrument was operated at a voltage of 45 kV and a current of 40 mA over a scan range 2-70 °2θ with a step size of 0.0201 °2θ and a time per step of 71.75 s. System suitability was performed daily for diffraction line position and peak and tube intensity using α-Alumina standard SRM 1976. Samples for XRPD analysis were prepared under ambient conditions with both the laboratory temperature and ambient percentage relative humidity (%RH) monitored. The average sample preparation time was approximately 2 min.

Routine XRPD acquisitions usually stop at 40 to 50 °2θ which may not capture the entire diffraction signal and thus scans to higher °2θ values such as 70 °2θ may allow other potential unique peaks to be identified[285,286]. This extended range may also provide valuable information to investigate the amorphous character by advanced analysis methods such as those using pairwise distribution function (PDF) algorithms[285,286]. PDF could be used to provide information on the local molecular structure and short range order for materials across the crystalline-amorphous continuum and this is a subject of further investigation by other researchers[285,286].

3.2.1.1 *XRPD data treatment method*

To obtain numerical response data for analysis, the acquired XRPD diffraction patterns were pre-processed using the PANalytical X'Pert HighScore Plus (version 3.0) software to separate the crystalline peak data from the background (baseline) and to identify the associated diffraction peaks.

Replicate XRPD patterns were averaged by combining the merge scans with simple sum and taking the mean value. A background search was performed on the average scan using the following parameters: automatic with granularity = 25 and bending factor (See APPENDIX 5 for more information about granularity and bending factor settings).

A peak search was carried out to automatically locate peak positions and peak intensities using the minimum of second derivative and the following search parameters (Table 3-2). The minimum of second derivative peak search method provides optimal results for scans with overlapping peaks[287]. The treated XRPD peak data (*.HPF) and background profile (*.RD) were then saved for further analysis.

Table 3-2 XRPD peak search parameters

Parameter	Value	Details and Comments
Minimum significance	15 or 5 for patterns with high noise values, *i.e.* milled materials	The significance of a peak is a measure of the probability that a peak found is not noise-induced. Only peaks with significance above the minimum significance are accepted by the peak search procedure.
Minimum tip width	0.05	The minimum and the maximum tip width are a measure of the width of the peaks to be found. The tip width is the width, where the 2nd derivative is < zero.
Maximum tip width	1.0	
Peak Base Width	2.0	The width of the peak base. It must be greater than the maximum peak tip width.

3.2.2 XRPD response analysis

Using the treated data a number of individual peak and general diffractogram responses were reported and tabulated for further data analysis and interpretation (Figure 3-1 and Table 3-3).

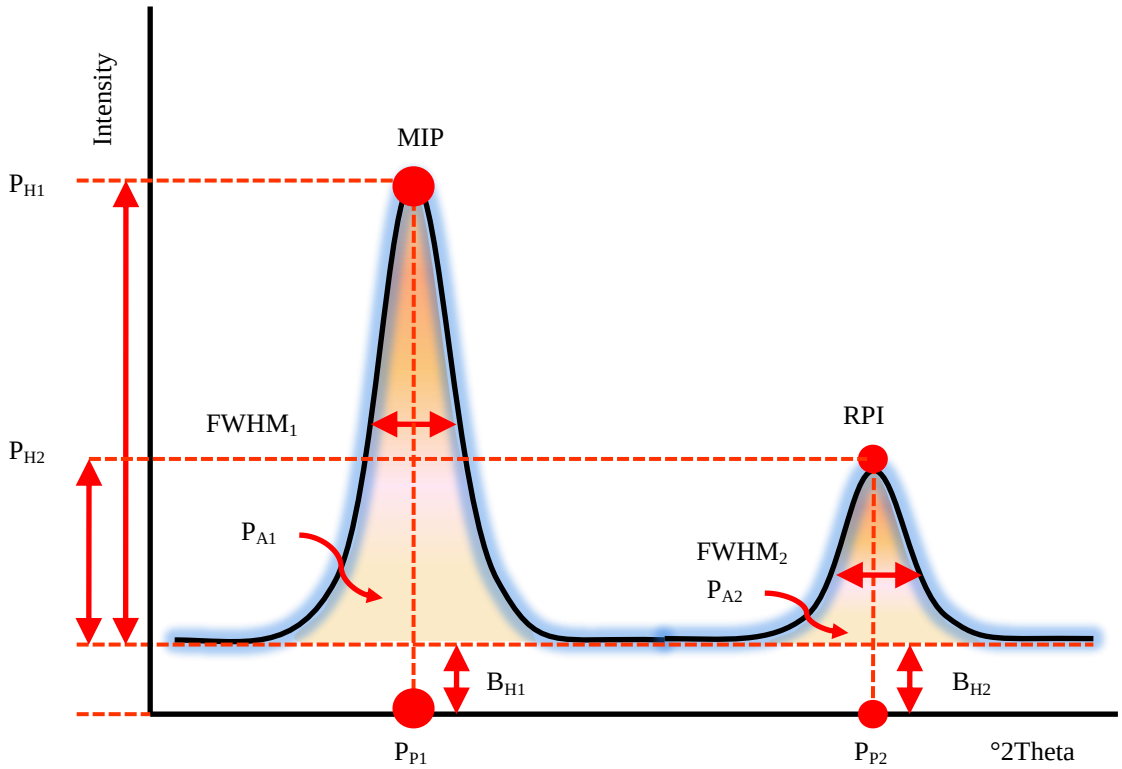

Figure 3-1 Reported and calculated responses for individual XRPD peak data
(See Table 3-3 for definitions of terms)

Table 3-3 XRPD responses: Definitions and calculations for individual peaks and whole diffractogram.

	Response	Details and Comments
Individual peak responses	Peak position (P_P)	Peak position of diffraction reflection [°2θ.] e.g. P_{P1} and P_{P2} refer to peak positions of peaks 1 and 2 respectively in Figure 3-1.
	Relative peak intensity (RPI)	% Intensity relative to the strongest peak. In X'Pert HighScore relative intensities are calculated on the basis of the net peak height. e.g. In Figure 3-1 the strongest intensity peak is peak 1 therefore the RPI for peak 2 = (PH2/PH1)*100.
	Peak height (P_H)	Intensity of the peak maximum in [counts or cts]. The peak height is determined by the composition and structure of the lattice, as well as instrumental factors (slit width, tube settings, tube age) e.g. P_{H1} and P_{H2} refer to peak height of peaks 1 and 2 respectively in Figure 3-1
	Background height (B_H)	Height of the background [counts or cts] influenced by sample preparation, instrument, air and crystallite properties (size, shape and lattice disorder). e.g. B_{H1} and B_{H2} refer to background height of peaks 1 and 2 respectively in Figure 3-1.
	Peak area (P_A)	Peak area in [cts$^{\times}$scan axis]. e.g. P_{A1} and P_{A2} refer to peak areas of peaks 1 and 2 respectively in Figure 3-1. Peak area is influenced by the lattice structure, instrumental factors and particle size.
	FWHM	Full Width at Half Maximum of a peak [°2θ.] The half-height width depends on the particle size, crystallite size and internal strains and instrument effects. FWHM in this research will be used as a measure of peak width.
	d-spacing	The *d*-spacing (inter-planar distances) of the peak [Å].
Diffractogram responses	Most intense peak (MIP)	The peak position of the peak with the highest intensity. This value is used in the determination of the relative peak intensities for all the other peaks. e.g. P_{H1} is the most intense peak in Figure 3-1.
	Significant peaks (SP)	List between 15-30 significant peaks based on relative peak intensities (RPI) to discriminate the material. Typically peaks above 5.0 % RPI were selected. However, for some materials the MIP is so intense it results in very low RPI's for the other peaks. In these cases a cut-off % RPI value of 0.5-2 % may have been used. The % RPI value used for peak selection was reported.
	Sum of net intensity signals for crystalline (X_I), background (B_I) and observed (T_I) [cts]	Net signal information for crystalline (X_I), background (B_I) and observed (T_I) obtained during the background search. These values are reported in the signal statistics section of the object inspector panel.
	Sum of Net peak (X_A), background (B_A) and gross areas (T_A) [cts*°2θ]	The net areas for peaks (X_A), background (B_A) and total areas (T_A) are calculated after performing the peak search. These values are reported in the peak statistics section of the object inspector panel.

3.3 Thermogravimetric analysis (TGA)

Thermogravimetric analysis is typically used to determine sample mass changes as a function of temperature[29,288,289]. These mass change events primarily represent the loss of volatiles or material decomposition. TGA of the bulk crystalline material was performed to demonstrate that the material was not a solvate or hydrate and to provide the upper temperature limit to be applied during DSC acquisition based on the observed degradation temperature.

It is important to note that TGA does not provide a direct indicator for the presence of disorder in materials but indirectly some valuable information can be ascertained. For example changes to surface disorder, particle size and levels of impurities maybe be

implied through changes to the mass loss profile and, or degradation temperatures[46,55,58]. Understanding the causes of these changes, especially the weight loss due to the presence of water that may have been sorbed as a consequence of processing or storage, can be used to highlight any potential solid state stability issues. The sorption of water either during processing or storage can be used to accelerate the crystallisation of any disordered surfaces and could lead to agglomeration and in worst cases new solid state forms[288,290]. It has been noted that a greater than 0.5 % w/w absorption of water could be indicative of the presence of a small level of amorphous content[250].

3.3.1 TGA acquisition method

TGA analyses were performed using a TA Instruments Q500 TGA (details in APPENDIX 4). The instrument was calibrated using a two point temperature calibration with alumel (CRM3-5291) and nickel (CRM2-8058) at a heating rate of 10 °C/min. All measurements were performed in a dry nitrogen environment with a constant purge gas flow of 60 mL/min. 5-15 mg of each material was placed on a tarred platinum sample rig with an aluminum pan insert and analysed at a heating rate of 10 °C/min from 20-350 °C (the typical temperature range for studying pharmaceutical organics[288,289]). Data points were collected every 0.5 s.

3.3.2 TGA response analysis

The acquired TGA thermograms were analysed using TA instruments Universal Analysis (version 4.5) software and the responses tabulated as described in Table 3-4 and illustrated in Figure 3-2.

Two weight loss measurements were selected to aid in the reporting of volatiles such as solvents or adsorbed water in the materials and to provide a measure of consistency in the reporting of percentage weight loss over a set temperature range (Table 3-4). Percentage weight loss below 50° C (WL_{50}) may be indicative of loosely bound volatiles present in the material[288]. While, percentage weight loss below 150 °C (WL_{150}) generally represents the total amount of both loose and strongly bound volatiles such as moisture or solvent as it also includes WL_{50}[288]. However, it must be noted that in some instances solvent loss may not occur until degradation occurs, *i.e.* for occluded solvents.

Table 3-4 Description of TGA responses to be reported

Response	Details and Comments
Number of weight loss events (#W_E)	Report the number of weight loss events occurring before degradation (T_d).
Weight loss event(s) (W_E)	Report in order: % weight loss ($WL_{\#}$), onset temperature of weight loss event ($O_{\#}$) and temperature range (start (S) to end (E)) in the format; WL, (O, range). Where the onset temperature cannot be calculated only the range is reported, *i.e.* WL, (range). If an unresolved weight loss event occurs at degradation this is denoted as "LoD".
% weight loss below 50° C (WL_{50})	% mass change (w/w) between start and 50 °C. This temperature range is fixed to allow comparison across materials. Weight loss below 50 °C generally represents loosely bound volatiles such as moisture or solvent.
% weight loss below 150 °C (WL_{150})	% mass change (w/w) between start and 150°C. This temperature range is fixed to allow comparison across materials. Weight loss below 150 °C generally represents the amount of volatiles such as moisture or solvent present (both loose and strongly bound). For materials which started to thermally degrade below 150 °C, WL_{150} could not be calculated so were be denoted as "D".
Degradation onset temperature, (T_d)	Extrapolated onset temperature for sample degradation (°C).

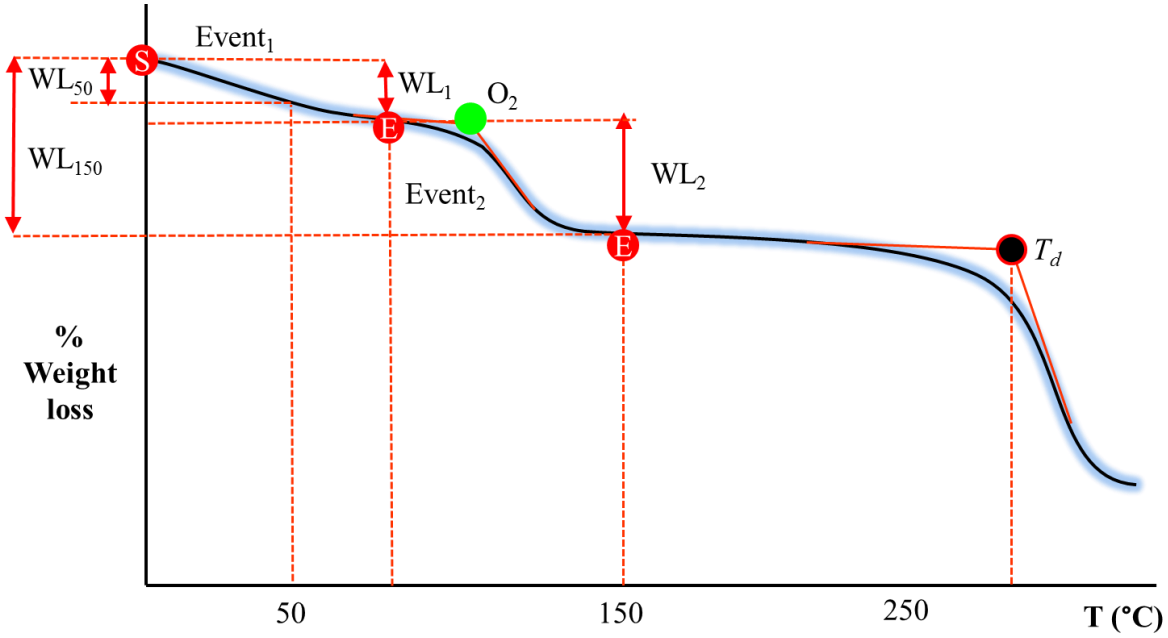

Figure 3-2 A hypothetical TGA thermogram describing the reported responses

See Table 3-4 for definitions of terms.
S = *Start point of event,* E= *End point of event, green circle is onset point* (O_2) *for the weight loss event* (WL_2)*, black circle is the onset point of degradation* (T_d).

3.4 Differential scanning calorimetry (DSC)

DSC provides information regarding the thermal properties of both crystalline and disordered material as a function of temperature[288,289,291]. DSC is a destructive technique and the responses obtained can be dependent on the parameters of acquisition such as heating rate, pan type and sample weight[288,289,291-296]. Solid-state form changes can also occur during acquisition, which may result in phases being identified that are not initially present in sample material[289,291-297]. Therefore, it is important that the correct

acquisition parameters are selected and reported alongside the resulting responses to ensure consistency in the interpretation. Information from the DSC thermogram is typically used to verify the solid state form identified by XRPD and vice versa, which can help to remove some of the ambiguity that can often occur during the interpretation of either results[19,29,30,175,193,288].

3.4.1 DSC acquisition method

The thermal properties of the materials were measured using a TA Instruments Q2000 DSC (details in APPENDIX 4) with an attached integrated refrigerated cooling system (RCS). The instrument was calibrated using a two point temperature and enthalpy calibration with indium (LGC2601) and lead (LGC2608) at a heating rate of 10 °C/min. All measurements were performed in a dry nitrogen environment with a constant purge gas flow of 50 mL/min. 1-2 mg of each material was accurately weighed into a standard aluminum pan and a lid placed on top before lightly crimping using a proprietary sealing press. The samples were heated at a rate of 10 °C/min from -10 °C to the respective end temperature based on the observed TGA degradation temperatures. These endpoints were selected to reduce the occurrence of degradation in the DSC cell which could interfere with the analysis of subsequent samples. Data points were collected every 0.2 s. Samples for DSC analysis were prepared under ambient conditions with both the laboratory temperature and RH monitored. The average sample preparation time was approximately 2 min.

A heating rate of 10 °C/min was chosen as this provides a good balance between sensitivity and resolution as well as allowing a reasonable acquisition time for organic pharmaceutical materials[289,291,297].

3.4.2 DSC response analysis

A DSC thermogram may contain a number of different thermal events as shown in Figure 3-3. These thermal events can be endothermic (heat absorbed), exothermic (heat released) or involve a change in heat capacity (change in baseline). In some cases the observed event may have an associated weight gain or losses, which can be verified by TGA analysis (Table 3-5).

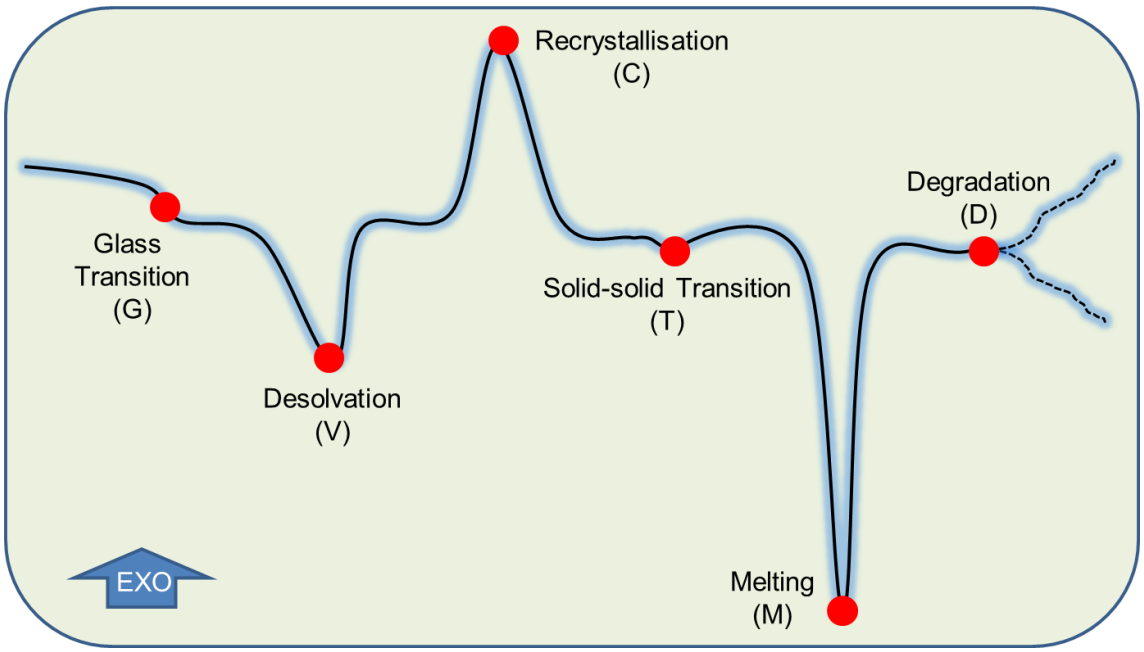

Figure 3-3 ***A hypothetical DSC thermogram depicting a number of thermal events that may be observed***

Table 3-5 ***Classification of thermal events as endothermic or exothermic***

Event	Weight gain	Weight loss	Endothermic	Exothermic
Absorption	Yes	-	-	Yes
Desorption	-	Yes	Yes	-
Dehydration/desolvation	-	Yes	Yes	-
Vaporisation	-	Yes	Yes	-
Sublimation	-	Yes	Yes	-
Decomposition/degradation	-	Yes	Yes	Yes
Oxidative degradation	-	Yes	-	Yes
Dissolution	-	-	Yes	-
Melting	-	-	Yes	-
Solid state transition	-	-	Yes*	Yes**
Enthalpic recovery	-	-	Yes	-

** Enantiotropic reversible, ** Monotropic irreversible*

For each thermal event there are a number of responses which can be used to both define and quantify the thermal event as illustrated in Figure 3-4, Figure 3-5 and Table 3-6. For each acquired DSC thermogram the thermal events were reported and the relative responses tabulated using the Universal Analysis software (version 4.5). Occluded solvents (solvents trapped in crystal lattice) and gas generated as a result of thermal degradation can be released during melting (M) and degradation (D), but as these observations coincide with those events they are likely to be unresolved. In this research, volatile (V) events in the DSC refers only to desolvation of liquids that occur before melting or degradation.

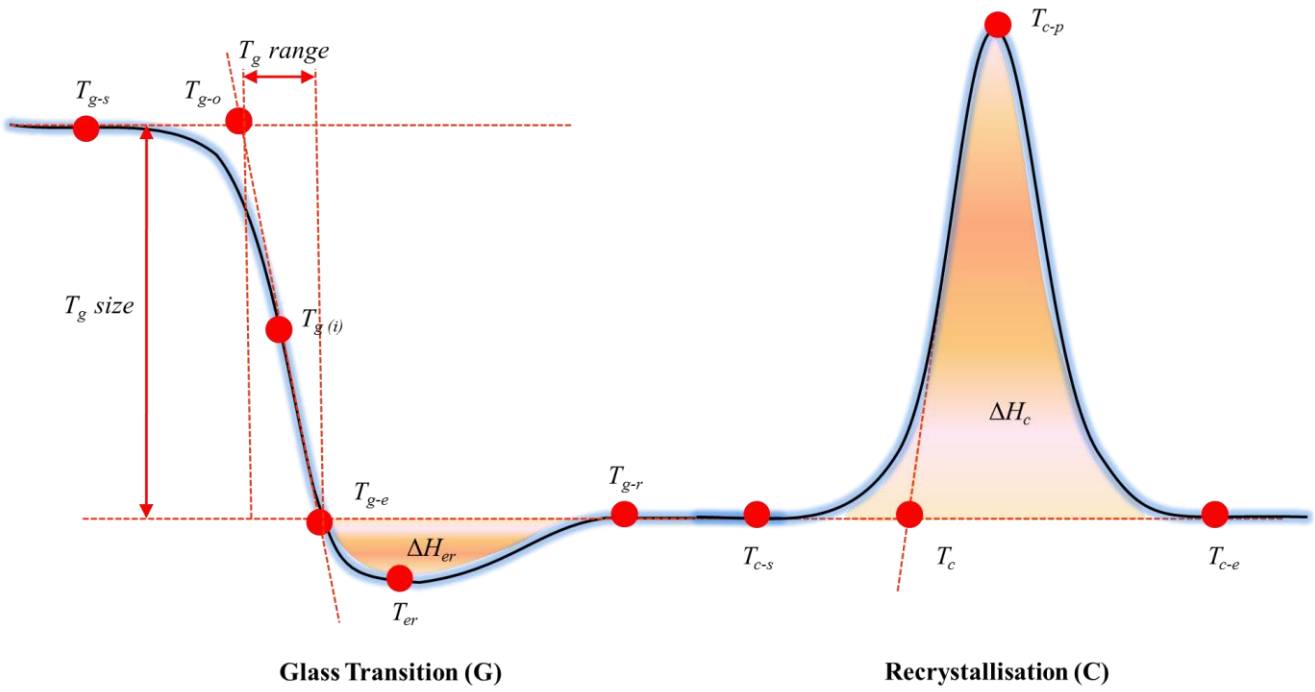

Figure 3-4 Depictions of glass transition (G) and recrystallisation events (C) with associated responses.

(See Table 3-6 for definitions of terms). Exothermic is up.

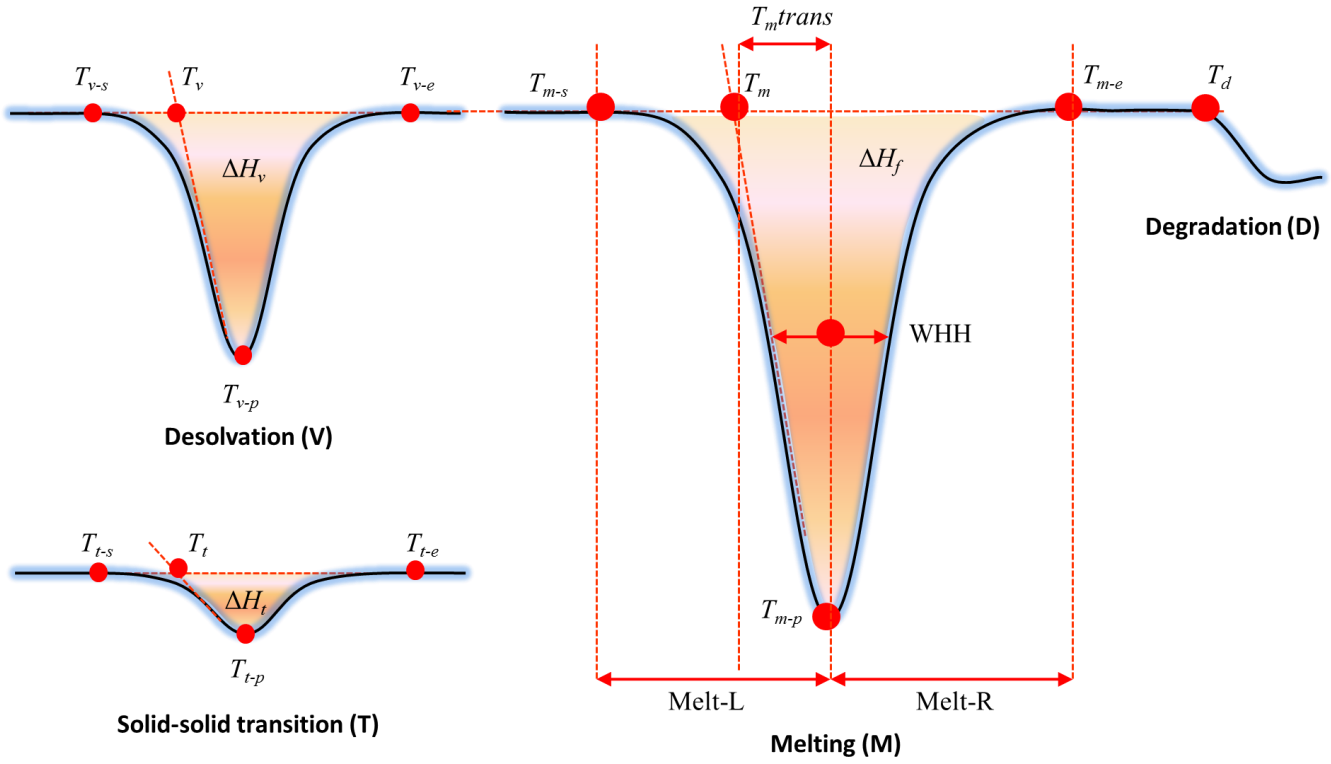

Figure 3-5 Depictions of desolvation (V), solid-solid transition (T) and melting (M) and degradation (D) event with their associated responses

(See Table 3-6 for definitions of terms). Exothermic is up.

Table 3-6 Description of reported DSC responses for different thermal events

Property/event	Response	Details and Comments
# events	$G_{\#}V_{\#}C_{\#}T_{\#}M_{\#}D_{\#}$	The number of occurrences for each type of thermal event
Glass transition (G)	$T_{g\text{-}s}$ & $T_{g\text{-}e}$	Start and end temperatures of glass transition respectively (°C)
	$T_{g\text{-}0}$	Extrapolated onset temperature of glass transition (°C)
	$T_g(i)$	Glass transition temperature (°C) inflexion point
	$T_{g\text{-}r}$	Temperature at which curve returns to baseline (°C)
	T_{er}	Peak temperature of enthalpic recovery (°C)
	T_g *size*	Size of glass transition or heat capacity (J/(g°C))
	T_g *range*	Temperature range of glass transition (°C) (equation [3-1])
	ΔH_{er}	Enthalpic recovery (J/g)
Desolvation (V) before melting or degradation	$T_{v\text{-}s}$, T_v, $T_{v\text{-}p}$ & $T_{v\text{-}e}$	Start, onset, peak and end temperatures of desolvation respectively (°C)
	ΔH_v	Heat of desolvation (J/g)
Recrystallisation (C)	$T_{c\text{-}s}$, T_c, $T_{c\text{-}p}$ &$T_{c\text{-}e}$	Start, onset, peak and end temperatures of crystallisation respectively (°C)
	ΔH_c	Heat of crystallisation (J/g)
Solid-solid transition (T)	$T_{t\text{-}s}$,T_t, $T_{t\text{-}p}$ &$T_{t\text{-}e}$	Start, onset, peak and end temperatures of transition respectively (°C)
	ΔH_t	Transition enthalpy (J/g)
Melting (M)	T_m	Extrapolated onset temperature of melting (°C)
	$T_{m\text{-}s}$ & $T_{m\text{-}e}$	Start and end temperatures of melting respectively (°C)
	$T_{m\text{-}p}$	Peak temperature of melting (°C)
	WHH	Width at half peak height (°C)
	T_m*trans*	Temperature range of melting (°C) (equation [3-2])
	ΔH_f	Heat of fusion (J/g)
	Melt-L	Total temperature range for melting to occur (°C) (equation [3-3])
	Melt-R	Total temperature range for material to recover after melting (°C) (equation [3-4])
	SYM	Measure of peak shape (equation [3-5])
Degradation (D)	T_d	Onset temperature of degradation (°C)

3.4.2.1 *Calculations*

Temperature range of glass transition, T_g *range* (°C) is given by:

$$T_g\,range = T_{g\text{-}e} - T_{g\text{-}0} \qquad [3\text{-}1]$$

where $T_{g\text{-}e}$ and $T_{g\text{-}0}$ are the end and extrapolated onset temperatures of glass transition respectively.

Temperature range of melting, T_m*trans* (°C) is given by:

$$T_m trans = T_{m\text{-}p} - T_m \qquad [3\text{-}2]$$

where $T_{m\text{-}p}$ and T_m are the peak and extrapolated onset temperatures of melting respectively.

Total temperature range for melting to occur, Melt-L (°C) is given by:

$$\text{Melt-L} = T_{m\text{-}p} - T_{m\text{-}s} \qquad [3\text{-}3]$$

where $T_{m\text{-}p}$ and $T_{m\text{-}s}$ are the peak and start temperatures of melting respectively.

Total temperature range for material to recover after melting, Melt-R (°C) is given by:

$$\text{Melt-R} = T_{m\text{-}e} - T_{m\text{-}p} \quad [3\text{-}4]$$

where $T_{m\text{-}e}$ and $T_{m\text{-}p}$ are the end and peak temperatures of melting respectively.

Measure or symmetry of peak shape (SYM) is given by:

$$\text{SYM} = \text{Melt-L} / \text{Melt-R} \quad [3\text{-}5]$$

3.5 Microscopy methods

Microscopy methods in the context of this research refer to both polarised light microscopy (PLM) and scanning electron microscopy (SEM) used to obtain preliminary estimations of particle size and shape. The choice of which microscopic method to use is dependent on the size of particles and the particle property information that is required.

Light microscopy is typically used to acquire optical crystallographic information such as crystal size, shape (habit) and agglomeration for particles greater than 1 µm in size[29,103,298,299]. However, when the sample is viewed under crossed-polarised light on a rotating stage (PLM) a qualitative check for crystallinity can be employed[29,30,103,298,299]. This is because most crystals are optically anisotropic and are birefringent, exhibiting different indices of refraction that is dependent upon the direction of vibration and transmission of the light passing through them[103,298]. Anisotropic crystals appear white to highly colored under cross polarised light and as the microscope stage is rotated the intensity of light will decrease to zero (crystal appears dark)[103,299]. These dark positions are called “extinction” positions and occur when a refractive index of the crystal coincides with the polarised light from the polariser[30,103,299]. Optical isotropic materials such as non-crystalline materials and cubic crystals exhibit identical optical properties in all directions and are described as non-birefringent. When these materials are viewed under cross-polarised light they appear dark like the field of the microscope, whatever their position[103,298,299].

SEM can also be used to provide particulate information about the material such as crystal shape (habit), agglomeration and particle size but can also provide additional information on crystal morphology, surface topography and extent of agglomeration due to its higher magnification and resolution, and greater depth of field and surface sensitivity (contrast) than that of optical microscopy [91,93,281].

When a material is subjected to a mechanical process such as ball-milling or micronisation, changes to the crystal habit and particle size can be monitored quickly

using microscopic methods. It is important to note that chemical and solid-state phase changes cannot be inferred directly or unambiguously by microscopy alone[300]. It is often up to the interpreters' experience to discern the information and then reach qualitative conclusions. Therefore it is important that any inferences with respect to the presence of disorder is made in conjunction with information provided by more direct measures of disorder using techniques such as XRPD and DSC.

3.5.1 PLM acquisition method

Any measurement must be representative of the bulk powder being analysed therefore the sample container was inverted end-over-end 20 times before a small sample of the material (approximately 20 mg) was removed using a spatula and placed in a 1 mL glass vial containing 1 mL of silicone oil (200/200 CS fluid, Dow Corning, Batch 000005E888, Lot L8-105). The suspension was then mixed using a vortex mixer (details in APPENDIX 4) for 15 s at medium speed. Two drops of suspension were then placed onto a glass slide. A metal wire was used to lightly disperse the particles in a few drops of silicon oil before a cover slip was applied. At least 3 images of each slide were acquired using a Zeiss Axioplan2 microscope (details in APPENDIX 4) with attached 5x, 10x and 20x objective lenses and transmitted light. Each slide was also viewed under polarised light and the stage rotated around at 90 degree angles to observe for the presence/absence of birefringence. Images were acquired under ambient conditions, with both the laboratory temperature and RH being monitored. The average sample preparation and acquisition time was approximately 5 min.

3.5.2 SEM acquisition method

The sample container was inverted end-over-end 20 times. Using a small plastic paintbrush a few milligrams of sample powder was sprinkled onto a carbon coated sample stub from a height of about 1-2 cm. Excess sample was tapped off the stub. The stub was then coated with a gold/palladium metal film using an argon-plasma sputter coater (details in APPENDIX 4) set at 20 mA for 3 min.

SEM images of the sample material were obtained using a high resolution FEI Quanta 200 SEM instrument (details in APPENDIX 4) operating under high vacuum, 0.45Torr pressure a voltage of 3.2-5 kV, an electron column spot size of 5.0 and a working distance of approximately 10 mm. Images were obtained at magnifications of 1000x (50 µm), 500x (100 µm), 100x (500 µm).

3.5.3 Microscopy response analysis

The microscopic images obtained using the PLM or SEM methods were qualitatively analysed using the Image Pro plus software (version 4.0). No image analysis was performed but rather a visual inspection was carried out to establish the primary particle habit and size, birefringence (PLM only), the extent of particle association (if any), along with surface characteristics (Table 3-7).

Table 3-7 Description of the microscopy responses to be reported

Response	Details and Comments
Primary particle shape or habit	As described and illustrated in Figure 3-6.
Particle surface characteristics and condition	As described and illustrated in Figure 3-7.
Birefringence (PLM Only)	For crystalline material extinction (darkening) observed upon rotation under polarised light. Disordered and cubic (isotropic) materials remain dark upon rotation.
Typical primary linear particle size (µm) & range	The longest linear dimension from edge to edge of a particle oriented parallel to the ocular scale as shown in Figure 3-8. This is an estimated value representing the average which is determined by manual calculation using the Image Pro plus (version 4.0) software.
Particle association (secondary crystal habits)	Primary particles can be associated into a collection of particles as described and illustrated in Figure 3-9.
Typical agglomerated particle size (µm) & range	The longest linear dimension from edge to edge for a mass of associated particles as shown in Figure 3-8. This is an estimated value representing the average which is determined by manual calculation using the Image Pro plus (version 4.0) software.

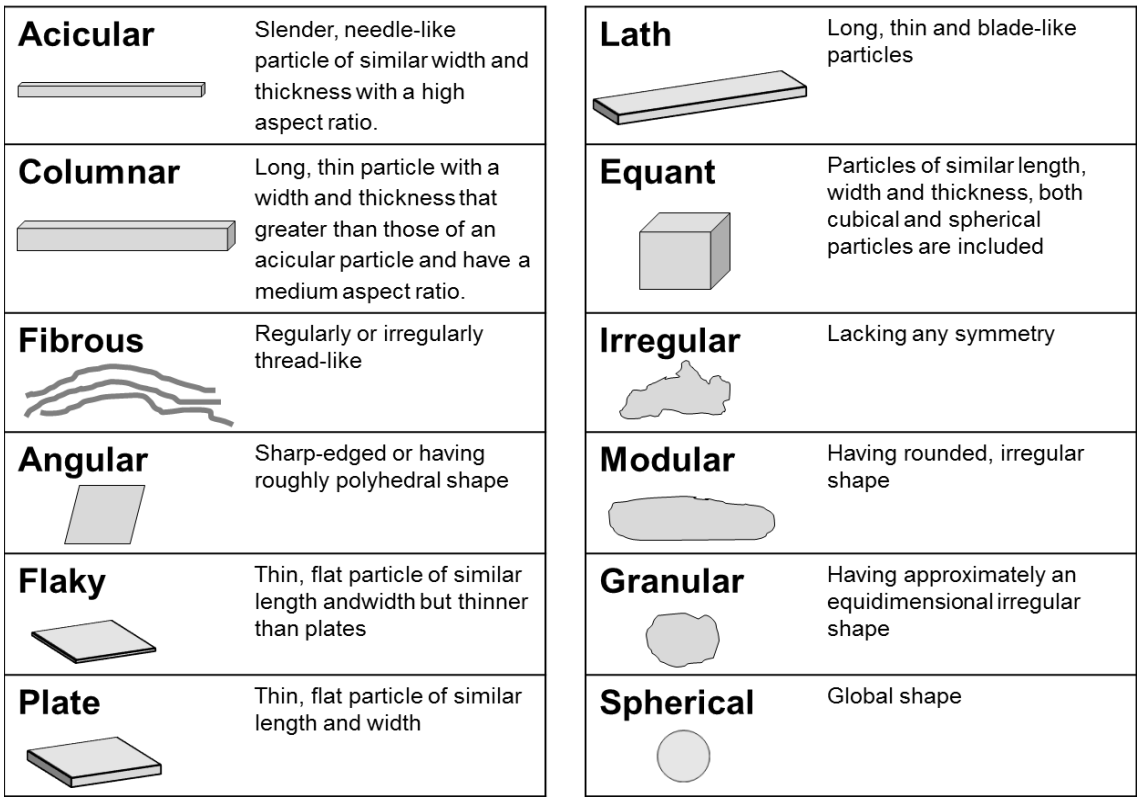

Figure 3-6 General descriptors for individual primary particles (Adapted[29])

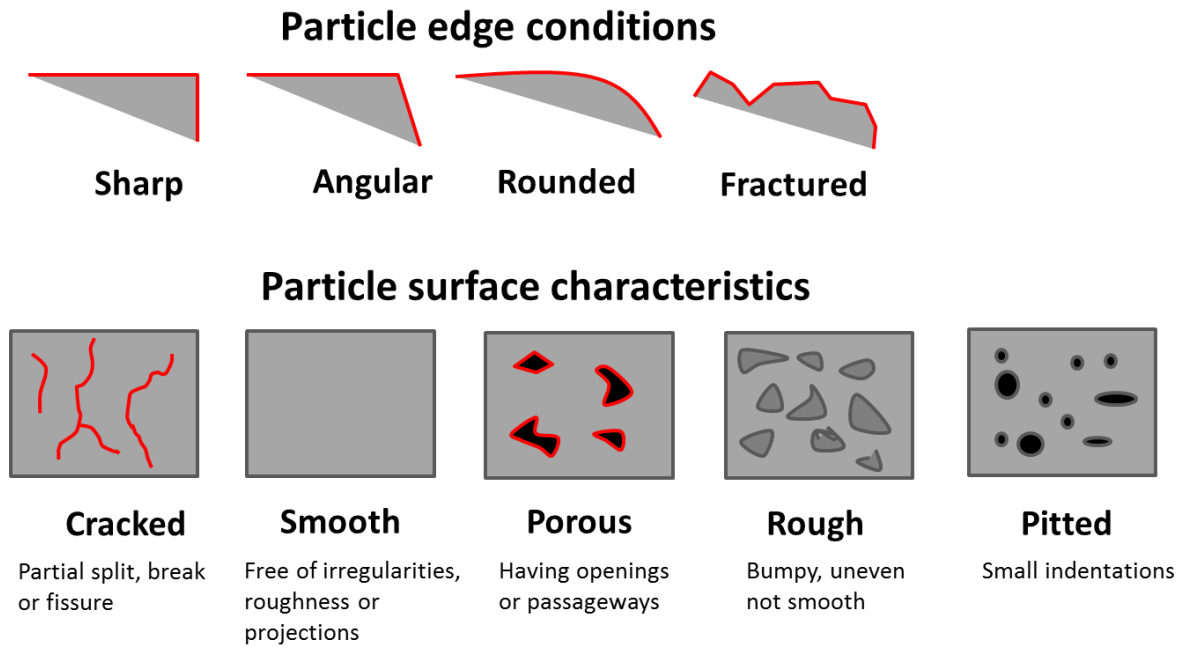

Figure 3-7 Particle edge conditions and surface characteristics (Adapted[29])

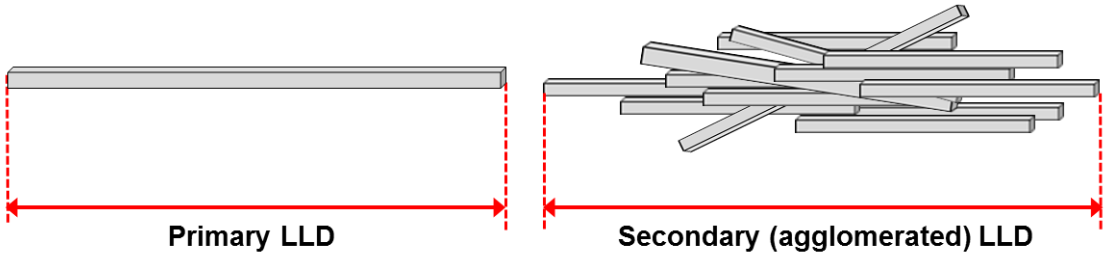

Figure 3-8 Longest linear dimensions (LLD) for primary and agglomerated particles

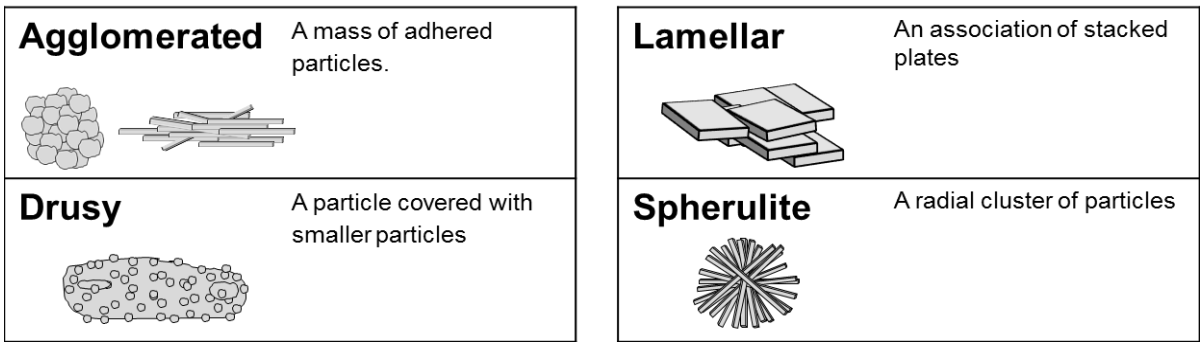

Figure 3-9 General descriptors for particle association of primary particles (Adapted[29])

3.6 Laser particle size analysis (PSA)

Laser diffraction is a commonly used particle sizing technique within the pharmaceutical industry on account of its speed of analysis, ability to handle a range of sample presentations and sizes, and ease of data presentation[301-303]

Unlike two dimensional microscopy methods which are number based and uses the longest linear dimension (length) as the defining particle size measure, particle size analysis by laser diffraction is a volume based three dimensional measurement technique which is sensitive to small changes in the amount of large material in the sample[301]. In the case of microscopic numerical distributions the fines may be over emphasised, and conversely for laser particle size volume distributions the coarse particles may be over emphasised[301].

It is also important to note that particle size analysis by laser diffraction does not measure particle size directly, but rather the property measured is the angular distribution of scattered light which is then converted into an approximation of homogenous spheres to give a particle size distribution based on either the Mie or Fraunhöfer theory[301]. However, the majority of pharmaceutical substances are non-spherical, and will therefore be measured over all orientations, resulting in a broadening in the measured size distribution. In addition, if particles are textured, they will tend to give enhanced weighting to the fine end of the distribution[301].

The two theories of light scattering - the Fraunhöfer theory and the Mie theory each make assumptions relating to physical attributes of the particles and the interaction of light with matter[301,302]. The Mie theory assumes that all the particles are spherical and translucent whereas the Fraunhöfer theory assumes that particles are spherical and opaque. In this research only the Fraunhöfer theory has been applied since it does not require knowledge of the refractive index of the materials being investigated[301,302]. As the particle sizes (>1 μm) being investigated are significantly greater than the wavelength of the laser light the Fraunhöfer approximation can be suitably applied to derive the particle size distribution[304,305].

As laser particle size analysis cannot distinguish between single particles and agglomerated particles care must be taken when preparing samples for analysis and when interpreting the results[303]. It is for this reason that results from laser particle size analysis should be viewed in conjunction with microscopy study information to evaluate

the accuracy of the values, or at the very least provide an understanding whether it is the primary or secondary particles that have been measured[301-303].

3.6.1 PSA acquisition method

Under ambient conditions, the sample container was inverted end-over-end 20 times before six aliquots of approximately 50 mg of sample were placed in clear ASPIROS sample tubes and capped. The samples were then analysed in the dry state using a Sympatec HELOS laser light diffraction particle size analyser with an attached RODOS dry disperser and an ASPIROS dry dispersion unit (details in APPENDIX 4). The samples were dispersed with compressed air at 1 bar with a feed velocity of 40.00 mm/s.

The choice of lens used depended on the qualitative assessment of the linear particle size range defined using an appropriate microscopic technique (sections 3.5.1 or 3.5.2). Table 3-8 defines the acceptable particle range for each lens type R1 to R8.

Table 3-8 Sympatec HELOS Lens Table

Lens No.	Lens focal length (mm)	Particle size range (µm)
R1	20	0.18 – 35
R2	50	0.45 – 87.5
R3	100	0.9 – 175
R4	200	1.8 – 350
R5	500	4.5 – 875
R6	1000	9.0 – 1750
R7	2000	18 – 3500
R8	5000	45 – 8750

In between aliquot runs, silicon carbide was used to clean the dispersing line. Different size ranges of silicon carbide standards were also used to check instrument performance and the accuracy of each lens.

3.6.2 PSA response analysis

Particle size analysis was performed using the WINDOX 5.0 software (Sympatec GmbH). The particle size distributions can be plotted as a log-normal distribution curve cumulative distribution by volume vs. logarithm particle size, or density distribution, (q3*) versus logarithm particle size, whereby particle size responses could be calculated and tabulated[302,306] (Table 3-9).

Table 3-9 Description of the particle size analysis responses to be reported

Response	Description
D_{10} (µm)	Lower decile *i.e.*10% of the particles by volume are below this size & 90% above.
D_{50} (µm)	Median *i.e.* 50% of the particles by volume are below this size & 50% above.
D_{90} (µm)	Upper decile *i.e.* 90% of the particles by volume are below this size & 10% above
Span	Is a numerical indication of the width of the distribution (see equation [3-6])
Mode(s)	Represents the most common value of the frequency distribution, *i.e.* the highest point or peaks in the curves
SMD (µm)	Surface mean diameter or Sauter mean diameter
VMD (µm)	Volume mean diameter, the larger the particles the greater the value
Sm (cm^2/g)	Surface area, the more fines there are the greater the value

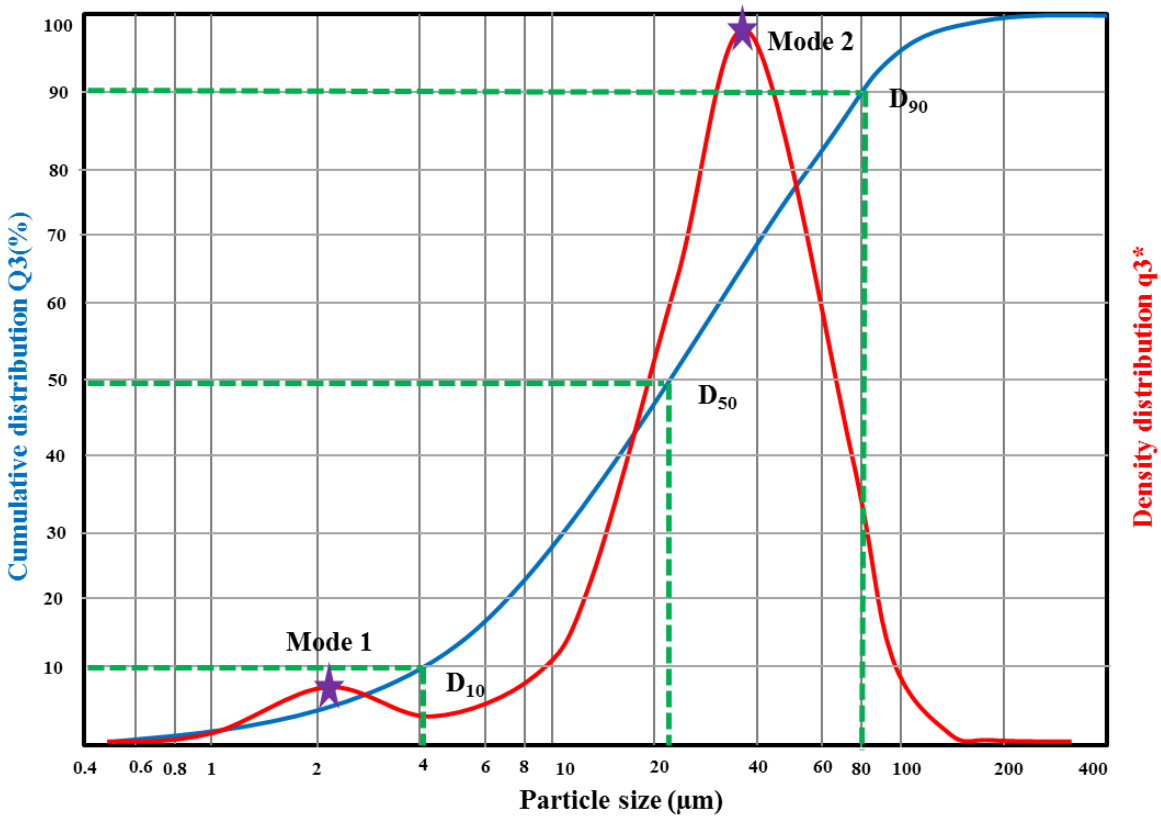

Figure 3-10 Example of a bimodal particle size distribution, illustrating some key responses D_{10}, D_{50}, D_{90} and modal positions) as described in Table 3-9

3.6.2.1 *Calculations*

Numerical width of the particle size distribution. Span is given by:

$$\text{Span} = \frac{D_{90} - D_{10}}{D_{50}} \qquad [3\text{-}6]$$

Where D_{10}, D_{50} and D_{90} are the lower, median and upper decile particle size values.

3.7 Gravimetric vapour sorption (GVS)

It is important to understand the moisture sorption properties of materials, as water can alter the solid state form, affect bulk and mechanical properties and can cause chemical interactions[18,24,190,191,252,290,307,308].

Water can interact at the surface of materials (adsorption) or it can penetrate into the internal bulk structure (absorption) resulting in the formation of crystal hydrates[290]. Typically water is adsorbed at the surface of crystalline materials due to the close packing and high degree of order within the crystal lattice forming only 2-3 mono-layers of water molecules and resulting in moisture sorption of typically less than 2% (w/w). However, for materials that have been size-reduced but are still crystalline the amount of water adsorption may increase due to the larger available surface area[290,309 310].

For amorphous or disordered materials, water adsorption can be significant as it involves dissolution of water molecules into the solid mass. It has been noted that a 0.5 % w/w absorption of water could be indicative of the presence of a small level of amorphous content[250]. For materials subjected to mechanical process such as ball-milling or micronisation the introduction of defects allows the ingress (adsorption) of moisture initially at the surface which is then absorbed into the internal structure of the solid[290]. In these cases water acts as a plasticiser, reducing the value of the T_g allowing either surface re-ordering or bulk recrystallisation depending on the location, the amount of water adsorbed, the temperature and the relative humidity[19,65,85,249-252,290,311]. This recrystallisation event can be observed in the GVS run as a mass loss as %RH is maintained at an elevated level[312,313]. It has been suggested that for every 1% w/w water present the T_g can be lowered by approximately 10 °C as was shown for amorphous indomethacin[254].

Moisture vapour sorption techniques are typically utilised to better understand both the amount and the kinetics of moisture adsorption/desorption of materials and in the detection of amorphous phases[18,24,190,191,252,290,307,308]. The detection of the presence of amorphous and disordered phases is achieved by measuring the release of adsorbed vapor from the amorphous phase when it crystallises rather than directly measuring properties of the amorphous phase, such as the T_g[18,24,190,191,252,307,308]. However, to quantify the amount of disorder or amorphous phase present the use of calibration standards are typically used[18,24,190,191,252,307,308]. This can be problematic as it cannot be guaranteed that the standard is 100% amorphous or that the moisture sorption process of

the standard reflects that of the sample, *i.e.* absorption from a spray dried standard versus adsorption from a ball-milled sample maybe different. This could result in an over estimation of the actual amount of amorphous material present[309]. It is therefore better to rely on correlating instrument responses with product performance rather than use inappropriate standards.

3.7.1 GVS acquisition method

Moisture sorption/desorption properties of the materials were investigated using a Surface Measurement Systems DVS-1 instrument (details in APPENDIX 4). Approximately 10-20 mg of sample was weighed into a quartz sample holder and held for 15 min at 30 %RH and 25 °C to equilibrate before a two cycle adsorption/desorption run was initiated using a dm/dt of 0.02 $\%min^{-1}$ with a time interval range of 15 to 120 min and a nitrogen gas flow of 200 $mLmin^{-1}$. The % RH was then adjusted at 10 %RH intervals within the adsorption/desorption ranges as shown in Table 3-10.

The DVS instrument is sensitive to electrostatic charge so where possible electrostatic charge was dissipated before analysis using a Zerostat 3 electrostatic discharge gun.

The instrument was calibrated using saturated NaCl reference salt and a weight check performed before use. Due to the length of acquisition (+10 h), replicate analysis was not performed.

Table 3-10 %RH ranges for sorption/desorption

Adsorption/ Desorption cycles	% RH range (increase at 10 %RH intervals)
Adsorption 1 (ADS1)	30 to 90
Desorption 1 (DES1)	90 to 0
Adsorption 2 (ADS2)	0 to 90
Desorption 2 (DES2)	90 to 0
Adsorption 3 (ADS3)	0 to 30

From the literature "drying" the sample is often the first step in the GVS analysis[290,314]. However, "drying" can potentially alter the solid state properties of the sample if for example water is present, then the removal of water could destabilise the crystal lattice resulting in the generation of amorphous material[290,310,314]. Therefore, in this research 30 %RH was selected as the starting RH as this represents a close approximation to the typical environmental RH of the laboratory and is unlikely to alter the initial solid state form of the material being analysed.

3.7.2 GVS response analysis

The acquired data was exported from the SMS DVS 1 software version 3.01 to Excel© where the data was plotted as % RH as a function of time, with an overlay plot of the percentage change in sample mass (dry) this is referred to as a kinetics plot (Figure 3-11[A]). The value for % change in sample mass (dry) at a given %RH is calculated relative to the value at 0 %RH, *i.e.* point C in Figure 3-11[A].

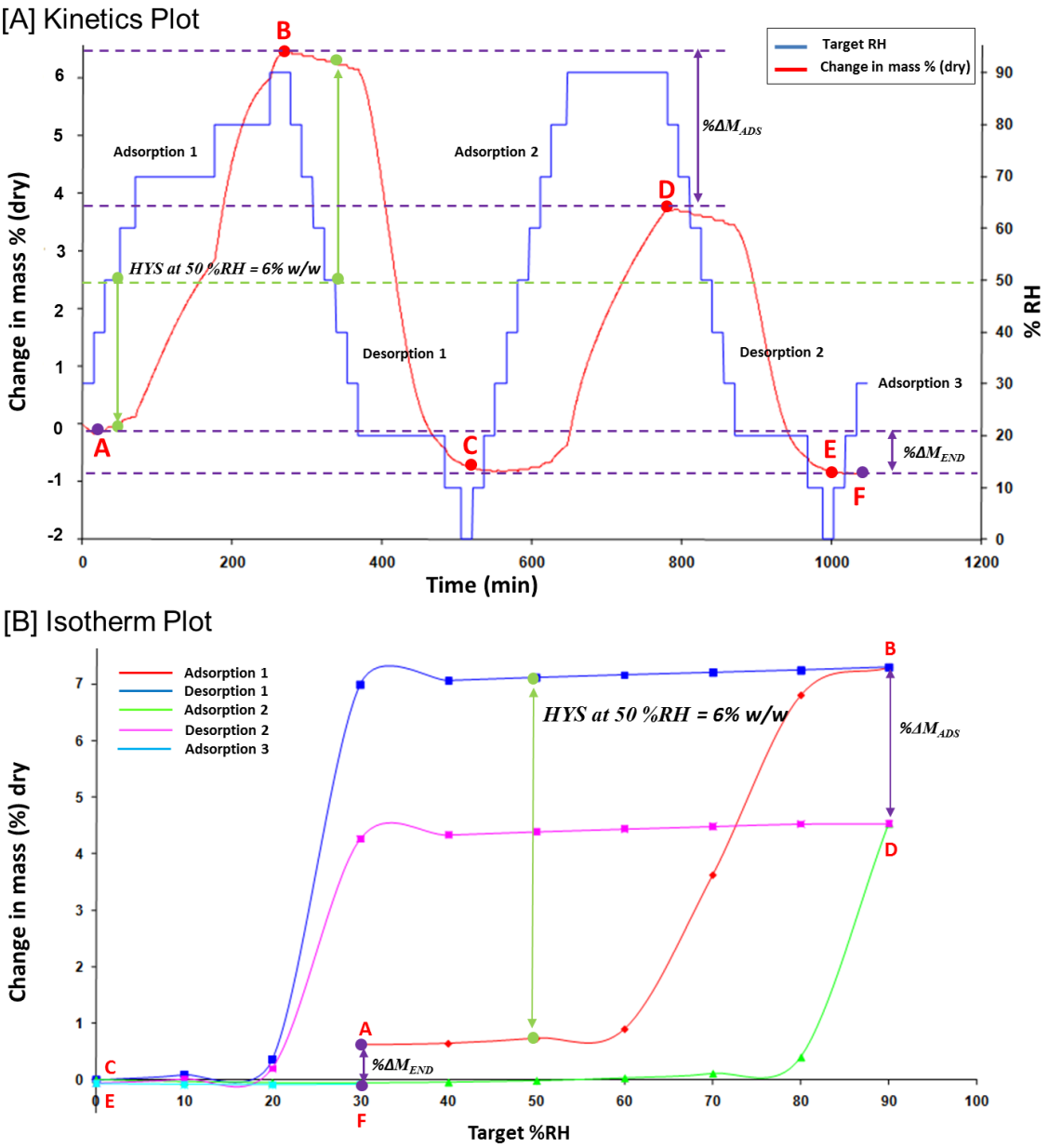

Figure 3-11 GVS kinetics [A] and isotherm [B] plots showing the moisture adsorption/desorption profile for ball-milled caffeine

Points A to F represent the start to end points of the adsorption/desorption cycles. Please refer to Table 3-11 for definitions of other responses.

An isotherm plot is also obtained which represents the change in sample mass % (dry) as a function of target %RH (Figure 3-11[B]) and can be used to visualise changes in moisture adsorption/desorption profiles at different %RH values. Table 3-11 describes

the associated GVS responses that are tabulated and reported to aid in characterising the moisture sorption properties of the study materials.

Table 3-11 Description of GVS responses to be reported

Response	Details
$M_{\#}$, (%)	Equilibrium % change in mass (dry) at different %RH values # = A, B, C, D, E, F (see Figure 3-11) *A* represents the initial point at 30 %RH and reflects the amount of moisture initially present. However, an elevated value could also be due to an electrostatic charge so need to compare with TGA results *B* represents point at 90 % RH (end of first adsorption) *C* represents point at 0 % RH (end of first desorption and dry) *D* represents point at 90 % RH (end of second adsorption) *E* represents point at 0 % RH (end of second desorption and dry) *F* represents final point at 30 %RH (end of third adsorption)
M_{END}, (%)	Represents the difference in % change in mass (dry) from the starting point (A) to the end point (F) during the run. If this value is large *i.e.* greater than ±1 then this may indicate that moisture has been retained or absorbed and that the solid state form of the material being analysed may have changed.
M_{ADS}, (%)	Represents the difference in equilibrium % change in mass between points B and D, *i.e.* At 90 %RH for adsorption cycles 1 and 2.
ADS#, DES#	Represents the adsorption and desorption cycle number # respectively. ADS1 30-90 %RH or points A to B DES1 90-0 %RH or points B to C ADS2 0-90 %RH or points C to D DES2 90-0 %RH or points D to E ADS3 0-30 %RH or points E to F
M_{MAX1}, M_{MAX2} (%)	Maximum equilibrium % change in mass (dry) during adsorption cycles 1 (ADS1) and 2 (ADS2) respectively.
ADS (%)	Represents the difference in the maximum equilibrium % change in mass (dry) during adsorption cycles 1 (ADS1) and 2 (ADS2) respectively. A large positive value infers irreversible moisture sorption or that a crystallisation event may have occurred in ADS1 (equation [3-7])
Moles of water at x %RH (M_{water})	Moles of water at a specified %RH value calculated using equation [3-8]
HYS at x %RH, (%)	Hysteresis is the difference in change in mass at a defined target %RH value (x) between the desorption and adsorption cycle. Calculated using equation [3-9]
$\%RH_{xtal}$ (%RH)	%RH value where a mass loss is observed as %RH value is maintained representing %RH for recrystallisation. ND (not detected) reported if not observed
M_{xtal} (%)	Value for % mass loss observed during recrystallisation at $\%RH_{xtal,}$ ND (not detected) reported if not observed

3.7.2.1 *Calculations*

The difference in the maximum equilibrium % change in mass (dry) (*ADS*) during adsorption cycles 1 (ADS1) and 2 (ADS2) respectively is given by:

$$ADS\,(\%) = (M_{MAX1} - M_{MAX2}) \qquad [3\text{-}7]$$

where M_{MAX1} and M_{MAX2} represent the mmaximum equilibrium % change in mass (dry) during adsorption cycles 1 (ADS1) and 2 (ADS2) respectively.

Moles of water at a specified %RH value ($M_{\#}$) is given by:

$$\text{Moles of water } (M_{water}) = \frac{M_{\#}}{\left(\frac{Mw_{water}}{Mw_{water}+M_w}\right) \text{ x } 100} \quad [3\text{-}8]$$

where $M_{\#}$ represents the % mass change at a specified %RH point or the maximum, Mw_{water} is the molecular weight of water (18.016) and M_w is the molecular weight or mass of the study material.

Hysteresis at a specified %RH value (*HYS at X %RH*) is given by:

$$HYS\ at\ X\ \%RH = (M_{\#desorption} - M_{\#adsorption}) \quad [3\text{-}9]$$

where $M_{\#}$ represents the percentage change in mass at a defined target %RH value (X) for the respective desorption and adsorption cycle.

3.8 High pressure liquid chromatography (HPLC)

A fast gradient HPLC method developed within GSK[315] was used to provide an estimate of the degree of chemical purity of the input study materials and to qualitatively identify the presence of any degradants as a result of mechanical processing. It is not intended that this method be quantitative nor was it validated.

3.8.1 HPLC acquisition method

A sample solution was prepared by weighing approximately 5 mg of study material into a 2ml amber HPLC autosampler vial containing 1.5 mL 50% (v/v) acetonitrile:water. A blank solution containing 1.5 mL 50% (v/v) acetonitrile: water solution was also prepared. The samples were then mixed well and analysed by UV using an Agilent 1100 series HPLC fitted with a diode array (details in APPENDIX 4). A gradient system was used with initial conditions 1 $mLmin^{-1}$ flow rate and Mobile phase A consisting of 0.05 % v/v trifluoroacetic acid (TFA) in water. At 8 min the mobile phase was switched to 95 % Mobile phase B (0.0 5% v/v TFA in acetonitrile) and 5 % mobile phase A. A Phenomenex Luna C18 (2), 50 x 2.0 mm, 3 µm column was used with a column temperature of 40 °C and an injection volume of 1 µL.

The wavelength selected for each material was determined initially by identifying the maximum absorbance peak (λmax) using A diode array detector. All solvents and reagents used were of HPLC grade, filtered and degassed before use.

3.8.2 HPLC response analysis

Integration of the area beneath any peaks in the acquired chromatograms was determined automatically using the peak integration settings as defined in Table 3-12.

For each integrated peak the retention time (RT), peak width, peak area, peak height and area % were reported. However, only RT and relative area % were utilised for characterising the material in this research. The peak with highest %area was designated the primary peak; any other peaks were referred to as secondary peaks.

Table 3-12 HPLC integration parameters

Time	Event	Value
Initial	Slope Sensitivity	35.0
Initial	Peak Width	0.02
Initial	Area Reject	1.00
Initial	Peak Height Reject	0.40
Initial	Shoulders	OFF
Initial	Integration	OFF
0.50	Integration	ON
8.50	Integration	OFF

3.9 Fourier transform infra-red spectroscopy (FTIR)

Fourier transform infrared spectroscopy is a well-established technique that is typically used to qualitatively identify and deduce the physical structure, conformation and chemical nature of the materials[30,316,317]. FTIR can also be used to identify differences in the solid state forms of materials as a result of processing and shows great sensitivity to polar bonds such as O-H, C=O and N-H. Hence, FTIR is a good tool to investigate the presence of water and changes in H-bonding[317,318].

Solid powder samples can be prepared using Nujol® mulls or KBR disks but this type of preparation can influence the solid state form of the materials[317]. By using an Attenuated Total Reflectance (ATR) accessory no sample preparation is required, as the sample can be analysed directly and has the added advantage that the influence of particle size is reduced compared to other techniques such as XRPD[317].

3.9.1 FTIR acquisition method

Under ambient conditions, the sample container was inverted end-over-end 20 times before 1-10mg of study material was placed on the ATR accessory of a PE Spectrum One FT-IR Spectrometer (details in APPENDIX 4). An applied pressure reading of 20 was applied and an interferogram representing 32 scans obtained over the 4000 – 650 cm^{-1} range, with a resolution 2.00 cm^{-1}. All samples were measured in triplicate and the spectra averaged. Both the laboratory temperature and %RH were monitored during sample preparation.

3.9.2 FTIR response analysis

The acquired IR spectra, representing transmittance as a function of wavenumber were analysed using the Omnic E.S.P. v5.1 software. The transmittance data was normalised by setting the maximum value of the spectrum to 1, allowing the spectra to be overlaid and easily compared. A peak search was performed and the results tabulated. Interpretation of the spectrum and assignment of the peaks to the group frequencies of the molecule was achieved using correlation tables and a review of the relevant literature[318].

3.10 Conclusion

A set of core test techniques is described in this chapter which will be employed to characterise a number of important molecular, particulate and bulk properties of the selected study materials before and after mechanical comminution.

The utilisation of this core test set of analytical methods should provide a reasonably comprehensive means of assessing any disorder that might occur to the crystal structure of the model materials as a consequence of mechanical comminution under standardised conditions.

4 Characterisation of input materials: Response analysis

4.1 Introduction

Ten selected materials were identified using the strategy outlined previously (Chapter 2), as being a suitable set of model materials to investigate the effects of mechanical processing on potential disorder. It was anticipated on the basis of the current literature that these materials might span a range that might encompass those with a higher propensity for PID through to those with a lower propensity. However before subjecting these compounds to mechanical comminution the initial solid state properties of these materials would require characterisation so as to provide a baseline to which changes in the analytical responses could be compared, and the relevance of the amount of change defined. Therefore, the main objectives of the work described here were to: (i) classify the study materials into different particle size fractions and (ii) characterise the selected size fractions using the core test methods described earlier (Chapter 3).

Classification would be effected by sieving so that similar size fractions could be selected with a view to reducing the potential influence of particle size on the generation of PID during the later planned comminution phase of the project. This fractionation process would also act to deaggregate the materials and promote sample homogeneity. . For each input material, the analytical property responses (APRs) from the core test methods will act as references that can be used to compare with the responses measured using the corresponding mechanically comminuted materials.

It was also planned to estimate and quantify where possible the amount of experimental and technique variation in the observed APRs.

4.2 Methods

4.2.1 Size fractionation by mechanical sieving

A nest of sieves (Table 4-1) (Endecott Ltd, London UK) was used to separate the material into a series of particle fractions using a Retsch mechanical agitation sieve assembly (details in APPENDIX 4)[319]. Approximately 25 g of bulk material received ‘as-is’ from the suppliers was added to the top sieve (425 micron). The sieving assembly was then securely fastened and shaken for 10 min with an amplitude setting of 1.50 mm and an interval time of 10 s[319]. The laboratory temperature and relative humidity (%RH) were also recorded at the time of sieving. Material from each sieve

was then transferred to an amber glass container and weighed. The amount of retained material in each sieve was expressed as a percentage of the initial input weight (% w/w).

Any electrostatic charge generated via sieving was then dissipated by placing the sealed container under a stream of ionized air for 15 min using a SIMCO Sentry ionizing air blower. The material was then stored at 20-25 °C, 0 %RH away from light.

Table 4-1 Analytical sieves and particle size fractions used to separate the study materials into different fractions[319]

Sieve Size (µm)	US Sieve No.	Frame/Mesh	Size range (µm)	Size class ID
425	40	Brass/Brass	>425	A4
212	70	Brass/Stainless steel	212 – 425	A1
125	120	Brass/ Stainless steel	125 – 212	A2
Receiver	N/A	Brass	<125	A3

4.2.2 Laser particle size analysis (PSA)

The particle size distributions for the sieved fractions for each of the study materials were obtained and analysed using the methods described in Section 3.6.1 and 3.6.2 respectively. For the selected sieved fraction, six replicates were analysed. For the other sieved fractions only three replicates were measured and analysed. The amount of variation in the responses was estimated based on the relative standard deviation (RSD) values. The particle size distributions were plotted as normalised density distribution (q3*) versus logarithm particle size obtained by dividing each q3* value by the highest q3* value observed.

4.2.3 Microscopy methods

PLM and SEM images for the selected sieved fractions of the study materials were obtained and analysed using the methods described in Section 3.5.

4.2.4 X-ray powder diffraction (XRPD)

4.2.4.1 *Acquisition and response analysis*

X-ray powder diffraction patterns for the selected sieved fractions of the study materials were obtained and analysed using the methods described in Section 3.2.1 and 3.2.2 respectively. Three replicates were obtained and an estimate of the amount of apparent variation observed in the responses quantified using the relative standard deviation (RSD) and range values. APPENDIX 6 illustrates the process used to investigate this variation using a worked example. For each material a single representative reference XRPD pattern was obtained by averaging the three replicates (method 3.2.1.1). The solid-state form of this XRPD pattern was confirmed by comparing it to the simulated

XRPD pattern of the respective CSD reference for each material as described in section 4.2.4.2.

4.2.4.2 *Confirmation of the solid state form by XRPD*

A simulated reference XRPD pattern for the CSD reference for each material was obtained using the CSD CrystalWeb software[320]. This file was first saved in *.Cif format and then converted to Bruker format (*.Raw) using the CSD Mercury (v2.3) software. The Bruker format file was then finally converted to a PHILIPS binary scan (*.RD) using PANalytical X'Pert HighScore Plus (v 3.0) and used to confirm the solid-state identity of the study materials. This was achieved by qualitatively matching (overlaying) the data treated XRPD diffractogram of the study material with that of the simulated XRPD reference pattern (Table 4-2).

Table 4-2 CSD references[320] used to generate simulated XRPD reference patterns for the study materials

Material	Crystallographic Reference (CSD)[320]
γ-Indomethacin	INDMET03
Salbutamol sulphate	SALBUT
Loperamide HCl	WAWVOH
Caffeine	NIWFEE03
Methyl paraben	CEBGOF01

Material	Crystallographic Reference (CSD)[320]
Sulfadiazine	SULDAZ02
Sulfamerazine	SLFNMA02
Acetaminophen	HXACAN11
Phenacetin	PYRAZB21
Acetylsalicylic acid	ACSALA01

4.2.5 Fourier transform infra-red spectroscopy (FTIR)

FTIR spectra for the selected sieved fractions of the study materials were obtained and analysed using the methods described in Section 3.9.1 and 3.9.2 respectively.

4.2.6 Thermogravimetric analysis (TGA)

TGA thermograms for the selected sieved fractions of the study materials were obtained and analysed using the methods described in Section 3.3.1 and 3.3.2 respectively. Each study material was analysed in triplicate and the responses averaged. The amount of variation in the responses was estimated using the relative standard deviation (RSD) values for % weight loss events or range values (°C) for temperature responses.

4.2.7 Differential scanning calorimetry (DSC)

DSC thermograms for the selected sieved fractions of the study materials were obtained and analysed using the methods described in Section 3.4.1 and 3.4.2 respectively. To reduce the potential for DSC contamination between sequential measurements the final analysis temperature for each material was selected based on the degradation temperature observed during the TGA analysis (Table 4-3). Six replicate sample preparations for each study material were prepared, acquired, analysed and the DSC

responses averaged. The amount of variation in the responses was estimated using either the range values (°C) for temperature responses or the relative standard deviations (RSD) observed for other types of DSC responses such as enthalpies.

Table 4-3 End point temperatures used during DSC acquisition for the study materials based on TGA data to reduce DSC cell contamination

Material	End-point temp (° C)
γ-Indomethacin	200
Salbutamol sulphate	250
Loperamide HCl	240
Caffeine	240
Methyl paraben	135

Material	End-point temp (° C)
Sulfadiazine	250
Sulfamerazine	260
Acetaminophen	200
Phenacetin	150
Acetylsalicylic acid	150

4.2.8 High pressure liquid chromatography (HPLC)

The wavelength of maximum absorbance (λmax) was obtained for each study material using the method described in Section 3.8.1. This wavelength was then used to determine the HPLC responses of the selected study materials using the method described in Section 3.8.2. Samples after DSC analysis were also examined using the HPLC method for some materials to demonstrate the suitability of the method to detect the presence of thermal and/or induced degradants.

4.2.9 Gravimetric vapour sorption (GVS)

Moisture sorption profiles for the selected sieved fractions of the study materials were obtained and analysed using the methods described in Section 3.7.1 and 3.7.2 respectively. Due to the length of time that was required to acquire these moisture sorption profiles, replicate analysis was not performed.

4.3 Results and discussion

4.3.1 Sieve fractionation

Historically, many investigators use materials as they are received from the suppliers, without carrying out any pre-processing procedures to ensure homogeneity in some of the physical properties, such as particle size or morphology (crystal habit). The potential problem in following this approach is that the material may exhibit a wide range of particle properties such as size or morphology (habit) and these may give rise to a wide range of analytical responses when characterised. Sieving the material can reduce the inherent variation in the bulk but quite often, the efficiency of sieving is not investigated[247,248]. These assumptions could lead to misinterpretations during characterisation and the possibility of the misidentification of correlations between the properties.

Therefore, the initial bulk materials as received from the suppliers in this reseach were first sieved and then separated into the different particle size fractions as shown in Table 4-4. The decision on which particle size class to use as the input for comminution processing was made based on the amounts retained in each sieve fraction and where possible, the same particle size class (PSC) for all the study materials was chosen. The minimum amount per size fraction to allow for characterisation and processing was 5 g (20 % of the 25 g input). Sieve fractions with less than 5 g were rejected and no further characterisation or processing was carried out on these.

Table 4-4 Sieving results for the 10 study materials (25 g bulk input), showing the amount of material collected per sieve fraction.

	Amount per sieve fraction (g)				
Material	<125 µm Size class A3	125-212 µm Size class A2	212-425 µm Size class A1	>425 µm Size class A4	Comments
Acetaminophen	1 (4%)	12 (48%)	3 (12%)	8 (30%)	electrostatic
γ-Indomethacin	1 (4%)	15 (60%)	8 (30%)		electrostatic
Loperamide HCl	6 (24%)	12 (48%)	5 (20%)		electrostatic
Salbutamol sulphate	6 (24%)	10 (40%)	5 (20%)	3 (12%)	sieves well
Methyl paraben	1 (4%)	14 (56%)	6 (24%)		electrostatic
Phenacetin	1 (4%)	20 (80%)	1 (4%)		electrostatic
Caffeine	1 (4%)	18 (72%)	4 (16%)		electrostatic
Acetylsalicylic acid	1 (4%)	18 (72%)	4 (16%)		sieves well
Sulfamerazine	3 (12%)	19 (76%)	1 (4%)		electrostatic
Sulfadiazine	1 (4%)	2 (8%)	19 (76%)		electrostatic

Value in brackets represents the percentage of the sieved fraction relative to the 25 g input bulk. Red indicates insufficient material to be used as the input for mechanical processing. Green shaded cell indicates the size class selected for further testing.

It can be seen from Table 4-4 that the most common sieved size fractions were between 125-212 µm (size class A2). This size class was selected to be used as the input material for the majority of the study materials. However, for sulfadiazine there was insufficient material in the A2 class, hence the 212-425 µm (A1 size class) fraction was selected. For a number of materials there were difficulties in sieving due to generated electrostatic charges. This charge was effectively dissipated using an ionized air flow after sieving (refer to section 4.2.1). It is has also been reported in the literature that relative humidity and temperature can affect the sieving process through the absorption of moisture to the material, which can result in larger or agglomerated particles[319]. However, in this study the sieving process was performed with relative humidities and temperatures recorded between 20-35 %RH and 21-26 °C respectively, so it is unlikely that the environmental conditions would have affected the sieving process.

4.3.2 Laser particle size analysis (PSA) and microscopy

To verify the particle sizes of the sieved fractions, the fractions containing material greater than 5 g were analysed by PSA and microscopy (Table 4-5 and Table 4-6 respectively).

Table 4-5 Particle size analysis summary for the sieved study materials

Material	PSC	n	D_{10} (µm)	D_{50} (µm)	D_{90} (µm)	Span	SMD	VMD	Sm (cm^2/g)	No. Mode
Acetaminophen	A2	6	3.58 (1)	23.5 (1)	132 (3)	5.48 (3)	10.3	47.5	5854	3
γ-Indomethacin	A1	3	8.07 (1)	75.4 (0)	250 (1)	3.20 (0)	20.2	106	2982	2
	A2	6	4.87 (7)	24.4 (3)	94.7 (5)	3.68 (6)	10.6	38.8	5690	2
Loperamide HCl	A1	3	5.03 (9)	216 (0)	343 (0)	1.57 (0)	17.0	182	3541	2
	A2	6	1.71 (7)	17.1 (9)	139 (6)	8.05 (6)	5.5	43.3	11021	3
	A3	3	1.51 (2)	12.3 (5)	51.4 (4)	4.05 (4)	4.60	20.6	13039	2
Salbutamol sulphate	A1	3	79.2 (9)	234 (3)	359 (4)	1.20 (4)	59.5	227	1012	1
	A2	6	47.5 (6)	144 (1)	267 (5)	1.52 (5)	50.4	153	1194	1
	A3	3	10.4 (7)	71.6 (2)	145 (1)	1.88 (1)	18.1	77.5	3323	1
Methyl paraben	A1	3	54.2 (12)	222 (1)	338 (1)	1.28 (3)	95.0	215	632	2
	A2	6	16.6 (3)	63.7 (4)	157 (3)	2.21 (3)	36.4	76.7	1650	2
Phenacetin	A2	6	8.25 (6)	34.3 (3)	96.2 (3)	2.56 (1)	15.3	44.8	3941	1
Caffeine	A2	6	2.93 (13)	23.7 (17)	147 (8)	6.13 (9)	8.0	51.0	7613	3
Acetylsalicylic acid	A2	6	115 (1)	203 (2)	346 (4)	1.13 (4)	121	217	495	2
Sulfamerazine	A2	6	13.0 (2)	33.8 (1)	67.0 (1)	1.60 (1)	19.7	37.5	3044	1
Sulfadiazine	A1	6	2.73 (11)	10.6 (13)	42.8 (8)	5.48 (3)	6.1	17.0	10151	2

n – Number of replicates, RSD values for the respective particle size and span values are shown in brackets. Red values indicate where the particle size did not match the expected sieve class. PSC: Particle sieve class, SMD: Surface mean diameter, VMD: Volume mean diameter, Sm: Surface area, No. Mode: Number of modes. For further definitions of the terms please refer to Table 3-9.

All the sieved fractions for the study materials exhibited birefringence by polarised light microscopy, indicating that the materials appeared crystalline (Table 4-6). However, particle size analysis by laser diffraction revealed that for a number of materials the particle size did not match that of the expected sieve class (shown as red in Table 4-5). These differences can most likely be attributed to the presence or breaking of

agglomerates, or due to other material properties such as crystal morphology and, or electrostatic charges generated during the sieving process. A brief description of the microscopy and particle size analyses for the materials follows.

For acetaminophen, phenacetin, sulfamerazine and caffeine only the A2 sieved fractions were obtained in sufficient quantities to be used as the input materials for mechanical comminution (Table 4-4). However, the particle sizes for these fractions were lower than expected considering the size of the sieve employed, *i.e.* 125-212 µm (Table 4-5). A potential reason for this lower than expected particle size maybe due to the observed electrostatic charge generated during sieving. This electrostatic charge may have caused smaller particles to "clump" together forming agglomerates, which prevented the smaller particles passing through the sieve. However, when analysed by laser particle size and in some cases microscopy these agglomerates start to breakup into the primary particles, hence the smaller primary particles are measured.

The particle size distributions for the A2 sieved fractions of acetaminophen and caffeine were multimodal with large span values, indicating broad distributions (Figure 4-1). The particle size distribution for caffeine also indicated the presence of agglomerates which suggests that these agglomerates are fairly robust and are not fully dispersed during particle size analysis. Both phenacetin and sulfamerazine exhibited mono-modal particle size distributions (Figure 4-1).

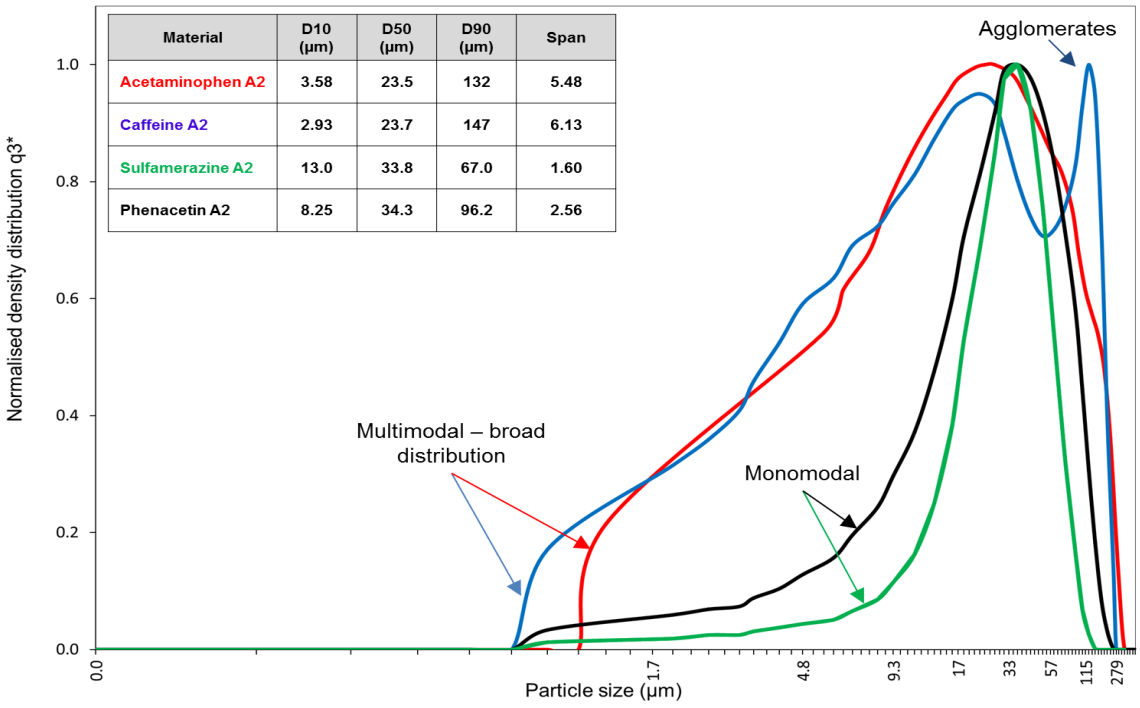

Figure 4-1 ***Particle size distributions for the A2 sieved fractions of acetaminophen (red), caffeine (blue), sulfamerazine (green) and phenacetin (black)***

Table 4-6 Microscopy analysis for the sieved fractions of the study materials

Material	PSC	Tech	Crystal habit	Edge	Surface	BiFr	1° LLD (µm)	1° range (µm	Agg	Agg size (µm)	Agg range (µm)
Acetaminophen	A2	PLM	Acicular & columnar	Rounded	Smooth	Yes	50	50-200	Agg	200	100-400
		SEM	Acicular & columnar	Fractured	Rough	N/A	50	10-150	Drusy	ND	ND
Indomethacin	A1	PLM	Irregular & plates	Fractured	Rough & cracked	Yes	200	10-425	Drusy	300	100-425
	A2	PLM	Irregular	Fractured	Rough	Yes	25	10-150	Drusy	200	100-400
		SEM	Irregular & plates	Fractured	Rough & cracked	N/A	50	10-250	Drusy	ND	ND
Loperamide HCl	A1	PLM	Irregular	Fractured	Rough & cracked	Yes	20	10-75	Agg	300	50-425
	A2	PLM	Irregular	Fractured	Rough & cracked	Yes	20	10-150	Agg	150	50-200
		SEM	Irregular	Fractured	Rough & pitted	N/A	25	5-100	Drusy	ND	ND
	A3	PLM	Irregular	Fractured	Rough & cracked	Yes	5	5-50	Agg	50	20-50
		SEM	Irregular	Fractured	Rough & pitted	N/A	5	5-50	Agg	50	20-125
Salbutamol sulphate	A1	PLM	Acicular & columnar	Angular	Smooth	Yes	350	10-400	Agg	400	200-500
		SEM	Acicular & columnar	Angular	Smooth & slightly cracked	N/A	250	10-400	Drusy & agg	ND	ND
	A2	PLM	Acicular & columnar	Angular	Smooth	Yes	150	10-300	Agg	200	50-400
		SEM	Acicular & columnar	Angular	Smooth & slightly cracked	N/A	125	5-450	Drusy & agg	ND	ND
	A3	PLM	Irregular & columnar	Angular	Smooth	Yes	75	5-200	ND	ND	ND
		SEM	Irregular & columnar	Angular	Smooth	N/A	75	5-150	Drusy	ND	ND
Methyl paraben	A1	PLM	Irregular	Fractured	Rough	Yes	10	5-25	Agg	200	100-450
	A2	PLM	Irregular	Fractured	Rough	Yes	50	25-150	Agg	75	50-225
		SEM	Irregular	Fractured	Rough	N/A	50	10-250	Agg	ND	ND
Phenacetin	A2	PLM	Irregular plates	Fractured	Smooth	Yes	50	25-150	Agg	350	100-400
		SEM	Broken plates	Fractured	Smooth	N/A	75	10-200	Drusy	ND	ND
Caffeine	A2	PLM	Acicular	Fractured	Rough	Yes	25	10-100	Agg	75	50-150
		SEM	Irregular	Fractured	Rough	N/A	25	5-50	Agg	ND	ND
Acetylsalicylic acid	A2	PLM	Modular	Rounded	Smooth	Yes	200	200-400	ND	ND	ND
		SEM	Modular	Rounded with Fractures	Cracked	N/A	200	150-500	ND	ND	ND
Sulfamerazine	A2	PLM	Columnar	Fractured	Smooth	Yes	50	10-100	ND	ND	ND
		SEM	Irregular & broken columnar	Rounded with Fractures	Rough with some cracks	N/A	75	5-100	Slight drusy	ND	ND
Sulfadiazine	A1	PLM	Acicular	Sharp	Smooth	Yes	25	10-75	ND	ND	ND
		SEM	Acicular	Sharp	Smooth	N/A	50	10-200	Agg	ND	ND

PSC: sieve particle size class or sieve fraction, Tech: technique, BiFr: birefringence, 1°LLD: primary particle longest linear dimension, 1° range: primary particle size range, Agg: agglomeration, Agg size: agglomeration particle size, Agg range: agglomerate particle size range. ND: not determined. For further definitions of the terms please refer to Table 3-7 and Figure 3-6 to Figure 3-9.

Microscopy analysis for all four materials supported the observations made by laser particle size (Figure 4-2). For example, there are two different crystal habits observed in samples of acetaminophen which vary in particle size along with the presence of

agglomeration which accounts for the large span value. Microscopy images for caffeine also show the presence of agglomerates.

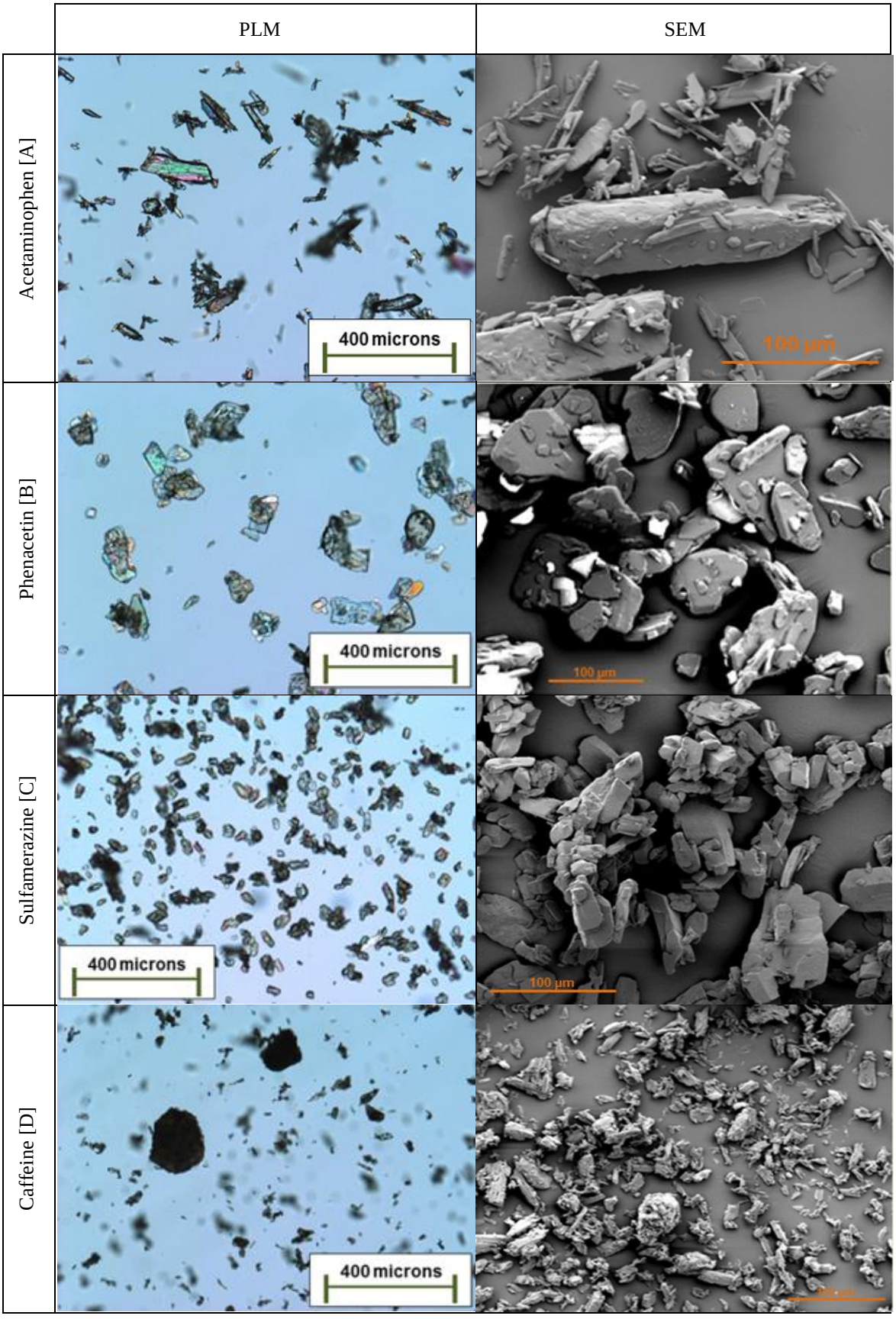

Figure 4-2 Microscopic images for the A2 sieved fractions of acetaminophen [A], phenactin [B], sulfamerazine [C] and caffeine [D]

Three sieved fractions of loperamide HCl were analysed by microscopy and laser particle size. The particle sizes for the sieve fractions A1, and A3 were consistent with the size of sieve employed (Table 4-5). However, for the A2 sieve fraction, particle sizes were smaller than expected (Table 4-5). PLM images for all of the fractions show that the primary particles were small but that they formed agglomerates in the A1 and A2 fractions (Figure 4-3), and these agglomerates were not dispersed during particle size analysis (Figure 4-3 [A] and [B]). The particle size distributions for all three sieved fractions A1, A2 and A3 were bimodal with large span values for the sieved fractions A2 and A3 (Figure 4-4).

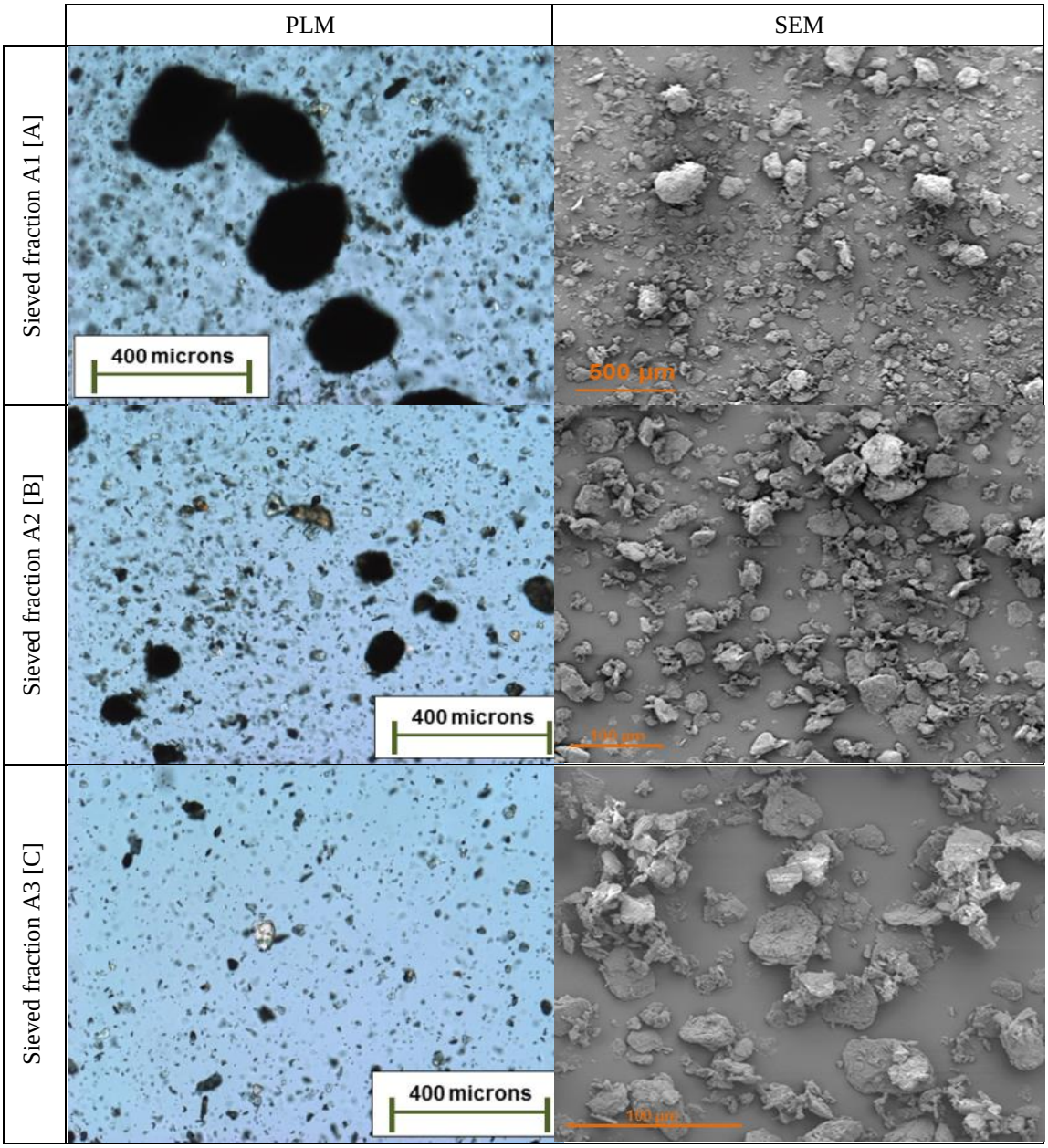

Figure 4-3 Microscopic images for loperamide HCl sieved fractions A1, A2 and A3

PLM images for sieved fractions A1 [A], and A2 [B] illustrate the presence of agglomerates and the smaller irregular primary particles.

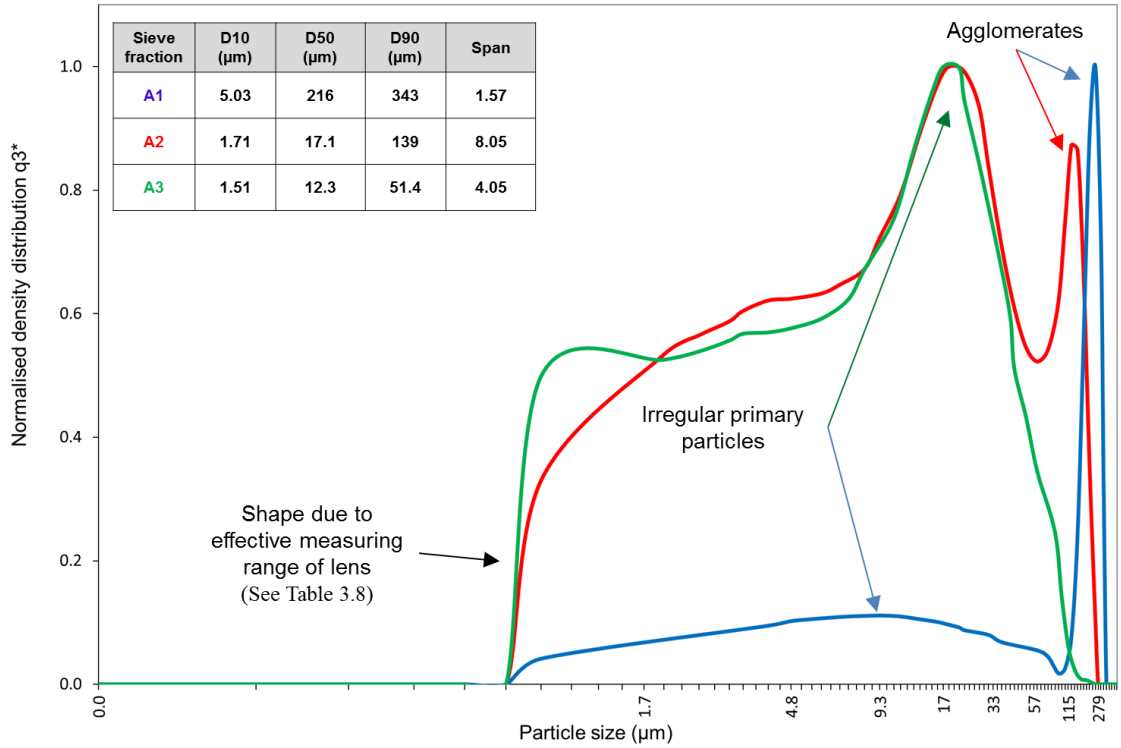

Figure 4-4 ***Particle size distributions for loperamide HCl sieved fractions A1 (blue), A2 (red) and A3 (green)***

The two sieve fractions for methyl paraben were analysed and shown to be predominately agglomerated (Table 4-5 and Table 4-6), while the A2 sieved fraction for acetylsalicylic acid exhibits a mono-modal particle size distribution where the particle size was consistent with the type of sieve used (Table 4-5 and Figure 4-5 [A]).

Only the A1 sieved fraction was obtained in sufficient quantity for sulfadiazine (Table 4-4). Analysis by laser diffraction and microscopy showed that the particles retained in the A1 sieved fraction were smaller than expected (Table 4-5 and Figure 4-5 [B]). Sieving of sulfadiazine resulted in an electrostatic charge which caused the material to "clump" and be retained in the upper sieve. During PSA analysis these agglomerates were dispersed and only the primary particles were measured.

The two sieved fractions, A1 and A2 for indomethacin were analysed by microscopy and laser particle size (Table 4-5 and Table 4-6 respectively). The A1 fraction consisted predominately of large plates with attached (drusy) smaller particles (Figure 4-6 [A]), while the A2 sieved fraction consisted predominately of irregular particles with some weak agglomeration through electricstatic charging. The degree of agglomeration appears to be reduced during particle size analysis (Figure 4-6 [B]).

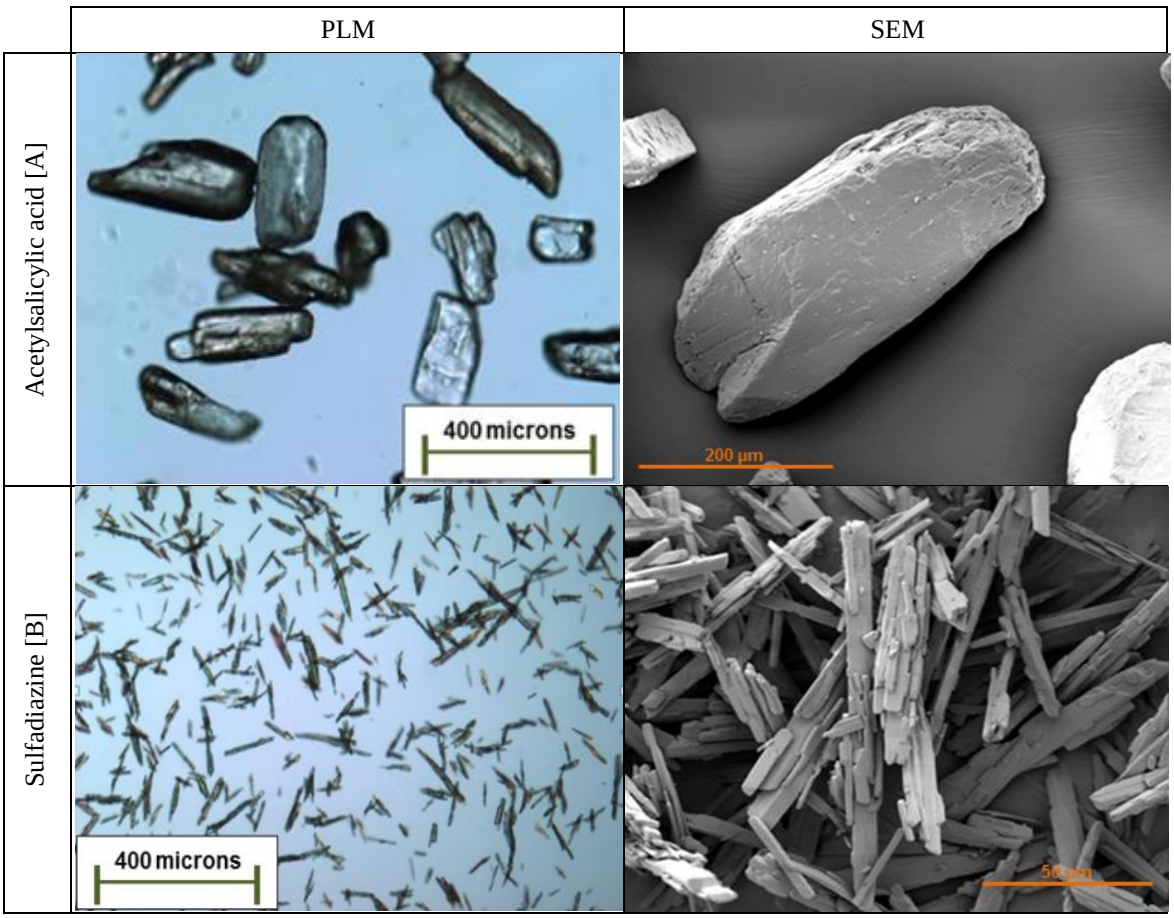

Figure 4-5 ***Microscopic images for sieved fractions A2 for acetylsalicylic acid [A] & sieved fraction A1 for sulfadiazine [B]***

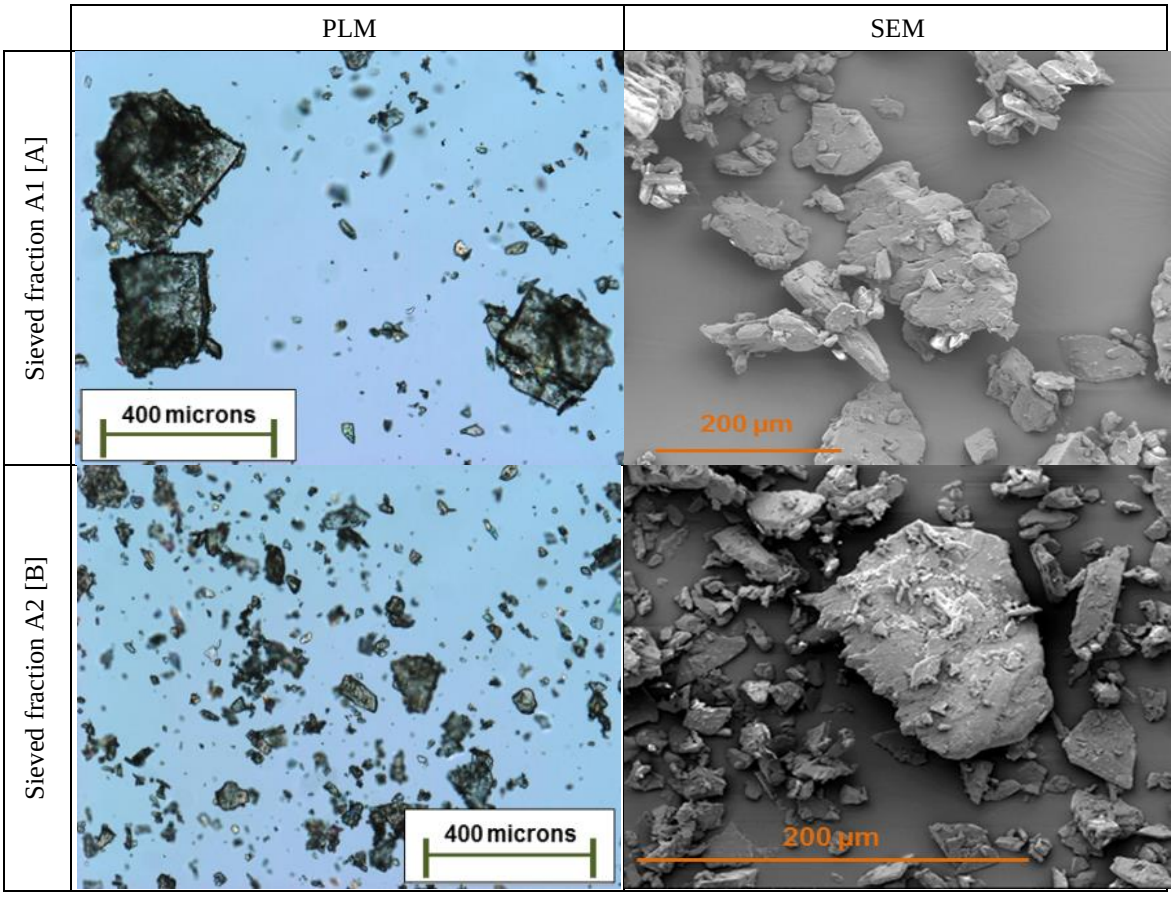

Figure 4-6 ***Microscopic images for indomethacin sieved fractions A1[A] & A2 [B].***

Three sieved fractions for salbutamol sulphate were obtained and analysed by laser particle size and microscopy (Table 4-5 and Table 4-6 respectively). The particle sizes for all three fractions were consistent with size of the sieves used and were shown to have monomodal particle size distributions (Figure 4-7 and Figure 4-8). Within sieve fraction A1 the particles were predominately agglomerated (Figure 4-8 [A]), while sieve fractions A2 and A3 consisted mainly of primary particles with some smaller particles attached, *i.e.* appear drusy (Figure 4-8 [B] & [C]).

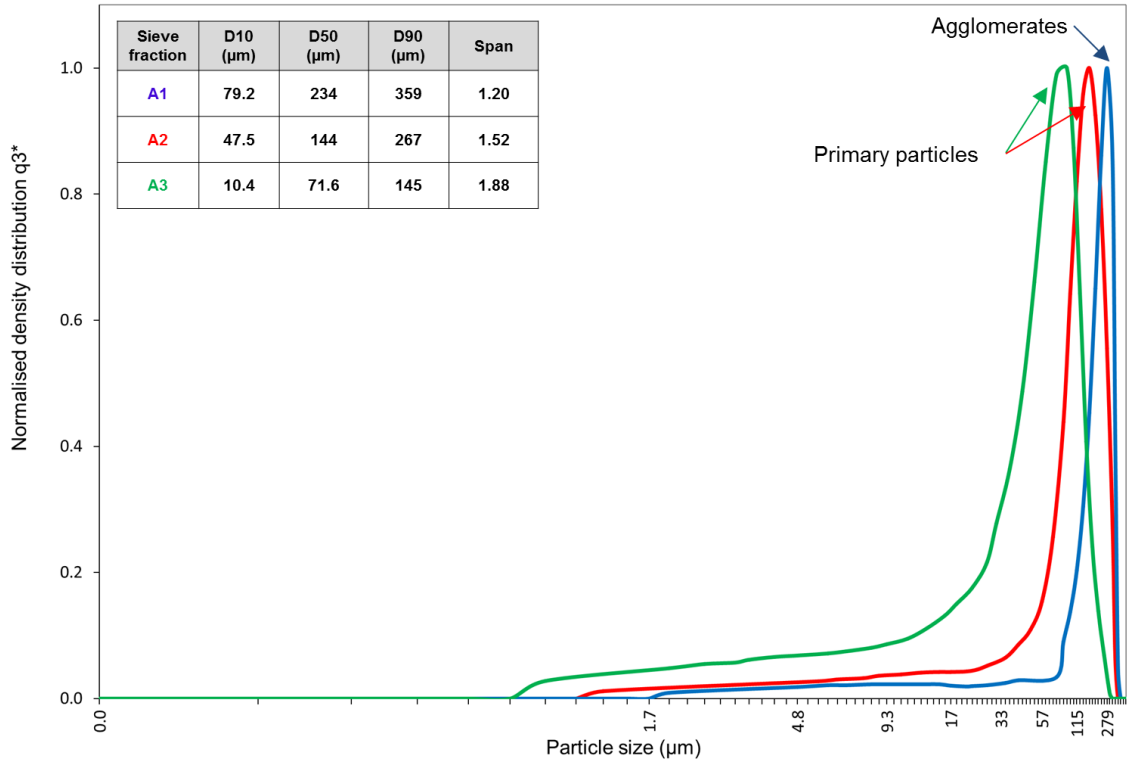

Figure 4-7 ***Particle size distributions for salbutamol sulphate sieved fractions A1 (blue), A2 (red) and A3 (green)***

Based on the particle size and microscopy results, the selected sieved fractions which were to be used as the input material during mechanical comminution were reclassified to reflect the actual particle size and agglomeration present, as it has been shown based on the data presented, that in practice the actual particle size of a material does not necessarily match the sieve fraction employed. The presence of agglomeration and generated electrostatic charges can influence particle retention during sieving and can result in a less predictable sieving process, *i.e.* results in a different particle size range from that expected.

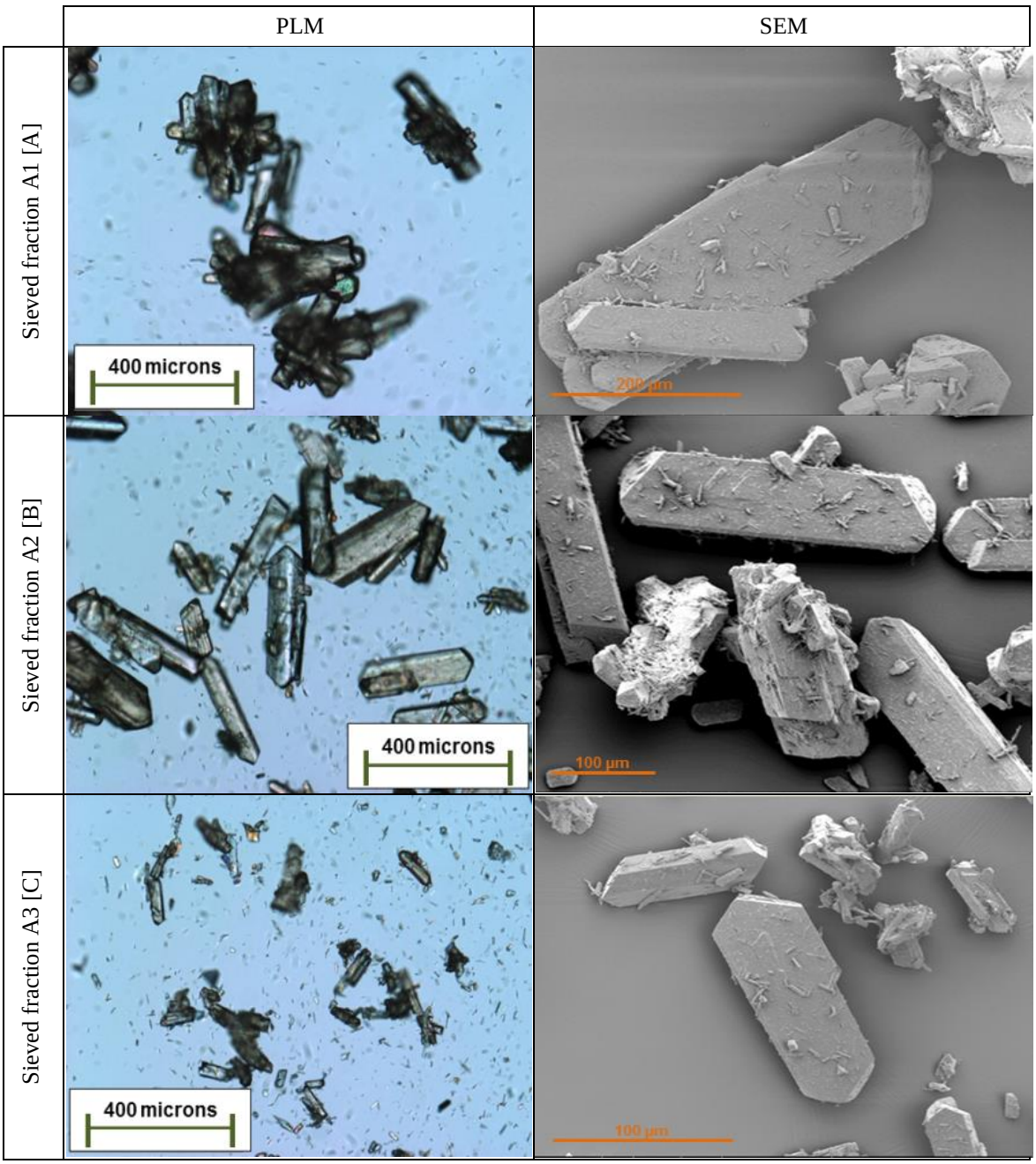

Figure 4-8 Microscopic images for salbutamol sulphate sieved fractions A1, A2 and A3

PLM images for PSC-A1 [A] illustrate the presence of agglomerates. PLM images for PSC-A2 [B] and PSC-A3 [C] illustrates the presence of primary particles with smaller attached particles (drusy).

The new size classifications for the materials were defined using the designator codes outlined in Table 4-7. These are based on the material's D_{50}, D_{90} and span values. For example the A2 sieved fraction for acetaminophen, which has D_{50}, D_{90} and span values of 23.5 µm, 132 µm and 5.5 respectively would have a size classification code (SCC) of S1B3 (Table 4-8). In some cases the sieved fractions for the study materials contained a significant amount of agglomerated material which was not easily dispersed during particle size analysis, these materials were further designated with an asterisk * (Table 4-8).

Table 4-7 Size classification designation codes

D_{50}		D_{90}		Span	
Size (µm)	Designation Code	Size (µm)	Designation Code	Size	Designation Code
< 50	1	< 100	A	< 2	1
50 - 100	2	100 - 200	B	2 - 5	2
> 100	3	> 200	C	> 5	3

Table 4-8 Size reclassification for the selected sieved fractions for the study materials

Material	Size class based on Sieve used	D_{50}	D_{90}	Span	Size class based on PSA & microscopy (SCC)
Acetaminophen	A2	23.5	132	5.5	S1B3
Indomethacin	A2	24.4	94.7	3.7	S1A2
Loperamide HCl	A2	17.1	139	8.0	S1B3*
Salbutamol sulphate	A2	144	267	1.5	S3C1
Acetylsalicylic acid	A2	203	346	1.1	S3C1
Sulfamerazine	A2	33.8	67.0	1.6	S1A1
Phenacetin	A2	34.3	96.2	2.6	S1A2
Caffeine	A2	23.7	147	6.1	S1B3*
Methyl paraben	A2	63.7	157	2.2	S2B2*
Sulfadiazine	A1	10.6	42.8	5.5	S1A3

** indicates the presence of a significant amount of agglomerated particles*

4.3.3 X-ray powder diffraction (XRPD)

For each material a single representative XRPD pattern was obtained by averaging three replicates and the XRPD responses investigated. Table 4-9 provides details for the peak position and height of the most intense peak (MIP) and the %RPI significance value which was used to select the number of significant peaks for each material. This value was selected for each material based on the respective MIP height intensities as defined in APPENDIX 6 (worked example step 3). It was observed that for some materials (salbutamol sulphate, acetylsalicylic acid, phenacetin, caffeine, and methyl paraben) the MIP peak intensities were significantly larger than that observed for others. Large MIP peak height values reflect the particle size present in the material and the influence that particle size has on the XRPD responses[29,280]. However, based on this observation, loperamide HCl would have been expected to have had higher peak intensities, similar to caffeine which has the same size classification and observed particle sizes but this proved not to be the case. A likely reason for this could have been due to the dispersion of the loperamide HCl agglomerates during the XRPD sample preparation, while for caffeine the agglomerates remained intact.

Table 4-9 XRPD information for the selected study materials

Material	SCC	MIP (° 2θ)	MIP Height (cts)	% RPI Significance value	No. Significant peaks
Acetaminophen	S1B3	18.23	31181	5.0	17
γ-Indomethacin	S1A2	19.68	24805	5.0	32
Loperamide HCl	S1B3*	16.29	43235	5.0	23
Salbutamol sulphate	S3C1	10.60	297687	1.0	24
Acetylsalicylic acid	S3C1	15.65	714853	0.5	25
Sulfamerazine	S1A1	14.67	34175	5.0	21
Phenacetin	S1A2	13.72	298635	1.0	17
Sulfadiazine	S1A3	23.07	64213	5.0	15
Caffeine	S1B3*	12.01	138861	1.0	23
Methyl paraben	S2B2*	26.25	101681	2.0	24

SCC: size classification code, MIP: Most intense peak. Size class as defined in Table 4-7. cts: Counts. %RPI: % relative peak intensity

For each study material the average XRPD diffraction pattern was qualitatively compared to the simulated powder diffractograms constructed using the respective CSD reference data (see section 4.2.4.2 (Table 4-10)).

All of the study materials appeared crystalline, as assessed by XRPD. However, in a few cases the acquired XRPD pattern did not match that of the simulated powder diffractogram of the initial CSD reference (coloured red in Table 4-10).

Table 4-10 CSD Reference and solid-state forms for selected input materials

Material	Initial crystallographic (CSD) reference	Acquired XRPD concordant with crystallographic (CSD) reference	Solid-state form of study material
γ-Indomethacin	INDMET03	INDMET	Crystalline
Acetaminophen	HXACAN11	HXACAN19	Crystalline
Methyl paraben	CEBGOF01	CEBGOF	Crystalline
Salbutamol sulphate	SALBUT	SALBUT	Crystalline
Loperamide HCl	WAWVOH	WAWVOH	Crystalline
Caffeine	NIWFEE03	NIWFEE03	Crystalline
Sulfadiazine	SULDAZ02	SULDAZ02	Crystalline
Sulfamerazine	SLFNMA02	SLFNMA02	Crystalline
Phenacetin	PYRAZB21	PYRAZB21	Crystalline
Acetylsalicylic acid	ACSALA01	ACSALA01	Crystalline

Red entries indicate materials where the acquired XRPD diffractogram did not match the initial CSD reference

The crystallographic CSD references (from Chapter 2) for each material were initially selected based on their respective R-factor values, with the lowest R-factor value being selected[238]. However, in practice this entry may not be "truly" representative of the crystal lattice of the material purchased. Differences in preferred orientation and the

temperature at which single crystal data were collected could account for these discrepancies.

For those materials which did not match the initial crystallographic CSD reference the acquired XRPD diffractograms were compared to other simulated XRPD patterns for CSD entries of the same structural family. For example the XRPD diffractogram for bulk γ-Indomethacin was concordant with that of the simulated powder pattern for INDMET (R= 5.9 %) but not INDMET03 (R= 4.4 %) even though the latter had the slightly lower R-factor value (Figure 4-9). In this example, differences in peak intensities could account for some of the discrepancies as there was an indication of some degree of preferred orientation being present, *i.e.* differences in the most intense peak (MIP) and in the intensities of other peaks.

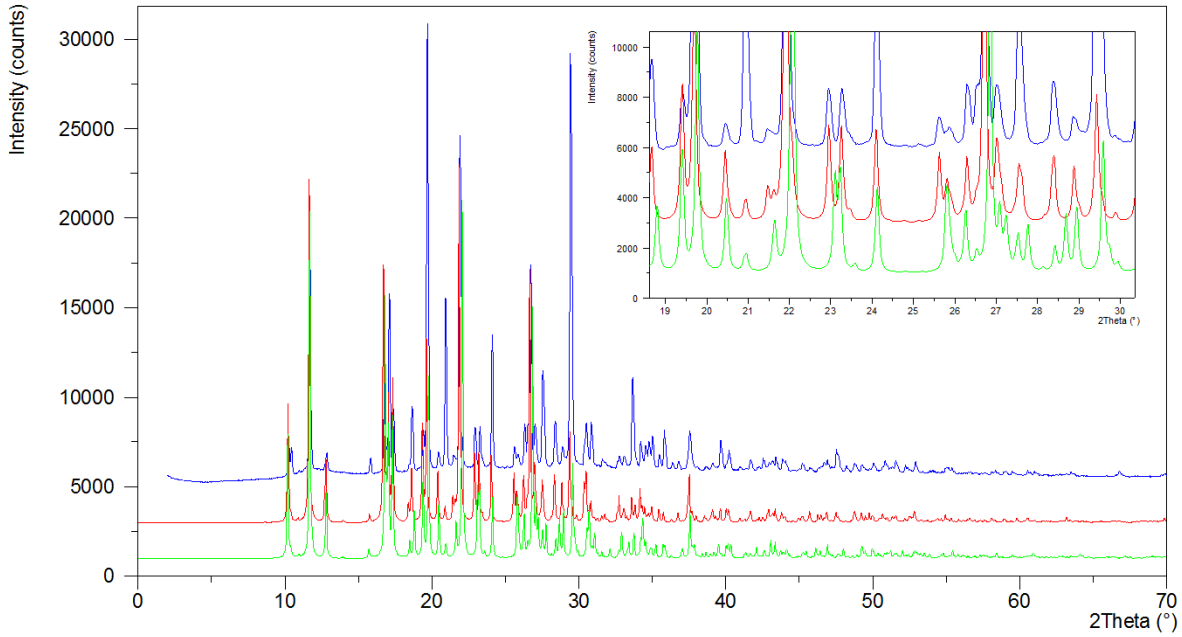

Figure 4-9 ***XRPD diffractograms for sieved γ-indomethacin (blue) and the reference simulated XRPD diffractograms INDMET (red) and INDMET03 (green).***
Differences in the patterns can be seen between 20 and 30 ° 2Theta (insert)

The amount of variation in the XRPD responses was also investigated. An overlay of the replicate XRPD patterns revealed only small differences in the peak, but other differences such as shifts in peak position, variations in background height, peak widths (FWHM) and peak areas were not so apparent. For example, in Figure 4-10, the replicate XRPD patterns for acetylsalicylic acid are overlaid. It can be seen that the only discernible difference between the replicates is in the peak heights and then only for a few peaks. However, numerical analysis of the variation in the replicate XRPD peak responses allows the amount of variation between replicates to be more readily identified and quantified. Variation (expressed as RSDs) in peak and background

height, peak width and area were calculated (similar to worked example in Appendix 6) to be 20, 12, 15 and 19 % respectively (inserted table in Figure 4-10). These RSDs and peak position ranges can be used to define acceptable tolerance levels for further investigations.

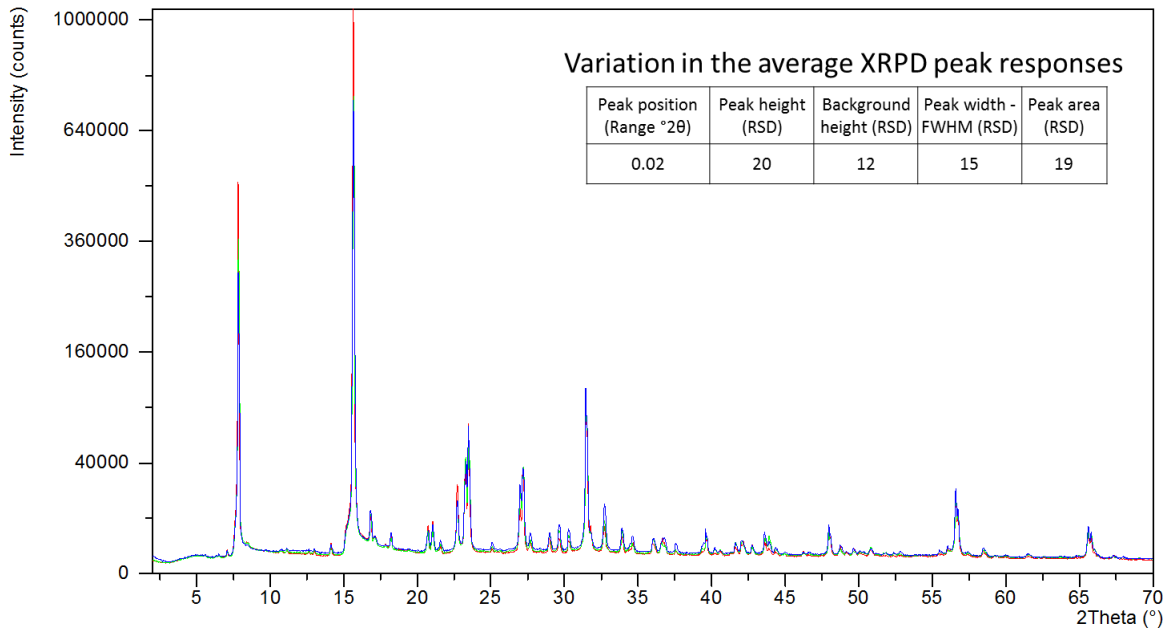

Figure 4-10 Overlaid XRPD diffraction patterns for three replicates (red, blue & green) of acetylsalicylic acid

Table 4-11, illustrates the observed variation in the average XRPD peak responses for the selected study materials calculated using the process defined in APPENDIX 6.

Table 4-11 Calculated variation in the average XRPD peak responses for the study materials

Material	SCC	n	Peak position (Range °2θ)	Peak height (RSD)	Background height (RSD)	Peak width - FWHM (RSD)	Peak area (RSD)
Acetaminophen	S1B3	3	0.02	15	4	15	19
γ-Indomethacin	S1A2	3	0.01	16	7	14	19
Loperamide HCl	S1B3*	3	0.02	12	5	10	17
Salbutamol sulphate	S3C1	3	0.03	16	7	16	18
Acetylsalicylic acid	S3C1	3	0.02	20	12	15	19
Sulfamerazine	S1A1	3	0.01	6	8	10	14
Phenacetin	S1A2	3	0.04	16	16	9	20
Sulfadiazine	S1A3	3	0.02	13	4	9	17
Caffeine	S1B3*	3	0.03	11	20	19	18
Methyl paraben	S2B2*	3	0.03	14	11	15	19

SCC: size classification code, Range and RSD values calculated using the process defined in APPENDIX 6.
n: number of replicates. RSD: relative standard deviation

The magnitude of the variation in the XRPD responses between replicates can be attributed to the physical properties of the materials. For example large particle sizes and particle morphologies such as plates, columnar and acicular can cause differences in the replicate responses as a result of preferred orientation generated during sample

preparation[29,280]. Other factors such as the amount of sample and silicone grease used during sample preparation could also influence the observed levels of variation in the XRPD peak responses, so care must be taken to minimise these influences[29,280]. Based on the RSD values (Table 4-11) for the average XRPD peak responses peak height, background height, peak width (FWHM) and peak area values, a limit of not greater than 20 % to the amount of variation (RSD value) that can typically be expected between replicates can be applied. While variation in the peak positions was found to be less than 0.05 °2θ for both the calculated average and individual peak positions.

The XRPD analysis applied in this research separates the background from the peak data, enabling a background profile to be visualised (Figure 4-11 and APPENDIX 5). It is important to note that this background profile represents not only the amount of disorder and microcrystalline material present but also background scattering due to the instrument and sample preparation (APPENDIX 5).

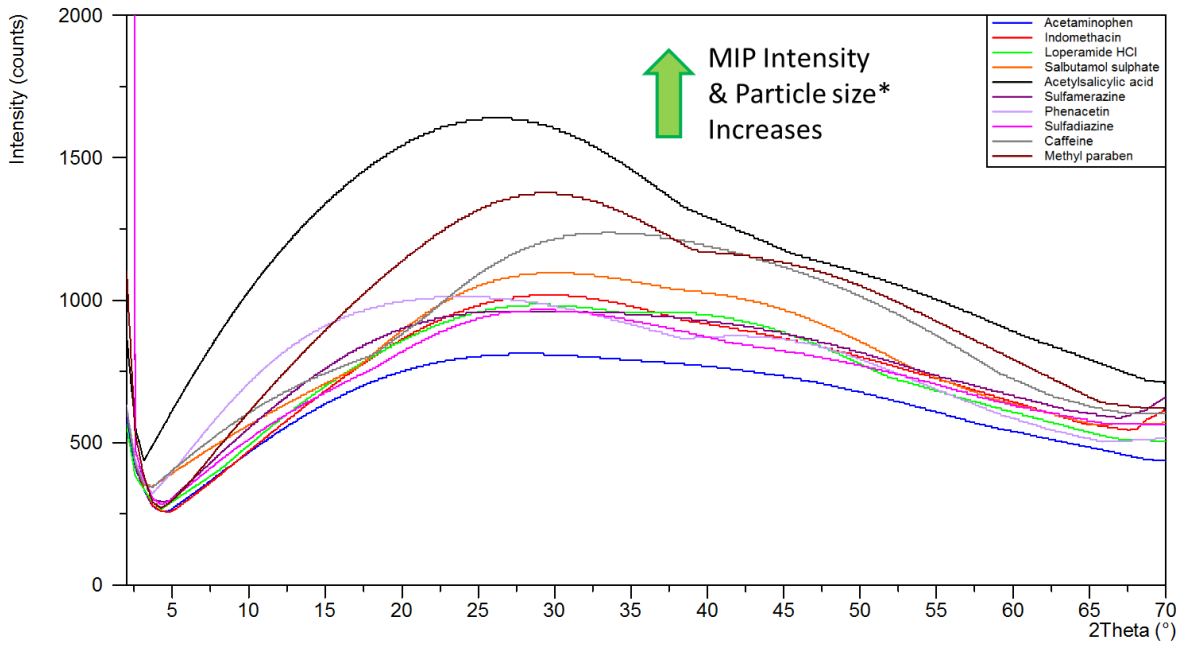

Figure 4-11 Average XRPD background profiles for the study materials (n=3 replicates)
** Particle size refers to the overall size including agglomeration.*

As illustrated in Figure 4-11, particle size and peak intensities appear to influence the height of the background profiles for crystalline materials: the larger the particle size and intensities of the MIPs the larger the background profiles. For example, acetylsalicylic acid and methyl paraben which have large particle sizes (size class S3C1) exhibit high intensity crystalline peaks (MIP >100 k cts) by XRPD compared to that of acetaminophen, which is comprised of smaller particles and has less intense XRPD peaks. However, caffeine has a larger background profile than other materials of similar particle size class due to the presence and the strength of agglomeration.

It is postulated that for materials exhibiting disorder, changes in the XRPD responses will occur over the whole of the XRPD pattern and not just in a few individual peaks. Changes in XRPD responses for only a few individual peaks are most likely due to orientation effects as a result of processing, such as a reduction in particle size rather than the presence of disorder. It is for this reason that it was proposed to investigate the changes in the average XRPD responses across the whole XRPD pattern in comminuted materials compared to those of the input material.

4.3.4 Fourier transform infra-red spectroscopy (FTIR)

FTIR spectra for the sieved study materials were obtained and shown to be concordant with those reported in the literature and from online databases (Table 4-12), confirming the solid state form purity observed by XRPD (Table 4-10). There appeared to be only small differences, but these generally arose as a consequence of differences in the sample preparations between the reference and acquired IR spectra, *i.e.* Nujol mull or KBr disc versus ATR used in this research respectively.

Table 4-12 Frequency assignment of IR peaks for the study materials

Material	Frequency assignment	FTIR Reference
Acetaminophen	3323 cm^{-1} (NH stretch), 3161cm^{-1} (H-bonded OH stretch), 1650 cm^{-1} (C=O amide stretching), 1562 cm^{-1} (N–H in-plane bending), 1328 cm^{-1} (O–H bending), 1259 cm^{-1} (C–O stretch), 1225 cm^{-1} (C–N amide stretch)	321-326
γ-Indomethacin	3023 cm^{-1} (O-H stretch), 1714 cm^{-1} (C=O stretch of cyclic dimer), 1690 cm^{-1} (C=O amide stretch),1613 cm^{-1} (N-H stretch),1478 cm^{-1} (C-C stretch)	45,212,325,327,328
Loperamide HCl	2959 cm^{-1} (C-H aromatic stretch),1623 cm^{-1} (C=O stretch tertiary amide),1484 cm^{-1} (C-C aromatic stretch), 1448 cm^{-1} (C-O-H stretch)	278,329-332
Salbutamol sulphate	3474 cm^{-1} (O-H stretch), 3409 cm^{-1} (N-H stretch), 1616 cm^{-1} (C-N stretch), 1507 cm^{-1} (C-N stretch), 1496 cm^{-1} (O-H bend), 1205 cm^{-1} (C-O phenolic stretch), 1112 cm^{-1} (C-O stretch), 1078 cm^{-1} (secondary alcoholic C–O stretch)	219,246,247,333
Acetylsalicylic acid	1750 cm^{-1} (C=O acetyl stretch ester), 1680 cm^{-1} (C=O stretch carboxylic acid),1605 cm^{-1} (C=C aromatic), 1482 cm^{-1} (C=C aromatic)	334
Sulfamerazine	3498 cm^{-1} (NH_2 stretch), 3482 cm^{-1} (NH_2 stretch), 1641 cm^{-1} (NH_2 scissoring), 1628 cm^{-1} (NH_2 scissoring), 1326 cm^{-1} (S=O stretch), 1304 cm^{-1} (Aromatic-N stretch), 1150 cm^{-1} (S=O stretch)	335-337
Phenacetin	3283 cm^{-1} (N-H stretch), 3073 cm^{-1} (aromatic-H stretch), 2928 cm^{-1} (C-H stretch amide), 2885 cm^{-1} (C-H stretch), 1658 cm^{-1} (C=O stretch), 1645 cm^{-1} (C-NH deformation), 1480 cm^{-1} (C-H bend), 1265 cm^{-1} (C-N stretch)	325,326
Sulfadiazine	3424 cm^{-1} (NH_2 stretch), 3356 cm^{-1} (NH_2 stretch),1653 cm^{-1} (NH_2 scissoring), 1580 cm^{-1} (NH_2 scissoring), 1326 cm^{-1} (S=O stretch), 1153 cm^{-1} (S=O stretch),	338
Caffeine	1694 cm^{-1} (C=O stretch), 1599 cm^{-1} (C-N stretch), 1547 cm^{-1} (C-N stretch),	339
Methyl paraben	3285 cm^{-1} (O-H stretch) 1678 cm^{-1} (C=O stretch), 1513 cm^{-1} (Phenol C-O stretch), 1433 cm^{-1} (Enol C-O stretch)	340

4.3.5 Thermogravimetric analysis (TGA) and differential scanning calorimetry (DSC)

The thermal properties for the selected sieved fractions were determined by TGA (Table 4-13) and DSC analysis (Table 4-14). Overall the onset temperatures of melting (T_m) for

the materials were consistent with those cited in the literature and/from databases[232,320,341] (Table 4-14). All of the materials appeared anhydrous, as determined by TGA and the very small WL_{50} and WL_{150} values. A number of materials, such as phenacetin, exhibit a broad weight loss event associated with thermal degradation below 150 °C. For caffeine this broad weight loss event is associated with sublimation[216,342,343]. As a consequence of such degradation occurring below 150°C, WL_{150} values could not be calculated and these materials are denoted with a D in Table 4-13. All materials exhibited degradation below 290 °C and these degradation temperatures were used to select the appropriate end-point temperatures when the DSC studies were undertaken. The small amount of weight loss observed, *i.e.* below 0.5% (w/w) for WL_{50} and WL_{150} for the materials is likely to be due to experimental noise. As these values are relatively small, any variation between the replicates resulted in large RSD values being obtained. Therefore, any WL_{50} and WL_{150} values less than 0.5% (w/w) are denoted as < 0.5% for later studies.

Table 4-13 Summary of average TGA responses for the sieved study materials

Material	WL_{50} % w/w (RSD)	WL_{150} % w/w (RSD)	T_d ° C (range)	Comments
Acetaminophen	0.07 (0)	0.30 (3)	235 (2.1°C)	No weight loss events observed before degradation
γ-Indomethacin	0.05 (0)	0.20 (25)	266 (0.3°C)	No weight loss events observed before degradation
Loperamide HCl	0.12 (25)	0.29 (17)	262 (3.2°C)	No weight loss events observed before degradation
Salbutamol sulphate	0.09 (33)	0.24 (21)	197 (0.2°C)	Unresolved weight loss event is observed on degradation
Acetylsalicylic acid	0.07 (29)	D	126 (3.1°C)	Unresolved weight loss event is observed on degradation, Degradation starts below 150 °C
Sulfamerazine	0.07 (14)	0.15 (27)	255 (3.1°C)	No weight loss events observed before degradation
Phenacetin	0.10 (20)	D	198 (0.9°C)	Degradation starts below 150 °C
Sulfadiazine	0.20 (10)	0.49 (4)	263 (0.3°C)	Unresolved weight loss event is observed on degradation
Caffeine	0.17 (6)	D	201 (1.6°C)	Sublimation starts below 150 °C
Methyl paraben	0.03 (33)	D	115 (1.8°C)	Unresolved weight loss events observed on degradation, Degradation starts below 150 °C

Number of replicates n = 3, WL_{50}: % Weight loss (w/w) below 50° C. WL_{150}: % Weight (w/w) loss below 150 °C. D: Degrades below 150 °C, T_d: Degradation temperature (°C). Please refer to Table 3-4 for further descriptions of the terms

Table 4-14 Summary of average DSC responses for the sieved study materials

Material	Lit.T_m* °C	T_m °C (range)	ΔH_f J/g (RSD)	WHH °C (range)	$T_{m\text{-}p}$ °C (range)	$T_m trans$ °C (range)	T_d °C (range)	Comments
Acetaminophen	168-172	169.0 (0.1°C)	185 (1.1)	0.9 (0.4°C)	169.7 (0.3°C)	0.6 (0.3°C)	ND	
γ-Indomethacin	158-162	159.5 (0.3°C)	107 (0.9)	1.3 (0.3°C)	160.5 (0.4°C)	1.0 (0.2°C)	ND	
Loperamide HCl	228	227.2 (1.4°C)	90 (2.2)	2.3 (0.4°C)	229.3 (1.6°C)	2.2 (0.7°C)	235.5 (2.5°C)	Potential melt degradation
Salbutamol sulphate	198	196.7 (2.6°C)	165 (1.8)	8.9 (1.2°C)	204.1 (0.7°C)	7.4 (2.3°C)	204.1** (0.6°C)	Potential melt degradation
Acetylsalicylic acid	134	139.3 (1.2°C)	169 (2.4)	2.6 (1.5°C)	141.2 (3.3°C)	1.9 (2.5°C)	146.4 (2°C)	Potential melt degradation
Sulfamerazine	236	235.9 (1.4°C)	141 (2.8)	1.3 (0.4°C)	236.9 (0.1°C)	1.0 (1.5°C)	ND	
Phenacetin	135	134.4 (0.7°C)	170 (3.5)	1.2 (0.6°C)	135.5 (0.8°C)	1.1 (1.3°C)	ND	
Sulfadiazine	251	261.3 (3°C)	169 (4.1)	0.8 (0.2°C)	261.5 (2.8°C)	0.2 (0.7°C)	266.8 (2.8°C)	Potential melt degradation
Caffeine	238	236 .0 (0.2°C)	NC	NC	236.4 (0.1°C)	0.5 (0.2°C)	236.4** (0.1°C)	Transition at 146 °C observed, melt-sublimination
Methyl paraben	127	125.8 (0.3°C)	165 (2.4)	1.2 (0.5°C)	127 (0.9°C)	1.2 (0.7°C)	ND	

Number of replicates n = 6, ND: Not detected, NC: Not calculated, T_d: Degradation temperature (°C), T_m: Onset of melting temperature (°C), $T_m trans$: Melting transition range (°C), ΔH_f: Heat of fusion (J/g), WHH*: width at half peak height (°C), $T_{m\text{-}p}$: Peak melting temperature (°C). Please refer to Table 3-6 for further descriptions of the terms*
** Literature T_m*[232,320,341]
*** $T_{m\text{-}p}$ value used to represent T_d as material melts-degrades or melt-sublimes*

For some materials the first derivative signal in the TGA can indicate that unresolved weight loss events may be occurring upon degradation which may coincide with melting, *i.e*. melt-degradation event. For example the first derivative signals for the TGA and DSC analyses of salbutamol sulphate (Figure 4-12) suggested multiple unresolved events occurred around the melt at 198 °C and decomposition at 204 °C events. Melting occurs initially, involving the dissociation of the sulphate, followed immediately by degradation[1,19,297]. Typically, materials that exhibit melt-degradation events have larger WHH and $T_m trans$ values as shown for salbutamol sulphate and acetylsalicylic acid (Table 4-14). These materials also typically exhibit more variation in their DSC responses as shown by the RSD and range values (Table 4-14). Based on the observed variations in the DSC responses for the materials, temperature values for the same material should fall within 4 °C for materials exhibiting unresolved melt-degradation events and 2 °C for materials that have resolved melting events. However, it should be noted that, in cases where the melt-degradation or sublimation events cannot be resolved, values for WHH and heats of fusion (ΔH_f) may not be accurately determined. For these materials, $T_{m\text{-}p}$ values can be used to indicate the start of degradation and $T_m trans$ values can be used as an indicator of melting broadness. For

example, WHH and ΔH_f could not be determined for caffeine, which exhibits a melt sublimation event around 236 °C, hence, $T_{m\text{-}p}$ of 238 °C was used to indicate the start of degradation temperature with a $T_m trans$ value of 1.6 °C to describe melting broadness (Table 4-14). An endothermic event representing a form II to form I solid-state transition for caffeine was also observed around 145 °C consistent with literature observations[216,217,342,343] (Figure 4-13).

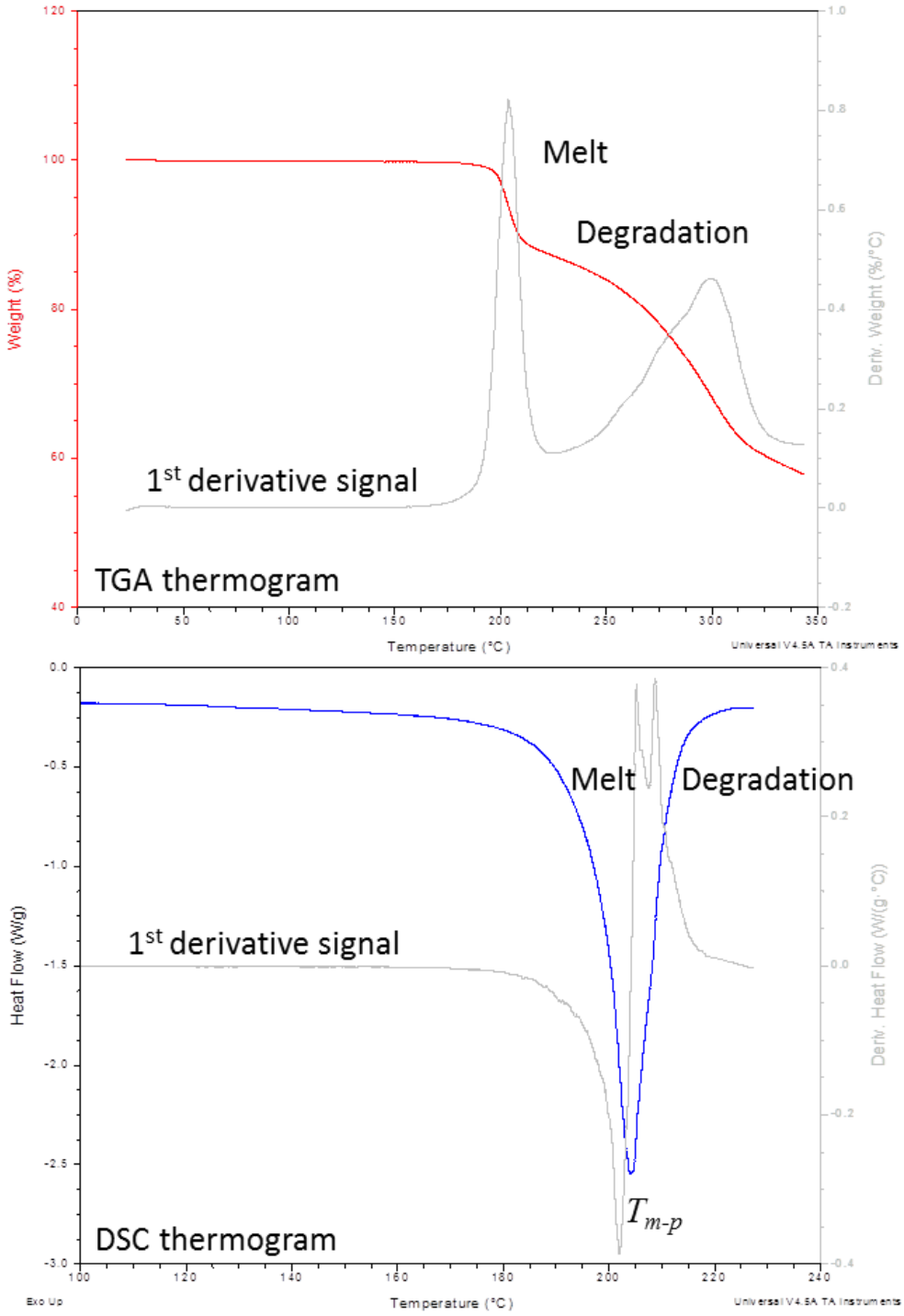

Figure 4-12 TGA and DSC thermograms for salbutamol sulphate

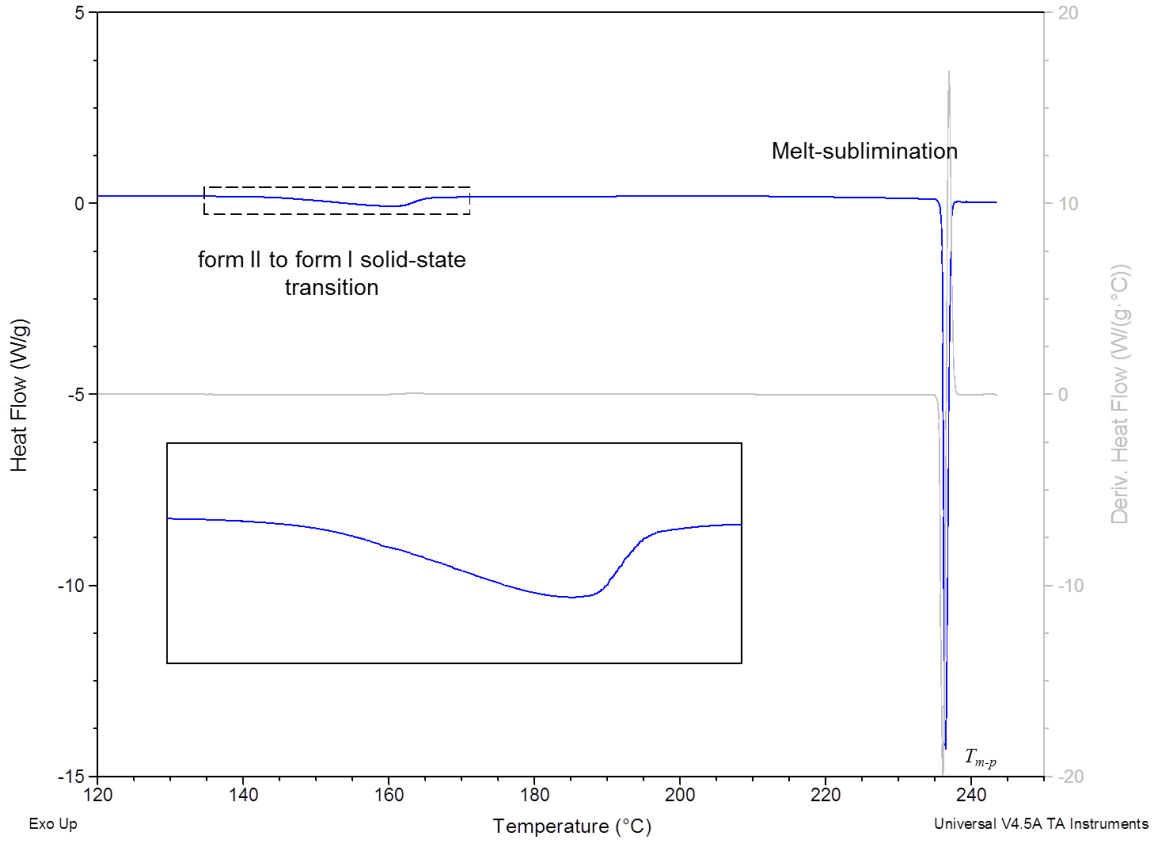

Figure 4-13 DSC thermogram for caffeine

When interpreting DSC data, it is important to consider the effects of other material properties and sample preparation on the observed DSC responses[288,289]. Large sample weights may cause thermal lags and event broadening while particle size can affect heat transfer properties. The larger the particle size the smaller the surface area, therefore the material will be in contact with the sample pan less resulting in less heat transfer. A thermal gradient can also occur within the sample, whereby smaller particles can melt first resulting in broader, unresolved or split peaks depending on the size of particles present[288,289]. It has also been shown that sample weights can influence DSC responses[288,289] and therefore, so as to minimise the influence of sample weight on the thermal responses, sample weights were kept at a minimum during the current study. Accordingly, only 1-2 mg of each material was employed and particle size was measured and taken into consideration during interpretation.

4.3.6 High pressure liquid chromatography (HPLC)

A fast gradient HPLC method[315] was used to first identify the wavelength of maximum absorbance (λmax) using a diode array detector for each study material (Table 4-15). This wavelength was then used to identify the retention times of the major peak and that of any other peaks for each study material (Table 4-15).

Table 4-15 Summary of HPLC results for the selected sieved fractions of the study material

Material	Max absorbance Wavelength λmax (nm)	No. Peaks	Primary peak RT, min (% area in brackets)	Other Peaks RT, min (% area in brackets)
Acetaminophen	240	1	1.56 (100)	--
γ-Indomethacin	240	3	5.33 (99.65)	5.71 (0.05), 6.35 (0.3)
Loperamide HCl	220	3	4.53 (99.8)	2.57 (0.07), 4.26 (0.13)
Salbutamol sulphate	225	2	1.88 (99.8)	2.61 (0.2)
Acetylsalicylic acid	235	2	2.91 (99.4)	3.09 (0.6)
Sulfamerazine	240	3	2.06 (99.76)	1.77 (0.08), 3.10 (0.16)
Phenacetin	245	4	3.17 (99.5)	2.06 (0.03), 3.48 (0.27), 3.57 (0.2)
Sulfadiazine	265	1	1.67 (100)	--
Caffeine	265	1	2.27 (100)	--
Methyl paraben	260	1	3.04 (100)	--

To demonstrate the suitability of the HPLC method in detecting thermal degradants, post-DSC samples were analysed at the selected wavelengths for indomethacin, loperamide HCl, salbutamol sulphate and caffeine (Table 4-16). These results demonstrate that the HPLC method was capable of detecting thermal degradants of the material understudy. Though the primary peak was reduced by only 3.45% in area for the DSC sample of indomethacin seven new peaks were observed, suggesting that some thermal degradation had occurred. The material following DSC analysis was also discoloured (light brown) which further indicates thermal degradation had occurred. For the DSC sample of loperamide HCl, the primary peak was reduced by 8.7% in area and another identified peak (RT 2.57 min) increased in area 1.84%. Eleven new peaks were observed verifying the TGA and DSC interpretation that the melting of loperamide HCl is closely followed by degradation. HPLC analysis of the DSC sample for salbutamol sulphate also verified that a melt-degradation event occurs, as the area of the primary peak was reduced by 43.1% and another identified peak (RT 2.60 min) increased in area by 19.8%. There were also 20 new peaks observed. However, HPLC analysis of post-DSC caffeine did not detect any degradation products as a consequence of the melt-sublimation event.

From the HPLC results, it can be seen that all materials were of high purity, but upon melting, degradation may occur for a number of materials which could impact chemical purity. For these materials the use of quench-cooling to generate amorphous materials or standards could potentially introduce thermal degradants and influence any acquired analytical responses. Hence, quench-cooling was not used in this thesis.

Table 4-16 Summary of HPLC results for samples analysed after DSC analysis

Material	No. Peaks	Primary peak RT, min (% area in brackets)	Reference Peaks RT, min (% area in brackets)	New Peaks RT, min (% area in brackets)
γ-Indomethacin	9	5.34 (96.2)	6.35 (0.3)	3.09 (0.22), 4.58 (0.37), 4.76 (0.12), 4.96 (0.69), 6.53 (0.25), 6.82 (1.72), 6.92 (0.08)
Loperamide HCl	13	4.54 (91.08)	2.57 (1.91)	1.9 (0.18), 3.16 (0.15), 3.61 (0.44), 4.46 (0.18), 4.76 (1.53), 4.96 (1.41), 5.13 (0.33), 5.88 (0.94), 6.13 (0.28), 6.72 (0.41), 6.82 (1.16)
Salbutamol sulphate	22	1.89 (56.7)	2.60 (20.04)	1.67 (4.19), 2.02 (0.24), 2.19 (1.75), 2.26 (0.28), 2.30 (0.18), 2.34 (0.33), 2.41 (0.41), 2.48 (1.40), 2.53 (0.36), 2.73 (0.79), 2.83 (3.82), 2.91 (1.80), 3.00 (1.74), 3.09 (0.68), 3.11 (0.77), 3.19 (0.62), 3.23 (0.22), 3.38 (2.57), 3.46 (0.55), 3.50 (0.53)
Caffeine	1	2.27 (100)		--

4.3.7 Gravimetric vapour sorption (GVS)

Moisture sorption profiles for the selected study materials were obtained and the responses tabulated (Table 4-17). These results verify the TGA, DSC and FTIR observations that initially the materials appear anhydrous and further show that after a two moisture sorption/desorption cycles little or no moisture sorption is observed indicating that the input materials are moisture stable between 0-90 % RH (Table 4-17). A representative moisture sorption profile illustrating the moisture sorption stability of the materials is shown in Figure 4-14 for indomethacin which exhibits a reversible change in mass of less than 0.1 % over the 0-90 %RH range.

Table 4-17 Summary of GVS results for the study material sieved fractions

Material	M_A	M_B	M_C	M_D	M_E	ΔM_F	M_{END}	M_{MAX1}	M_{MAX2}	ΔMAX	M_{ADS}
Acetaminophen	0.04	0.07	0.00	0.03	0.01	0.01	-0.03	0.07	0.03	0.03	0.03
γ-Indomethacin	0.02	0.09	0.00	0.09	0.00	0.02	0.00	0.09	0.09	0.00	0.00
Loperamide HCl	0.05	0.13	0.00	0.12	0.00	0.03	-0.01	0.13	0.12	0.01	0.01
Salbutamol sulphate	-0.01	0.04	0.00	0.04	0.00	0.00	0.01	0.04	0.04	0.00	0.00
Acetylsalicylic acid	0.00	0.01	0.00	0.01	0.00	0.00	0.00	0.01	0.01	0.00	0.00
Sulfamerazine	0.06	0.22	0.00	0.20	-0.07	0.00	-0.06	0.22	0.20	0.03	0.03
Phenacetin	0.00	0.10	0.00	0.10	0.00	0.00	0.00	0.10	0.10	0.00	0.00
Sulfadiazine	-0.05	0.07	0.00	0.06	-0.01	0.00	0.05	0.07	0.06	0.01	0.01
Caffeine	-0.01	0.13	0.00	0.11	0.00	0.02	0.03	0.13	0.11	0.02	0.02
Methyl paraben	0.00	0.02	0.00	0.01	0.00	0.00	0.00	0.02	0.01	0.01	0.01

$M_{\#}$: % mass change at %RH points A (30%RH, B (90%RH), C (0%RH), D (90%RH), E (0%RH), and F (30%RH), $M_{END:}$ difference between final (F) and initial (A) values. M_{MAX1} and M_{MAX1} are the maximum % mass change observed during first and second adsorption intervals (ADS1 and ADS2). ΔMAX is the difference in M_{MAX1} and M_{MAX1} values. M_{ADS} is the difference in % change in mass between points B and D, i.e. at 90 %RH for adsorption cycles 1 and 2. Please refer to Table 3-11 for further descriptions of the terms

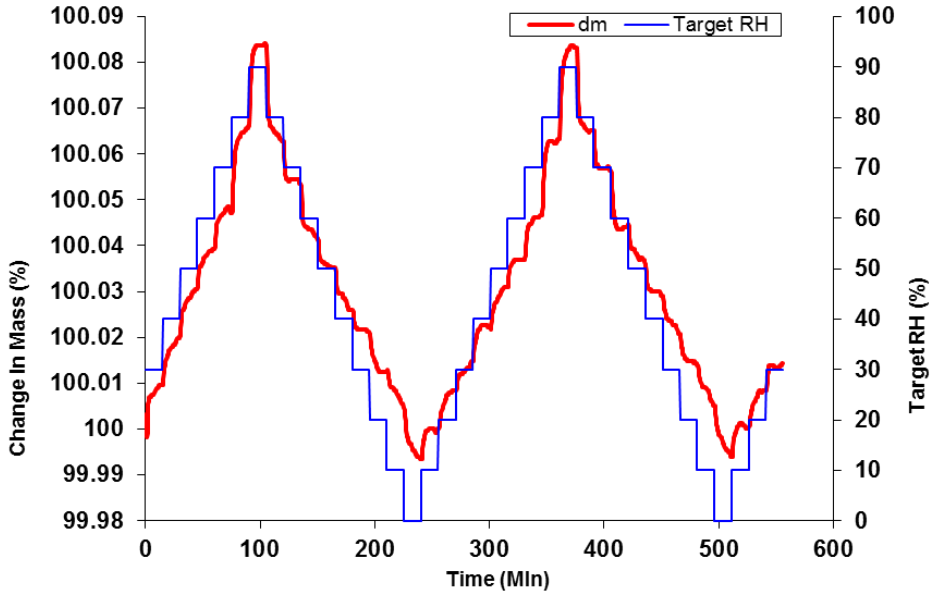

Figure 4-14 Two-cycle GVS moisture sorption profile for γ-indomethacin

4.4 Conclusions

In this chapter, the ten selected study materials were classified into different particle size fractions by mechanical sieving and the sieving efficiency investigated using a combination of laser particle size and optical and electron microscopy. It was shown that the sieving process was effective in separating the materials into different particle size fractions. However, these particle size fractions were not necessarily consistent with the mesh size used (Table 4-5). For each study material one sieved fraction was selected and defined with respect to particle size using a novel approach according to their microscopy and particle size values (Table 4-8). The selected sieved fractions for the materials were then successfully characterised using the core test methods (XRPD, IR, TGA, DSC, HPLC and GVS). The analytical property responses (APRs) from these core techniques demonstrated that the all the sieved powders were highly crystalline as shown by the intense and sharp diffraction peaks in the powder X-ray patterns and the observance of birefringence under a polarized-light microscope. Additionally, all materials were shown to be anhydrous as indicated by the relatively small mass changes in their TGA thermograms and GVS moisture sorption profiles. The APRs from these core tests will also act as reference values that will be used to compare with the responses of the corresponding mechanically comminuted materials. The amount of experimental and instrumental variations in the observed APRs was also estimated and these values will be used to define what constitutes a marked change in the analytical responses during the comparative response analysis (CRA) of the processed material in Chapter 6.

5 Mechanical comminution of input materials

5.1 Introduction

Ten study materials have been fractionated into different particle size fractions by sieving and one of the fractions was then selected and characterised using the core test methods (Chapter 4). These selected fractions were then used as the input material to be mechanically comminuted by ball-milling and jet-milling (micronisation) under varying operating parameters.

An overview of the mechanical comminution process was given previously (Section 1.4.2) along with an introduction to the principles of ball- and jet-milling with respect to their uses within the pharmaceutical industry (Sections 1.4.3 and 1.4.4).

The primary aim of this chapter was to obtain mechanically comminuted material which can then be used to investigate the respective analytical property responses (APRs) using the core test methods as described in Chapter 3. It is envisioned that different levels of PID may be obtained by employing both ball- and jet-milling for materials that maybe susceptible to PID and this variation can translate into different analytical response levels which can be investigated using the core test methods.

5.2 Input materials

The materials selected (sieved fractions) to be used as the input materials for both the ball-milling and micronisation processes are given in Table 4-8.

5.3 Mechanical comminution methods

5.3.1 Ball-milling methods (Mill-A & Mill-B)

Two ball-milling methods utilising primarily different ball sizes, milling frequencies and periods were employed to mechanically comminute the input materials using the conditions as outlined in Table 5-1 to potentially generate different levels of PID in materials that maybe susceptible to PID. These methods will commonly be referred to as the high frequency (Mill-A) and low frequency (Mill-B) milling methods.

Method Mill-A, is a high energy comminution process that vibrates a larger milling ball at a higher frequency, for a longer period then method Mill-B, hence, method mill-A is more likely to generate PID of the two methods.

Table 5-1 Ball-milling method conditions and operating parameters

Process	Variable	Method Mill-A	Method Mill-B
Milling Jar preparation	Jar size (cm^3)	50	50
	Ball size (mm)	20	15
	Number of balls	1	1
	Charge size (g)	2	2
Milling parameters	Cycle mill time (min)	5	5
	Cycle pause/cool time (min)	2	2
	No. cycles	12	6
	Total mill time (min)	60	30
	Cryogenic cooling with liquid nitrogen	Yes	Yes
	Frequency (Hz)	25	15

For each ball-milling method (Table 5-1), 2 g of the input material were weighed (charged) into a stainless-steel milling jar with the appropriate sized stainless-steel milling ball. The milling jars were then sealed inside a glove box purged with dry nitrogen gas to minimise surface adsorption of atmospheric water which has the potential to promote recrystallisation during milling. The sealed milling jars were then immersed in a Dewar containing liquid nitrogen for 15 min. Following cryo-cooling the milling jars were fixed into place on the MM301 Retsch bench-top mixer-mill (details in APPENDIX 4) and milled using the operational parameters as outlined in Table 5-1. Materials were milled at 5 min intervals with a 2 min pause between milling cycles to reduce any localised temperature build-up[22]. After every 15 min of milling time, the milling jars were re-immersed in a Dewar containing liquid nitrogen for 5 min.

At the completion of milling, the milling jars were placed in a glove box purged with dry nitrogen gas and the comminuted material transferred to a pre-weighed glass container before sealing. The %RH within the glove box was shown to be 3-5 %RH as determined using a portable %RH meter (details in APPENDIX 4). To ensure homogeneity of the materials for analysis, the containers were mixed using a spiral mixer (details in APPENDIX 4) for 5 min prior to the start of analysis using the core test methods. In addition, in order to aid in the dissipation of any generated electrostatic charge the sealed containers were placed in front of a SIMCO sentry ionizing air blower (details in APPENDIX 4) for 10 min.

Throughout the milling process the environmental relative humidity (%RH) and temperature were monitored and recorded. Any material observations were also recorded, such as electrostatic behaviour, change in colour and general handling. The

ratio of milling ball weight to charge (*BCR*) and % yield were also reported for each material using the equations given below:

$$BCR = \frac{\text{Milling ball weight (g)}}{\text{Charge weight (g)}} \quad [5\text{-}1]$$

$$\%\ \text{yield} = \frac{\text{Weight of milled material (g)}}{\text{Charge weight (g)}} \text{ x } 100 \quad [5\text{-}2]$$

For each study material, the selected sieved fractions were milled using both ball-milling methods (Mill-A and Mill-B) at least once. However, to demonstrate repeatability of the milling process, the milling of acetaminophen, indomethacin and salbutamol sulphate were performed in duplicate and on different days. In addition to the methods described above, salbutamol sulphate was also ball-milled using method Mill-A without cooling in liquid nitrogen to control the milling temperature, with a view to investigate whether or not limited or no temperature control can affect PID generation; all the other method parameters and timings remained the same for this investigation.

5.3.2 Jet-milling (micronisation) method (JM-A)

Jet micronisation was performed only once for each study material using the process described below.

In a Class II cabinet with a dry nitrogen gas atmosphere, approximately 1 g of input material was manually feed into a JETPHARMA MC One jet-mill microniser (details in APPENDIX 4) over a 4 min period. Micronisation was performed using a venturi (feed) and ring (grind) pressure of 8 and 6 bar respectively with nitrogen as the carrier gas[344]. Micronisation was stopped approximately 1-2 min after the final addition of material.

At the completion of micronisation the collection vessel was disassembled in a glove box purged with dry nitrogen gas and the micronised material transferred to a pre-weighed glass container before sealing. The %RH within the glove box was shown to be 3-5 %RH, as determined using a portable %RH meter (APPENDIX 4). To ensure homogeneity of the materials for analysis, the contents of the containers were mixed using a spiral mixer (details in APPENDIX 4) for 5 min prior to the start of analysis. In addition, in order to aid in the dissipation of any electrostatic charge the sealed containers were placed in front of a SIMCO sentry ionizing air blower (details in APPENDIX 4) for 10 min.

Throughout the micronisation process the environmental relative humidity (%RH) and temperature were monitored and recorded. Any material observations were also recorded, such as electrostatic behaviour, change in colour and general handling. The amount of time taken to feed the charge and total micronisation time were reported for each material and the feed rate (*FR*) and % yield calculated using the equations given below:

$$FR\ (\text{gmin}^{-1}) = \frac{\text{Charge weight (g)}}{\text{Feed time (min)}} \quad [5\text{-}3]$$

$$\%\ \text{yield} = \frac{\text{Weight of micronised material (g)}}{\text{Charge weight (g)}} \times 100 \quad [5\text{-}4]$$

5.4 Results & discussion

The potential for crystalline pharmaceutical material to undergo mechanically activation or disordering has been investigated for a number of materials[137,160,192,221]. However, these studies involved variations in milling time and intensity to produce complete disordering of the crystalline material so as to generate the amorphous state. In the current study, a more systematic and controlled investigation into the milling and micronisation behaviour was performed. The same mechanical comminution process and operational parameters were employed for all of the study materials to mimic the "reality" of generating unintentional induced disorder, rather than over-processing with the intent to completely collapse the crystal lattice. To this end, two ball-milling methods, involving low and high frequency were employed to comminute mechanically the input materials. These methods differed not only in their operational frequency but also in the size of the milling balls used and in the time of milling (Table 5-1). It is proposed that by ensuring the same processing conditions are employed for each material, the relative amounts of any observed disorder can be compared across the materials. In addition by designing the study to ensure that different processing conditions were applied to the same material, any difference in the levels of PID that might be generated for materials with the propensity for PID could be assessed as a function of the selected conditions.

All of the materials were cryogenic ball-milled using liquid nitrogen to ensure that milling occurred below room temperature. Milling below room temperature is thought to reduce the conversion of any generated transient disordered solid to another more stable form during the milling process. The low temperature might also be expected to

render the sample more brittle (less elastic) and therefore more amenable to size reduction[137,146,160,191,192,221,247,345]. However, for one milling investigation involving salbutamol sulphate, cryogenic ball-milling was not performed with a view to investigating any differences between this material and the material cryogenic ball-milled. Salbutamol sulphate was chosen for this investigation as it has been reported previously to exhibit PID[1,20,21,246,247,275-277], has a low T_g (°C) and has been shown to exhibit a melt-degradation event (Section 4.3), hence, any increase in internal milling temperature could affect PID generation as well as chemical and solid state form stability. The importance of local %RH and temperature has been highlighted by the investigation by Burnett *et al.*[311] in which the recrystallisation of disordered salbutamol sulphate was studied using GVS at different temperatures. It was found that as temperature was increased the amount %RH required to initiate recrystallisation decreased. Therefore, by ensuring the milling temperature is controlled using liquid nitrogen and using a dry nitrogen atmosphere to charge the milling jars, precautions have been taken to reduce the influence of local %RH and milling temperatures to cause recrystallisation of any transient or permanent PID material during ball-milling.

Table 5-2 summaries the post milling observations along with the reported *BCR* and % yield values for the study materials ball-milled using the two methods. In general, the high frequency ball-mill method generated material which was more electrostatic. The most notable observation was for γ-indomethacin, which upon milling changes colour from white to bright yellow and formed lumps and a hard layer that encased the milling ball (Figure 5-1).

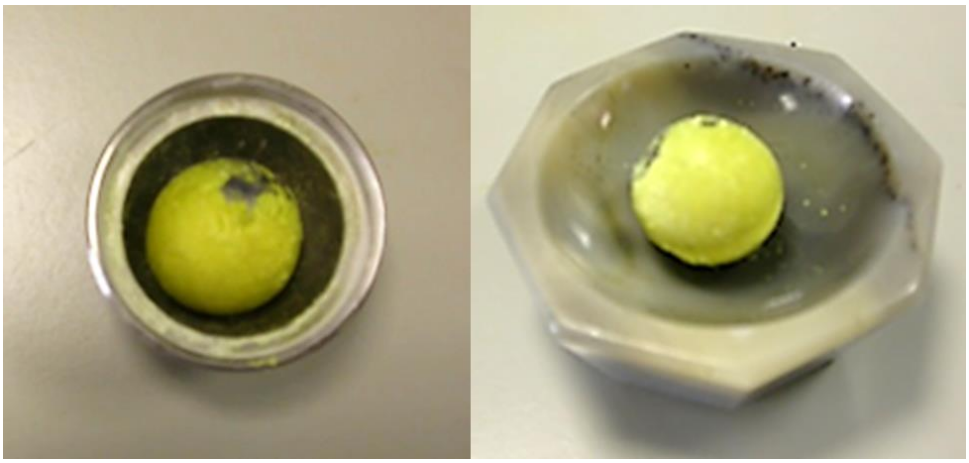

Figure 5-1 Post milling images of the milling ball for γ-indomethacin after high frequency ball-milling (method Mill-A)

Table 5-2 Summary of reported observations and % yields for the cryogenic ball-milling of the study materials

Material	Mill method	Mill batch ID	Ball/Charge ratio (*BCR*)	% yield	Observations post ball-milling	Electrostatic
Acetaminophen	Mill-A1	1-MA1	16	81	White powder, no colour change	Yes
	Mill-A2	1-MA2	16	89	White powder, no colour change	Yes
	Mill-B1	1-MB1	7	85	White powder, no colour change	Yes
	Mill-B2	1-MB2	7	83	White powder, no colour change	Yes
γ-Indomethacin	Mill-A1	11-MA1	16	65	Colour change- yellow clumpy powder	Yes
	Mill-A2	11-MA2	15	72	Colour change from white free-flowing to a yellow clumpy powder	Yes
	Mill-B1	11-MB1	7	87	Colour change- yellow powder	Slightly
	Mill-B2	11-MB2	7	81	Colour change- yellow powder	Slightly
Salbutamol sulphate	Mill-A1	24-MA1	16	72	White powder, no colour change	Yes
	Mill-A2	24-MA2	15	89	White powder, no colour change	Yes
	Mill-A3*	24-MA3	15	89	White powder, no colour change	Yes
	Mill-B1	24-MB1	7	88	White powder, no colour change	Slightly
	Mill-B2	24-MB2	7	88	White powder, no colour change	Slightly
Loperamide HCl	Mill-A1	14-MA1	16	79	White powder, no colour change	Yes
	Mill-B1	14-MB1	7	91	White powder, no colour change	Slightly
Acetylsalicylic acid	Mill-A1	33-MA1	16	75	White powder, no colour change	No
	Mill-B1	33-MA2	7	88	White powder, no colour change	Slightly
Sulfamerazine	Mill-A1	54-MA1	16	87	White powder, no colour change	Yes
	Mill-B1	54-MA2	7	88	White powder, no colour change	Slightly
Phenacetin	Mill-A1	69-MA1	16	88	White powder, no colour change	Yes
	Mill-B1	69-MA2	7	91	White powder, no colour change	Slightly
Sulfadiazine	Mill-A1	87-MA1	16	88	White powder, more free flowing after milling	No
	Mill-B1	87-MA2	7	90	White powder, no colour change	No
Caffeine	Mill-A1	88-MA1	16	79	White powder, no colour change	No
	Mill-B1	88-MA2	7	84	White powder, no colour change	No
Methyl paraben	Mill-A1	140-MA1	16	89	White powder, no colour change	No
	Mill-B1	140-MA2	7	92	White powder, no colour change	No

** milled without liquid nitrogen*

To demonstrate reproducibility of the milling processes, acetaminophen, indomethacin and salbutamol sulphate were milled in duplicate and on different days using both Mill-A and Mill-B methods. These materials were chosen as they reflect the potential extremes when milled, from stable crystalline (acetaminophen[160,221]) to disordered (γ-indomethacin[148,160,178,212,221,268,271] and salbutamol sulphate[1,20,21,246,247,275-277]). The % yields for all materials were fairly similar and generally high, which is expected, as the ball-milling process is a closed comminution process (Section1.4.3) with all the material retained within the milling jars. Any material lost is due to retention of material on the sides of the milling jar and around the milling balls as was illustrated for γ-

indomethacin (Figure 5-1). Any material adhering to either the milling ball or jar was scraped off gently and included in the final yield.

Micronisation of the materials was performed under a dry nitrogen atmosphere, to reduce the effects of environmental RH. Though the local environment (laboratory) was generally held at a constant temperature, it was noted that during the micronisation process, heat was generated by this high energy process. This was detected as an increase in temperature within the collection vessels at the end of the micronisation process. Initially the temperature at the start of micronisation was around 25 ± 5 °C but this rose to 35 ± 2 °C at the end of micronisation. Based on this observation it is likely that the temperature within the grinding ring could be markedly higher and as a consequence this could have affected the extent of any PID that might have been generated. This slightly contradicts previous assumptions that jet-milling with air as the grinding media can help to cool or dissipate any generated heat thereby avoiding excessive heat and contamination during its operation[180].

It has been noted in the literature that low temperature milling is more efficient in generating amorphous material than at room temperature[146,345], hence, at elevated temperatures any transient meta-stable phases or solid-state forms may be lost, which might not be detected.

The degree of comminution obtained by micronisation depends on the critical milling parameters. The most important parameters are feed rate, feed pressure and grind pressure[21,344]. Micronisation feed and grind pressures of 8 and 6 bar respectively were selected based on pharmaceutical industry guidance[344] and on investigations by Brodka-Pfeiffer *et al.*[21], in which salbutamol sulphate was micronised at different pressures. It was shown that a grind pressure of 6 bar was effective to achieve a potentially respirable particle size distribution, with only a small amount of generated disorder. Above 6 bar the effect of the grind pressure decreased as, once a certain pressure has been reached, no further increase in the maximum jet speed (sonic velocity) can be obtained[21]. Feed pressure is generally set at a higher value than the grinding pressure and must be sufficient to prevent any clogging. In this study feed pressure was set at 8 bar based on manufacturer and industry reccomendations[344]. By applying similar low feed rates across the materials, 0.23 to 0.29 $gmin^{-1}$ (Table 5-3), the amounts of material introduced within the grinding chamber were similar, thus particles would readily be accelerated upon entry. If the material concentration inside the grinding chamber was too large then a decrease in inter-particulate acceleration distance would result, giving

rise to coarser particles[21]. The amount of micronised material (% yield) collected for all the materials were similar but lower than those obtained by ball-milling (Table 5-3).

Table 5-3 Summary of reported observations and % yields for the micronisation of the study materials using method JM-A

Material	Mill batch ID	Feed time (min)	Feed rate, *FR* ($gmin^{-1}$)	Process time (min)	% yield	Observations post micronisation	Electrostatic
Acetaminophen	1-X1	4.5	0.23	6.0	69	No colour change, but induced agglomeration	Very
γ-Indomethacin	11-X1	4.2	0.26	5.2	69	Colour change from white to slightly yellow	Yes
Salbutamol sulphate	24-X1	4.0	0.22	5.0	58	No colour change	Yes
Loperamide HCl	14-X1	4.3	0.25	5.3	69	Colour change from white to slightly grey	Yes
Acetylsalicylic acid	33-X1	4	0.28	5.0	52	No colour change	Yes
Sulfamerazine	54-X1	4	0.26	5.0	68	Colour change from white to slightly off-white	Yes
Phenacetin	69-X1	3.8	0.27	4.8	71	No colour change	Yes
Sulfadiazine	87-X1	5	0.26	6.0	68	No colour change, more free flowing	Slightly
Caffeine	88-X1	3.7	0.29	4.7	60	No colour change	Yes
Methyl paraben	140-X1	3.5	0.29	4.5	67	No colour change	No

The majority of the micronised materials were electrostatically charged which may have been accentuated by the dry nitrogen atmosphere environment employed during the process (Table 5-3). The most charged was acetaminophen which resulted in agglomeration of the material. However, applying an ionizing airflow to this material tended to dissipate this electrostatic charge and reduce agglomeration. Some micronised materials also exhibited a limited amount of colour change (Table 5-3), γ-indomethacin, became slightly yellow when micronised but the final colour was much less intense than that for the ball-milled samples. For loperamide HCl and sulfamerazine there was some slight discoloration from the white powdered input material, which could be indicative of thermal or chemical changes (Table 5-3).

5.5 Conclusions

In this chapter the selected study materials were successfully mechanically comminuted by ball-milling using two different conditions and by jet micronisation. Characterisation of these processed materials follows in the proceeding chapters (Chapter 6 and 7).

6 Characterisation of mechanically comminuted material

6.1 Introduction

In the previous chapter the ten model materials were mechanically comminuted to produce material with potentially differing amounts of PID depending on the comminution process and the material's inherent propensity for PID.

The aim of this chapter was to characterise the selected materials that were comminuted mechanically previously (Chapter 5) using the described core test methods (Chapter 3). The APRs obtained from each core test method would then be compared to those of the relative input materials that were analysed under standard conditions (Chapter 4). It was planned to do this using a novel approach termed comparative response analysis (CRA). Based on the CRA evaluations, the relative amounts of change in each APR obtained from the individual analytical techniques could then be defined and quantified and used to determine if the comminution processes were successful in generating material that encompassed the whole amorphous-crystalline continuum.

6.2 Materials

Table 6-1 lists the mechanically comminuted study materials that were characterised using the core test methods (Chapter 3). At least three batches of each material, one from each comminution method (Mill-A, Mill-B and JM-A) were characterised.

Table 6-1 Mechanically comminuted material characterised using the core test methods

	Particle size class of input material		Number of batches per milling method			
Material	PSC	SCC	Mill-A	Mill-B	JM-A	Total No. batches
Acetaminophen	A2	S1B3	2	2	1	5
γ-Indomethacin	A2	S1A2	2	2	1	5
Salbutamol sulphate	A2	S3C1	2 & 1**	2	1	6
Loperamide HCl	A2	S1B3*	1	1	1	3
Acetylsalicylic acid	A2	S3C1	1	1	1	3
Sulfamerazine	A2	S1A1	1	1	1	3
Phenacetin	A2	S1A2	1	1	1	3
Sulfadiazine	A1	S1A3	1	1	1	3
Caffeine	A2	S1B3*	1	1	1	3
Methyl paraben	A2	S2B2*	1	1	1	3

** indicates the presence of a significant amount of agglomerated particles,* ** Milled without liquid nitrogen.

PSC: particle size class based on sieved fraction, SCC: size classification code Mill-A high frequency ball-mill method A, Mill-B: low frequency ball-mill method B. JM-A: jet micronisation method A. Methods are described in 5.3.1 and 5.3.2 respectively

6.3 Methods

To ensure that the comminuted materials were analysed consistently and efficiently the materials were analysed using the same order of techniques immediately after completion of the comminution process. Typically the analysis protocol was started within 30 min of completing the comminution process (Table 6-2). For the first four techniques, samples were prepared quickly (less 3 min each) and acquisition initiated before starting sample preparation for the remaining techniques. These four techniques were selected first as any disorder present could be either directly observed, or would identify the presence of water. The latter, if present could affect the stability of the solid-state phase or form present in the comminuted material.

Table 6-2 Order of analysis for the characterisation of mechanically comminuted material

Order of analysis	Technique	Acquisition and RA methods - see section	CRA method - see section
1	X-ray powder diffraction (XRPD)	3.2.1 3.2.2 6.3.1	6.3.1.2
2	Thermogravimetric analysis (TGA)	3.3.1 3.3.2 6.3.2.1	6.3.2.2
3	Differential scanning calorimetry (DSC)	3.4.1 3.4.2 6.3.3.1	6.3.3.2
4	Gravimetric vapour sorption (GVS)	3.7.1 3.7.2 6.3.6.1	6.3.6.2
5	Laser particle size analysis (PSA)	3.6.1 3.6.2 6.3.4.1	6.3.4.2
6	Scanning electron microscopy (SEM)	3.5.2 3.5.3 6.3.5.1	6.3.5.2
7	Fourier transform infra-red spectroscopy (FTIR)	3.9.1 3.9.2 6.3.7.1	6.3.7.2
8	High pressure liquid chromatography (HPLC)	3.8.1 3.8.2 6.3.8.1	6.3.8.2

To ensure homogeneity of the comminuted material prior to analysis, each material was thoroughly mixed using a spiral mixer and any electrostatic charge was dissipated (Section 5.3). Exposure to the environment was also minimised as much as practically possible during sample preparation procedures and the temperature and %RH monitored and recorded.

For each analytical technique, the acquisition and response analysis method along with the CRA process are described in each section. The CRA process for each technique defines the relevance of the amount of change between the analytical responses of the material being investigated (comminuted material) and that of the input/reference material. The limits to define the level of relevance for changes in the APRs for the individual techniques are based on the observed variations in the responses for the input/reference materials as reported earlier (Chapter 4) as well as applicable pharmaceutical industry and instrument supplier recommendations.

6.3.1 X-ray powder diffraction (XRPD)

6.3.1.1 *XRPD acquisition and response analysis*

X-ray powder diffraction patterns for mechanically comminuted materials were obtained using the method described in Section 3.2.1. For each comminuted material, three replicate sample preparations were prepared and a single representative XRPD pattern obtained by averaging the replicates using the PANalytical X'Pert HighScore Plus (version 3.0) software (Section 3.2.1.1). The averaged XRPD patterns were then analysed using the processes described in Section 3.2.2 and the individual peak responses tabulated using five peak descriptors; peak position (P_P), peak height or intensity (P_H), peak width (P_W), peak area (P_A) and background height (B_H). These five XRPD peak descriptors or responses, best represent the key indicators to describe individual peak characteristics and changes in these values will be investigated as part of the comparative response analysis process.

6.3.1.2 *Comparative response analysis of XRPD diffractograms*

CRA between the responses of the comminuted material XRPD diffractogram and those of the input/reference material were determined by investigating the changes between responses in the individual peak characteristics of the most significant peaks in the input and comminuted material averaged across the whole XRPD diffractogram. Any changes to the MIP positions and MIP intensities were also determined.

The XRPD diffractograms of the comminuted and input/reference were overlaid using the PANalytical's X'Pert Data viewer (v1.3) and the peaks inspected visually in conjunction with the tabulated peak lists. The presence or absence of the significant peaks (peaks with % RPI above the defined % RPI value) in both diffractograms was determined by peak matching using a similar method to Patel *et al.*[346] and defined using novel peak designators, as described below. The labeling of the peaks is illustrated in Figure 6-1. If a significant input/reference peak was absent in the XRPD diffractogram

for the comminuted material, these were denoted with an **A**. If a new peak was observed in the comminuted material, these were designated with a **N**. However, if a comminuted material peak had broadened or merged such that it overlaid a number of reference peaks and could not be resolved, then these were denoted with an **M** along with the peak position value for the maxima of the broadened peak (see Figure 6-1).

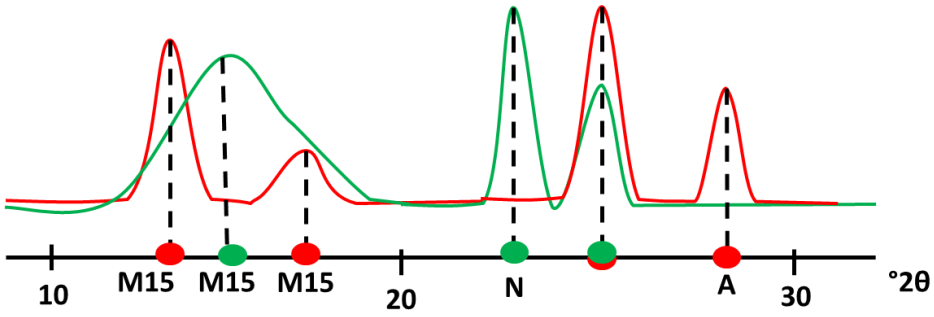

Figure 6-1 ***Example of an overlaid reference (red) and comminuted (green) XRPD diffractogram illustrating the labeling of the peaks.***

M refers to merged or broadened peaks and the value represents the peak position of the maxima of the broadened/merged peak. N represents a new peak not present in the reference and A represents an absent reference peak.

For each significant peak tabulated, changes in the five key XRPD peak descriptor values and the MIP position and MIP intensity (height) were determined using the equations defined below and the amount of change in the peak descriptor responses were then qualified using the limits defined in Table 6-3.

Average changes in individual peak position (ΔP_P) and average peak shifting ($Av\Delta P_P$) across the whole diffractogram are given by:

$$\Delta P_P\ (°2\theta) = \text{Sample peak position } P_P - \text{Reference peak position } P_P \quad [6\text{-}1]$$

$$Av\Delta P_P\ (°2\theta) = \frac{\text{Sum of changes in individual peak shifts } \Delta P_P}{\text{number of significant peaks in sample}} \quad [6\text{-}2]$$

Percentage changes in the individual peak responses (%Δ"*RSP*") and average peak responses (AvΔ"*RSP*") across the whole diffractogram are given by the general equations:

$$\%\Delta\text{“}RSP\text{”}\ (\%) = \left(\frac{\text{Sample peak “}RSP\text{” - Reference “}RSP\text{”}}{\text{Reference “RSP”}}\right) \text{x } 100 \quad [6\text{-}3]$$

$$Av\Delta\text{“}RSP\text{”}\ (\%) = \frac{\text{Sum of \% changes in individual peak “}RSP\text{”}}{\text{number of significant peaks in sample}} \quad [6\text{-}4]$$

where "*RSP*" can be peak height (P_H), peak widths (P_W using FWHM), peak areas (P_A) or background height (B_H).

Percentage change in MIP intensity ($\%\Delta MIP_H$) is given by:

$$\%\Delta MIP_H(\%) = \left(\frac{\text{Sample MIP height (cts)} - \text{Reference MIP height (cts)}}{\text{Reference MIP height (cts)}}\right) \times 100) \quad [6\text{-}5]$$

Table 6-3 Qualitative relevance of CRA values for key XRPD peak descriptors over the whole XRPD diffractogram

XRPD Response	Average amount of change (Δ) across all peaks	Qualitative relevance of the amount of change in XRPD responses and observations of comminuted material
Peak position P_P	A few new peaks (N)	Some new peaks observed suggesting presence of a new solid state form
	All new peaks (N)	Suggests presence of a new solid state form
	Merged peaks (M)	Some reference peaks broadened or merged
	A few Absent peaks (A)	Some reference peaks missing in sample XRPD
	No peaks present (A)	Suggests material is XRPD amorphous
	$-0.03 < Av\Delta P_P < 0.03$	Peak positions remains relatively unchanged
	$Av\Delta P_P > 0.03$	Peaks generally shifted to the higher angles inferring contraction of the unit cell[347]
	$Av\Delta P_P < -0.03$	Peaks generally shifted to the lower angles inferring expansion of the unit cell[347]
Peak height P_H	$-20\% < Av\Delta P_H < 20\%$	Peak heights remains relatively unchanged
	$Av\Delta P_H < -20\%$	Reduced peak heights observed
	$Av\Delta P_H > 20\%$	Increased peak heights observed
Peak widths P_W	$-20\% < Av\Delta P_W < 20\%$	Peak widths remains relatively unchanged
	$Av\Delta P_W < -20\%$	Peaks becoming narrower and more sharper
	$Av\Delta P_W > 20\%$	Peaks becoming broader
Peak areas P_A	$-20\% < Av\Delta P_A < 20\%$	Peak areas remains relatively unchanged
	$Av\Delta P_A < -20\%$	A decrease in overall peak areas observed
	$Av\Delta P_A > 20\%$	An increase in overall peak areas observed
Background height B_H	$-20\% < Av\Delta B_H < 20\%$	Background height remains relatively unchanged
	$Av\Delta B_H < -20\%$	A decrease in background height observed
	$Av\Delta B_H > 20\%$	An increase in background height observed
MIP position MIP_P	Different MIP	Change in MIP may suggest the presence of preferred orientation or a new solid state form
	No Change	MIP remains the same
MIP height MIP_H	$-20\% < \%\Delta MIP_H < 20\%$	MIP height remains relatively unchanged
	$\%\Delta MIP_H < -20\%$	Intensity of MIP decreased
	$\%\Delta MIP_H > 20\%$	Intensity of MIP increased

$Av\Delta P_P$*: amount of average peak shifting.* $Av\Delta P_H$*: % change in average peak height.* $Av\Delta P_W$*: % change in average peak width (*FWHM*). AvΔP*$_A$*: % change in average peak area.* $Av\Delta B_H$*: % change in average background height*

In Table 6-3 the threshold limits for changes in the peak descriptors were based on the replicate analysis of the input materials using values selected just above the calculated instrumental and sample preparation variance (Table 4-11).

6.3.1.3 *Qualitative classification of solid state phase based on changes in XRPD responses*

Using the observed changes in the XRPD responses (CRA values) and the relative threshold limits as defined in Table 6-3, the comminuted materials could be qualitatively classified as being crystalline, microcrystalline, disordered or X-ray amorphous using novel definitions and decision tree (Table 6-4 and Figure 6-2).

Table 6-4 ***Qualitative classification of solid-state phase present based on changes in XRPD responses over the whole XRPD diffratogram***

Solid state phase	XRPD characteristics of comminuted material	Illustrative XRPD
Crystalline (Concordant with reference)	XRPD diffractogram is identical to a reference with same MIP, peak positions, similar %RPIs, peak widths and background heights	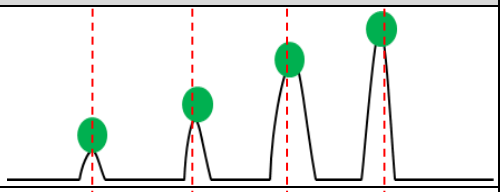
Crystalline (preferred orientation)	XRPD diffractogram is similar to a reference with similar peak positions. However, MIP and peak heights are different	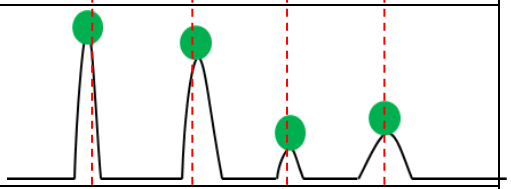
Crystalline (mixed solid state forms)	XRPD diffractogram contains new peaks along with peaks concordant with the reference	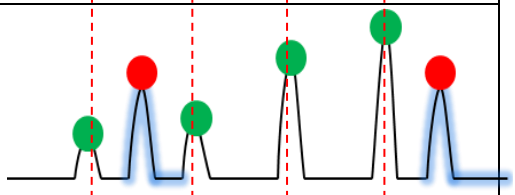
Crystalline (New solid state form)	XRPD diffractogram contains all new peaks	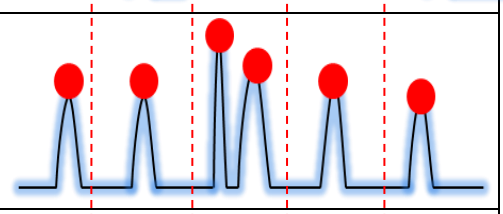
Microcrystalline (Due to decrease in particle size not an increase in disorder.)	XRPD diffractogram has similar peak positions as the reference. However, MIP is different, peaks are broader and the background height may be increased.	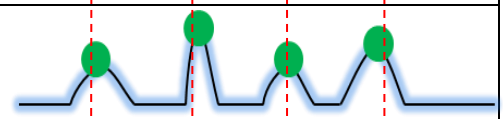
Disordered	Peaks have generally shifted and broadened with a decrease in height. The background height has also increased	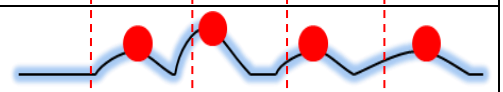
X-ray amorphous	A “halo” or large background is observed in the XRPD diffractogram with no discernable peaks implying complete disorder of the crystal lattice	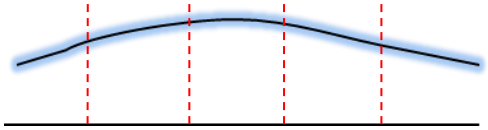

Green dots identify agreement in peak positions while red dots signify new peaks or shifts in peak positions

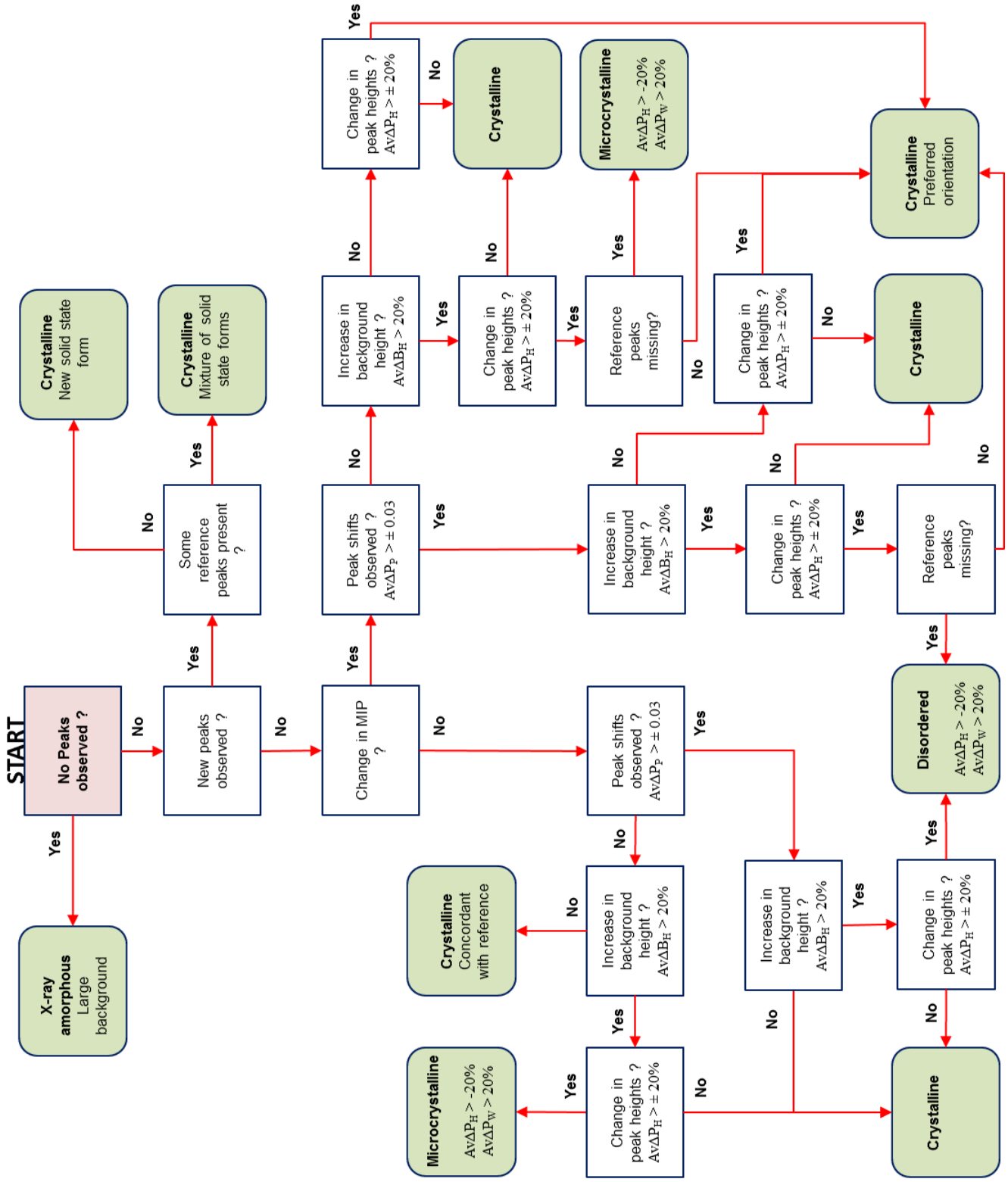

Figure 6-2 Decision tree for the qualitative classification of solid state phases by XRPD

$Av\Delta P_P$*: amount of average peak shifting.* $Av\Delta P_H$*: % change in average peak height.* $Av\Delta P_W$*: % change in average peak width (*FWHM*).* $Av\Delta B_H$*: % change in average background height.* MIP*: Most intense peak.*

6.3.2 Thermogravimetric analysis (TGA)

6.3.2.1 *TGA acquisition and response analysis*

TGA thermograms for the mechanically comminuted materials were obtained and analysed using the methods described in Sections 3.3.1 and 3.3.2 respectively. Each study material was analysed in duplicate and the responses averaged.

Based on the TGA analysis of the input/reference material (Chapter 4) any observed weight loss below 0.5% (w/w) for WL_{50} and WL_{150} is assumed to be due to experimental noise and was therefore reported as "< 0.5% (w/w)". For materials which started to thermally degrade below 150 °C, WL_{150} values could not be calculated and so these were denoted as "D".

6.3.2.2 *Comparative response analysis of TGA thermograms*

CRA was performed by comparing the differences in the weight loss profiles and thermal responses of the comminuted material TGA thermogram with those of the input/reference obtained under the same acquisition conditions (Section 3.3.1). The amount of change in four key TGA responses was determined using the equations defined below and the qualitative relevance of these changes defined (Table 6-5).

Change in % weight loss below 50 °C (ΔWL_{50}) is given by:

$$\Delta WL_{50}\,(\%) = \text{Sample } WL_{50} - \text{Reference } WL_{50} \qquad [6\text{-}6]$$

if either the sample or reference WL_{50} value is less than 0.5 % w/w, then 0.5 is used in the equation for either or both values.

Change in % weight loss below 150 °C (ΔWL_{150}) is given by:

$$\Delta WL_{150}\,(\%) = \text{Sample } WL_{150} - \text{Reference } WL_{150} \qquad [6\text{-}7]$$

if either the sample or reference WL_{150} value is less than 0.5 % w/w, then 0.5 is used in the equation for either or both values.

For both ΔWL_{50} and ΔWL_{150} a negative value indicates a decrease in weight loss, *i.e.* the reference had more volatiles (moisture) present, while a positive value indicates that the comminuted material being examined had more volatile (moisture) material present.

Shift in degradation temperature (ΔT_d) is given by:

$$\Delta T_d\,(^\circ\text{C}) = \text{Sample } T_d - \text{Reference } T_d \qquad [6\text{-}8]$$

A negative value indicates a shift to lower temperature and therefore a potential decrease in thermal stability which can be indicative of the presence of amorphous or

disordered phases. While a positive value indicates a shift to a higher temperature and potentially an increase in thermal stability.

In Table 6-5 the threshold limits for defining the qualitative relevance of the amount of change in TGA responses and observations were selected using values just above the calculated instrumental and sample preparation variance using data from the replicate analysis of the input materials and pharmaceutical industry recommendations[288] (Table 4-13).

Table 6-5 Qualitative relevance of CRA values for key TGA responses

TGA Response	Amount of change Δ	Qualitative relevance of the amount of change in TGA responses and observations of comminuted material
Change in number of weight loss events $\#W_E$	$\Delta\#W_E = 0$	No change in number of events
	$\Delta\#W_E$ negative	Indicates a decrease in number of events and may suggest some volatile/moisture has been removed
	$0 < \Delta\#W_E < 3$	Suggests a small increase in number of events and may suggest moisture may have been absorbed or the sample is less stable
	$\Delta\#W_E > 3$ or continuous weight loss	May infer large thermal instability
Change in weight loss (% w/v) below 50°C WL_{50}	$-0.25 < \Delta WL_{50} < 0.25$	No change in weight loss below 50 °C
	$\Delta WL_{50} < -0.25$	A decrease in weight change may indicate reference contained volatiles
	$0.25 < \Delta WL_{50} < 1.0$	Some loosely bound volatile (moisture) present
	$\Delta WL_{50} > 1.0$	Marked loosely bound volatile (moisture) present
Change in weight loss (% w/v) below 150°C WL_{150}	$-0.25 < \Delta WL_{150} < 0.25$	No change in weight loss below 150 °C
	$\Delta WL_{150} < -0.25$	A decrease in weight change may indicate reference contained volatiles or moisture
	$0.25 < \Delta WL_{150} < 1.0$	Some bound volatile (moisture) present
	$\Delta WL_{150} > 1.0$	Marked bound volatile (moisture) present
	Degrades below 150°C	WL_{150} cannot be determined so denoted as "D"
Shift in degradation temperature T_d (°C)	$-5 < \Delta T_d < 5$	No change in thermal degradation temperature
	$\Delta T_d > 5$	Improved thermal stability
	$-5 < \Delta T_d < -10$	A decrease in thermal stability
	$\Delta T_d > -10$	Marked decrease in thermal stability

$\Delta\#W_E$: change in number of weight loss events observed, ΔWL_{50}: change in weight loss below 50°C, ΔWL_{150}: change in weight loss below 150°C, ΔT_d: change in degradation temperature.

6.3.3 Differential scanning calorimetry (DSC)

6.3.3.1 *DSC acquisition and response analysis*

DSC thermograms for the mechanically comminuted materials were obtained and analysed using the methods described in Sections 3.4.1 and 3.4.2 respectively. Each study material was analysed in triplicate and the responses averaged.

As a number of materials exhibit melt-degradation the typical indicator for peak broadness, width at half peak height (WHH) value cannot be determined. Hence, $T_m trans$ which represents the temperature range of melting was used as an indicator of the broadness of the melting event.

6.3.3.2 *Comparative response analysis of DSC thermograms*

CRA of the acquired DSC thermograms was performed by comparing the differences in the thermal responses associated with five major thermal events; melting (M), degradation (D), volatile loss (V), glass transition (G) and recrystallisation (C) of the comminuted sample DSC thermogram with that of the input/reference obtained under the same acquisition conditions (Section 3.4.1).

Two general equations (equations [6-9] and [6-10]**)** can be derived to compare the thermal responses, allowing the qualitative relevance of these changes to be defined for each type of thermal event, G, V, C, M, and D that maybe present (Table 6-6).

Shifts in temperature responses (Δ"*T*") are defined by:

$$\Delta\text{“}T\text{”}\ (^\circ\text{C}) = \text{Sample “}T\text{”} - \text{Reference “}T\text{”} \qquad [6\text{-}9]$$

where "*T*" can be melting onset (T_m), temperature range of melting ($T_m trans$), degradation onset (T_d), desolvation onset (T_v), or crystallisation onset (T_c).

Percentage changes in enthalpic responses (%Δ"*H*") are defined by:

$$\%\Delta\text{“}H\text{”}\ (\text{J/g}) = \left(\frac{\text{Sample “}H\text{” - Reference “}H\text{”}}{\text{Reference “}H\text{”}}\right) \times 100 \qquad [6\text{-}10]$$

where "*H*" can be heat of desolvation (ΔH_v), heat of crystallisation (ΔH_c), or the heat of fusion (ΔH_f).

In Table 6-6 the threshold limits for defining the qualitative relevance of the amount of change in DSC responses and observations were selected using values just above the calculated instrumental and sample preparation variance using data from the replicate analysis of the input materials and pharmaceutical industry recommendations[288] (Table 4-14).

Table 6-6 Qualitative relevance of CRA values for the DSC thermal responses

DSC event	DSC Response or observation	Amount of change Δ	Qualitative relevance of the amount of change in DSC responses and observations of comminuted material
M	No melt	No melt observed	Infers presence of disorder*.
	More than one melt	Additional melting event(s) observed	May suggest presence of a new form*.
	Melting onset, T_m	$\Delta T_m < \pm 3$ °C	Effectively no change in melting onset.
		$\Delta T_m > -3$ °C	A decrease in melting onset as a result of impurities or thermal degradants or it may indicate the presence of a new form*.
		$\Delta T_m > 3$ °C	An increase in melting onset as a result of improved solid state purity or it may indicate the presence of a new solid state form*.
	Melting transition range, $T_m trans$	$\Delta T_m trans < \pm 3$ °C**	Effectively no change in melting transition range.
		$\Delta T_m trans > -3$ °C**	Melting transition range narrower as a result of improved solid state purity or a change in particle size.
		$\Delta T_m trans > 3$ °C**	Melting transition range broadened as a result of a decrease in solid state purity , crystallinity or a change in particle size.
	Heat of fusion, H_f	$\%\Delta H_f < \pm 25$ %**	Effectively no change in heat of fusion.
		$\%\Delta H_f > -25$ %**	Heat of fusion reduced as a result of a decrease in solid state purity or crystallinity.
		$\%\Delta H_f > 25$ %**	Heat of fusion increased as a result of improved solid state purity or crystallinity.
D	No degradation	No degradation observed	Material thermally stable over DSC acquisition range. If degradation event has been removed this may indicate the material has become more thermally stable.
	New degradation	New degradation event observed	New degradation event observed inferring decreased thermal stability.
	Degradation onset, T_d	$\Delta T_d < \pm 3$ °C	No change in thermal degradation temperature.
		$\Delta T_d > -3$ °C	A decrease in thermal degradation due to impurities or increased disorder.
		$\Delta T_d > 3$ °C	Higher degradation may infer increased thermal stability due to new form if a new T_m observed or improved crystallinity.
V	No volatile event	No volatile event observed	No solvent/moisture present respectively.
	New volatile event	New volatile event observed	Could infer the presence of absorbed water.
	Volatile loss onset, T_v	$\Delta T_v < \pm 3$ °C	No change in volatile onset.
		$\Delta T_v > \pm 3$ °C	Infers a shift in temperature of volatile loss This could be related to changes in particle size and/or strengths of solvent absorption.
	Heat of desolvation, H_V	$\%\Delta H_V < \pm 25$ %**	Effectively no change in the heat of desolvation.
		$\%\Delta H_V > -25$ %**	Amount of solvent/moisture present has decreased.
		$\%\Delta H_V > 25$ %**	Amount of solvent/moisture present has increased.
G	No glass transition event	No glass transition observed	No glass transition observed over the analysis temperature range selected or ca not be discerned.
	New glass transition event	New glass transition observed	If a glass transition event is observed a recrystallisation event is likely to be observed as well. Infers presence of disorder.
C	No new crystallisation	No new recrystallisation event observed	No new recrystallisation event observed over the analysis temperature range.
	New crystallisation event	New recrystallisation observed	Recrystallisation may result in the same solid state form or a new form with a corresponding new T_m. May infer the presence of disorder.

M*: melting events.* D*: degradation events.* V*: volatile loss events.* G*: glass transition events.* C*: recrystallisation event.* ΔT_m*: Shift in melting onset.* $\Delta T_m trans$*: change in Melting transition range.* $\%\Delta H_f$*: % Change in heat of fusion.* ΔT_d*: change in degradation onset.* ΔT_v*: change in volatile loss onset.* $\%\Delta H_v$*: % Change in heat of desolvation.*

** Check XRPD for confirmation of presence of another solid state form*

*** Applicable only if referring to the same reported event*

The appearance of new glass transition (G) and/or crystallisation (C) events provides direct evidence to support the presence of disorder in material following comminution. However, it must be noted that the absence of a T_g event does not exclude the presence of disorder, as the presence of a recrystallisation event can also possibly suggest some degree of disorder[22]. Changes in the melting (M) and degradation (D) events can provide information regarding the solid-state form initially present or recrystallised during the DSC analysis run. As described in Section 3.4.2, volatile (V) events refer only to events associated with the desolvation of liquids that occur before melting or degradation. Therefore, changes in volatile responses such as shifts in the onset of desolvation (ΔT_v) or percentage change in heats of desolvation ($\%\Delta H_v$) can provide information about the presence and potential bound strength of the observed solvent. Interpretation of volatile (solvent) components in DSC thermograms should be made in conjunction with the TGA data to confirm their presence. For example the presence of a new volatile loss (endotherm) after storage or ball-milling may suggest the presence of absorbed water. This can be confirmed by observing a weight loss event in the TGA thermogram over a similar temperature range as the event in the DSC thermogram.

6.3.3.3 *Qualitative classification of solid-state phase based on changes in DSC responses*

Using the observed changes in the DSC responses and the relative threshold limits defined in Table 6-6, the comminuted materials could be qualitatively classified as being crystalline, microcrystalline, disordered or DSC amorphous using novel definitions and decision tree (Table 6-7 and Figure 6-3).

Table 6-7 Qualitative classification of solid-state phase present based on changes in DSC responses

Initial solid-state phase	DSC characteristics of comminuted material
Crystalline (Concordant with reference)	DSC thermogram is identical to a reference with the same DSC responses.
Crystalline (Improved crystallinity same form)	DSC thermogram with the same DSC events as reference but with increased ΔH_f.
Crystalline (Improved crystallinity additional form present)	DSC thermogram with similar DSC events as reference but with increased ΔH_f for same T_m as the reference and an additional T_m.
Crystalline (mixed solid-state forms)	DSC thermogram contains a new T_m along with a T_m concordant with the reference or evidence of a solid-state transition.
Crystalline (New solid-state form)	DSC thermogram contains a new T_m.
Mixed Phase A	Same crystalline form with some disorder present.
Mixed Phase B	Potentially a new crystalline form with some disorder present.
Mixed Phase C	Potentially a mixture of crystalline forms with some disorder present.
Disordered	Potentially a large amount disorder of the crystal lattice with a T_g observed.
DSC amorphous	DSC thermogram with no discernable events (multiple unresolved thermal events) implying significant amount of disorder of the crystal lattice – confirm by other techniques such as XRPD.

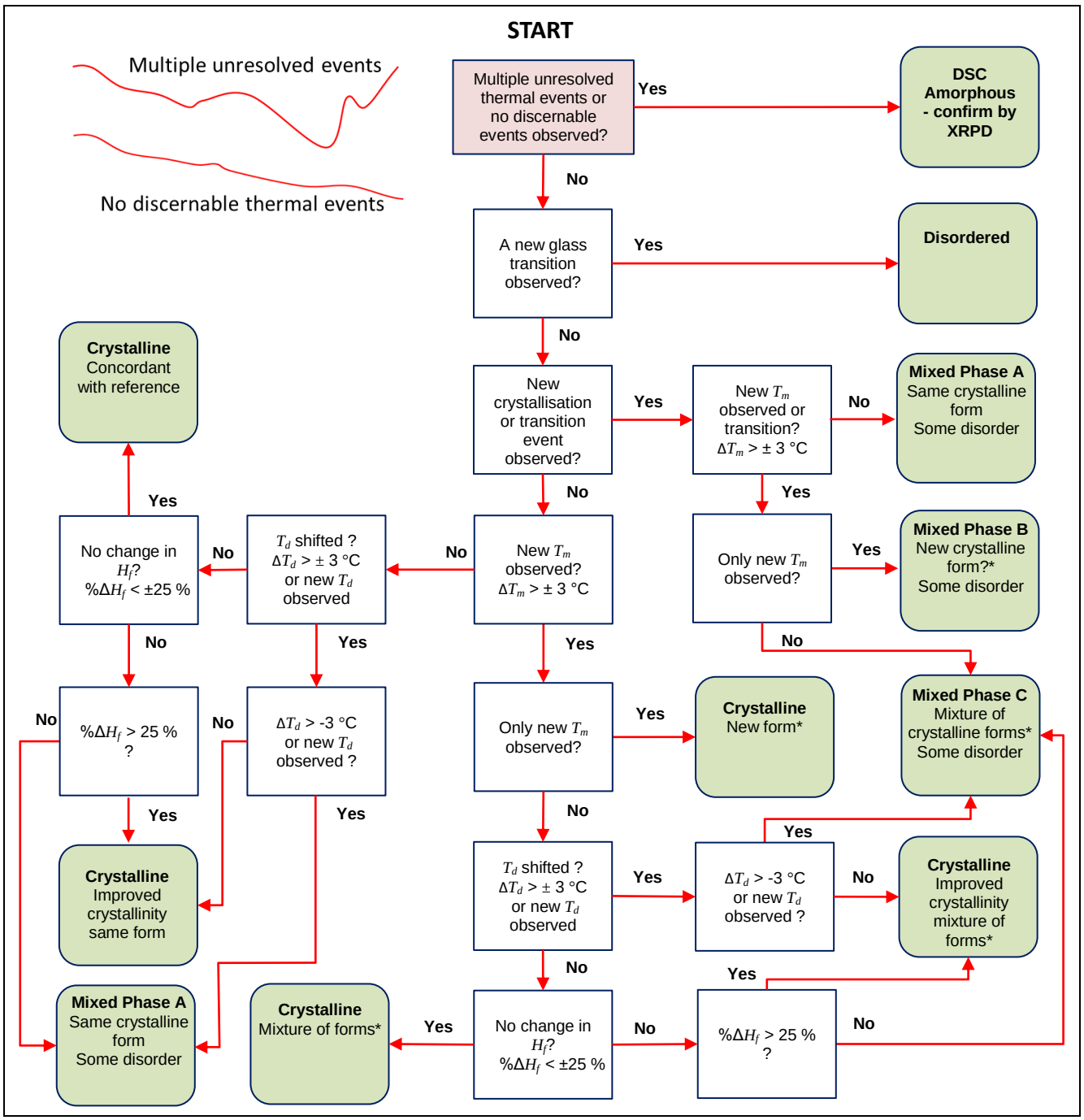

Figure 6-3 ***Decision tree for the qualitative classification of solid state phases by DSC using CRA values (comparison between processed and input DSC thermograms & responses)***

ΔT_m: Shift in melting onset. $\%\Delta H_f$: % Change in heat of fusion. ΔT_d: change in degradation onset.
** confirm by XRPD*

6.3.4 Laser particle size analysis (PSA)

6.3.4.1 *PSA acquisition and response analysis*

Particle size distributions (PSD) and responses for the mechanically comminuted materials were obtained and analysed using the methods described in Sections 3.6.1 and 3.6.2 respectively. Six replicates of each study material were analysed and the responses averaged. The particle size distributions were plotted as normalised density distribution

(q3*) versus logarithm particle sizes, obtained by dividing each q3* value by the highest q3* value observed.

6.3.4.2 *Comparative response analysis of particle size distributions*

CRA was performed by comparing the differences in the particle size distributions and responses of the comminuted material with those of the input/reference obtained under the same acquisition conditions (Section 3.6.1). The amount of change in the PSA responses was determined by overlaying the relevant particle size distributions and by using the equations defined below. The qualitative relevance of these changes could then be defined (Table 6-8).

Changes in particle size response values (ΔD#) were determined by:

$$\Delta D\# = \text{Sample } D\# - \text{Reference } D\# \quad [6\text{-}11]$$

where D# can be D_{10} (µm), D_{50} (µm), D_{90} (µm) values,

The degree of change in the particle size responses (F_{RSP}) was given by:

$$F_{RSP} = \frac{\text{Reference } P_{RSP}}{\text{Sample } P_{RSP}} \quad [6\text{-}12]$$

where P_{RSP} can be span, volume mean diameter (VMD) in (µm), or surface area (Sm) in (cm^2g^{-1}) values. VMD and Sm values were selected as they give a measure of the amount of large particles and sub-micron fines within the material upon comminution respectively.

Table 6-8 Qualitative relevance of CRA values for the PSA responses

PSA response	Amount of change Δ	Qualitative relevance of the amount of change in PSA responses and observations of comminuted material
Decile% of particles D_{10}, D_{50}, D_{90}	ΔD# a negative value	Particle size reducing for defined percentage of particles
	ΔD# a positive value	Particle size increasing for defined percentage of particles. May infer agglomeration has occurred as a result of or during the comminution process
Number of modes	Increases	Particle size distribution becoming more poly-modal
	Decreases	Particle size distribution becoming more uniform
Span	$F_{span} \sim 1$	similar width of particle size distribution
	$F_{span} < 1$	Width of particle size distribution is broader
	$F_{span} > 1$	Width of particle size distribution is narrower
Volume mean diameter, VMD	$F_{VMD} \sim 1$	Similar amount of larger particles present
	$F_{VMD} > 1$	The size of larger particles is decreasing
	$F_{VMD} < 1$	The size of larger particles is increasing
Surface area, SM	$F_{Sm} \sim 1$	Similar amount (size) of fines (sub-micron) present
	$F_{Sm} < 1$	The number (size) of fines (sub-micron) present is increasing
	$F_{Sm} > 1$	The number (size) of fines (sub-micron) present is decreasing

ΔD#: *Changes in particle size response values for* D_{10}, D_{50}, D_{90}, F_{span}*: the degree of change in span,* F_{VMD}*: the degree of change in volume mean diameter,* F_{Sm}*: the degree of change in surface area*

6.3.5 Scanning electron microscopy (SEM)

6.3.5.1 *SEM acquisition and response analysis*

Only SEM images for the mechanically comminuted materials were obtained and analysed using the methods described in Sections 3.5.2 and 3.5.3. PLM images were not acquired as the comminution processes results in the large reduction in particle size (potentially to a particle size of less than 10 µm) and therefore PLM was not deemed an appropriate technique to investigate primary particle morphology for these materials.

Due to the nature of the technique, numerical analysis of the particles with respect to particle size is difficult to determine by SEM as there are a limited number of particles analysed. Therefore, SEM analysis was restricted to reporting qualitative or descriptor responses such as particle, surface and edge morphology.

6.3.5.2 *Comparative response analysis of SEM images*

CRA of the acquired SEM micrographs was performed by qualitatively comparing the differences in microscopic responses of the comminuted material against those of the input/reference material obtained under the same acquisition conditions (Section 3.5.2). This CRA process for SEM was restricted to only the descriptor responses and the qualitative relevance for these changes defined (Table 6-9).

Table 6-9 Qualitative relevance of changes in particulate morphology by SEM analysis

SEM response	Qualitative relevance of the amount of change in SEM responses and observations of comminuted material
Primary particle shape or habit	A different crystal habit suggests process has caused a morphological change.
Particle surface characteristics	Changes in surface characteristics as a result of a process may indicate the effect of the process on the material, e.g. a transformation from cracked, porous, rough or pitted surfaces to smooth may indicate some degree of recrystallisation has occurred, whilst a change from a smooth to cracked, porous, rough or pitted surface suggests the material has or is fracturing..
Particle edge characteristics	Changes in edge characteristics as a result of a process may indicate how the process affects the material, e.g. a transformation from fractured to sharp, rounded or angular form may suggest some degree of recrystallisation has occurred or material has sheared, whilst a change from a sharp, rounded or angular form to a fractured form suggests fracturing has occurred.
Particle association (secondary crystal habits)	The observance of agglomeration may indicate electrostatic affects, particle binding through moisture sorption or the effects of processing resulting in particle fusing.

6.3.6 Gravimetric vapour sorption (GVS)

6.3.6.1 *GVS acquisition and response analysis*

Moisture sorption profiles for the mechanically comminuted materials were obtained and analysed using the methods described in Sections 3.7.1 and 3.7.2 respectively. Due to the length of time to acquire these moisture sorption profiles, replicate analyses were not performed.

6.3.6.2 *Comparative response analysis of moisture sorption profiles*

Comparative response analysis of the acquired moisture sorption profiles was performed by comparing the differences in GVS responses for the comminuted material against those of the input/reference material obtained under the same acquisition conditions (Section 3.7.1). The amount of change in the GVS responses was determined using the equations defined below and the qualitative relevance of these changes defined (Table 6-10).

Table 6-10 Qualitative relevance of changes in moisture sorption properties by GVS analysis

GVS response	Amount of change Δ	Qualitative relevance of the amount of change in GVS responses and observations after comminution
Initial % mass change, M_A	$\Delta M_A \sim 0$ %	Similar amount of moisture present initially
	$\Delta M_A > 0.5$ %	Amount of moisture initially present increased or may be due to an electrostatic charge so need to refer to TGA data for confirmation. Increased moisture sorption may indicate presence of disorder or could be due to increased surface area
Equilibrium % mass changes at defined %RH points, M_B, M_C, M_D, M_E, M_F	-0.5 % $< \Delta M_{\#} < 0.5$ %	Similar amount of moisture present at defined %RH
	$\Delta M_{\#}$ reduced more than -0.5 %	Moisture sorption decreased at defined %RH
	$\Delta M_{\#} > 0.5$ %	Moisture sorption increased at defined %RH
Difference in % mass change over run, M_{END}	-0.5 % $< M_{END} < 0.5$ % for sample	No irreversible moisture sorption observed during the analysis
	$M_{END} > 0.5$ % for sample	May indicate that moisture has been retained or absorbed (irreversible process) and that the solid state form of the material being analysed may have changed
	M_{END} reduced more than -0.5 % for sample	May indicate that any initial moisture or electrostatic charge has been removed
Maximum % change in mass during adsorption cycles, M_{MAX1} or M_{MAX2}	-0.5 % $< \Delta M_{MAX\#} < 0.5$ %	Similar amount of moisture uptake observed during adsorption cycle
	$\Delta M_{MAX\#} > 0.5$ %	Amount of moisture uptake observed during adsorption cycle has increased suggesting increased surface area or disorder
	$\Delta M_{MAX\#}$ reduced more than -0.5 %	Amount of moisture uptake observed during adsorption cycle has decreased suggesting material may have a smaller surface area
Difference in % change in mass during adsorption cycles1 and 2, *ADS*	-0.5 % $< ADS < 0.5$ % for sample	No difference in moisture uptake between the adsorption cycles for a given sample (equation [3-7])
	ADS reduced more than -0.5 % for sample	Uptake of moisture during adsorption cycle 1 (ADS1) is less than that during the second adsorption cycle (ADS2) (equation [3-7])
	ADS > 0.5 % for sample	Uptake of moisture during adsorption cycle 1 (ADS1) is greater than that during the second adsorption cycle (ADS2) suggesting recrystallisation or the irreversible formation of a hydrate (equation [3-7])
%RH and % mass loss for recrystallisation event, $\%RH_{xtal}$ (%RH) and M_{xtal}, (%)	Recrystallisation observed	The observation of a mass loss as %RH is increased or maintained at an elevated value ($\%RH_{xtal}$) is indicative of recrystallisation and infers that disorder was initially present. The size of the mass change (M_{xtal}) may also reflect the degree of disorder present

ΔM_A: % change in mass (dry) at initial 30%RH. $\Delta M_{\#}$: % change in mass (dry) at different %RH values # = B (90%), C (0%), D (90%), E (0%) and F (30%). Please refer to Table 3-11 for full definitions of the responses

Comparative difference in % change in mass at a defined %RH value ($\Delta M_{\#}$) is given by;

$$\Delta M_{\#}\ (\%) = \text{Sample } M_{\#} - \text{Reference } M_{\#} \quad [6\text{-}13]$$

where $M_{\#}$ is the equilibrium % change in mass (dry) at different %RH values # = A (30%), B (90%), C (0%), D (90%), E (0%) and F (30%) (See Figure 3-11).

Comparative difference in maximum equilibrium % change in mass (dry) during adsorption cycles *($\Delta M_{MAX\#}$)* between the sample and reference is given by;

$$\Delta M_{MAX\#}\ (\%) = \text{Sample } M_{MAX\#} - \text{Reference } M_{MAX\#} \quad [6\text{-}14]$$

where # = 1 or 2, *i.e.* adsorption cycle 1 or 2 respectively

6.3.6.3 *Qualitative classification of solid state phase based on changes in GVS responses*

Using the observed changes in the GVS responses and the relative threshold limits defined in Table 6-10 the comminuted materials could be qualitatively classified as being crystalline or disordered using a novel decision tree and definitions (Table 6-11 and Figure 6-4).

Table 6-11 Qualitative classification of solid state phase present based on changes in GVS responses

Initial solid-state phase	GVS characteristics of comminuted material
Crystalline (reversible moisture adsorption)	GVS moisture sorption profile similar to that of the reference, exhibiting reversible moisture adsorption/desorption cycles. No effective difference in %mass at end of the run compared to the start ($-0.5\% < M_{END} < 0.5\%$) and little difference in the adsorption profile.
Crystalline (loss of initial moisture or electrostatic charge)	Small ($\Delta M_{MAX1} < 0.5\%$) irreversible moisture sorption/desorption observed ($M_{END} < -0.5\%$). Infers Loss of initial moisture or electrostatic charge
Crystalline (irreversible moisture adsorption)	Small ($\Delta M_{MAX1} < 0.5\%$) irreversible moisture sorption/desorption observed ($M_{END} > 0.5\%$).
Disordered	Recrystallisation observed as an expulsion of water from the solid at elevated %RH. Note that recrystallisation by moisture sorption may not occur for all disordered materials. For some materials heat maybe also required or a different solvent.
Disordered (or increased surface area)	An increase ($\Delta M_{MAX1} > 0.5\%$) in the amount of moisture adsorbed during the first adsorption cycle can infer the presence of disorder or it could be as a result of increased surface area as a consequence of a comminution process.

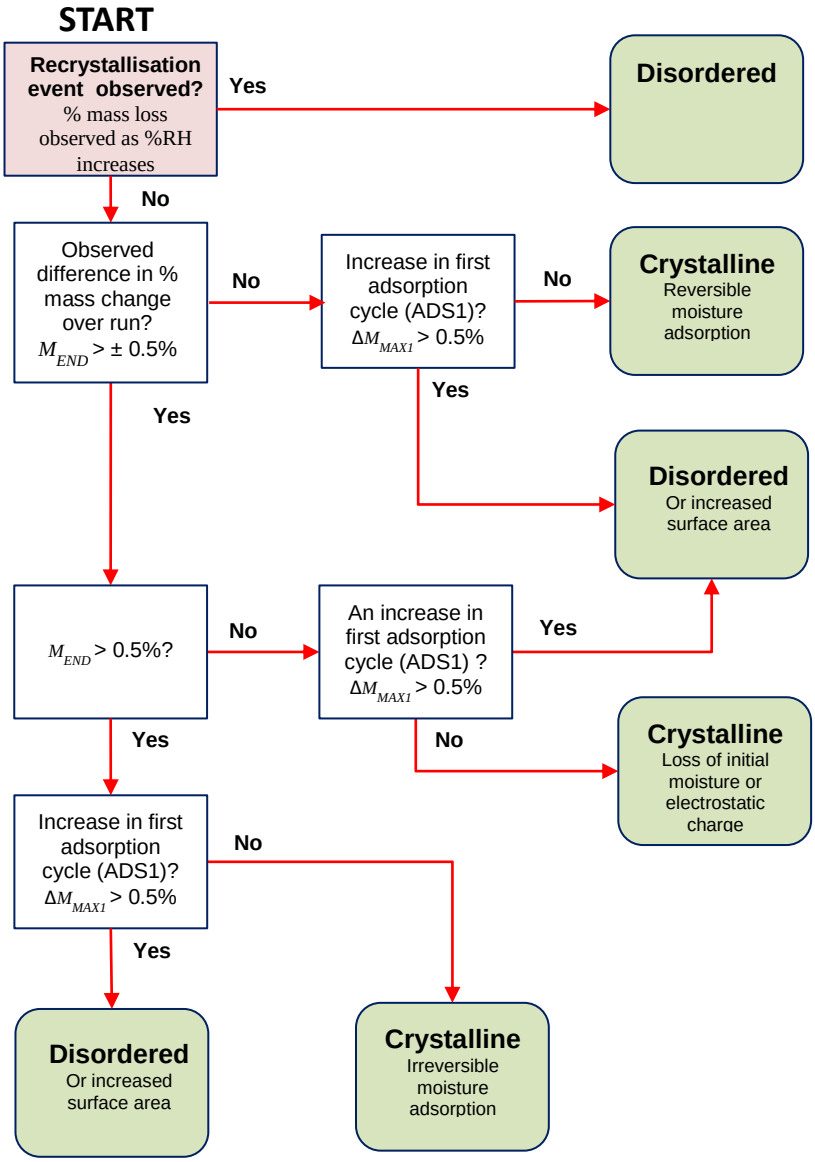

Figure 6-4 Decision tree for the qualitative classification of solid-state phase by GVS using CRA values

6.3.7 Fourier transform infra-red spectroscopy (FTIR)

6.3.7.1 *FTIR acquisition and response analysis*

FTIR spectra for the mechanically comminuted materials were obtained and analysed using the methods described in Sections 3.9.1 and 3.9.2 respectively. Each study material was prepared and analysed in triplicate and the spectra averaged and normalised.

6.3.7.2 *Comparative response analysis of FTIR spectra*

The average normalised FTIR spectra for the comminuted materials were qualitatively compared to the spectra of the relevant input material acquired using the same conditions (Sections 3.9.1 and 3.9.2). The presence of new peaks and/or missing peaks were noted and the vibrational frequencies assigned appropriately using correlation tables and relevant literature references[318].

6.3.8 High pressure liquid chromatography (HPLC)

6.3.8.1 *HPLC acquisition and response analysis*

The λmax for each study material (Table 6-12) was used to obtain the HPLC chromatograms for the mechanically comminuted materials using the method described in Section 3.8.2.

Table 6-12 λmax values for the study materials

Material	Max absorbance wavelength λmax (nm)	Material	Max absorbance wavelength λmax (nm)
Acetaminophen	240	Sulfamerazine	240
γ-Indomethacin	240	Phenacetin	245
Loperamide HCl	220	Sulfadiazine	265
Salbutamol sulphate	225	Caffeine	265
Acetylsalicylic acid	235	Methyl paraben	260

λmax determined in Section 4.2.8

6.3.8.2 *Comparative response analysis of HPLC chromatograms*

Comparative response analysis for the HPLC responses of the comminuted material was performed by comparing the HPLC responses for the sample material against those of the input/reference material obtained under the same acquisition conditions (Section 3.8.2). The amount of change in the HPLC responses was determined using the equations defined below and the qualitative relevance of these changes defined (Table 6-13).

Table 6-13 Qualitative relevance CRA values for the HPLC responses

HPLC response	Amount of change Δ	Qualitative relevance of the amount of change in GVS responses and observations after comminution
Peaks, #peaks	Δ#peaks > 1	Presence of new peaks infers an increase in impurities or degradants as a result of comminution
	Δ#peaks > -1	Decrease in number of observed peaks may suggest improved purity
Primary peak retention time, RT	ΔRT~ 0 %	Same primary peak observed
	ΔRT > ± 0.2	New primary peak observed which infers new chemical identity present
Primary peak % area	Δ%area - negative value	Suggests chemical purity is reduced
	Δ%area - positive value	Suggests chemical purity is improved

Change in retention time, ΔRT (min) for primary peak is given by:

$$\Delta RT\ (min) = Sample\ RT - Reference\ RT \quad [6\text{-}15]$$

Change in percentage area for HPLC peaks, Δ%area (%) is given by:

$$\Delta\%area\ (\%) = Sample\ \%area - Reference\ \%area \quad [6\text{-}16]$$

Change in number of peaks (Δ#peaks) is given by:

$$\Delta\#peaks = Total\ \#\ peaks\ in\ sample - Total\ \#\ peaks\ in\ reference \quad [6\text{-}17]$$

6.4 Results & discussion

6.4.1 X-ray powder diffraction (XRPD)

For each comminuted material a single representative XRPD pattern was obtained by averaging the acquired XRPD diffractograms from three sample preparations. The averaged XRPD patterns were then analysed, and the individual peak responses tabulated using five peak descriptors; peak position (P_P), peak height or intensity (P_H), peak width (P_W), peak area (P_A) and background height (B_H). Average differences between the individual peak characteristics of the input/reference and comminuted material for the most significant peaks over the whole XRPD diffractogram, along with any changes to the MIP positions and MIP intensities was assessed using a novel comparative response analysis process (Section 6.3.1.2). These values are reported in Table 6-14 along with the determined solid-state classification made using the novel decision tree (Section 6.3.1.3).

It can be seen from Table 6-14 that that the XRPD methodology and novel analysis processes were able to discern differences between the materials comminuted under the same and also under different conditions. Comminution resulted in the generation of different solid-state phases. These results confirm that the comminution processes were successful in generating materials that encompassed the whole amorphous-crystalline continuum.

Acetaminophen, methyl paraben, caffeine, acetylsalicylic acid, sulfadiazine, and phenacetin were all classified as crystalline based on their XRPD responses regardless of the type of comminution process employed (Table 6-14). A number of these comminuted materials also exhibited preferred orientation effects as illustrated in Figure 6-5 for micronised phenacetin. A few peaks in the XRPD diffractogram for the input material of phenacetin were sharp and of very high intensity, *i.e.* over 40000 cts, while other peaks appear much smaller, suggesting some form of texture or preferred orientation exists, *i.e.* alignment of crystallite particles in the same direction causing some peaks to appear much higher in intensity than others).

Ball-milling indomethacin at low and high frequencies appeared to result in microcrystalline and disordered material respectively (Table 6-14). However, micronised γ-indomethacin remained crystalline and exhibited preferred orientation, *i.e.* change in MIP and peak intensities.

Table 6-14 CRA for XRPD responses of the comminuted materials (comparing responses from averaged XRPD diffractogram to those of the input)

Material	Batch ID	Changes in average peak responses across diffractogram					Change in MIP?	$\%\Delta MIP_H$ (%)	New peaks	Absent/ Merged peaks	Solid-state classification
		Postion $Av\Delta P_P$ (°2θ)	Height $Av\Delta P_H$ (%)	Background $Av\Delta B_H$ (%)	Area $Av\Delta P_A$ (%)	Width $Av\Delta P_W$ (%)					
Acetaminophen	1-MA1	0.00	59	14	213	40	Yes	-8	No	No	Crystalline – preferred orientation
	1-MA2	-0.01	39	19	195	48	Yes	-15	No	No	Crystalline – preferred orientation
	1-MB1	-0.01	69	27	342	62	Yes	18	No	No	Crystalline – preferred orientation
	1-MB2	0.00	85	21	395	57	Yes	25	No	No	Crystalline – preferred orientation
	1-X1	-0.03	-7	-12	9	16	Yes	-22	No	No	Crystalline
γ-Indomethacin	11-MA1	-0.04	-67	44	-47	68	Yes	-79	No	Yes	Disordered
	11-MA2	-0.03	-57	31	-11	119	Yes	-75	No	Yes	Disordered
	11-MB1	-0.01	-37	27	9	87	Yes	-65	No	Yes	Microcrystalline
	11-MB2	0.01	-49	25	-6	99	Yes	-70	No	Yes	Microcrystalline
	11-X1	-0.01	-36	-27	-31	12	Yes	-43	No	Yes	Crystalline – preferred orientation
Salbutamol sulphate	24-MA1	NPD	NPD	NPD	NPD	NPD	NPD	NPD	NPD	NPD	X-ray amorphous
	24-MA2	NPD	NPD	NPD	NPD	NPD	NPD	NPD	NPD	NPD	X-ray amorphous
	24-MA3	NPD	NPD	NPD	NPD	NPD	NPD	NPD	NPD	NPD	X-ray amorphous
	24-MB1	0.00	-73	28	-57	73	Yes	-96	No	Yes	Microcrystalline
	24-MB2	0.00	-79	22	-66	76	Yes	-97	No	Yes	Microcrystalline
	24-X1	-0.02	-70	-31	-69	15	Yes	-92	No	No	Crystalline – preferred orientation
Loperamide HCl	14-MA1	NPD	NPD	NPD	NPD	NPD	NPD	NPD	NPD	NPD	X-ray amorphous
	14-MB1	-0.07	-64	49	44	271	Yes	-90	No	Yes	Disordered
	14-X1	-0.03	-66	1	4	148	No	-88	No	Yes	Crystalline
Acetylsalicylic acid	33-MA1	-0.09	-63	-26	-59	93	No	-96	No	No	Crystalline
	33-MB1	-0.05	-55	-16	-23	67	No	-94	No	No	Crystalline
	33-X1	-0.07	-62	-43	-54	36	No	-95	No	No	Crystalline
Sulfamerazine	54-MA1	-0.06	31	21	115	67	Yes	-69	Some	Yes	Crystalline mixture of forms
	54-MB1	0.02	-48	51	-1	124	Yes	-74	No	Yes	Microcrystalline
	54-X1	-0.01	-51	-6	8	147	Yes	-77	No	Yes	Crystalline – preferred orientation

Material	Batch ID	Changes in average peak responses across diffractogram					Change in MIP?	$\%\Delta MIP_H$ (%)	New peaks	Absent/ Merged peaks	Solid-state classification
		Postion $Av\Delta P_P$ (°2θ)	Height $Av\Delta P_H$ (%)	Background $Av\Delta B_H$ (%)	Area $Av\Delta P_A$ (%)	Width $Av\Delta P_W$ (%)					
Phenacetin	69-MA1	0.03	60	28	191	48	Yes	-81	No	No	Crystalline – preferred orientation
	69-MB1	0.00	52	13	137	30	No	-80	No	No	Crystalline – concordant with reference
	69-X1	0.01	35	-14	118	59	Yes	-89	No	No	Crystalline – preferred orientation
Sulfadiazine	87-MA1	0.01	-3	-1	129	109	Yes	-88	No	Yes	Crystalline
	87-MB1	0.01	-4	21	118	88	Yes	-87	No	Yes	Crystalline
	87-X1	-0.03	31	-7	67	-8	Yes	-77	No	Yes	Crystalline – preferred orientation
Caffeine	88-MA1	0.03	-53	7	4	90	Yes	-67	No	Yes	Crystalline – preferred orientation
	88-MB1	0.03	-48	11	-18	41	No	-65	No	Yes	Crystalline
	88-X1	-0.02	-58	-30	-47	20	No	-63	No	Yes	Crystalline – concordant with reference
Methyl paraben	140-MA1	0.02	-3	-6	-3	2	No	-37	No	No	Crystalline – concordant with reference
	140-MB1	0.02	-28	-18	-21	17	No	-53	No	No	Crystalline – concordant with reference
	140-X1	-0.01	-53	-31	-50	9	No	-60	No	No	Crystalline – concordant with reference

NPD: *no peaks detected,* $Av\Delta P_P$*: amount of average peak shifting.* $Av\Delta P_H$*: % change in average peak height.* $Av\Delta P_W$*: % change in average peak width (FWHM).* $Av\Delta P_A$*: % change in average peak area.*$Av\Delta B_H$*: % change in average background height.* MIP*: most intense peak,* $\%\Delta MIP_H$*: % change in MIP height. #-MA#: high frequency ball-mill method A, #-MB#: low frequency ball-mill method B. #-X#: jet micronisation method A.*

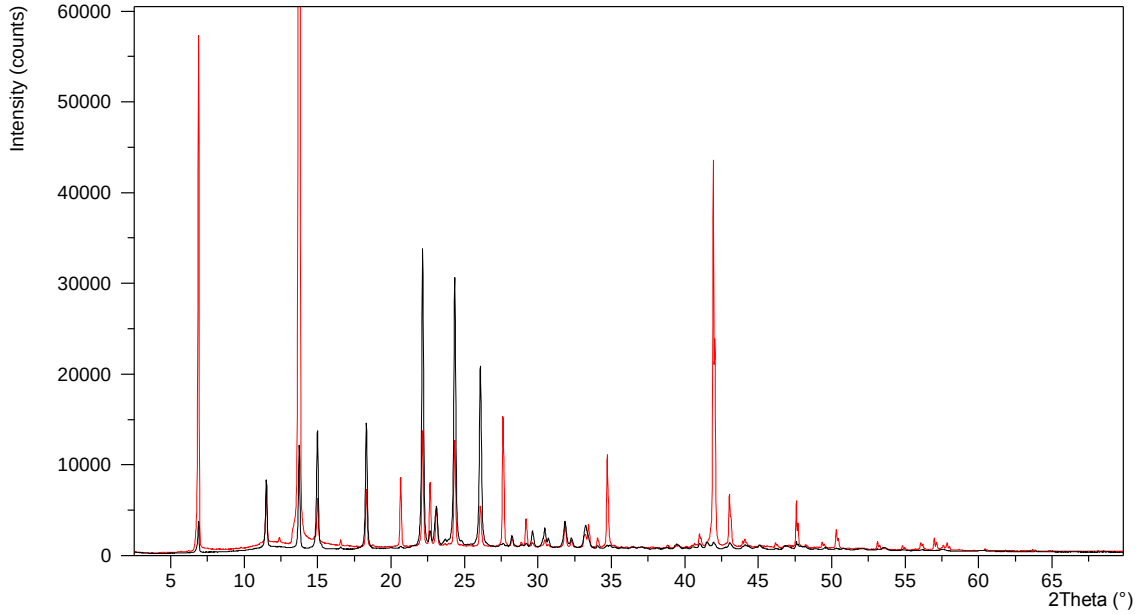

Figure 6-5 XRPD diffractograms for the input/reference (red) and micronised (JM-A) (black) phenacetin illustrating preferred orientation effects

High frequency ball-milling, of salbutamol sulphate and loperamide HCl resulted in X-ray amorphous material (Figure 6-6 and Figure 6-7), while low frequency ball-milling resulted in microcrystalline material for salbutamol sulphate in accordance with the XRPD solid-state phase classification decision tree (Section 6.3.1.3), *i.e.* no peak shifting was observed, however, the MIP was different and overall the peaks were broader and reduced in height, whilst the background heights were elevated (Table 6-14 and Figure 6-7). Low frequency ball-milling of loperamide on the other hand generated disordered material, as there was significant peak shifting, a different MIP, broader and smaller peaks and an overall increase in the background profile (Table 6-14 and Figure 6-6).

Micronisation of either salbutamol sulphate or loperamide HCl did not generate any evidence of PID by XRPD, though peak heights were markedly reduced, and the background height profiles for both materials appeared to be similar or reduced in height with respect to the back ground heights of their input materials as illustrated by the black lines in the inserts for Figure 6-6 and Figure 6-7. Based on the XRPD responses, both of these comminuted materials were classified as being crystalline using the novel XRPD solid-state phase decision tree (Section 6.3.1.3).

The observed solid-state phases for both salbutamol sulphate and loperamide HCl illustrate that both of these materials appear to be susceptible to PID by mechanical comminution and that high frequency ball-milling is more likely to generate PID than micronisation. This is in agreement with literature observations[2].

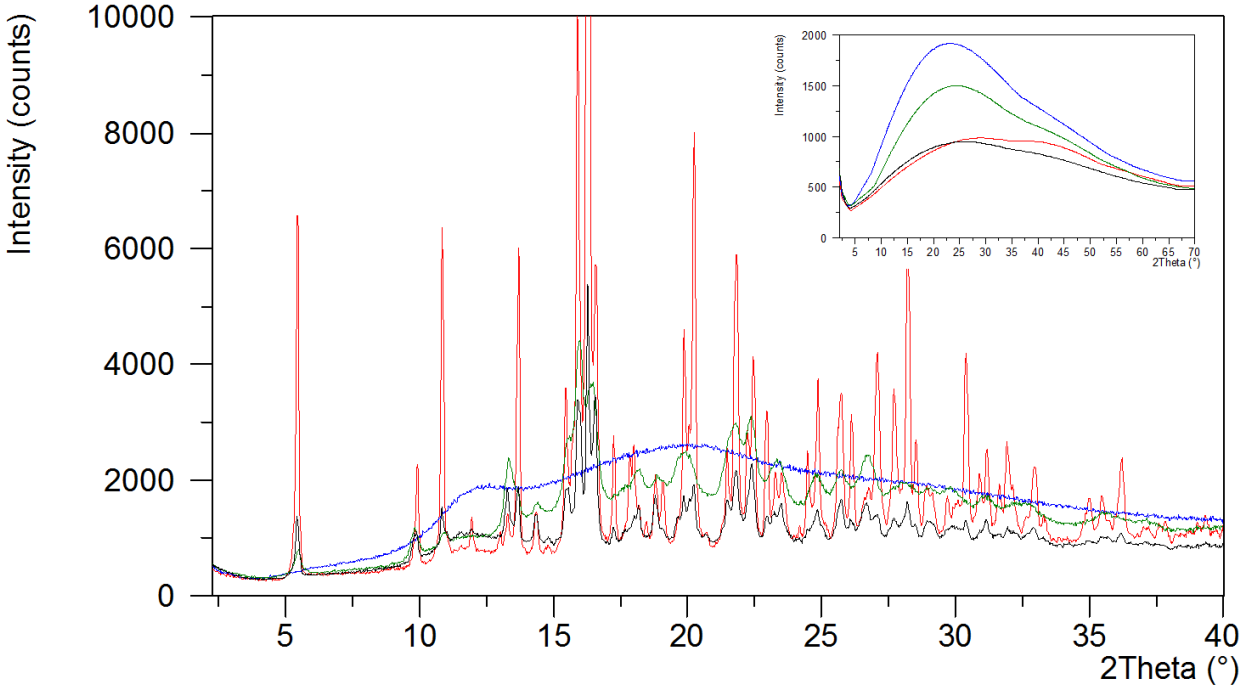

Figure 6-6 ***XRPD diffractograms for the comminuted materials of loperamide HCl by high frequency ball-milling (blue), low frequency ball-milling (green) and micronisation (black) compared to the input material (red).***

The insert illustrates the increased background heights of the ball-milled materials relative to the input and micronised materials.

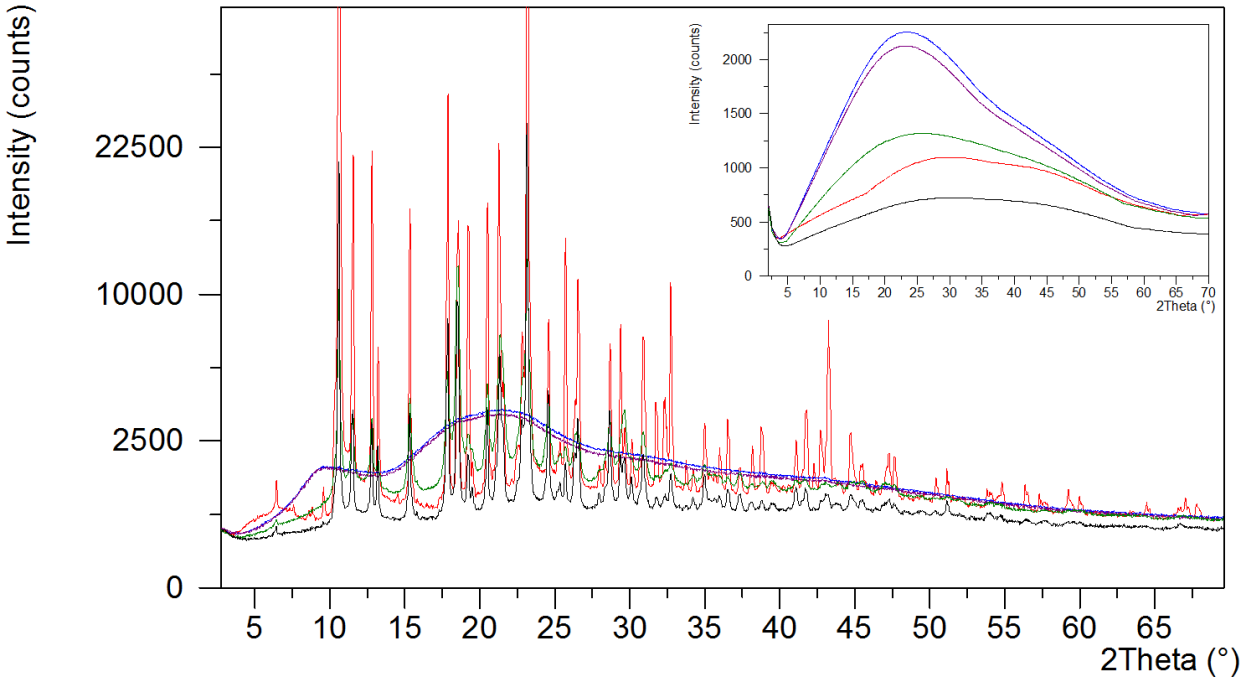

Figure 6-7 ***XRPD diffractograms for the comminuted materials of salbutamol sulphate by high frequency ball-milling with liquid nitrogen (blue) at room temperature (purple), low frequency ball-milling Mill-B (green) and micronisation (black) compared to the input material (red).***

The insert illustrates the increased background heights of the ball-milled materials relative to the input and micronised materials

Reproducibility of the ball-milling processes for acetaminophen, indomethacin and salbutamol sulphate was demonstrated by the identical XRPD responses for Mill-A1/2 and Mill-B1/2 samples. High frequency ball-milling with and without liquid nitrogen

for salbutamol sulphate illustrated that milling temperature did not have an effect on the resulting sold-state form or phase as in both cases an X-ray amorphous material was generated (Figure 6-7 blue with liquid nitrogen and purple without liquid nitrogen).

High frequency ball-milling of sulfamerazine resulted in material containing extra XRPD peaks. These extra peaks were consistent with those of sulfamerazine Form II[117,348,349] determined using the simulated XRPD pattern for Form II (CSD reference SLFNMA01[348]) and the process described in 4.2.4.2 (Figure 6-8).

The presence of a mixture of two solid-state forms, Form I and Form II for ball-milled sulfamerazine was concordant with earlier studies that demonstrated ball-milling sulfamerazine can result in several form solid-state transformations, *i.e.* transformations from Form I to amorphous to Form II and then back to Form I[349-351].

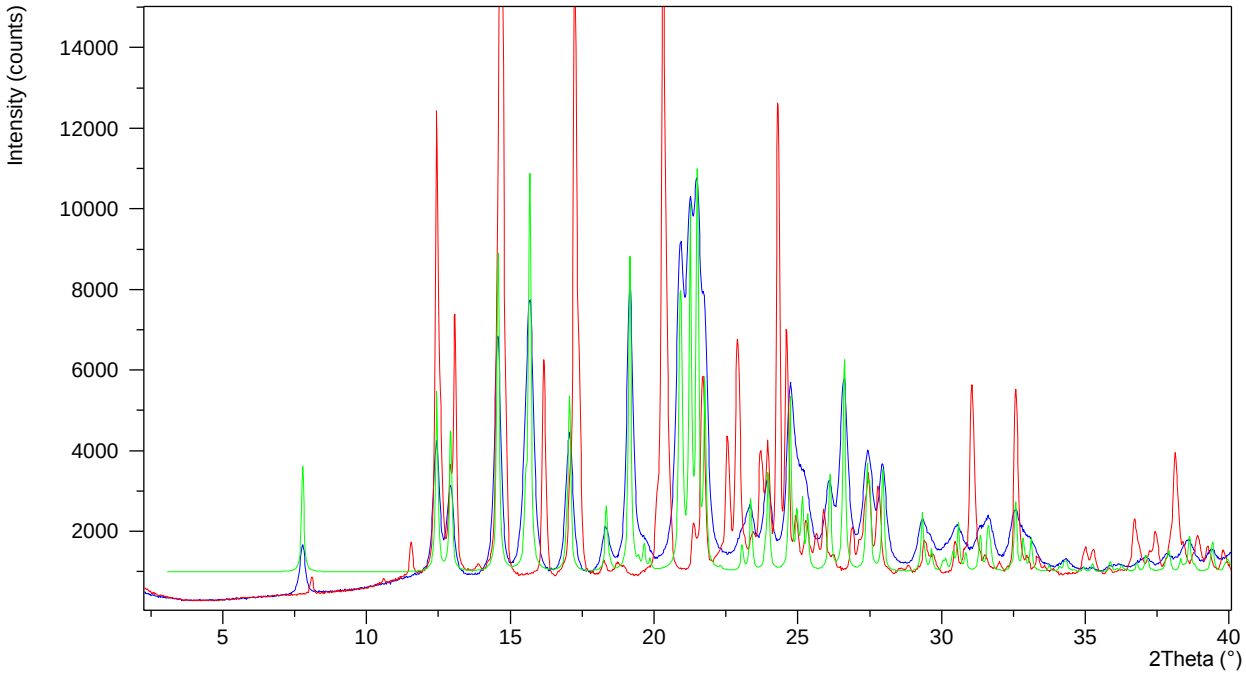

Figure 6-8 ***XRPD diffractograms for sulfamerazine. Ball-milled (Mill-A, blue) appears to be a mixture of the Form 1 reference (red) and the simulated XRPD pattern for Form II, SLFNMA01[348] (green)***

6.4.2 Thermogravimetric analysis (TGA)

TGA thermograms for the mechanically comminuted materials were obtained and the responses compared to those of the input materials (Figure 6-9 and Table 6-15).

The majority of the materials remained anhydrous with no apparent change in the TGA responses regardless of the type of comminution method employed. However, increased weight loss events below 50 °C were observed for ball-milled loperamide HCl and salbutamol sulphate suggesting the presence of absorbed moisture and potentially

increased disorder. It can be suggested that a reduction in particle size or the presence of degradants could also account for these observations, as it has been noted that by decreasing the particle size, surface areas can increase, thereby increasing the potential for greater moisture adsorption at crystal surfaces[290,309,310]. However, of the three comminution processes, micronisation would most likely result in smaller particle sizes and as there is very little adsorption observed for both micronised loperamide HCl and salbutamol sulphate it more likely that the observed weight losses are due to the presence of disorder or degradants, rather than as a consequence in particle size reduction. The observed weight loss events were more pronounced for the high frequency ball-milled materials of loperamide HCl and salbutamol sulphate, which may suggest the presence of more disorder present or the presence of degradants ((Figure 6-9 and Table 6-15). Furthermore, the thermal degradation temperatures (T_d) for ball-milled salbutamol sulphate were markedly reduced, which also suggests the presence of disorder or degradants (Figure 6-9 and Table 6-15), as the greater the degree of disorder present, the greater the molecular mobility and therefore the lower the activation energy for degradation. Conversely, for acetaminophen the degradation temperature actually increased which may suggest a potential improvement in thermal stability and an improvement in crystal ordering ((Figure 6-9 and Table 6-15).

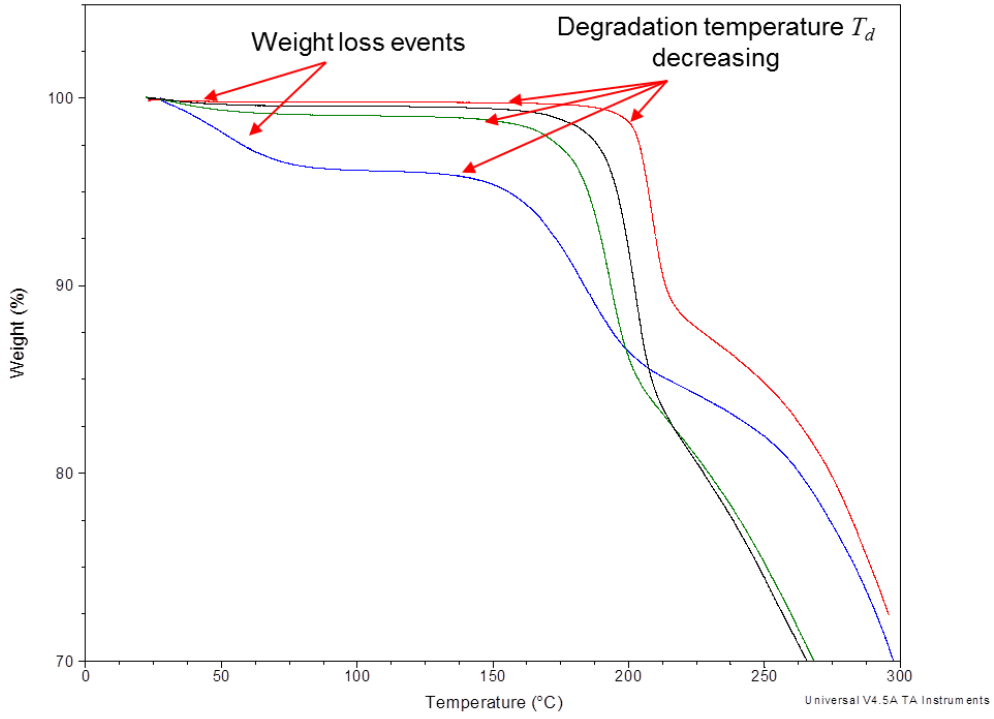

Figure 6-9 ***TGA thermograms for the comminuted materials of salbutamol sulphate by high frequency ball-milling (blue), low frequency ball-milling (green) and micronisation (Black) compared to the input material (red).***

Weight loss below 50 °C is increased for the ball-milled samples

Table 6-15 Average TGA responses and CRA of the comminuted materials

		Average TGA responses					TGA CRA			
Material	Batch ID	#W_E	WL_{50} (% w/w)	WL_{150} (% w/w)	T_d (° C)	Other WL events %WL (T range)	ΔW_E	ΔW_{L50} % w/w	ΔWL_{150} % w/w	ΔT_d ° C
Acetaminophen	Input	0	<0.5	<0.5	235	--	--	--	--	--
	1-MA1	0	<0.5	<0.5	246	--	0	0	0	11
	1-MA2	0	<0.5	<0.5	247	--	0	0	0	12
	1-MB1	0	<0.5	<0.5	246	--	0	0	0	11
	1-MB2	0	<0.5	<0.5	246	--	0	0	0	11
	1-X1	0	<0.5	<0.5	240	--	0	0	0	5
γ-Indomethacin	Input	0	<0.5	<0.5	266	--	--	--	--	--
	11-MA1	0	<0.5	0.52	264	--	0	0	0	-2
	11-MA2	0	<0.5	0.50	264	--	0	0	0	-2
	11-MB1	0	<0.5	<0.5	264	--	0	0	0	-2
	11-MB2	0	<0.5	<0.5	265	--	0	0	0	-1
	11-X1	0	<0.5	<0.5	265	--	0	0	0	-1
Salbutamol sulphate	Input	0	<0.5	<0.5	197	LoD	--	--	--	--
	24-MA1	1	1.79	D	161	3.93 (23-100), LoD	1	1.29	D	-36
	24-MA2	1	1.90	D	163	3.93 (23-100), LoD	1	1.40	D	-34
	24-MA3	1	1.13	D	163	2.72 (23-100), LoD	1	0.63	D	-34
	24-MB1	1	0.69	D	182	0.95 (21-100), LoD	1	0.19	D	-15
	24-MB2	1	0.74	D	181	1.15 (24-100), LoD	1	0.24	D	-16
	24-X1	1	<0.5	<0.5	191	<0.5 (23-100), LoD	0	0	0	-6
Loperamide HCl	Input	0	<0.5	<0.5	262	--	--	--	--	--
	14-MA1	1	1.37	2.39	258	2.22 (27-100)	1	0.87	1.89	-4
	14-MB1	1	0.74	1.21	258	1.14 (27-100)	1	0.24	0.71	-4
	14-X1	0	<0.5	<0.5	258	--	0	0	0	-4
Acetylsalicylic acid	Input	0	<0.5	D	126	LoD	--	--	--	--
	33-MA1	0	<0.5	D	125	D	0	0	D	-1
	33-MB1	0	<0.5	D	125	D	0	0	D	-1
	33-X1	0	<0.5	D	126	D	0	0	D	0
Sulfamerazine	Input	0	<0.5	<0.5	255	--	--	--	--	--
	54-MA1	0	<0.5	<0.5	256	--	0	0	0	1
	54-MB1	0	<0.5	<0.5	257	--	0	0	0	2
	54-X1	0	<0.5	<0.5	255	--	0	0	0	0
Phenacetin	Input	0	<0.5	D	198	D	--	--	--	--
	69-MA1	0	<0.5	D	198	D	0	0	D	0
	69-MB1	0	<0.5	D	199	D	0	0	D	1
	69-X1	0	<0.5	D	197	D	0	0	D	-1
Sulfadiazine	Input	0	<0.5	<0.5	263	LoD	--	--	--	--
	87-MA1	0	<0.5	<0.5	256	LoD	0	0	0	-7
	87-MB1	0	<0.5	<0.5	257	LoD	0	0	0	-6
	87-X1	0	<0.5	<0.5	257	LoD	0	0	0	-6
Caffeine	Input	0	<0.5	D	201	D	--	--	--	--
	88-MA1	1	1.09	D	203	1.28 (27-100), D	1	0.59	0	2
	88-MB1	0	<0.5	D	203	D	0	0	0	2
	88-X1	0	<0.5	D	203	D	0	0	0	2
Methyl paraben	Input	0	<0.5	D	115	LoD	--	--	--	--
	140-MA1	0	<0.5	D	110	D	0	0	0	-5
	140-MB1	0	<0.5	D	111	D	0	0	0	-4
	140-X1	0	<0.5	D	112	D	0	0	0	-3

Each material analysed in duplicate, #W_E*: Number of weight loss events observed before degradation,* $WL_{50:}$ *% Weight loss (w/w) below 50° C.* WL_{150}*: % Weight (w/w) loss below 150 °C.* D*: Degrades below 150 °C,* T_d*:* Degradation temperature (°C). *WL events: Defined weight loss over a given temperature range i.e. %WL (T range)*. LoD: unresolved or weight loss observed at degradation. *#-MA#: high frequency ball-mill method A, #-MB#: low frequency ball-mill method B. #-X#: jet micronisation method A. Please refer to* Table 3-4 *for further descriptions of the term.*

6.4.3 Differential scanning calorimetry (DSC)

DSC thermograms for the mechanically comminuted materials were obtained and the responses (Table 6-16) compared to those of the input materials (Table 6-17). The amount of change in the DSC responses were assessed and used to define the solid-state phase present using the novel process outlined in Section 6.3.3.3.

For a number of materials; acetaminophen, acetylsalicylic acid, phenacetin and methyl paraben, applying different comminution processes had little effect on the observed DSC thermograms and responses. An example of this can be seen in Figure 6-10 of the DSC thermograms for the comminuted materials of acetaminophen, which appeared to be similar to that of the input material.

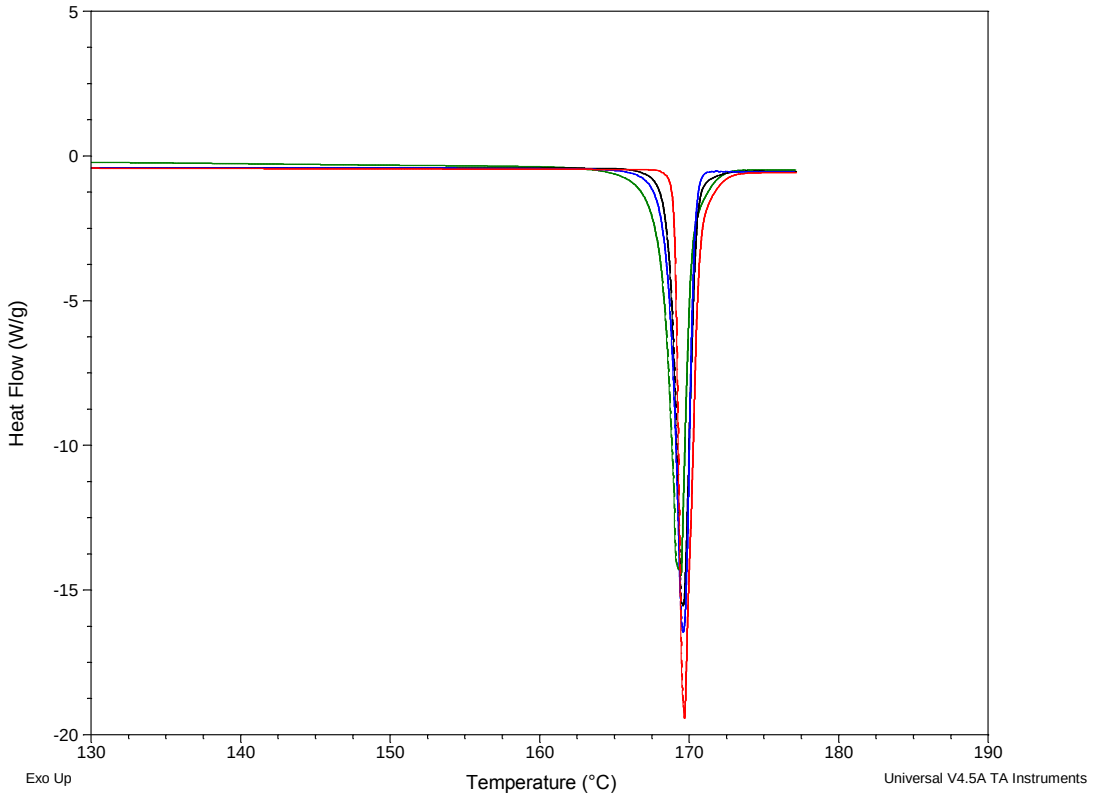

Figure 6-10 DSC thermograms for the comminuted materials of acetaminophen ball-milled at high frequency (blue), at low frequency (green) and micronised (black) compared to the input material (red)

Table 6-16 Average DSC responses for the comminuted materials

			Glass transition events (G)		Volatile events (V)		Crystallisation events (C)		Transition events (T)		Melting events (M)					Degradation (D)	Comments
Material	Batch ID	Events	T_g (°C)	T_g *size* (J/(g°C))	T_v (°C)	ΔH_v (J/g)	T_c (°C)	ΔH_c (J/g)	T_t (°C)	ΔH_t (J/g)	T_m (°C)	ΔH_f (J/g)	WHH (°C)	T_m*trans* (°C)	$T_{m\text{-}p}$ (°C)	T_d (° C)	
Acetaminophen	Input	M	--	--	--	--	--	--	--	--	169.0	185	0.90	0.6	169.7	--	
	1-MA1	M	--	--	--	--	--	--	--	--	168.7	175	1.34	1.2	169.9	--	
	1-MA2	M	--	--	--	--	--	--	--	--	168.6	179	1.27	1.1	169.7	--	
	1-MB1	M	--	--	--	--	--	--	--	--	168.4	187	1.10	1.0	169.4	--	
	1-MB2	M	--	--	--	--	--	--	--	--	168.4	187	0.90	1.0	169.4	--	
	1-X1	M	--	--	--	--	--	--	--	--	168.7	179	1.16	0.9	169.6	--	
γ-Indomethacin	Input	M	--	--	--	--	--	--	--	--	159.5	107	1.30	1.0	160.5	--	
	11-MA1	GCM	45.3	0.345	--	--	70.3	22.3	--	--	157.5	106	1.35	1.7	159.2	--	Glass transition & crystallisation observed
	11-MA2	GCM	42.9	0.285	--	--	66.1	18.2	--	--	156.9	101	1.82	1.9	158.8	--	Glass transition & crystallisation observed
	11-MB1	CM	--	--	--	--	53.4	5.4	--	--	156.6	104	2.17	2.7	159.2	--	crystallisation observed
	11-MB2	CM	--	--	--	--	57.9	1.6	--	--	156.9	103	2.17	2.5	159.4	--	crystallisation observed
	11-X1	M	--	--	--	--	--	--	--	--	158.8	103	1.13	1.2	159.9	--	
Salbutamol sulphate	Input	MD	--	--		--		--	--	--	196.7	165	8.9	7.4	204.1	204.2*	
	24-MA1	VC2MD	60-65 /120°C	--	30.2	--	114.4, 135.9**	--	--	--	151.5	NC	NC	26.9	178.4	178.4*	Volatile loss and two crystallisation events observed, melt-degradation
	24-MA2	VC2MD	60-65 /120°C	--	41.7	--	118.1, 148.6**	--	--	--	151.3	NC	NC	26.8	178.1	178.1*	Volatile loss and two crystallisation events observed, melt-degradation
	24-MA3	VC2MD	60-65 /120°C	--	58.5	--	116.6, 149.0**	--	--	--	149.0	NC	NC	29.3	178.2	178.2*	Volatile loss and two crystallisation events observed, melt-degradation
	24-MB1	VC2MD	--	--	4.9	--	116.3, 138.8**	--	--	--	166.7	NC	NC	29.9	196.5	196.5*	Volatile loss and two crystallisation events observed, melt-degradation
	24-MB2	VC2MD	--	--	13.6	--	115.8, 138.2**	--	--	--	166.8	NC	NC	30.5	197.3	197.3*	Volatile loss and two crystallisation events observed, melt-degradation
	24-X1	VCMD	--	--	3.4	--	98.9**	--	--	--	187.3	NC	NC	14.4	201.7	201.7*	Volatile loss and crystallisation events observed, melt-degradation
Loperamide HCl	Input	MD	--	--	--	--	--	--	--	--	227.2	90	2.30	2.2	229.3	235.5	Degradation soon after melt
	14-MA1	GVCMD	120.8	0.265	21.2	71	166.7	68.7	--	--	223.7	82	2.55	3.3	227.9	235.5	Degradation soon after melt
	14-MB1	VMCD	--	--	11.5	40.9	132.4	11.1	--	--	221.4	75	3.73	4.4	225.9	235.7	Degradation soon after melt
	14-X1	VMCD	--	--	4.3	14.3	114.9	8	--	--	224.3	80	2.76	3.4	227.5	235.6	Degradation soon after melt

Material	Batch ID	Events	Glass transition events (G)		Volatile events (V)		Crystallisation events (C)		Transition events (T)		Melting events (M)					Degradation (D)	Comments
			T_g (°C)	T_g *size* (J/(g°C))	T_v (°C)	ΔH_v (J/g)	T_c (°C)	ΔH_c (J/g)	T_t (°C)	ΔH_t (J/g)	T_m (°C)	ΔH_f (J/g)	WHH (°C)	T_m*trans* (°C)	$T_{m\text{-}p}$ (°C)	T_d (° C)	
Acetylsalicylic acid	Input	MD	--	--	--	--	--	--	--	--	139.3	169	2.60	1.9	141.2	146.4	Degradation soon after melt
	33-MA1	MD	--	--	--	--	--	--	--	--	138.4	173	1.99	2.4	140.8	147.2	Degradation soon after melt
	33-MB1	MD	--	--	--	--	--	--	--	--	139.0	173	1.83	2.2	141.2	149.0	Degradation soon after melt
	33-X1	MD	--	--	--	--	--	--	--	--	138.7	171	1.84	1.9	140.6	146.4	Degradation soon after melt
Sulfamerazine	Input	M	--	--	--	--	--	--	--	--	235.9	141	1.30	1.0	236.9	--	
	54-MA1	TM	--	--	--	--	--	--	142.3	9.6	234.7	196	1.48	1.9	236.6	--	Form II to Form I transition
	54-MB1	M	--	--	--	--	--	--	--	--	234.4	144	1.58	1.9	236.3	--	
	54-X1	M	--	--	--	--	--	--	--	--	234.4	142	1.48	1.9	236.3	--	
Phenacetin	Input	M	--	--	--	--	--	--	--	--	134.4	170	1.20	1.1	135.5	--	
	69-MA1	M	--	--	--	--	--	--	--	--	133.8	174	1.08	1.2	135.0	--	
	69-MB1	M	--	--	--	--	--	--	--	--	134.2	180	1.02	0.8	135.1	--	
	69-X1	M	--	--	--	--	--	--	--	--	134.2	173	1.19	1.0	135.1	--	
Sulfadiazine	Input	MD	--	--	--	--	--	--	--	--	261.3	169	0.8	0.2	261.5	266.8	Degradation soon after melt
	87-MA1	MD	--	--	--	--	--	--	--	--	256.9	233	1.51	1.8	258.7	262.0	Degradation soon after melt
	87-MB1	MD	--	--	--	--	--	--	--	--	255.7	240	1.99	2.3	258.0	261.4	Degradation soon after melt
	87-X1	MD	--	--	--	--	--	--	--	--	258.7	176	1.04	1.0	259.7	261.2	Degradation soon after melt
Caffeine	Input	TMD	--	--	--	--	--	--	146	19.6	236.0	NC	NC	0.5	236.4	236.4*	Form II to Form I transition observed, melt-sublimation
	88-MA1	VTMD	--	--	8.2	NC	--	--	116.1	4.1	236.0	NC	NC	0.4	236.4	236.4*	volatile loss first, Form II to Form I transition then melt/sublimation
	88-MB1	TMD	--	--	--	--	--	--	120.9	12.6	236.0	NC	NC	0.5	236.5	236.5*	Form II to Form I transition observed, melt-sublimation
	88-X1	TMD	--	--	--	--	--	--	137.8	18.8	235.9	NC	NC	0.6	236.5	236.5*	Form II to Form I transition observed, melt-sublimation
Methyl paraben	Input	M	--	--	--	--	--	--	--	--	125.8	165	1.20	1.2	127 .0	--	
	140-MA1	M	--	--	--	--	--	--	--	--	125.2	177	0.82	0.7	125.9	--	
	140-MB1	M	--	--	--	--	--	--	--	--	125.5	176	0.84	0.7	126.2	--	
	140-X1	M	--	--	--	--	--	--	--	--	125.5	170	0.83	0.8	126.3	--	

All comminuted material were analysed at least in duplicate. Events: M-melt, D-Degradation, T-transition, V-volatile. ND: Not detected, NC: Not calculated, T_d: Degradation temperature (°C), T_m: Onset of melting temperature (°C), $T_m$trans: Melting transition range (°C), ΔH_f: Heat of fusion (J/g), WHH: width at half peak height (°C), $T_{m\text{-}p}$: Peak melting temperature (°C). T_g: Glass transition temperature, T_c: Recrystallisation onset temperature, ΔH_c: Heat of crystallisation, T_v: Onset of endothermic volatile event, ΔH_v: Heat of desolvation, ND: Not detected, NC: Not calculated. #-MA#: high frequency ball-mill method A, #-MB#: low frequency ball-mill method B. #-X#: jet micronisation method A. Please refer to Table 3-4 or further descriptions of the terms

** $T_{m\text{-}p}$ value used to represent T_d as material melts-degrades or melt-sublimes.**$T_{c\text{-}p}$ used instead of T_c due to unresolved thermal events*

Table 6-17 CRA for DSC responses of the comminuted materials

Material	Batch ID	Glass transition events (G)	Crystallisation event (C)	Volatile event (V)	Melting events (M)				Degradation (D)		Comments & solid-state phase classification
					Melting event	ΔT_m (°C)	$\%\Delta H_f$ (%)	$\Delta T_m trans$ (°C)	Degradation event	ΔT_d (° C)	
Acetaminophen	1-MA1	ND	--	ND	--	-0.3	-5.4	0.6	ND	--	Crystalline concordant with reference
	1-MA2	ND	--	ND	--	-0.4	-3.2	0.5	ND	--	Crystalline concordant with reference
	1-MB1	ND	--	ND	--	-0.6	1.1	0.4	ND	--	Crystalline concordant with reference
	1-MB2	ND	--	ND	--	-0.6	1.1	0.4	ND	--	Crystalline concordant with reference
	1-X1	ND	--	ND	--	-0.3	-3.2	0.3	ND	--	Crystalline concordant with reference
γ-Indomethacin	11-MA1	New	New	ND	--	-2.0	-0.9	0.7	ND	ND	Disordered
	11-MA2	New	New	ND		-2.6	-5.6	0.9	ND	ND	Disordered
	11-MB1	ND	New	ND		-2.9	-2.8	1.7	ND	ND	Mixed Phase A – same crystalline form with some disorder
	11-MB2	ND	New	ND		-2.6	-3.7	1.5	ND	ND	Mixed Phase A – same crystalline form with some disorder
	11-X1	ND	ND	ND	--	-0.7	-3.7	0.2	ND	ND	Crystalline concordant with reference
Salbutamol sulphate	24-MA1	Maybe 60-65/120°C	New	New	Multiple unresolved events	-45.2	NC	19.5	New	-25.8	DSC amorphous
	24-MA2	Maybe 60-65/120°C	New	New	Multiple unresolved events	-45.4	NC	19.4	New	-26.1	DSC amorphous
	24-MA3	Maybe 60-65/120°C	New	New	Multiple unresolved events	-47.7	NC	21.9	New	-26.0	DSC amorphous
	24-MB1	ND	New	New	Large shift or new	-30.0	NC	22.5	--	-7.7	Mixed Phase A – same crystalline form with some disorder*
	24-MB2	ND	New	New	Large shift or new	-29.9	NC	23.1	--	-6.9	Mixed Phase A – same crystalline form with some disorder*
	24-X1	ND	New	New	Large shift or new	-9.4	NC	7.0	--	-2.5	Mixed Phase A – same crystalline form with some disorder*
Loperamide HCl	14-MA1	New	New	New	shifted or new	-3.5	-8.9	1.1	--	0.0	Disordered
	14-MB1	ND	New	New	shifted or new	-5.8	-16.7	2.2	--	0.2	Mixed Phase A – same crystalline form with some disorder*
	14-X1	ND	New	New		-2.9	-11.1	1.2	--	0.1	Mixed Phase A – same crystalline form with some disorder
Acetylsalicylic acid	33-MA1	ND	ND	ND	--	-0.9	2.4	0.5	--	0.8	Crystalline concordant with reference
	33-MB1	ND	ND	ND	--	-0.3	2.4	0.3	--	2.6	Crystalline concordant with reference
	33-X1	ND	ND	ND	--	-0.6	1.2	0.0	--	0	Crystalline concordant with reference
Sulfamerazine	54-MA1	ND	ND	ND	New transition event	-1.2	39.0	0.9	ND	ND	Mixed Phase C – maybe mixture of crystalline forms with some disorder*
	54-MB1	ND	ND	ND	--	-1.5	2.1	0.9	ND	ND	Crystalline concordant with reference
	54-X1	ND	ND	ND	--	-1.5	0.7	0.9	ND	ND	Crystalline concordant with reference

Material	Batch ID	Glass transition events (G)	Crystallisation event (C)	Volatile event (V)	Melting events (M)				Degradation (D)		Comments & solid-state phase classification
					Melting event	ΔT_m (°C)	$\%\Delta H_f$ (%)	$\Delta T_m trans$ (°C)	Degradation event	ΔT_d (° C)	
Phenacetin	69-MA1	ND	ND	ND	--	-0.6	2.4	0.1	ND	ND	Crystalline concordant with reference
	69-MB1	ND	ND	ND	--	-0.2	5.9	-0.3	ND	ND	Crystalline concordant with reference
	69-X1	ND	ND	ND	--	-0.2	1.8	-0.1	ND	ND	Crystalline concordant with reference
Sulfadiazine	87-MA1	ND	ND	ND	shifted or new	-4.4	37.9	1.6	--	-4.8	Mixed Phase A – same crystalline form with some disorder*
	87-MB1	ND	ND	ND	shifted or new	-5.6	42.0	2.1	--	-5.4	Mixed Phase A – same crystalline form with some disorder*
	87-X1	ND	ND	ND		-2.6	4.1	0.8	--	-5.6	Mixed Phase A – same crystalline form with some disorder*
Caffeine	88-MA1	ND	ND	New	--	0.0	NC	-0.1	--	0.0	Mixed Phase A – same crystalline form with some disorder
	88-MB1	ND	ND	ND	--	0.0	NC	0.0	--	0.1	Mixed Phase A – same crystalline form with some disorder
	88-X1	ND	ND	ND	--	-0.1	NC	0.1	--	0.1	Mixed Phase A – same crystalline form with some disorder
Methyl paraben	140-MA1	ND	ND	ND	--	-0.6	7.3	-0.5	ND	ND	Crystalline concordant with reference
	140-MB1	ND	ND	ND	--	-0.3	6.7	-0.5	ND	ND	Crystalline concordant with reference
	140-X1	ND	ND	ND	--	-0.3	3.0	-0.4	ND	ND	Crystalline concordant with reference

** confirmed by XRPD, ND: Not detected, NC: Not calculated, ΔT_d: shift in degradation temperature (°C), ΔT_m: shift in onset of melting temperature (°C), $T_m trans$: change in melting transition range (°C), $\%\Delta H_f$: % change in Heat of fusion (%).#-MA#: high frequency ball-mill method A, #-MB#: low frequency ball-mill method B. #-X#: jet micronisation method A. Please refer to Table 3-4 for further descriptions of the terms*

For γ-indomethacin, salbutamol sulphate and loperamide HCl comminuted by different processes and conditions, the DSC thermograms and responses suggest that a different solid-state phase or form maybe present (Table 6-17). However, the XRPD diffractograms for these materials (Section 6.4.1) did not indicate the presence of a new solid-state form, therefore it can be inferred that the observed changes in the DSC responses are likely as a result of solid-state phase changes and that there is disorder present.

Comminution of γ-indomethacin by different processes and conditions resulted in the generation of materials that encompassed the whole amorphous-crystalline continuum (Table 6-17). High frequency ball-milling (Mill-A) generated disordered material as indicated by the presence of glass transition and recrystallisation events consistent with that cited in the literature[254,352-354]. In comparison, no glass transition event was observed for material comminuted by low frequency ball-milling (Mill-B) but some degree of disorder could be inferred from the observance of a crystallisation event (Figure 6-11). However, γ-indomethacin appeared to remain crystalline when micronised (JM-A) with respect to the DSC thermogram and associated responses (Figure 6-11).

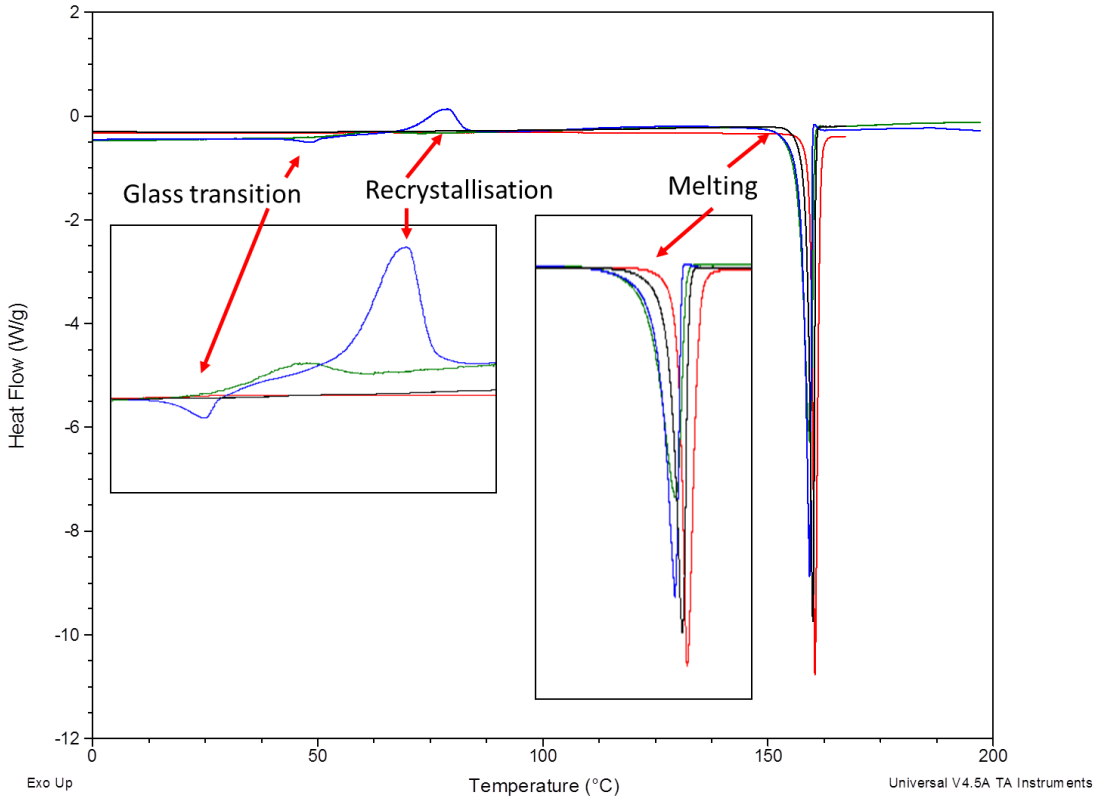

Figure 6-11 ***DSC thermograms for the comminuted materials of indomethacin ball-milled at high frequency (blue), at low frequency (green) and micronised (Black) compared to the input material (red)***

High frequency ball-milling of loperamide HCl resulted in the generation of disordered material as shown by the presence of a high temperature glass transition (121 °C), recrystallisation events and an observed volatile (moisture) loss (Figure 6-12). It has been suggested that the high temperature of the glass transition is due to the stabilisation of the amorphous state by the formation of a salt[355]. This type of elevated T_g has also been demonstrated for indomethacin using a sodium salt which increased the T_g from 45 °C to 121 °C[356,357]. Confirmation of the volatile (moisture) loss is shown by the overlaid weight loss event in the TGA thermogram and degradation also appears to occur soon after melting (Figure 6-12). Both low frequency ball-milling and micronisation of loperamide HCl resulted in recrystallisation and volatile loss events, along with an observed shift in the melting onsets of their respective DSC thermograms. These observations suggest that some degree of disorder was present but more so for the low frequency ball-milled material than micronised (Figure 6-13).

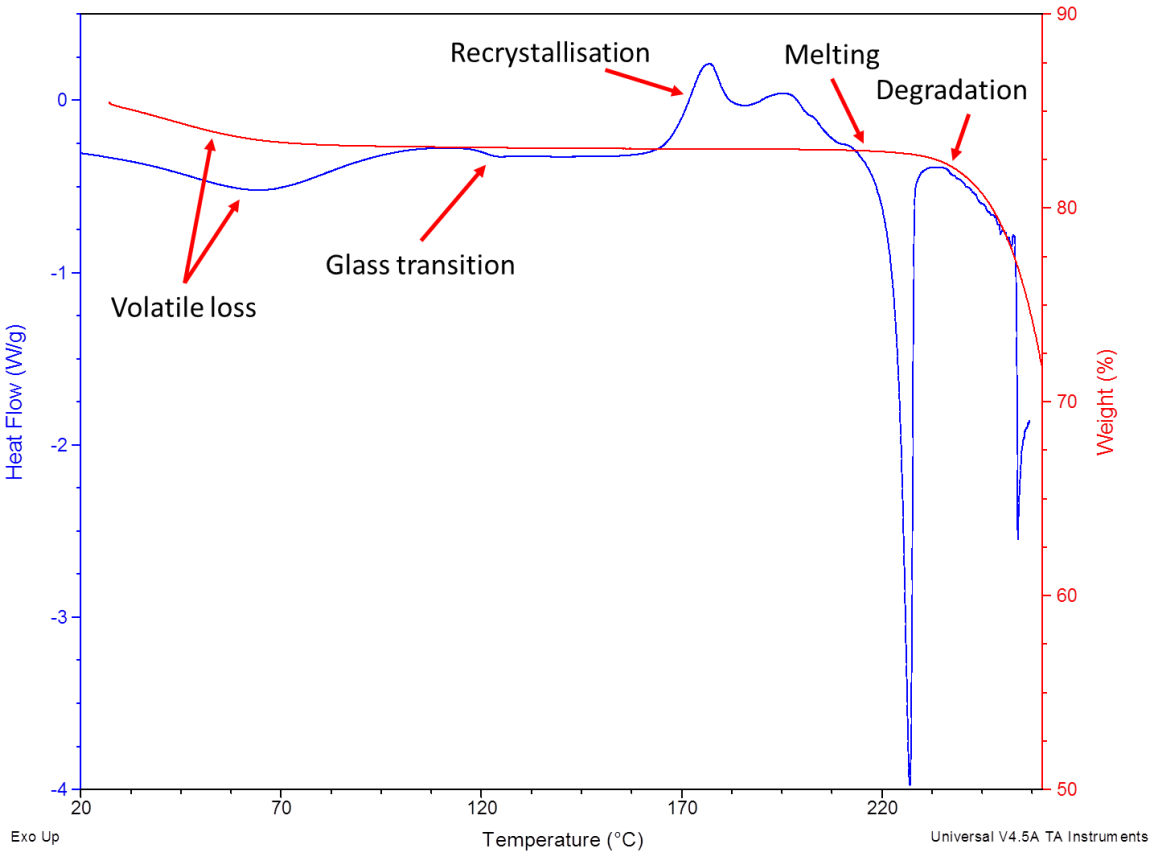

Figure 6-12 Overlaid DSC (blue) and TGA (red) thermograms for high frequency ball-milled loperamide HCl

Overlaid TGA thermogram verifies the events associated with weight losses such as volatile (moisture loss) and degradation.

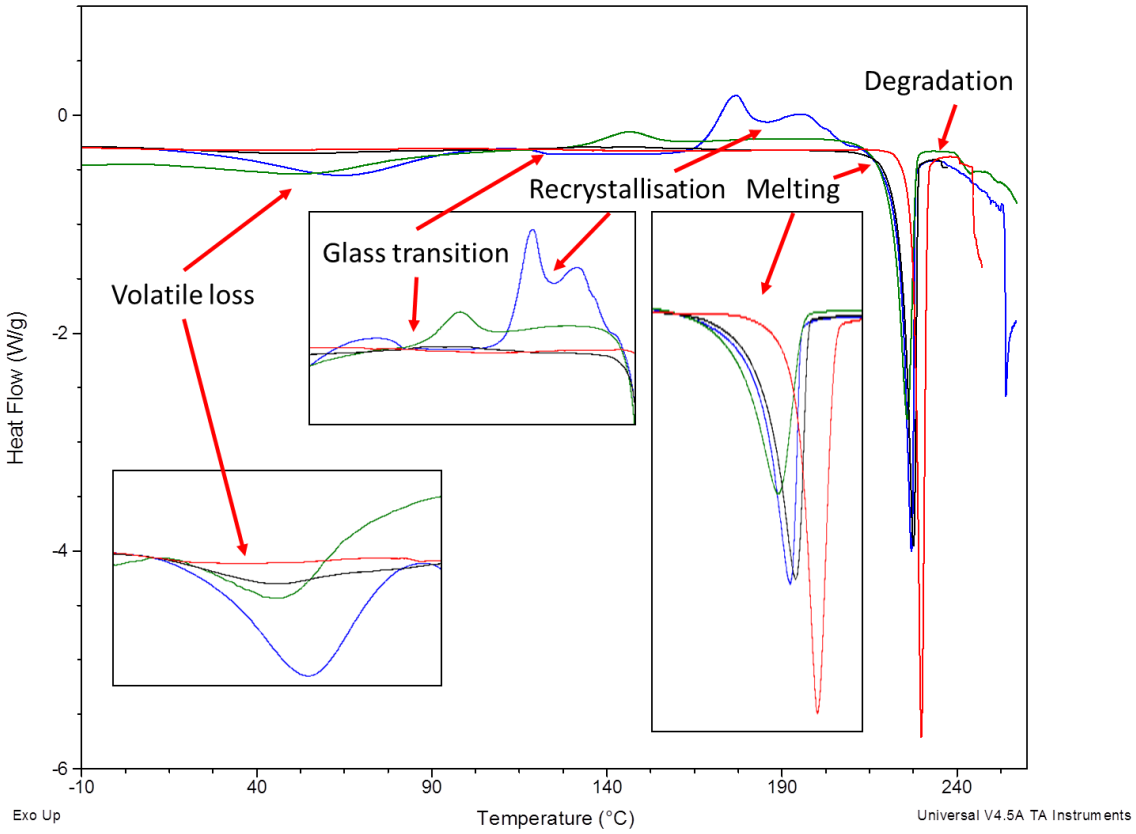

Figure 6-13 DSC thermograms for the comminuted materials of loperamide HCl ball-milled at high frequency (blue), at low frequency (green) and micronised (black) compared to the input material (red)

DSC analysis of the high frequency ball-milled material of salbutamol sulphate exhibited multiple unresolved events (Table 6-16, Figure 6-14). Overlaying the TGA and DSC thermograms assisted in defining these events (Figure 6-14). A weight loss event observed below 80 °C in the TGA thermogram coincided with the broad endotherm in the DSC between 0 and 100 °C, suggesting the loss of absorbed moisture over this range. Potentially the T_g for salbutamol sulphate may fall within this region, as it has been noted to occur around 60-65 °C when there is moisture the present[19,247,358]. However, amorphous salbutamol sulphate prepared by spray or freeze drying has a T_g around 120 °C which likely represents the dry T_g[359] and this may also be present in the acquired DSC thermogram (Figure 6-14). Therefore, following the volatile (moisture) loss and "wet T_g" there is a potential restructuring of the molecule given rise to the "dry T_g" prior to recrystallisation[19,21]. The material then melt-degrades[1,19,297,358] at a much lower temperature than that of the crystalline input material, with an observed shift of 45 °C. Based on these observations it can be concluded that high frequency ball-milled salbutamol sulphate is predominately disordered and can be classed as "DSC amorphous" in accordance to the novel solid-state classification process (Section 6.3.3.3.).

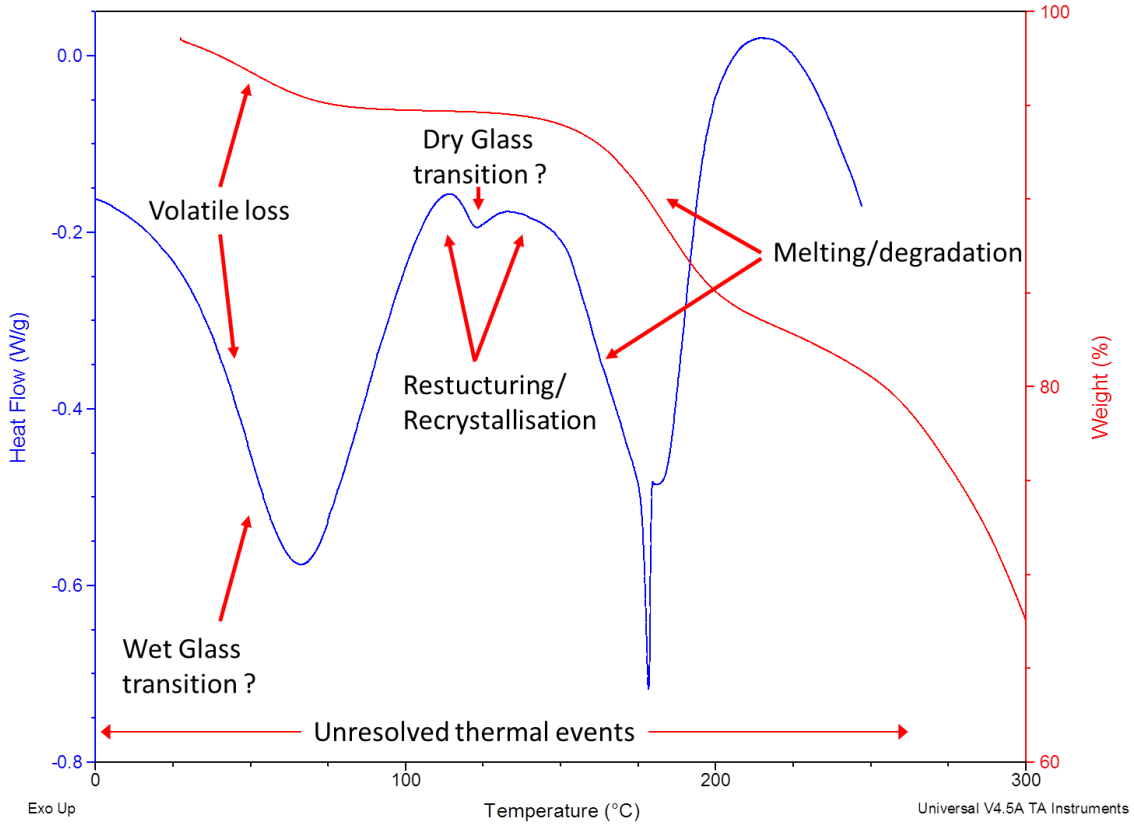

Figure 6-14 Overlaid DSC (blue) and TGA (red) thermograms for high frequency ball-milled (Mill-A1) salbutamol sulphate

The DSC thermogram exhibits multiple unresolved thermal events while the overlaid TGA thermogram verifies the events associated with weight losses such as volatile (moisture loss) and degradation.

Lower frequency ball-milling and micronisation of salbutamol sulphate also appears to generate some level of disorder, though to a much lower degree than higher frequency ball-milling, as shown by their respective DSC thermograms and responses (Figure 6-15 and Table 6-17). For each of these materials, volatile (moisture) loss and recrystallisation events were observed alongside a significant decrease in the melt-degradation onset temperatures.

It is postulated that the observed large decrease in T_m for the comminuted materials of salbutamol sulphate maybe due to the decrease in particle size, the presence of thermal degradants or due to increased levels of lattice disordering.

Information relating to changes in the solid state form or phase present can be discerned by changes in melting responses ΔT_m, $\Delta T_m trans$ and ΔH_f. For materials which don't melt-degrade then T_m should stay the same for a crystalline materials with the same solid state form. However, if impurities such as thermal degradants are generated as a result of mechanical processing then T_m could be reduced. If disorder is introduced as a form of a phase impurity, the remaining crystalline material will melt at the same T_m but

the heat of fusion could be reduced proportionally to the amount of disorder present. However, if unresolved crystallisation-melting occurs then the change in ΔH_f for the melting peak may not be as pronounced.

For materials such as salbutamol sulphate which melt-degrade, then the decrease in T_m could be due to the introduction of disorder into the material as a consequence of the comminution process. The generated disorder decreases the lattice strength thereby lowering the amount of energy (and temperature) required to initiate melting. The amount of decrease observed therefore is proportional to both the amount of energy applied during the comminution process and the degree of induced disorder. For salbutamol sulphate, high frequency ball-milling gave the largest shift in T_m followed by lower frequency ball-milling and then micronisation. As discussed in Section 1.4.2 ball-milling is a high impact and high input energy process, where the material is isolated in the same chamber for a prolonged period of time and subjected to prolonged impacts. In comparison, micronisation exposes the material to only limited high impact processes until the particle is reduced in size so that it can be collected. Therefore, it is more likely that more disorder will be generated by ball-milling than by micronisation and this can be observed by the decrease in T_m as shown by the comminuted materials of salbutamol sulphate[2] (Table 6-17). These observed shifts are more pronounced in materials which melt-degrade[360].

The fact that micronisation, which in general results in smaller particle sizes had the lowest decrease in T_m also supports the suggestion that disorder is responsible for the decrease T_m and also suggests that the decrease in particle size is not the cause for this observed shift in T_m.

As the level of disorder increases for a given melt-degradation material, the amount of thermal degradants may also increase which can influence the degree of observed T_m shifting. When ball-milling at room temperature there is no effective temperature control, therefore the likelihood of generating thermal degradants is higher than ball-milling using liquid nitrogen. For salbutamol sulphate ball-milled at high frequency with (Mill-A1/2) and without (Mill-A3) liquid nitrogen there were no significant differences in the DSC responses and in both cases “DSC amorphous” material was generated (Figure 6-15 and Table 6-17). This implies that the observed decrease in T_m is most likely due to the level of disorder generated as a consequence of the comminution process rather than due to the presence of thermal degradants, as cryogenic ball-milling

should have been sufficient to control the temperature at such a level so as to limit any localised melt-degradation and thereby, prevent the generation of thermal degradants.

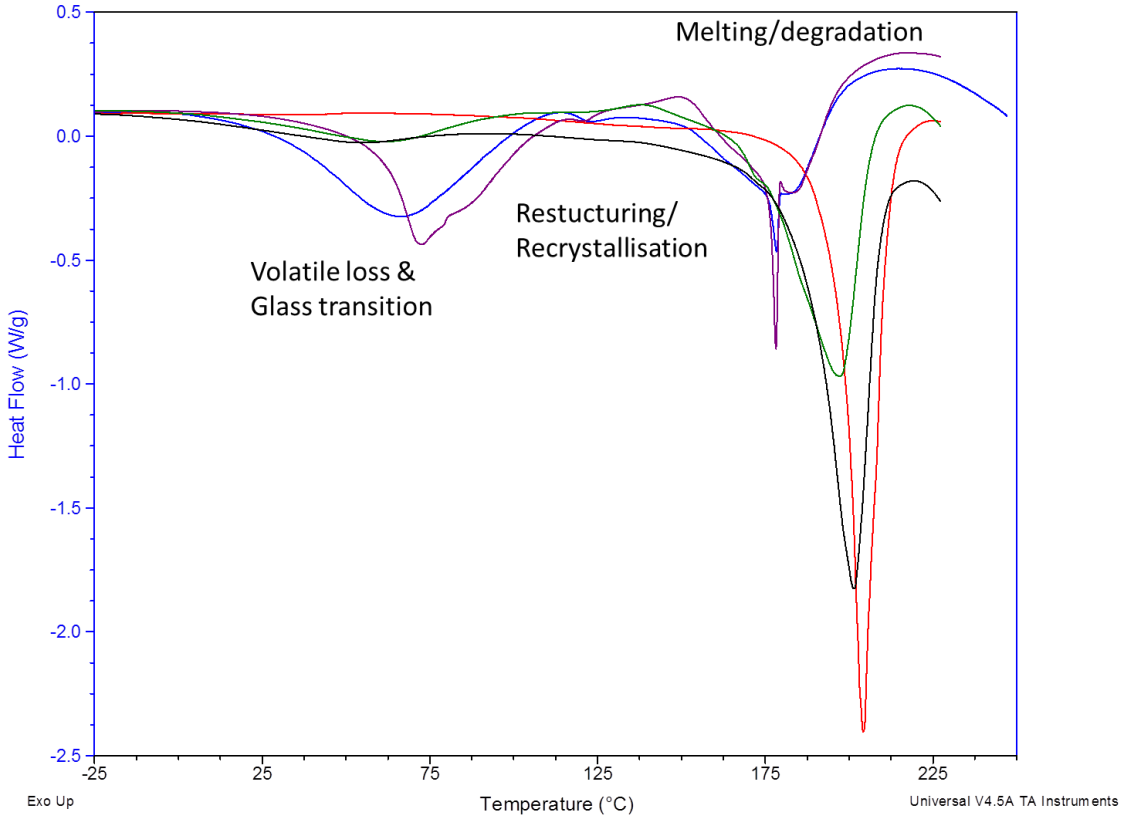

Figure 6-15 DSC thermograms for the comminuted materials of salbutamol sulphate by high frequency ball-milling with liquid nitrogen (blue) at room temperature (purple), low frequency ball-milling (green) and micronisation (Black) compared to the input material (red).

A small degree of disorder was induced in comminuted sulfadiazine, as inferred from the observed small shift in T_m, the broadening of the melting event and the decrease in degradation temperature (Table 6-17). It should be noted that ΔH_f values actually increase, which may suggest that particle size is influencing the observations. However, the DSC responses for the micronised material are less affected than the ball-milled materials, so it less likely that particle size is influencing these observations and hence the changes in the thermograms are more likely to be due to the presence of disorder (Figure 6-16).

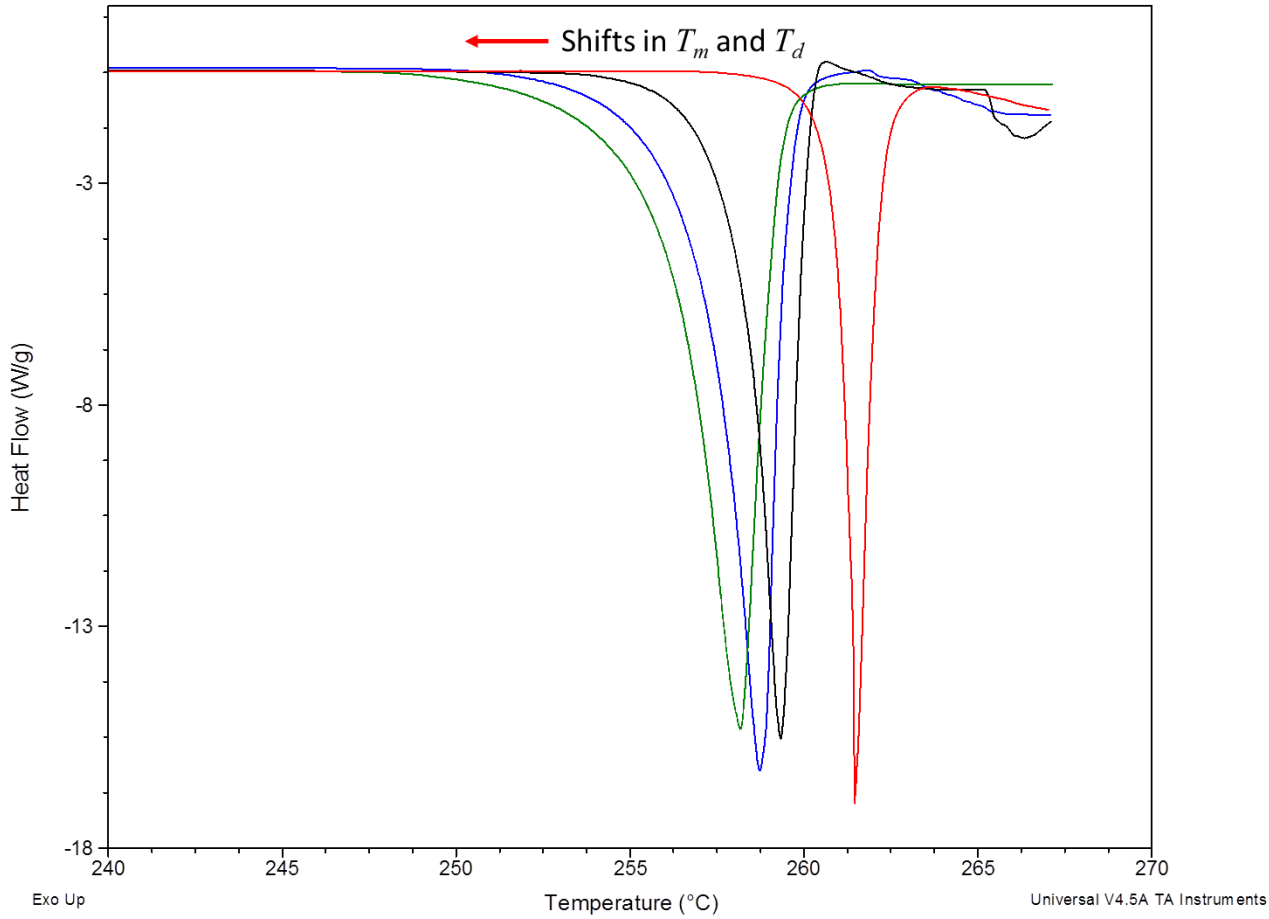

Figure 6-16 DSC thermograms for the comminuted materials of sulfadiazine by high frequency ball-milling (blue), low frequency ball-milling (green) and micronisation (black) compared to the input material (red).

The high frequency ball-milling of sulfamerazine resulted in an observed solid-state transition at 142 °C from Form II to Form I, consistent with the author's previous observations[350,351] and those from the literature[336,361,362] (Figure 6-17). This polymorph transition is thought to arise as a consequence of ball-milling, whereby the material is transformed through a series of transitions from Form I to amorphous to Form II and then back to Form I[349-351]. The solid-state phase present will depend on both the type of comminution process and the length of the comminution process employed. In this case high frequency ball-milling imparted sufficient energy and was of sufficient duration to convert some of the material from Form I to amorphous and then to Form II at the completion of the process. When analysed by DSC, disorder is only inferred to have occurred in the sulfamerazine subjected to high frequency comminution due to the presence of Form II, as there are no other indications of its presence (Figure 6-17).

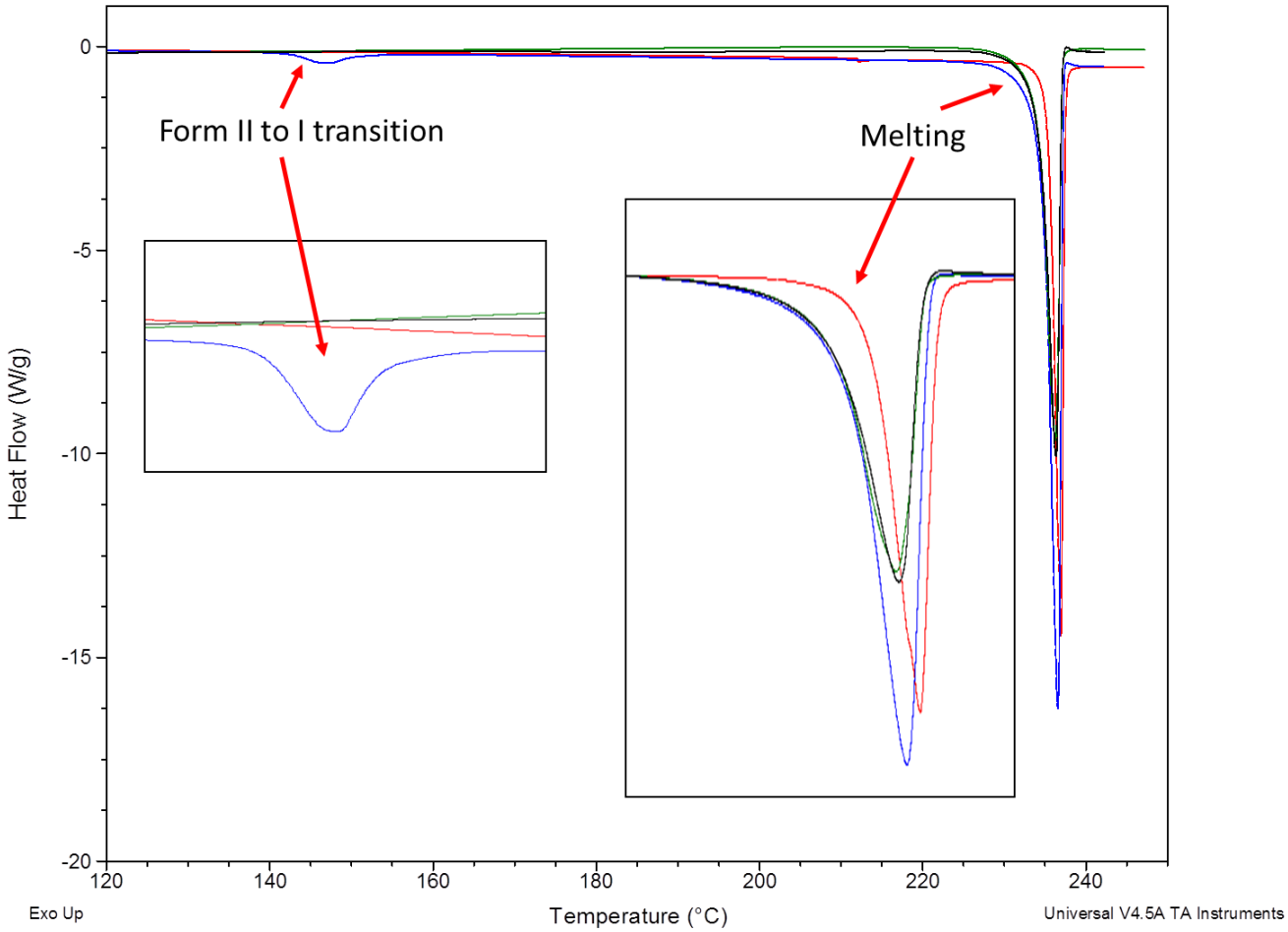

Figure 6-17 ***DSC thermograms for the comminuted materials of sulfamerazine by high frequency ball-milling (blue), low frequency ball-milling (green) and micronisation (black) compared to the input material (red).***

DSC analysis of the comminuted materials of caffeine show that all the processed materials exhibit similar DSC thermograms to that of the input material, *i.e.* a Form II to Form I solid-state transition[216,342,343] and a melt-sublimation event (Table 6-16). However, for the high frequency ball-milled material an endothermic loss of moisture also occurs (as verified by the TGA thermogram, Figure 6-18) followed by a shift in the solid-state transition temperature (Table 6-16).. These findings suggest that a small degree of disorder may have been generated. In fact, all the comminution processes for caffeine appear to have caused a shift in the solid-state transition temperature. The more aggressive the process, the greater the shift, but in all cases the melt-sublimation temperature remained the same (Figure 6-19 and Table 6-16).

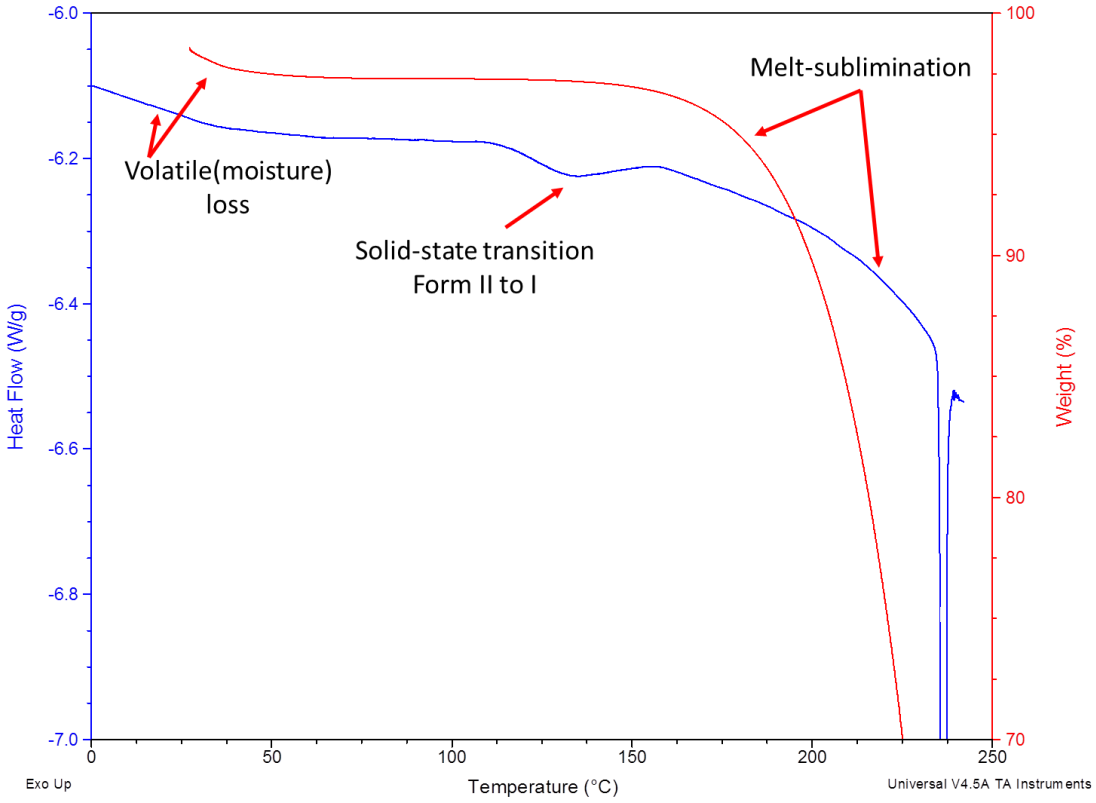

Figure 6-18 Overlaid DSC (blue) and TGA (red) thermograms for high frequency ball-milled caffeine

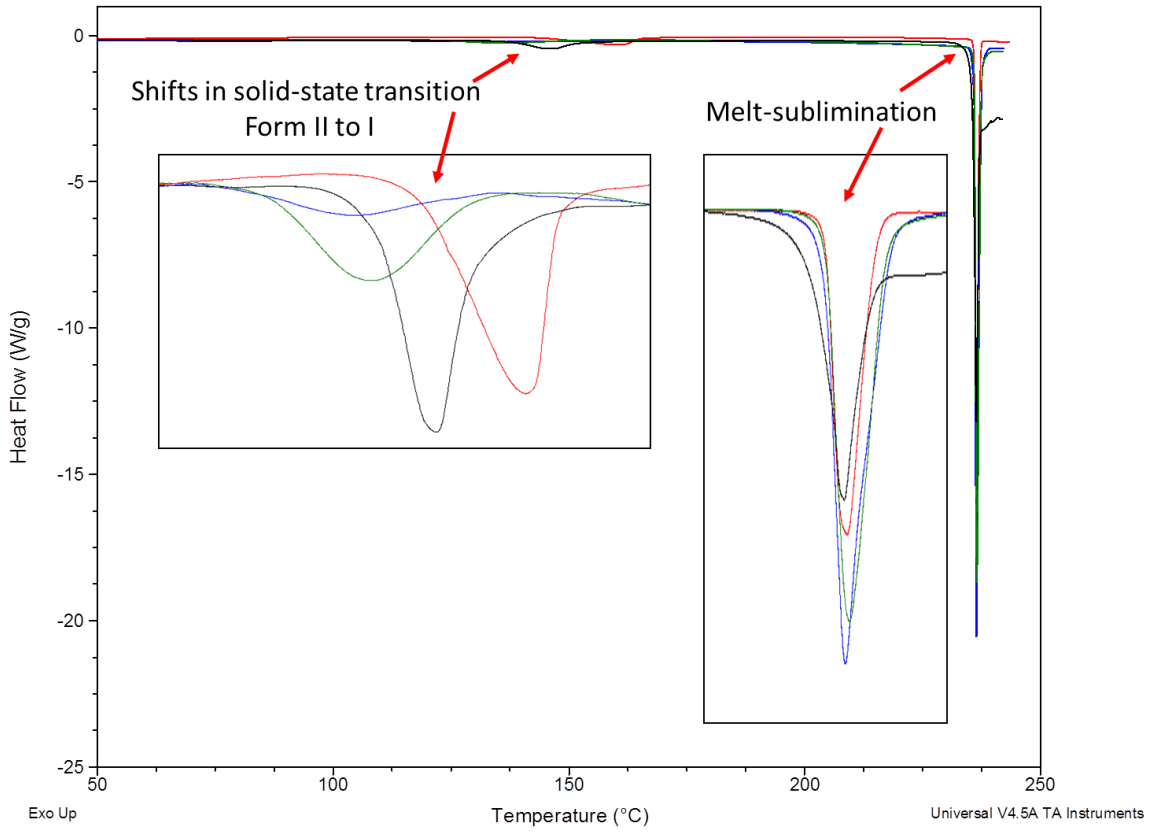

Figure 6-19 DSC thermograms for the comminuted materials of caffeine by high frequency ball-milling (blue), low frequency ball-milling (green) and micronisation (black) compared to the input material (red).

6.4.4 Laser particle size analysis (PSA)

The particle size distributions (PSDs) and responses for the mechanically comminuted materials were compared to those of the input materials (Table 6-18).

During comminution, particle size is generally reduced, which can increase the surface area of the material and therefore result in greater moisture adsorption. This sorption of water can occur along disordered surfaces forming inter-particle bridges or cause fusion of particles resulting in an increase in particle size due to agglomeration or recrystallisation[19,20,288,290]. Agglomeration can also result as a consequence of electrostatic charging induced by the milling/micronisation process[363].

In general ball-milling produced only moderate effects in reducing the particle size of the comminuted materials and often resulted in a broadening of the PSDs (Table 6-18). Micronisation on the other hand was effective in reducing the particle size for all the materials, and generated the same PSD regardless of the type of material comminuted.

High frequency ball-milling of acetaminophen did not reduce the particle size of the material, but instead resulted in larger or agglomerated particles as illustrated in Figure 6-20 and Table 6-18. Low frequency milling was more successful in reducing the particle size but the PSD was broad and larger particles still remain (Figure 6-20 and Table 6-18). When micronised, the particle size of acetaminophen was significantly reduced (D_{90} < 5 µm) giving rise to a narrower (F_{span} >1) mono-modal PSD (Figure 6-20 and Table 6-18).

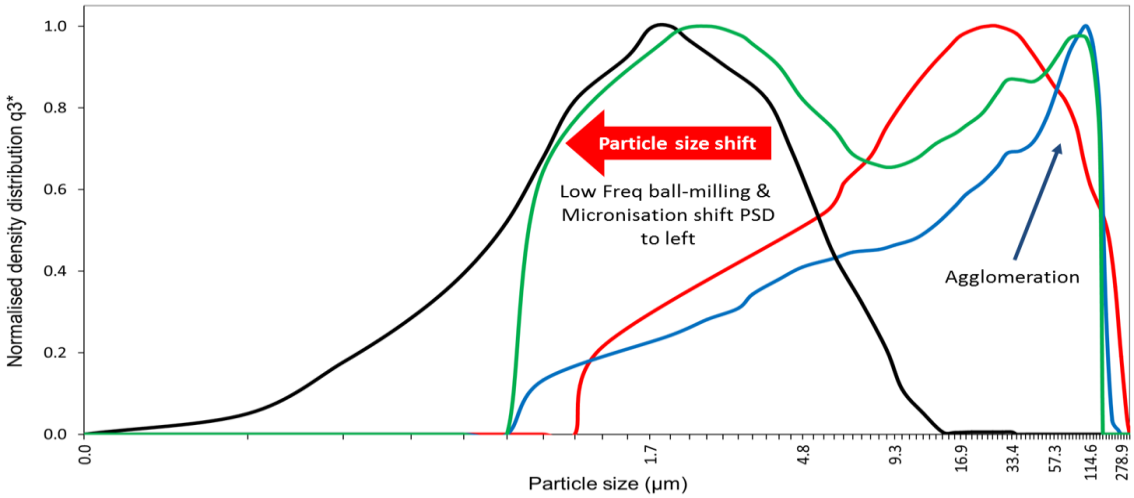

Figure 6-20 ***Average particle size distributions for the comminuted materials of acetaminophen by high frequency ball-milling (blue), low frequency ball-milling (green) and micronisation (black) compared to the input material (red).***
Note: below 2µm, particle size distribution shape differs between comminuted materials due to the size of lens used.

Table 6-18 Average particle size responses and CRA of the comminuted materials

		PSA responses								PSA CRA						
Material	Batch ID	n	D_{10} (µm)	D_{50} (µm)	D_{90} (µm)	Span (µm)	VMD (µm)	Sm (cm^2/g)	No. Mode	ΔD_{10}	ΔD_{50}	ΔD_{90}	Δmodes	F_{span}	F_{VMD}	F_{Sm}
Acetaminophen	Input	6	3.58	23.5	132	5.5	47.5	5854	3	--	--	--	--	--	--	--
	1-MA1	6	2.87	32.5	132	4.0	51.4	7300	3	-0.71	8.94	-0.64	0	1.38	0.92	0.80
	1-MA2	6	2.82	33.8	130	3.8	50.5	7382	3	-0.76	10.2	-2.17	0	1.45	0.94	0.79
	1-MB1	6	1.24	11.0	102	9.1	32.2	15426	4	-2.34	-12.5	-30.9	1	0.60	1.47	0.38
	1-MB2	6	1.22	9.98	102	10.1	31.8	15703	4	-2.36	-13.6	-30.1	1	0.54	1.50	0.37
	1-X1	6	0.79	2.05	5.53	2.3	2.76	37980	1	-2.80	-21.5	-127	-2	2.37	17.2	0.15
γ-Indomethacin	Input	6	4.87	24.4	94.7	3.7	38.8	5690	2	--	--	--	--	--	--	--
	11-MA1	6	2.19	18.3	115	6.2	39.4	9557	3	-2.68	-6.13	20.6	1	0.60	0.99	0.60
	11-MA2	6	1.90	14.8	76.7	5.1	27.7	11388	4	-2.97	-9.63	-18.0	2	0.73	1.40	0.50
	11-MB1	6	1.51	14.9	115	7.6	41.0	12436	4	-3.36	-9.53	20.3	2	0.48	0.95	0.46
	11-MB2	6	1.40	13.4	97.3	7.2	32.6	13951	4	-3.47	-11.0	2.54	2	0.51	1.19	0.41
	11-X1	6	0.60	1.74	3.77	1.8	2.02	47978	2	-4.27	-22.7	-91.0	0	2.02	19.2	0.12
Loperamide HCl	Input	6	1.71	17.15	139	8.0	43.3	11021	3	--	--	--	--	--	--	--
	14-MA1	6	1.22	7.06	86.6	12.1	25.8	16649	4	-0.50	-10.1	-52.7	1	0.66	1.68	0.66
	14-MB1	6	1.29	9.34	89.0	9.4	28.1	15233	4	-0.42	-7.81	-50.3	1	0.85	1.54	0.72
	14-X1	6	0.52	1.40	3.19	1.9	1.67	56618	2	-1.20	-15.7	-136	-1	4.20	26.0	0.19
Salbutamol sulphate	Input	6	47.5	144	267	1.5	152.7	1194	1	--	--	--	--	--	--	--
	24-MA1	6	1.45	11.8	103	8.6	32.6	13424	4	-46.1	-133	-164	3	0.18	4.68	0.09
	24-MA2	6	1.35	10.4	98.4	9.4	30.8	14506	4	-46.2	-134	-169	3	0.16	4.95	0.08
	24-MA3	6	1.24	9.06	94.0	10.2	25.4	16152	4	-46.3	-135	-173	3	0.15	6.01	0.07
	24-MB1	6	1.12	6.97	87.3	12.4	26.4	17780	4	-46.4	-137	-180	3	0.12	5.78	0.07
	24-MB2	6	0.93	6.58	87.0	13.1	20.7	21721	4	-46.6	-138	-180	3	0.12	7.37	0.05
	24-X1	6	0.60	1.58	3.78	2.0	1.96	49925	2	-46.9	-143	-263	1	0.75	78.0	0.02
Acetylsalicylic acid	Input	6	115	203	346	1.1	217	495	2	--	--	--	--	--	--	--
	33-MA1	6	1.52	13.5	102	7.5	33.8	12624	4	-113	-190	-244	2	0.15	6.41	0.04
	33-MB1	6	1.03	5.96	93.4	15.5	27.8	19518	4	-114	-197	-252	2	0.07	7.80	0.03
	33-X1	6	0.75	1.55	2.92	1.4	1.73	45563	1	-114	-202	-343	-1	0.81	125	0.01

		PSA responses								PSA CRA						
Material	Batch ID	n	D_{10} (µm)	D_{50} (µm)	D_{90} (µm)	Span (µm)	VMD (µm)	Sm (cm^2/g)	No. Mode	ΔD_{10}	ΔD_{50}	ΔD_{90}	Δmodes	F_{span}	F_{VMD}	F_{Sm}
Sulfamerazine	Input	6	13.0	33.8	67	1.6	37.5	3044	1	--	--	--	--	--	--	--
	54-MA1	6	1.27	9.21	98.3	10.5	30.0	15380	4	-11.7	-24.6	31.4	3	0.15	1.25	0.20
	54-MB1	6	1.95	27.2	127	4.6	47.8	9612	4	-11.0	-6.61	60.0	3	0.35	0.78	0.32
	54-X1	6	0.54	1.79	4.38	2.1	2.19	49188	1	-12.4	-32.0	-62.6	0	0.74	17.1	0.06
Phenacetin	Input	6	8.3	34.3	96.2	2.6	44.8	3941	1	--	--	--	--	--	--	--
	69-MA1	6	1.56	11.7	96.5	8.1	30.8	12760	4	-6.70	-22.7	0.31	3	0.31	1.45	0.31
	69-MB1	6	2.04	16.0	53.1	3.2	22.8	10114	2	-6.21	-18.3	-43.1	1	0.80	1.96	0.39
	69-X1	6	0.72	1.95	4.22	1.8	2.27	41917	1	-7.54	-32.4	-92.0	0	1.43	19.7	0.09
Sulfadiazine	Input	6	2.7	10.6	42.8	3.8	17.0	10151	2	--	--	--	--	--	--	--
	87-MA1	6	1.81	22.0	153	6.9	52.1	10376	4	-0.92	11.4	111	2	0.55	0.33	0.98
	87-MB1	6	1.86	27.4	171	6.2	59.3	9869	4	-0.87	16.8	128	2	0.61	0.29	1.03
	87-X1	6	0.66	2.06	4.61	1.9	2.43	42614	1	-2.07	-8.56	-38.2	-1	1.97	7.00	0.24
Caffeine	Input	6	2.9	23.7	147	6.1	51.0	7613	3	--	--	--	--	--	--	--
	88-MA1	6	3.29	32.6	141	4.23	54.0	6754	3	0.36	8.82	-5.95	0	1.45	0.94	1.13
	88-MB1	6	1.86	42.2	143	3.37	58.5	9317	3	-1.07	18.5	-3.31	0	1.82	0.87	0.82
	88-X1	6	0.75	1.73	3.46	1.57	2.23	43212	2	-2.18	-22.0	-143	-1	3.90	22.9	0.18
Methyl paraben	Input	6	16.6	63.7	157	2.2	76.7	1650	2	--	--	--	--	--	--	--
	140-MA1	6	3.33	27.8	115	4.03	44.6	6850	3	-13.3	-35.9	-41.7	1	0.55	1.72	0.24
	140-MB1	6	3.60	29.7	141	4.63	52.4	6436	3	-13.0	-34.0	-16.0	1	0.48	1.46	0.26
	140-X1	6	2.63	8.05	26.1	2.89	11.6	13536	2	-14.0	-55.6	-131.0	0	0.76	6.60	0.12

n – Number of replicates. D#: particle size for decile #. VMD: volume mean diameter, Sm: Surface area, No. Mode: number of modes. Span: width of particle distribution.
$\Delta D_{\#}$: changes in particle size for decile #. Δmodes: change in the number of modes. F_{span}: degree of change in span. F_{VMD}: degree of change in volume mean diameter. F_{Sm}: degree of change in surface area. #-MA#: high frequency ball-mill method A, #-MB#: low frequency ball-mill method B. #-X#: jet micronisation method A
For further definitions of the terms please refer to Table 3-9.

For indomethacin and phenacetin, ball-milling resulted in material with a broad multi-modal PSD in which particle size was not significantly reduced. However, when micronised the resulting PSD of the product was narrower and mono-modal with the majority of the particles (D_{90}) being less than 3-4 µm (Table 6-18).

The input material for loperamide HCl exhibited agglomeration which upon ball-milling was moderately reduced along with the overall particle size. However, some agglomeration still remains (Table 6-18 and Figure 6-21). When micronised a narrow mono-modal PSD for loperamide HCl was produced, in which the majority of the particles (D_{90}) were less than 3 µm (Table 6-18 and Figure 6-21).

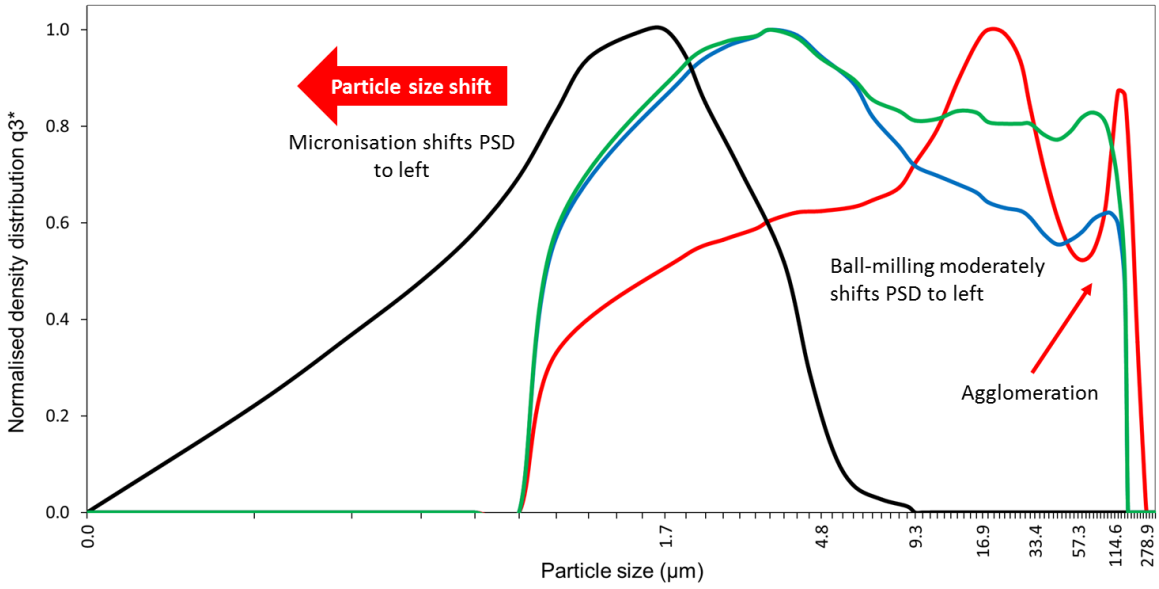

Figure 6-21 ***Average particle size distributions for the comminuted materials of loperamide HCl by high frequency ball-milling (blue), low frequency ball-milling (green) and micronisation (black) compared to the input material (red).***

Note: below 2µm, particle size distribution shape differs between comminuted materials due to the size of lens used

The input material for salbutamol sulphate was large with a mono-modal PSD (Table 6-18). The particle size was effectively reduced when ball-milled using high or low frequency but the PSD was fairly broad and multi-modal (Table 6-18 and Figure 6-22). The particle size of micronised salbutamol sulphate on the other hand was significantly reduced with the majority of particles (D_{90}) being less than 3 µm (Table 6-18 and Figure 6-22).

Ball-milling acetylsalicylic acid was also effective in reducing the particle size but the resultant material was found to have a broad and multi-modal PSD. Micronisation, was more effective than ball-milling in changing particle sizes and distributions resulting in a mono-modal PSD with the majority of the particles (D_{90}) being less than 2 µm (Table 6-18).

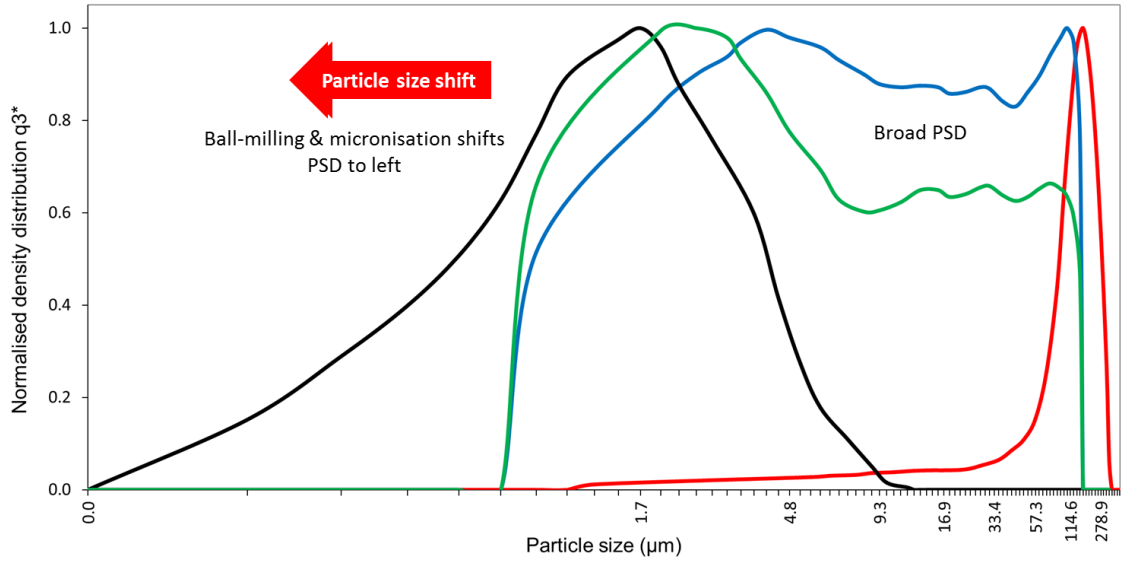

Figure 6-22 ***Average particle size distributions for the comminuted materials of salbutamol sulphate by high frequency ball-milling (blue), low frequency ball-milling (green) and micronisation (black) compared to the input material (red).***

Note: below 2µm, particle size distribution shape differs between comminuted materials due to the size of lens used

Like salbutamol sulphate, the input material for sulfamerazine was also mono-modal. When ball-milled, the overall particle sizes of the comminuted material were reduced. However, some larger particles were observed which may suggest either particle growth or agglomeration as a consequence of the comminution process had occurred (Table 6-18 and Figure 6-23). This is consistent with the XRPD and DSC analysis which suggests a solid-state transformation had occurred, therefore large particles maybe as a result of recrystallisation that may have occurred during milling. Upon micronisation a narrow mono-modal PSD was observed with the majority of the particles (D_{90}) being less than 4 µm (Table 6-18 and Figure 6-23).

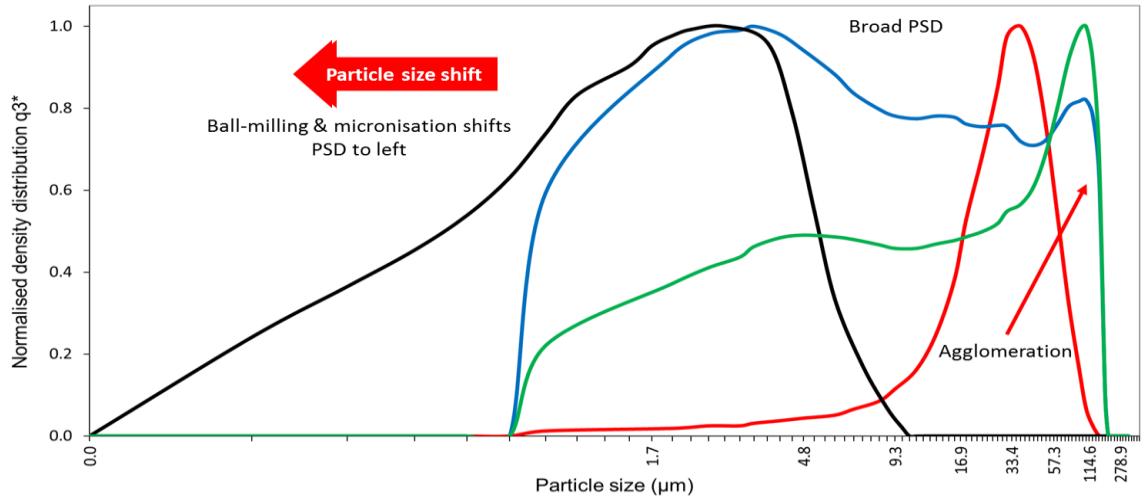

Figure 6-23 ***Average particle size distributions for the comminuted materials of sulfamerazine by high frequency ball-milling (blue), low frequency ball-milling (green) and micronisation (black) compared to the input material (red).***

Note: below 2µm, particle size distribution shape differs between comminuted materials due to the size of lens used

Both high and low frequency ball-milling had little effect in reducing the particle size of sulfadiazine, and instead introduced agglomerates into the powder (Table 6-18 and Figure 6-24). When micronised, a narrow mono-modal PSD was observed with the majority of the particles (D_{90}) being less than 4 µm (Table 6-18 and Figure 6-24).

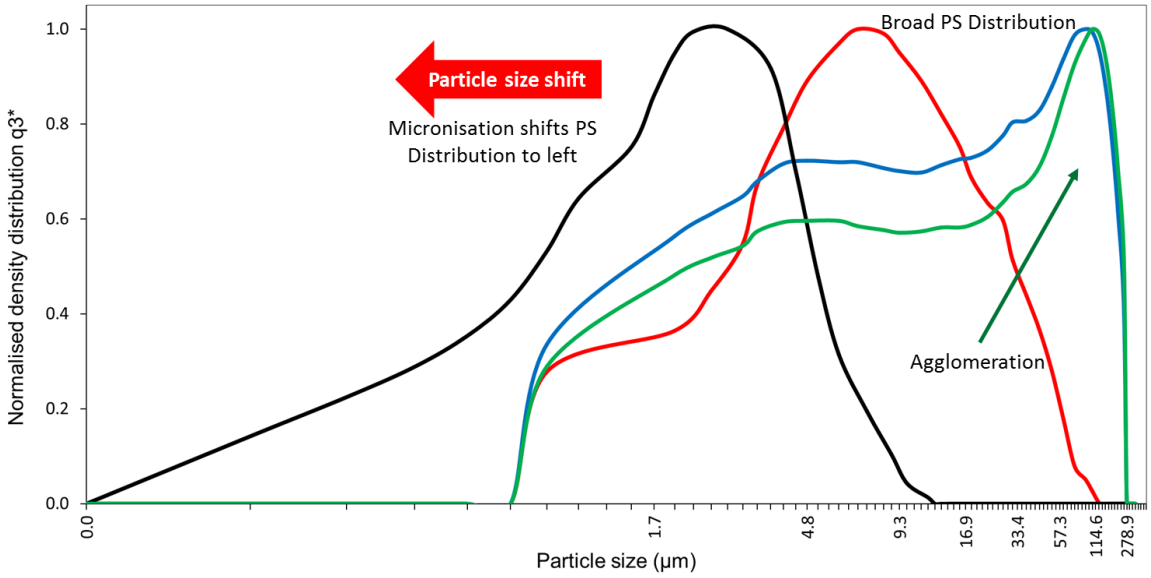

Figure 6-24 ***Average particle size distributions for the comminuted materials of sulfadiazine by high frequency ball-milling (blue), low frequency ball-milling (green) and micronisation (black) compared to the input material (red).***

Note: below 2µm, particle size distribution shape differs between comminuted materials due to the size of lens used

Ball-milling methyl paraben had a moderate effect in reducing the particle size, but still resulted producing a material with a broad multi-modal PSD. When the input material was micronised, the particle size was only reduced to less than 30 µm, the smallest reduction of all the micronised materials which typically had particle sizes less than 10 µm (Table 6-18).

The input material for comminuted caffeine was initially agglomerated. Ball-milling of this material had little effect on either reducing the particle size or altering the PSD (Table 6-18 and Figure 6-25). However, when micronised the PSD was narrowed and resulted in a majority of particles (D_{90}) being less than 3 µm.

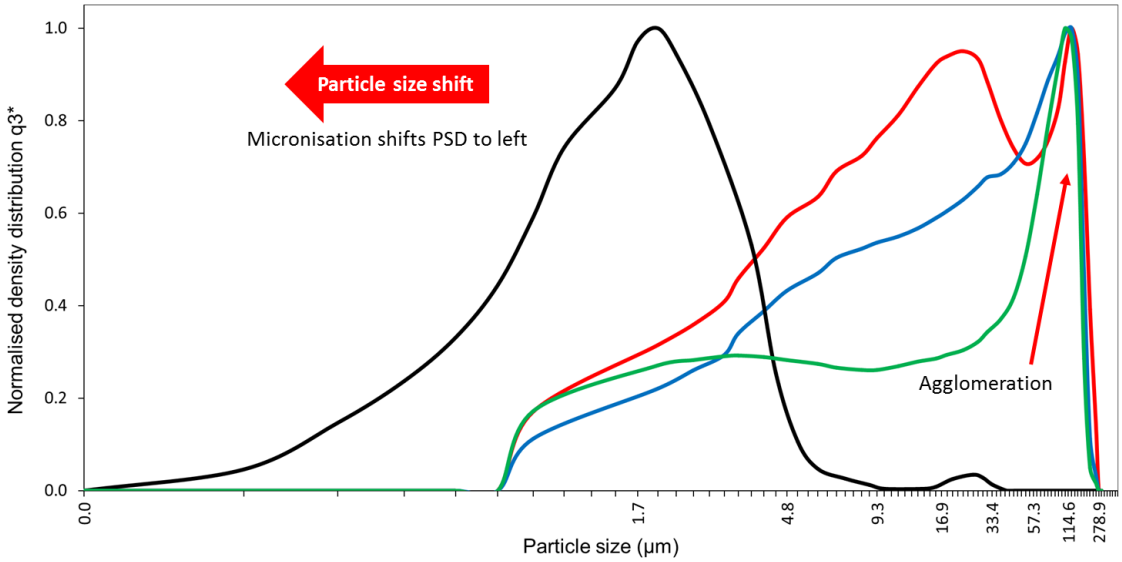

Figure 6-25 ***Average particle size distributions for the comminuted materials of caffeine by high frequency ball-milling (blue), low frequency ball-milling (green) and micronisation (black) compared to the input material (red).***

Note: below 2µm, particle size distribution shape differs between comminuted materials due to the size of lens used

6.4.5 Scanning electron microscopy (SEM)

SEM analysis of the comminuted materials showed that the particles in general exhibited irregular particle morphologies with rough surfaces, fractured edges and were agglomerated and drusy *i.e.* coated with finer particles (Table 6-19). An example of this agglomeration for the comminuted materials can be seen in Figure 6-26 for sulfadiazine, where particle size appears to increase upon ball-milling due to agglomeration of smaller particles. This is consistent with the observed PSD for this material (Table 6-18 and Figure 6-24). Based on this observation it would be expected that T_m may have increased as the particle size has increased[288,289]. However, DSC analysis for this material (Section 6.4.3) showed that T_m had in fact slightly decreased in temperature, which may suggest the presence of some disorder. It is proposed that during the milling process the input sulfadiazine particles were reduced in size with some disorder introduced onto their surfaces. These smaller particles then fused together via recrystallisation of the disordered regions to form agglomerates[19], as depicted in Figure 6-26[B] without changing the solid-state form of the final comminuted material, as the XRPD diffractogram was concordant with input (Section 6.4.1).

Table 6-19 SEM analysis of the comminuted materials

		SEM responses			
Material	Batch ID	Crystal habit	Edge	Surface	Agglomeration
Acetaminophen	Input	Acicular & columnar	Fractured	Rough	Drusy
	1-MA1	Irregular	Fractured	Rough	Agg & Drusy
	1-MA2	Irregular	Fractured	Rough	Agg & Drusy
	1-MB1	Irregular	Fractured	Rough	Agg & Drusy
	1-MB2	Irregular	Fractured	Rough	Agg & Drusy
	1-X1	Acicular	Rounded	Smooth	Agg
Indomethacin	Input	Irregular & plates	Fractured	Rough & cracked	Drusy
	11-MA1	Irregular	Fractured	Rough	Agg & Drusy
	11-MA2	Irregular	Fractured	Rough	Agg & Drusy
	11-MB1	Irregular	Fractured	Rough	Agg & Drusy
	11-MB2	Irregular	Fractured	Rough	Agg & Drusy
	11-X1	Irregular	Fractured	Rough	Agg & Drusy
Loperamide HCl	Input	Irregular	Fractured	Rough & pitted	Agg
	14-MA1	Irregular	Fractured	Rough	Agg & Drusy
	14-MB1	Irregular	Fractured	Rough	Agg & Drusy
	14-X1	Irregular	Fractured	Rough	Agg & Drusy
Salbutamol sulphate	Input	Acicular & columnar	Angular	Smooth & slightly cracked	Drusy & agg
	24-MA1	Irregular	Fractured	Rough	Agg & Drusy
	24-MA2	Irregular	Fractured	Rough	Agg & Drusy
	24-MA3	Irregular	Fractured	Rough	Agg & Drusy
	24-MB1	Irregular	Fractured	Rough	Agg & Drusy
	24-MB2	Irregular	Fractured	Rough	Agg & Drusy
	24-X1	Irregular	Fractured	Rough	Agg & Drusy
Acetylsalicylic acid	Input	Modular	Rounded with Fractures	Cracked	ND
	33-MA1	Irregular	Fractured	Rough	Agg & Drusy
	33-MB1	Irregular	Fractured	Rough	Agg & Drusy
	33-X1	Irregular	Fractured	Rough	Agg & Drusy
Sulfamerazine	Input	Irregular & broken columnar	Rounded with Fractures	Rough with some cracks	Slight drusy
	54-MA1	Irregular	Fractured	Rough	Agg & Drusy
	54-MB1	Irregular	Fractured	Rough	Agg & Drusy
	54-X1	Irregular	Fractured	Rough	Agg & Drusy
Phenacetin	Input	Broken plates	Fractured	Smooth	Drusy
	69-MA1	Irregular	Fractured	Rough	Agg & Drusy
	69-MB1	Irregular	Fractured	Rough	Agg & Drusy
	69-X1	Irregular	Fractured	Rough	Agg & Drusy
Sulfadiazine	Input	Acicular	Sharp	Smooth	Agg
	87-MA1	Irregular	Fractured	Rough	Agg & Drusy
	87-MB1	Irregular	Fractured	Rough	Agg & Drusy
	87-X1	Irregular	Fractured	Rough	Agg & Drusy
Caffeine	Input	Irregular	Fractured	Rough	Agg
	88-MA1	Acicular	Sharp	Smooth	Agg
	88-MB1	Acicular	Sharp	Smooth	Agg
	88-X1	Acicular	Rounded	Smooth	Agg
Methyl paraben	Input	Irregular	Fractured	Rough	Agg
	140-MA1	Irregular	Fractured	Rough	Agg & Drusy
	140-MB1	Irregular	Fractured	Rough	Agg & Drusy
	140-X1	Irregular	Fractured	Rough	Agg & Drusy

Agg: agglomeration, For further definitions of the terms please refer to Table 3-7 and Figure 3-6 to Figure 3-9. #-MA#: high frequency ball-mill method A, #-MB#: low frequency ball-mill method B. #-X#: jet micronisation method A

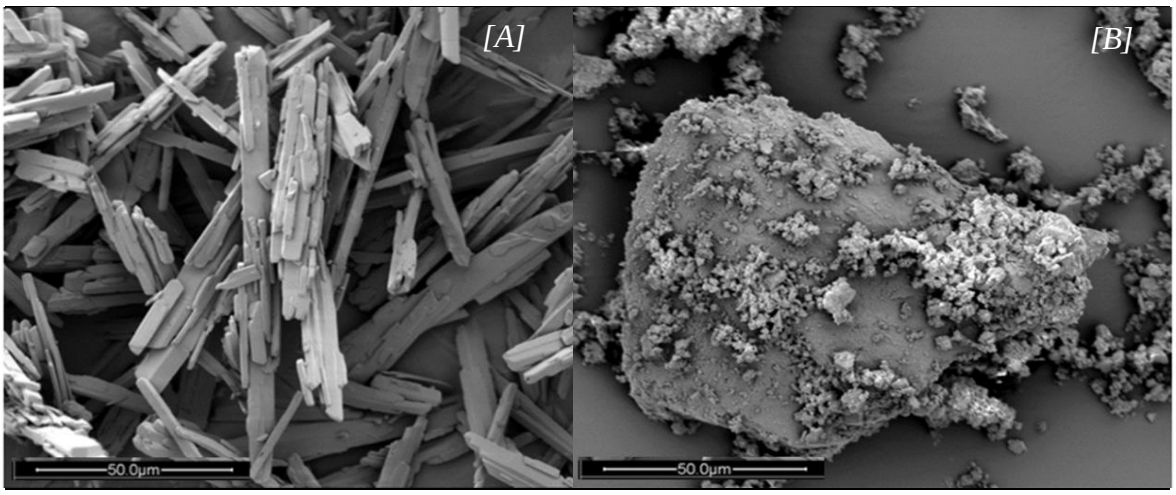

Figure 6-26 SEM micrographs for sulfadiazine: (A) input/reference, (B) high frequency ball-milled

Unlike the other comminuted materials, ball-milled caffeine appears acicular with sharp ends (edges) and smooth surfaces (Figure 6-27[C]), whilst jet-micronised caffeine appeared acicular with rounded edges Figure 6-27[D]). These changes in primary morphology of caffeine from irregular particles with fractured edges to smaller acicular, smooth particles may indicate that the material has undergone a solid-state form transition or recrystallisation (from sublimation) during the mechanical comminution processes. However, there is no conclusive evidence from XRPD (Section 6.4.1) or DSC (Section 6.4.3) to suggest a solid-state transformation was or had occurred as analysis is performed after comminution not during the milling process. However, the presence of a volatile peak (moisture) in the DSC and a weight loss in the TGA (Table 6-15) suggests a disruption to the crystal surface whereby, moisture can absorb and potentially lead to recrystallisation and the observed changes in crystal morphology[19] (Figure 6-27). These observations are also consistent with the particle size data obtained for the comminuted materials of caffeine (Table 6-18 and Figure 6-25), *i.e.* the ball-milled material appears larger due to recrystallisation and agglomeration while the micronised material appears smaller. It is likely that agglomeration for caffeine occurs where particles are in contact during crystallisation resulting in inter-particle bridging or fusion[19].

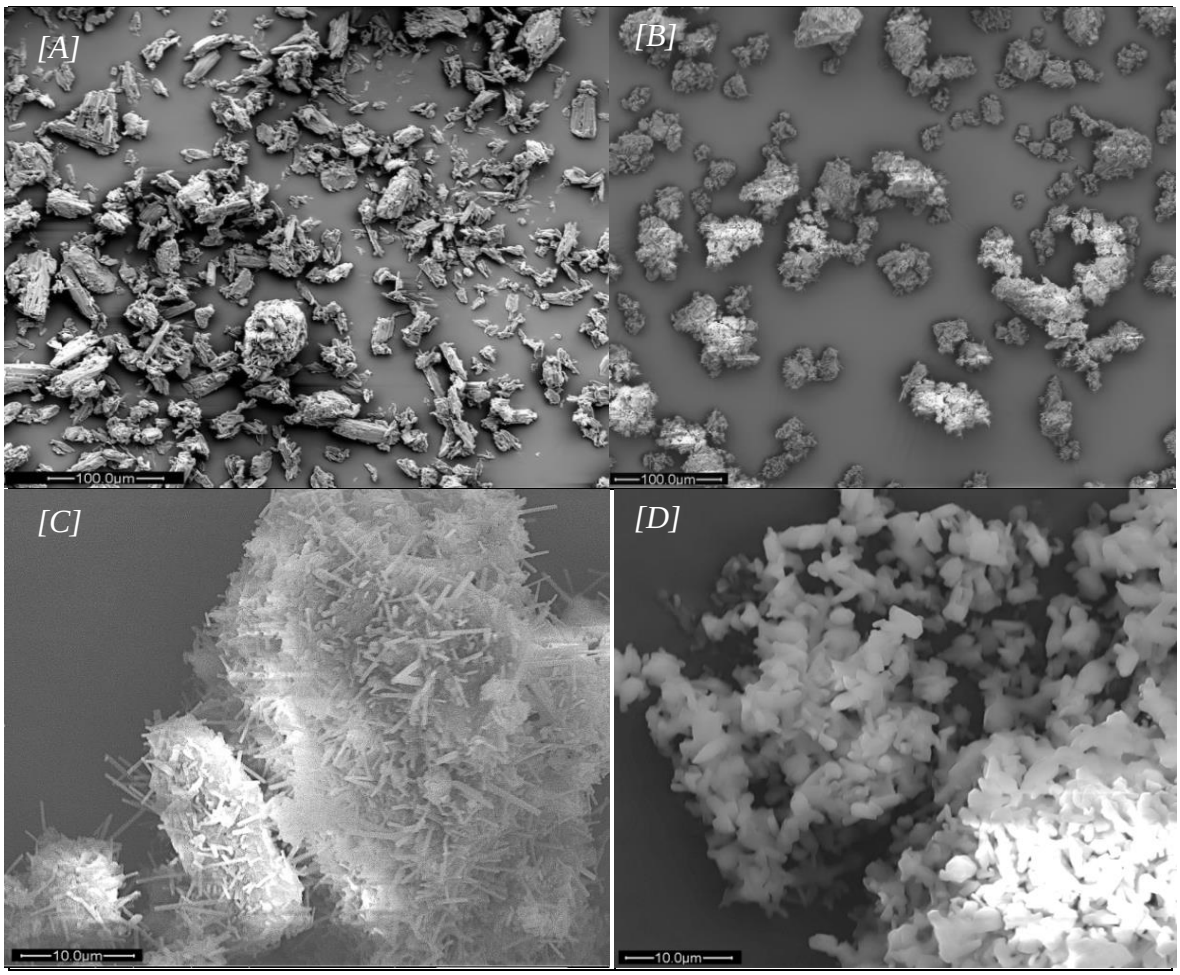

Figure 6-27 SEM micrographs of caffeine - the input (A), high frequency ball-milled (B & C) and jet –milled (D)

6.4.6 Gravimetric vapour sorption (GVS)

Moisture sorption profiles and associated responses were obtained for the mechanically comminuted materials and compared to those of the input materials (Table 6-20). For the comminuted materials of acetylsalicylic acid, phenacetin, methyl paraben and acetaminophen very little reversible moisture sorption occurred (less than 0.2% w/w) and the materials can be defined as being crystalline and moisture stable. The high frequency ball-milled phenacetin illustrates the typical kinetic and isotherm plots for this type of material (Figure 6-28).

Materials exhibiting surface disorder can be identified by observing recrystallisation events or large increases in adsorbed water from their moisture sorption profiles. These recrystallisation events are recognised by a continuous mass increase at specific %RH value as water molecules are adsorbed by the disordered surface. This is followed by an expulsion of water from the crystal lattice which is represented as a mass loss[20,276]. An example of this can be seen in the kinetics and isotherm plots for ball-milled salbutamol sulphate (Figure 6-29).

Table 6-20 GVS responses and CRA of the comminuted materials

		GVS responses												GVS CRA			
Material	Batch ID	M_A	M_B	M_C	M_D	M_E	M_F	M_{END}	M_{MAX1}	M_{MAX2}	*ADS*	$\%RH_{XTAL}$	M_{XTAL}	ΔMA	ΔM_{MAX1}	ΔM_{MAX2}	Comments
Acetaminophen	Input	0.04	0.07	0.00	0.03	0.01	0.01	-0.03	0.07	0.03	0.03	ND	ND	--	--	--	--
	1-MA1	0.02	0.13	0.00	0.13	0.00	0.03	0.01	0.13	0.13	0.00	ND	ND	-0.03	0.06	0.10	Crystalline stable reversible moisture sorption
	1-MA2	0.02	0.14	0.00	0.14	0.00	0.04	0.02	0.14	0.14	0.00	ND	ND	-0.02	0.07	0.10	Crystalline stable reversible moisture sorption
	1-MB1	0.03	0.10	0.00	0.09	-0.01	0.02	-0.01	0.10	0.09	0.01	ND	ND	-0.01	0.03	0.05	Crystalline stable reversible moisture sorption
	1-MB2	0.03	0.09	0.00	0.09	0.00	0.03	0.00	0.09	0.09	-0.01	ND	ND	-0.02	0.02	0.06	Crystalline stable reversible moisture sorption
	1-X1	-0.02	0.08	0.00	0.06	0.00	0.01	0.03	0.08	0.06	0.02	ND	ND	-0.06	0.01	0.03	Crystalline stable reversible moisture sorption
γ-Indomethacin	Input	0.02	0.09	0.00	0.09	0.00	0.02	0.00	0.09	0.09	0.00	ND	ND	--	--	--	--
	11-MA1	0.49	1.42	0.00	1.29	0.00	0.28	-0.22	1.42	1.29	0.13	ND	ND	0.48	1.33	1.20	Disordered (or increased surface area)
	11-MA2	0.51	1.40	0.00	1.31	0.00	0.29	-0.23	1.40	1.31	0.09	ND	ND	0.50	1.31	1.22	Disordered (or increased surface area)
	11-MB1	0.13	0.37	0.00	0.31	0.00	0.11	-0.02	0.37	0.31	0.06	ND	ND	0.12	0.28	0.22	Crystalline stable reversible moisture sorption
	11-MB2	0.14	0.38	0.00	0.32	0.00	0.12	-0.02	0.38	0.32	0.06	ND	ND	0.13	0.29	0.23	Crystalline stable reversible moisture sorption
	11-X1	-0.07	0.18	0.00	0.17	0.00	0.06	0.12	0.18	0.17	0.01	ND	ND	-0.08	0.09	0.08	Crystalline stable reversible moisture sorption
Loperamide HCl	Input	0.05	0.13	0.00	0.12	0.00	0.03	-0.01	0.13	0.12	0.01	ND	ND	--	--	--	--
	14-MA1	2.28	9.23	0.01	9.18	0.08	2.41	0.13	9.23	9.18	0.05	ND	ND	2.23	9.10	9.05	Disordered (or increased surface area)
	14-MB1	1.33	1.88	0.00	1.41	0.00	0.52	-0.81	3.01	1.41	1.60	90	3.46	1.28	2.88	1.29	Disordered
	14-X1	0.43	0.96	0.00	0.84	0.00	0.24	-0.18	0.96	0.84	0.12	90	1.08	0.38	0.83	0.72	Disordered
Salbutamol sulphate	Input	-0.01	0.04	0.00	0.04	0.00	0.00	0.01	0.04	0.04	0.00	ND	ND	--	--	--	--
	24-MA1	4.42	1.37	0.00	1.18	-0.02	0.18	-4.24	7.62	1.18	6.45	60	9.76	4.43	7.59	1.14	Disordered
	24-MA2	4.44	1.21	0.00	1.04	-0.01	0.11	-4.32	7.64	1.04	6.59	60	9.62	4.45	7.60	1.01	Disordered
	24-MA3	4.81	1.11	0.00	0.96	-0.01	0.11	-4.70	8.48	0.96	7.52	60	9.74	4.83	8.44	0.93	Disordered
	24-MB1	1.03	0.79	0.00	0.66	-0.02	0.21	-0.82	1.18	0.66	0.52	50	1.33	1.04	1.14	0.62	Disordered
	24-MB2	1.02	0.79	0.00	0.67	0.00	0.20	-0.82	1.02	0.67	0.35	50	1.25	1.03	0.98	0.63	Disordered
	24-X1	0.64	0.30	0.00	0.28	-0.01	0.10	-0.55	0.65	0.28	0.36	50	0.68	0.66	0.61	0.25	Disordered or electrostatic

		GVS responses												GVS CRA			
Material	Batch ID	M_A	M_B	M_C	M_D	M_E	M_F	M_{END}	M_{MAX1}	M_{MAX2}	ADS	$\%RH_{XTAL}$	M_{XTAL}	ΔMA	ΔM_{MAX1}	ΔM_{MAX2}	Comments
Acetylsalicylic acid	Input	0.00	0.01	0.00	0.01	0.00	0.00	0.00	0.01	0.01	0.00	ND	ND	--	--	--	--
	33-MA1	0.00	0.13	0.00	0.10	0.00	0.02	0.02	0.13	0.10	0.03	ND	ND	0.00	0.12	0.09	Crystalline stable reversible moisture sorption
	33-MB1	0.01	0.08	0.00	0.07	0.00	0.01	0.00	0.08	0.07	0.01	ND	ND	0.01	0.07	0.06	Crystalline stable reversible moisture sorption
	33-X1	-0.49	0.04	0.00	0.01	-0.02	-0.01	0.48	0.04	0.01	0.03	ND	ND	-0.50	0.03	0.00	Crystalline stable reversible moisture sorption
Sulfamerazine	Input	0.06	0.22	0.00	0.20	-0.07	0.00	-0.06	0.22	0.20	0.03	ND	ND	--	--	--	--
	54-MA1	0.36	0.85	0.00	0.81	0.00	0.24	-0.13	0.85	0.81	0.04	ND	ND	0.30	0.63	0.61	Disordered (or increased surface area)
	54-MB1	0.25	0.71	0.00	0.66	0.00	0.19	-0.06	0.71	0.66	0.04	ND	ND	0.19	0.48	0.47	Crystalline stable reversible moisture sorption
	54-X1	0.18	0.45	0.00	0.42	0.00	0.12	-0.06	0.45	0.42	0.03	ND	ND	0.12	0.23	0.23	Crystalline stable reversible moisture sorption
Phenacetin	Input	0.00	0.10	0.00	0.10	0.00	0.00	0.00	0.10	0.10	0.00	ND	ND	--	--	--	--
	69-MA1	0.04	0.21	0.00	0.20	0.00	0.03	-0.01	0.21	0.20	0.01	ND	ND	0.04	0.12	0.10	Crystalline stable reversible moisture sorption
	69-MB1	0.04	0.09	0.00	0.10	0.00	0.01	-0.03	0.09	0.10	-0.01	ND	ND	0.04	-0.01	0.00	Crystalline stable reversible moisture sorption
	69-X1	0.10	0.10	0.00	0.12	0.02	0.03	-0.07	0.10	0.12	-0.02	ND	ND	0.10	0.01	0.02	Crystalline stable reversible moisture sorption
Sulfadiazine	Input	-0.05	0.07	0.00	0.06	-0.01	0.00	0.05	0.07	0.06	0.01	ND	ND	--	--	--	--
	87-MA1	0.31	1.20	0.00	1.03	0.00	0.24	-0.08	1.20	1.03	0.17	ND	ND	0.37	1.13	0.97	Disordered (or increased surface area)
	87-MB1	0.25	0.98	0.00	0.83	0.00	0.19	-0.06	0.98	0.83	0.15	ND	ND	0.30	0.91	0.77	Disordered (or increased surface area)
	87-X1	0.03	0.27	0.00	0.24	0.00	0.06	0.03	0.27	0.24	0.03	ND	ND	0.08	0.20	0.18	Crystalline stable reversible moisture sorption
Caffeine	Input	-0.01	0.13	0.00	0.11	0.00	0.02	0.03	0.13	0.11	0.02	ND	ND	--	--	--	--
	88-MA1	0.62	7.30	0.00	4.53	-0.07	-0.09	-0.70	7.30	4.53	2.76	ND	ND	0.63	7.17	4.42	Disordered (or increased surface area)
	88-MB1	0.11	0.80	0.00	0.72	0.00	0.09	-0.01	0.80	0.72	0.08	ND	ND	0.12	0.67	0.61	Disordered (or increased surface area)
	88-X1	-0.12	0.15	0.00	0.14	0.00	0.02	0.15	0.15	0.14	0.02	ND	ND	-0.11	0.02	0.03	Crystalline stable reversible moisture sorption
Methyl paraben	Input	0.00	0.02	0.00	0.01	0.00	0.00	0.00	0.02	0.01	0.01	ND	ND	--	--	--	--
	140-MA1	0.02	0.08	0.00	0.07	0.00	0.01	-0.01	0.08	0.07	0.01	ND	ND	0.02	0.06	0.06	Crystalline stable reversible moisture sorption
	140-MB1	0.04	0.09	0.00	0.06	0.00	0.01	-0.03	0.09	0.06	0.03	ND	ND	0.03	0.07	0.04	Crystalline stable reversible moisture sorption
	140-X1	-0.10	0.04	0.00	0.03	0.00	0.00	0.10	0.04	0.03	0.00	ND	ND	-0.10	0.02	0.02	Crystalline stable reversible moisture sorption

$M_{\#}$: % mass change at %RH points A (30%RH, B (90%RH), C (0%RH), D (90%RH), E (0%RH), and F (30%RH), $M_{END:}$ difference between final (F) and initial (A) values. M_{MAX1} and M_{MAX1} are the maximum % mass change observed during first and second adsorption intervals (ADS1 and ADS2). ΔMAX is the difference in M_{MAX1} and M_{MAX1} values. M_{ADS} is the difference in % change in mass between points B and D, i.e. At 90 %RH for adsorption cycles 1 and 2. #-MA#: high frequency ball-mill method A, #-MB#: low frequency ball-mill method B. #-X#: jet micronisation method A. Please refer to Table 3-11 for further descriptions of the terms

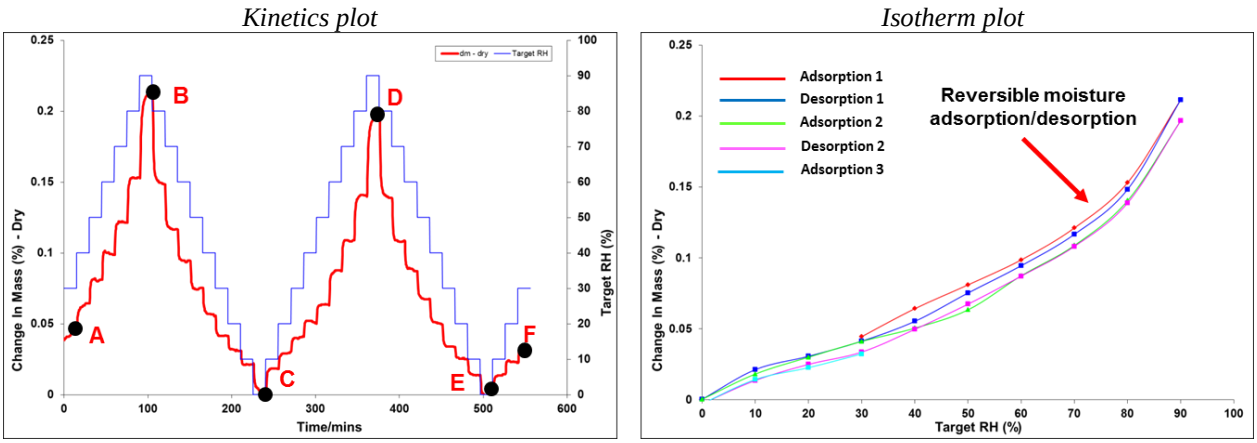

Figure 6-28 GVS kinetics and isotherm plots showing the reversible moisture adsorption/desorption profile for high frequency ball-milled phenacetin.
Points A to F refer to the equilibrium endpoints at %RH values from the start to end of the adsorption/desorption cycles

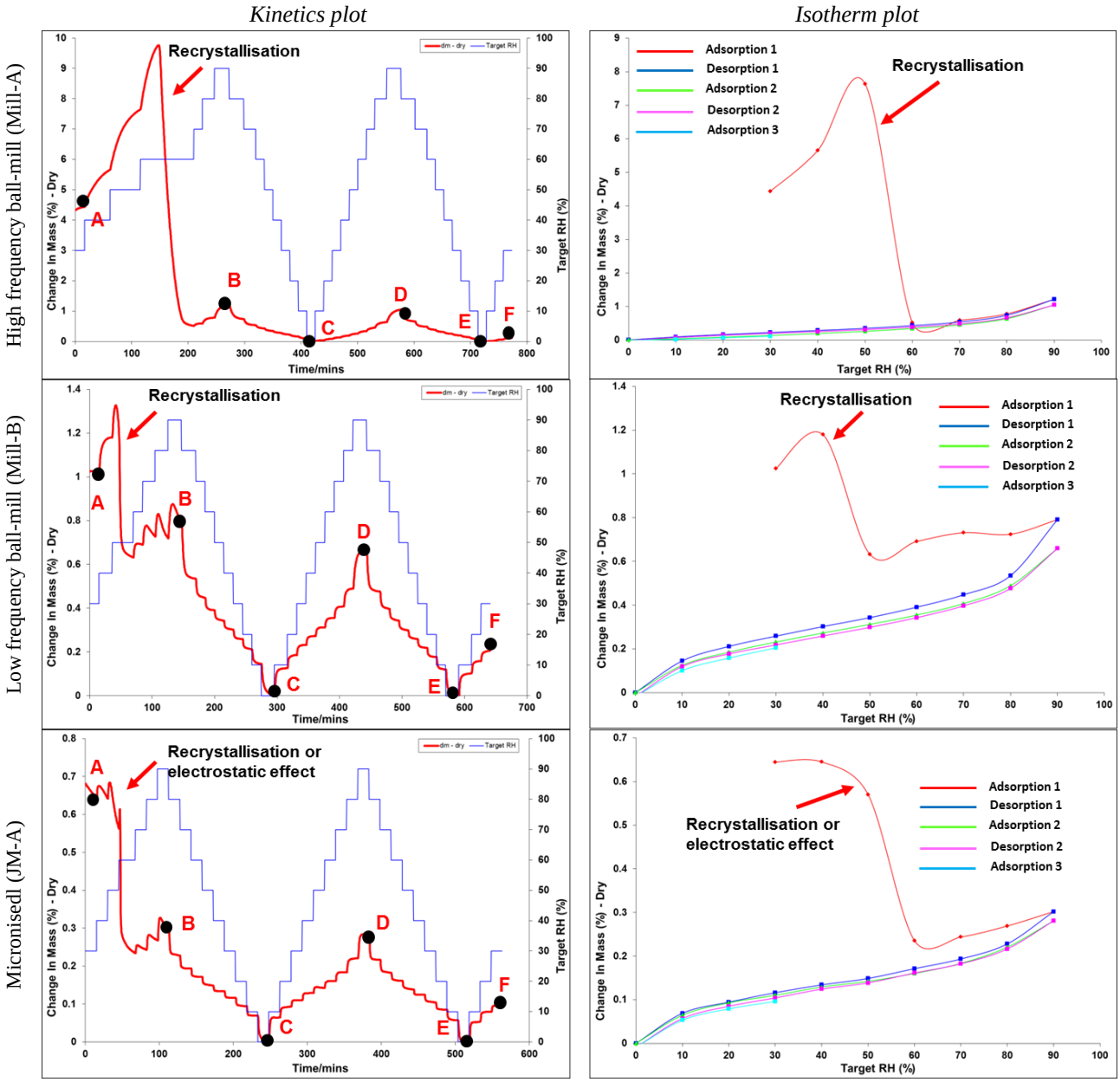

Figure 6-29 GVS kinetics and isotherm plots for the comminuted materials of salbutamol sulphate
Points A to F refer to the equilibrium endpoints at %RH values from the start to end of the adsorption/desorption cycles

Both high and low frequency ball-milling of salbutamol sulphate appeared to generate surface disorder with recrystallisation occurring at 50-60 %RH, consistent with previous literature observations[1,21,246,364]. There is also some suggestion of a small amount of disorder for micronised salbutamol sulphate, as a mass loss is observed which could be interpreted as a recrystallisation event. However, it is more likely that this observation is due to electrostatic charges rather than disorder, as there was no increase in water adsorption prior to this event and it can be seen that as %RH increases the electrostatic charge is dissipated[365] which would account for the observed mass loss (Figure 6-29).

Surface disorder maybe distinguished from bulk disorder by the amount of moisture adsorbed and the observation that a recrystallisation event maybe present. Bulk disordered materials typically absorb relatively more moisture and may or may not exhibit a recrystallisation event[255]. An example of this distinction can be seen in the moisture sorption profiles for ball-milled loperamide HCl (Figure 6-30). High frequency ball-milling did not result in an observed recrystallisation in the GVS kinetics plot, but instead the material absorbed 9 % (w/w) moisture reversibly during the first and second adsorption cycles (points B & D Figure 6-30) and it can be inferred that this is due to the presence of bulk disorder. In contrast, low frequency ball-milling results in only surface disorder with the observance of a recrystallisation event only at high %RH, *i.e.* 90% RH (Figure 6-30).

It should be noted that loperamide HCl can form a tetrahydrate, but only when immersed completely in an aqueous environment[331]. In the latter case the amount of moisture sorption was approximately 14.5% (w/w)[331]. For the bulk disordered material of loperamide HCl, it is postulated that moisture is readily and reversibly absorbed without recrystallisation or formation of the tetrahydrate and that this highly disordered material remains amorphous even after multiple adsorption/desorption cycles. This was confirmed by investigating the solid-state form/phase post-GVS by XRPD using the method described in Section 3.2.1 (Figure 6-31). This XRPD diffractogram post-GVS showed that the material remained amorphous, suggesting that moisture sorption by itself is not sufficient to facilitate a solid-state transformation of the bulk disordered material but rather the addition of heat is required for recrystallisation to occur, as was shown in the DSC thermogram for the high frequency ball-milled material (Figure 6-12).

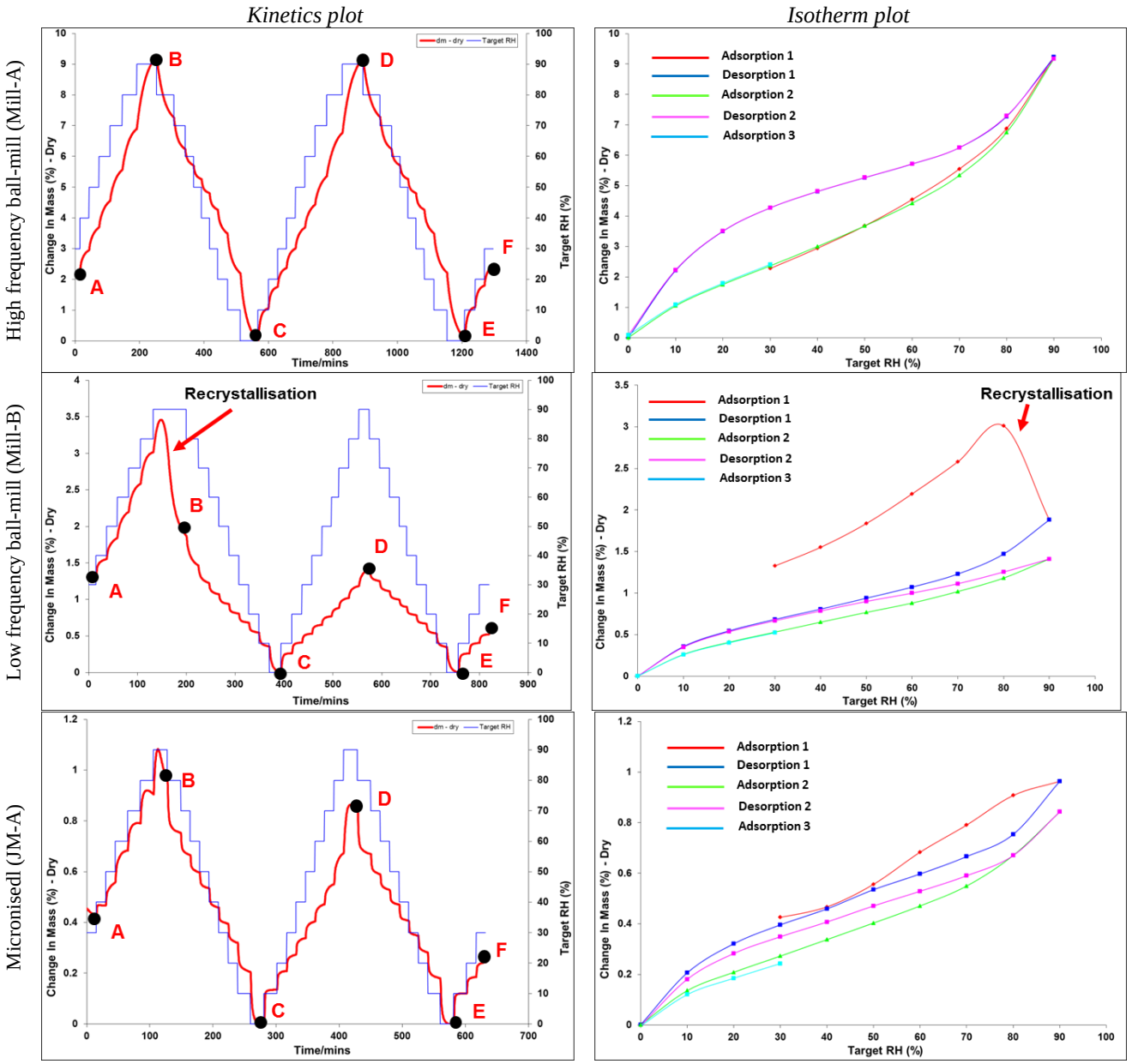

Figure 6-30 GVS kinetics and isotherm plots for the comminuted materials of loperamide HCl
Points A to F refer to the equilibrium endpoints at %RH values from the start to end of the adsorption/desorption cycles

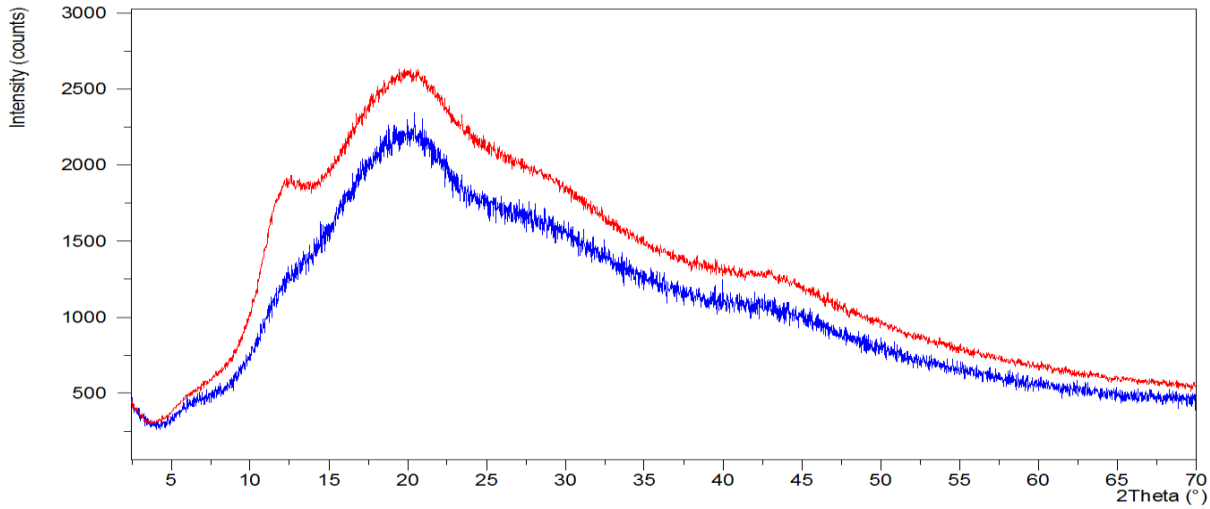

Figure 6-31 XRPD diffractograms for the high frequency ball-milled samples of loperamide HCl before GVS analysis (red) and post-GVS (blue)

Reducing the particle size of loperamide HCl by micronisation did not result in an increase in moisture sorption. This further verifies that it is the presence of disorder that is responsible for the observed moisture adsorption increase and not the increase in particle surface area due to size reduction (Table 6-20).

For other comminuted materials such as γ-indomethacin disorder may have been generated by high frequency ball-milling, as indicated by the increase in moisture sorption. In contrast, low frequency ball-milling and micronisation did not appear as disruptive with the resulting material remaining crystalline after processing, as little moisture sorption was observed (Table 6-20).

Ball-milling of sulfamerazine and sulfadiazine also resulted in a small amount of surface disorder as indicated by the relative small amount of moisture sorption observed. However, micronisation of these materials did not cause any change in the moisture sorption profiles suggesting that reducing the particle size did not have any significant influence (Table 6-20).

Of all the comminuted materials, only high frequency ball-milling of caffeine appeared to result in the formation of a hydrate but this was only produced during GVS analysis (Figure 6-32). Significant changes to the moisture sorption profile for this material were observed. These changes are likely due to lattice disordering, resulting in irreversible moisture adsorption/desorption. The material appears to readily convert to a hydrated form above 60 %RH and water is desorbed below 30 %RH. However, the material does not readsorb the same amount of moisture during the second adsorption cycle, suggesting that another hydrated form may be generated (Figure 6-32). Low frequency ball-milling, and to some degree micronisation, resulted in only a small amount of moisture sorption, suggesting that these materials remained predominately crystalline. Micronised caffeine also appeared to be electrostatically charged but this did not appear to affect the overall amount of moisture adsorbed (Figure 6-32).

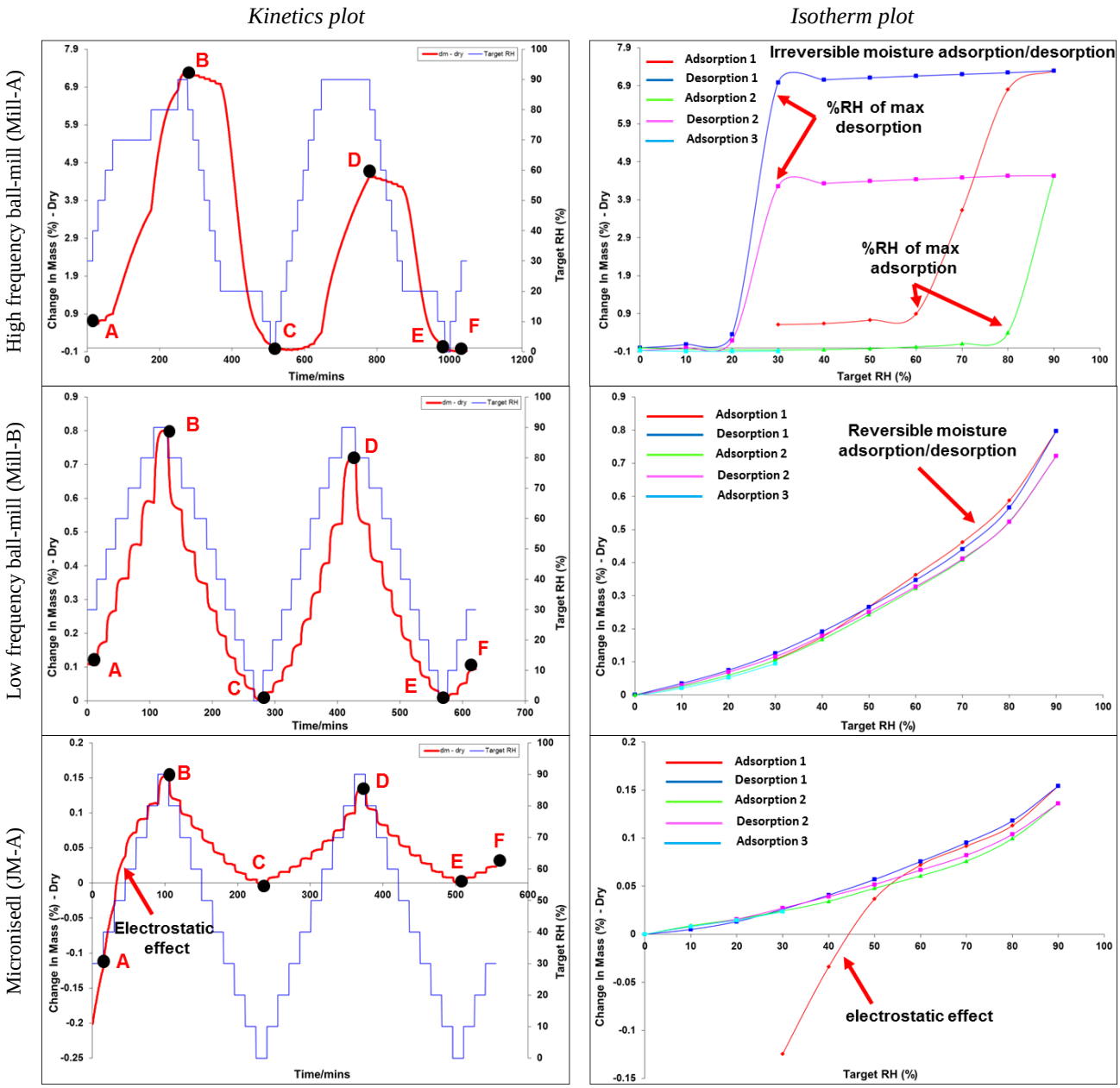

Figure 6-32 GVS kinetics and isotherm plots for the comminuted materials of caffeine

Points A to F refer to the equilibrium endpoints at %RH values from the start to end of the adsorption/desorption cycles

6.4.7 Fourier transform infra-red spectroscopy (FTIR)

Infrared spectra for the mechanically comminuted materials were obtained and compared to those of the input/reference materials (Table 6-21).

Table 6-21 Frequency assignment of FTIR peaks and CRA of the comminuted materials

		FTIR Response	FTIR CRA
Material	Batch ID	Observed key vibrations	Observed changes
Acetaminophen	Input	3323 cm^{-1} (NH stretch), 3161cm^{-1} (H-bonded OH stretch), 1650 cm^{-1} (C=O amide stretching), 1562 cm^{-1} (N–H in-plane bending), 1328 cm^{-1} (O–H bending), 1259 cm^{-1} (C–O stretch), 1225 cm^{-1} (C–N amide stretch)	_
	1-MA1	3324 cm-1 (NH stretch), 3162cm-1 (H-bonded OH stretch), 1653 cm-1 (C=O amide stretching), 1564 cm-1 (N–H in-plane bending), 1328 cm-1 (O–H bending), 1260 cm-1 (C–O stretch), 1226 cm-1 (C–N amide stretch)	No change, concordant with input/reference spectra
	1-MA2	3324 cm-1 (NH stretch), 3161cm-1 (H-bonded OH stretch), 1653 cm-1 (C=O amide stretching), 1563 cm-1 (N–H in-plane bending), 1328 cm-1 (O–H bending), 1260 cm-1 (C–O stretch), 1226 cm-1 (C–N amide stretch)	No change, concordant with input/reference spectra
	1-MB1	3325 cm-1 (NH stretch), 3162cm-1 (H-bonded OH stretch), 1653 cm-1 (C=O amide stretching), 1564 cm-1 (N–H in-plane bending), 1328 cm-1 (O–H bending), 1260 cm-1 (C–O stretch), 1227 cm-1 (C–N amide stretch)	No change, concordant with input/reference spectra
	1-MB2	3323 cm^{-1} (NH stretch), 3162cm^{-1} (H-bonded OH stretch), 1650 cm^{-1} (C=O amide stretching), 1562 cm^{-1} (N–H in-plane bending), 1328 cm^{-1} (O–H bending), 1259 cm^{-1} (C–O stretch), 1226 cm^{-1} (C–N amide stretch)	No change, concordant with input/reference spectra
	1-X1	3325 cm-1 (NH stretch), 3162cm-1 (H-bonded OH stretch), 1652 cm-1 (C=O amide stretching), 1563 cm-1 (N–H in-plane bending), 1328 cm-1 (O–H bending), 1259 cm-1 (C–O stretch), 1226 cm-1 (C–N amide stretch)	No change, concordant with input/reference spectra
γ-Indomethacin	Input	3023 cm^{-1} (O-H stretch), 1714 cm^{-1} (C=O stretch of cyclic dimer), 1690 cm^{-1} (C=O amide stretch),1613 cm^{-1} (N-H stretch),1478 cm^{-1} (C-C stretch)	_
	11-MA1	3023 cm-1 (O-H stretch), 1715cm-1 (C=O stretch of cyclic dimer), 1691 cm-1 (C=O amide stretch),1613 cm-1 (N-H stretch),1479 cm-1 (C-C stretch)	No change, concordant with input/reference spectra
	11-MA2	3023 cm-1 (O-H stretch), 1714 cm-1 (C=O stretch of cyclic dimer), 1691 cm-1 (C=O amide stretch),1613 cm-1 (N-H stretch),1479 cm-1 (C-C stretch)	No change, concordant with input/reference spectra
	11-MB1	3023 cm-1 (O-H stretch), 1715cm-1 (C=O stretch of cyclic dimer), 1691 cm-1 (C=O amide stretch),1613 cm-1 (N-H stretch),1479 cm-1 (C-C stretch)	No change, concordant with input/reference spectra
	11-MB2	3023 cm-1 (O-H stretch), 1715 cm-1 (C=O stretch of cyclic dimer), 1691 cm-1 (C=O amide stretch),1613 cm-1 (N-H stretch),1479 cm-1 (C-C stretch)	No change, concordant with input/reference spectra
	11-X1	3023 cm-1 (O-H stretch), 1716 cm-1 (C=O stretch of cyclic dimer), 1691 cm-1 (C=O amide stretch),1614 cm-1 (N-H stretch),1479 cm-1 (C-C stretch)	No change, concordant with input/reference spectra
Salbutamol sulphate	Input	3474 cm-1 (O-H stretch), 3409 cm-1 (N-H stretch), 1616 cm-1 (C-N stretch), 1507 cm-1 (C-N stretch), 1496 cm-1 (O-H bend), 1205 cm-1 (C-O phenolic stretch), 1112 cm-1 (C-O stretch), 1078 cm-1 (secondary alcoholic C–O stretch)	_
	24-MA1	Broad 3500 cm^{-1} to 2200cm-1, 1614 cm^{-1} and 1510 cm^{-1} (C-N stretch), 1501 cm^{-1} (O-H bend), 1201 cm^{-1} (C-O phenolic stretch), 1115 cm^{-1} (C-O stretch), Broad 1078 cm^{-1} (secondary alcoholic C–O stretch)	broadening and shifts of a number of peaks in the FTIR spectrum bands in the region 3500 to 2200 cm^{-1} and 1700 to 700 cm^{-1}
	24-MA2	Broad 3500 cm^{-1} to 2200cm-1, 1613 cm^{-1} and 1509 cm^{-1} (C-N stretch), 1500 cm^{-1} (O-H bend), 1201 cm^{-1} (C-O phenolic stretch), 1115 cm^{-1} (C-O stretch), Broad 1078 cm^{-1} (secondary alcoholic C–O stretch)	broadening and shifts of a number of peaks in the FTIR spectrum bands in the region 3500 to 2200 cm^{-1} and 1700 to 700 cm^{-1}
	24-MA3	Broad 3500 cm^{-1} to 2200cm-1, 1614 cm^{-1} and 1507 cm^{-1} (C-N stretch), 1502 cm^{-1} (O-H bend), 1202 cm^{-1} (C-O phenolic stretch), 1115 cm^{-1} (C-O stretch), Broad 1078 cm^{-1} (secondary alcoholic C–O stretch)	broadening and shifts of a number of peaks in the FTIR spectrum bands in the region 3500 to 2200 cm^{-1} and 1700 to 700 cm^{-1}
	24-MB1	3473 cm^{-1} (O-H stretch), 1616 cm^{-1} and 1507 cm^{-1} (C-N stretch), 1496 cm^{-1} (O-H bend), 1206 cm^{-1} (C-O phenolic stretch), 1112 cm^{-1} (C-O stretch), 1079 cm^{-1} (secondary alcoholic C–O stretch)	No change, concordant with input/reference spectra
	24-MB2	3472 cm^{-1} (O-H stretch), 1617 cm^{-1} and 1508 cm^{-1} (C-N stretch), 1498 cm^{-1} (O-H bend), 1206 cm^{-1} (C-O phenolic stretch), 1112 cm^{-1} (C-O stretch), 1079 cm^{-1} (secondary alcoholic C–O stretch)	No change, concordant with input/reference spectra
	24-X1	3474 cm^{-1} (O-H stretch), 1617 cm^{-1} and 1508 cm^{-1} (C-N stretch), 1497 cm^{-1} (O-H bend), 1207 cm^{-1} (C-O phenolic stretch), 1113 cm^{-1} (C-O stretch), 1078 cm^{-1} (secondary alcoholic C–O stretch)	No change, concordant with input/reference spectra

		FTIR Response	FTIR CRA
Material	Batch ID	Observed key vibrations	Observed changes
Loperamide HCl	Input	2959 cm^{-1} (C-H aromatic stretch),1623 cm^{-1} (C=O stretch tertiary amide),1484 cm^{-1} (C-C aromatic stretch), 1448 cm^{-1} (C-O-H stretch)	–
	14-MA1	Broad 3500 cm-1 to 2200cm-1, 1628 cm^{-1} (C=O stretch tertiary amide), broad 1494cm^{-1}, 1449 cm^{-1} (C-O-H stretch)	Water present , peak broadening and peak shifts observed
	14-MB1	2959 cm^{-1} (C-H aromatic stretch),1624 cm^{-1} (C=O stretch tertiary amide),1485 cm^{-1} (C-C aromatic stretch), 1448 cm^{-1} (C-O-H stretch)	Some slight broadening and shifts observed
	14-X1	2959 cm^{-1} (C-H aromatic stretch),1624 cm^{-1} (C=O stretch tertiary amide),1485 cm^{-1} (C-C aromatic stretch), 1449 cm^{-1} (C-O-H stretch)	No change, concordant with input/reference spectra
Acetylsalicylic acid	Input	1750 cm^{-1} (C=O acetyl stretch ester), 1680 cm^{-1} (C=O stretch carboxylic acid),1605 cm^{-1} (C=C aromatic), 1482 cm^{-1} (C=C aromatic)	–
	33-MA1	1751 cm^{-1} (C=O acetyl stretch ester), 1682 cm^{-1} (C=O stretch carboxylic acid),1606 cm^{-1} (C=C aromatic), 1483 cm^{-1} (C=C aromatic)	No change, concordant with input/reference spectra
	33-MB1	1751 cm^{-1} (C=O acetyl stretch ester), 1682 cm^{-1} (C=O stretch carboxylic acid),1606 cm^{-1} (C=C aromatic), 1483 cm^{-1} (C=C aromatic)	No change, concordant with input/reference spectra
	33-X1	1751 cm^{-1} (C=O acetyl stretch ester), 1682 cm^{-1} (C=O stretch carboxylic acid),1606 cm^{-1} (C=C aromatic), 1483 cm^{-1} (C=C aromatic)	No change, concordant with input/reference spectra
Sulfamerazine	Input	3498 cm^{-1} and 3482 cm^{-1} (NH_2 stretch), 1641 cm^{-1} and 1628 cm^{-1} (NH_2 scissoring), 1326 cm^{-1} and 1150 cm^{-1} (S=O stretch), 1304 cm^{-1} (Aromatic C-N stretch)	–
	54-MA1	3498 cm^{-1} and 3482 cm^{-1} (NH_2 stretch), 1641 cm^{-1} and 1628 cm^{-1} (NH_2 scissoring), 1326 cm^{-1} and 1150 cm^{-1} (S=O stretch), 1304 cm^{-1} (Aromatic C-N stretch)	Some new peaks for Form II and some peak shifts. Remainder, concordant with peaks for input/reference spectra
	54-MB1	3498 cm^{-1} and 3485 cm^{-1} (NH_2 stretch), 3458 cm-1 (NH2 stretch Form II), 1644 cm^{-1} and 1630 cm^{-1} (NH_2 scissoring), 1323 cm^{-1} and 1149 cm^{-1} (S=O stretch), 1301 cm^{-1} (Aromatic C-N stretch)	No change, concordant with input/reference spectra
	54-X1	3497 cm^{-1} and 3483 cm^{-1} (NH_2 stretch), 1641 cm^{-1} and 1629 cm^{-1} (NH_2 scissoring), 1327 cm^{-1} and 1151 cm^{-1} (S=O stretch), 1304 cm^{-1} (Aromatic C-N stretch)	No change, concordant with input/reference spectra
Phenacetin	Input	3283 cm^{-1} (N-H stretch), 3073 cm^{-1} (aromatic-H stretch), 2928 cm^{-1} (C-H stretch amide), 2885 cm^{-1} (C-H stretch), 1658 cm^{-1} (C=O stretch), 1645 cm^{-1} (C-NH deformation), 1480 cm^{-1} (C-H bend), 1265 cm^{-1} (C-N stretch)	–
	69-MA1	3281 cm^{-1} (N-H stretch), 3073 cm^{-1} (aromatic-H stretch), 2928 cm^{-1} (C-H stretch amide), 2884 cm^{-1} (C-H stretch), 1658 cm^{-1} (C=O stretch), 1645 cm^{-1} (C-NH deformation), 1482 cm^{-1} (C-H bend), 1266 cm^{-1} (C-N stretch)	No change, concordant with input/reference spectra
	69-MB1	3281 cm^{-1} (N-H stretch), 3073 cm^{-1} (aromatic-H stretch), 2928 cm^{-1} (C-H stretch amide), 2885 cm^{-1} (C-H stretch), 1659 cm^{-1} (C=O stretch), 1645 cm^{-1} (C-NH deformation), 1482 cm^{-1} (C-H bend), 1266 cm^{-1} (C-N stretch)	No change, concordant with input/reference spectra
	69-X1	3282 cm^{-1} (N-H stretch), 3073 cm^{-1} (aromatic-H stretch), 2928 cm^{-1} (C-H stretch amide), 2886 cm^{-1} (C-H stretch), 1659 cm^{-1} (C=O stretch), 1645 cm^{-1} (C-NH deformation), 1482 cm^{-1} (C-H bend), 1266 cm^{-1} (C-N stretch)	No change, concordant with input/reference spectra
Sulfadiazine	Input	3424 cm^{-1} (NH_2 stretch), 3356 cm^{-1} (NH_2 stretch),1653 cm^{-1} (NH_2 scissoring), 1580 cm^{-1} (NH_2 scissoring), 1326 cm^{-1} (S=O stretch), 1153 cm^{-1} (S=O stretch),	–
	87-MA1	3424 cm^{-1} (NH_2 stretch), 3355 cm^{-1} (NH_2 stretch),1653 cm^{-1} (NH_2 scissoring), 1580 cm^{-1} (NH_2 scissoring), 1326 cm^{-1} (S=O stretch), 1152 cm^{-1} (S=O stretch),	No change, concordant with input/reference spectra
	87-MB1	3424 cm^{-1} (NH_2 stretch), 3355 cm^{-1} (NH_2 stretch),1652 cm^{-1} (NH_2 scissoring), 1580 cm^{-1} (NH_2 scissoring), 1326 cm^{-1} (S=O stretch), 1153 cm^{-1} (S=O stretch),	No change, concordant with input/reference spectra
	87-X1	3424 cm^{-1} (NH_2 stretch), 3355 cm^{-1} (NH_2 stretch),1653 cm^{-1} (NH_2 scissoring), 1579 cm^{-1} (NH_2 scissoring), 1326 cm^{-1} (S=O stretch), 1153 cm^{-1} (S=O stretch),	No change, concordant with input/reference spectra
Caffeine	Input	1694 cm^{-1} (C=O stretch), 1599 cm^{-1} (C-N stretch), 1547 cm^{-1} (C-N stretch),	–
	88-MA1	1696cm^{-1} (C=O stretch), 1599 cm^{-1} (C-N stretch), 1548 cm^{-1} (C-N stretch),	No change, concordant with input/reference spectra
	88-MB1	1697 cm^{-1} (C=O stretch), 1599 cm^{-1} (C-N stretch), 1548 cm^{-1} (C-N stretch),	No change, concordant with input/reference spectra
	88-X1	1697 cm^{-1} (C=O stretch), 1599 cm^{-1} (C-N stretch), 1550cm^{-1} (C-N stretch),	No change, concordant with input/reference spectra

		FTIR Response	FTIR CRA
Material	Batch ID	Observed key vibrations	Observed changes
Methyl paraben	Input	3285 cm^{-1} (O-H stretch) 1678 cm^{-1} (C=O stretch), 1513 cm^{-1} (Phenol C-O stretch), 1433 cm^{-1} (Enol C-O stretch)	–
	140-MA1	3287 cm^{-1} (O-H stretch) 1678 cm^{-1} (C=O stretch), 1513 cm^{-1} (Phenol C-O stretch), 1433 cm^{-1} (Enol C-O stretch)	No change, concordant with input/reference spectra
	140-MB1	3285 cm^{-1} (O-H stretch) 1678 cm^{-1} (C=O stretch), 1513 cm^{-1} (Phenol C-O stretch), 1433 cm^{-1} (Enol C-O stretch)	No change, concordant with input/reference spectra
	140-X1	3287 cm^{-1} (O-H stretch) 1678 cm^{-1} (C=O stretch), 1513 cm^{-1} (Phenol C-O stretch), 1433 cm^{-1} (Enol C-O stretch)	No change, concordant with input/reference spectra

Red – changes in observed vibrations. #-MA#: high frequency ball-mill method A, #-MB#: low frequency ball-mill method B. #-X#: jet micronisation method A.

The FTIR spectra for the comminuted materials of acetylsalicylic acid, phenacetin, sulfadiazine, caffeine, γ-indomethacin, methyl paraben and acetaminophen were concordant with the FTIR spectra of the respective input material, as illustrated in Figure 6-33 for indomethacin. These observations indicate that there were no significant changes to the physical structure, conformation and/or chemical nature of the materials.

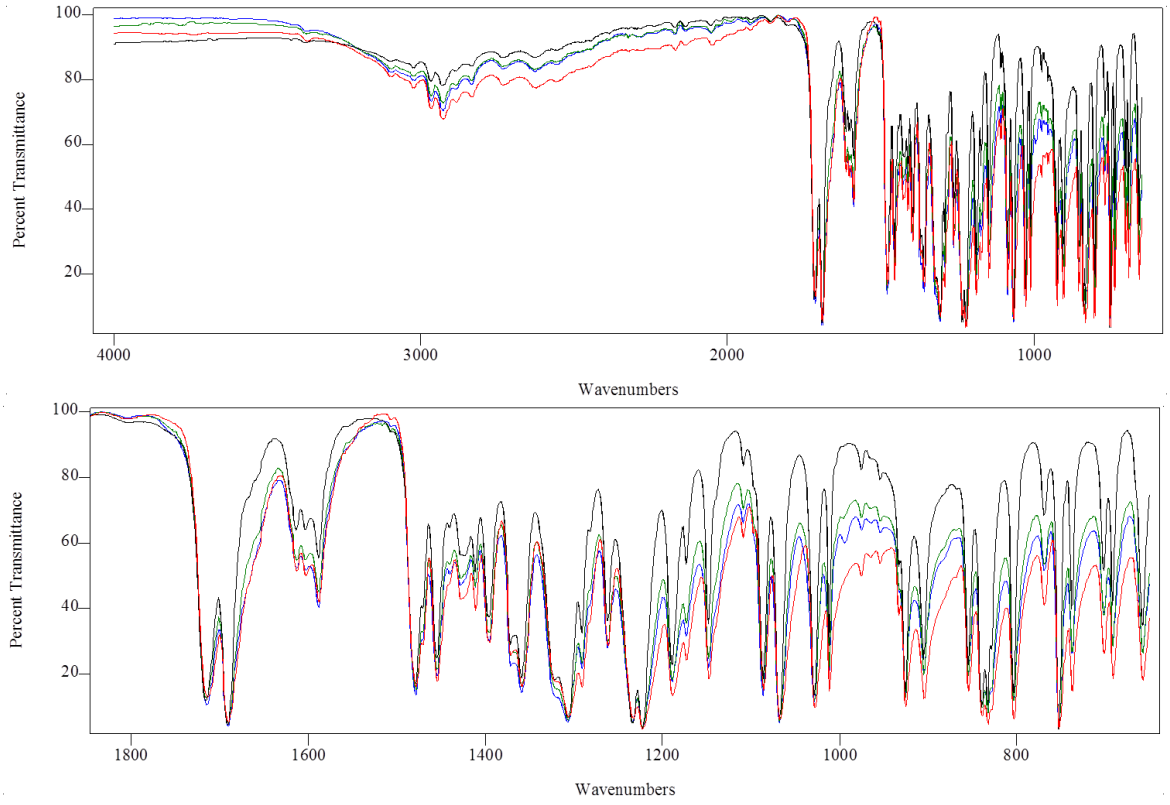

Figure 6-33 Overlay of the normalised FTIR spectra for the comminuted materials of γ-indomethacin by high frequency ball-milling (Blue), low frequency ball-milling (Green) and micronisation (Black) compared to the Input/reference material (Red).

FTIR can also be used to identify differences in the solid-state forms of the materials as a result of processing and shows great sensitivity to polar bonds such as O-H, C=O and N-H, hence, FTIR provides a good tool to investigate the presence of water and changes in any H-bonding[317,318]. This is illustrated by the FTIR spectra for the comminuted

materials for salbutamol sulphate (Figure 6-34) and loperamide HCl (Figure 6-35). High frequency ball-milling of salbutamol sulphate with and without liquid nitrogen resulted in peak broadening and shifts in a number of FTIR peaks s in the region 3500 to 2200 cm^{-1} and 1700 to 700 cm^{-1} which were consistent with observations from the literature, suggesting the presence of disorder, and a small amount of adsorbed water[219,247,366] (Figure 6-34). The FTIR spectra for low frequency ball-milled and micronised salbutamol sulphate were generally consistent with that of the spectrum of the input material, therefore, these processes did not appear to alter the H-bonding pattern or change the chemical nature of the material.

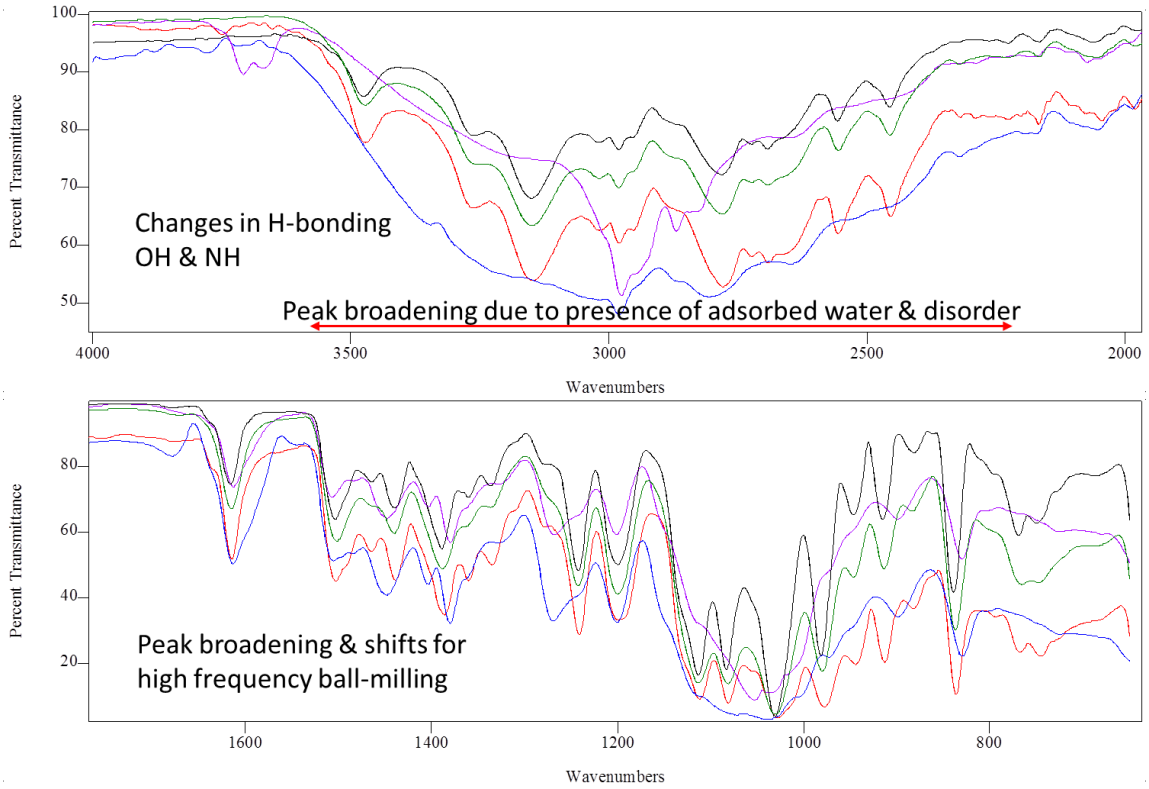

Figure 6-34 Overlay of the normalised FTIR spectra of the comminuted materials of salbutamol sulphate by high frequency ball-milling with liquid nitrogen (blue) at room temperature (purple), low frequency ball-milling Mill-B (green) and micronisation (black) compared to the input material (red).

The FTIR spectra for the comminuted materials of loperamide HCl are shown Figure 6-35. For the high frequency ball-milled material the presence of water and disorder can be inferred from the broad band between 3600 and 3100 cm^{-1} and the observed peak broadening and shifts. A small amount of peak broadening and peak shifts was observed for low frequency ball-milled loperamide HCl, suggesting that a small amount of disorder was possibly present. However, the FTIR spectra for the micronised material was concordant with that of the input material.

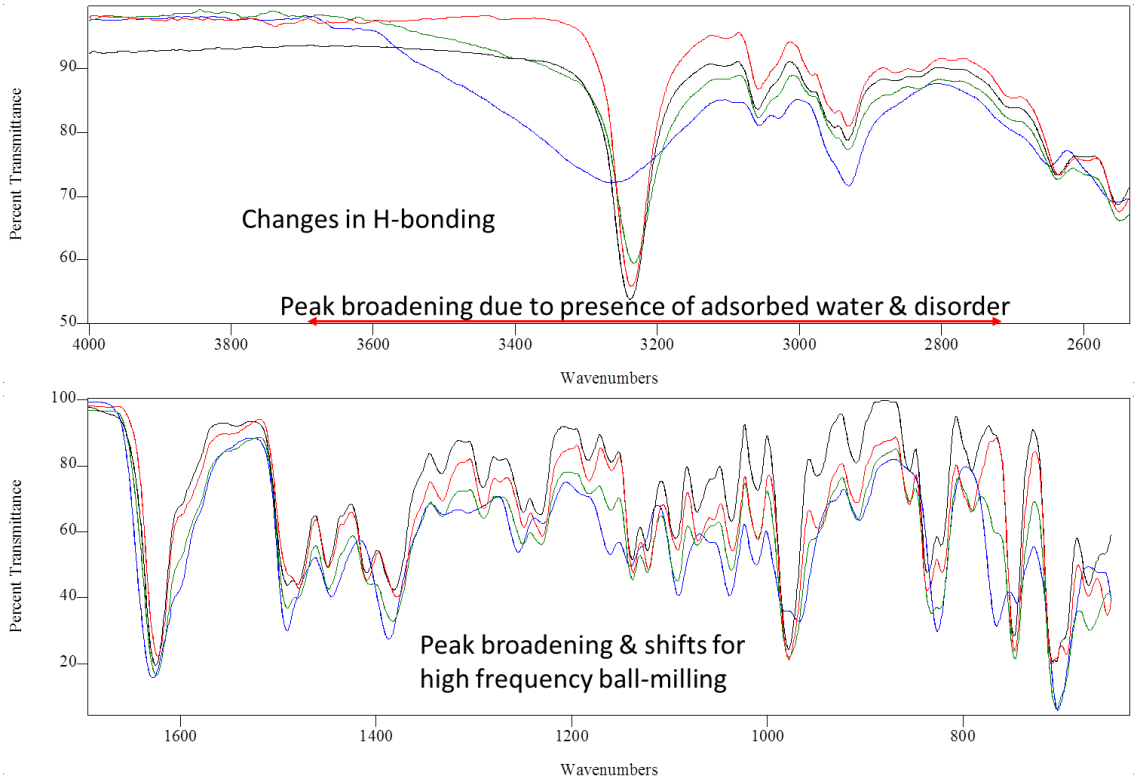

Figure 6-35 Overlay of the normalised FTIR spectra of the comminuted materials of loperamide HCl by high frequency ball-milling (blue), low frequency ball-milling (green) and micronisation (black) compared to the input material (red).

Several polymorphs of sulfamerazine are known to exist and it has been shown that mechanical processing can induce solid-state transformations via the amorphous phase[349-351]. Additional vibrations were observed in the IR spectrum for high frequency ball-milled sulfamerazine consistent with those of Form II[157,184146,173] and shifts in peaks suggesting changes in the intermolecular interactions (H-bonding) of the molecule[146,173] (Figure 6-36 and Table 6-21). Typically Form I sulfamerazine exhibits split vibrational stretches at 3498/3482 cm^{-1} for asymmetric stretching of NH_2 and 1641/1628 cm^{-1} for NH_2 scissoring. While Form II, shows only single vibrations around 3458 cm^{-1} and1644 cm^{-1} for these stretches respectively. This confirms the observations made using other methods such as XRPD (Figure 6-8) and DSC (Figure 6-17) of the presence of a mixture of Form I and Form II sulfamerazine in the sample after high frequency ball-milling[336,361,362].

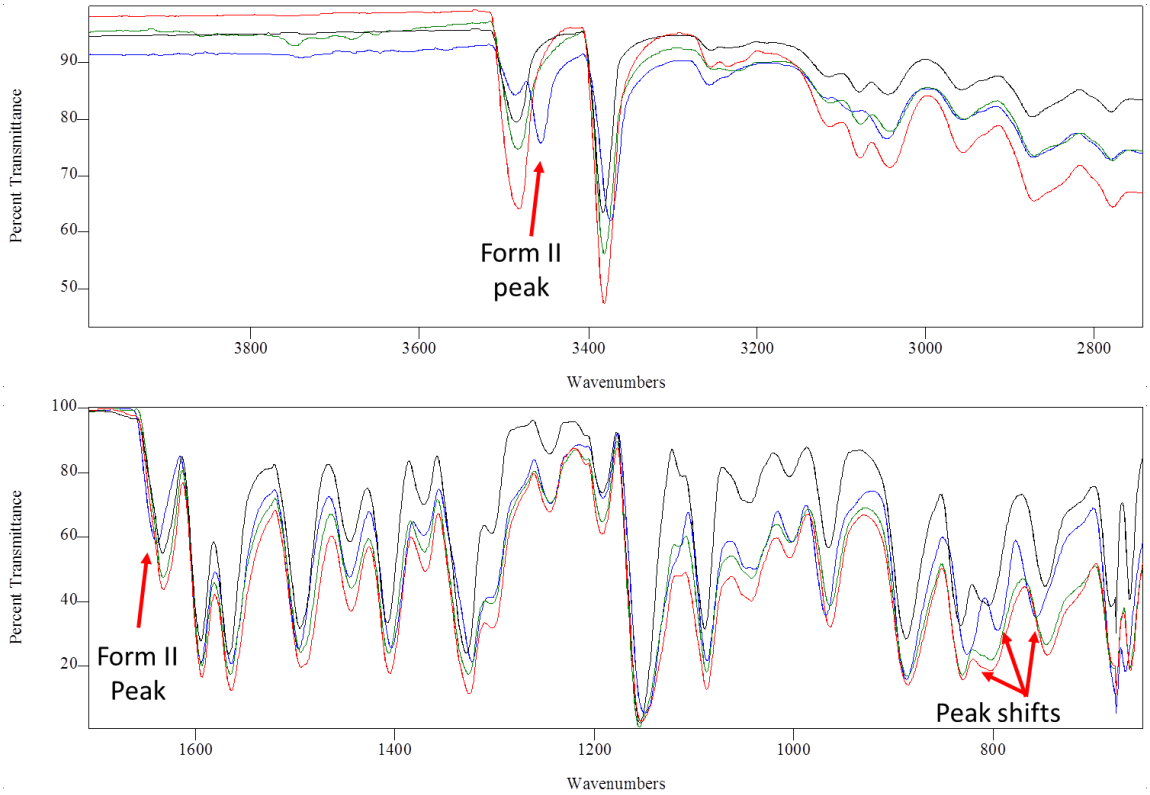

Figure 6-36 ***Overlay of the normalised FTIR spectra of the comminuted materials of sulfamerazine by high frequency ball-milling (blue), low frequency ball-milling (green) and micronisation (black) compared to the input material (red).***

6.4.8 High pressure liquid chromatography (HPLC)

As discussed in Section 1.4, mechanical processes can be of high energy and can impart large amounts of stress to the material being processed. These stresses can result in the formation of impurities such as those generated by thermal degradation. This is especially important when investigating the generation of amorphous materials as these are often associated with temperature changes. In a number of historical studies involving the production of amorphous materials by melt-quenching or ball-milling, the assessment of final chemical purity has often not been investigated[160,205,208,221,257,367-369].

In the current study, the final chemical purity or the presence of impurities was assessed by HPLC to add a degree of confidence to the conclusion that the response changes observed as a consequence of different comminution processes are due to the presence of disorder rather than to changes in chemical purity. *e.g.* shifts in T_m and T_d, etc.. To this end, the HPLC chromatograms and associated responses were obtained for the mechanically comminuted materials and compared to those of the input/reference materials (Table 6-22).

Table 6-22 Summary of HPLC responses and CRA of the comminuted materials

		HPLC responses			HPLC CRA	
Material	Batch ID	No. peaks	Primary peak RT min (% area)	Other Peaks RT min (% area)	Δ No. peaks	ΔRT & (Δ%area)
Acetaminophen	Input	1	1.56 (100)	ND	--	--
	1-MA1	1	1.56 (100)	ND	0	0 (0)
	1-MA2	1	1.55 (100)	ND	0	0 (0)
	1-MB1	1	1.55 (100)	ND	0	0 (0)
	1-MB2	1	1.55 (100)	ND	0	0 (0)
	1-X1	1	1.55 (100)	ND	0	0 (0)
γ-Indomethacin	Input	3	5.33 (99.7)	5.71 (<0.1), 6.35 (0.3)	--	--
	11-MA1	2	5.34 (99.7)	6.35 (0.3)	-1	0 (0)
	11-MA2	2	5.34 (99.7)	6.35 (0.3)	-1	0 (0)
	11-MB1	3	5.34 (99.6)	5.71 (<0.1), 6.35 (0.3),	0	0 (-0.1)
	11-MB2	2	5.34 (99.7)	6.36 (0.3)	-1	0 (0)
	11-X1	2	5.34 (99.7)	6.35 (0.3)	-1	0 (0)
Salbutamol sulphate	Input	2	1.88 (99.8)	2.61 (0.2)	--	--
	Post-DSC	22	1.89 (56.7)	2.60 (20.04), **2.30** (0.18), **2.41** (0.41), **2.53** (0.36)	20	0 (-43.1)
	24-MA1	5	1.88 (99.4)	2.61 (0.2), **2.29** (0.1), **2.41** (0.2), **2.53** (0.1)	3	0 (-0.4)
	24-MA2	5	1.88 (99.3)	2.61 (0.3), **2.29** (0.1), **2.41** (0.2), **2.53** (0.1)	3	0 (-0.5)
	24-MA3	5	1.87 (99.4)	2.61 (0.3), **2.29** (0.1), **2.41** (0.1), **2.53** (0.1)	3	0 (-0.4)
	24-MB1	2	1.88 (99.7)	2.60 (0.3)	0	0 (0)
	24-MB2	2	1.87 (99.7)	2.60 (0.3)	0	0 (0)
	24-X1	4	1.88 (99.5)	2.60 (0.3), **2.29** (0.1), **2.53** (0.1)	2	0 (-0.3)
Loperamide HCl	Input	3	4.53 (99.8)	2.57 (<0.1), 4.26 (0.1)	--	--
	14-MA1	3	4.53 (99.8)	2.56 (0.1), 4.26 (0.1)	0	0 (0)
	14-MB1	3	4.54 (99.8)	2.56 (<0.1) 4.27 (0.1)	0	0 (0)
	14-X1	3	4.52 (99.8)	2.56 (0.1), 4.26 (0.1)	0	0 (0)
Acetylsalicylic acid	Input	2	2.91 (99.4)	3.09 (0.6)	--	--
	33-MA1	2	2.91 (99.4)	3.09 (0.6)	0	0 (0)
	33-MB1	2	2.91 (99.4)	3.09 (0.6)	0	0 (0)
	33-X1	2	2.91 (99.4)	3.09 (0.6)	0	0 (0)
Sulfamerazine	Input	3	2.06 (99.8)	1.77 (<0.1), 3.10 (0.2)	--	--
	54-MA1	3	2.06 (99.8)	1.77 (<0.1), 3.10 (0.2)	0	0 (0)
	54-MB1	3	2.06 (99.8)	1.77 (<0.1), 3.10 (0.2)	0	0 (0)
	54-X1	3	2.06 (99.8)	1.77 (<0.1), 3.09 (0.2)	0	0 (0)
Phenacetin	Input	4	3.17 (99.5)	2.06 (<0.1), 3.48 (0.3), 3.57 (0.2)	--	--
	69-MA1	1	3.17 (100)	ND	-3	0 (0.5)
	69-MB1	2	3.17 (99.5)	3.48 (0.5),	-2	0 (0)
	69-X1	2	3.17 (99.5)	3.48 (0.4)	-2	0 (0)
Sulfadiazine	Input	1	1.67 (100)	ND	--	--
	87-MA1	1	1.68 (100)	ND	0	0 (0)
	87-MB1	1	1.68 (100)	ND	0	0 (0)
	87-X1	1	1.68 (100)	ND	0	0 (0)
Caffeine	Input	1	2.27 (100)	ND	--	--
	88-MA1	1	2.27 (100)	ND	0	0 (0)
	88-MB1	1	2.27 (100)	ND	0	0 (0)
	88-X1	1	2.27 (100)	ND	0	0 (0)
Methyl paraben	Input	1	3.04 (100)	ND	--	--
	140-MA1	1	3.04 (100)	ND	0	0 (0)
	140-MB1	1	3.04 (100)	ND	0	0 (0)
	140-X1	1	3.04 (100)	ND	0	0 (0)

RT: retention time (min), Δ#peaks: Change in number of observed peaks between sample and reference, ND: Not detected, ΔRT & Δ%area: change in retention time and % area of primary peak. Red identifies identical peaks in comminuted material (Mill-A1 & JM-A) for salbutamol sulphate with those from the post-DSC sample
#-MA#: high frequency ball-mill method A, #-MB#: low frequency ball-mill method B. #-X#: jet micronisation method A

For the majority of the comminuted materials the estimated chemical purity, as indicated by the peak retention time and % area for the primary peak remained the same and no degradation (additional) peaks were observed. However, some additional peaks were observed for high frequency ball-milled and micronised salbutamol sulphate.

It has been postulated that the process of ball-milling can cause "amorphisation" of a material due to collisions of the milling balls resulting in localised increases in temperature or the creation of "hot points"[72]. These local hot points may exceed the melting temperature of the compound and the sudden return to room temperature after the impact would then act as a quench mechanism, thereby generating amorphous material by a melt/quench process[72]. This phenomenon was investigated by ball-milling salbutamol sulphate with and without liquid nitrogen (temperature control). However, in both cases a predominately amorphous material was generated and HPLC analysis showed peaks indicative of the presence of a small amount of impurities similar to those obtained post-DSC. Nevertheless, the overall estimated purity remained relatively high, *i.e.* % area of the primary peak was only reduced by 0.5% and this could account for some of the decreases in the observed DSC responses (Table 6-17). However, it is most likely the presence of disorder that has the biggest impact on observed APRs.

6.4.9 General discussion

Compared to other pharmaceutical processes such as spray and freeze drying which can often result in "100%" amorphous content, detecting disorder as a result of milling and micronisation can be challenging, as the level of disorder present can vary depending on the energy applied. Therefore a combination of techniques should be employed to increase the probability of detection and to mitigate the potential for misinterpreting the solid-state phase present by using only one or two techniques in isolation[16,17,119,185,186].

The selected study materials were subjected to ball milling at two different levels of impact and by micronisation using a fluid jet-mill (Chapter 5). The analytical responses of the comminuted materials have been reported here, using a number of different characterisation techniques, which have been referred to as the core test methods. The responses from these core test methods were then compared to those of the input material using a novel approach called CRA. The qualitative relevance of these changes was then defined with respect to the solid-state phase present for each of the comminuted materials. This CRA approach provided a more consistent and data driven classification process to define the solid-state phase present, rather than employing an

approach that relied solely on the knowledge, experience and interpretation of the investigator. Based on the CRA values, novel solid-state phase classifications or decision trees were applied to those core test methods which can detect the presence of disorder directly; these were designated the 'primary' disorder detection methods such as XRPD, DSC and GVS (Sections 6.3.1.3, 6.3.3.3 and 6.3.6.3 respectively). Other core test methods such as TGA, HPLC, FTIR and SEM, on the basis of the results obtained here, may be categorised as 'secondary' disorder detection methods, as it proved more difficult to discriminate between disordered and crystalline phases present in the materials. Solid-state phase decision trees were not created for these 'secondary' detection methods, instead, these methods were employed to provide supplementary or supportive evidence for the presence of disorder indirectly. For example, TGA was used to determine the change in sample mass as a function of temperature[288,289,370]. These mass change events primarily represented the loss of volatiles or material decomposition. Changes to surface disorder, particle size and levels of impurities could be inferred through changes to the mass loss profile and, or degradation temperatures[33-36]. Understanding the causes of these changes especially the weight loss due to the presence of water that may have been sorbed as a consequence of processing or storage can be used to highlight any potential solid state stability issues. The sorption of water either during processing or storage can be used to accelerate the crystallisation of any disordered surfaces and could lead to agglomeration and in worst case, transformation to new solid states[288,290].

Using the combined information from the primary and secondary disorder detection methods, the solid-state phase present for each comminuted material was qualitatively defined and summarised in tabular form. An example is shown in Table 6-23 for comminuted loperamide HCl and in APPENDIX 7 for all of the study materials.

For the 'primary' detection methods, XRPD, GVS and DSC, the solid-state phase identified was colour coded to represent the phase present, red for disordered, orange for microcrystalline or little to some degree of disorder present, while crystalline materials were colour coded green. With respect to moisture sorption information obtained by DSC, TGA and GVS the presence of moisture was commented on. For the GVS analysis data, "observed" refers to any large change in moisture uptake (ΔM_{ADS1}) greater than 0.5 % (w/w).

Table 6-23 Summary of the solid-state phase present in the comminuted materials of loperamide HCl

			Solid-state phase classifications and analytical response observations		
Material Property	Technique	DM	Mill-A***	Mill-B***	JM-A
Phase detection & identification	XRPD	1	X-ray Amorphous	Disordered	Crystalline
	GVS	1	Disordered	Disordered	Disordered
	DSC	1	Disordered	Mixed Phase B – maybe new crystalline form some disorder	Mixed Phase A – same crystalline form with some disorder
Moisture sorption	GVS	1	Observed (9.01%)	Observed (2.88 %)	Observed (0.83 %)
	DSC	1	Observed	Observed	Observed
	TGA	2	Observed (1.37 %)	Observed (0.74 %)	Not observed
Chemical purity	HPLC	2	Concordant with Ref.	Concordant with Ref.	Concordant with Ref.
	FTIR	2	Disorder - Broadening, water & shifts	Some disorder - slight broadening and shifts	Concordant with Ref.
Particle size	PSA	2	Broad multi-modal agglomeration D_{50} < 7 µm	Broad multi-modal agglomeration D_{50} < 10 µm	mono-modal D_{50} < 2 µm
	SEM	2	Irregular, fractured, rough, agglomerated & drusy	Irregular, fractured, rough, agglomerated & drusy	Irregular, fractured, rough, agglomerated & drusy
Solid-state phase present			Disordered	Some disorder	Crystalline –little disorder

DM – detection method; 1:primary disorder detection technique. 2: secondary disorder detection technique
Mill-A: high frequency ball-mill method A, Mill-B: low frequency ball-mill method B. JM-A: jet-mill method A.
Phase indicated by colour Crystalline, Microcrystalline or little/some disorder, Disordered

Solid-state phase colour coding was not applied to 'secondary' disorder detection methods but the information from these techniques were summarised to help support the final phase classification. This final designation of the solid-state phase present for each comminuted material was qualitatively determined by considering the number of colour codes (Table 6-24) for the solid-state phase identified by the techniques, XRPD, GVS and DSC.

Table 6-24 Colour coding for classifying the final solid-state phase present in comminute materials

No. colours from primary detection methods			Final solid-state phase identification	Solid-state phase identification colour code
			Disordered	
			Some disorder	
			Some disorder or microcrystalline	
			Some disorder or microcrystalline	
			Crystalline- little disorder or microcrystalline	
			Little disorder or microcrystalline	
			Crystalline- little disorder	
			Crystalline - little disorder or microcrystalline	
			Crystalline	

In the example given in Table 6-23 for the qualitative solid-state phase identification for the comminuted materials of loperamide HCl, it can be seen that for the high frequency

ball-milled material all three primary detection methods identified disorder being present (3 reds), hence this material was classified as being disordered. For low frequency ball-milling, both XRPD and GVS detected disorder (2 reds) but CRA for DSC only suggested that some disorder was present (orange). Therefore, the final material was designated as having "some disorder" (2 reds - 1 orange). CRA for the XRPD responses for micronised loperamide HCl suggests the material was crystalline (green) but disordered (red) by GVS and a mixture of phases from the DSC data (orange), hence the final solid-state phase designation for this material was crystalline with a little disorder present.

Defining the presence of mainly crystalline or disordered materials can be easily performed. However, defining a mixture of phases or the presence of microcrystalline material can be more difficult. In this research, a consistent approach has been applied to assist with classifying microcrystalline material using XRPD data. Microcrystalline refers to a material which is crystalline but the particle size has been significantly reduced, such that it may appear disordered by XRPD analysis, *i.e.* it may exhibit different MIP, broader peaks and the background heights may have increased. However, unlike disordered material there is no apparent peak shifting observed in the XRPD diffractogram.

A summary of the final solid-state phases identified for all the comminuted materials is given in Table 6-25. It can be seen that the three comminution processes produced materials that encompassed the whole amorphous-crystalline continuum, and the designated solid-state phases were consistent with the observed PID assessment previously reported in the literature (Table 2-8), but the degree of disorder was dependent on the comminution process employed. Materials such as acetaminophen, acetylsalicylic acid, phenacetin and methyl paraben were resistant to PID regardless of the comminution process employed. For other materials such as sulfamerazine, sulfadiazine and caffeine some disorder was observed upon ball-milling but there was little or none induced when they were micronised. In the case of sulfamerazine, high frequency ball-milling resulted in the generation of a small amount of Form II via the amorphous phase[336,361,362].

Table 6-25 Summary of the identified solid-state phase present in the comminuted materials

Material	Process	Literature PID (from Table 2-8)	Solid-state phase present	**Primary detection colour codes**
Acetaminophen	Mill-A	No[160,221]	Crystalline	
	Mill-B		Crystalline	
	JM-A		Crystalline	
Phenacetin	Mill-A	No[265]	Crystalline	
	Mill-B		Crystalline	
	JM-A		Crystalline	
Methyl paraben	Mill-A	No[255]	Crystalline	
	Mill-B		Crystalline	
	JM-A		Crystalline	
Acetylsalicylic acid	Mill-A	No[160,221,266,267]	Crystalline	
	Mill-B		Crystalline	
	JM-A		Crystalline	
Sulfamerazine	Mill-A	Some [270,271]	Some disorder – some new form	
	Mill-B		Microcrystalline - little disorder	
	JM-A		Crystalline	
Sulfadiazine	Mill-A	Some[221,270]	Crystalline – little disorder	
	Mill-B		Crystalline – little disorder	
	JM-A		Crystalline – little disorder	
Caffeine	Mill-A	Some[217,269]	Crystalline – little disorder	
	Mill-B		Crystalline – little disorder	
	JM-A		Crystalline – little disorder	
γ-Indomethacin	Mill-A	Yes[148,160,178,212,221,268,271]	Disordered	
	Mill-B		Microcrystalline - little disorder	
	JM-A		Crystalline	
Salbutamol sulphate	Mill-A	Yes[1,20,21,246,247,275-277]	Disordered	
	Mill-B		Microcrystalline - some disorder	
	JM-A		Crystalline - little disorder	
Loperamide HCl	Mill-A	Yes[278]	Disordered	
	Mill-B		Some disorder	
	JM-A		Crystalline – little disorder	

Crystalline, *Microcrystalline – little disorder*, *Disordered*

Mill-A: high frequency ball-mill method A, Mill-B: low frequency ball-mill method B. JM-A: jet micronisation method A. Summary of information from the primary and secondary disorder detection methods and the solid-state phase identified for each comminuted material can be found in APPENDIX 7.

For the remainder of the materials: loperamide HCl, salbutamol sulphate and γ-indomethacin different solid-state phases were observed depending on the comminution process employed. The level of disorder appeared to be proportional to the relative amount of energy imparted by the comminution process. Ball-milling in general had a greater tendency to induce disorder than micronisation, as it is a "closed system" (Section 1.4.3) as the material is constantly exposed to a number of high energetic forces (stresses). Micronisation on the other hand is an "open system" where material flows into the grinding chamber via a pressure gradient where it is size reduced and then

removed, once the desired particle size is attained. This final size is dependent on the operating parameters employed (Section 1.4.4). Based on the CRA responses and solid-state phase classification of the comminuted materials, the comminution processes were ranked in order of their tendency to cause PID from lowest to highest: micronisation (JM-A) < low frequency ball-milling (Mill-B) < high frequency ball-milling (Mill-A). This order also reflects the efficiency of the comminution processes in reducing particle size without causing PID, with micronisation (JM-A) being the most efficient, followed by low frequency ball-milling (Mill-B) and high frequency ball-milling (Mill-A) being the least efficient process. It is also important to note that, based on these observations the use of ball-milling to model the process of micronisation should be done with caution as the potential properties of the ball-milled material, such as levels of PID, particle size, agglomeration, etc. may not reflect that of the micronised material.

In general the comminution processes did not appear to cause significant degradation within the materials, which suggests that any observed changes in the analytical responses were most likely due to physical changes, such as reductions in particle size or the generation of PID. However, in the case of salbutamol sulphate, a small level of degradation was detected by HPLC but the estimated overall purity was not significantly reduced.

The novel qualitative CRA approach described here provides a more consistent and systematic approach to define the solid-state phase present in any given material subjected to a comminution process. However, the CRA values and qualitative colour coding of the solid-state phase present provides only a gross indication of the changes in the properties but is not definitive enough to be able to discriminate different levels of disorder. By redefining the CRA threshold levels for the technique responses specific to the presence of disorder, the amount of disorder may be able to be semi-quantified allowing better disorder identification and a better understanding of the impact a comminution process may have on a respective material to cause PID. This will be investigated in Chapter 7.

6.5 Conclusions

The characterisation of the mechanically comminuted study materials successfully demonstrated that the novel approach comprising of CRA and the use of solid-state phase decision trees, for the primary disorder detection methods of XRPD, DSC and GVS, could be used to effectively define changes in the individual technique responses,

as well as aid in appropriately classifying the solid-state phase of the resulting material. Using this approach it was demonstrated that the three comminution processes generated material that encompassed the whole amorphous-crystalline continuum and also showed that differences could be detected in the nature of the materials produced from the different comminution processes. Additionally, it was also shown that the comminution processes appeared to be HPLC pure, *i.e.* milling processes did not result in increased degradation apart from a very small amount for salbutamol sulphate.

7 Process disorder analysis (PDA) for mechanically comminuted materials

7.1 Introduction

Qualitatively assessing the presence of disorder can be somewhat subjective as such determination relies on the analyst's experience and interpretation[23,244,245,247]. Typically the presence of amorphous material as a consequence of mechanical processing can be characterised qualitatively by defining one or a combination of the following: the presence of an amorphous halo by XRPD, a T_g and recrystallisation by DSC and/or an observed recrystallisation in GVS moisture sorption profiles[6,7,23,160,221,242-247,280]. Such an assessment gives no indication of the degree of induced disorder. However, the amount of disorder is typically determined using only a single response from a given technique and a number of 'standards' to construct a calibration curve[137,199,369-371], despite these 'standards' being specific to the individual material, thereby making it harder to make comparisons between materials.

It has been successfully shown by the studies described in Chapter 6 that the novel CRA process based on the differences between analytical responses for the comminuted materials and those of the respective inputs could be used to classify qualitatively the presence of PID. However, this process has its limitations in that it may not be definitive enough to discriminate different levels of disorder. For example, high frequency ball-milling of indomethacin, loperamide HCl and salbutamol sulphate were all classified as being disordered using the CRA process but defining the relative amount of disordering and which of the three was the most affected by the ball-milling process could not be easily distinguished (Table 6-25). Comminution of salbutamol sulphate and loperamide HCl by low frequency ball-milling also exhibited "some disorder" but this also could not be quantified, nor could the materials be ranked according to the relative level of PID detected. However, an attempt to achieve this was made through the colour coding scheme based on the CRA results (Section 6.4.9), *i.e.* the greater the number red boxes, the more likely disorder is present (Table 6-25). This approach, even with its limitations provided a consistent and reproducible approach to defining the solid-state phase present which can be transferable between analysts and investigators working in different laboratories.

To be able to fully discriminate inter-, intra-material and processing differences a semi-quantitative approach is proposed, in which the amount of disorder may be first semi-

quantified by redefining the CRA threshold levels for the individual technique responses specific to the presence of disorder. This new process will be referred to as response disorder analysis (RDA). The RDA values from a number of techniques can then be combined into a single normalised value by a process designated process disorder analysis (PDA) enabling more information regarding the nature of the disorder to be deduced, as the responses represent information from multiple properties of the material not just a single property. To date, there has been no quantitative approach that has incorporated the responses from multiple techniques into a singular value to define a certain property such as the presence of disorder or amorphous character.

The objective for this chapter was to develop further the analytical approach introduced previously (Chapter 6) incorporating multiple responses from various techniques to determine the level of disorder present in a material as a consequence of mechanical comminution processes allowing semi-quantitative discrimination between materials and processing conditions.

7.2 Methods

7.2.1 Overview of analytical approach to identify and quantify the presence of disorder

The novel analytical approach to determine and semi-quantify the amount of disorder present as a consequence of a comminution process is outlined in Figure 7.1.

Once comminuted, the materials were characterised using the core test methods and individual responses, both qualitative and quantitative were obtained (RA) (Chapter 6). The responses for each technique were then compared to those of the initial input material by CRA (Section 6.3), and the relative amount of change in responses with respect to the presence of disorder could then assessed by RDA and a technique disorder score determined ($D_{Technique}$) (Sections 7.2.2 to 7.2.4). In this study only XRPD, DSC and GVS will be assessed by RDA, as these three techniques represent the 'primary' disorder detection methods and can also provide information for a number of other important properties, such as molecular structure, thermal behaviour, purity and moisture sorption.

The technique disorder scores, $D_{Technique}$ were then combined into a single normalised process disorder score (D_{Pro}), which represents the relative amount of disorder present as a result of a defined process (Section 7.2.5). This process disorder score combines the

information from changes in multiple analytical responses and techniques into a single value, enabling materials to be ranked according to the relative level of disorder present and may allow discrimination between the comminution processes with respect to the relative amount of disorder that they may induce.

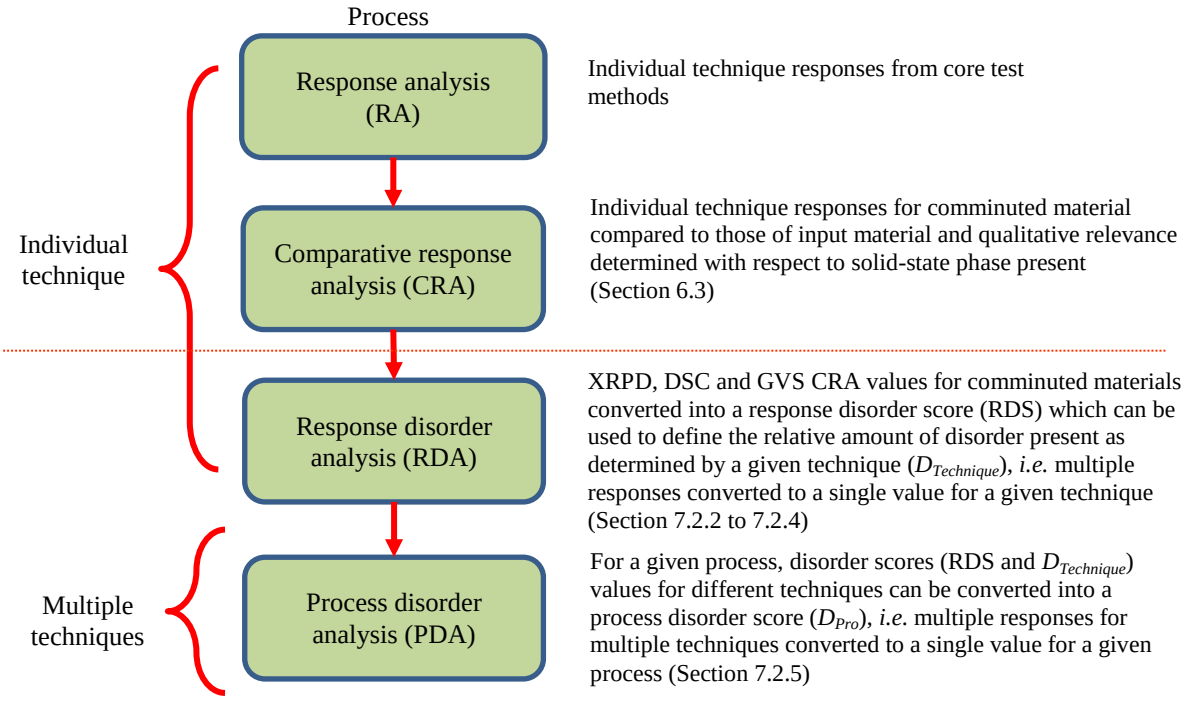

Figure 7-1 ***A novel analytical approach to define disorder as a consequence of a comminution process.***
Red dashed line shows the distinction between the processes to characterise the solid-state phase of the material (above the line) to those specific to determine relative disorder (below the line)

7.2.2 Response disorder analysis for X-ray powder diffraction (XRPD)

Using the XRPD CRA values for the different comminuted materials (Table 6-14), the amount of observed change in the responses over the whole XRPD diffractogram were assessed with respect to any perceived PID to give a response disorder score (R_{XRPD}). R_{XRPD} values were determined using Table 7.1. The magnitude of the RDS values reflect the changes in the peak characteristics over the whole XRPD diffractogram, such as shifts in peak positions (P_P), changes in peak (P_H) and background heights (B_H), as well as changes in peak widths (P_W) and were weighted to reflect the likelihood of PID being present.

Changes in peak positions, the MIP and the presence of new peaks cannot be directly related to disorder; hence these responses have a lower maximum score of 2 or 3. While the reduction in the number of peaks, decreased peak heights and/or increased

background heights as well as increased peak widths may be more indicative for the presence of disorder, hence they have higher maximum scores, 5, 7 or 9.

Table 7-1 RDS score values (R_{XRPD}) for key XRPD peak descriptors P_p, P_H, B_H, P_W, MIP and changes in number of peaks

Step	CRA parameter	CRA value	Response disorder score R_{XRPD}	RDS ID
1	Number of peaks reduced? (missing or merged)	No	0	R_{XRPD1}
		Yes	5	
		All new peaks	5	
		No peaks observed	7	
2	New peaks observed?	No new peak or no peaks observed	0	R_{XRPD2}
		Yes	2	
3	Average °2θ shift in peak positions across all peaks(AvP_P)	-0.03 to 0.03 (no change)	0	R_{XRPD3}
		> ±0.03 (observed shift)	3	
		No peaks observed or all new peaks	3	
4	Change in MIP?	No	0	R_{XRPD4}
		Yes	3	
		No peaks observed or all new peaks	3	
5	Average % change in peak heights across all peaks(AvP_H)	> -20 % (relatively unchanged or increased)	0	R_{XRPD5}
		-20 to -30 % (slight decrease)	2	
		-30 to -40 % (small decrease)	5	
		All new peaks observed	5	
		-40 to -50 % (large decrease)	7	
		Reduced more than -50 % (marked decrease)	9	
		No peaks observed	9	
6	Average % change in background heights across all peaks(AvB_H)	< 20 % (relatively unchanged or reduced)	0	R_{XRPD6}
		20 to 30 % (slight increase)	2	
		30 to 40 % (small increase)	5	
		All new peaks observed	5	
		40 to 50 % (large increase)	7	
		> 50 % (marked increase)	9	
		No peaks observed	9	
7	Average % change in peak widths across all peaks(AvP_W)	< 20 % (relatively unchanged or reduced)	0	R_{XRPD7}
		20 to 30 % (slight increase)	2	
		30 to 50 % (small increase)	5	
		All new peaks observed	5	
		50 to 100 % (large increase)	7	
		> 100% (marked increase)	9	
		No peaks observed	9	

Proceed stepwise from step1 to 7, summing the RDS *score (*R_{XRPD1} *to* R_{XRPD7}*) for the comminuted material using the relevant CRA values*

Average changes in peak areas (P_A) were not included in the calculation of R_{XRPD} as changes in this response could be misinterpreted and skew R_{XRPD} values. Increases in peak areas could arise due to peak merging or they could increase as a result of

increases crystallinity, *i.e.* increases in peak heights and peak widths, consequently the inclusion of peak areas could skew the RDS by over-emphasising the importance of the peak height and peak width information.

The RDS values were then converted to a technique disorder score (D_{XRPD}) using equation [7-1], which represents the total degree of observed disorder in the XRPD diffractogram as a consequence of a defined comminution process.

$$\text{XRPD disorder score } (D_{XRPD}) = \left(\frac{R_{XRPD}}{40}\right) \text{x } 10 \qquad [7\text{-}1]$$

where R_{XRPD} is the sum of $R_{XRPD\,1}$ to $R_{XRPD\,7}$ out of 40, the maximum score.

D_{XRPD} was therefore calculated as a value between 0 and 10 (Table 7-2); where, 0 represents no perceived observation of PID and 10, represents a marked degree of inferred disorder based on the changes in the XRPD responses. The D_{XRPD} values can also be represented by a colour code, green representing a low probability of disorder being present, orange a medium probability and red representing a high probability of disorder being present (Table 7-2).

Table 7-2 XRPD Disorder classification using D_{XRPD} values

D_{XRPD} value	Likelihood that disorder is present. The larger the value the more significant the disorder present	Colour code
0.0 to 3.0	Low probability of disorder being present – low levels of disorder	
3.1 to 7.0	Medium probability of disorder being present – some disorder present	
7.1 to 10.0	High probability of disorder being present – marked levels of disorder present	

A worked example of the method used to calculate D_{XRPD} is shown using the CRA values for high frequency ball-milled γ-indomethacin, batch 11-MA1 (Table 7-3).

Table 7-3 Calculated R_{XRPD} score for γ-indomethacin (11-MA1) using determined CRA values

	CRA values for γ-indomethacin						
	Missing/merged peaks?	New peaks?	$Av\Delta P_P$ (°2θ)	Change in MIP?	$Av\Delta P_H$ (%)	$Av\Delta B_H$ (%)	$Av\Delta P_W$ (%)
	Yes	No	-0.04	Yes	-67	44	68
RDS*	5	0	3	3	9	7	7
RDS ID	R_{XRPD1}	R_{XRPD2}	R_{XRPD3}	R_{XRPD4}	R_{XRPD5}	R_{XRPD6}	R_{XRPD7}

** RDS values determined using Table 7-1, CRA values from Table 6-14. Refer to appendix 8 for an overlay of the XRPD diffractogram of 11-MA1 and the input.*

The XRPD diffractogram of milled γ-indomethacin (Appendix 8), was found to have missing or merged peaks but no new peaks were observed, and hence a R_{XRPD1} value of

5 and a R_{XRPD2} of 0 were allotted respectively. There was also an observed average peak shift ($Av\Delta P_P$) greater than ± 0.03, hence R_{XRPD3} was given a value of 3. An observed change in MIP, a marked reduction in peak height ($Av\Delta P_H$) of -67 %, and a large increase in background height ($Av\Delta B_H$) of 44% resulted in RDS values of 3, 9 and 7 for R_{XRPD4}, R_{XRPD5} and R_{XRPD6} respectively. A large increase in peak width ($Av\Delta P_W$) of 68% was also observed generating a R_{XRPD7} value of 7. Summing all the values for R_{XRPD1} to R_{XRPD7} gave a total R_{XRPD} value of 34 and substituting this value into equation [7-1] produced a D_{XRPD} score of 8.5 for high frequency ball-milled γ-indomethacin.

7.2.3 Response disorder analysis for differential scanning calorimetry (DSC)

Using the DSC CRA values for the different comminuted materials (Table 6-17) the amount of observed change in the responses over the whole DSC thermogram were assessed with respect towards PID, to give a response disorder score (R_{DSC}). R_{DSC} values were determined using Table 7.4 and reflect the average changes in the thermal responses with respect to the presence of disorder.

Table 7-4 RDS score values (R_{DSC}) for key DSC responses based on CRA values

Step	CRA parameter	CRA value	Response disorder score R_{DSC}	RDS ID
1	Observed volatile?	No	0	R_{DSC1}
		Yes	5	
2	Observed glass transition event?	No	0	R_{DSC2}
		Yes	10	
3	New crystallisation or transition event observed?	No	0	R_{DSC3}
		Yes	10	
4	Average shift in melting temperature (ΔT_m) °C	> -3.0 °C	0	R_{DSC4}
		-3 to -10 °C	3	
		Decreased more than -10 °C	5	
5	Average change in degradation temperature (ΔT_d)	> -3.0 °C	0	R_{DSC5}
		-3 to -10 °C	5	
		Decreased more than -10 °C	10	

Proceed stepwise from step1 to 5, summing the RDS *score (*$R_{DSC\,1}$ *to* R_{DSC5}*) for the comminuted material using the relevant CRA values.*

The maximum RDS values for the responses were weighted with respect to likelihood that they indicate the presence of disorder. The presence of a T_g, a new recrystallisation or transition event and decreases in T_d values strongly suggests the presence of disorder, hence these responses have higher maximum RDS values (10). While, decreases in T_m and the presence of moisture (volatile) can indicate some disorder, it is not conclusive; hence these responses have lower maximum RDS values (5). Additionally, if disorder

was present and the material recrystallised to the same solid-sate form as the input, no change in T_m would be observed. By reducing the maximum RDS value for changes in T_m the RDS values are weighted (or skewed) more towards the responses more indicative of disorder.

Previous researchers Rani *et al.* (2006)[23] estimated the degree of crystallinity by DSC using the ratio of ΔH_f of sample and that of a 100% crystal sample. However this approach is not suitable for materials where ΔH_f cannot be calculated easily, *i.e.* melt-degradation materials or those that sublime, such as salbutamol sulphate or caffeine. Therefore, changes in ΔH_f were not included in the RDS calculations as some of the study materials melt-degrade, hence changes in this response were not able to be determined.

The RDS values were then converted to a technique disorder score (D_{DSC}) using equation [7-2], which represents the total degree of observed disorder in the DSC thermogram as a consequence of a defined comminution process.

$$\text{DSC disorder score } (D_{DSC}) = \left(\frac{R_{DSC}}{40}\right) \text{x } 10 \qquad [7\text{-}2]$$

where R_{DSC} is the sum of R_{DSC1} to R_{DSC5} out of 40, the maximum score.

D_{DSC} was therefore calculated as a value between 0 and 10; where, 0 represents no perceived observation of PID and 10, represents a marked degree of inferred disorder based on the changes in the DSC responses (Table 7-5).

Table 7-5 DSC Disorder classification using D_{DSC} values

D_{DSC} value	Likelihood that disorder is present. The larger the value the more significant the disorder present	Colour code
0.0 to 3.0	Low probability of disorder being present – low levels of disorder	
3.1 to 7.0	Medium probability of disorder being present – some disorder present	
7.1 to 10.0	High probability of disorder being present – marked levels of disorder present	

A worked example of the method used to calculate D_{DSC} is shown using the CRA values for high frequency ball-milled loperamide HCl (Table 7-6).

Table 7-6 Calculated R_{DSC} score for loperamide HCl (14-MA1) using determined CRA values

	CRA values for loperamide HCl				
	Observed volatile?	Observed glass transition event?	New crystallisation or transition event observed?	Average shift in melting temperature (ΔTm) °C	Average change in degradation temperature (ΔT_d)
	Yes	Yes	Yes	-3.5	0
RDS*	5	10	10	3	0
RDS ID	R_{DSC1}	R_{DSC2}	R_{DSC3}	R_{DSC4}	R_{DSC}

** RDS values determined using Table 7-4. RA and CRA values from Table 6-16 and 6-17 respectively. Refer to Figure 6-12 for an overlay of the DSC thermogram of 14-MA1 and the input*

A volatile (moisture) desolvation event was observed for loperamide HCl (Figure 6-12), hence R_{DSC1} was assigned a value of 5. This material also exhibited a glass transition and a recrystallisation event; therefore both R_{DSC1} and R_{DSC3} were assigned values of 10. T_m was reduced slightly hence the R_{DSC4} was allotted a value of 3 but there was no change in the degradation temperature as a consequence of ball-milling, *i.e.* R_{DSC5} was 0. Summing all the values for R_{DSC1} to R_{DSC5} gave a total D_{RDS} value of 28. Substituting this value into equation [7-2] gave a D_{DSC} score of 7.0 for high frequency ball-milled loperamide HCl.

7.2.4 Response disorder analysis for Gravimetric vapour sorption (GVS)

Using the GVS CRA values for the different comminuted materials (Table 6-20), the amount of observed change in the moisture sorption responses were assessed with respect to any perceived PID to provide a response disorder score (R_{GVS}). R_{GVS} values were determined using Table 7.7 and reflect the changes in the moisture sorption responses with respect to the presence of disorder. Only two responses were selected to investigate the presence of disorder, the observation of a recrystallisation event and changes in the maximum moisture adsorption during the first adsorption cycle (ΔM_{MAX1}).

Recrystallisation events are observed as a mass loss event as the %RH is maintained at an elevated level[312,313], and were assigned a R_{GVS} value of 10. Further evidence for the presence of disorder can be inferred to by the change in the maximum moisture adsorption during the first adsorption cycle (ΔM_{MAX1}). The magnitude of ΔM_{MAX1} provides a relative estimate to the magnitude of disorder and an estimate of moisture adsorption as a consequence of the comminution process.

Table 7-7 RDS score values (R_{GVS}) for key GVS responses based on CRA values

Step	CRA parameter	CRA value	Response disorder score R_{GVS}	RDS ID
1	Observed recrystallisation?	No	0	R_{GVS1}
		Yes	10	
2	Maximum % change in mass during adsorption cycle 1 (ΔM_{MAX1})	< 0.25 %	0	R_{GVS2}
		0.25 to 0.5 %	3	
		0.5 to 2.0 %	5	
		2.0 to 5.0 %	7	
		> 5.0 %	10	

Proceed stepwise from step1 to 2, summing the RDS *score (*$R_{GVS\,1}$ *to* R_{GVS2}*) for the comminuted material using the relevant CRA values.*

The RDS values (R_{GVS1} and R_{GVS2}) were then converted to a technique disorder score (D_{GVS}) using equation [7-3], which represents the total degree of observed disorder in the GVS moisture sorption profile as a consequence of a defined comminution process.

$$\text{GVS disorder score } (D_{GVS}) = \left(\frac{R_{GVS}}{20}\right) \text{x } 10 \qquad [7\text{-}3]$$

where R_{GVS} is the sum of R_{GVS1} and R_{GVS2} out of 20, the maximum score

D_{GVS} is therefore calculated as a value between 0 and 10; where, 0 represents no perceived observation of PID and 10, represents a marked degree of inferred disorder based on the changes in the GVS responses (Table 7-8).

Table 7-8 GVS Disorder classification using D_{GVS} values

D_{GVS} value	Likelihood that disorder is present. The larger the value the more significant the disorder present	Colour code
0.0 to 3.0	Low probability of disorder being present – low levels of disorder	
3.1 to 7.0	Medium probability of disorder being present – some disorder present	
7.1 to 10.0	High probability of disorder being present – marked levels of disorder present	

A worked example of the method used to calculate D_{GVS} is shown using the CRA values for low frequency ball-milled salbutamol sulphate (Table 7-9).

Table 7-9 Calculated R_{GVS} score for salbutamol sulphate using determined CRA values

	CRA values for salbutamol sulphate	
	Observed recrystallisation?	Maximum % change in mass during adsorption cycle 1 (ΔM_{MAX1})
	Yes	1.14
RDS*	10	5
RDS ID	R_{GVS1}	R_{GVS2}

** RDS values determined using Table 7-7. RA and CRA values from Table 6-20. Refer to Figure 6-29 for the kinetic and isotherm plots.*

A recrystallisation event was observed for low frequency ball-milled salbutamol sulphate (Figure 6-29), hence a R_{GVS1} value of 10 was assigned, whilst a change of 1.14% was observed for ΔM_{MAX1} and therefore a R_{GVS2} value of 5 was allocated. Summing the values for $R_{GVS\,1}$ and R_{GVS2} gave a total R_{GVS} value of 15. Substituting this value into equation [7-3] produced a D_{GVS} score of 7.5 for low frequency ball-milled salbutamol sulphate.

7.2.5 Process disorder analysis (PDA)

In the previous sections (7.2.2 to 7.2.4), the relative amount of change in individual responses for the techniques XRPD, DSC and GVS were converted to response disorder scores. These response RDS values were then combined and converted into disorder scores D_{XRPD}, D_{DSC} and D_{GVS} for the individual techniques. The magnitude of these technique disorder scores was thought to reflect the respective potential of each of these techniques to indicate the presence of disorder induced by any given process.

By combining the individual RDS scores for the three techniques, XRPD, DSC and GVS an overall response disorder score (P_{RDS}) can be determined for a given process (Equation [7-4]).

$$\text{Total process RDS } (P_{RDS}) = R_{XRPD} + R_{DSC} + R_{GVS} \qquad [7\text{-}4]$$

The individual technique contributions to P_{RDS} were weighted based on their potential to detect the presence of disorder. Both the XRPD and DSC contributions have a maximum value of 40, whilst the GVS contribution is only 20. The decreased weighting for the GVS P_{RDS} value reflects the number of individual responses involved in disorder scoring, *i.e.* only two responses are employed, the observation of recrystallisation and changes to ΔM_{MAX1} compared to 7 for XRPD and 5 for DSC.

P_{RDS} as calculated, produced a value between 0 and 100, the larger the value of P_{RDS}, the more significant or likely that disorder is present (Table 7-10).

Table 7-10 Disorder classification using P_{RDS} values

P_{RDS} value	Likelihood that disorder is present. The larger the value the more significant the disorder present	Colour code
0 to 30	Low probability of disorder being present – low levels of disorder	
31 to 70	Medium probability of disorder being present – some disorder present	
71 to 100	High probability of disorder being present – marked levels of disorder present	

By dividing the P_{RDS} value by 10, a value which represents the disorder for a given process can be calculated (D_{Pro}) (Equation [7-5]).

$$\text{Process disorder score } (D_{Pro1}) = \frac{R_{XRPD} + R_{DSC} + R_{GVS}}{10} \quad [7\text{-}5]$$

The larger the value of D_{Pro1}, the more significant or likely that disorder is present (Table 7-11).

Table 7-11 Disorder classification using D_{Pro} values

D_{Pro} value	Likelihood that disorder is present. The larger the value the more significant the disorder present	Colour code
0.0 to 3.0	Low probability of disorder being present – low levels of disorder	
3.1 to 7.0	Medium probability of disorder being present – some disorder present	
7.1 to 10.0	High probability of disorder being present – marked levels of disorder present	

Alternatively D_{Pro} can be determined by taking the average of the individual technique disorder scores D_{XRPD}, D_{DSC} and D_{GVS} (Equation [7-6]). In this approach each technique disorder score has equal weighting.

$$\text{Process disorder score } (D_{Pro2}) = \frac{D_{XRPD} + D_{DSC} + D_{GVS}}{3} \quad [7\text{-}6]$$

The larger the value of D_{Pro2}, the more significant or likely that disorder is present (Table 7-11).

By comparing the two approaches to calculate D_{Pro} the effect of technique contribution (weighting or no weighting) to the overall disorder score could be investigated.

7.3 Results & discussion

7.3.1 Response disorder analysis for X-ray powder diffraction (XRPD)

The total degree of observed disorder in the XRPD diffractogram as a consequence of a given comminution process can be described and semi-quantified using the technique disorder score, D_{XRPD}. This value reflects the changes in the XRPD responses over the whole diffractogram with respect to any perceived PID that these changes may infer (Table 7-12 and Figure 7-2). The higher the score the more likely that disorder is present.

The previously described novel XRPD phase classification (Table 6-3) successfully categorised the solid-state phases produced in comminuted materials but was limited when it came to discriminate differences in the amount of disorder present within a defined solid-state phase class. For example, a number of comminuted materials were identified as being crystalline (Table 6-14) but further separation of these materials could not be achieved. However, by modifying the tolerance ranges for changes in the XRPD responses with respect to PID, differences between the crystalline materials could now be discerned (Table 7-12). Furthermore, based on the D_{XRPD} values, some materials which were initially classified as crystalline could now be reclassified as containing some degree of disorder based on their XRPD responses, *e.g.* micronised sulfamerazine and loperamide HCl, high frequency ball-milled caffeine, sulfadiazine and sulfamerazine, low frequency ball-milled sulfadiazine and caffeine and all of the comminuted materials for acetylsalicylic acid (Table 7-12).

The data obtained using other comminuted materials, such as ball-milled γ-indomethacin, loperamide HCl and salbutamol sulphate when processed resulted in high D_{XRPD} values (> 7.0) and these powders were classified as containing high levels of disorder. Replicate comminution process results obtained for salbutamol sulphate, indomethacin and acetaminophen also produced D_{XRPD} values, confirming the reproducibility of both the comminution processes and the novel disorder scoring methods.

Table 7-12 R_{XRPD} and D_{XRPD} values for the comminuted materials

Material	Batch ID	Individual RDS values*							R_{XRPD} ǂ	D_{XRPD} ϕ	XRPD phase classification from Chapter 6 Δ
		R_{XRPD1}	R_{XRPD2}	R_{XRPD3}	R_{XRPD4}	R_{XRPD5}	R_{XRPD6}	R_{XRPD7}			
Acetaminophen	1-MA1	0	0	0	3	0	0	5	8	2.0	Crystalline
	1-MA2	0	0	0	3	0	0	5	8	2.0	Crystalline
	1-MB1	0	0	0	3	0	2	7	12	3.0	Crystalline
	1-MB2	0	0	0	3	0	2	7	12	3.0	Crystalline
	1-X1	0	0	0	3	0	0	0	3	0.8	Crystalline
γ-Indomethacin	11-MA1	5	0	3	3	9	7	7	34	8.5	Disordered
	11-MA2	5	0	0	3	9	5	9	31	7.8	Disordered
	11-MB1	5	0	0	3	5	2	7	22	5.5	Microcrystalline
	11-MB2	5	0	0	3	7	2	7	24	6.0	Microcrystalline
	11-X1	5	0	0	3	5	0	0	13	3.3	Crystalline
Salbutamol sulphate	24-MA1	7	0	3	3	9	9	9	40	10.0	X-ray Amorphous
	24-MA2	7	0	3	3	9	9	9	40	10.0	X-ray Amorphous
	24-MA3	7	0	3	3	9	9	9	40	10.0	X-ray Amorphous
	24-MB1	5	0	0	3	9	2	7	26	6.5	Microcrystalline
	24-MB2	5	0	0	3	9	2	7	26	6.5	Microcrystalline
	24-X1	0	0	0	3	9	0	0	12	3.0	Crystalline
Loperamide HCl	14-MA1	7	0	3	3	9	9	9	40	10.0	X-ray Amorphous
	14-MB1	5	0	3	3	9	7	9	36	9.0	Disordered
	14-X1	5	0	0	0	9	0	9	23	5.8	Crystalline
Acetylsalicylic acid	33-MA1	0	0	3	0	9	0	7	19	4.8	Crystalline
	33-MB1	0	0	3	0	9	0	7	19	4.8	Crystalline
	33-X1	0	0	3	0	9	0	5	17	4.3	Crystalline
Sulfamerazine	54-MA1	5	2	3	3	0	2	7	22	5.5	Crystalline mixture of forms
	54-MB1	5	0	0	3	7	9	9	33	8.3	Microcrystalline
	54-X1	5	0	0	3	9	0	9	26	6.5	Crystalline
Phenacetin	69-MA1	0	0	0	3	0	2	5	10	2.5	Crystalline
	69-MB1	0	0	0	0	0	0	2	2	0.5	Crystalline
	69-X1	0	0	0	3	0	0	7	10	2.5	Crystalline
Sulfadiazine	87-MA1	5	0	0	3	0	0	9	17	4.3	Crystalline
	87-MB1	5	0	0	3	0	2	7	17	4.3	Crystalline
	87-X1	5	0	0	3	0	0	0	8	2.0	Crystalline
Caffeine	88-MA1	5	0	0	3	9	0	7	24	6.0	Crystalline
	88-MB1	5	0	0	0	7	0	5	17	4.3	Crystalline
	88-X1	5	0	0	0	9	0	0	14	3.5	Crystalline
Methyl paraben	140-MA1	0	0	0	0	0	0	0	0	0.0	Crystalline
	140-MB1	0	0	0	0	2	0	0	2	0.5	Crystalline
	140-X1	0	0	0	0	9	0	0	9	2.3	Crystalline

** Determined using Table 7-1, R_{XRPD} ǂ: combined total RDS value for XRPD responses, D_{XRPD} ϕ : XRPD disorder score calculated using equation [7-1]. Δ: XRPD classification reported in Table 6-14. Colours for D_{XRPD} values are defined in Table 7-2*
#-MA#: high frequency ball-mill method A, #-MB#: low frequency ball-mill method B. #-X#: jet micronisation method A.

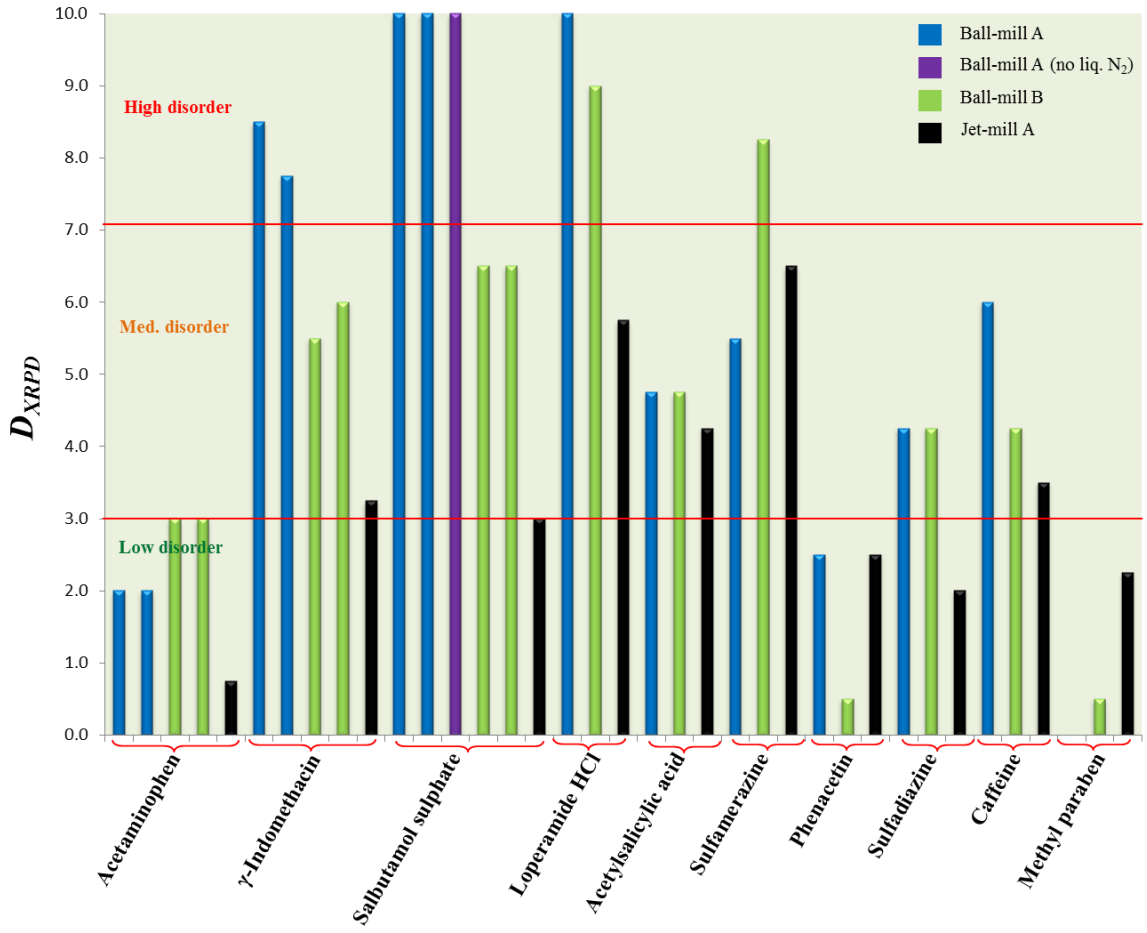

Figure 7-2 Summary plot of D_{XRPD} values for the comminuted materials

Of the three comminution processes, high frequency ball-milling (ball-mill A) appeared to result in higher levels of disorder for a given material (Table 7-12 and Figure 7-2). This observation is more apparent in those materials that appear to be more susceptible to PID such as milled γ-indomethacin, loperamide HCl, salbutamol sulphate and caffeine. In the case of sulfamerazine, low frequency ball-milling (ball-mill B) appeared to cause higher levels of PID than high frequency ball-milling (Table 7-12 and Figure 7-2). This can be misleading in some respects, as the level of disorder is not only dependent on the amount of disorder generated as a consequence of the comminution process but also on when the sample is analysed. For high frequency ball-milled sulfamerazine, disorder is generated within the material, but as the comminution progresses this disordered phase is transformed into a new solid-state form. When a sample of the comminuted material was analysed by XRPD only a moderate degree of disorder was apparent but peaks attributable to a new solid-state form were observed. However, low frequency ball-milled sulfamerazine (ball-mill B) appeared to have higher levels of disorder present (Table 7-12 and Figure 7-2). This is due to shorter milling time, therefore when a sample of this material was analysed by XRPD the

comminution process had been halted before the material had transformed into a new solid-state form, hence a relatively higher degree of disorder was observed.

For materials which had previously been classified as microcrystalline using the approach outlined in Section 6.3.1.3, the D_{XRPD} values by themselves were not sufficient to allow appropriate classification of microcrystalline material (Table 7-12). The materials appeared to have moderate levels of disorder (D_{XRPD} values between 4 and 7). Microcrystalline material must be defined using a multi-technique approach and classification rules such as those defined in Table 6-4 and Figure 6-2.

7.3.2 Response disorder analysis for differential scanning calorimetry (DSC)

DSC analysis of a sample containing both crystalline and disordered phases can be directly identified if the acquisition parameters are chosen correctly. However, interpretation of DSC thermograms can be somewhat complex due to the potential number of thermal events that can occur simultaneously or sequentially due to the semi-independent nature of each transformation. This means that interpretation of the thermogram to calculate and score the degree of perceived induced disorder may require a matrix analysis approach to provide a holistic view of what is occurring rather than depending on the analysis and interpretation of individual thermal responses. To this end, the total degree of observed disorder in the DSC thermogram as a consequence of a given comminution process can be described and quantified using the technique disorder score, D_{DSC}. This value reflects the combined observed changes in a number of thermal responses between the comminuted material and those of the input material with respect to any perceived PID (Table 7-13 and Figure 7-3). The higher the score the more likely that disorder is present.

In Chapter 6, the solid-state phases of the comminuted materials were successfully identified using the novel classification process based on changes in their respective DSC responses (Table 6-17). However, as in the case of the XRPD analysis, this approach was limited when it came to discriminate differences in the amount of disorder present within a defined solid-state phase class. By modifying the ranges applied to assess changes in a defined response specific to the inference of PID, the comminuted materials could be further discriminated and compared.

Table 7-13 **R_{DSC} *and* D_{DSC} *values for the comminuted materials***

Material	Batch ID	Individual RDS values*					R_{DSC} ǂ	D_{DSC} ϕ	DSC phase classification from Chapter 6 Δ
		R_{DSC1}	R_{DSC2}	R_{DSC3}	R_{DSC4}	R_{DSC5}			
Acetaminophen	1-MA1	0	0	0	0	0	0	0.0	Crystalline
	1-MA2	0	0	0	0	0	0	0.0	Crystalline
	1-MB1	0	0	0	0	0	0	0.0	Crystalline
	1-MB2	0	0	0	0	0	0	0.0	Crystalline
	1-X1	0	0	0	0	0	0	0.0	Crystalline
γ-Indomethacin	11-MA1	0	10 (G_D 0.345)	10 (X_D 22.3)	0	0	20	5.0 (G_D 0.345 X_D 22.3)	Disordered
	11-MA2	0	10 (G_D 0.285)	10 (X_D 18.2)	0	0	20	5.0 (G_D 0.28) X_D 18.2)	Disordered
	11-MB1	0	0	10 (X_D 5.4)	0	0	10	2.5 (X_D 5.4)	Mixed Phase A - crystalline some disorder
	11-MB2	0	0	X_D 1.6)	0	0	10	2.5 (X_D 1.6)	Mixed Phase A - crystalline some disorder
	11-X1	0	0	0	0	0	0	0.0	Crystalline
Salbutamol sulphate	24-MA1	5	10	10	5	10	40	10.0	DSC amorphous
	24-MA2	5	10	10	5	10	40	10.0	DSC amorphous
	24-MA3	5	10	10	5	10	40	10.0	DSC amorphous
	24-MB1	5	0	10	5	5	25	6.3	Mixed Phase A - crystalline some disorder x
	24-MB2	5	0	10	5	5	25	6.3	Mixed Phase A - crystalline some disorder x
	24-X1	5	0	10	3	2	20	5.0	Mixed Phase A - crystalline some disorder x
Loperamide HCl	14-MA1	5	10 (G_D 0.265)	10 (X_D 60.7)	3	0	28	7.0 (G_D 0.265 X_D 60.7)	Disordered
	14-MB1	5	0	10 (X_D 11.1)	3	0	18	4.5 (X_D 11.1)	Mixed Phase A - crystalline some disorder x
	14-X1	5	0	10 (X_D 8.0)	0	0	15	3.8 (X_D 8.0)	Mixed Phase A - crystalline some disorder x
Acetylsalicylic acid	33-MA1	0	0	0	0	0	0	0.0	Crystalline
	33-MB1	0	0	0	0	0	0	0.0	Crystalline
	33-X1	0	0	0	0	0	0	0.0	Crystalline
Sulfamerazine	54-MA1	0	0	10 (T 9.6)	0	0	10	2.5 (T 9.6)	Mixture of crystalline forms- some disorder x
	54-MB1	0	0	0	0	0	0	0.0	Crystalline
	54-X1	0	0	0	0	0	0	0.0	Crystalline
Phenacetin	69-MA1	0	0	0	0	0	0	0.0	Crystalline
	69-MB1	0	0	0	0	0	0	0.0	Crystalline
	69-X1	0	0	0	0	0	0	0.0	Crystalline
Sulfadiazine	87-MA1	0	0	0	3	5	8	2.0	Mixed Phase A - crystalline some disorder x
	87-MB1	0	0	0	3	5	8	2.0	Mixed Phase A - crystalline some disorder x
	87-X1	0	0	0	0	5	5	1.3	Mixed Phase A - crystalline some disorder x
Caffeine	88-MA1	5	0	0	0	0	5	1.3	Mixed Phase A - crystalline some disorder
	88-MB1	0	0	0	0	0	0	0.0	Mixed Phase A - crystalline some disorder
	88-X1	0	0	0	0	0	0	0.0	Mixed Phase A - crystalline some disorder
Methyl paraben	140-MA1	0	0	0	0	0	0	0.0	Crystalline
	140-MB1	0	0	0	0	0	0	0.0	Crystalline
	140-X1	0	0	0	0	0	0	0.0	Crystalline

** Determined using Table 7-4, [x]solid-state confirmed by XRPD.* R_{DSC} ǂ*: combined total RDS value for DSC responses,* D_{DSC} ϕ *: DSC disorder score calculated using equation [7-2].* Δ**:** *DSC classification reported in Table 6-17. (*G_D *#): size of* T_g *in J/(g°C), (*X_D *#):size of* ΔH_c *in J/g, (T #): size of transition* ΔH_t *in J/g.#-MA#: high frequency ball-mill method A, #-MB#: low frequency ball-mill method B. #-X#: jet micronisation method A.*

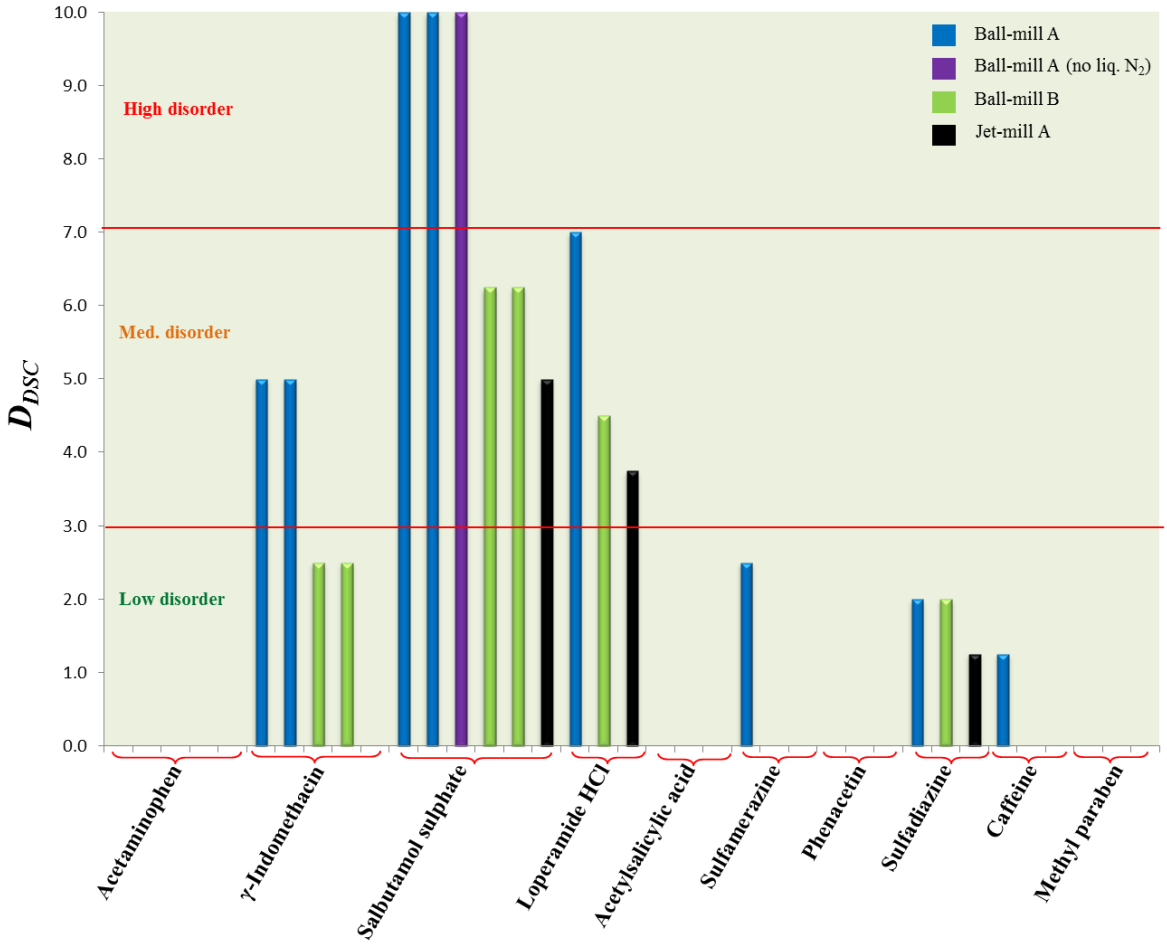

Figure 7-3 Summary plot of D_{DSC} values for the comminuted materials

For a number of comminuted materials: acetaminophen, acetylsalicylic acid, phenacetin, methyl paraben, low frequency ball and jet-milled sulfamerazine and caffeine and jet-milled γ-indomethacin there were no changes in their DSC responses which could infer the presence of disorder, hence these materials were assigned D_{DSC} values of 0 (Table 7-13 and Figure 7-3).

For other comminuted materials, such as sulfadiazine changes in T_m and T_d suggests a low presence of disorder and this resulted in a D_{DSC} value of less than 2 being obtained (Table 7-13 and Figure 7-3). The observation of a new desolvation event in some cases can also imply the presence of disorder. When this new desolvation event occurs below 100 °C this is most likely to be due to the removal of adsorbed moisture, as a consequence of surface disorder. For example, high frequency ball-milled caffeine exhibits a desolvation event representing the removal of adsorbed moisture that was not observed in the input material (Table 6-16). However, no other events such as T_g or recrystallisation were observed that may suggest disorder, hence this material was only assigned a D_{DSC} value of only1.3 (Table 7-13 and Figure 7-3).

It is important to note that the D_{DSC} value is a normalised estimate of the likelihood of disorder being present and should not be considered an absolute value of the amount of disorder present. For example, the observance of a glass transition or recrystallisation event can provide evidence for the presence of disorder but the presence of these phenomena alone cannot fully quantify the amount of disorder present. This is because the size of the T_g or ΔH_c have not been included in the disorder analysis as they are generally new events, and as such are absent in the input. However, the size of these responses should be reported where they are available along with the D_{DSC} value to assist in discriminating differences between different comminution processes and to investigate batch to batch variation for the same employed comminution process. For example the comminution of loperamide HCl by the three processes resulted in material with differing D_{DSC} values (Table 7-13 and Figure 7-3). All three comminuted materials produced DSC thermograms exhibiting a new recrystallisation event and hence they were given R_{DSC3} values of 10. However, the actual values for ΔH_c showed that the material subjected to high frequency ball-milling (ball-mill A) had the largest recrystallisation event and was also the only material exhibiting a glass transition event. Accordingly, the material processed in this way is most likely to contain more disorder than the low frequency ball-milled and jet-milled material. As the D_{DSC} values also follows this trend in the enthalpies, this demonstrates that the novel RDA process (Section 7.2.3) is effective in discriminating different levels of disorder.

This trend in the effect of the comminution processes to induce disorder can also be seen in the comminuted samples of salbutamol sulphate and γ-indomethacin (Table 7-13 and Figure 7-3). In the case of salbutamol sulphate, high frequency ball-milling resulted in D_{XRPD} values of 10 and this material was classified as containing high levels of disorder. The magnitude of either T_g or ΔH_c for the comminuted materials of salbutamol sulphate were not reported as these events could not be resolved sufficiently. The ball-milled γ-indomethacin exhibited different levels of disorder as shown by the relative changes in their DSC responses. New recrystallisation events were observed in both high and low frequency ball-milled materials but the ΔH_c values for these events differed between the processes, ΔH_c ~20J/g and ~ 4 J/g for high and low frequency ball-milling respectively (Table 7-13). High frequency ball-milled samples also exhibited a T_g which was absent in the low frequency ball-milled materials. When a RDA was applied to these materials, D_{DSC} values were obtained that reflected the relative levels of disorder present and confirmed the validity of the RDA approach in discriminating

differences between processes and relative levels of disorder, *i.e.* D_{DSC} values of 5.0 and 2.5 for high and low frequency ball-milled materials respectively.

For some materials disorder can be inferred as a consequence of the appearance of a solid-state form. For these materials the comminution process mechanically activates the material disrupting the molecular structure in which disorder can occur, as comminution progresses molecular then re-ordering can result in the generation of a new solid-state form. Therefore, depending upon when comminution is halted different solid-state forms or phases may be observed. For example a solid-state transition of Form II to Form I was observed for high frequency ball-milled sulfamerazine which was not observed in the input material or in the low frequency or jet-milled sample. It is most likely that this solid-state transition is a result of induced disorder being generated during comminution[350,360-362]. Consequently, high frequency ball-milled sulfamerazine was assigned a R_{DSC3} score of 10.

D_{DSC} values for replicate samples subject to comminution for salbutamol sulphate, indomethacin and acetaminophen were also consistent. This confirmed the reproducibility of both the comminution processes and the novel disorder scoring methods (Table 7-13 and Figure 7-3).

It can be seen from the results presented in Table 7-13 that the novel response disorder approach defined here is effective in defining both the presence of disorder based on changes in the DSC responses and also in discriminating between the different levels of disorder present for materials comminuted by different processes.

7.3.3 Response disorder analysis for Gravimetric vapour sorption (GVS)

The total degree of observed disorder in the moisture sorption profile as a consequence of a given comminution process can be described and semi-quantified using the technique disorder score, D_{GVS}. This value reflects the relative observed thermal response changes between the comminuted material and those of the input material with respect to any perceived PID changes (Table 7-14 and Figure 7-4). The higher the score the more likely that disorder is present.

Although GVS RDA utilises changes in only two responses to detect and semi-quantify the presence of disorder, the resulting D_{GVS} values were sufficient to discriminate differences between the materials and comminution processes (Table 7-14 and Figure 7-4). These D_{GVS} values were generally consistent with the GVS phase classification as determined previously (Table 6-20). However, like DSC, the observance of a new recrystallisation event in the moisture sorption profile cannot quantify the level of disorder and hence, the M_{xtal} (%) value should also be reported. M_{xtal} (%) is the value for % mass loss observed during recrystallisation.

No disorder was induced by milling, as based upon the relative changes to the GVS responses that were observed for the comminuted materials of acetaminophen, acetylsalicylic acid, phenacetin and methyl paraben (Table 7-14 and Figure 7-4). Additionally, samples of jet-milled γ-indomethacin, sulfamerazine, sulfadiazine and caffeine did not exhibit any disorder when only the changes to their respective GVS responses are considered (Table 7-14 and Figure 7-4). However, low amounts of moisture sorption (ΔM_{MAX1}) were observed when the ball-milled samples of γ-indomethacin, sulfamerazine, sulfadiazine and low frequency ball-milled caffeine were analysed. This implied that there may have been a small amount of disorder generated as a consequence of the comminution processes and these materials were assigned R_{GVS} values of 3 to 5. There was also observed a marked increase in moisture sorption when caffeine was subjected to high frequency ball-milling (Table 6.20) with the value of ΔM_{MAX1} being 7.17 % , which may suggest the presence of disorder.

Table 7-14 **R_{GVS} *and* D_{GVS} *values for the comminuted materials***

Material	Batch ID	Individual RDS values*		R_{GVS} ǂ	D_{GVS} ϕ	GVS phase classification from Chapter 6 Δ
		R_{GVS1}	R_{GVS2}			
Acetaminophen	1-MA1	0	0	0	0.0	Crystalline reversible moisture sorption
	1-MA2	0	0	0	0.0	Crystalline reversible moisture sorption
	1-MB1	0	0	0	0.0	Crystalline reversible moisture sorption
	1-MB2	0	0	0	0.0	Crystalline reversible moisture sorption
	1-X1	0	0	0	0.0	Crystalline reversible moisture sorption
γ-Indomethacin	11-MA1	0	5	5	2.5	Disordered/increased surface area
	11-MA2	0	5	5	2.5	Disordered/increased surface area
	11-MB1	0	3	3	1.5	Crystalline reversible moisture sorption
	11-MB2	0	3	3	1.5	Crystalline reversible moisture sorption
	11-X1	0	0	0	0.0	Crystalline reversible moisture sorption
Salbutamol sulphate	24-MA1	10 (X_G 9.76)	10	20	10.0 (X_G 9.76)	Disordered
	24-MA2	10 (X_G 9.62)	10	20	10.0 (X_G 9.62)	Disordered
	24-MA3	10 (X_G 9.74)	10	20	10.0 (X_G 9.74)	Disordered
	24-MB1	10 (X_G 1.33)	5	15	7.5 (X_G 1.33)	Disordered
	24-MB2	10 (X_G 1.25)	5	15	7.5 (X_G 1.25)	Disordered
	24-X1	10 (X_G 0.68)	5	15	7.5 (X_G 0.68)	Disordered or electrostatic
Loperamide HCl	14-MA1	0	10 (A_G 9.10)	10	5.0 (A_G 9.10)	Disordered/increased surface area
	14-MB1	10 (X_G 3.46)	7 (A_G 2.88)	17	8.5 (X_G 3.46) (A_G 2.88)	Disordered
	14-X1	10 (X_G 1.08)	5 (A_G 0.72)	15	7.5 (X_G 1.08) (A_G 0.72)	Disordered
Acetylsalicylic acid	33-MA1	0	0	0	0.0	Crystalline reversible moisture sorption
	33-MB1	0	0	0	0.0	Crystalline reversible moisture sorption
	33-X1	0	0	0	0.0	Crystalline reversible moisture sorption
Sulfamerazine	54-MA1	0	3	3	1.5	Disordered/increased surface area
	54-MB1	0	3	3	1.5	Crystalline reversible moisture sorption
	54-X1	0	0	0	0.0	Crystalline reversible moisture sorption
Phenacetin	69-MA1	0	0	0	0.0	Crystalline reversible moisture sorption
	69-MB1	0	0	0	0.0	Crystalline reversible moisture sorption
	69-X1	0	0	0	0.0	Crystalline reversible moisture sorption
Sulfadiazine	87-MA1	0	5	5	2.5	Disordered/increased surface area
	87-MB1	0	5	5	2.5	Disordered/increased surface area
	87-X1	0	0	0	0.0	Crystalline reversible moisture sorption
Caffeine	88-MA1	0	10 (A_G 7.17)	10	5.0 (A_G 7.17)	Disordered/increased surface area
	88-MB1	0	5	5	2.5	Disordered/increased surface area
	88-X1	0	0	0	0.0	Crystalline reversible moisture sorption
Methyl paraben	140-MA1	0	0	0	0.0	Crystalline reversible moisture sorption
	140-MB1	0	0	0	0.0	Crystalline reversible moisture sorption
	140-X1	0	0	0	0.0	Crystalline reversible moisture sorption

** Determined using Table 7-7 X solid-state confirmed by XRPD.* R_{GVS} ǂ*: combined total RDS value for GVS responses,* D_{GVS} ϕ *: GVS disorder score calculated using equation [7-3].* Δ*: GVS classification reported in Table 6-20. (*X_G *#): size of* M_{xtal} *in %, (*A_G *#): size of* $\Delta M_{MAX1.}$ *#-MA#: high frequency ball-mill method A, #-MB#: low frequency ball-mill method B. #-X#: jet micronisation method A.*

For salbutamol sulphate, all the comminuted samples exhibited high values for D_{GVS} due to the observation of a recrystallisation event and a large moisture adsorption during the first adsorption cycle. However, differences in the M_{xtal} values for the comminution processes do suggest that there may have been differences in the respective level of disorder present. High frequency ball-milling resulted in the largest M_{xtal} values followed by low frequency ball-milling and micronisation (Table 7-14).

Comminution of loperamide HCl by high frequency ball-milling produced lower D_{GVS} values than anticipated as no recrystallisation event was observed compared to that induced by other processes. Instead the material absorbed 9% (w/w) moisture reversibly during the first and second adsorption cycles, which can be indicative of the production of bulk disorder[255]. In the case of disorder generated by high frequency ball-milling, it has been demonstrated that moisture sorption by itself is not sufficient to facilitate a solid-state transformation of the bulk disordered material but rather the addition of heat is required for recrystallisation to occur. This was shown in the DSC thermogram for the high frequency ball-milled material (Figure 6-12).

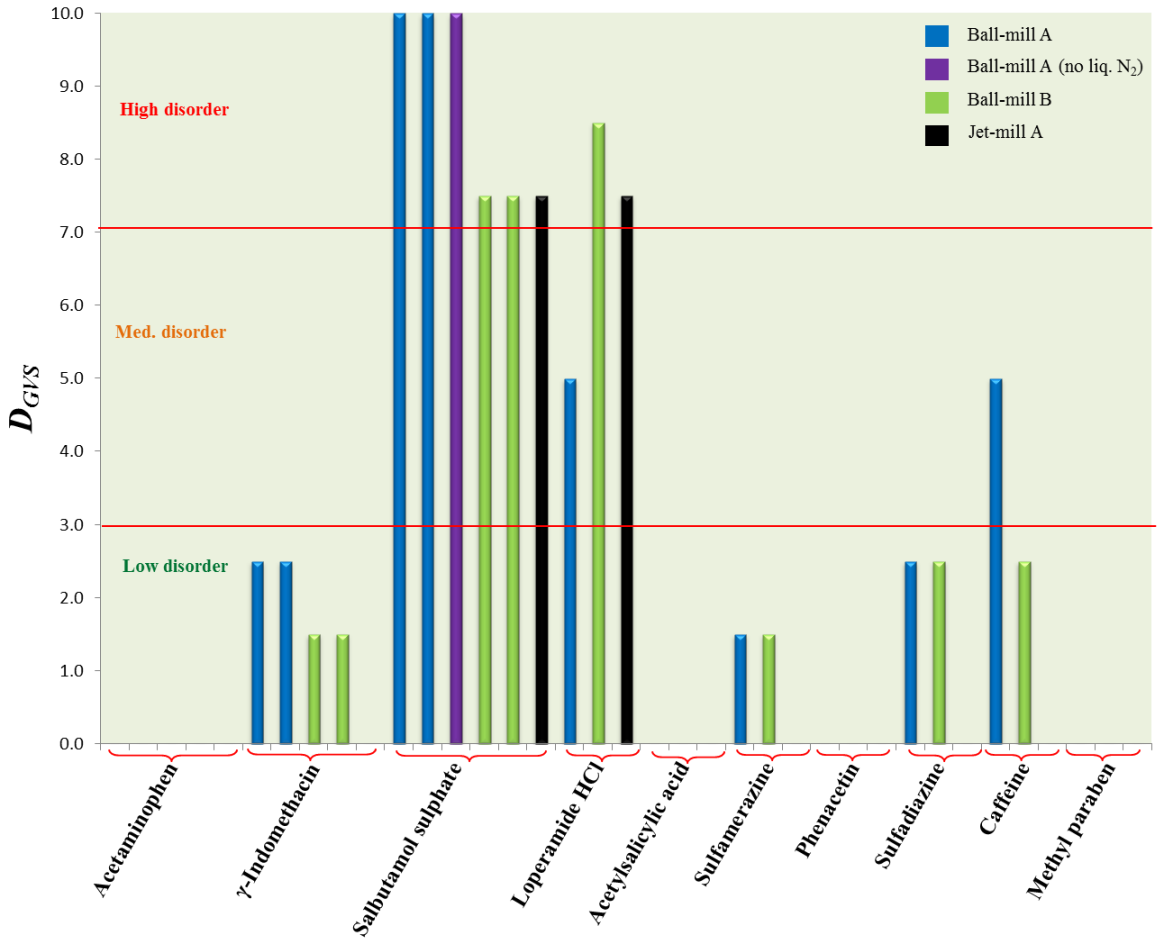

Figure 7-4 Summary plot of D_{GVS} values for the comminuted materials

D_{GVS} values that were obtained for replicate samples of comminuted salbutamol sulphate, indomethacin and acetaminophen were also consistent, confirming the reproducibility of both the comminution processes and the novel disorder scoring methods (Table 7-14 and Figure 7-4).

7.3.4 General discussion

To be able to fully discriminate between inter-, intra-material and processing differences in the degree of PID, a semi-quantitative approach was investigated. In this approach the amount of disorder in comminuted materials could be semi-quantified as a result of redefining the original CRA threshold levels from Chapter 6 for the individual technique responses specific to the presence of disorder. This enabled RDS values for the individual technique responses to be generated. These individual technique-specific RDS values were then combined to give P_{RDS} scores which were then converted into a disorder score for the individual technique, *i.e.* D_{XRPD}, D_{DSC} and D_{GVS}. The technique disorder scores were then combined to give a single normalised value, D_{Pro}, the magnitude of which represents the relative disorder present in the material as a result of a given pharmaceutical unit process. By using the relative combined changes between the individual technique responses of the comminuted material and those of the respective input the overall degree of PID can be defined multivariately instead of univariately and without the need for producing standard mixtures and calibration curves.

7.3.4.1 P_{RDS} *and* $D_{Technique}$ *scores*

In this study only RDS values for XRPD, DSC and GVS were used as these three techniques represent the 'primary' disorder detection methods in the core test set (Chapter 3). However, it is recommended that the full core test set is applied when characterising materials following comminution to provide a complete overview of the solid-state properties of the resulting material, such as monitoring changes in particle size, morphology and chemical purity.

The individual technique RDA and disorder values for the comminuted materials are summarised in Table 7-15 and Figure 7-5 along with the overall process RDA (P_{RDS}).

Table 7-15 Summary of technique response and process disorder scores for the comminuted materials

Material	Mill batch ID	RDA						PDA	Overview CRA solid-state phase classification*	Lit PID**
		R_{XRPD} (40)	R_{DSC} (40)	R_{GVS} (20)	D_{XRPD}	D_{DSC}	D_{GVS}	P_{RDS}		
Acetaminophen	1-MA1	8	0	0	2.0	0.0	0.0	8	Crystalline	No
	1-MA2	8	0	0	2.0	0.0	0.0	8	Crystalline	
	1-MB1	12	0	0	3.0	0.0	0.0	12	Crystalline	
	1-MB2	12	0	0	3.0	0.0	0.0	12	Crystalline	
	1-X1	3	0	0	0.8	0.0	0.0	3	Crystalline	
Methyl paraben	140-MA1	0	0	0	0.0	0.0	0.0	0	Crystalline	No
	140-MB1	2	0	0	0.5	0.0	0.0	2	Crystalline	
	140-X1	9	0	0	2.3	0.0	0.0	9	Crystalline	
Phenacetin	69-MA1	10	0	0	2.5	0.0	0.0	10	Crystalline	No
	69-MB1	2	0	0	0.5	0.0	0.0	2	Crystalline	
	69-X1	10	0	0	2.5	0.0	0.0	10	Crystalline	
Acetylsalicylic acid	33-MA1	19	0	0	4.8	0.0	0.0	19	Crystalline	No
	33-MB1	19	0	0	4.8	0.0	0.0	19	Crystalline	
	33-X1	17	0	0	4.3	0.0	0.0	17	Crystalline	
Sulfadiazine	87-MA1	17	8	5	4.3	2.0	2.5	30	Crystalline – little disorder	Some
	87-MB1	17	8	5	4.3	2.0	2.5	30	Crystalline – little disorder	
	87-X1	8	5	0	2.0	1.3	0.0	13	Crystalline – little disorder	
Sulfamerazine	54-MA1	22	10	3	5.5	2.5	1.5	35	Some disorder - some new form	Some
	54-MB1	33	0	3	8.3	0.0	1.5	36	Microcrystalline - little disorder	
	54-X1	26	0	0	6.5	0.0	0.0	26	Crystalline	
Caffeine	88-MA1	24	5	10	6.0	1.3	5.0 (A_G 7.17)	39	Crystalline – little disorder	Some
	88-MB1	17	0	5	4.3	0.0	2.5	22	Crystalline – little disorder	
	88-X1	14	0	0	3.5	0.0	0.0	14	Crystalline – little disorder	
γ-Indomethacin	11-MA1	34	20	5	8.5	5.0 (G_D 0.345 X_D 22.3)	2.5	59	Disordered	Yes
	11-MA2	31	20	5	7.8	5.0 (G_D 0.285 X_D 18.2)	2.5	56	Disordered	
	11-MB1	22	10	3	5.5	2.5 (X_D 5.4)	1.5	35	Microcrystalline - little disorder	
	11-MB2	24	10	3	6.0	2.5 (X_D 1.6)	1.5	37	Microcrystalline - little disorder	
	11-X1	13	0	0	3.3	0.0	0.0	13	Crystalline	
Loperamide HCl	14-MA1	40	28	10	10.0	7.0 (G_D 0.265 X_D 60.7)	5.0 (A_G 9.10)	78	Disordered	Yes
	14-MB1	36	18	17	9.0	4.5 (X_D 11.1)	8.5 (X_G 3.46 A_G 2.88)	71	Some disorder	
	14-X1	23	15	15	5.8	3.8 (X_D 8.0)	7.5 (X_G 1.08 A_G 0.72)	53	Crystalline – little disorder	
Salbutamol sulphate	24-MA1	40	40	20	10.0	10.0	10.0 (X_G 9.76)	100	Disordered	Yes
	24-MA2	40	40	20	10.0	10.0	10.0 (X_G 9.62)	100	Disordered	
	24-MA3	40	40	20	10.0	10.0	10.0 (X_G 9.74)	100	Disordered	
	24-MB1	26	25	15	6.5	6.3	7.5 (X_G 1.33)	66	Microcrystalline - some disorder	
	24-MB2	26	25	15	6.5	6.3	7.5 (X_G 1.25)	66	Microcrystalline - some disorder	
	24-X1	12	20	15	3.0	5.0	7.5 (X_G 0.68)	47	Crystalline - little disorder	

R_{XRPD}, R_{DSC} and R_{GVS}: combined total RDS value for XRPD, DSC and GVS responses respectively. D_{XRPD}, D_{DSC} and D_{GVS}: XRPD, DSC and GVS disorder scores calculated using equations [7-1], [7-2] and [7-3] respectively. P_{RDS}*: Process response disorder score..* G_D *#): size of* T_g *in J/(g°C),* (X_D *#):size of* ΔH_c *in J/g (T #): size of transition* ΔH_t *in J/g* (X_G *#): size of* M_{xtal} *in %,* (A_G *#): size of* $\Delta M_{MAX1.}$ ** from Table 6-25, ** from table 2-8. .#-MA#: high frequency ball-mill method A, #-MB#: low frequency ball-mill method B. #-X#: jet micronisation method A.*

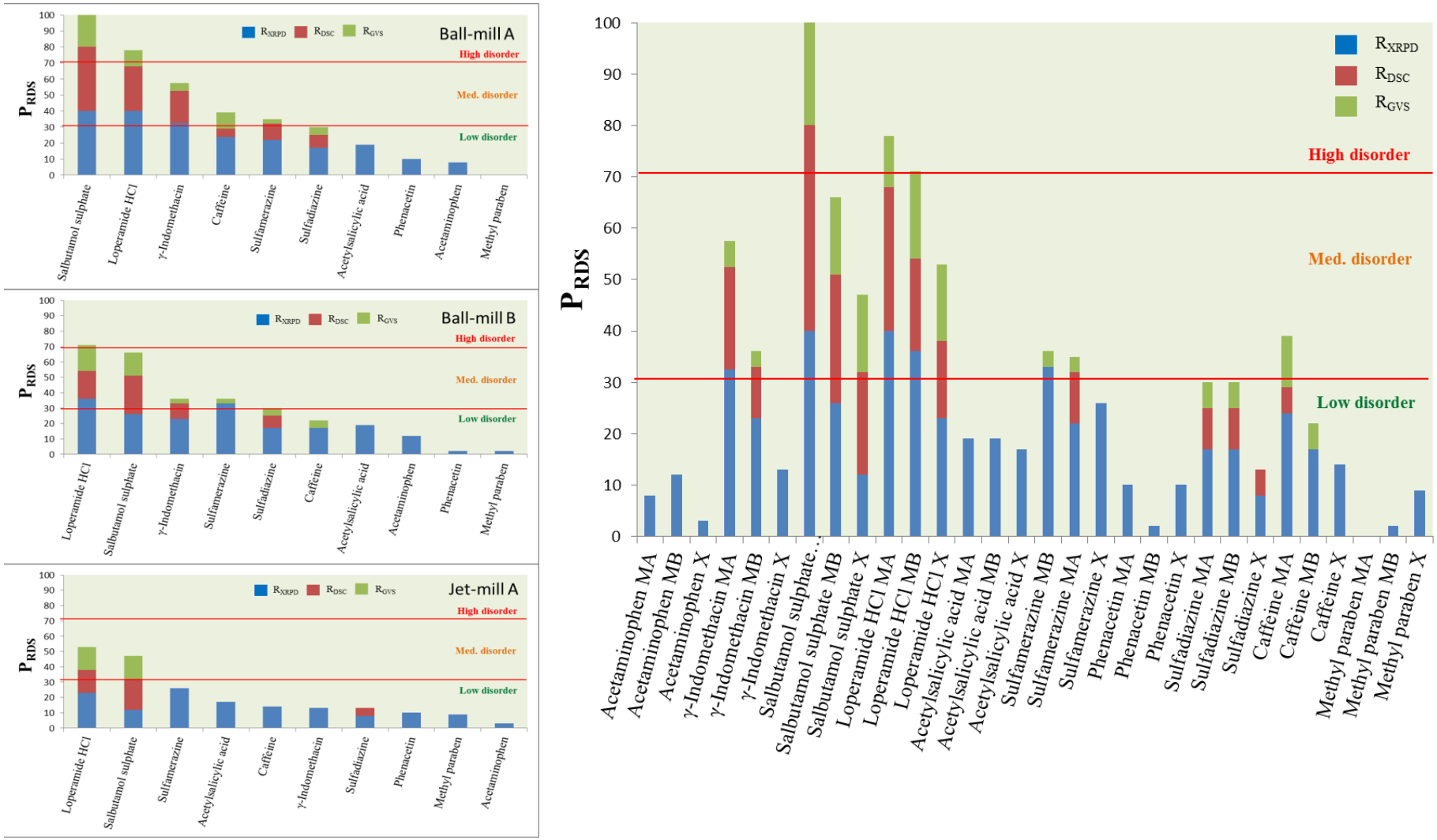

Figure 7-5 Plots of P_{RDS} values for the comminuted materials

Plots on the left show the P_{RDS} values for the three comminuted processes, while the plot on the right shows a summary of the P_{RDS} values across the comminuted materials
MA: high frequency ball-mill method A, MB: low frequency ball-mill method B. X: jet micronisation method A.

P_{RDS} values are a combination of the individual technique response disorder scores using the XRPD, DSC and GVS techniques, *i.e.* R_{XRPD}, R_{DSC} and R_{GVS} respectively. The individual technique contributions to the overall P_{RDS} score were weighted based on the number of responses used by each technique to infer the presence of disorder. R_{XRPD} and R_{DSC} values use a number of responses are employed, hence they provide a higher contribution or weight (with a maximum score of 40 allotted for each) to the overall P_{RDS} score compared to GVS, which only utilises only two responses (with a maximum of score of 20).

In general the overall response disorder scores (P_{RDS}) for the comminuted materials were low, with acetaminophen, methyl paraben and phenacetin exhibiting the lowest values with P_{RDS} values of less than 12 (Table 7-15). Only a few materials such as high frequency ball-milled γ-indomethacin, salbutamol sulphate and ball-milled loperamide HCl exhibited high P_{RDS} values greater than 70, which indicated the presence of marked disorder (Table 7-15). Of all the comminution processes, high frequency ball-milling appeared to generate the greatest level disorder with respect to the magnitude of the P_{RDS} values, followed by low frequency ball-milling and then jet-milling (Figure 7-5 and Table 7-15). In general, the calculated P_{RDS} values (Table 7-15) agreed with the initial qualitative CRA solid-state phase classifications (Table 6-25). However, there were some exceptions to this observation and these were attributed to the increased resolution power of the RDA and PDA processes to discriminate the disorder within the comminuted materials. This will be discussed further in the proceeding pages.

R_{XRPD} values were obtained for most of the comminuted materials which implies that XRPD analysis could detect some degree of disorder in these materials (Figure 7-5 and Table 7-15). However, it is important to note that the R_{XRPD} values represent not only changes in the XRPD responses for disordered material but also those associated with microcrystalline materials (Section 3.2). During a comminution process, material is mechanically broken down (ground) into smaller fragments with a consequential increase in surface area to produce particles within a specified particle size range (Section 1.4.2 and Figure 1-14). However, comminution can result in microcrystalline material, which may also contain some degree of disorder that can be difficult to define by XRPD analysis alone (Figure 7-6). With the addition of RDA scores by DSC and GVS analysis, the presence of disorder can be further discriminated and the solid-state phase present better defined (Figure 7-6).

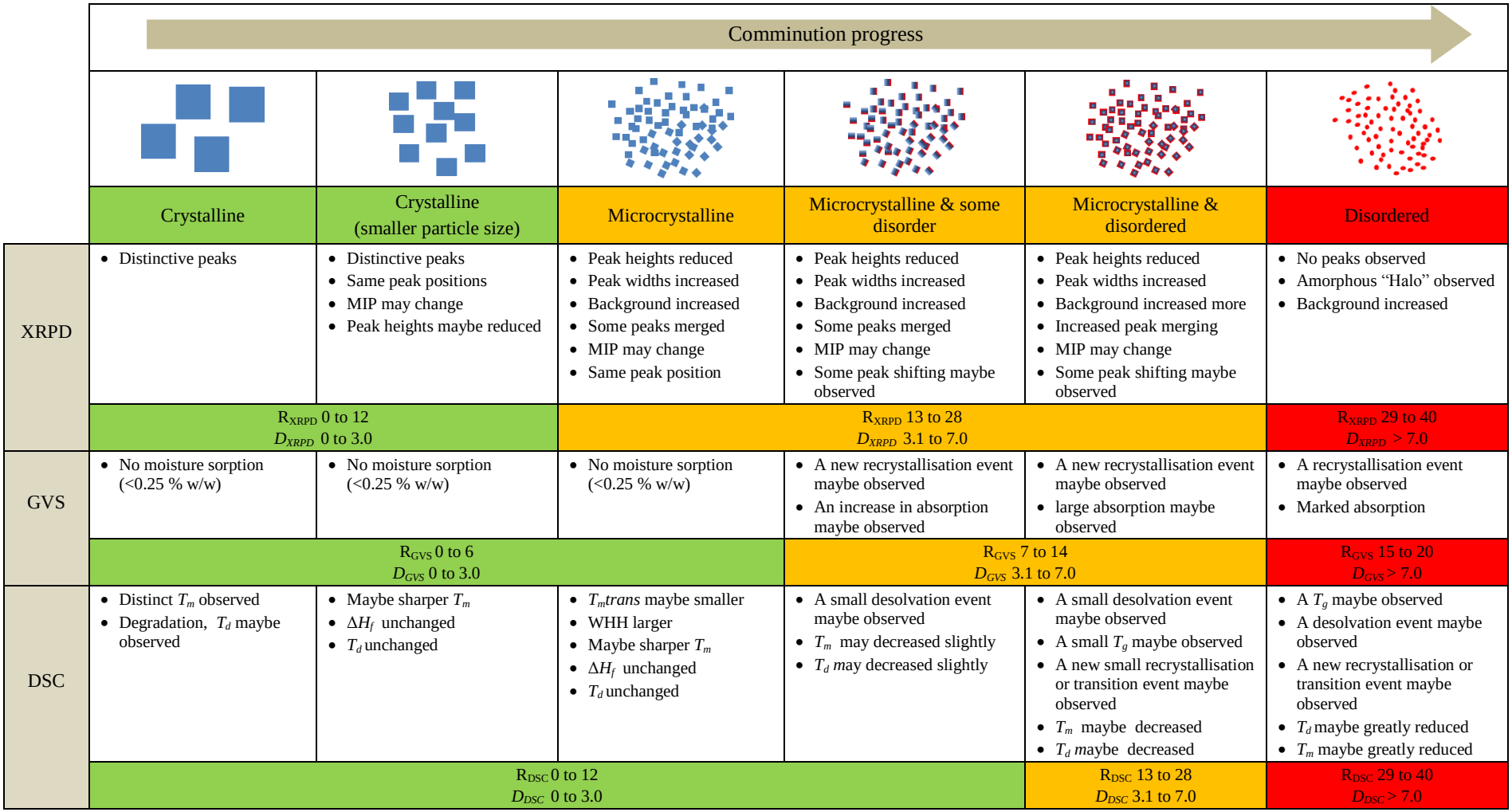

Figure 7-6 Technique response observations and RDA scores for different solid-state phase materials that could be generated during the comminution of an anhydrous crystalline input material

MIP: Most intense peak, R_{XRPD}, R_{DSC} *and* R_{GVS}*: combined total RDS value for XRPD, DSC and GVS responses respectively.* D_{XRPD}, D_{DSC} *and* D_{GVS}*: XRPD, DSC and GVS disorder scores calculated using equations [7-1], [7-2] and [7-3] respectively.* T_d*: Degradation temperature (°C),* T_m*: Onset of melting temperature (°C),* T_m*trans: Melting transition range (°C),* ΔH_f*: Heat of fusion (J/g),* WHH*: width at half peak height (°C),*

For example, ball-milled materials of sulfadiazine have R_{XRPD} values of 17 which implied the presence of some disorder (Table 7-15). However, XRPD analysis alone cannot discriminate whether the relative changes in the XRPD responses are a consequence of generated microcrystalline product, the presence of disordered material or a mixture of both. By including the RDA values and observations for the DSC and GVS data, the solid-state phase present can be better defined. The presence of a small amount of disorder in ball-milled sulfadiazine samples is indicated by the observed decreases in T_m and T_d during DSC analysis (R_{DSC} 8, D_{DSC} 2.0) and change in moisture sorption (ΔM_{MAX1}) observed during GVS analysis (R_{GVS} 5, D_{GVS} 2.5). However, the overall amount of disorder present as a consequence of ball-milling is low with a P_{RDS} value of 30, hence this material is likely to be microcrystalline with a very small amount of disorder present.

For the comminuted materials of acetylsalicylic acid (R_{XRPD} 17 to 19) and jet-milled sulfamerazine (R_{XRPD} 26), R_{XRPD} values may have suggested the presence of some disorder (Table 7-15). However, relative changes in their DSC and GVS responses did not support the presence of disorder, *i.e.* R_{DSC} and R_{GVS} values were 0 (Table 7-15). Therefore, it is most likely that the relative changes observed in the XRPD responses for these two materials were due to the presence of microcrystalline material generated as a consequence of the comminution processes and not due to disorder. P_{RDS} scores for these materials were low, below 31, hence these materials were designated as being crystalline.

Low frequency ball-milled γ-indomethacin was initially classified as being microcrystalline with a small amount of disorder using the CRA approach (Table 6-25). This was further confirmed using the new RDA and PDA approaches. A R_{XRPD} value of 23 (Average D_{XRPD} ~5.8) was determined based on the relevant changes to the XRPD responses, *i.e.* the merging of peaks, change in MIP, small decrease in peak heights, slight increase in background profile and a large increase in peak widths (Table 7-12). This R_{XRPD} value implies the presence of some disorder, microcrystalline material or a mixture of both, but using these data alone are insufficient to determine which of these is actually present. With the inclusion of the DSC and GVS data, a small level of recrystallisation and an increase in moisture sorption was observed giving rise to R_{DSC} and R_{GVS} scores of 10 and 3 respectively (Table 7-15). Hence, low frequency ball-

milled γ-indomethacin was thought likely to consist of microcrystalline material with a small amount of disorder.

It can be seen from examples given, relying on only one technique such as XRPD to define and discriminate the presence and degree of disorder present as a consequence of a comminution process may not be sufficient. By using multiple techniques and responses both the presence and relative amounts of disorder can be better determined and the probability of detecting disorder can be greatly enhanced.

This can be further illustrated using RDA analysis for jet-milled salbutamol sulphate. RDA analysis of the XRPD data (R_{XRPD} of 12, D_{XRPD} of 3.0) did not identify high levels of disorder present in the sample. Instead changes in the XRPD responses were most likely caused by the decrease in particle size of the comminuted material and this resulted in a change in MIP and a marked decrease in peak heights (Table 7-12). However, when changes in the DSC and GVS responses are included in the disorder assessment, higher levels of disorder are identified, *i.e*. values of 20 and 15 were determined for R_{DSC} and R_{GVS} respectively (Table 7-15). The reason for this discrepancy could be due to the sensitivities of the individual techniques in detecting disorder for this particular material or level of disorder, *i.e.* both the GVS and DSC methods were more sensitive than that of XRPD in this case.

It must be noted that the amount of recrystallisation observed in the DSC could not be calculated for salbutamol sulphate due to the presence of unresolved thermal events. However, visually, the recrystallisation observed in the DSC thermogram for the jet-milled salbutamol sulphate sample was much lower than that observed for the ball-milled materials (Figure 6-15). The combined P_{RDS} value for jet-milled salbutamol sulphate was 47, suggesting that there was some degree of disorder present which would not have been identified if just XRPD analysis was used alone.

The ball-milling of sulfamerazine resulted in material that exhibited changes in the XRPD diffractogram consistent with the presence of disorder. Interestingly, this was more so for the low frequency ball-milled material (R_{XRPD} of 33) compared to high frequency ball-milled material (R_{XRPD} of 22). As discussed earlier (Section 7.3.1), this observation was most likely due to the transformation kinetics of the disordered phase and not due to inaccuracies of the RDA method. Limited disorder was suggested with

the addition of DSC and GVS data as shown by their R_{DSC} and R_{GVS} values (Table 7-15).

In the case of high frequency ball-milled caffeine, RDA for the XRPD data suggested the presence of some disorder (R_{XRPD} of 24). However, DSC analysis only showed a small loss of volatile solvent (R_{DSC} of 5) but GVS analysis indicated that the moisture sorption properties of this material was greatly enhanced which may imply the presence of increased surface disorder (R_{GVS} of 10). Overall, the P_{RDS} for high frequency ball-milled caffeine was 39, which suggested there was only a small amount of disorder present.

7.3.4.2 D_{Pro} scores

The total amount of disorder present (D_{Pro}) in a material as a consequence of a given pharmaceutical process was calculated by two different approaches to investigate the effect of scaling of the individual technique contributions to the overall disorder score.

In the first approach, process P_{RDS} values were converted into D_{Pro1} values using equation [7-5], where the maximum individual RDS contributions of R_{XRPD}, R_{DSC} and R_{GVS} were weighted towards the XRPD and DSC values. While in the second approach the process disorder score, D_{Pro2} was calculated by averaging the technique disorder scores, D_{XRPD}, D_{DSC} and D_{GVS} using equation [7-6]. In this approach the individual technique contributions were treated equally.

The D_{Pro} values for the comminuted materials determined by both approaches are summarised in Table 7-16 and Figure 7-7. Using the D_{Pro} values, the comminuted materials can be separated and ranked into three classes of materials which reflect the solid-state phase present (Figure 7-11).

Only three materials, high frequency ball-milled salbutamol sulphate and high and low frequency ball-milled loperamide HCl exhibited D_{Pro} scores above 7 and were categorised as being disordered (Table 7-16 and Figure 7-11). These results are in agreement with the CRA classification (Table 6-25) and the literature observations that demonstrated that these materials exhibit PID when comminuted (Table 2-8).

Table 7-16 Summary of process disorder scores for the comminuted materials

Material	Process	Process scores			PDA solid-state phase classification	Overview CRA solid-state phase classification *	Lit PID**
		P_{RDS}	D_{Pro1}	D_{Pro2}			
Methyl paraben	MA	0	0.0	0.0	Crystalline	Crystalline	No
	MB	2	0.2	0.2	Crystalline	Crystalline	
	X	9	0.9	0.8	Crystalline	Crystalline	
Acetaminophen	MA	8	0.8	0.7	Crystalline	Crystalline	No
	MB	12	1.2	1.0	Crystalline	Crystalline	
	X	3	0.3	0.3	Crystalline	Crystalline	
Phenacetin	MA	10	1.0	0.8	Crystalline	Crystalline	No
	MB	2	0.2	0.2	Crystalline	Crystalline	
	X	10	1.0	0.8	Crystalline	Crystalline	
Acetylsalicylic acid	MA	19	1.9	1.6	Crystalline	Crystalline	No
	MB	19	1.9	1.6	Crystalline	Crystalline	
	X	17	1.7	1.4	Crystalline	Crystalline	
Sulfadiazine	MA	30	3.0	2.9	Microcrystalline – little disorder	Crystalline – little disorder	Some
	MB	30	3.0	2.9	Microcrystalline – little disorder	Crystalline – little disorder	
	X	13	1.3	1.1	Crystalline	Crystalline – little disorder	
Caffeine	MA	39 (A_G 7.17)	3.9	4.1	Little disorder	Crystalline – little disorder	Some
	MB	22	2.2	2.3	Crystalline	Crystalline – little disorder	
	X	14	1.4	1.2	Crystalline	Crystalline	
Sulfamerazine	MA	35 (T 9.6)	3.5	3.2	Little disorder	Some disorder - some new form	Some
	MB	36	3.6	3.3	Little disorder	Microcrystalline - little disorder	
	X	26	2.6	2.2	Crystalline	Crystalline	
γ-Indomethacin	MA	58 (G_D 0.315,X_D 20.3)ǂ	5.8	5.2	Some disorder	Disordered	Yes
	MB	36 (X_D 3.5)ǂ	3.6	3.3	Microcrystalline with disorder	Microcrystalline - little disorder	
	X	13	1.3	1.1	Crystalline	Crystalline	
Loperamide HCl	MA	78 (G_D 0.265, X_D 60.7, A_G 9.10)	7.8	7.3	Disordered	Disordered	Yes
	MB	71 (X_D 11.1, X_G 3.46, A_G 2.88)	7.1	7.3	Disordered	Some disorder	
	X	53 (X_G 1.08, A_G 0.72)	5.3	5.7	Some disorder	Crystalline – little disorder	
Salbutamol sulphate	MA	100 (X_G 9.69) ǂ	10.0	10.0	Disordered	Disordered	Yes
	MB	66 (X_G 1.29) ǂ	6.6	6.8	Some disorder	Microcrystalline - some disorder	
	X	47 (X_G 0.68)	4.7	5.2	Microcrystalline with disorder	Crystalline - little disorder	

ǂ *Average value from replicate processes.* D_{XRPD}, D_{DSC} *and* D_{GVS}*: XRPD, DSC and GVS disorder scores calculated using equations [7-1], [7-2] and [7-3] respectively.* P_{RDS}*: Process response disorder score.* D_{Pro1} *and* D_{Pro2} *: process disorder score calculated using equation s [7-5]and [7-6] respectively.* from Table 6-25, ** from table 2-8.* (G_D *#): size of* T_g *in J/(g°C),* (X_D *#):size of* ΔH_c *in J/g,* (T *#): size of transition* ΔH_t *in J/g.* (X_G *#): size of* M_{xtal} *in %,* (A_G *#): size of* $\Delta M_{MAX1.}$
M: high frequency ball-mill method A, MB: low frequency ball-mill method B. X: jet micronisation method A.

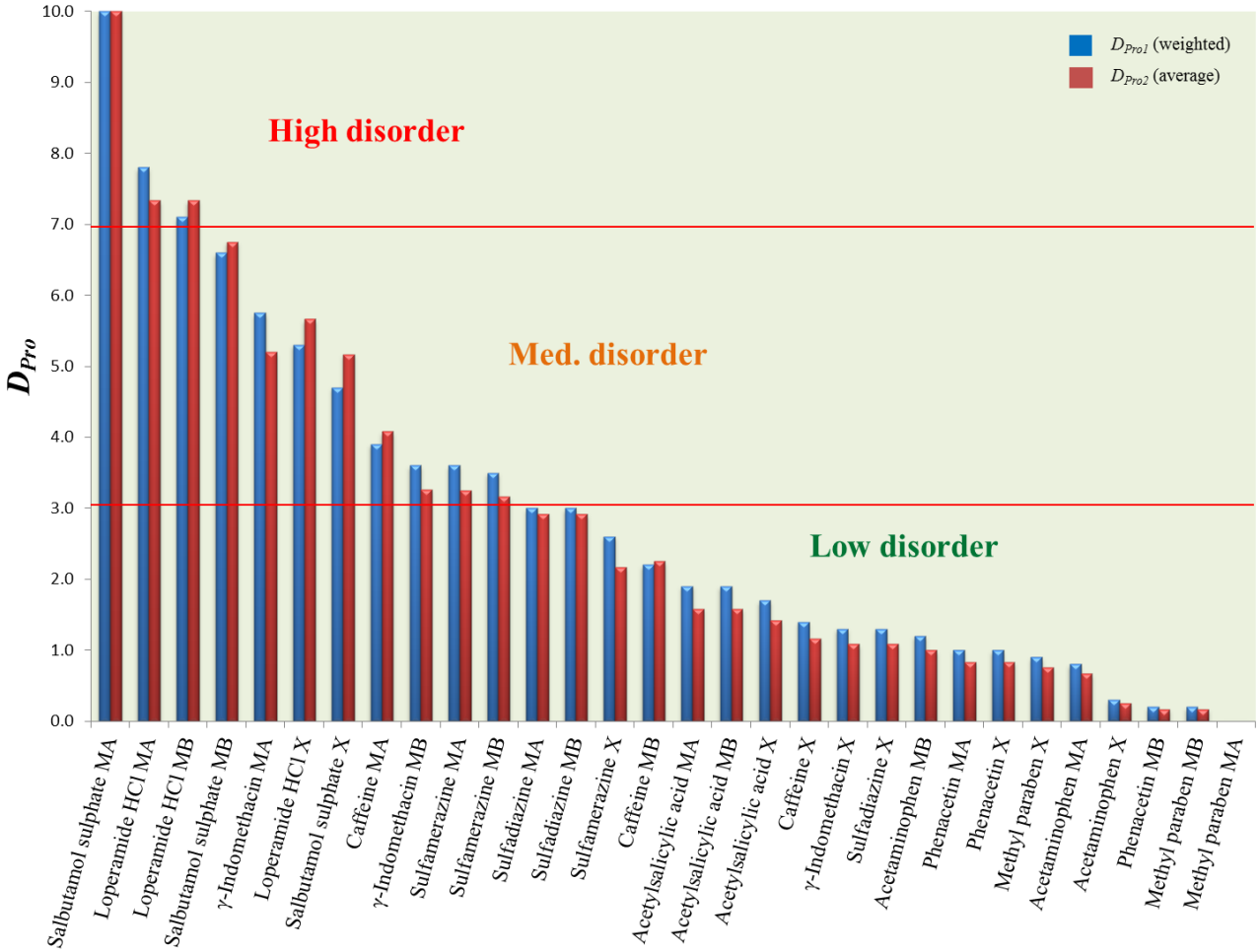

Figure 7-7 Calculated D_{Pro} scores using weighted and average approaches for the comminuted materials

MA: high frequency ball-mill method A, MB: low frequency ball-mill method B. X: jet micronisation method A. D_{Pro1}(weighted): process disorder score calculated using equation [7-5], D_{Pro2}(average): process disorder score calculated using equation [7-6],

When comparing the D_{Pro} values calculated by the two different approaches for the same material, it can be seen that the weighted approach appears to be better at discriminating between the comminution processes for materials containing higher degrees of disorder (Figure 7-11). For example, D_{Pro1} values of 7.8 and 7.1 were calculated using the weighted approach for high and low frequency ball-milled loperamide respectively, but the D_{Pro2} values were identical (D_{Pro2} of 7.3) when calculated using the average approach (Table 7-16 and Figure 7-11). However, the reported ΔH_c values for recrystallisation from the DSC thermograms (Table 7-13), suggests high frequency ball-milled loperamide HCl (ΔH_c of 60.7 J/g) is more disordered than the low frequency ball-milled sample (ΔH_c of 11.1 J/g). Therefore, the weighted approach appears to be better at discriminating between the comminution processes and quantify the relative levels of disorder present.

A number of materials appear to have some level of disorder with D_{Pro} values between 3 and 7 such as: ball-milled sulfamerazine, γ-indomethacin, high frequency ball-milled caffeine, jet-milled loperamide HCl and salbutamol sulphate and low frequency ball-milled salbutamol sulphate (Table 7-16). For these materials, the method by which the D_{Pro} values were calculated had minimal impact to the overall PID ranking or to amounts of relative disorder estimated to be present. The relative levels of disorder present in the comminuted materials were in agreement with the CRA classification (Table 6-25) and those from literature observations that demonstrated that these materials exhibit some degree of PID when comminuted (Table 2-8).

Literature observations[221,270] for sulfadiazine suggested that this material may exhibit some degree of disorder when comminuted. This was confirmed using the CRA approach (Table 6-25) in chapter 6. However, these approaches only provide a qualitative assessment of disorder. When the new RDA and PDA approaches were applied to assess the degree of disorder present as a consequence of the three comminution processes a relatively low D_{Pro} value of less than 3.0 was obtained (Table 7-16). This illustrates the effectiveness of the new processes in quantifying the relative levels of disorder present, as it can remove some of the ambiguity concerning the degree of disorder by providing a numerical value, allowing better comparisons to be made between both different material types and processes.

7.4 Conclusions

The development of a novel analytical approach to determine the level of disorder present in a material as a consequence of a comminution process has been described.

To date, there has been no quantitative approach reported that has incorporated the responses from multiple techniques into a single value to define a certain property such as the presence of disorder or amorphous character.

The validity and verification of the novel analytical approach to determine disorder has been further demonstrated through its application in characterising the resulting comminuted materials. It has been successfully shown that this approach will allow materials of differing chemical and crystallographic properties to be ranked according to the relative level of disorder being present, and that the approach can differentiate the effectiveness of different comminution processes in generating PID.

8 General discussion and conclusions

8.1 General discussion

Pharmaceutical medicines are most frequently manifested as solid dosage forms which are manufactured using a number of different pharmaceutical unit operations or processes. Such processes often impose a number of thermal and mechanical stresses upon the formulation, comprising of an API and associated excipients (Figure 1-11). The forces associated with mechanical processing may inadvertently cause process-induced phase transformations[11,12] (such as the generation of lattice disorder or PID[17-28]) to any crystalline components within the formulation, which is a significant concern to the pharmaceutical industry[17-28,65] as it may ultimately change the intended pharmaceutical product's physiochemical stability and therapeutic performance[13-17]. The extent of this disorder will depend on the type and conditions of the pharmaceutical unit process employed and upon the intrinsic properties of the materials involved. Typically Particle size reduction or comminution by milling or micronisation is often required to enhance the bioavailability of pharmaceutical solids as a consequence of it conferring increased dissolution rate or solubility[1-4] upon the API. For an inhaled pharmaceutical powder, the overall size is also a major determinant of its site of deposition in the airways after aerosolised delivery[372-376]. However, such size reduction unit operations have the highest risk of generating PID due to their intense mechanical nature and the associated high processing input energies that are required[5-10]. It is therefore important to develop strategies to control, characterise and optimise the particle properties to ensure the safety and quality of the final product.

Knowledge of the molecular structure and mechanical properties of the input material and the potential pre-existing structural flaws could enable the development of more robust pharmaceutical comminution processes and lead to a better understanding of the potential for certain materials to undergo PID. However, currently the propensity of crystalline materials to become disordered or the extent to which this might proceed as a function of imposed processing conditions is poorly understood[137,160,192,221,264]. Recent studies have made attempts to correlate the presence of disorder with known material properties, in order to predict their disordering potential or propensity[160,221,264]. However, the materials employed in these studies have potentially been over-processed in an attempt to force the generation of "pure" amorphous phases using different processes and/or conditions. Additionally, differences in milling times were not taken

into account when interpreting and modelling any property-phase relationships[160,221]. Continuingly milling for excessive periods effectively forces the material to become "amorphous" and treats all those materials that exhibit amorphous behaviour identically, regardless of the time it may have taken to induce this disorder. It can be argued that it is more appropriate to mill all the materials for the same period of time using the same operational conditions or include a weighting/scale factor that takes into account the time required to generate disorder. This time period could be classed as a measure of the materials PID resistance or susceptibility under standardized conditions. The shorter the time period, the lower the PID resistance, and the greater the susceptibility of the material to PID.

In recent years methods to define "pure" crystalline and "pure" amorphous materials has vastly improved[11,12,14,15,17,31]. Nevertheless, the detection and quantification of the relative amounts of solid-state phases across the amorphous-crystalline continuum within a given material is still not readily achieved

Typically the qualitative detection of PID is performed using individual techniques such as XRPD, DSC and GVS[21,28,88,175,190-193], which can produce somewhat subjective results since such determinations rely on the analyst's experience and interpretation[23,244,245,247]. Conversely, quantifying the amount of disorder present within a solid material depends greatly on the sensitivity of the technique. It is also typically only achieved with the use of single analytical responses and employing calibration curves constructed using mixtures of "pure" amorphous and crystalline standards that can be both problematic and complex to generate[23,24,65,87,194-198]. For example, in a number of earlier studies, investigators made the assumptions that the analytical responses from a potential disordered material being investigated were the same as those of an amorphous standard[18,24,190,191,252,307,308]. However, this may not always be the case, as the "pure" amorphous standards were typically generated using a different process from than that being applied to the material being investigated, *e.g.* amorphous standards generated by spray drying (bulk disorder) will exhibit different moisture sorption properties/responses when analysed by GVS than disordered ball-milled samples (surface disorder). The use of such standards can therefore result in errors in the estimation of the amount of amorphous material present[309]. Additionally a number of previous studies generated amorphous standards by the process of "melt-quenching", which is the process of melting the materials followed by a rapid cooling so as to "trap"

or isolate the amorphous form[56,63,271]. This is in effect, the formation of a kinetamorph, where different cooling and process parameters may give rise to a different polyamorphic form (Section 1.1.2). However, amorphous standards prepared in this manner will also be bulk disordered and as such may exhibit different analytical responses compared to mechanically comminuted materials where disorder is mainly located upon the surface[56,63,279]. Furthermore, it is important to check the chemical purity post-processing to ensure no impurities have been introduced that could interfere with the analytical response measurements. However, historically this has not always the case[158,205,208,221,257,367-369]. This is especially important for materials that exhibit a melt-degradation events such as salbutamol sulphate[1,19,297] as the amorphous materials prepared by melt-quenching are more likely to contain thermal degradants.

To address the need for an effective method to both detect and quantify levels of induced disorder in a material as a consequence of a given mechanical process, a novel analytical approach was investigated that negated the need for standard mixtures or calibration curves. This provided the main research focus for this thesis (Section 1.5).

To develop this new analytical approach a model set of ten pharmaceutical materials that encompassed the whole of the amorphous-crystalline continuum were selected using a defined set of criteria (Table 2-4). This systematic selection process, which does not appear to have been utilized previously, ensured materials were chosen not only based on the literature assessments of their propensity for PID by mechanical comminution, but also ensured that the materials selected had sufficient diversity in their structural and molecular properties. For example, diversities in their H-bond donor and acceptor capabilities, molecular weights, melting onset temperatures, LogP, solubilities, molecular space group numbers and the number of rotatable bonds etc (Table 2-9). Mechanical properties were not included in the selection criteria, due to the difficulty in obtaining this information for all materials either from the literature or from databases. Additionally, there are no mechanical property prediction software programs available, unlike those for solubility and H-bond properties.

Of the materials selected, four were selected from the literature that appeared to be resistant to PID, acetaminophen[158,221], methyl paraben[255], phenacetin[265] and acetylsalicylic acid[158,221,266,267]. Three materials were selected from the literature that exhibited some disorder: caffeine[217,269], sulfadiazine[221,270] and sulfamerazine[270,271], and finally three materials were selected from the literature that appeared mainly disordered

when mechanically comminuted: salbutamol sulphate[1,20,21,246,247,275-277], γ-indomethacin[141,158,178,212,221,268,271] and loperamide hydrochloride[278].

Prior to subjecting the compounds to mechanical comminution, the materials were classified into different particle size fractions by mechanical sieving and the sieving efficiency investigated using a combination of techniques (PSA, SEM and PLM) (Section 4.3.2). Sieving the materials can reduce the inherent variation in the bulk as unsieved materials can exhibit a wide range of particle properties, such as size or morphology (habit) and these may give rise to a wide range of analytical responses when characterised.

It was noted that many investigators use materials as received from the supplier without performing any pre-processing steps, such as particle size fractionation. Alternatively, if the materials are sieved, then assumptions are often made that the particle size fractions obtained will always match the mesh sizes employed[247,248]. However, data obtained in the current study have shown that despite the sieving process being effective in separating the materials into different particle size fractions, the final particle sizes did not necessarily correlate precisely with the sieve size used (Table 4-5). Such differences were most likely attributable to the presence or breaking of agglomerates, other material properties such as crystal morphology, or electrostatic charges generated during the sieving process that caused particle retention. Such behaviour is typified by loperamide HCl, caffeine and methyl paraben whereby, fairly strong agglomerates remained (Table 4-6).

For each study material only one sieved fraction was selected for further investigation thereby reducing the potential range of analytical response variability as a consequence of particle size (Table 4-8). The selected sieved fractions for the materials were then successfully characterised using a set of core analytical test methods comprising of XRPD, GVS, DSC, TGA, SEM, PLM, PSA, HPLC, and FTIR (Chapter 4). The analytical responses from these core techniques demonstrated that all the sieved powders were highly crystalline and anhydrous. Furthermore, the analytical responses from these core tests became the reference values that were then used to compare to the responses of the corresponding mechanically comminuted materials.

Unlike previous studies[160,221] where different comminution conditions were applied to different materials, all the materials in this thesis were comminuted the same way and for the same length of time. This regimen allowed the relative amounts of any observed

disorder to be compared between materials and also between processes and or conditions for the same material.

Three mechanical comminution methods involving cryogenic vibrating ball-milling and air jet-milling (fluid energy mill or micronisation) were employed to generate different levels of PID for the selected study materials using varying but standardised parameters (Chapter 5). Any variation in PID within the material might then be reasonably attributable to the different processing conditions. Such changes could, in turn be investigated using the core analytical test methods. Of the comminution processes employed, two comprised cryogenic ball-milling methods, which involved low and high frequency impaction using different ball sizes and milling periods, performed whilst cooling at the temperature of liquid nitrogen (Table 5-1). These methods were referred to as the high frequency (Mill-A) and low frequency (Mill-B) milling methods. Method Mill-A, was a high energy comminution process that vibrated a larger milling ball at a higher frequency and for a longer period then method Mill-B, hence, method mill-A was the more likely of the two techniques to generate the most PID.

Cryogenic ball-milling using liquid nitrogen was used to ensure that milling occurred below room temperature as it has been noted in the literature that low temperature milling can be more efficient in generating amorphous material compared to room temperature[146,345]. This may be attributed in part to the materials being rendered more brittle (less elastic) at low temperatures and therefore more amenable to size reduction processes and hence induced disorder[137,146,160,191,192,221,247,345]. Additionally, precautions were taken to reduce the influence of local %RH to cause recrystallisation[311] of any transient meta-stable phases or solid-state forms during and after ball-milling by using a dry nitrogen atmosphere to charge and discharge the milling jars. Similarly, jet-milling or micronisation of the materials was performed under a dry nitrogen atmosphere, to reduce the effects of environmental %RH. However, an increase in the temperature of 10 °C in the collection vessel was observed during the micronisation process, which partially contradicts previous assumptions that jet-milling using air as a component of the grinding media can help to cool or dissipate any generated heat[180].

The degree of comminution obtained by micronisation depends on the critical milling parameters: feed rate, feed pressure and grind pressure[21,344]. Micronisation feed and grind pressures of 8 and 6 bar respectively were selected[11,344] so as to prevent clogging and to ensure a maximum jet speed (sonic velocity) could be obtained[21]. The feed rates

were similar for all materials, ranging from 0.23 to 0.29 $gmin^{-1}$ (Table 5-3), allowing the materials to be readily be accelerated upon entry into the grinding chamber. If the material concentration inside the grinding chamber was too large then a decrease in inter-particulate acceleration distance would result, giving rise to coarser particles[21].

Following comminution, most materials were electrostatically charged especially those processed by high frequency ball-milling or micronisation. However, by applying an ionizing airflow to these materials the electrostatic charges tended to dissipate. For some materials a colour change was observed upon comminution, the most notable of these was for γ-indomethacin[377], which upon high frequency ball-milling changed colour from white to bright yellow and formed lumps and a hard layer that encased the milling ball (Figure 5-1). Similar, although less-intense colour changes, were also observed for the low frequency ball-milled and micronised materials.

Once comminuted, the materials were characterised using the core analytical test methods and the technique responses compared to those obtained for the input materials by a new approach called comparative response analysis (CRA) (Chapter 6). This approach allowed a systematic and consistent process, in which the amount of change in the individual technique responses could be determined and the qualitative relevance of these changes with respect to the solid-state phase present for each of the comminuted materials to be defined. This is advocated to be an improvement on previous methods to define the solid-state phase in materials which solely relied on the analyst's experience and interpretation using single techniques and/or responses[23,244,245,247].

Based on the CRA values, novel solid-state phase classifications or decision trees were developed and applied to those core test methods which could detect the presence of disorder directly; these were referred to as the 'primary' disorder detection methods XRPD, DSC and GVS. The other test methods were classed as 'secondary' disorder detection methods as it was concluded that the results generated by the latter methods could not be employed solely to infer the presence of disorder. However, such 'secondary' methods can be used to provide supplementary or supportive evidence for the presence of disorder indirectly.

By using the combined information from the primary and secondary disorder detection methods, the solid-state phase present for each comminuted material could be qualitatively defined (Table 6-25).

Four materials, acetaminophen, acetylsalicylic acid, phenacetin and methyl paraben appeared resistant to PID regardless of the comminution process employed which was consistent with the initial literature PID classifications (Table 6-25).

Three other materials, sulfamerazine, sulfadiazine and caffeine exhibited some degree of disorder when ball-milled but not when micronised which is in general agreement with the initial literature PID classifications (Table 6-25). However, in the case of sulfamerazine, high frequency ball-milling resulted in the generation of a small amount of Form II material via the amorphous phase which was consistent with previous studies[336,349-351,361,362]. This new solid-state form is thought to arise as a consequence of ball-milling, whereby the material is transformed through a series of transitions from Form I to amorphous to Form II. If the comminution process were to continue then the material would then revert back to Form I. The comminution of sulfamerazine highlights an important observation in that the identification of the presence of disorder typically relies on disorder being present at the time of analysis. This means, therefore, that disorder may have already have been generated but such changes may then have been transformed to another solid-state as the comminution process progresses. By using the CRA methods and combining the results from multiple techniques, the probability of identifying either the presence or remnants (effects) of disorder would likely to be greatly enhanced.

For loperamide HCl, salbutamol sulphate and γ-indomethacin different solid-state phases were observed depending on the comminution process employed. The level of disorder present appeared to be proportional to the relative amount of energy imparted by the comminution process. Ball-milling in general had a greater tendency to induce disorder than micronisation, hence the comminution processes could be ranked in order of their tendency to cause PID from lowest to highest: micronisation (JM-A) < low frequency ball-milling (Mill-B) < high frequency ball-milling (Mill-A). This order also reflects the efficiency of the comminution processes in reducing particle size without causing PID, with micronisation (JM-A) being the most efficient and ball-milling (Mill-B and Mill-A) being least efficient of the processes investigated.

It has been postulated that the process of ball-milling can cause “amorphisation” of a material via melt-quenching at localised “hot spots” where there is no temperature control during the comminution process[72]. This phenomenon was investigated by ball-milling salbutamol sulphate at high frequency with and without temperature control

using liquid nitrogen. Salbutamol sulphate was chosen for this investigation as it has a T_g that has been shown to be affected by the presence of water, around 65 °C when "wet" [19,247,358] or 120 °C if "dry" [359], and has been shown to exhibit a melt-degradation event[1,19,297], hence, any increase in internal milling temperature could affect PID generation as well as chemical purity. High frequency ball-milling salbutamol sulphate with and without temperature control resulted in a predominately amorphous material but the overall estimated chemical purity remained relatively high with only a 0.5 % observed drop in the primary peak area by HPLC analysis. This implied that the observed "amorphisation" of salbutamol sulphate was most likely due to the mechanical disordering of the molecules and not because of melt-quenching at localised "hot spots". This was consistent with other studies which also refute the local heating theory for amorphous generation[5,7,242].

Using the novel CRA procedure (Chapter 6) the solid-state phases present in the comminuted materials were identified and defined and were in general, in agreement with the initial literature PID classifications (Table 6-25). For example, acetaminophen appeared not to generate PID when subjected to mechanical comminution processes as observed by Wildfong *et al.* (2006)[160]. However, for other materials such as γ-indomethacin which had been initially classified as being sucepitble to PID when mechanically comminuted[148,160,178,212,221,268,271], the solid-state phase classification using the CRA approach depended on the comminution process employed. However, it must be noted that the initial literature PID classification was based on observations from a number of studies that used different comminution conditions and milling periods from those employed in this current study to ensure complete amorphisation of γ-indomethacin. For example, Wildfong *et al.* (2006)[160] and Lin *et al.* (2009)[221] used a cryogenic impact mill to generate amorphous γ-indomethacin afer 3 h milling, while Otsuka *et al.* (1994)[148] ball-milled at 4 °C for 10h generate the amorphous form. In all these examples, complete disorder was assumed by the demonstration of a diffuse halo in XRPD patterns without detectable diffraction peaks and also verified by the presence of a glass transition in the DSC thermograms[148,160, 221].

Using the CRA approach, the high frequency ball-milling of γ-indomethacin resulted in material classified as being disordered which was consistent with the literature PID classification. While low frequency ball-milling generated microcrystalline material

with a small level of disorder present and micronisation did not alter the solid-state phase, *i.e.* micronised γ-indomethacin appeared to be remain crystalline.

The comminution of γ-indomethacin successfully demonstrates that the different comminuted materials can be classified into different solid-state phase classes based on relative changes to their technique responses. However, there are some limitations in using the CRA approach, in that the process cannot discriminate the degree of disorder within a certain class, *i.e.* which materials were more disordered than others with a solid-state phase class. However, some attempt to achieve a degree of disorder scaling was made by developing a colour-coding scheme. This procedure employed the qualitative CRA results obtained from the XRPD, DSC and GVS experiments (Section 6.4.9) and assigning a colour (red, orange or green) corresponding to the degree of change. The greater the number red boxes, the more likely disorder is present (Table 6-25).

The CRA results further demonstrated that the three comminution processes successfully produced materials that encompassed the whole amorphous-crystalline continuum and that the defined solid-state phases were consistent with those reported from the literature (Table 6-25).

In order to improve the discrimination of the resultant degree of induced disorder the data were further processed to develop a procedure, termed response disorder analysis (RDA) (Chapter 7). This was achieved by redefining the CRA threshold levels for the individual technique responses so that they were specific to the presence of disorder. This allowed the relative amount of disorder present in the comminuted materials to be semi-quantified and generated response disorder scores (RDS) for the individual technique responses. These individual RDS values were then combined to give an overall RDS score for the technique, ($R_{Technique}$). In this study only RDS values for XRPD (R_{XRPD}), DSC (R_{DSC}) and GVS (R_{GVS}) were used as these three techniques represent the 'primary' disorder detection methods in the core analytical methods test set.

The maximum sum of the individual RDS for each technique was weighted depending on the number of inherent specific responses associated with each technique that can be used to identify disorder. For example, both XRPD and DSC have a number of responses that are specific to identifying disorder in a compound, so that the maximum

sum of their individual RDS values was 40, while for GVS the maximum sum was 20, as it only allowed two different responses specific to disorder to be determined.

To enable comparisons between the relative amounts of disorder detected by each technique to be made, the weighted $R_{Technique}$ values were converted to technique disorder scores ($D_{Technique}$). It is important to note that the $D_{Technique}$ values are normalised estimates of the likelihood of disorder being present as determined by observed response changes using the given technique and should not be considered as absolute values for the amount of disorder present. $D_{Technique}$ values were allocated a maximum value of 10, the higher the value the greater the relative amount of disorder detected by the given technique.

When comparing $D_{Technique}$ values between different comminution processes, it may be advantageous to also quote the observed magnitude of certain responses, *i*.e. the size of the T_g and ΔH_c responses from the DSC response analysis, or the size of M_{xtal} (%) and ΔM_{MAX1} responses from the GVS analyses. For example, the comminution of loperamide HCl by the three different comminution processes (Mill-A, Mill-B and JM-A) resulted in material with differing D_{DSC} values, 7.0, 4.5 and 3.8 and values for ΔH_c of 60.7, 11.1 and 8.0 J/g respectively. Therefore, the high frequency ball-milled sample contained more disorder than the low frequency ball-milled or jet-milled materials as indicated by the D_{DSC} values and verified by the magnitudes of the recrystallisation enthalpies.

Though disorder could be detected to some degree in most of the comminuted materials by XRPD analysis alone, it is important to note that observed changes in the XRPD responses may not necessarily be completely due to the presence of disorder. The presence of microcrystalline material may also result in similar changes and lead to D_{XRPD} values between 3 and 7 being obtained. Therefore, relying on only one technique such as XRPD to define and discriminate the presence of disorder as a consequence of a comminution process may not be sufficient, but with the addition of the R_{DSC} and R_{GVS} values the presence of disorder could be further verified and the solid-state phase present confirmed (Figure 7.6).

The process of determining the relative amount of disorder as a consequence of a defined comminution process, was referred to as process disorder analysis (PDA), and involved combining either the individual technique RDS values of the three techniques,

R_{XRPD}, R_{DSC} and R_{GVS} to give an overall process response disorder score (P_{RDS}) or the use of $D_{Technique}$ scores to give an overall process disorder score (D_{Pro}).

The P_{RDS} values were scored out of 100, the higher the value the greater the relative degree of disorder present. These calculated P_{RDS} values for the comminuted materials (Table 7-15) generally correlated well with the initial qualitative CRA solid-state phase and the literature PID classifications (Table 6-25). However, there were some exceptions that could be attributed to the increased resolution power of the RDA and PDA processes to discriminate the disorder within the comminuted materials. For example, high frequency ball-milled γ-indomethacin had initially been classified as being disordered by the CRA process and the PID literature review but the combined XRPD, DSC and GVS RDS values obtained using the PDA process produced a P_{RDS} value of only 58. This suggested that although there was some disorder present in the sample, the material was not completely disordered. Though γ-indomethacin does form an amorphous material when subjected to a mechanical process, the degree of disorder induced is dependent upon the comminution process and the relative operating conditions employed. For example, Wildfong *et al.* (2006)[160] cryogenically milled indomethacin for 3 h to generate amorphous γ-indomethacin, while Chieng *et al.* (2009)[212] ball-milled for only 60 min in a 25 mL volume stainless-steel milling jar containing two 12 mm diameter stainless-steel balls and at a milling frequency of 30 Hz to generate material that appeared predominately disordered. In both cases the degree of disorder present was assessed based on qualitative analysis of the XRPD and DSC data, *i.e.* the presence of an amorphous XRPD "halo" and a glass transition in the DSC thermogram[160, 212].

For other materials such as ball-milled caffeine the increased resolution power of the RDA process enabled the degree of disorder present to be better defined. In addition the better discrimination power associated with this factor allowed the effects of the different comminution processes to generate PID to be determined. The CRA values suggested the material derived from both the ball-milling processes for caffeine was predominately crystalline with only a small amount of disorder induced in the samples (Table 6-25), which was in agreement with observations from the literature[217,269]. However, the degree of PID as a result of these two processes could not be distinguished, but by using the RDA and PDA approaches the calculated P_{RDS} values for these comminuted materials indicated that different levels of disorder were present but

the overall the amount of disorder present was low. The high frequency ball-milled sample generated material having a P_{RDS} value of 39, confirming the presence of some disorder. The low frequency ball-milled sample had less disorder present with a calculated P_{RDS} value of only 22, hence this material was classified as being crystalline (Table 7-15).

The total amount of disorder present (D_{Pro}) in a material as a consequence of a given pharmaceutical process was calculated by two different approaches to investigate the effect of scaling of the individual technique contributions to the overall process disorder score.

In the first approach the D_{Pro} values were calculated using process P_{RDS} values that were weighted with respect to the number of response contributions of the individual techniques. In the second approach the D_{Pro} values were calculated by averaging the individual technique disorder scores, D_{XRPD}, D_{DSC} and D_{GVS}. In this approach the individual technique contributions were treated equally.

When comparing the calculated D_{Pro} values by the two different approaches for the same material, it was observed that the weighted approach appeared to provide a better discrimination between the comminution processes for materials containing higher degrees of disorder (Table 7-16 and Figure 7-7).

As with the CRA approach, the PDA process also differentiated between the comminuted materials on the basis of the solid-state phase present. However, the PDA process has the additional advantage in that the materials could also be ranked in accordance to their D_{Pro} or P_{RDS} values, which appeared to reflect the relative degree of disorder present (Table 7-16 and Figure 7-7). Based on the D_{Pro} or P_{RDS} values, the materials were ranked from highest to lowest with respect to the general degree of disorder determined across all the comminution processes: salbutamol sulphate > loperamide HCl > γ-indomethacin > sulfamerazine > caffeine > sulfadiazine > acetylsalicylic acid > phenacetin > acetaminophen > methyl paraben. This order also reflected the general susceptibility of the materials to PID by mechanical comminution processes.

Of all the comminution processes, high frequency ball-milling appeared to generate the greatest level disorder based on the magnitude of the P_{RDS} and D_{Pro} values, followed by low frequency ball-milling and then jet-milling.

The validity and verification of the novel analytical approach to determine the relative degree of disorder present in materials as a consequence of a mechanical comminution process has been successfully demonstrated here through its application in characterising the resulting comminuted materials from the three different milling and micronisation processes. It has also been successfully shown that this approach will allow materials of differing chemical and crystallographic properties to be ranked according to the relative level of disorder being present, and that the approach can differentiate the effectiveness of different comminution processes in generating PID.

8.2 Recommendations for future work

It is important to note that this study should be viewed as developing the first iteration of the CRA, RDA and PDA processes and it is anticipated that as the understanding of the relationship of technique responses with observed disorder develops, so a better knowledge of the CRA and RDA limits for the individual technique responses will evolve. In order to provide a starting point for future work, an analytical protocol has been developed (Appendix 9) that outlines the general process for defining disorder in a material as a consequence of a pharmaceutical process or unit operation. It is envisaged that this protocol will assist future researchers when investigating and expanding the novel approaches described in this thesis.

Currently the described RDA and PDA approaches employed data derived from the primary disorder detection techniques of XRPD, DSC and GVS but in future studies data from other analytical techniques could also be incorporated such as those from Raman spectroscopy, solid state NMR, dynamic mechanical analysis, inverse gas chromatography and solution calorimetry. However it should be noted that further improvements could also be made to the current RDA and PDA methods by investigating the potential enhancement in detecting disorder using the current primary disorder detection techniques of XRPD, DSC and GVS. For example, the use of transmission or capillary XRPD may reduce some preferred orientation effects. Nevertheless, some care will always be required in data interpretation since a grinding of the material is typically required as part of the sample preparation for these methods. The use of high speed DSC could also be applied to increase the sensitivity for disorder detection. However such use could be at the expense of thermal resolution and such events as the loss of volatiles may be lost. Additionally modulated DSC (MDSC) could possibly be used but this type of analysis typically requires long run times and very

small heating rates. Accordingly, any transient solid-state forms or phases could be lost during the period of analysis and the stability of the material should be investigated prior to performing MDSC analysis. Improvements to the GVS analysis method could also be made by investigating the potential use of %RH ramps instead of %RH steps etc. Should any technique be modified however, it is important to note that the sensitivities and instrumental variances could change, hence modification to the CRA and RDA response criteria maybe warranted.

To further validate the analytical CRA, RDA and PDA approaches using the same standardised ball-milling and micronisation comminution processes as described in this thesis, other study materials should also be investigated such as: (i) materials that encompass the amorphous-crystalline continuum, (ii) different polymorphic forms of a given material, (iii) different crystal morphologies and particle sizes of a given material, (iv) materials that exhibit melt-degradation and (v) different salts of a given material. The latter would enable the investigation of the influence of a counter-ion on the stability of the crystal lattice to restrict the susceptibility for PID during mechanical processing[253]. Additionally, verification of the benefits of the RDA/PDA processes could be investigated for a given material by comparing the calculated relative disorder values using the RDA/PDA processes with those obtained using a more traditional approach that employs standard mixtures and calibration curves.

It is also envisaged that the current set of materials might be used as a standard model set to investigate different pharmaceutical unit operations or changes in operating parameters. Alternatively a subset of materials that encompasses the amorphous-crystalline continuum could be used. For example acetaminophen (crystalline), sulfadiazine and caffeine (some disorder) and loperamide HCl (disordered). Some examples of the different ball milling conditions that could be investigated are: size of the milling balls, the number of balls, different charge ratios, different vibration frequencies and mill duration. While different micronisation conditions may include different feed rates and pressure differentials between the feed and grind pressures.

The CRA, RDA and PDA processes could also be applied to investigating and monitoring stability samples post-comminution. Samples at different stability time-points could be compared to either the responses of the input material or to the responses of the comminuted material at time zero (*i.e.* directly after milling). This would result in a single value being obtained at each time point and set of conditions

that represent all the results from the stability tests not just the result from a single technique. Changes in this value at different time points could then be used to measure the change in stability of the solid-state phase.

By using the RDA and PDA processes the relative amount of disorder present in a material as a consequence of mechanical comminution can be estimated. However, it is also important to be able to relate the amount of disorder to any effect on product performance. For example, a future study may involve using an API with different levels of calculated disorder to formulate a tablet and then determine whether any changes with respect to performance parameters occur (e.g. disintegration, dissolution, and bioavailability).

The CRA, RDA and PDA processes should be applied to a much larger number of materials that encompass the whole range of the amorphous-crystalline continuum with a view to establishing any correlations between the level of observed PID and the inherent and derived crystalline properties. It might then be possible ultimately predict the propensity for PID that might be induced by a given pharmaceutical process. Such predictive capacity might not only lead to a better understanding of the crystalline state but also that of the disordered state. This could help to minimise and mitigate the risk of process induced phase transformations during pharmaceutical manufacturing, and assist in candidate drug selection.

8.3 Concluding remarks

A relative estimate of the degree of PID inadvertently generated as a consequence of a defined comminution process could be obtained by application of the novel analytical approaches as developed in the current study. These approaches utilised the combined differences between the individual technique responses for the comminuted materials to those of the respective inputs allowing changes from multiple techniques to be incorporated into a singular value to define a certain property such as the presence of disorder or amorphous character.

This approach provides the developmental pharmaceutical scientist with a more consistent and efficient means to define and quantify the presence of PID without the need of standard mixtures and calibration curves and can lead to better understanding of the generation of PID and the comminution process, allowing appropriate mitigation strategies to be implemented.

APPENDIX 1. Risk statement codes

Risk Statement codes[234]- Risk statement codes for materials to be excluded from selection coloured red

R1 Explosive when dry.
R2 Risk of explosion by shock, friction, fire or other source of ignition.
R3 Extreme risk of explosion by shock, friction, fire or other sources of ignition.
R4 Forms very sensitive explosive metallic compounds.
R5 Heating may cause an explosion.
R6 Explosive with or without contact with air.
R7 May cause fire.
R8 Contact with combustible material may cause fire.
R9 Explosive when mixed with combustible material.
R10 Flammable.
R11 Highly flammable.
R12 Extremely flammable.
R13 Extremely flammable liquefied gas
R14 Reacts violently with water.
R15 Contact with water liberates extremely flammable gases.
R16 Explosive when mixed with oxidizing substances.
R17 Spontaneously flammable in air.
R18 In use, may form inflammable/explosive vapour-air mixture.
R19 May form explosive peroxides.
R20 Harmful by inhalation.
R21 Harmful in contact with skin.
R22 Harmful if swallowed.
R23 Toxic by inhalation.
R24 Toxic in contact with skin.
R25 Toxic if swallowed.
R26 Very toxic by inhalation.
R27 Very toxic in contact with skin.
R28 Very toxic if swallowed.
R29 Contact with water liberates toxic gas.
R30 Can become highly flammable in use.
R31 Contact with acids liberates toxic gas.
R32 Contact with acid liberates very toxic gas.
R33 Danger of cumulative effects.
R34 Causes burns.
R35 Causes severe burns.
R36 Irritating to eyes.
R37 Irritating to respiratory system.
R38 Irritating to skin.
R39 Danger of very serious irreversible effects.
R40 Limited evidence of a carcinogenic effect.
R41 Risk of serious damage to the eyes.
R42 May cause sensitization by inhalation.
R43 May cause sensitization by skin contact.
R44 Risk of explosion if heated under confinement.
R45 May cause cancer.
R46 May cause heritable genetic damage.
R47 May cause birth defects
R48 Danger of serious damage to health by prolonged exposure.
R49 May cause cancer by inhalation.
R50 Very toxic to aquatic organisms.
R51 Toxic to aquatic organisms.
R52 Harmful to aquatic organisms.
R53 May cause long-term adverse effects in the aquatic environment.
R54 Toxic to flora.
R55 Toxic to fauna.
R56 Toxic to soil organisms.
R57 Toxic to bees.
R58 May cause long-term adverse effects in the environment.
R59 Dangerous to the ozone layer.
R60 May impair fertility.
R61 May cause harm to the unborn child.
R62 Risk of impaired fertility.
R63 Possible risk of harm to the unborn child.
R64 May cause harm to breastfed babies.
R65 Harmful: may cause lung damage if swallowed.
R66 Repeated exposure may cause skin dryness or cracking.
R67 Vapours may cause drowsiness and dizziness.
R68 Possible risk of irreversible effects.

R20/21: Harmful by inhalation and in contact with skin.
R20/21/22: Harmful by inhalation, in contact with skin and if swallowed.
R20/22: Harmful by inhalation and if swallowed.
R21/22: Harmful in contact with skin and if swallowed.
R23/24/25: Toxic by inhalation, in contact with skin and if swallowed.
R23/25: Toxic by inhalation and if swallowed.
R26/27/28: Very toxic by inhalation, in contact with skin and if swallowed.
R26/28: Very toxic by inhalation and if swallowed.
R36/37: Irritating to eyes and respiratory system.
R36/37/38: Irritating to eyes, respiratory system and skin.
R36/38: Irritating to eyes and skin.
R37/38: Irritating to respiratory system and skin.
R42/43: May cause sensitization by inhalation and skin contact.
R48/22: Harmful: danger of serious damage to health by prolonged exposure if swallowed.
R50/53: Very toxic to aquatic organisms may cause long-term adverse effects in the aquatic environment.
R51/53: Toxic to aquatic organisms, may cause long-term adverse effects in the aquatic environment.
R52/53: Harmful to aquatic organisms may cause long-term adverse effects in the aquatic environment.

APPENDIX 2. PCA model data for final material selection

ID	CMPD	Mw	Z	CCV	CD	Mv	Mrv	MrR	Par	RI	ST	Pz	TPSA	RB	LogP	Sol	HA	HD	Tm
C1	Acetaminophen	151.17	4	651.428	1.541	162.86	98.10	42	326	1.618	52.8	1.68E-23	49.3	1	0.54	4.5	**2**	**2**	171
C140	Methyl paraben	152.15	12	2126.445	1.426	177.20	106.70	40	327.1	1.547	45.7	1.58E-23	46.6	2	1.97	1.3	**2**	**1**	127
C69	Phenacetin	179.22	4	961.356	1.238	240.34	144.77	52	407.4	1.548	39	2.05E-23	38.3	3	1.5	1.3	**2**	**1**	135
C39	Naproxen	230.26	2	604.172	1.266	302.09	181.88	67	504.6	1.608	47.4	2.64E-23	46.5	3	3.26	0.093	3	**1**	152
C33	Acetylsalicylic acid	180.16	4	854.229	1.457	213.56	123.65	45	370.9	1.550	49.8	1.77E-23	63.6	3	1.39	2.7	**3**	**1**	136
C88	Caffeine	194.19	20	4277.013	1.448	213.85	134.11	50	364.5	1.679	55.7	2.00E-23	58.4	0	0.11	21.5	**3**	**0**	234
C86	Sulfathiazole	255.32	8	2116.277	1.603	264.53	159.28	63	493.7	1.704	83	2.52E-23	121.7	3	0.69	0.56	**4**	**2**	201
C87	Sulfadiazine	250.30	4	1098.375	1.558	274.59	160.65	63	504.4	1.679	82.6	2.50E-23	106.4	3	-0.05	0.45	**5**	**2**	251
C118	Sulfamethoxazole	253.28	8	2253.793	1.413	281.72	179.25	62	502.3	1.641	70.9	2.48E-23	106.6	3	1.03	0.82	**4**	**2**	170
C54	Sulfamerazine	264.31	8	2606.485	1.347	325.81	196.22	68	542.6	1.660	75.4	2.69E-23	106.4	3	0.38	0.54	**5**	**2**	236
C24	Salbutamol sulphate	337.39	8	2900.802	1.321	362.60	255.40	68	550	1.566	49.2	2.69E-23	72.7	5	0.19	33.1	**6**	**5**	198
C11	γ-Indomethacin	357.79	2	847.865	1.401	423.93	255.38	95	707.6	1.619	47.4	3.75E-23	68.5	4	4.3	0.016	**5**	**1**	160
C34	Ursodeoxycholic acid	392.58	8	4352.173	1.198	544.02	327.69	110	905.9	1.543	46	4.35E-23	77.8	4	3.39	0.031	4	**3**	203
C14	Loperamide hydrochloride	513.51	4	2627	1.298	656.75	395.62	138	1067.1	1.600	49.8	5.45E-23	43.8	7	5.62	0.0056	**5**	**1**	234

Xvar ID	Property
CMPD	Compound name/ID
Mw	Molar weight (M_w) (g/mol)
CCV	Calculated (unit) cell volume (CCV)
Z	Z
CD	Cell Density (g/cm³)
Mv	Molecular volume
Mrv	Molar Volume (cm³)
MrR	Molar refractivity * (cm³)
Par	Parachor * (cm³)
RI	Index of refraction*

Xvar ID	Property
ST	Surface tension* (dyne/cm)
Pz	Polarizability * (cm³)
TPSA	Topological Polar Surface Area*
RB	No. rotatable bonds*
LogP	LogP*
Sol	Solubility * (mg/ml)
HA	H-bond acceptors*
HD	H-bond donors*
Tm	Melting temperature (°C)
PID	Literature PID

APPENDIX 3. Supplier, therapeutic classification and use for the final 10 selected materials

Bulk material	Supplier	Batch No. & Purity (% w/w)	Therapeutic classification and use
γ-Indomethacin 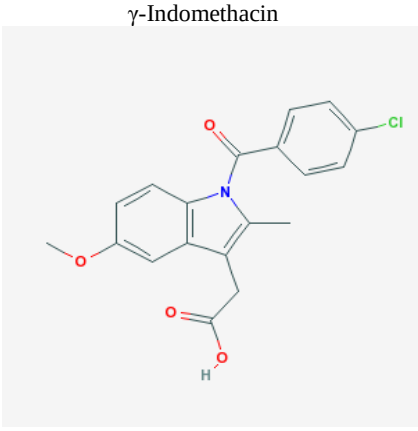	Sigma-Aldrich	115K0689 (99.0%)	A non-steroidal anti-inflammatory agent (NSAID) with analgesic, antipyretic, and platelet-inhibitory actions. Used in the treatment of chronic arthritic conditions, pain and inflammation
Salbutamol sulphate 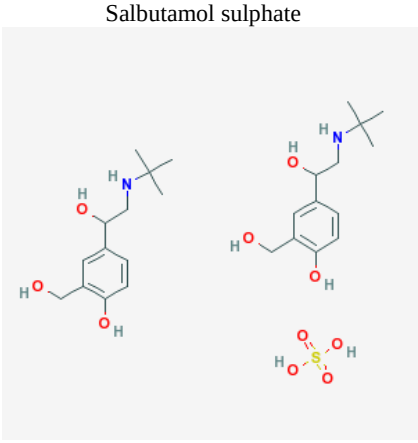	GSK (Ware)	R355888 (99.0%)	A short-acting beta-2 adrenergic agonist that is used as a bronchodilator agent to treat asthma.
Loperamide HCl 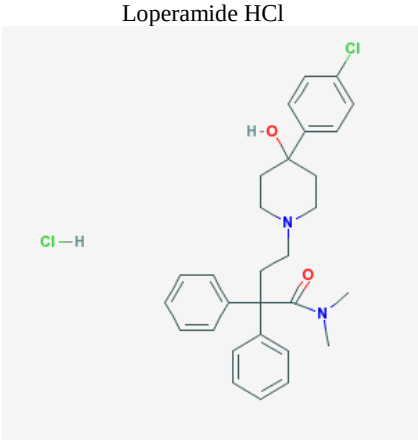	MP Biomedical	7585E (98%)	Gastrointestinal agent – antidiarrheal

Bulk material	Supplier	Batch No. & Purity (% w/w)	Therapeutic classification and use
Caffeine 	Sigma-Aldrich	1378801 (>99.0%)	A central nervous system (CNS) stimulant and a phosphodiesterase inhibitor.
Sulfamerazine 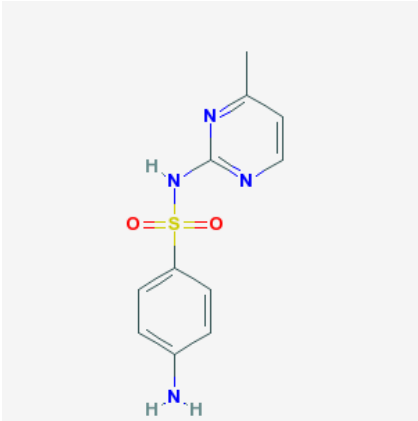	Sigma-Aldrich	068K1130 (>99.0%)	Anti-infective agent used as an antibacterial agent
Sulfadiazine 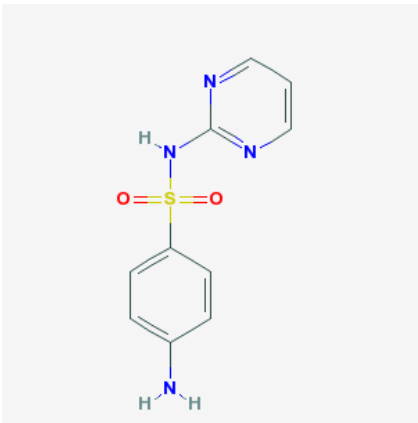	MP Biomedical	3423E (99.0%)	Anti-infective and antiprotozoal agent
Methyl paraben 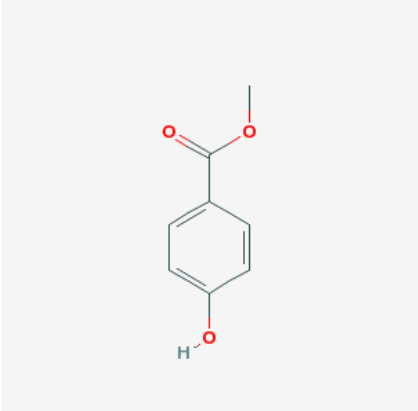	Fisher Scientific	A0257407 (99.0%)	Pharmaceutical excipient used as a preservative

Bulk material	Supplier	Batch No. & Purity (% w/w)	Therapeutic classification and use
Acetaminophen 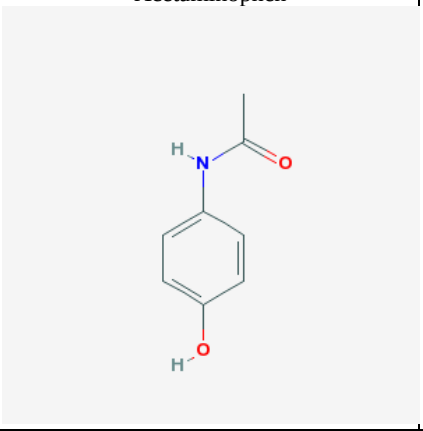	Sigma-Aldrich	1272987 (99.0%)	Analgesic antipyretic derivative of acetanilide. It has weak anti-inflammatory properties and is used as a common analgesic
Phenacetin 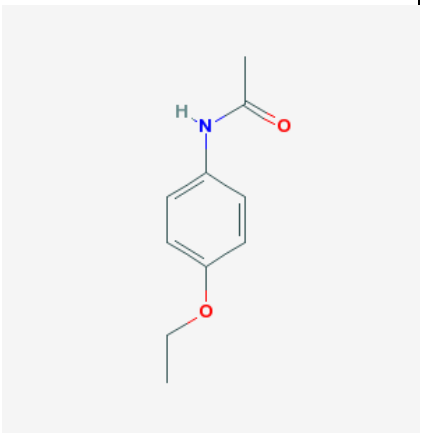	Sigma-Aldrich	S4263199 (>98%)	Formerly used as an analgesic
Acetylsalicylic acid 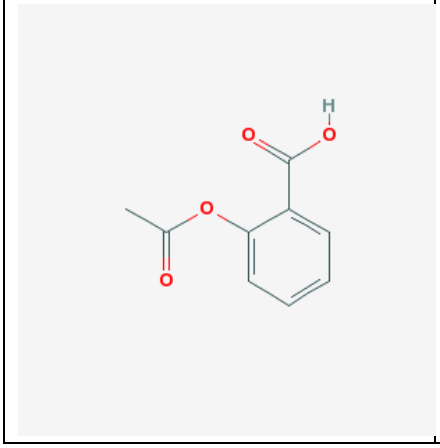	Sigma-Aldrich	048K0015 (>99.0%)	A NSAID analgesic used in the treatment of mild to moderate pain. It has anti-inflammatory and antipyretic properties and acts as an inhibitor of cyclooxygenase and platelet aggregation

APPENDIX 4. Experimental Equipment

Technique/Process	Instrument	Supplier	Serial Number
XRPD	CubiX PRO Fast diffractometer (PW3800/00 with a Cu LFF X-ray tube (PW3373/00)	PANalytical, Almelo, Netherlands	DY753
TGA	Q500 TGA	TA Instruments (Crawley, UK)	0500-0057
DSC	Q2000 DSC	TA Instruments (Crawley, UK)	Q2000-060
PLM	Axioplan2 microscope	Zeiss	35091-65
SEM	FEI Quanta 200	FEI	XTE 13/D7513
SEM coater	Au/Pd sputter coater model 108A	Agar	A2096
GVS	DVS-1 vapour sorption instrument	Surface Measurement Systems (SMS), Alperton, UK	010726
PSA	HELOS (system H0933)	Sympatec	56
HPLC	1100 series HPLC	Aligent	
FTIR	Spectrum One FT-IR Spectrometer	Perkin Elmer	58880
Sieving	Retsch sieve shaker	Retsch GmbH, Rheinische Straße, Haan, Germany	9 0503 019
Ball-mill	MM301,	Retsch	125041013M
Microniser	McOne microniser	JetPharma	19000C0418/08
Mixer	REAX Vortex Top Mixer	Heidolph	N/A
Mixer	Spiramix 5	Denley	N/A
Balance	MC5 microbalance (6 place)	Sartorius	13110100
Balance	ME 215S balance 5 place	Sartorius	13507552
RH meter	Portable relative humidity meter, ms1	Novasina	0105013/2
Antistatic	Sentry ionizing air blower	SIMCO Industrial static control	N/A
Antistatic	Zerostat 3 electrostatic discharge gun	Zerostat	N/A

APPENDIX 5. Appropriate settings for the determination of the background (baseline) in the XRPD Data treatment process.

A typical XRPD pattern for a crystalline material will consist of two principal components; the crystalline peaks and the background component (Figure A4-1). However, it is important to note that the size of the background component will depend on the amount of amorphous or disorder and microcrystalline material present as well as any background scattering due to the instrument and sample preparation etc.

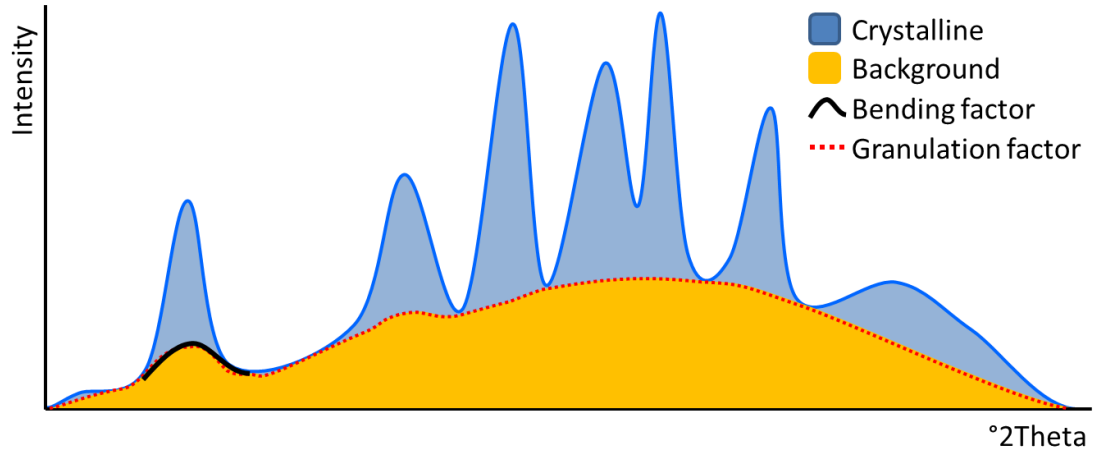

Figure A4-1 Two components (crystalline and background) of an XRPD diffractogram depicting bending and granulation factors

To determine appropriately the crystalline attributes such as peak position, relative intensity and area a background or baseline determination need to be performed. This background search can be performed using proprietary software such as PANalytical's X'Pert HighScore Plus (version 3.0) software. But before the background can be determined appropriate data analysis settings typically have to be selected. For the X'Pert HighScore Plus software used in this research, arbitrary settings for granularity and bending factor are first selected before performing the background determination for a given XRPD diffractogram[287].

Granularity refers to the size of the intervals used during the background determination and should be of a sufficient size such that the baseline follows that expected for the crystalline component (red dashed line Figure A4-1). The larger the granularity value (1-100), the wider the size of the interval and the broader the baseline[287]. The bending factor adjusts the curvature of the background (black curve in Figure A4-1). The higher the bending factor value, the greater the curvature.

Choosing a too low a granularity value may cause an under estimation of the crystalline peak responses and could lead to an over estimation of the background contribution[287]. This effect is illustrated by the size of the red arrow line in Figure A4-2. As the amount of disorder or amorphous content increases, the potential over estimation of the background increases as a result of selecting a lower granularity factor.

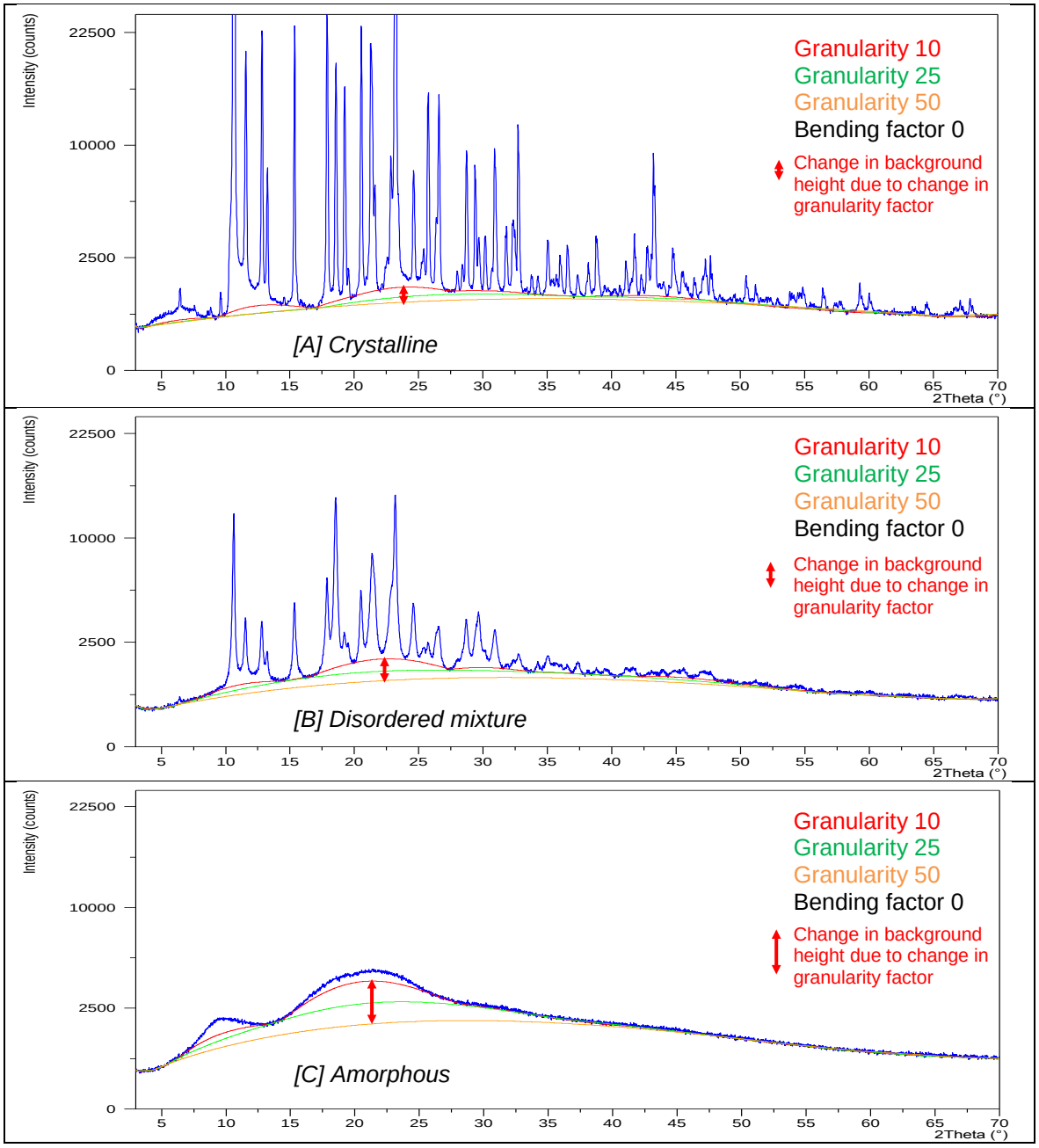

Figure A4-2 XRPD diffractograms depicting the effect of the granularity value in determining the background for [A] crystalline, [B] a disordered mixture and [C] an amorphous material

The most important factor when selecting the appropriate settings is consistency. The same settings need to be applied when comparing results for different materials as well as different processing conditions. This will ensure that the integrated areas and

observed responses are reported consistently allowing them to be utilized for comparative analysis purposes.

For the purposes of this research a granularity value of 25 with a bending factor of 0 have been selected as appropriate settings to determine the background (baseline) for the acquired XRPD diffractograms.

Once the background has been determined the sum of net intensity values for the crystalline peaks, the background (disorder, microcrystalline and instrument components) and the total observed signals can be obtained from the object inspector panel and reported (Table A4-1).

Table A4-1 Sum of net intensity values and calculated XRPD components based on different granularity value settings.

		Crystalline		Crystalline/amorphous		Mostly amorphous	
Granularity		10	25	10	25	10	25
Sum of net intensity	Peaks (X)	5005652	5130720	1459524	1791419	402622	986836
	Background (B)	4368972	4243903	5532350	5200455	5891151	5306937
	Observed (T)	9374623	9374623	6991874	6991874	6293774	6293774
Ratio X/T (Crystalline)		0.53	0.55	0.21	0.26	0.06	0.16
Ratio B/T (Background)		0.47	0.45	0.79	0.74	0.94	0.84
Ratio X/B		1.15	1.21	0.26	0.34	0.07	0.19
Ratio B/X		0.87	0.83	3.79	2.90	14.63	5.38

Differences in the net intensity ratios can be used to provide an estimate of the reduction of crystallinity in a material as a result of a process. For example in Table A4-1, as the amount of amorphous material increases, so do the ratios for B/T and B/X, while the ratios for X/T and X/B decrease (Table A4-1). It is important to note that the calculated values for the components of the XRPD diffractograms should be treated as gross estimates and not absolute values. As the amount of background scattering due to the instrument and other sample affects have not been accounted for or subtracted from the signals. Hence, the individual contributions of the different components maybe over or under exaggerated which could result in erroneously over or under integrating of the total sample diffraction signal.

APPENDIX 6. XRPD response variation investigation

The amount of apparent variation between replicates observed in the XRPD peak responses as a result of sample preparation, acquisition and instrument parameters was investigated using the procedure outlined below and the XRPD data obtained for three replicates for sulfamerazine as a worked example.

The overlay of the three XRPD replicates for sulfamerazine in Figure A6-1 shows that there is very little differences between them, with only some minor variation in peak height intensity. On closer inspection of the reported data and using the process outlined below, the amount of variation in the XRPD responses can be quantified. It can be seen that there is only a small amount of variation in the XRPD responses as indicated by the low RSD's (< 15%) and the small average range for the peak position values (0.01 °2Th) .

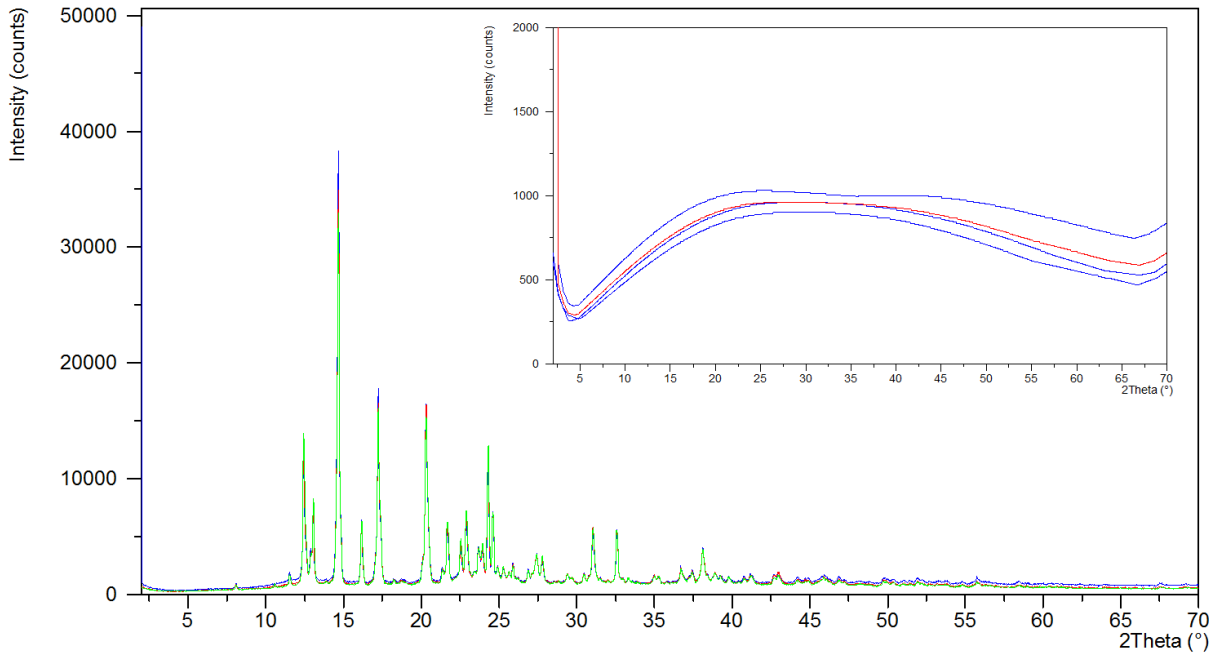

Figure A6-1. XRPD diffractograms for the three replicates of the input sulfamerazine material. *The Insert shows the determined background profiles for the three replicates in blue and that for the calculated average XRPD pattern in red*

1. For each replicate and calculated average XRPD pattern, the XRPD responses were tabulated using the methods described in Section 3.2.1 and 3.2.2 (Table A6-1 to A6-4). The MIP is highlighted in yellow.

Table A6- 1 Reported XRPD responses for sulfamerazine input material replicate 1

Pos. [°2Th.]	Rel. Int. [%]	Height [cts]	Backgr.[cts]	d-spacing [Å]	FWHM Left [°2Th.]	Area [cts*°2Th.]
11.55	4.4	1611.22	704.05	7.66255	0.026705	28.6851
12.42	28.7	10586.58	744.64	7.12668	0.0984	1027.604
12.91	11.8	4371.555	766.7	6.85568	0.164542	479.5366
13.06	17.0	6268.22	773.25	6.77777	0.07872	486.7482
14.67	100.0	36914.24	839.06	6.03805	0.07872	2866.514
16.15	14.9	5504.965	891.57	5.48806	0.0984	534.3486
17.23	45.6	16824.93	924.63	5.14623	0.07872	1306.512
20.29	41.2	15198.74	992.42	4.37681	0.11808	1770.35
21.39	3.6	1312.238	1006.93	4.16403	0.0984	127.3746
21.66	11.6	4279.237	1010.59	4.10364	0.15744	664.594
22.52	8.3	3058.607	1018.33	3.94778	0.0984	296.8888
22.87	13.8	5096.922	1020.75	3.88893	0.17712	890.5343
23.67	8.3	3068.6	1024.84	3.75855	0.11808	357.4305
23.94	8.5	3145.375	1025.83	3.71681	0.0984	305.3111
24.29	31.6	11681.03	1026.76	3.66369	0.11808	1360.607
24.59	16.6	6111.35	1027.3	3.61994	0.11808	711.8501
24.91	5.8	2133.998	1027.72	3.57408	0.251166	273.2116
25.28	5.1	1872.744	1027.83	3.52327	0.140249	175.1009
25.64	3.8	1403.071	1027.78	3.47457	0.1263	118.1387
25.89	4.5	1651.842	1027.57	3.44181	0.11808	192.4066
26.87	3.2	1167.077	1026.03	3.31797	0.11808	135.9411
27.44	6.8	2522.536	1024.66	3.25004	0.11808	293.825
27.78	5.4	1978.266	1023.78	3.21199	0.13776	268.8331
29.40	2.1	776.1166	1018.54	3.03804	0.15744	120.5361
31.02	12.0	4441.464	1012.66	2.88318	0.13776	603.5654
32.56	12.2	4490.159	1006.82	2.75036	0.13776	610.1827
35.10	1.3	482.5252	996.98	2.55672	0.47232	224.8181
36.73	3.5	1279.426	997.39	2.44697	0.23616	298.0551
37.44	2.8	1046.458	998.72	2.40192	0.15744	162.5218
38.10	8.1	2991.712	999.75	2.36172	0.11808	348.4746
38.90	4.0	1469.809	1000.68	2.31552	0.125553	123.0258
39.79	2.9	1063.974	1001.2	2.26554	0.048895	34.682
41.19	2.1	791.7665	1000.75	2.19166	0.23616	184.4499
43.03	2.0	751.8278	997.2	2.10226	0.55104	408.6736
45.93	1.7	617.2333	983.98	1.97578	0.47232	287.5814
49.88	1.2	443.5289	951.33	1.82843	0.62976	275.532

Table A6- 2 Reported XRPD responses for sulfamerazine input material replicate 2

Pos. [°2Th.]	Rel. Int. [%]	Height [cts]	Backgr.[cts]	d-spacing [Å]	FWHM Left [°2Th.]	Area [cts*°2Th.]
11.50	2.0	659.4543	594.68	7.6949	0.09	39.5673
12.42	33.6	11381.92	635.14	7.12426	0.0984	1104.805
13.07	19.7	6660.609	662.14	6.77608	0.07872	517.2185
14.67	100.0	33849.89	725.28	6.03781	0.0984	3285.696
16.15	15.7	5306.775	777.22	5.48944	0.13776	721.1554
17.23	46.3	15668.75	811.36	5.14647	0.0984	1520.913
18.86	0.9	304.0215	855.8	4.70567	0.7872	236.0829
20.29	44.6	15092.89	887.8	4.37626	0.11808	1758.02
21.39	5.8	1961.637	907.92	4.15351	0.124368	162.643
21.68	15.0	5078.192	912.58	4.0995	0.15744	788.6771
22.53	9.9	3334.388	924.74	3.94678	0.13776	453.1211
22.87	16.5	5592.64	929.13	3.88783	0.17712	977.146
23.68	8.9	3016.535	938.05	3.75665	0.11808	351.366
23.95	9.8	3326.373	940.59	3.71633	0.0984	322.8799
24.29	34.4	11639.44	943.64	3.66411	0.13776	1581.723
24.59	17.8	6027.955	946.06	3.61968	0.11808	702.1362
24.92	6.3	2117.869	948.49	3.57317	0.251166	354.6239
25.29	3.8	1276.458	950.84	3.52203	0.15744	198.2424
25.89	4.8	1636.297	954.2	3.44122	0.11808	190.5958
27.01	3.9	1322.605	958.63	3.30123	0.310271	273.5772
27.45	7.2	2431.852	959.82	3.24874	0.13776	330.4724
27.78	6.4	2175.41	960.55	3.2116	0.13776	295.6237
29.41	2.5	845.9543	961.97	3.03742	0.15744	131.3823
30.48	4.0	1346.809	961.35	2.93286	0.043224	38.8097
31.02	14.0	4753.514	960.64	2.88322	0.15744	738.2524
32.56	13.3	4486.966	957.32	2.7505	0.13776	609.7487
34.97	1.8	606.8247	948.48	2.56606	0.47232	282.7318
36.71	4.0	1349.48	939.37	2.44845	0.1968	261.9791
37.45	3.1	1042.888	934.73	2.40152	0.15744	161.9674
38.10	8.8	2971.108	930.28	2.3617	0.0984	288.3956
38.90	4.7	1575.848	924.44	2.31528	0.179073	188.1279
39.27	3.5	1167.17	921.54	2.29451	0.043121	33.5528
39.71	1.1	376.7007	917.9	2.26986	0.09	22.602
41.20	2.1	704.2089	904.44	2.19092	0.1968	136.7104
43.01	2.9	973.2185	885.55	2.10319	0.47232	453.442
45.91	1.8	615.6275	849.02	1.97666	0.3936	239.0276
49.85	1.2	403.0612	787.87	1.82923	0.62976	250.3923
55.78	1.2	413.67	677.66	1.64798	0.31488	128.4914

Table A6- 3 Reported XRPD responses for sulfamerazine input material replicate 3

Pos. [°2Th.]	Rel. Int. [%]	Height [cts]	Backgr.[cts]	d-spacing [Å]	FWHM Left [°2Th.]	Area [cts*°2Th.]
8.09	1.3	413.1377	402.41	10.92409	0.15744	64.163
10.54	0.4	139.7935	509.63	8.39351	0.09	8.3876
11.54	3.5	1110.646	551.79	7.66657	0.0984	107.8068
12.42	41.3	13110.75	587.5	7.12555	0.11808	1527.14
13.07	23.5	7473.25	612.84	6.77626	0.0984	725.4035
14.67	100.0	31778.25	672.5	6.03936	0.11808	3701.53
16.15	17.3	5486.641	722.5	5.48954	0.13776	745.5979
17.23	48.0	15252.43	755.52	5.14761	0.0984	1480.502
18.26	1.4	438.2874	784.06	4.85859	0.09	26.2972
18.82	0.9	286.1457	798.17	4.71526	0.09	17.1687
20.29	44.0	13994.57	830.39	4.37735	0.15744	2173.45
21.39	5.8	1850.721	850.17	4.15424	0.124368	43.3319
21.66	16.1	5112.313	854.47	4.10357	0.15744	793.9763
22.53	12.1	3845.608	866.68	3.94647	0.13776	522.5924
22.88	19.7	6251.825	870.97	3.88723	0.15744	970.9501
23.67	9.4	2996.792	879.44	3.75866	0.11808	349.0664
23.95	11.1	3520.581	882.03	3.71584	0.11808	410.0772
24.29	37.6	11954.42	884.95	3.66398	0.13776	1624.525
24.60	19.6	6214.698	887.29	3.61906	0.11808	723.888
24.93	6.8	2156.039	889.64	3.57212	0.205191	294.933
25.28	4.8	1527.005	891.79	3.52302	0.0984	148.2213
25.88	4.4	1403.039	894.96	3.44332	0.11808	163.4259
26.86	3.6	1130.408	898.8	3.31976	0.13776	153.6149
27.44	8.1	2575.802	900.37	3.25076	0.11808	300.0294
27.78	7.6	2416.496	901.14	3.21095	0.13776	328.3857
29.41	2.6	812.7604	902.66	3.03702	0.15744	126.2271
30.48	4.2	1333.836	902.28	2.93321	0.041027	36.4824
31.01	14.2	4498.134	901.73	2.88379	0.15744	698.5902
32.55	14.4	4563.358	898.91	2.75107	0.13776	620.13
35.00	3.5	1109.377	890.49	2.56402	0.058902	43.5629
35.29	2.1	673.8705	889.11	2.54353	0.15744	104.6566
36.70	4.3	1350.828	881.37	2.44874	0.15744	209.7925
37.44	3.2	1020.138	876.47	2.40209	0.15744	158.4343
38.10	9.3	2938.037	871.6	2.36199	0.11808	342.2226
38.90	4.9	1540.9	865.11	2.31536	0.158206	162.5194
39.24	3.6	1148.232	862.06	2.2959	0.049159	37.6305
39.79	3.5	1109.714	856.95	2.26548	0.040468	29.9385
41.22	2.4	754.9661	842.1	2.19021	0.1968	146.5641
43.02	2.2	709.0392	820.15	2.10277	0.47232	330.3556
45.93	1.9	612.5115	777.84	1.97602	0.3936	237.8178
55.79	1.3	426.4833	602.12	1.64792	0.31488	132.4714

Table A6- 4 Reported XRPD responses for the calculated average XRPD pattern for sulfamerazine

Pos. [°2Th.]	Rel. Int. [%]	Height [cts]	Backgr.[cts]	d-spacing [Å]	FWHM Left [°2Th.]	Area [cts*°2Th.]
8.10	1.2	405.1344	459.23	10.91562	0.09	24.3081
11.54	3.3	1120.206	620.49	7.66792	0.0984	108.7346
12.42	34.2	11688.55	658.53	7.12545	0.0984	1134.569
13.06	19.9	6790.498	685.22	6.77671	0.07872	527.3048
14.67	100.0	34175.29	747.45	6.03834	0.0984	3317.282
16.15	15.9	5437.88	798.47	5.48886	0.11808	633.4043
17.23	46.5	15903.38	831.57	5.14672	0.07872	1234.951
18.21	1.1	380.7452	858.29	4.87181	0.09	22.8447
18.86	0.9	304.9836	874.08	4.70643	0.7872	236.83
20.29	43.2	14764.93	903.93	4.37675	0.13776	2006.455
21.38	5.5	1892.509	921.94	4.1556	0.257816	325.2791
21.66	14.0	4790.505	925.98	4.10277	0.15744	743.9974
22.53	10.0	3412.075	936.61	3.94705	0.13776	463.6783
22.87	16.5	5629.656	940.27	3.88807	0.17712	983.6135
23.44	4.8	1627.458	945.49	3.79501	0.289979	314.6195
23.67	8.8	3002.981	947.36	3.75822	0.11808	349.7872
23.95	9.8	3336.417	949.4	3.71639	0.0984	323.8549
24.29	34.4	11756.52	951.7	3.66389	0.11808	1369.399
24.59	17.9	6102.972	953.46	3.61964	0.11808	710.8742
24.92	6.3	2153.381	955.19	3.57301	0.170874	245.3048
25.28	3.8	1305.947	956.75	3.52292	0.15744	202.8222
25.64	4.5	1539.023	958.12	3.47462	0.140838	144.5019
25.89	4.7	1595.155	958.9	3.44181	0.11808	185.8036
26.87	3.3	1133.139	961.12	3.31775	0.11808	131.988
27.44	7.4	2518.414	961.81	3.24998	0.13776	342.2356
27.78	6.4	2190.936	962.08	3.21149	0.13776	297.7336
29.41	2.4	811.759	961.8	3.03745	0.15744	126.0716
30.48	3.8	1289.838	960.68	2.93309	0.135736	116.7182
31.02	13.4	4576.854	959.91	2.88336	0.15744	710.8159
32.55	13.2	4507.283	957.08	2.7506	0.13776	612.5097
35.11	1.5	521.0271	950.35	2.55602	0.47232	242.7569
36.73	3.7	1263.529	944.47	2.44689	0.23616	294.3517
37.44	3.0	1032.032	941.36	2.40184	0.15744	160.2814
38.10	8.7	2985.395	938.2	2.3618	0.0984	289.7823
38.89	6.2	2101.917	934.02	2.31581	0.115523	161.8799
39.25	3.4	1145.406	931.95	2.2955	1.019054	778.1535
39.79	3.2	1077.258	928.65	2.2657	0.036529	26.2341
40.73	1.2	402.6698	922.29	2.21534	0.09	36.2403
41.20	2.1	729.3008	918.82	2.19102	0.1968	141.5816
43.02	2.3	799.256	903.49	2.1027	0.47232	372.3894
45.94	1.7	584.3146	872.25	1.97549	0.47232	272.2438
55.79	1.3	457.0247	723.88	1.64788	0.31488	141.958

2. For each replicate, the peak positions were aligned and compared to the calculated average XRPD pattern. Red indicates peaks that are absent with respect to the other replicates and the calculated average XRPD pattern. (Table A6-5)

Table A6-5 Alignment of peaks for 3 replicate XRPD samples of sulfamerazine and the calculated average XRPD pattern.

Replicate 1		Replicate 2		Replicate 3		Average XRPD	
Pos. [°2Th.]	Rel. Int. [%]	Pos. [°2Th.]	Rel. Int. [%]	Pos. [°2Th.]	Rel. Int. [%]	Pos. [°2Th.]	Rel. Int. [%]
				8.09	1.3	8.10	1.2
				10.54	0.4		
11.55	4.4	11.50	2.0	11.54	3.5	11.54	3.3
12.42	28.7	12.42	33.6	12.42	41.3	12.42	34.2
12.91	11.8						
13.06	17.0	13.07	19.7	13.07	23.5	13.06	19.9
14.67	100.0	14.67	100.0	14.67	100.0	14.67	100.0
16.15	14.9	16.15	15.7	16.15	17.3	16.15	15.9
17.23	45.6	17.23	46.3	17.23	48.0	17.23	46.5
				18.26	1.4	18.21	1.1
		18.86	0.9	18.82	0.9	18.86	0.9
20.29	41.2	20.29	44.6	20.29	44.0	20.29	43.2
21.34	3.6	21.39	5.8	21.39	5.8	21.38	5.5
21.66	11.6	21.68	15.0	21.66	16.1	21.66	14.0
22.52	8.3	22.53	9.9	22.53	12.1	22.53	10.0
22.87	13.8	22.87	16.5	22.88	19.7	22.87	16.5
						23.44	4.8
23.67	8.3	23.68	8.9	23.67	9.4	23.67	8.8
23.94	8.5	23.95	9.8	23.95	11.1	23.95	9.8
24.29	31.6	24.29	34.4	24.29	37.6	24.29	34.4
24.59	16.6	24.59	17.8	24.60	19.6	24.59	17.9
24.91	5.8	24.92	6.3	24.93	6.8	24.92	6.3
25.28	5.1	25.29	3.8	25.28	4.8	25.28	3.8
25.64	3.8					25.64	4.5
25.89	4.5	25.89	4.8	25.88	4.4	25.89	4.7
26.87	3.2			26.86	3.6	26.87	3.3
		27.01	3.9				
27.44	6.8	27.45	7.2	27.44	8.1	27.44	7.4
27.78	5.4	27.78	6.4	27.78	7.6	27.78	6.4
29.40	2.1	29.41	2.5	29.41	2.6	29.41	2.4
		30.48	4.0	30.48	4.2	30.48	3.8
31.02	12.0	31.02	14.0	31.01	14.2	31.02	13.4
32.56	12.2	32.56	13.3	32.55	14.4	32.55	13.2
		34.97	1.8	35.00	3.5		
35.10	1.3					35.11	1.5
				35.29	2.1		
36.73	3.5	36.71	4.0	36.70	4.3	36.73	3.7
37.44	2.8	37.45	3.1	37.44	3.2	37.44	3.0
38.10	8.1	38.10	8.8	38.10	9.3	38.10	8.7
38.90	4.0	38.90	4.7	38.90	4.9	38.89	6.2
39.79	2.9	39.27	3.5	39.24	3.6	39.25	3.4
		39.71	1.1	39.79	3.5	39.79	3.2
						40.73	1.2
41.19	2.1	41.20	2.1	41.22	2.4	41.20	2.1
43.03	2.0	43.01	2.9	43.02	2.2	43.02	2.3
45.93	1.7	45.91	1.8	45.93	1.9	45.94	1.7
49.88	1.2	49.85	1.2				
		55.78	1.2	55.79	1.3	55.79	1.3

3. The most significant peaks were selected based on a minimum relative intensity value of the average XRPD pattern;

    a. If the most intense peak (MIP) height was less than 100k cts then peaks with a relative intensity > 5% were selected

    b. If MIP height is greater than 100k cts in size then peaks with a relative intensity value of greater than 0.5,1.0 or 2.0 % were selected

For sulfamerazine the MIP is at 14.67 °2Theta with a peak height less than 100K cts. Therefore a relative intensity limit value of 5.0 % was used to select 21 significant peaks for the calculated average XRPD pattern (Table A6- 6).

Table A6- 6 Selected significant peaks for sulfamerazine using a 5.0% RI limit

	Replicate 1		Replicate 2		Replicate 3		Average XRPD	
Peak	Pos. [°2Th.]	Rel. Int. [%]	Pos. [°2Th.]	Rel. Int. [%]	Pos. [°2Th.]	Rel. Int. [%]	Pos. [°2Th.]	Rel. Int. [%]
1	12.42	28.7	12.42	33.6	12.42	41.3	12.42	34.2
2	13.06	17.0	13.07	19.7	13.07	23.5	13.06	19.9
3	14.67	100.0	14.67	100.0	14.67	100.0	14.67	100.0
4	16.15	14.9	16.15	15.7	16.15	17.3	16.15	15.9
5	17.23	45.6	17.23	46.3	17.23	48.0	17.23	46.5
6	20.29	41.2	20.29	44.6	20.29	44.0	20.29	43.2
7	21.34	3.6	21.39	5.8	21.39	5.8	21.38	5.5
8	21.66	11.6	21.68	15.0	21.66	16.1	21.66	14.0
9	22.52	8.3	22.53	9.9	22.53	12.1	22.53	10.0
10	22.87	13.8	22.87	16.5	22.88	19.7	22.87	16.5
11	23.67	8.3	23.68	8.9	23.67	9.4	23.67	8.8
12	23.94	8.5	23.95	9.8	23.95	11.1	23.95	9.8
13	24.29	31.6	24.29	34.4	24.29	37.6	24.29	34.4
14	24.59	16.6	24.59	17.8	24.60	19.6	24.59	17.9
15	24.91	5.8	24.92	6.3	24.93	6.8	24.92	6.3
16	27.44	6.8	27.45	7.2	27.44	8.1	27.44	7.4
17	27.78	5.4	27.78	6.4	27.78	7.6	27.78	6.4
18	31.02	12.0	31.02	14.0	31.01	14.2	31.02	13.4
19	32.56	12.2	32.56	13.3	32.55	14.4	32.55	13.2
20	38.10	8.1	38.10	8.8	38.10	9.3	38.10	8.7
21	38.90	4.0	38.90	4.7	38.90	4.9	38.89	6.2

4. The amount of variation in peak position was estimated using the average range value at each identified peak position and then reporting the average overall value

Table A6- 7 Variation in peak positions for the 3 replicates of sulfamerazine

	Replicate 1	Replicate 2	Replicate 3	
Peak	Pos. [°2Th.]	Pos. [°2Th.]	Pos. [°2Th.]	Range [°2Th.]
1	12.42	12.42	12.42	0.00
2	13.06	13.07	13.07	0.00
3	14.67	14.67	14.67	0.00
4	16.15	16.15	16.15	0.00
5	17.23	17.23	17.23	0.00
6	20.29	20.29	20.29	0.01
7	21.39	21.39	21.39	0.00
8	21.66	21.68	21.66	0.02
9	22.52	22.53	22.53	0.01
10	22.87	22.87	22.88	0.01
11	23.67	23.68	23.67	0.01
12	23.94	23.95	23.95	0.01
13	24.29	24.29	24.29	0.00
14	24.59	24.59	24.60	0.01
15	24.91	24.92	24.93	0.01
16	27.44	27.45	27.44	0.02
17	27.78	27.78	27.78	0.01
18	31.02	31.02	31.01	0.01
19	32.56	32.56	32.55	0.01
20	38.10	38.10	38.10	0.00
21	38.90	38.90	38.90	0.00
			Overall Average	**0.01**

5. An estimate of the variation in the peak XRPD responses for the three replicates at each peak position was obtained using the relative standard deviation (RSD) values for the peak responses; peak height (cts), background height (cts), peak width - FWHM (°2theta) and peak area (cts.2°Theta). The total observed variation in the peak responses over the whole XRPD profile was then estimated by taking the average of the individual RSD values calculated at each peak position.

Table A6- 8 Reported XRPD responses for the 3 replicates of sulfamerazine and calculated RSD values

	Replicate 1	Replicate 2	Replicate 3		Replicate 1	Replicate 2	Replicate 3	
Peak	Height [cts]	Height [cts]	Height [cts]	RSD	Backgr.[cts]	Backgr.[cts]	Backgr.[cts]	RSD
1	10586.58	11381.92	13110.75	11	744.64	635.14	587.5	12
2	6268.22	6660.609	7473.25	9	773.25	662.14	612.84	12
3	36914.24	33849.89	31778.25	8	839.06	725.28	672.5	11
4	5504.965	5306.775	5486.641	2	891.57	777.22	722.5	11
5	16824.93	15668.75	15252.43	5	924.63	811.36	755.52	10
6	15198.74	15092.89	13994.57	5	992.42	887.8	830.39	9
7	1312.238	1961.637	1850.721	20	1006.93	907.92	850.17	9
8	4279.237	5078.192	5112.313	10	1010.59	912.58	854.47	9
9	3058.607	3334.388	3845.608	12	1018.33	924.74	866.68	8
10	5096.922	5592.64	6251.825	10	1020.75	929.13	870.97	8
11	3068.6	3016.535	2996.792	1	1024.84	938.05	879.44	8
12	3145.375	3326.373	3520.581	6	1025.83	940.59	882.03	8
13	11681.03	11639.44	11954.42	1	1026.76	943.64	884.95	7
14	6111.35	6027.955	6214.698	2	1027.3	946.06	887.29	7
15	2133.998	2117.869	2156.039	1	1027.72	948.49	889.64	7
16	2522.536	2431.852	2575.802	3	1024.66	959.82	900.37	6
17	1978.266	2175.41	2416.496	10	1023.78	960.55	901.14	6
18	4441.464	4753.514	4498.134	4	1012.66	960.64	901.73	6
19	4490.159	4486.966	4563.358	1	1006.82	957.32	898.91	6
20	2991.712	2971.108	2938.037	1	999.75	930.28	871.6	7
21	1469.809	1575.848	1540.9	4	1000.68	924.44	865.11	7
			Overall Average	6			Overall Average	8

Peak	Replicate 1	Replicate 2	Replicate 3		Replicate 1	Replicate 2	Replicate 3	
1	FWHM Left [°2Th.]	FWHM Left [°2Th.]	FWHM Left [°2Th.]	RSD	Area [cts*°2Th.]	Area [cts*°2Th.]	Area [cts*°2Th.]	RSD
2	0.0984	0.0984	0.11808	11	1027.604	1104.805	1527.14	22
3	0.07872	0.07872	0.0984	13	486.7482	517.2185	725.4035	23
4	0.07872	0.0984	0.11808	20	2866.514	3285.696	3701.53	13
5	0.0984	0.13776	0.13776	18	534.3486	721.1554	745.5979	17
6	0.07872	0.0984	0.0984	12	1306.512	1520.913	1480.502	8
7	0.11808	0.11808	0.15744	17	1770.35	1758.02	2173.45	12
8	0.0984	0.124368	0.124368	13	127.3746	162.643	43.3319	55
9	0.15744	0.15744	0.15744	0	664.594	788.6771	793.9763	10
10	0.0984	0.13776	0.13776	18	296.8888	453.1211	522.5924	27
11	0.17712	0.17712	0.15744	7	890.5343	977.146	970.9501	5
12	0.11808	0.11808	0.11808	0	357.4305	351.366	349.0664	1
13	0.0984	0.0984	0.11808	11	305.3111	322.8799	410.0772	16
14	0.11808	0.13776	0.13776	9	1360.607	1581.723	1624.525	9
15	0.11808	0.11808	0.11808	0	711.8501	702.1362	723.888	2
16	0.251166	0.251166	0.205191	11	273.2116	354.6239	294.933	14
17	0.11808	0.13776	0.11808	9	293.825	330.4724	300.0294	6
18	0.13776	0.13776	0.13776	0	268.8331	295.6237	328.3857	10
19	0.13776	0.15744	0.15744	8	603.5654	738.2524	698.5902	10
20	0.13776	0.13776	0.13776	0	610.1827	609.7487	620.13	1
21	0.11808	0.0984	0.11808	10	348.4746	288.3956	342.2226	10
	0.125553	0.179073	0.158206	17	123.0258	188.1279	162.5194	21
			Overall Average	10			Overall Average	14

Therefore estimates of the variation in XRPD responses for sulfamerazine would be on average 0.01°2Th for changes in peak position, 6 % in peak heights, 8 % in the background heights, 10 % in peak widths (FWHM) and 14 % in peak areas over the whole XRPD pattern,

APPENDIX 7. Summary of solid-state phase present in comminuted materials.

Table A7- 1 Summary of the solid-state phase present in the comminuted materials of acetaminophen

			Solid-state phase classifications and analytical response observations		
Material Property	Technique	DM	Mill-A***	Mill-B***	JM-A
Phase detection & identification	XRPD	1	Crystalline Form 1 – preferred orientation	Crystalline Form 1 – preferred orientation	Crystalline Form 1 – preferred orientation
	GVS	1	Crystalline	Crystalline	Crystalline
	DSC	1	Crystalline Form 1	Crystalline Form 1	Crystalline Form 1
Moisture sorption	GVS	1	Reversible moisture sorption (0.06 %)	Reversible moisture sorption (0.03 %)	Reversible moisture sorption (0.01 %)
	DSC	1	Not observed	Not observed	Not observed
	TGA	2	Not observed - concordant with Ref.	Not observed - concordant with reference	Not observed - concordant with reference
Chemical purity	HPLC	2	Concordant with reference	Concordant with reference	Concordant with reference
	FTIR	2	Concordant with reference	Concordant with reference	Concordant with reference
Particle size	PSA	2	Agglomerated D_{50} < 35 µm	Agglomerated D_{50} < 12 µm	Mono-modal D_{50} < 2 µm
	SEM	2	Irregular, fractured, rough, agglomerated & drusy	Irregular, fractured, rough, agglomerated & drusy	acicular, rounded smooth, agglomerated
Solid-state phase present			Crystalline	Crystalline	Crystalline

DM – detection method; 1: primary disorder detection technique. 2: secondary disorder detection technique
**Summary from 2 replicate process runs, i.e. two batches*
Mill-A: high frequency ball-mill method A, Mill-B: low frequency ball-mill method B. JM-A: jet-mill method A.
Phase indicated by colour Crystalline, Microcrystalline – little/some disorder, Disordered

Table A7- 2 Summary of the solid-state phase present in the comminuted materials of γ-indomethacin

			Solid-state phase classifications and analytical response observations		
Material Property	Technique	DM	Mill-A***	Mill-B***	JM-A
Phase detection & identification	XRPD	1	Disordered	Microcrystalline	Crystalline γ Form– preferred orientation
	GVS	1	Disordered	Crystalline	Crystalline
	DSC	1	Disordered	Mixed Phase A – same crystalline form with some disorder	Crystalline - concordant with reference
Moisture sorption	GVS	1	Observed (1.32 %)	Reversible moisture sorption (0.29 %)	Reversible moisture sorption (0.09 %)
	DSC	1	Not observed	Not observed	Not observed
	TGA	2	Not observed - concordant with reference	Not observed - concordant with reference	Not observed - concordant with reference
Chemical purity	HPLC	2	Concordant with reference	Concordant with reference	Concordant with reference
	FTIR	2	Concordant with reference	Concordant with reference	Concordant with reference
Particle size	PSA	2	Broad multi-modal D_{50} < 20 µm	Broad multi-modal D_{50} < 15 µm	Mono-modal D_{50} < 2 µm
	SEM	2	Irregular, fractured, rough, agglomerated & drusy	Irregular, fractured, rough, agglomerated & drusy	Irregular, fractured, rough, agglomerated & drusy
Solid-state phase present			Disordered	Microcrystalline – little disorder	Crystalline

DM – detection method; 1: primary disorder detection technique. 2: secondary disorder detection technique
**Summary from 2 replicate process runs, i.e. two batches*
Mill-A: high frequency ball-mill method A, Mill-B: low frequency ball-mill method B. JM-A: jet-mill method A.
Phase indicated by colour Crystalline, Microcrystalline – little/some disorder, Disordered

Table A7- 3 Summary of the solid-state phase present in the comminuted materials of salbutamol sulphate

			Solid-state phase classifications and analytical response observations		
Material Property	Technique	DM	Mill-A***	Mill-B***	JM-A
Phase detection & identification	XRPD	1	X-ray Amorphous	Microcrystalline	Crystalline – preferred orientation
	GVS	1	Disordered	Disordered	Crystalline -electrostatic
	DSC	1	DSC amorphous	Mixed Phase C – maybe mixture of crystalline forms with some disorder	Mixed Phase C – maybe mixture of crystalline forms with some disorder
Moisture sorption	GVS	1	Observed (7.60 %)	Observed (1.06 %)	Observed (0.61 %)
	DSC	1	Observed	Observed	Observed
	TGA	2	Observed (1.85 %)	Observed (0.72 %)	Observed <0.5%
Chemical purity	HPLC	2	Small degradation	Concordant with reference	Small degradation
	FTIR	2	Disorder - Broadening & shifts	Concordant with reference	Concordant with reference
Particle size	PSA	2	Broad multi-modal D_{50} < 12 µm	Broad multi-modal D_{50} < 7 µm	Mono-modal D_{50} < 2 µm
	SEM	2	Irregular, fractured, rough, agglomerated & drusy	Irregular, fractured, rough, agglomerated & drusy	Irregular, fractured, rough, agglomerated & drusy
Solid-state phase present			Disordered	Microcrystalline -some disorder	Crystalline –little disorder

DM – detection method; 1: primary disorder detection technique. 2: secondary disorder detection technique
**Summary from 2 replicate process runs, i.e. two batches*
Mill-A: high frequency ball-mill method A, Mill-B: low frequency ball-mill method B. JM-A: jet-mill method A.
Phase indicated by colour Crystalline, Microcrystalline – little/some disorder, Disordered

Table A7- 4 Summary of the solid-state phase present in the comminuted materials of loperamide HCl

			Solid-state phase classifications and analytical response observations		
Material Property	Technique	DM	Mill-A***	Mill-B***	JM-A
Phase detection & identification	XRPD	1	X-ray Amorphous	Disordered	Crystalline
	GVS	1	Disordered	Disordered	Disordered
	DSC	1	Disordered	Mixed Phase B – maybe new crystalline form some disorder	Mixed Phase A – same crystalline form with some disorder
Moisture sorption	GVS	1	Observed (9.01%)	Observed (2.88 %)	Observed (0.83 %)
	DSC	1	Observed	Observed	Observed
	TGA	2	Observed (1.37 %)	Observed (0.74%)	Not observed
Chemical purity	HPLC	2	Concordant with reference	Concordant with reference	Concordant with reference
	FTIR	2	Disorder - Broadening, water & shifts	Some disorder - slight broadening and shifts	Concordant with reference
Particle size	PSA	2	Broad multi-modal agglomeration D_{50} < 7 µm	Broad multi-modal agglomeration D_{50} < 10 µm	mono-modal D_{50} < 2 µm
	SEM	2	Irregular, fractured, rough, agglomerated & drusy	Irregular, fractured, rough, agglomerated & drusy	Irregular, fractured, rough, agglomerated & drusy
Solid-state phase present			Disordered	Some Disorder	Crystalline –little disorder

DM – detection method; 1: primary disorder detection technique. 2: secondary disorder detection technique
Mill-A: high frequency ball-mill method A, Mill-B: low frequency ball-mill method B. JM-A: jet-mill method A.
Phase indicated by colour Crystalline, Microcrystalline – little/some disorder, Disordered

Table A7- 5 Summary of the solid-state phase present in the comminuted materials of acetylsalicylic acid

			Solid-state phase classifications and analytical response observations		
Material Property	Technique	DM	Mill-A***	Mill-B***	JM-A
Phase detection & identification	XRPD	1	Crystalline	Crystalline	Crystalline
	GVS	1	Crystalline	Crystalline	Crystalline
	DSC	1	Crystalline - concordant with reference	Crystalline - concordant with reference	Crystalline - concordant with reference
Moisture sorption	GVS	1	Reversible moisture sorption (0.12 %)	Reversible moisture sorption (0.07 %)	Reversible moisture sorption (0.03 %)
	DSC	1	Not observed	Not observed	Not observed
	TGA	2	Not observed	Not observed	Not observed
Chemical purity	HPLC	2	Concordant with reference	Concordant with reference	Concordant with reference
	FTIR	2	Concordant with reference	Concordant with reference	Concordant with reference
Particle size	PSA	2	Broad multi-modal D_{50} < 15 µm	Broad multi-modal D_{50} < 6 µm	Mono-modal D_{50} < 2 µm
	SEM	2	Irregular, fractured, rough, agglomerated & drusy	Irregular, fractured, rough, agglomerated & drusy	Irregular, fractured, rough, agglomerated & drusy
Solid-state phase present			Crystalline	Crystalline	Crystalline

DM – detection method; 1: primary disorder detection technique. 2: secondary disorder detection technique
Mill-A: high frequency ball-mill method A, Mill-B: low frequency ball-mill method B. JM-A: jet-mill method A.
Phase indicated by colour Crystalline, Microcrystalline – little/some disorder, Disordered

Table A7- 6 Summary of the solid-state phase present in the comminuted materials of sulfamerazine

			Solid-state phase classifications and analytical response observations		
Material Property	Technique	DM	Mill-A***	Mill-B***	JM-A
Phase detection & identification	XRPD	1	Crystalline mixture of Forms I & II	Microcrystalline	Crystalline – preferred orientation
	GVS	1	Disordered	Crystalline	Crystalline
	DSC	1	Mixed Phase C – maybe mixture of crystalline forms with some disorder	Crystalline - concordant with reference	Crystalline - concordant with reference
Moisture sorption	GVS	1	Observed (0.63 %)	Reversible moisture sorption (0.45 %)	Reversible moisture sorption (0.23 %)
	DSC	1	Not observed	Not observed	Not observed
	TGA	2	Not observed	Not observed	Not observed
Chemical purity	HPLC	2	Concordant with reference	Concordant with reference	Concordant with reference
	FTIR	2	Some peaks for Form II and some peak shifts.	Concordant with reference	Concordant with reference
Particle size	PSA	2	Broad multi-modal agglomeration D_{50} < 10 µm	Broad multi-modal agglomeration D_{50} < 30 µm	Mono-modal D_{50} < 2 µm
	SEM	2	Irregular, fractured, rough, agglomerated & drusy	Irregular, fractured, rough, agglomerated & drusy	Irregular, fractured, rough, agglomerated & drusy
Solid-state phase present			Some disorder – some new form	Microcrystalline	Crystalline

DM – detection method; 1: primary disorder detection technique. 2: secondary disorder detection technique
Mill-A: high frequency ball-mill method A, Mill-B: low frequency ball-mill method B. JM-A: jet-mill method A.
Phase indicated by colour Crystalline, Microcrystalline – little/some disorder, Disordered

Table A7- 7 Summary of the solid-state phase present in the comminuted materials of phenacetin

			Solid-state phase classifications and analytical response observations		
Material Property	Technique	DM	Mill-A***	Mill-B***	JM-A
Phase detection & identification	XRPD	1	Crystalline – preferred orientation	Crystalline – concordant with reference	Crystalline – preferred orientation
	GVS	1	Crystalline	Crystalline	Crystalline
	DSC	1	Crystalline - concordant with reference	Crystalline - concordant with reference	Crystalline - concordant with reference
Moisture sorption	GVS	1	Reversible moisture sorption (0.12 %)	Reversible moisture sorption (0 %)	Reversible moisture sorption (0.01 %)
	DSC	1	Not observed	Not observed	Not observed
	TGA	2	Not observed	Not observed	Not observed
Chemical purity	HPLC	2	Concordant with reference	Concordant with reference	Concordant with reference
	FTIR	2	Concordant with reference.	Concordant with reference	Concordant with reference
Particle size	PSA	2	Broad multi-modal D_{50} < 12 µm	Broad multi-modal D_{50} < 16 µm	Mono-modal D_{50} < 2 µm
	SEM	2	Irregular, fractured, rough, agglomerated & drusy	Irregular, fractured, rough, agglomerated & drusy	Irregular, fractured, rough, agglomerated & drusy
Solid-state phase present			Crystalline	Crystalline	Crystalline

DM – detection method; 1: primary disorder detection technique. 2: secondary disorder detection technique
Mill-A: high frequency ball-mill method A, Mill-B: low frequency ball-mill method B. JM-A: jet-mill method A.
Phase indicated by colour Crystalline, Microcrystalline – little/some disorder, Disordered

Table A7- 8 Summary of the solid-state phase present in the comminuted materials of sulfadiazine

			Solid-state phase classifications and analytical response observations		
Material Property	Technique	DM	Mill-A***	Mill-B***	JM-A
Phase detection & identification	XRPD	1	Crystalline	Crystalline	Crystalline – preferred orientation
	GVS	1	Disordered	Disordered	Crystalline
	DSC	1	Mixed Phase C – maybe mixture of crystalline forms with some disorder	Mixed Phase C – maybe mixture of crystalline forms with some disorder	Mixed Phase C – maybe mixture of crystalline forms with some disorder
Moisture sorption	GVS	1	Observed (1.13 %)	Observed (0.91 %)	Reversible moisture sorption (0.20 %)
	DSC	1	Not observed	Not observed	Not observed
	TGA	2	Not observed	Not observed	Not observed
Chemical purity	HPLC	2	Concordant with reference	Concordant with reference	Concordant with reference
	FTIR	2	Concordant with reference	Concordant with reference	Concordant with reference
Particle size	PSA	2	Broad multi-modal agglomeration D_{50} < 22 µm	Broad multi-modal agglomeration D_{50} < 28 µm	Mono-modal D_{50} < 2 µm
	SEM	2	Irregular, fractured, rough, agglomerated & drusy	Irregular, fractured, rough, agglomerated & drusy	Irregular, fractured, rough, agglomerated & drusy
Solid-state phase present			Crystalline –little disorder	Crystalline –little disorder	Crystalline

DM – detection method; 1: primary disorder detection technique. 2: secondary disorder detection technique
Mill-A: high frequency ball-mill method A, Mill-B: low frequency ball-mill method B. JM-A: jet-mill method A.
Phase indicated by colour Crystalline, Microcrystalline – little/some disorder, Disordered

Table A7- 9 Summary of the solid-state phase present in the comminuted materials of caffeine

			Solid-state phase classifications and analytical response observations		
Material Property	Technique	DM	Mill-A***	Mill-B***	JM-A
Phase detection & identification	XRPD	1	Crystalline – preferred orientation	Crystalline	Crystalline – concordant with reference
	GVS	1	Disordered	Disordered	Crystalline
	DSC	1	Mixed Phase A – same crystalline form with some disorder	Mixed Phase A – same crystalline form with some disorder	Mixed Phase A – same crystalline form with some disorder
Moisture sorption	GVS	1	Observed (0.63 %)	Observed (0.12 %)	Reversible moisture sorption (0 %)
	DSC	1	Observed	Not observed	Not observed
	TGA	2	Observed (1.09 %)	Not observed	Not observed
Chemical purity	HPLC	2	Concordant with reference	Concordant with reference.	Concordant with reference
	FTIR	2	Concordant with reference	Concordant with reference	Concordant with reference
Particle size	PSA	2	Broad multi-modal agglomeration D_{50} < 35 µm	Broad multi-modal agglomeration D_{50} < 45 µm	Mono-modal D_{50} < 2 µm
	SEM	2	Acicular, sharp, smooth, agglomerated	Acicular, sharp, smooth, agglomerated	Acicular, rounded, smooth, agglomerated
Solid-state phase present			Crystalline –little disorder	Crystalline –little disorder	Crystalline

DM – detection method; 1: primary disorder detection technique. 2: secondary disorder detection technique
Mill-A: high frequency ball-mill method A, Mill-B: low frequency ball-mill method B. JM-A: jet-mill method A.
Phase indicated by colour Crystalline, Microcrystalline – little/some disorder, Disordered

Table A7- 10 Summary of the solid-state phase present in the comminuted materials of methyl paraben

			Solid-state phase classifications and analytical response observations		
Material Property	Technique	DM	Mill-A***	Mill-B***	JM-A
Phase detection & identification	XRPD	1	Crystalline – concordant with reference	Crystalline – concordant with reference	Crystalline – concordant with reference
	GVS	1	Crystalline	Crystalline	Crystalline
	DSC	1	Crystalline – concordant with reference	Crystalline – concordant with reference	Crystalline – concordant with reference
Moisture sorption	GVS	1	Reversible moisture sorption (0.06 %)	Reversible moisture sorption (0.07 %)	Reversible moisture sorption (0.02 %)
	DSC	1	Not observed	Not observed	Not observed
	TGA	2	Not observed	Not observed	Not observed
Chemical purity	HPLC	2	Concordant with reference	Concordant with reference	Concordant with reference
	FTIR	2	Concordant with reference	Concordant with reference	Concordant with reference
Particle size	PSA	2	Broad multi-modal D_{50} < 30 µm	Broad multi-modal D_{50} < 30 µm	Mono-modal D_{50} < 8 µm
	SEM	2	Irregular, fractured, rough, agglomerated & drusy	Irregular, fractured, rough, agglomerated & drusy	Irregular, fractured, rough, agglomerated & drusy
Solid-state phase present			Crystalline	Crystalline	Crystalline

DM – detection method; 1: primary disorder detection technique. 2: secondary disorder detection technique
Mill-A: high frequency ball-mill method A, Mill-B: low frequency ball-mill method B. JM-A: jet-mill method A.
Phase indicated by colour Crystalline, Microcrystalline – little/some disorder, Disordered

APPENDIX 8. Overlay of the XRPD diffractograms for high frequency ball-milled indomethacin (11-MA1) and its input.

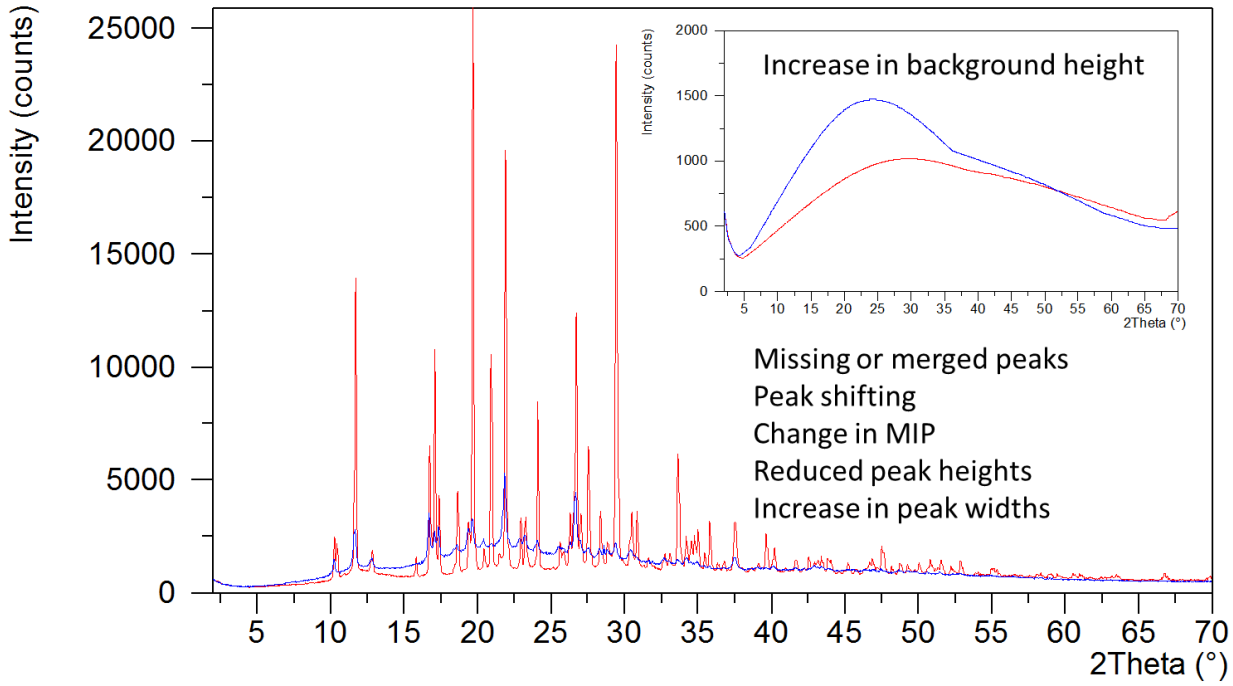

Blue – high frequency ball-milled γ-indomethacin, batch 11-MA1. Red – input γ-indomethacin. Insert depicts overlay of background profiles for the two materials

APPENDIX 9. General analytical protocol to identify and quantify relative disorder in pharmaceutical materials

Step 1: Define the study intent and or objective.

- Define the purpose of the investigation and what it is hoped to achieve, e.g. investigate the degree of PID that may be generated as a consequence of jet-milling using different micronisation parameters to achieve a particle size of X90 of 5 µm.

Step 2: Define the appropriate core test methods.

- Define the primary and secondary disorder detection methods that will be used, e.g. the table below lists some recommended techniques that should be employed to ensure the adequate characterisation of a material properties.

Primary disorder detection methods	Secondary disorder detection methods
XRPD DSC GVS	TGA PLM/SEM FTIR HPLC PSA

- Define the acquisition parameters for each technique and the responses that will be reported.
- Determine the instrumental variances and operational tolerances, e.g. signal to noise values, background heights of blanks etc.

Step 3: Perform any appropriate pre-processing on the bulk.

- e.g. sieving, or recrystallisation.

Step 4: Characterise the input material (RA).

- Using the core test methods determine the responses for the input material.
- Determine the sample and material variance in the responses.
- Determine the criteria limits for the individual technique responses to allow appropriate identification of the solid-state phase, *i.e.* define the CRA limits.
- Determine appropriate RDA limits for the responses of the primary disorder detection methods.

Step 5: Process the input material.

- Process the material using the appropriate parameters under defined conditions.

Step 6: Characterise the processed material (RA).

- Using the core test methods determine the responses for the processed material.

Step 7: Perform CRA on processed material.

- For each of the core test methods compare the responses of the processed material (from Step 6) with those of the input material (from step 4).
- Using the CRA response limits identify the solid-state phase present.

Step 8: Determine relative levels of disorder using RDA and PDA approaches.

- Perform a RDA for each of the identified primary disorder detection methods, determining the $R_{Technique}$ and $D_{Technique}$ scores.
- Perform PDA for each process being investigated, determining the overall P_{RDS} and D_{Pro} values.
- Define and classify the relative amount of PID generated along with the solid-state phase present in the material based on the overall P_{RDS} and D_{Pro} values for the given process.

References

1. Begat P, Young PM, Edge S, Kaerger JS, Price R 2003. The effect of mechanical processing on surface stability of pharmaceutical powders: visualization by atomic force microscopy. JPharmSci 92(3):611-620.
2. Chikhalia V, Forbes RT, Storey RA, Ticehurst M 2006. The effect of crystal morphology and mill type on milling induced crystal disorder. EurJ Pharm Sci 27(1):19-26.
3. Mackin L, Sartnurak S, Thomas I, Moore S 2002. The impact of low levels of amorphous material (<5%) on the blending characteristics of a direct compression formulation. International Journal of Pharmaceutics 231(2):213-226.
4. Rasenack N, Muller BW 2004. Micron-size drug particles: common and novel micronization techniques. Pharm DevTechnol 9(1):1-13.
5. Willart JF, Caron V, Lefort R, Danode F, Provost D, Descamps M 2004. Athermal character of the solid state amorphization of lactose induced by ball milling. Solid State Communications 132(10):693-696.
6. Willart JF, De Gusseme A, Hemon S, Odou G, Danede F, Descamps M 2001. Direct crystal to glass transformation of trehalose induced by ball milling. Solid State Communications 119(8-9):501-505.
7. Willart JF, Descamps M 2008. Solid state amorphization of pharmaceuticals. Mol Pharm 5(6):905-920.
8. Willart JF, Dujardin N, Dudognon E, Danede F, Descamps M 2010. Amorphization of sugar hydrates upon milling. CarbohydrRes 345(11):1613-1616.
9. Willart JF, Hedoux A, Guinet Y, Danede F, Paccou L, Capet F, Descamps M 2006. Metastability release of the form alpha of trehalose by isothermal solid state vitrification. J PhysChem B 110(23):11040-11043.
10. Willart JF, Carpentier L, Dande F, Descamps M 2012. Solid-state vitrification of crystalline griseofulvin by mechanical milling. Journal of Pharmaceutical Sciences 101(4):1570-1577.
11. Zhang G, Law D, Schmitt e, Qiu Y 2004. Phase transformation considerations during process development and manufacture of solid oral dosage forms. Advanced Drug Delivery Reviews 56(3):371-390.
12. Morris KR, Griesser UJ, Eckhardt CJ, Stowell JG 2001. Theoretical approaches to physical transformations of active pharmaceutical ingredients during manufacturing processes. AdvDrug DelivRev 48(1):91-114.
13. Specifications for New Drug Substances and Products: Chemical Substances, 1999. International Conference on Harmonization Q6A Guideline, ed.
14. Huang LF, Tong WQ 2004. Impact of solid state properties on developability assessment of drug candidates. AdvDrug DelivRev 56(3):321-334.
15. Pfeiffer R, Stowell J, Byrn S. 1999. Introduction to the Solid sate chemistry of Drugs. 2 ed.: SSCI Inc., West Laffayette.
16. Venkatesh S, Lipper RA 2000. Role of the development scientist in compound lead selection and optimization. J PharmSci 89(2):145-154.
17. Vippagunta SR, Brittain HG, Grant DJ 2001. Crystalline solids. AdvDrug DelivRev 48(1):3-26.
18. Saleki-Gerhardt A, Ahlneck C, Zografi G 1994. Assessment of disorder in crystalline solids. International Journal of Pharmaceutics 101(3):237-247.
19. Ward GH, Schultz RK 1995. Process-induced crystallinity changes in albuterol sulfate and its effect on powder physical stability. Pharm Res 12(5):773-779.
20. Brodka-Pfeiffer K, Hausler H, Grass P, Langguth P 2003. Conditioning following powder micronization: influence on particle growth of salbutamol sulfate. Drug DevIndPharm 29(10):1077-1084.

21. Brodka-Pfeiffer K, Langguth P, Grass P, Hausler H 2003. Influence of mechanical activation on the physical stability of salbutamol sulphate. EurJPharmBiopharm 56(3):393-400.
22. Feng T, Bates S, Carvajal MT 2009. Toward understanding the evolution of griseofulvin crystal structure to a mesophase after cryogenic milling. IntJ Pharm 367(1-2):16-19.
23. Rani M, Govindarajan R, Surana R, Suryanarayanan R 2006. Structure in dehydrated trehalose dihydrate--evaluation of the concept of partial crystallinity. Pharm Res 23(10):2356-2367.
24. Mackin L, Zanon R, Park JM, Foster K, Opalenik H, Demonte M 2002. Quantification of low levels (<10%) of amorphous content in micronised active batches using dynamic vapour sorption and isothermal microcalorimetry. IntJPharm 231(2):227-236.
25. Dudognon E, Willart JF, Caron V, Capet F, Larsson T, Descamps M 2006. Formation of budesonide/[alpha]-lactose glass solutions by ball-milling. Solid State Communications 138(2):68-71.
26. Feng T, Pinal R, Carvajal M 2008. Process induced disorder in crystalline materials: Differentiating defective crystals from the amorphous form of griseofulvin. Journal of Pharmaceutical Sciences 97(8):3207-3221.
27. Font J, Muntasell J, Cesari E 1997. Amorphization of organic compounds by ball milling. Materials Research Bulletin 32(12):1691-1696.
28. Shakhtshneider TP 1997. Phase transformations and stabilization of metastable states of molecular crystals under mechanical activation. Solid State Ionics 101-103(2):851-856.
29. Ondarza-Rovira R 2002. Lattice-parameter determination from the interaction of short femtosecond laser pulses with crystalline solids. Acta Crystallographica Section A: Foundations of Crystallography 58(1):27-32.
30. Kim CD, Pillet S, Wu G, Fullagar WK, Coppens P 2002. Excited-state structure by time-resolved X-ray diffraction. Acta Crystallographica Section A: Foundations of Crystallography 58(2):133-137.
31. Craig D, Royall PG, Kett VL, Hopton ML 1999. The relevance of the amorphous state to pharmaceutical dosage forms: glassy drugs and freeze dried systems. IntJPharm 179(2):179-207.
32. Hancock BC, Shalaev EY, Shamblin SL 2002. Polyamorphism: a pharmaceutical science perspective. J PharmPharmacol 54(8):1151-1152.
33. Rodriguez-Spong B, Price CP, Jayasankar A, Matzger AJ, Rodriguez-Hornedo N 2004. General principles of pharmaceutical solid polymorphism: a supramolecular perspective. AdvDrug DelivRev 56(3):241-274.
34. Shalaev EY, Zografi G. 2002. The concept of ``structure ' ' in amorphous solids from the perspective of the pharmaceutical sciences. In Levine H, editor Progress in amorphous food and pharmaceutical systems, ed., London, UK: The Royal Society of Chemistry. p 11-30.
35. Stevenson CL, Bennett DB, Lechuga-Ballesteros D 2005. Pharmaceutical liquid crystals: the relevance of partially ordered systems. J PharmSci 94(9):1861-1880.
36. Martin A. 1993. States of matter. ed., PA,: Lea and Febiger.
37. Nangia A 2008. Conformational polymorphism in organic crystals. AccChem Res 41(5):595-604.
38. Bernstein J, Davey RJ, Henck JO 1999. Concomitant Polymorphs. AngewChem IntEd Engl 38(23):3440-3461.
39. Grant D. 1999. Theory and origin of polymorphism. In Brittain HG, editor Polymorphism in Pharmaceutical Solids, ed., New York: Marcel Dekker. p 1-33.
40. Byrn S, Pfeiffer R, Stowell J. 1999. Solid State Chemistry of Drugs. 2 ed., West Lafayette.: SSCI. p 249.

41. Desiraju GR 2002. Hydrogen bridges in crystal engineering: interactions without borders. AccChem Res 35(7):565-573.

42. Yu L 2001. Amorphous pharmaceutical solids: preparation, characterization and stabilization. AdvDrug DelivRev 48(1):27-42.

43. Tang XC, Pikal MJ, Taylor LS 2002. A spectroscopic investigation of hydrogen bond patterns in crystalline and amorphous phases in dihydropyridine calcium channel blockers. Pharm Res 19(4):477-483.

44. Andronis V, Zografi G 2000. Crystal nucleation and growth of indomethacin polymorphs from the amorphous state. Journal of Non-Crystalline Solids 271(3):236-248.

45. Taylor LS, Zografi G 1997. Spectroscopic characterization of interactions between PVP and indomethacin in amorphous molecular dispersions. Pharm Res 14(12):1691-1698.

46. Champagnon B, Martinet C, Coussa C, Deschamps T 2007. Polyamorphism: Path to new high density glasses at ambient conditions. Journal of Non-Crystalline Solids 353(44-46):4208-4211.

47. Craig D, Kett V, Murphy J, Price D 2001. The measurement of small quantities of amorphous material--should we be considering the rigid amorphous fraction? PharmRes 18(8):1081-1082.

48. Molteni C, Martonak R 2005. Polyamorphism in silicon nanocrystals under pressure. Chemphyschem 6(9):1765-1768.

49. Angell CA 2004. Amorphous water. AnnuRevPhysChem 55:559-583.

50. Johari GP, Andersson O 2004. Water's polyamorphic transitions and amorphization of ice under pressure. J Chem Phys 120(13):6207-6213.

51. Sheng HW, Liu HZ, Cheng YQ, Wen J, Lee PL, Luo WK, Shastri SD, Ma E 2007. Polyamorphism in a metallic glass. NatMater 6(3):192-197.

52. Winkel K, Elsaesser MS, Mayer E, Loerting T 2008. Water polyamorphism: reversibility and (dis)continuity. J Chem Phys 128(4):044510.

53. Pikal MJ, Lukes AL, Lang JE, Gaines K 1978. Quantitative crystallinity determinations for beta-lactam antibiotics by solution calorimetry: correlations with stability. J Pharm Sci 67(6):767-773.

54. Mishima O, Suzuki Y 2002. Propagation of the polyamorphic transition of ice and the liquid-liquid critical point. Nature 419:599-603.

55. van TM, Ree FH 1993. High-pressure liquid-liquid phase change in carbon. PhysRevB CondensMatter 48(6):3591-3599.

56. Yonemochi E, Inoue Y, Buckton G, Moffat A, Oguchi T, Yamamoto K 1999. Differences in crystallization behavior between quenched and ground amorphous ursodeoxycholic acid. Pharm Res 16(6):835-840.

57. Kercogonek J, Srcic S, Mohar M, mid-Korbar J 1991. Some physicochemical properties of glassy felodipine. International Journal of Pharmaceutics 68(1-3):25-33.

58. Yoshioka M, Hancock BC, Zografi G 1994. Crystallization of indomethacin from the amorphous state below and above its glass transition temperature. J PharmSci 83(12):1700-1705.

59. Surana R, Pyne A, Suryanarayanan R 2004. Effect of preparation method on physical properties of amorphous trehalose. Pharm Res 21(7):1167-1176.

60. Surana R, Pyne A, Suryanarayanan R 2004. Effect of aging on the physical properties of amorphous trehalose. Pharm Res 21(5):867-874.

61. Ueno Y, Yonemochi E, Tozuka Y, Yamamura S, Oguchi T, Yamamoto K 1998. Characterization of amorphous ursodeoxycholic acid prepared by spray-drying. J Pharm Pharmacol 50(11):1213-1219.

62. Yamaguchi T, Nishimura M, Okamoto R, Takeuchi T, Yamamoto K 1992. Glass formation of 4″-O-(4-methoxyphenyl) acetyltylosin and physicochemical stability of the amorphous solid. International Journal of Pharmaceutics 85(1–3):87-96.
63. Yonemochi E, Ueno Y, Ohmae T, Oguchi T, Nakajima S, Yamamoto K 1997. Evaluation of amorphous ursodeoxycholic acid by thermal methods. Pharm Res 14(6):798-803.
64. Hilfiker R. 2006. Polymorphism in the pharmaceutical industry. ed., Weinheim, Germany: Wiley-VCH.
65. Hancock BC, Zografi G 1997. Characteristics and significance of the amorphous state in pharmaceutical systems. J Pharm Sci 86(1):1-12.
66. Kearns KL, Swallen SF, Ediger MD, Wu T, Sun Y, Yu L 2008. Hiking down the energy landscape: progress toward the Kauzmann temperature via vapor deposition. The journal of physical chemistry B 112(16):4934-4942.
67. C. A. Angell DRM, M. Oguni 1986. The Kauzmann Paradox, Metastable Liquids, and Ideal Glasses: A Summary. Ann NY Acad Sci 484:241-247.
68. Kauzmann W 1948. Chem Rev 43:219-256.
69. Hodge IM 1995. Physical Aging in Polymer Glasses. Science 267:1945-1947.
70. Gaskell P 1986. Dynamic aspects of structural change in liquids and glasses,. Annals NY AcadSci Vol 484:66-80.
71. Threlfall T 1995. Analyst 120:2435-2460.
72. De Gusseme A, Neves C, Willart JF, Rameau A, Descamps M 2008. Ordering and disordering of molecular solids upon mechanical milling: The case of fananserine. Journal of Pharmaceutical Sciences 97(11):5000-5012.
73. Descamps M, Willart JF, Dudognon E, Caron V 2007. Transformation of pharmaceutical compounds upon milling and comilling: the role of T(g). J Pharm Sci 96(5):1398-1407.
74. Lefebvre J, Willart JF, Caron V, Lefort R, Affouard F, Danede F 2005. Structure determination of the 1/1 alpha/beta mixed lactose by X-ray powder diffraction. Acta CrystallogrB 61(4):455-463.
75. Lefort R, De Gusseme A, Willart JF, Danede F, Descamps M 2004. Solid state NMR and DSC methods for quantifying the amorphous content in solid dosage forms: an application to ball-milling of trehalose. IntJ Pharm 280(1-2):209-219.
76. Platteau C, Lefebvre J, Affouard F, Willart JF, Derollez P, Mallet F 2005. Structure determination of the stable anhydrous phase of alpha-lactose from X-ray powder diffraction. Acta CrystallogrB 61(2):185-191.
77. Bauer-Brandl A 1996. Polymorphic transitions of cimetidine during manufacture of solid dosage forms. International Journal of Pharmaceutics 140(2):195-206.
78. Slade L, Levine H 1988. Non-equilibrium behavior of small carbohydratewater systems. Pure ApplChem 60:1841.
79. Ediger MD, Angell CA, Nagel S 1996. Supercooled Liquids and Glasses. JPhysChem 100:13200-13212.
80. Angell CA 1996. The glass transition. Current Opinion in Solid State and Materials Science 1(4):578-585.
81. Angell CA 1997. Why C1 = 16-17 in the WLF equation is physical--and the fragility of polymers. Polymer 38(26):6261-6266.
82. Threlfall TL 1995. Analysis of organic polymorphs. A review. Analyst 120(10):2435-2460.
83. Shalaev EY, Shalaeva M, Zografi G 2002. The effect of disorder on the chemical reactivity of an organic solid, tetraglycine methyl ester: change of the reaction mechanism. J Pharm Sci 91(2):584-593.

84. Huttenrauch R, Fricke S, Zielke P 1985. Mechanical activation of pharmaceutical systems. Pharm Res 2:302-306.
85. Saleki-Gerhardt A, Zografi G 1994. Non-isothermal and isothermal crystallization of sucrose from the amorphous state. Pharm Res 11(8):1166-1173.
86. Chandrasekhar S. 1992. Liquid crystals. 2 ed., Cambridge: Cambridge University Press.
87. Yoshioka M, Hancock BC, Zografi G 1995. Inhibition of indomethacin crystallization in poly(vinylpyrrolidone) coprecipitates. J Pharm Sci 84(8):983-986.
88. Ward S, Perkins M, Zhang JX, Roberts CJ, Madden CE, Luk SY, Patel NES 2005. Identifying and mapping surface amorphous domains. Pharmaceutical Research 22(7):1195-1202.
89. Haleblian J, McCrone W 1969. Pharmaceutical applications of polymorphism. J Pharm Sci 58(8):911-929.
90. Haleblian JK 1975. Characterization of habits and crystalline modification of solids and their pharmaceutical applications. J Pharm Sci 64(8):1269-1288.
91. Byrn S, Pfeiffer R, Stowell J. 1999. Solid State Chemistry of Drugs. 2 ed., West Lafayette.: SSCI.
92. Brittain HG. 1995. Overview of physical characterization methodology. In Brittain HG, editor Physical characterization of pharmaceutical solids, ed., New York: Marcel Dekker. p 1-35.
93. Brittain HG. 2011. Characterization of Pharmaceutical Compounds in the Solid State. In Scypinski SAaS, editor Separation Science and Technology Handbook of Modern Pharmaceutical Analysis, Volume 10 ed.: Academic Press. p 11-58.
94. Lohani S, Grant D. 2006. Thermodynamics of polymorphs. In Hilfiker R, editor Polymorphism in the pharmaceutical industry, ed., Weinheim, Germany: Wiley-VCH. p 21-41.
95. Byrn SR, Pfeiffer RR, Stephenson G, Grant DJW, Gleason WB 1994. Solid-State Pharmaceutical Chemistry. Chemistry of Materials 6(8):1148-1158.
96. Buckingham AD. 1999. Crystal Engineering: the Design and Application of Functional Solids. In Seddon KR, Zaworotko M, editors. NATO Science Series C Vol539, ed., Boston: Kluwer Academic. p 49-68.
97. Etter MC 1991. Hydrogen bonds as design elements in organic chemistry. Journal of Physical Chemistry 95(12):4601-4610.
98. Kitaigorodskii AI. 1961. Organic Chemical Crystallography. ed., New York: Consultant's Bureau.
99. Etter MC, MacDonald JC, Bernstein J 1990. Graph-set analysis of hydrogen-bond patterns in organic crystals. Acta CrystallogrB 46 (2):256-262.
100. Galek PTA, Fabian L, Allen FH 2009. Persistent hydrogen bonding in polymorphic crystal structures. Acta Crystallographica Section B 65(1):68-85.
101. Brittain HGB, S. 1999. Structural aspects of polymorphism. In Brittain HG, editor Polymorphism in Pharmaceutical Solids, ed., New York: Marcel Dekker. p 73-124.
102. Myerson AS. 1999. Crystallization Basics. In Myerson AS, editor Molecular Modeling Applications in Crystallization, ed., Cambridge: Cambridge University Press. p 55.
103. Byrn S, Pfeiffer R, Stowell J. 1999. Solid State Chemistry of Drugs. 2 ed., West Lafayette.: SSCI. p 63-64.
104. Chan LL, Lidstone EA, Finch KE, Heeres JT, Hergenrother PJ, Cunningham BT 2009. A Method for Identifying Small-Molecule Aggregators Using Photonic Crystal Biosensor Microplates. JALA - Journal of the Association for Laboratory Automation 14(6):348-359.
105. Buerger M. 1956. Elementary Crystallography. ed., New York: John Wiley & Sons.
106. Hilton H. 1963. Mathmatical Crystallography. ed., New York: Dover.

107. Datta S, Grant DJ 2004. Crystal structures of drugs: advances in determination, prediction and engineering. NatRev Drug Discov 3(1):42-57.

108. 2014. A Hypertext Book of Crystallographic Space Group Diagrams and Tables. ed.: Birkbeck College, University of London. . p A Hypertext Book of Crystallographic Space Group Diagrams and Tables.

109. Han T. 1987. International Tables for Crystallography. ed., Boston, MA: International Union of Crystallography.

110. Kitaigorodskii AI. 1973. Molecular crystals and molecules. ed., New York: Academic Press.

111. Docherty RM, P. 1999. The study of molecular materials using computational chemistry. In Myerson AS, editor Molecular modeling applications in crystallization, ed., Cambridge: Cambridge University press. p 108-117.

112. Dauber P, Hagler A 1980. Crystal packing, hydrogen bonding, and the effect of crystal forces on molecular conformation. Accounts of Chemical Research 13(4):105-112.

113. Boldyreva EV, Shakhtshneider TP, Vasilchenko MA, Ahsbahs H, Uchtmann H 2000. Anisotropic crystal structure distortion of the monoclinic polymorph of acetaminophen at high hydrostatic pressures. Acta CrystallogrB 56 (2):299-309.

114. Vasilchenko M, Shakhtshneider T, Naumov D, Boldyrev V 1996. Topochemistry of the Initial Stages of the Dissolution of Single Crystals of Acetaminophen. Journal of Pharmaceutical Sciences 85:929-934.

115. Shekunov BY, Aulton R, Adama-Acquah R, Grant DJ 1996. Effect of temperature on crystal growth and crystal properties of paracetamol. JChemSoc, Faraday Trans 92:439-444.

116. Picker-Freyer KM, Liao X, Zhang G, Wiedmann TS 2007. Evaluation of the compaction of sulfathiazole polymorphs. J Pharm Sci 96(8):2111-2124.

117. Sun C, Grant DJ 2001. Influence of crystal structure on the tableting properties of sulfamerazine polymorphs. PharmRes 18(3):274-280.

118. Sun CC, Kiang YH 2008. On the identification of slip planes in organic crystals based on attachment energy calculation. J Pharm Sci 97(8):3456-3461.

119. Roberts R, Rowe R, York P 1994. The relationship between indentation hardness of organic solids and their molecular structure. Journal of Materials Science 29:2289-2296.

120. Roberts R, Rowe R, York P 1995. The relationship between the fracture properties; tensile strength and critical stress intensity factor of organic solids and their molecular structure. IntJPharm 125:157-162.

121. Feng Y, Grant DJ, Sun CC 2007. Influence of crystal structure on the tableting properties of n-alkyl 4-hydroxybenzoate esters (parabens). J Pharm Sci 96(12):3324-3333.

122. Callister W. 2003. Materials science and engineering: An introduction. 6 ed., New York: Wiley.

123. Zeng XM, Martin GP, Marriott C, Pritchard J 2000. The influence of carrier morphology on drug delivery by dry powder inhalers. IntJ Pharm 200(1):93-106.

124. Newman A, Brittain HG. 1995. Particle morphology:optical and electron microscopies. In Brittain HG, editor physical characterization of pharmaceutical solids, 2 ed., New York: Marcel Dekker Inc. p 127-148.

125. Byrn S, Pfeiffer R, Stowell J. 1999. Drugs as molecular solids. In Byrn S, Pfeiffer R, Stowell J, editors. Solid State Chemistry of Drugs 2ed., West Lafayette.: SSCI. p 12-15.

126. Myerson AS. 1999. Crystallization Basics. In Myerson AS, editor Molecular Modeling Applications in Crystallization, ed., Cambridge: Cambridge University Press. p 98-105.

127. Dirksen JA, Ring TA 1991. Fundamentals of crystallization- Kinetic effects on particle size distributions and morphology. Chemical Engineering Science 46:2389-2427.

128. Hooton JC, Jones MD, Harris H, Shur J, Price R 2008. The influence of crystal habit on the prediction of dry powder inhalation formulation performance using the cohesive-adhesive force balance approach. Drug Development & Industrial Pharmacy 34(9):974-983.

129. Weissbuch I, Addadi L, Leiserowitz L 1991. Molecular Recognition at Crystal Interfaces. Science 253(5020):637-645.

130. Weissbuch I, Leiserowitz L, Lahav M 2008. Direct assignment of the absolute configuration of molecules from crystal morphology. Chirality 20(5):736-748.

131. Weissbuch I, Torbeev VY, Leiserowitz L, Lahav M 2005. Solvent effect on crystal polymorphism: why addition of methanol or ethanol to aqueous solutions induces the precipitation of the least stable beta form of glycine. AngewChem IntEd Engl 44(21):3226-3229.

132. Burt HM, Mitchell AG 1981. Crystal defects and dissolution. International Journal of Pharmaceutics 9(2):137-152.

133. Byrn S, Pfeiffer R, Stowell J. 1999. Role of defects in solid-state reactions. In Byrn S, Pfeiffer R, Stowell J, editors. Solid State Chemistry of Drugs 2ed., West Lafayette.: SSCI. p 482-484.

134. Myerson AS. 1999. Crystal lattice defects. In Myerson AS, editor Molecular Modeling Applications in Crystallization, ed., Cambridge: Cambridge University Press. p 84-85.

135. Boldyrev V 1993. Reactivity of solids. Journal of Thermal Analysis 40:1041-1062.

136. Grant DJW, York P 1986. Entropy of processing: a new quantity for comparing the solid state disorder of pharmaceutical materials. International Journal of Pharmaceutics 30(2-3):161-180.

137. Chamarthy SP, Pinal R 2008. The nature of crystal disorder in milled pharmaceutical materials. Colloids and Surfaces A: Physicochemical and Engineering Aspects 331(1-2):68-75.

138. Wikipedia: Crystallographic defect, 2014. ed. *Accessed April 2014*

139. Bechard SR, Down GR 1992. Infrared imaging of pharmaceutical materials undergoing compaction. Pharmaceutical research 9(4):521-528.

140. Weber G. 2012. Influence of Temperature on the Compaction and Strength of Some Pharmaceutical Excipients ed., Department of Materials Science and Engineering, Drexel University, Philadelphia, PA, 19104.

141. Cespi M, Bonacucina G, Casettari L, Ronchi S, Palmieri GF 2013. Effect of temperature increase during the tableting of pharmaceutical materials. International Journal of Pharmaceutics 448(1):320-326.

142. Parrott EL 1974. Milling of pharmaceutical solids. Journal of Pharmaceutical Sciences 63(6):813-829.

143. Qiu Z, Stowell JG, Cao W, Morris KR, Byrn SR, Carvajal MT 2005. Effect of milling and compression on the solid-state Maillard reaction. J PharmSci 94(11):2568-2580.

144. Qiu Z, Stowell JG, Morris KR, Byrn SR, Pinal R 2005. Kinetic study of the Maillard reaction between metoclopramide hydrochloride and lactose. IntJ Pharm 303(1-2):20-30.

145. Otsuka M, Kaneniwa N 1986. Effect of seed crystals on solid-state transformation of polymorphs of chloramphenicol palmitate during grinding. J Pharm Sci 75(5):506-511.

146. Otsuka M, Matsumoto T, Kaneniwa N 1986. Effect of environmental temperature on polymorphic solid-state transformation of indomethacin during grinding. Chem Pharm Bull(Tokyo) 34(4):1784-1793.

147. Otsuka M, Matsumoto T, Kaneniwa N 1989. Effects of the mechanical energy of multi-tableting compression on the polymorphic transformations of chlorpropamide. J Pharm Pharmacol 41(10):665-669.

148. Otsuka.m, Otsuka K, Kaneniwa N 1994. Relation between polymorphic transformation pathway during grinding and the physicochemical properties of bulk powders for pharmaceutical preparations. Drug DevIndPharm 20:1649-1660.

149. Otte A, Carvajal MT 2011. Assessment of milling-induced disorder of two pharmaceutical compounds. Journal of Pharmaceutical Sciences 100(5):1793-1804.

150. Deng Z, Xu S, Li S 2008. Understanding a relaxation behavior in a nanoparticle suspension for drug delivery applications. International Journal of Pharmaceutics 351(1–2):236-243.

151. Bailey A 2008. Electrostatic phenomena during powder handling. Powder Technology 37 (1984):71-85.

152. Engers DA, Fricke MN, Storey RP, Newman AW, Morris KR 2006. Triboelectrification of pharmaceutically relevant powders during low-shear tumble blending. Journal of Electrostatics 64(12):826-835.

153. Han X, Ghoroi C, To D, Chen Y, Dav+© R 2011. Simultaneous micronization and surface modification for improvement of flow and dissolution of drug particles. International Journal of Pharmaceutics 415:185-195.

154. Ng WK, Kwek JW, Yuen A, Tan CL, Tan R 2010. Effect of milling on DSC thermogram of excipient adipic acid. AAPSPharmSciTech 11(1):159-167.

155. Burnett DJ, Khoo J, Naderi M, Heng JY, Wang GD, Thielmann F 2012. Effect of processing route on the surface properties of amorphous indomethacin measured by inverse gas chromatography. AAPS PharmSciTech 13(4):1511-1517.

156. Pu Y, Mazumder M, Cooney C 2009. Effects of electrostatic charging on pharmaceutical powder blending homogeneity. Journal of Pharmaceutical Sciences 98(7):2412-2421.

157. Adi H, Kwok PCL, Crapper J, Young PM, Traini D, Chan H-K 2010. Does electrostatic charge affect powder aerosolisation? Journal of Pharmaceutical Sciences 99(5):2455-2461.

158. Kulvanich P, Stewart P 1987. An evaluation of the air stream Faraday cage in the electrostatic charge measurement of interactive drug systems. Int J Pharm 36:243-252.

159. Staniforth JN, Rees JE 1982. Electrostatic charge interactions in ordered powder mixes. J Pharm Pharmacol 34:69-76.

160. Wildfong PL, Hancock BC, Moore MD, Morris KR 2006. Towards an understanding of the structurally based potential for mechanically activated disordering of small molecule organic crystals. J Pharm Sci 95(12):2645-2656.

161. Hagan JT 1981. Impossibility of fragmenting small particles: brittle—ductile transition. Journal of Materials Science 16(10):2909-2911.

162. Kendall K 1975. The impossibility of comminuting small particles by compression. Nature 272:710-711.

163. Roberts RJ, Rowe RC 1999. Brittle-ductile transitions in organic solids during comminution: a practical demonstration. The Journal of pharmacy and pharmacology 51(6):751-752.

164. Larsson I, Kristensen HG 2000. Comminution of a brittle/ductile material in a Micros Ring Mill. Powder Technology 107(1-2):175-178.

165. Roberts RJ, Rowe RC 1987. Brittle/ductile behaviour in pharmaceutical materials used in tabletting. International Journal of Pharmaceutics 36(2–3):205-209.

166. Lin M-C, Duncan-Hewitt WC 1994. Deformation kinetics of acetaminophen crystals. International Journal of Pharmaceutics 106(3):187-200.

167. Duncan-Hewitt WC, Mount DL, Yu A 1994. Hardness anisotropy of acetaminophen crystals. Pharm Res 11(5):616-623.

168. Shekunov BY, York P 2000. Crystallization processes in pharmaceutical technology and drug delivery design. Journal of Crystal Growth 211(1–4):122-136.

169. Heiskanen K 1995. On the difficulties of implementing particle size control in particulate processes. Powder Technology 82(1):13-19.

170. Steele G. 2004. Preformulation as an aid to product design in early drug development. In Gibson M, editor Pharmaceutical Preformulation and Formulation: A Practical Guide from Candidate Drug Selection to Commercial Dosage Form, ed., Boca Raton: Interpharm/CRC. p 175-289.

171. Ray Y-C, Jiang T-S, Wen CY 1987. Particle attrition phenomena in a fluidized bed. Powder Technology 49(3):193-206.

172. Hilden LR, Morris KR 2004. Physics of amorphous solids. Journal of Pharmaceutical Sciences 93(1):3-12.

173. Martin G, Bellon P 1997. "Driven alloys,". Solid State Physics, 50:189-331.

174. Okamoto PR, Lam NQ, Rehn LE 1999. Physics of crystal-to-glass transformations. Solid State Phys 52:1.

175. Crowley KJ, Zografi G 2002. Cryogenic grinding of indomethacin polymorphs and solvates: assessment of amorphous phase formation and amorphous phase physical stability. J Pharm Sci 91(2):492-507.

176. Feng T, Pinal R, Carvajal MT 2008. Process induced disorder in crystalline materials: Differentiating defective crystals from the amorphous form of griseofulvin. Journal of Pharmaceutical Sciences 97(8):3207-3221.

177. Karmwar P, Graeser K, Gordon KC, Strachan CJ, Rades T 2011. Investigation of properties and recrystallisation behaviour of amorphous indomethacin samples prepared by different methods. International Journal of Pharmaceutics 417(1ΓÇô2):94-100.

178. Patterson JE, James MB, Forster AH, Lancaster RW, Butler JM, Rades T 2005. The influence of thermal and mechanical preparative techniques on the amorphous state of four poorly soluble compounds. J Pharm Sci 94(9):1998-2012.

179. Botker JP, Karmwar P, Strachan CJ, Cornett C, Tian F, Zujovic Z, Rantanen J, Rades T 2011. Assessment of crystalline disorder in cryo-milled samples of indomethacin using atomic pair-wise distribution functions. International Journal of Pharmaceutics 417(1ΓÇô2):112-119.

180. Midoux N, Hošek P, Pailleres L, Authelin JR 1999. Micronization of pharmaceutical substances in a spiral jet mill. Powder Technology 104(2):113-120.

181. Teng S, Wang P, Zhu L, Young M-W, Gogos CG 2009. Experimental and numerical analysis of a lab-scale fluid energy mill. Powder Technology 195(1):31-39.

182. Mohanty B, Narasimhan KS 1982. Fluid energy grinding. Powder Technology 33(1):135-141.

183. Dobson B, Rothwell E 1969. Particle size reduction in a fluid energy mill. Powder Technology 3(1):213-217.

184. Ramanujam M, Venkateswarlu D 1969. Studies in fluid energy grinding. Powder Technology 3(1):92-101.

185. Perkins MC, Bunker M, James J, Rigby-Singleton S, Ledru J, Madden-Smith C, Luk S, Patel N, Roberts CJ 2009. Towards the understanding and prediction of material changes during micronisation using atomic force microscopy. EurJPharmSci 38(1):1-8.

186. James J, Crean B, Davies M, Toon R, Jinks P, Roberts CJ 2008. The surface characterisation and comparison of two potential sub-micron, sugar bulking excipients for use in low-dose, suspension formulations in metered dose inhalers. IntJ Pharm 361(1-2):209-221.

187. Feeley JC, York P, Sumby BS, Dicks H 1998. Determination of surface properties and flow characteristics of salbutamol sulphate, before and after micronisation. International Journal of Pharmaceutics 172(1-2):89-96.

188. Newell HE, Buckton G, Butler DA, Thielmann F, Williams DR 2001. The use of inverse phase gas chromatography to measure the surface energy of crystalline, amorphous, and recently milled lactose. Pharm Res 18(5):662-666.

189. Heng JY, Thielmann F, Williams DR 2006. The effects of milling on the surface properties of form I paracetamol crystals. Pharm Res 23(8):1918-1927.

190. Burnett D, Malde N, Williams D 2009. Characterizing amorphous materials with gravimetric vapour sorption techniques. Pharmaceutical Technology Europe 21(4):41-45.

191. Burnett DJ, Thielmann F, Booth J 2004. Determining the critical relative humidity for moisture-induced phase transitions. IntJPharm 287(1-2):123-133.

192. Crowley KJ, Zografi G 2001. The use of thermal methods for predicting glass-former fragility. Thermochimica Acta 380(2):79-93.

193. Planinsek O, Zadnik J, Kunaver M, Srcic S, Godec A 2010. Structural evolution of indomethacin particles upon milling: time-resolved quantification and localization of disordered structure studied by IGC and DSC. JPharmSci 99(4):1968-1981.

194. Ticehurst D, Basford A, Dallman I, Lukas M, Marshall V, Nichols G, Smith D 2000. Characterisation of the influence of micronisation on the crystallinity and physical stability of revatropate hydrobromide. International Journal of Pharmaceutics 193(2):247-259.

195. Ahmed H, Buckton G, Rawlins DA 1996. The use of isothermal microcalorimetry in the study of small degrees of amorphous content of a hydrophobic powder. International Journal of Pharmaceutics 130(2):195-201.

196. Saunders M, Podluii K, Shergill S, Buckton G, Royall P 2004. The potential of high speed DSC (hyper-DSC) for the detection and quantification of small amounts of amorphous content in predominantly crystalline samples. IntJ Pharm 274(1-2):35-40.

197. Hogan SE, Buckton G 2000. The quantification of small degrees of disorder in lactose using solution calorimetry. International Journal of Pharmaceutics 207(1–2):57-64.

198. Buckton G, Darcy P 1995. The use of gravimetric studies to assess the degree of crystallinity of predominantly crystalline powders. International Journal of Pharmaceutics 123(2):265-271.

199. Al-Hadithi D, Buckton G, Brocchini S 2004. Quantification of amorphous content in mixed systems: amorphous trehalose with lactose. Thermochimica Acta 417(2):193-199.

200. Alie J, Menegotto J, Cardon P, Duplaa H, Caron A, Lacabanne C, Bauer M 2004. Dielectric study of the molecular mobility and the isothermal crystallization kinetics of an amorphous pharmaceutical drug substance. JPharmSci 93(1):218-233.

201. Ambarkhane AV, Pincott K, Buckton GB 2005. The use of inverse gas chromatography and gravimetric vapour sorption to study transitions in amorphous lactose. International Journal of Pharmaceutics 294(1-2):129-135.

202. Andronis V, Zografi G 1997. Molecular mobility of supercooled amorphous indomethacin, determined by dynamic mechanical analysis. Pharm Res 14(4):410-414.

203. Andronis V, Zografi G 1998. The molecular mobility of supercooled amorphous indomethacin as a function of temperature and relative humidity. Pharm Res 15(6):835-842.

204. Angberg M 1995. Lactose and thermal analysis with special emphasis on microcalorimetry. Thermochimica Acta 248:161-176.

205. Bates S, Zografi G, Engers D, Morris K, Crowley K, Newman A 2006. Analysis of amorphous and nanocrystalline solids from their X-ray diffraction patterns. Pharm Res 23(10):2333-2349.

206. Abiad MG, Gonzalez DC, Mert B, Campanella OH, Carvajal MT 2010. A novel method to measure the glass and melting transitions of pharmaceutical powders. IntJPharm 396(1-2):23-29.

207. Alem N, Beezer AE, Gaisford S 2010. Quantifying the rates of relaxation of binary mixtures of amorphous pharmaceuticals with isothermal calorimetry. IntJPharm 399(1-2):12-18.

208. Alonzo DE, Zhang GG, Zhou D, Gao Y, Taylor LS 2010. Understanding the behavior of amorphous pharmaceutical systems during dissolution. PharmRes 27(4):608-618.

209. Bhugra C, Shmeis R, Pikal MJ 2008. Role of mechanical stress in crystallization and relaxation behavior of amorphous indomethacin. Journal of Pharmaceutical Sciences 97(10):4446-4458.

210. Buckton G, Ambarkhane A, Pincott K 2004. The use of inverse phase gas chromatography to study the glass transition temperature of a powder surface. Pharm Res 21(9):1554-1557.

211. Carstensen JT, Morris T 1993. Chemical stability of indomethacin in the solid amorphous and molten states. JPharmSci 82(6):657-659.

212. Chieng N, Aaltonen J, Saville D, Rades T 2009. Physical characterization and stability of amorphous indomethacin and ranitidine hydrochloride binary systems prepared by mechanical activation. European Journal of Pharmaceutics and Biopharmaceutics 71(1):47-54.

213. Correia NT, Ramos JJ, Descamps M, Collins G 2001. Molecular mobility and fragility in indomethacin: a thermally stimulated depolarization current study. PharmRes 18(12):1767-1774.

214. Desprez S, Descamps M 2006. Transformations of glassy indomethacin induced by ball-milling. Journal of Non-Crystalline Solids 352(42-49):4480-4485.

215. Luisi BS, Medek A, Liu Z, Mudunuri P, Moulton B 2012. Milling-induced disorder of pharmaceuticals: One-phase or two-phase system? Journal of Pharmaceutical Sciences 101(4):1475-1485.

216. Descamps M, Correia NT, Derollez P, Danede F, Capet F 2005. Plastic and Glassy Crystal States of Caffeine. The Journal of Physical Chemistry B 109(33):16092-16098.

217. Pirttimaki J, Laine E, Ketolainen J, Paronen Pi 1993. Effects of grinding and compression on crystal structure of anhydrous caffeine. International Journal of Pharmaceutics 95(1-3):93-99.

218. Chaumeil JC 1998. Micronization: a method of improving the bioavailability of poorly soluble drugs. Methods FindExpClinPharmacol 20(3):211-215.

219. Grisedale LC, Jamieson MJ, Belton PS, Barker SA, Craig M 2011. Characterization and quantification of amorphous material in milled and spray-dried salbutamol sulfate: A comparison of thermal, spectroscopic, and water vapor sorption approaches. Journal of Pharmaceutical Sciences 100(8):3114-3129.

220. Zhou D, Zhang GGZ, Law D, Grant DJW, Schmitt EA 2008. Thermodynamics, molecular mobility and crystallization kinetics of amorphous griseofulvin. Molecular Pharmaceutics 5(6):927-936.

221. Lin Y, Cogdill RP, Wildfong PLD 2009. Informatic calibration of a materials properties database for predictive assessment of mechanically activated disordering potential for small molecule organic solids. Journal of Pharmaceutical Sciences 98(8):2696-2708.

222. Lin SY, Lin HL, Li MJ 2003. Reproducibility of temperature response and long-term stability of thermo-responsive membrane prepared by adsorption of binary liquid crystals. Journal of Membrane Science 225(1-2):135-143.

223. Fletcher DA, McMeeking RF, Parkin D 1996. The United Kingdom Chemical Database Service. Journal of Chemical Information and Computer Sciences 36(4):746-749.

224. 2011. NIST Chemistry WebBook, NIST Standard Reference Database Number 69, http://webbook.nist.gov/chemistry/. ed. *Accessed April 2014*

225. Knox C, Law V, Jewison T, Liu P, Ly S, Frolkis A, Pon A, Banco K, Mak C, Neveu V, Djoumbou Y, Eisner R, Guo AC, Wishart DS 2011. DrugBank 3.0: a comprehensive

resource for 'omics' research on drugs. Nucleic Acids Res 39(Database issue):D1035-D1041.

226. 2011. MSDS Xchange. http://www.msdsxchange.com/english/index.cfm, ed. *Accessed April 2014*
227. 2011. Sigma-Aldrich. http://www.sigmaaldrich.com/sigma-aldrich/home.html ed. *Accessed April 2014*
228. 2011. Fisher Scientific. http://www.fisher.co.uk/, ed. *Accessed April 2014*
229. 2011. MP Biomedicals. wwwmpbiocom/, ed. *Accessed April 2014*
230. Tetko IV GJ, Todeschini R,Mauri A,Livingstone D,Ertl P,Palyulin VA,Radchenko EV,Zefirov NS,Makarenko AS,Tanchuk VY,Prokopenko VV. 2005. Virtual computational chemistry laboratory-design and description. J Comput Aided Mol Des 19(6):453-463.
231. 2005. VCCLAB - Virtual Computational Chemistry Laboratory. http://www.vcclab.org/, ed. *Accessed April 2014*
232. 2011. SpresiWeb 2.8, a Selective Chemical Synthesis and Reaction Database. http://www.spresi.com/, ed. *Accessed April 2014*
233. 2011. Marvin 5.4.0.1. ed.
234. 2011. Risk and safety statements. http://www.sigma.aldrich.com/sigma-aldrich/help/help-welcome/risk-and-safety-statements/risk-and-safetyhtml#indicationrisks, ed. *Accessed Aug 2011*
235. 2011. SIRI MSDS Index. http://hazard.com/msds/, ed. *Accessed April 2014*
236. van de SJ 2006. Searching the Cambridge Structural Database for the 'best' representative of each unique polymorph. Acta CrystallogrB 62(Pt 4):567-579.
237. 2011. The CSD SDfile. http://www.ccdc.cam.ac.uk/support/documentation/non.csd.formats/sdfilepdf, ed. p 5. *Accessed Aug 2011*
238. 2011. R-factors - A rough guide to the quality of structure determinations. http://wwwccdccamacuk/support/documentation/conquest/ConQuest/conquest3342html#231109, ed. *Accessed Aug 2011*
239. van de SJ, Motherwell S 2005. Searching the Cambridge Structural Database for polymorphs. Acta CrystallogrB 61(Pt 5):504-510.
240. Chu KA, Yalkowsky SH 2009. An interesting relationship between drug absorption and melting point. International Journal of Pharmaceutics 373(1-2):24-40.
241. 2011. Xemistry GmbH Cactvs. ed., http://85.214.71.72/. *Accessed Aug 2011*
242. Willart JF, Caron V, Descamps M 2007. Transformations of crystalline sugars upon milling. Journal of Thermal Analysis and Calorimetry 90(1):125-130.
243. Ng WK, Kwek JW, Tan RB 2008. Anomalous particle size shift during post-milling storage. Pharm Res 25(5):1175-1185.
244. Zhu HJ, Sacchetti M 2002. Solid state characterization of an neuromuscular blocking agent--GW280430A. IntJ Pharm 234(1-2):19-23.
245. Pedersen GP, F+ñldt P, Bergenst+Ñhl B, Kristensen HG 1998. Solid state characterisation of a dry emulsion: a potential drug delivery system. International Journal of Pharmaceutics 171(2):257-270.
246. Balani PN, Ng WK, Tan RB, Chan SY 2010. Influence of excipients in comilling on mitigating milling-induced amorphization or structural disorder of crystalline pharmaceutical actives. JPharmSci 99(5):2462-2474.
247. Balani PN, Wong SY, Ng WK, Widjaja E, Tan RB, Chan SY 2010. Influence of polymer content on stabilizing milled amorphous salbutamol sulphate. IntJPharm 391(1-2):125-136.
248. Yang W, Kwan CC, Ding YL, Ghadiri M, Roberts KJ 2007. Milling of sucrose. Powder Technology 174(1):14-17.

249. Zografi G 1988. States of Water Associated with Solids. Drug Development and Industrial Pharmacy 14(14):1905-1926.

250. Ahlneck C, Zografi G 1990. The molecular basis of moisture effects on the physical and chemical stability of drugs in the solid state. International Journal of Pharmaceutics 62(2-3):87-95.

251. Oksanen CA, Zografi G 1990. The relationship between the glass transition temperature and water vapor absorption by poly(vinylpyrrolidone). Pharm Res 7(6):654-657.

252. Hancock BC, Zografi G 1994. The relationship between the glass transition temperature and the water content of amorphous pharmaceutical solids. Pharm Res 11(4):471-477.

253. Tong P, Taylor LS, Zografi G 2002. Influence of alkali metal counterions on the glass transition temperature of amorphous indomethacin salts. Pharm Res 19(5):649-654.

254. Andronis V, Yoshioka M, Zografi G 1997. Effects of sorbed water on the crystallization of indomethacin from the amorphous state. J Pharm Sci 86(3):346-351.

255. Woodhead B. 2006. Internal GSK experiment (not public). ed.

256. Veber DF, Johnson SR, Cheng HY, Smith BR, Ward KW, Kopple KD 2002. Molecular Properties That Influence the Oral Bioavailability of Drug Candidates. Journal of Medicinal Chemistry 45(12):2615-2623.

257. Baird JA, Van Eerdenbrugh B, Taylor LS 2010. A classification system to assess the crystallization tendency of organic molecules from undercooled melts. Journal of Pharmaceutical Sciences 99(9):3787-3806.

258. Huang J, Kaul G, Cai C, Chatlapalli R, Hernandez-Abad P, Ghosh K, Nagi A 2009. Quality by design case study: an integrated multivariate approach to drug product and process development. IntJPharm 382(1-2):23-32.

259. Bartholomew DJ. 2010. Principal Components Analysis. In Peterson P, Baker E, McGaw B, editors. International Encyclopedia of Education (Third Edition), ed., Oxford: Elsevier. p 374-377.

260. Esbensen KH, Geladi P. 2009. 2.13 - Principal Component Analysis: Concept, Geometrical Interpretation, Mathematical Background, Algorithms, History, Practice. In Brown SD, Tauler R, Walczak B, editors. Comprehensive Chemometrics, ed., Oxford: Elsevier. p 211-226.

261. Wold S, Esbensen K, Geladi P 1987. Principal component analysis. Chemometrics and Intelligent Laboratory Systems 2(1–3):37-52.

262. Wang R, Fu Y, Lai L 1997. A New Atom-Additive Method for Calculating Partition Coefficients. Journal of Chemical Information and Computer Sciences 37(3):615-621.

263. 2011. Druglikeness. http://en.wikipedia.org/wiki/Druglikeness, ed. *Accessed Apr 2014*

264. Yu L, Reutzel-Edens SM, S.M. M, C.A 2000. Crystallization and Polymorphism of Conformationally Flexible Molecules: Problems, Patterns, and Strategies. OrgProcResDev 4:396-402.

265. Chattoraj S, Bhugra C, Telang C, Zhong L, Wang Z, Sun C. AAPS 2011, 2011.

266. Buckton G, Choularton A, Beezer AE, Chatham SM 1988. The effect of the comminution technique on the surface energy of a powder. International Journal of Pharmaceutics 47(1-3):121-128.

267. Olusanmi D, Ding Y, Ghadiri M, Roberts KJ. PARTEC2007, 2007.

268. Gupta MK, Vanwert A, Bogner RH 2003. Formation of physically stable amorphous drugs by milling with Neusilin. J Pharm Sci 92(3):536-551.

269. Mazel V, Delplace C, Busignies V, Faivre V, Tchoreloff P, Yagoubi N 2011. Polymorphic transformation of anhydrous caffeine under compression and grinding: a re-evaluation. Drug DevIndPharm.

270. Caron V, Hu Y, Tajber L, Erxleben A, Corrigan O, McArdle P, Healy A 2013. Amorphous Solid Dispersions of Sulfonamide/Soluplus-« and Sulfonamide/PVP Prepared by Ball Milling. AAPS PharmSciTech 14(1):464-474.

271. Chattoraj S, Bhugra C, Telang C, Zhong L, Wang Z, Sun C 2012. Origin of two modes of non-isothermal crystallization of glasses produced by milling. Pharm Res 29(4):1020-1032.

272. Erizal S, Yeyet Cahyati S, Nurono S, Auzal H 2008. Effect of Milling on Solid State Transformation of Sulfamethoxazole. International Journal of Pharmacology 4:140-144.

273. Takasuka M, Naki H 2001. IR and Raman spectral and X-ray structural studies of polymorphic forms of sulfamethoxazole. Vibrational Spectroscopy 25(2):197-2004.

274. Yang SS, Guillory JK 1972. Polymorphism in sulfonamides. JPharmSci 61(1):26-40.

275. Gaisford S, Dennison M, Tawfik M, Jones MD 2010. Following mechanical activation of salbutamol sulphate during ball-milling with isothermal calorimetry. IntJPharm 393(1-2):74-78.

276. Gorny M, Jakobs M, Mykhaylova V, Urbanetz NA 2007. Quantifying the degree of disorder in micronized salbutamol sulfate using moisture sorption analysis. Drug Development & Industrial Pharmacy 33(3):235-243.

277. Khalef N, Pinal R, Bakri A 2010. Limitations of amorphous content quantification by isothermal calorimetry using saturated salt solutions to control relative humidity: alternative methods. JPharmSci 99(4):2080-2089.

278. Woodhead B, Chui T. 2001. Solid state forms of Loperamide HCl: supporting patent information, Internal GSK Consumer Healthcare R&D study. ed.

279. Ito T, Byrn S, Chen X, Carvajal MT 2011. Thermal insight of mechanically activated bile acid powders. International Journal of Pharmaceutics 420(1):68-75.

280. Bhugra C, Rambhatla S, Bakri A, Duddu SP, Miller DP, Pikal MJ, Lechuga-Ballesteros D 2007. Prediction of the onset of crystallization of amorphous sucrose below the calorimetric glass transition temperature from correlations with mobility. J Pharm Sci 96(5):1258-1269.

281. Brittain HG, Bogdanowich SJ, Bugay DE, DeVincentis J, Lewen G, Newman AW 1991. Physical characterization of pharmaceutical solids. Pharm Res 8(8):963-973.

282. Alam S, Patel S, Bansal AK 2010. Effect of sample preparation method on quantification of polymorphs using PXRD. Pharm DevTechnol 15(5):452-459.

283. Dash AK, Khin-Khin A, Suryanarayanan R 2002. X-ray powder diffractometric method for quantitation of crystalline drug in microparticulate systems. I. Microspheres. JPharm Sci 91(4):983-990.

284. Kitahara S, Ishizuka T, Kikkoji T, Matsuda R, Hayashi Y 2004. Precision and detection limit of quality test for amorphous drug in powder X-ray diffractometry. IntJ Pharm 283(1-2):63-69.

285. Billinge SJ, Kanatzidis MG 2004. Beyond crystallography: the study of disorder, nanocrystallinity and crystallographically challenged materials with pair distribution functions. Chem Commun(Camb) (7):749-760.

286. Billinge SJ, Levin I 2007. The problem with determining atomic structure at the nanoscale. Science 316(5824):561-565.

287. X'Pert Highscore Plus online help 2009, V3.0. 3.0 ed.: PANalytical B.V.

288. Woodhead B. 2008. GSK Compendium of analytical procedures: Thermal Analysis. ed. p 16.

289. British Pharmacopoeia 2013. Appendix V M. Thermal analysis. 2013 ed. *Accessed Aug 2013*

290. British Pharmacopoeia 2013. Appendix IX M. Water-solid interactions: determination of sorption-desorption isotherms and of water activity. 2013 ed. *Accessed Aug 2013*

291. Interpreting DSC Data Glass Transition & Melting - TA traning seminar, 2004. In Instruments T, editor TA traning seminar, ed.

292. van Dooren AA, M³ller BW 1981. Influence of experimental variables on curves in differential scanning calorimetry. Part III. Effects on peak height, peak width, shape index and baseline displacement. Thermochimica Acta 49(2-3):175-183.

293. van Dooren AA, M³ller BW 1981. Influence of experimental variables on curves in differential scanning calorimetry. Part I. Study design and results of calibration checks. Thermochimica Acta 49(2-3):151-161.

294. van Dooren AA, M³ller BW 1981. Influence of experimental variables on curves in differential scanning calorimetry. Part II. Effects on baseline-related characteristics. Thermochimica Acta 49(2-3):163-173.

295. van Dooren AA, M³ller BW 1981. Influence of experimental variables on curves in differential scanning calorimetry. Part IV. Effects on peak-related temperatures and specific enthalpy. Thermochimica Acta 49(2-3):185-191.

296. Van Miltenburg JC, Cuevas-Diarte MA 1989. The influence of sample mass, heating rate and heat transfer coefficient on the form of DSC curves. Thermochimica Acta 156(2):291-297.

297. Woodhead B. 2008. Internal GSK investigation - TGMS investigation into the dissociation of pharmaceutical salts. ed.

298. Bradbury S, Evennett PJ. 1996. Contrast techniques in light microscopy. 01 ed.: Bios Scientific Publishers Ltd, Oxford, UK.

299. Davidson MW, Abramowitz M. 2002. Optical Microscopy. In Hornak J, editor Encyclopedia of Imaging Science and Technology, ed.: Wiley-Interscience, New York. p 1106-1141.

300. Gunter M 2004. The polarzed light microscope: should we teach the use of 19th century instrument in the 21st century. J Geo Ed 52(1):34-44.

301. Stockton B. 2010. GSK Compendium of Analytical Procedures CAP006 Particle Size Analysis. ed.

302. British Pharmacopoeia 2013, Appendix XVII P. Particle size analysis by laser light diffraction. 2013 ed. *Accessed Aug 2013*

303. Byrn S, Pfeiffer R, Stowell J. 1999. Particle size analysis. Solid State Chemistry of Drugs, 2 ed., West Lafayette.: SSCI. p 103-110.

304. ISO 13320-1, 1999Particle size analysis - Laser diffraction methods Part 1: General Principles. ed.

305. Brittain HG. 1995. Overview of physical characterization methodology. In Brittain HG, editor Physical characterization of pharmaceutical solids, ed., New York: Marcel Dekker. p 12-13.

306. British Pharmacopoeia 2013 Appendix XVII A. Particle size of powders. 2013 ed. *Accessed Aug 2013*

307. Hancock BC, Zografi G 1996. Effects of solid-state processing on water vapor sorption by aspirin. J Pharm Sci 85(2):246-248.

308. Young PM, Chiou H, Tee T, Traini D, Chan HK, Thielmann F, Burnett D 2007. The use of organic vapor sorption to determine low levels of amorphous content in processed pharmaceutical powders. Drug Development & Industrial Pharmacy 33(1):91-97.

309. Meenan E. 2010. GSK WD2010/00756/00 Training Module for Gravimetric Vapour Sorption (GVS). ed.

310. Reutzel-Edens SM, Newman A. 2006. Physical characterization of hygroscpicity in pharmaceutical solids. In Hilfiker R, editor Polymorphism in the pharmaceutical industry, ed., Weinheim, Germany: Wiley-VCH. p 235-258.

311. Burnett DJ, Thielmann F, Booth J 2004. Determining the critical relative humidity for moisture-induced phase transitions. International Journal of Pharmaceutics 2:123-133.

312. Hogan SE, Buckton G. 2001. The application of near infrared spectroscopy and dynamic vapor sorption to quantify low amorphous contents of crystalline lactose. PharmRes,, ed. p 112-116.

313. Buckton G, Darcy P 1995. The influence of additives on the recrystallisation of amorphous spray dried lactose. International Journal of Pharmaceutics 121(1):81-87.

314. Kontny MJ, Zografi G. 1995. Sorption of water by solids. In Brittain HG, editor Physical characterization of pharmaceutical solids, ed., New York: Marcel Dekker. p 387-415.

315. Weston H. 2009. M0004187v2 the CD generic fast gradient (8 minute) HPLC method for macro controlled open access systems. ed.

316. Byrn S, Pfeiffer R, Stowell J. 1999. Infrared Spectroscopy of solids. Solid State Chemistry of Drugs, 2 ed., West Lafayette.: SSCI. p 111.

317. Chalmers J, Dent G. 2006. Vibrational Spectroscopic methods in pharamaceutical solid-state characterization. In Hilfiker R, editor Polymorphism in the pharmaceutical industry, ed., Weinheim, Germany: Wiley-VCH. p 95-138.

318. Stockton B. 2003. GSK Method PDMH 2364/01 - Standard Analytical Method for Recording FT-IR Spectra. ed.

319. British Pharmacopoeia Appendix XVII B. Sieves and filters. 2013 ed. *Accessed Aug 2013*

320. CrstalWeb. https://cdsdlacuk/cweb, ed. *Accessed Aug 2011*

321. British Pharmacopoeia Volume V, Infrared Reference Spectra Paracetamol RS258. British Pharmacopoeia, 2013 ed. *Accessed Aug 2013*

322. NIST Acetaminophen Data IR spectra 103-90-2. NIST Standard Reference Database 69: NIST Chemistry WebBook, ed. *Accessed Aug 2013*

323. Wang S, Lin SY, wei YS 2002. Transformation of Metastable Forms of Acetaminophen Studied by Thermal Fourier Transform Infrared (FT-IR) Microspectroscopy. ChemPharmBull 50(2):153-156.

324. Bhavani K, Sankaranarayanan k, Jerome DS 2012. Biologically Essential Drug Material Crystallization and Characterization. International Journal of Scientific & Engineering Research 3(8):3.

325. Khan MSA 2010. PhD Thesis - Solid dispersions: Formulation, characterisation, permeability and genomic evaluation. Ashton University.

326. Burgina EB, Baltakhino VP, Boldyreva EV, Shakhtshneider TP 2004. Ir spectra of paracetamol and phenacetin: 1. Theoretical and experimental studies. Journal of Structural Chemistry 45(1):64-73.

327. British Pharmacopoeia 2013. Volume V, Infrared Reference Spectra Indometacin RS187. British Pharmacopoeia, 2013 ed.

328. Rezaei MA, Kebriaee ZA, Keshavarz M, Ahmadi A, Mohtat B 2010. Preparation and in-vitro evaluation of indomethacin nanoparticles. DARU 18(3):185-192.

329. Giordano F, Pavan M, Bettinetti GP, Pavesi L 1988. Solid state characterization and solubility enhancement of loperamide hydrochloride. Farmaco Prat 43(9):267-278.

330. Van Rompay J, Carter JE. 1990. Loperamide Hydrochloride. In Klaus F, editor Analytical Profiles of Drug Substances, Volume 19 ed.: Academic Press. p 341-365.

331. Woodhead B, Chui T. 2000. Physiochemical characterisation of loperamide hydrochloride crstal forms- part I , Internal SmithKline Beecham Consumer Healthcare R&D study, Weybridge, UK. ed.

332. Gautam SG, Rai JP, Billshaiya U, Jain N, Vikram P, Jain DK 2013. Formulation and evaluation of mouth dissolving tablet of loperamide. IJPSR 4(5):1782-1788.

333. British Pharmacopoeia 2013. Volume V, Infrared Reference Spectra Salbutamol sulphate RS315. British Pharmacopoeia, 2013 ed.

334. NIST 2013. Acetylsalicylic acid Data IR spectra 50-78-2. NIST Standard Reference Database 69: NIST Chemistry WebBook, ed. *Accessed Aug 2013*

335. NIST 2013. Sulfamerazine Data IR spectra 127-79-7. NIST Standard Reference Database 69: NIST Chemistry WebBook, ed. *Accessed Aug 2013*

336. Caria MR, Mohamed R 1992. Positive indentification of two orthorhombic polymorphs of sulfamerazine (C11H12N4O2S), their thermal analyses and structural comparison. Acta Crystallographica Section B 48(4):492-498.

337. Cao X, Sun C, Thamann TJ 2005. A study of sulfamerazine single crystals using atomic force microscopy, transmission light microscopy, and Raman spectroscopy. JPharmSci 94(9):1881-1892.

338. NIST 2013.Sulfadiazine Data IR spectra 68-35-9. NIST Standard Reference Database 69: NIST Chemistry WebBook, ed. *Accessed Aug 2013*

339. NIST 2013.Caffeine Data IR spectra 58-08-2. NIST Standard Reference Database 69: NIST Chemistry WebBook, ed. *Accessed Aug 2013*

340. NIST 2013. Methyl paraben Data IR spectra 99-76-3. NIST Standard Reference Database 69: NIST Chemistry WebBook, ed. *Accessed Aug 2013*

341. ChemSpider. http://www.chemspider.com/, ed. *Accessed Aug 2013*

342. Cesaro A, Starec G 1980. Thermodynamic properties of caffeine crystal forms. The Journal of Physical Chemistry 84(11):1345-1346.

343. Lehto VP, Laine E 1998. A kinetic study of polymorphic transition of anhydrous caffeine with microcalorimeter. Thermochimica Acta 317(1):47-58.

344. Batt I, Brown A. 2007. GSK First Intent Process Guide - micronisation. ed.

345. Dujardin N, Willart JF, Dudognon E, Hθdoux A, Guinet Y, Paccou L, Chazallon B, Descamps M 2008. Solid state vitrification of crystalline [alpha] and [beta]-D-glucose by mechanical milling. Solid State Communications 148(1-2):78-82.

346. Patel AD, Luner PE, Kemper MS 2001. Low-level determination of polymorph composition in physical mixtures by near-infrared reflectance spectroscopy. Journal of Pharmaceutical Sciences 90(3):360-370.

347. Thirunahari S, Aitipamula S, Chow PS, Tan RB 2010. Conformational polymorphism of tolbutamide: A structural, spectroscopic, and thermodynamic characterization of Burger's forms I-IV. JPharmSci 99(7):2975-2990.

348. Ravindra Acharya K, Kuchela KN, Kartha G 1982. Crystal structure of sulfamerazine. Journal of Crystallographic and Spectroscopic Research 12(4):369-376.

349. Davis T. 2011. Fingerprinting analysis of non-crystalline pharmaceutical compounds using high energy X-rays and the total scattering pair distribution function. Graduate School of Arts and Sciences, ed.: COLUMBIA UNIVERSITY.

350. Johnson M, Lake P, Woodhead B. 2009. Meeting to Determine Final List of Samples for the Pairwise Distribution Function (PDF) Studies. ed., Internal GSK Document: Glaxosmithkline.

351. Woodhead B, Lake P. 2010. Cryromilling and characteristaion of sulfamerazine, caffeine, cefuroxime axetil. ed.: Glaxosmithkline Tonbridge R&D.

352. Wu T, Sun Y, Li N, de Villiers MM, Yu L 2007. Inhibiting surface crystallization of amorphous indomethacin by nanocoating. Langmuir 23(9):5148-5153.

353. Wu T, Yu L 2006. Surface crystallization of indomethacin below Tg. Pharm Res 23(10):2350-2355.

354. Matsumoto T, Zografi G 1999. Physical properties of solid molecular dispersions of indomethacin with poly(vinylpyrrolidone) and poly(vinylpyrrolidone-co-vinyl-acetate) in relation to indomethacin crystallization. Pharm Res 16(11):1722-1728.

355. Weuts I, Kempen D, Verreck G, Peeters J, Brewster M, Blaton N, Van den Mooter G 2005. Salt formation in solid dispersions consisting of polyacrylic acid as a carrier and three basic model compounds resulting in very high glass transition temperatures and

constant dissolution properties upon storage. European Journal of Pharmaceutical Sciences 25(4-5):387-393.

356. Tong P, Zografi G 1999. Solid-state characteristics of amorphous sodium indomethacin relative to its free acid. Pharm Res 16(8):1186-1192.

357. Tong P, Zografi G 2001. A study of amorphous molecular dispersions of indomethacin and its sodium salt. J Pharm Sci 90(12):1991-2004.

358. Dhumal RS, Biradar SV, Paradkar AR, York P 2009. Particle engineering using sonocrystallization: Salbutamol sulphate for pulmonary delivery. International Journal of Pharmaceutics 368(1-2):129-137.

359. Mueannoom W, Srisongphan A, Taylor KMG, Hauschild S, Gaisford S 2012. Thermal ink-jet spray freeze-drying for preparation of excipient-free salbutamol sulphate for inhalation. Eur J Pharm Biopharm 80:149-155.

360. Woodhead B. 2010. Influences of sample and instrument parameters on DSC responses and thermograms - GSK Technical Expert Team Training presentation. ed.: GlaxoSmithKline.

361. Zhang GG, Gu C, Zell MT, Burkhardt RT, Munson EJ, Grant DJ 2002. Crystallization and transitions of sulfamerazine polymorphs. JPharmSci 91(4):1089-1100.

362. Caron V, Hu Y, Tajber L, Erxleben A, Corrigan O, McArdle P, Healy A 2013. Amorphous Solid Dispersions of Sulfonamide/Soluplus® and Sulfonamide/PVP Prepared by Ball Milling. AAPS PharmSciTech 14(1):464-474.

363. de Villiers MM 1995. Influence of cohesive properties of micronized drug powders on particle size analysis. J Pharm BiomedAnal 13(3):191-198.

364. Young PM, Price R 2004. The influence of humidity on the aerosolisation of micronised and SEDS produced salbutamol sulphate. EurJPharmSci 22(4):235-240.

365. Zeng XM, Martin GP, Marriott C. 2001. Particulate interations in dry powder formulations for inhaltion. ed., london: Taylor & Francis.

366. Grisedale LC, Belton PS, Jamieson MJ, Barker SA, Craig DQ 2012. An investigation into water interactions with amorphous and milled salbutamol sulphate: the development of predictive models for uptake and recrystallization. IntJ Pharm 422(1-2):220-228.

367. Ahmed H, Buckton G, Rawlins DA 1998. Crystallisation of partially amorphous griseofulvin in water vapour: determination of kinetic parameters using isothermal heat conduction microcalorimetry. International Journal of Pharmaceutics 167(1–2):139-145.

368. Aso Y, Yoshioka S, Kojima S 2001. Feasibility of using isothermal microcalorimetry to evaluate the physical stability of amorphous nifedipine and phenobarbital. Thermochimica Acta 380(2):199-204.

369. Bahl D, Bogner RH 2006. Amorphization of Indomethacin by Co-Grinding with Neusilin US2: amorphization kinetics, physical stability and mechanism. Pharm Res 23(10):2317-2325.

370. British Pharmacopoeia 2013. Appendix XVII O. Optical microscopy, 2013. 2013 ed. *Accessed Aug 2013*

371. British Pharmacopoeia 2013. Appendix XVII U. Crystallinity, 2013. 2013 ed. *Accessed Aug 2013*

372. Guenette E, Barrett A, Kraus D, Brody R, Harding L, Magee G 2009. Understanding the effect of lactose particle size on the properties of DPI formulations using experimental design. IntJPharm 380(1-2):80-88.

373. Shariare MH, de Matas M, York P 2011. Effect of crystallisation conditions and feedstock morphology on the aerosolization performance of micronised salbutamol sulphate. International Journal of Pharmaceutics 415:62-72.

374. Shoyele SA, Cawthorne S 2006. Particle engineering techniques for inhaled biopharmaceuticals. AdvDrug Deliv Rev 58(9-10):1009-1029.

375. Siekmeier R, Scheuch G 2008. Systemic treatment by inhalation of macromolecules--principles, problems, and examples. Journal of physiology and pharmacology : an official journal of the Polish Physiological Society 59 Suppl 6:53-79.

376. Weers JG, Tarara TE, Clark AR 2007. Design of fine particles for pulmonary drug delivery [Review]. Expert Opinion on Drug Delivery 4(3):297-313.

377. Tanabe S, Higashi K, Umino M, Limwikrant W, Yamamoto K, Moribe K 2012. Yellow coloration phenomena of incorporated indomethacin into folded sheet mesoporous materials. International Journal of Pharmaceutics 429:38-45.